

2008-03-18

An Investigation of the Electrical Short Circuit Characteristics of Tin Whiskers

Karim Joseph Courey

University of Miami, Karim.J.Courey@nasa.gov

Follow this and additional works at: https://scholarlyrepository.miami.edu/oa_dissertations

Recommended Citation

Courey, Karim Joseph, "An Investigation of the Electrical Short Circuit Characteristics of Tin Whiskers" (2008). *Open Access Dissertations*. 38.

https://scholarlyrepository.miami.edu/oa_dissertations/38

This Open access is brought to you for free and open access by the Electronic Theses and Dissertations at Scholarly Repository. It has been accepted for inclusion in Open Access Dissertations by an authorized administrator of Scholarly Repository. For more information, please contact repository.library@miami.edu.

UNIVERSITY OF MIAMI

AN INVESTIGATION OF THE
ELECTRICAL SHORT CIRCUIT CHARACTERISTICS
OF TIN WHISKERS

By

Karim J. Courey

A DISSERTATION

Submitted to the Faculty
of the University of Miami
in partial fulfillment of the requirements for
the degree of Doctor of Philosophy

Coral Gables, Florida

May 2008

©2008
Karim J. Courey
All Rights Reserved

UNIVERSITY OF MIAMI

A dissertation submitted in partial fulfillment
of the requirements of for the degree of
Doctor of Philosophy

AN INVESTIGATION OF THE ELECTRICAL SHORT CIRCUIT
CHARACTERISTICS OF TIN WHISKERS

Karim J. Courey

Approved:

Dr. Shihab Asfour
Professor and Associate Dean
College of Engineering

Dr. Terri A. Scandura
Dean of the Graduate School

Dr. Sohyung Cho
Assistant Professor of Industrial
Engineering

Dr. Moiez Tapia
Professor of Electrical and Computer
Engineering

Dr. Arzu Onar
Assistant Member
Department of Biostatistics
St. Jude Children's Research Hospital
Memphis, TN

COUREY, KARIM J

An Investigation of the Electrical Short
Circuit Characteristics of Tin
Whiskers.

(Ph.D., Industrial Engineering)
(May 2008)

Abstract of a dissertation at the University of Miami.

Dissertation supervised by Professor Shihab Asfour
No. of pages in the text. (254)

Existing risk simulations make the assumption that when a free tin whisker has bridged two adjacent exposed electrical conductors, the result is an electrical short circuit. This conservative assumption is made because shorting is a random event that has a currently unknown probability associated with it. Due to contact resistance electrical shorts may not occur at lower voltage levels. In these experiments, the effect of varying voltage on the breakdown of the contact resistance which leads to a short circuit was studied. From this data, the probability of an electrical short was estimated, as a function of voltage, given that a free tin whisker has bridged two adjacent exposed electrical conductors.

Also, three tin whiskers grown from the same Space Shuttle Orbiter card guide used in the aforementioned experiment were cross-sectioned and studied using a focused ion beam (FIB). The rare polycrystalline structure seen in the FIB cross section was confirmed using transmission electron microscopy (TEM). The FIB was also used to cross section two card guides to facilitate the measurement of the grain size of each card guide's tin plating to determine its finish.

NOTICE

This document was prepared under the sponsorship of the National Aeronautics and Space Administration. Neither the United States government nor any person acting on behalf of the United States government assumes any liability resulting from the use of the information contained in this document, or warrants that such use will be free from privately owned rights.

DEDICATION

I would like to dedicate this work to my wife Daphne and our children Michael and Elizabeth. I thank them for their support, understanding and patience during the coursework, research, and writing of this dissertation.

ACKNOWLEDGMENTS

I thank all of my committee members; Dr. Shihab Asfour, Dr. Arzu Onar, Dr. Moiez Tapia, and Dr. Sohyung Cho for their advice and guidance. I also thank Dr. Henning Leidecker of NASA and Jay Brusse of Perot Systems at Goddard Space Flight Center for sharing their vast knowledge on the topic of tin whiskers, and taking the time to answer the many questions posed throughout this experiment including, but not limited to, the whisker bending model, the use of a micromanipulator for whisker probing, and oxide breakdown theory.

In addition, I would also like to thank the managers at NASA who supported all of my doctoral studies including Steve Poulos, Armando Oliu, and Jon Cowart of Johnson Space Center, and Anne Gawronski of Kennedy Space Center. I also thank Jon Bayliss and Larry Ludwig of NASA at Kennedy Space Center for their support with LabVIEW software and experimentation, M. Clara Wright of NASA at Kennedy Space Center for her support with materials analysis, Zia Rahman with the Materials Characterization Facility, AMPAC, University of Central Florida (UCF) for his expertise in FIB and TEM operation and analysis, Mike Spates, Pete Marciniak, Sandy Loucks, James Neihoff, Pete Richiuso and Roy King of NASA Kennedy Space Center for their help with the fabrication/modification of the test equipment, Larry Batterson for his expertise in photography and digital imaging, Lindsay Keller of NASA Johnson Space Center for reviewing the diffraction patterns, Shaun Nerolich of United Space Alliance for his help with the cantilever beam model, and Mike Madden of United Space Alliance for his software expertise with probability model evaluation and breakdown voltage selection.

I also thank the librarians at the Kennedy Space Center Library who filled my many requests for non-electronic articles that I needed for the literature review: Beverly

Bush, Deborah Guelzow, Linda Holten-Hamilton, Lori Uffner, Susan Gray Byrd and
Melanie Carlson. I also want to thank the employees of the University of Miami Library;
Carmen Gaskell, John Renaud, Ron Figueroa for their help with inter-library loans
including overseas library loans, and the procurement of rare articles.

TABLE OF CONTENTS

LIST OF TABLES	ix
LIST OF FIGURES	x
CHAPTER 1: INTRODUCTION	1
Tin Whiskers.....	1
CHAPTER 2: REVIEW OF LITERATURE	3
Tin Whisker Phenomenon	3
The Purpose of Tin Plating in Electronics	6
Physical Tin Whisker Characteristics	6
Shapes	6
Length	7
Diameter	7
Growth Rate.....	7
Incubation Period.....	8
Growth Density	8
Electrical Tin Whisker Characteristics	9
Resistivity	9
Current Carrying Capability	9
Superconductivity	9
Mechanical Tin Whisker Characteristics	10
Elastic and Plastic Properties.....	10
Vibration and Shock	11
Other Types of Metal Whiskers.....	11
Failure Modes	12
Electrical Short Circuits	12
Metal Vapor Arcing.....	13
Loose Whiskers	14
Reflections.....	14
Failure Experiences	15
Medical	15
Power Plant.....	15
Computer Rooms.....	16
Military	16
Satellites	16
Extensive List of Metal Whisker Failures	17
Useful Applications of Metal Whiskers	17
Lead-Free Movement.....	17
WEEE and RoHS	18
Requested Exemptions	18
Other Legislation	19
Substitute Materials for Tin Lead Alloys	19

Complications from Lead-Free Materials.....	20
Growth Mechanism Theories	21
Dislocation.....	22
Recrystallization.....	22
Oxidation.....	24
Factors that Effect Tin Whisker Growth	25
Applied Stress.....	25
Internal Stresses.....	25
Substrate Material Selection.....	26
Environmental Stresses	26
Plating and Process Chemistry	27
Growth Mitigation Strategies	27
Alloying with Lead.....	27
Underlay	28
Conformal Coating.....	28
Physical Barriers.....	29
Tin Finish Selection (Matte vs. Bright).....	29
Thickness of Plating	29
Heat Treatments.....	30
Solder Dipping.....	30
Hot Tin Dipped Coating.....	31
Risk Assessments and the Probability of Electrical Shorts	31
 CHAPTER 3: PROOF OF CONCEPT EXPERIMENT.....	 33
Breakdown Voltage Experiment.....	33
Review Stage	33
Equipment List	36
Methods	37
Validation	42
Results	42
Focused Ion Beam (FIB) Analysis	53
Methods	53
Results	57
 CHAPTER 4: METHODOLOGY	 60
Full Experiment	60
Whisker Breakdown Voltage Experiment.....	60
Equipment	60
Improvements.....	61
Method of Sample Selection	63
Analysis of Sample Size.....	64
Validation	68
Data Analysis	68
Sample Preparation for Transmission Electron Microscopy (TEM).....	68

CHAPTER 5: RESULTS AND DISCUSSION.....	73
Full Experiment	73
Breakdown Voltage Experiment	73
Tin Whisker Current and Voltage Data and Breakdown Voltage Selection	73
Data Analysis	73
Explanation of the Linearity Seen in the Voltage and Current Charts.....	87
Tin Whisker Current Carrying Characteristics.....	90
Comparison of Proof of Concept and Full Experiment Results.....	91
Limitations	94
Transmission Electron Microscopy (TEM).....	95
Card Guide Cross Sections Using a FIB	97
CHAPTER 6: CONCLUSION	101
Future Work.....	104
LIST OF REFERENCES.....	106
APPENDIX A.....	116
Proof of Concept Experiment Breakdown Voltage Data	116
APPENDIX B.....	117
Proof of Concept Experiment Tin Whisker Data Graphs	117
APPENDIX C.....	135
Full Experiment Breakdown Voltage Data.....	135
APPENDIX D.....	143
Full Experiment Tin Whisker Data Graphs	143
APPENDIX E.....	243
Statistical Analysis for the Full Experiment.....	243
APPENDIX F.....	249
Diffraction Patterns.....	249
APPENDIX G.....	253
Comparative Statistical Analysis for the Proof of Concept.....	253

LIST OF TABLES

Table 3-1 Kolmogorov-Smirnov test	51
Table 5-1 Tin whisker current carrying characteristics from the full experiment	91

LIST OF FIGURES

Figure 2-1 Relay with cover removed	4
Figure 2-2 Tin whiskers growing on armature of a hermetically seals relay.....	4
Figure 2-3 Microcircuit.....	5
Figure 2-4 Tin whiskers between microcircuit leads.....	5
Figure 2-5 Failed relay from tin whisker induced metal vapor arc.....	14
Figure 3-1 Cantilever beam whisker model illustrating the mechanical load placed on a whisker by the micromanipulator probe.	35
Figure 3-2 Micromanipulator and card guide	37
Figure 3-3 Close up photo of micromanipulator probe and whiskers on card guide.....	38
Figure 3-4 The micromanipulator probe touching tin whisker number 20 growing from the card guide.	38
Figure 3-5 PXI chassis with computer, power supply, voltmeter, and currentmeter.....	39
Figure 3-6 Software screen capture for whisker number 27.....	40
Figure 3-7 Tin whisker test station	41
Figure 3-8 Cable interconnect diagram for the tin whisker test station.....	41
Figure 3-9 Electrical schematic for the tin whisker test station.....	42
Figure 3-10 Whisker voltage as a function of time plotted for whisker number 32, illustrating a single transition point.....	43
Figure 3-11 Whisker current as a function of time plotted for whisker number 32, illustrating a single transition point.....	44
Figure 3-12 Whisker voltage as a function of time plotted for whisker number 4, illustrating multiple transition points.	45
Figure 3-13 Whisker current as a function of time plotted for whisker number 4, illustrating multiple transition points.	45
Figures 3-14 Whisker voltage as a function of time plotted for whisker number 2, illustrating multiple transition points with intermittent contact.....	46

Figures 3-15 Whisker current as a function of time plotted for whisker number 2, illustrating multiple transition points with intermittent contact.....	47
Figure 3-16 Cumulative distribution of sample data and the fitted inverse gaussian (3-parameter) model as a function of voltage.....	48
Figure 3-17 Probability density function of inverse gaussian (3-parameter) model as a function of voltage with a histogram of the sample data.....	49
Figure 3-18 The probability-probability (P-P) plot shows how well the data follows the inverse gaussian (3-parameter) distribution.....	50
Figure 3-19 Load Applied to Whisker Lying Across Two Conductors.....	53
Figure 3-20 Stereomicroscope image showing tin whiskers on carbon tape mounted on a microscopy stub. Magnification: 18X.....	54
Figure 3-21 FIB image of a tin whisker on the carbon tape substrate that has been sputter coated with gold palladium (NASA/UCF).....	55
Figure 3-22 FIB image of tin whisker removed from card guide shows a fluted outer surface. Platinum was deposited on the surface prior to sectioning in order to preserve the region of interest (NASA/UCF).	56
Figure 3-23 FIB image of sectioned whisker after ion beam milling (NASA/UCF).....	57
Figure 3-24 FIB image of as-sectioned tin whisker shows apparent variation in grain orientation within the cross-section. Image was taken at a 52° angle from horizontal (NASA/UCF).....	58
Figure 3-25 FIB image of two as-sectioned tin whiskers that exhibited the expected single-crystal cross section. Image was taken 52° from horizontal (NASA/UCF).	59
Figure 4-1 Tin whisker test station - full experiment	61
Figure 4-2 Test station - tin whisker probing.....	62
Figure 4-3 Micromanipulator probe in contact with a tin whisker	63
Figure 4-4 ATVC 31 card guides.....	64
Figure 4-5 Simulated population for 3-parameter inverse gaussian distribution.....	65
Figure 4-6 Population summary statistics.....	65
Figure 4-7 Population values and the numerical summaries of 5000 samples for each of the quantities of interest.....	66

Figure 4-8 Smoothed histograms for sample size evaluation	67
Figure 4-9 FIB image showing a cross section of a tin whisker that has been created by milling out trenches on either side of section. Magnification: 8000X (NASA/UCF)	69
Figure 4-10 FIB image showing the in-situ needle approaching whisker and FIB section. Magnification: 650X (NASA/UCF)	70
Figure 4-11 FIB image showing removal of tin whisker section using the in-situ needle. Magnification: 3500X (NASA/UCF)	71
Figure 4-12 FIB image of tin whisker section mounted on copper grid for TEM. Magnification: 5000X (NASA/UCF)	72
Figure 5-1 Breakdown voltage individual value plot	74
Figure 5-2 ANOVA natural log transformed data (abbreviated)	75
Figure 5-3 ANOVA with outlier removed (abbreviated)	75
Figure 5-4 Individual value plot collapsing over card guides data not transformed	76
Figure 5-5 Individual value plot collapsing over card guides data transformed	77
Figure 5-6 P-P plot and correlation coefficient for weibull, lognormal, exponential and logistic	78
Figure 5-7 P-P plot and correlation coefficient for weibull, lognormal, exponential and logistic with outlier removed	79
Figure 5-8 Anderson-Darling (adjusted) and correlation coefficients	80
Figure 5-9 Hazard plot for breakdown voltage	83
Figure 5-10 P-P plot of tin whisker breakdown voltage with confidence intervals	84
Figure 5-11 Lognormal distribution analysis	85
Figure 5-12 Histogram tin whisker breakdown voltages with lognormal distribution	86
Figure 5-13 Tin whisker CDF of breakdown voltage for lognormal distribution	87
Figure 5-14 Electrical schematic for derivation of equations to explain the tin whisker voltage and current charts	88
Figure 5-15 Tin whisker number 137 graph of voltage versus time from the full experiment	89

Figure 5-16 Tin whisker number 137 graph of current versus time from the full experiment.....	90
Figure 5-17 TEM Image of the polycrystalline tin whisker and nomenclature used to identify the various grains (A-D). Magnification: 34000X (NASA/UCF).....	96
Figure 5-18 High-resolution TEM image of the amorphous region in the polycrystalline tin whisker between the uniform crystal lattices of regions A and B. The amorphous region is a low-angle grain boundary (NASA/UCF). Magnification: 1,000,000X.....	97
Figure 5-19 FIB ion channeling image of card guide 16 (ATVC S/N 31) cross section showing the distinct layers studied: the expected Cu-Be substrate with larger grains, the Sn plating with nm-sized grains, the Au-Pd sputter coating and finally the deposited Pt used to protect the region during FIB (NASA/UCF). Magnification: 15,000X.	99
Figure 5-20 FIB ion channeling image of card guide 15 (ATVC S/N 33) cross section showing the distinct layers studied: the expected Cu-Be substrate with larger grains, the Sn plating with nm-sized grains, the Au-Pd sputter coating and finally the deposited Pt used to protect the region during FIB (NASA/UCF). Magnification: 20,000X.	100

CHAPTER 1: INTRODUCTION

Tin Whiskers

Metal whiskers are filamentary growths which may develop on metal surfaces (Koonce & Arnold, 1953). Metal whiskers usually erupt from thin metal films that have been deposited on a substrate, and can grow in a variety of shapes including, straight, kinked, and curved (G. T. Galyon, 2005). Metal whiskers have grown on different metal films. Although a number of metal coatings have exhibited a propensity for whisker growth, the metal films that are most often referred to in the metal whisker literature are cadmium (Cobb, 1946), zinc and tin (Compton, Mendizza, & Arnold, 1951). Tin films deposited by electroplating are more prone to whiskering than hot dipped coatings (Harris, 1994). The physical dimensions of tin whiskers also exhibit a great deal of variability.

The maximum current that a whisker can carry before fusing open has been measured up 75mA (Hada, Morikawa, & Togami, 1978). Given the current-carrying capacity and the length that whiskers can grow, the potential for short circuits in electronics is a very real concern.

The failure modes caused by tin whiskers can be grouped into four different categories. The failure modes include: permanent short circuits in low current applications, transient short circuits in applications where current is high enough to cause the whisker to fuse open, metal vapor arcing in a vacuum, and debris/contamination resulting from vibration which frees loose whiskers that can interfere with optical surfaces or bridge exposed electrical conductors (Brusse, Ewell, & Siplon, 2002).

Metal whisker failures have been documented in commercial satellites, military, medical, and industrial/power applications as well as in computer rooms (Leidecker,

Brusse, Sampson, & Kadesch, 2006). Documented failures include heart pacemakers (Food and Drug Administration, 1986), apnea monitors (Downs, 1994), a nuclear reactor shutdown (Daddonna, 2005), computers in data centers with raised flooring (Brusse & Sampson, 2004), F-15 radar problems (Nordwall, 1986), patriot missile (Anoplate, 2000), in addition to a number of commercial satellites. Given the numerous documented failures, it is evident that whiskers can pose serious problems in high reliability systems that could result in loss of life as well as significant capital losses.

In addition, in an effort to protect the environment, lead-free legislation such as the European Union's reduction of hazardous substances (RoHS) has placed restrictions on the use of lead, and other hazardous materials (European Union, 2003a). To comply with RoHS, and other lead-free legislation, many manufacturers have converted to pure tin finishes. Given that the spacing between leads in electronics continues to decrease as well as the proliferation of pure tin finishes, improving our ability to assess the risk associated with tin whiskers remains an important area of study.

CHAPTER 2: REVIEW OF LITERATURE

Tin Whisker Phenomenon

While evaluating a number of aluminum alloys to improve the design of bearings, Hunsicker and Kempf studied an aluminum-tin alloy (Hunsicker & Kempf, 1947).

During these studies the authors noted:

An unexplained phenomenon which occurs in the solid state has been observed repeatedly in aluminum alloys containing tin. Microscopic examination of metallographic samples a day or more after preparation of the polished surface has revealed thin metallic filaments extending outward from the prepared surface. These filaments appear much like minute extrusions with a thickness or diameter in the range of 1 to 4 microns and a length which varies with the time and temperature during their formation.

As a result of this publication in 1947, the discovery of tin whiskers has been attributed to Hunsicker and Kempf (Jiang & Xian, 2006). Galyon described metallic whiskers as a filament shaped single crystalline surface eruption that grows from a metal surface that are most often found on thin metal films that were deposited on a substrate (G. T. Galyon, 2005).

The hermetically sealed relay shown in Figure 2-1 has an iron armature that was plated with pure tin (Leidecker et al., 2006). A close up photo of the tin whiskers on the armature is shown in Figure 2-2. Whiskers with length sufficient, ~ 3mm, to cause an internal short circuit were found in this relay (Leidecker et al., 2006).



Figure 2-1 Relay with cover removed

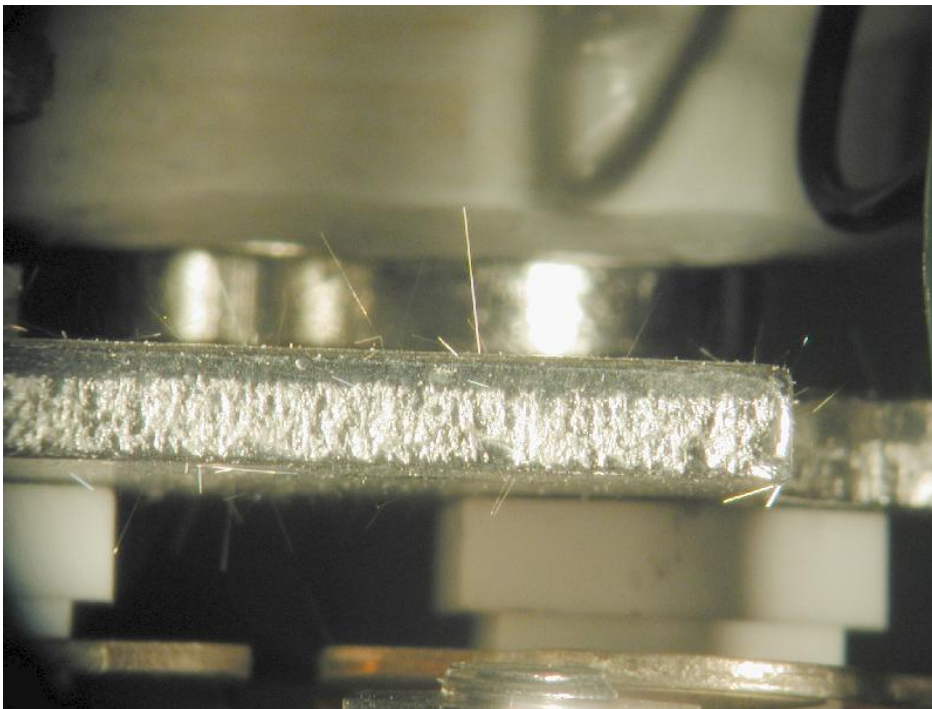


Figure 2-2 Tin whiskers growing on armature of a hermetically seals relay

Figure 2-3 shows a matte tin plated dual in-line package (DIP) integrated circuit (Leidecker et al., 2006). A close up photo of the leads illustrating the tin whiskers that caused a field failure of an electronic system that was used in the electrical power utility industry is shown in Figure 2-4 (Leidecker et al., 2006). Tin whiskers had caused a permanent short circuit in the IC (Leidecker et al., 2006). The photos in Figures 2-1, 2-2, 2-3 and 2-4 were provided courtesy of NASA EEE Parts and Packaging (NEPP) Program from the NASA Goddard Space Flight Center tin whisker (and other metal whisker) homepage (Leidecker et al., 2006).

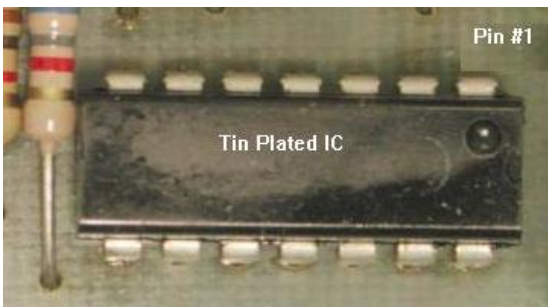


Figure 2-3 Microcircuit

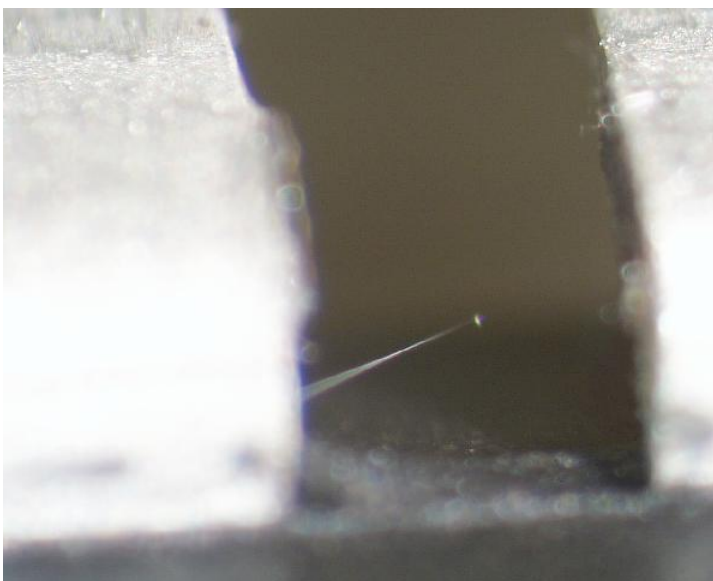


Figure 2-4 Tin whiskers between microcircuit leads

The Purpose of Tin Plating in Electronics

Electronics have traditionally used tin plating on leads to increase solderability and to prevent corrosion of the base metal (Nakadaira et al., 2001). Since the 1960's alloying the tin plating with as little as 1% lead has proven to be an effective tin whisker mitigation strategy while maintaining desirable qualities such as good solderability, low cost, appearance, and ease of plating process control (Arnold, 1966).

However, errors in process controls have allowed pure tin plating to slip through the supply chain even when it was prohibited by procurement specifications. Process escapes have resulted in tin whisker related failures, for example the relay used in military aircraft that failed due to metal vapor arcing caused by tin whiskers (Davy, 2002).

Physical Tin Whisker Characteristics

Shapes

Tin whiskers can grow in a variety of shapes. They are usually straight (Arnold, 1956). However, some whiskers have an offset where the direction of growth varies, and are often referred to as kinked (Arnold, 1956). Other whiskers have a spiral shape (Levy & Kammerer, 1955). The exterior of the whisker often has striations along the length of the whisker giving it a fluted shape and the appearance of being extruded (Arnold, 1956). Other surface eruptions that are not considered whiskers are nodules, flowers or hillocks, but these eruptions are usually significantly shorter ($<10 \mu\text{m}$) than whiskers, and thus present little risk of producing an electrical short circuit (Y. Fukuda, Osterman, & Pecht, 2007).

Length

In a 16 month study by Fukuda et al. the length distribution of whiskers was found to follow a lognormal probability density function (Y. Fukuda et al., 2007). In this experiment the bright tin finish consistently produced longer and denser whisker growth than matte tin (Y. Fukuda et al., 2007) with the longest measuring 166 μm in length. In an 18 month study by Fang et al the mean length was found to be 26.0 μm with a standard deviation of 11.4 μm (Fang, Osterman, & Pecht, 2006). Fang et al. measured the whiskers at the 8, 13 and 18 month intervals throughout the study. They determined that the rate of whisker length growth decreases with time and approaches an equilibrium state (Fang et al., 2006). Typical whiskers are between 1-500 μm in length (G. T. Galyon, 2005). However, very long tin whiskers have been measured up to 18mm in length (Nishimi, 2007).

Diameter

Tin whisker diameters can range from 0.006 μm to 10 μm (Leidecker & Brusse, 2006). However, typical whiskers are between 1-5 μm in diameter (G. T. Galyon, 2005). It is important to note that whiskers do not have a perfectly circular cross sectional area; therefore the term diameter is an approximation.

Growth Rate

Fisher et al. determined that by applying pressure up to 7,500 psi. the growth rate of whiskers may be accelerated up to 10,000 times (Fisher, Darken, & Carroll, 1954). Fisher et al. also noted that whisker growth can be described in three stages (Fisher et al., 1954):

It is shown that these whiskers may exhibit three stages of growth: (1) an induction period (sometimes unobservably small); (2) a period of constant growth rate, and (3) an abrupt transition to a much slower growth rate.

Fisher also noted that there is a great deal of variability in growth rate from a few millimeters per year to a millimeter in 16 minutes, and that growth rate was proportional to the applied pressure (Fisher et al., 1954).

Dunn's laboratory study found that whisker growth rates can vary from 0.029 nm/s to 0.230 nm/s (Dunn, Burke, & Battrick, 1987). Dunn also noted that the growth rate showed little or no correlation with the type of plating or the selection of substrate material (Dunn et al., 1987).

Incubation Period

The incubation period, the time before whisker growth is noted, can vary significantly from just days to years (Government Electronics and Information Technology Association, 2006). Chen and Wilcox noted that in pure tin or tin based electrodeposits, the incubation period was often quite long from months to years which made fundamental investigations difficult (Chen & Wilcox, 2005). Chen and Wilcox discovered a tin-manganese alloy coating that can be electrodeposited that has "extremely short incubation period of a few hours only, followed by a spectacularly rapid and profuse growth which will facilitate mechanistic studies allowing real-time observation" (Keming Chen & Wilcox, 2005).

Growth Density

Tu measured a growth density of 10^3 to 10^4 whiskers/cm² where the distribution was relatively uniform across the surface (Tu, 1973). Fukuda compared whisker density of two finishes, bright tin and matte tin, over three different substrate materials; Alloy 42, Brass and Copper (Y. Fukuda, 2005). Fukuda found that after 8 months the whisker density varied from 2000 whiskers/sqcm for matte tin over alloy 42 to nearly 6000 whiskers/sqcm for bright tin over bass.

Electrical Tin Whisker Characteristics

Resistivity

Dunn measured the electrical characteristics of four typical tin whiskers and found that the two smaller diameter whiskers that were tested had resistivity values of 10.8 $\mu\Omega\text{cm}$ and 11.4 $\mu\Omega\text{cm}$ which are very close to the resistivity of pure tin 11.3 $\mu\Omega\text{cm}$. However, the resistivity of the two larger diameter whiskers that were tested had resistivity values of 59.2 $\mu\Omega\text{cm}$ and 41.0 $\mu\Omega\text{cm}$ which are larger than the resistivity of pure tin (Dunn, 1987). Dunn attributed this difference to possible internal defects (Dunn, 1987).

Current Carrying Capability

Sabbagh reported that the burning-out current for a 3 mm long whisker was 10 mA (Sabbagh & McQueen, 1975). The diameter of the whisker was not reported. Hada found the current carrying capacity to be 10mA for whiskers with a 1 μm diameter, up to 30 mA for whiskers with a 2.5 μm diameter, and up to 75mA for whiskers with a 4 μm diameter (Hada et al., 1978).

Dunn reported a fusing current of 10 mA for a 1.1 μm diameter whisker, 20mA for a 1.5 μm diameter whisker, and the highest reading in his study was 32mA for a 3.0 μm whisker (Dunn, 1987). Given the current carrying capabilities of tin whiskers the potential for electrical short circuits is a real threat.

Superconductivity

Superconductivity can be explained as follows (Wikipedia, 2007b):

A phenomenon occurring in certain materials at extremely low temperatures, characterized by exactly zero electrical resistance and the exclusion of the interior magnetic field (the Meissner effect). The electrical resistivity of a metallic conductor decreases gradually as the temperature is lowered. However, in ordinary conductors such as copper

and silver, impurities and other defects impose a lower limit. Even near absolute zero a real sample of copper shows a non-zero resistance. The resistance of a superconductor, on the other hand, drops abruptly to zero when the material is cooled below its "critical temperature".

It is interesting to note that as early as 1955, Lutes and Maxwell found superconducting transitions in tin whiskers (Lutes & Maxwell, 1955). The sample was cooled using a liquid helium bath and the transition was most pronounced at 1.69°K (Lutes & Maxwell, 1955). While this electrical property is outside of the scope of this dissertation, it is interesting and further reading on the superconductivity of tin whiskers can be found in the following references: (Davis, 1966), (Meyer & Tidecks, 1977), and (Gluck, 1978).

Mechanical Tin Whisker Characteristics

Elastic and Plastic Properties

Herring and Galt tested the hypothesis that specimens of very small dimensions should have a greater range of elastic strain than the bulk metal (Herring & Galt, 1952). This is because they don't have any imperfections in the form of dislocations or because there are few dislocations present that cannot multiply to result in slip (Herring & Galt, 1952). Herring and Galt used tin whiskers to test this hypothesis. The tin whiskers that were tested had a very uniform diameter $1.8 \pm 0.1 \times 10^{-4}$ cm and were up to several millimeters in length (Herring & Galt, 1952). The results of their tests found that the elastic and plastic behavior was very close to what would be expected in a truly perfect crystal (Herring & Galt, 1952).

Powell and Skove performed tensile tests of tin whiskers of ten whiskers at room temperature (Powell & Skove, 1965). To perform the tensile tests the whiskers were removed from the substrate and glued to mounting points on the pulling apparatus (Powell & Skove, 1965). They obtained yield strains of 0.43 % to 2.94 % with an

average slightly greater than 1% (Powell & Skove, 1965). Powell and Skove concluded that whiskers are strong in tensile strength (Powell & Skove, 1965).

Vibration and Shock

Dunn tested tin whiskers by exposing them to vibration, using a vibration table, over a large frequency range from 10 to 2000 Hz (Dunn, 1987). This wide frequency range was selected because it approximates the range of vibration that a spacecraft would be subjected to from ground handling, through launch, to reentry (Dunn, 1987). Dunn determined by microscopic inspection that there was “no evidence of damaged or detached whiskers after exposure to this test” (Dunn, 1987).

Dunn also performed shock tests where the tin whisker samples exposed to 50 shocks at 2060 g (Dunn, 1987). Dunn reported “It is surprising to record that no examples of any damage to any whiskers we observed” (Dunn, 1987).

The results of the tests performed by Dunn differ from the findings of other researchers that “have observed component failure resulting from detached whiskers that lodged in areas creating critical short circuits” (Brusse et al., 2002). Nishimi also noted that loose tin whiskers were found in Space Shuttle Avionics hardware, further demonstrating that the potential for failure from loose tin whiskers is real (Nishimi, 2007).

Other Types of Metal Whiskers

Often considered the earliest publication on the metal whisker phenomenon, Cobb (1946) noted that cadmium deposits grew “straight, cylindrical, needle like crystals” known as whiskers (Cobb, 1946). In addition to cadmium, Arnold and Koonce noted that metal whiskers have been found to grow on zinc, nickel, lead, magnesium, palladium, platinum and iron at elevated temperatures (Arnold & Koonce, 1956). In their study, the

maximum exposure time was 2500 hr with temperatures ranging from 200 to 700 °C (Arnold & Koonce, 1956). The majority of whiskers were only 1-2 μ m in length which is much shorter than tin whiskers growing at room temperature (Arnold & Koonce, 1956). Arnold and Koonce stated that “no correlation was found between temperature and growth rate, maximum filament size, and the time required for initial growth” (Arnold & Koonce, 1956).

In Dunn’s book titled *Metallurgical Assessment of Spacecraft Parts, Materials and Processes* whiskers were also found to grow on molybdenum, tungsten and aluminum (Dunn, 1997). Chudnovsky et al. found that silver plating on power contacts grew profuse whiskers when exposed to sulfur rich environments (Chudnovsky, Swindler, & Thompson, 2001). Using Energy Dispersive X-ray Spectroscopy (EDS), they determined that most of the whiskers contained 97-99% silver with 1-3 % copper (Chudnovsky et al., 2001).

In the literature that I have reviewed, I have found only one reference to gold whiskers that were found by Teverovsky at NASA Goddard Space Flight Center (Teverovsky, 2003). The gold whiskers were found during SEM examination of a relay that had gold electroplating over a nickel substrate (Teverovsky, 2003). While gold whiskers are rare, it is important to note that whiskering is possible even with gold plating.

Failure Modes

Electrical Short Circuits

Hada determined the current carrying capacity of tin whiskers to be between 10 – 75mA (Hada et al., 1978). Electrical systems with current levels that exceed the current carrying capacity of the shorting whisker can experience a temporary or intermittent short

circuit until the whisker fuses open. When an electrical system has current levels that do not exceed the current carrying capacity of the shorting whisker, a permanent short circuit can result (M. Osterman, 2006).

Metal Vapor Arcing

Brusse et al. concisely described metal vapor (plasma) arcing in a vacuum as follows (Brusse et al., 2002):

In vacuum (reduced atmospheric pressure) a much more destructive short circuit phenomenon can occur. If currents of above a few amps are available and the supply voltage is above approximately 18V, the tin whisker may vaporize creating a plasma of tin ions that can conduct hundreds of amperes. An adequate supply of tin from the surrounding plated surface can help to sustain the arc until the available tin is consumed or the supply current is interrupted such as occurs when a protective fuse or circuit breaker interrupts the current flow (Van Westerhuyzen, Backes, Linder, Merrell, & Poeschel, 1992). This phenomenon is reported to have occurred on at least three on-orbit commercial satellites since 1998 resulting in blown fuses that have rendered the spacecraft non-operational (Brusse et al., 2002).

For many years the risk of metal vapor arcing from tin whiskers was thought to be limited to hardware operating in a vacuum. However, Davy in 2002 determined that the relay failure under investigation was likely due to a “self-sustaining arc at atmospheric pressure” (Davy, 2002). The relay that failed in atmospheric pressure is shown in Figure 2-5. The photo in Figure 2-5 was from Gordon Davy’s paper titled *Relay Failure Caused by Tin Whiskers* (Davy, 2002). In 2006, Mason and Eng demonstrated through experimentation that tin plasma could be generated at 28 vdc in 1 atm of air (Mason & Eng, 2006).



Figure 2-5 Failed relay from tin whisker induced metal vapor arc

Loose Whiskers

Whiskers can become detached from vibration and shock resulting in debris that can cause temporary or permanent short circuits or interfere with optics (Brusse et al., 2002). Nordwall reported that the USAF found loose tin whiskers floating freely in the cases of hermetically sealed military hybrid circuits (Nordwall, 1986). These whiskers caused intermittent problems that would disappear during routine troubleshooting (Nordwall, 1986).

Reflections

Puttlitz reported that tin whiskers can effect a high frequency RF (>6 GHz) circuit or fast digital circuits with a rise time of < 59 ps even when not creating a short circuit by acting as a antenna that affects the impedance of the circuit (Puttlitz & Galyon, 2007). The change of impedance can cause reflections (Puttlitz & Galyon, 2007).

Failure Experiences

Medical

The Food and Drug Administration (FDA) issued a recall after finding that a large number of pacemakers from a specific manufacturer were experiencing a high rate of failure. These failures were due to tin whiskers growing from the tin-plated case of the pacemaker crystal component. Tin whiskers caused a short circuit between the case and the crystal that caused the total failure of the pacemaker (Food and Drug Administration, 1986). Zinc whiskers caused the failure of an apnea monitor by causing leakage from rotary switch to ground (Downs, 1994). The manufacturer of the switch was aware that tin and cadmium could whisker, but did not know that zinc plating could also whisker (Downs, 1994). Apnea monitors are regularly used on adults recovering from anesthesia (Downs, 1994).

Power Plant

In 2005, a nuclear reactor shutdown at the millstone power plant was caused by tin whiskers (Daddonna, 2005). Fortunately the system failed in a safe condition (Daddonna, 2005). The whisker had bridged a trace causing a short that gave a false low-pressure reading that resulted in the shutdown (Daddonna, 2005).

Three relays failed at an overseas electric power company (Stevens, 2001). Without a control signal the relay closed which produced a false alarm that initiated a plant shutdown (Stevens, 2001). This type of relay was used reliably for many years (Stevens, 2001). However, when the supplier changed manufacturer sites, a change to pure tin plating was implemented (Stevens, 2001).

Computer Rooms

Brusse and Sampson reported that a NASA data center experienced at least 18 power supply failures over a one month period in mass memory storage devices that were recently installed (Brusse & Sampson, 2004). The cause of the short circuits was zinc whiskers that were growing on the underside of the raised floor tiles that were disturbed and dislodged during the installation of the new equipment (Brusse & Sampson, 2004). These loose whiskers were carried into the power supplies of the devices by the air conditioning under the raised floor that is used to cool the computers (Brusse & Sampson, 2004). A similar problem with zinc whiskers from raised floor tiles was experienced by the Australian Taxation Office (Crawford, 2004).

Military

Cadmium whiskers grew between the plates of variable condensers causing electrical shorts that resulted in the failure of aircraft radios (Cobb, 1946). The Navy's Phoenix air-to air missile system had experienced problems with whisker growth (Corbid, 1989). The tin whiskers were growing from the tin lining of a box that encloses the missile's target-detection system (Corbid, 1989).

Satellites

Silverstein reported that Hughes Space and Communication Company which built the HS601 Satellite experienced three failures of the computer that maintains the satellite's orientation toward earth (Silverstein, 1998). The failures were traced to tin whiskers growing from a switch (Silverstein, 1998). One of these failures caused a loss of pager, broadcast, and other transmissions across the United States (Silverstein, 1998). The following satellites were complete losses, when both the primary and secondary control processors failed: the GALAXY VII [PanAmSat] in November 2000, the

SOLIDARIDAD 1 [SatMex] in August 2000, and the GALAXY IIIIR [PanAmSat] in January 2006 (Leidecker et al., 2006). These on-orbit failures were attributed to tin whiskers that grew on pure tin plated relays (Leidecker et al., 2006).

Extensive List of Metal Whisker Failures

For an extensive listing of documented metal whisker failures in chronological order is provided in the following reference: (Leidecker & Brusse, 2006). For an extensive listing of the publicly reported whisker induced failures grouped by industry refer to the following reference: (Leidecker et al., 2006).

Useful Applications of Metal Whiskers

After learning of the costly damage that tin whisker growth can have on electronics, the question naturally arises; Are there any useful applications for tin whiskers? Egashira et al. found that tin oxide whiskers showed substantial changes in resistance when exposed to inflammable gases (Egashira, Matsumoto, Shimizu, & Iwanaga, 1988). Substantial gas sensitivity and good response time was found in whiskers with a diameter of 5 -10 μm (Egashira et al., 1988). However, the sensitivity is based on whisker size which poses the practical problem of growing whisker to a particular size (Egashira et al., 1988).

Lead-Free Movement

The European Union (EU) passed two pieces of legislation aimed at improving the environment: The directive 2002/95/EC of the European parliament and of the council of 27 January 2003 on the restriction of the use of certain hazardous substances in electrical and electronic equipment (RoHS) (European Union, 2003a), and the directive 2002/96/EC of the European parliament and of the council of 27 January 2003 on waste electrical and electronic equipment (WEEE) (European Union, 2003b).

WEEE and RoHS

Osterman summarized the salient points of the legislation as follows: The restriction of hazardous substances (RoHS) legislation prohibits the use of lead and other harmful substance (i.e. mercury, cadmium, chromium, PBBs (polybrominated biphenyls), and PBDEs (polybrominated diphenyl ethers)) in new electrical and electronic equipment put on the market after 1 July 2006 (M. Osterman, 2006). Pb-free is defined as <0.1% Pb by weight in homogeneous materials (M. Osterman, 2006). Compliance is attained through self-certification and market surveillance (M. Osterman, 2006). The defense, aerospace, and battery industries are not in scope, and RoHS also provides a means of applying for an exemption (M. Osterman, 2006).

The purpose of the waste electrical and electronic equipment (WEEE) legislation is to increase recycling and recovery of end-of-life electronics (M. Osterman, 2006). The manufacturers, sellers and distributors will be responsible for financing the collection, treatment, recovery and disposal of WEEE from private households deposited at collection facilities by 13 August 2005 (M. Osterman, 2006).

Requested Exemptions

Sony and Hewlett Packard (HP) have requested exemptions from RoHS to ensure the reliability of their products (Buetow, 2005). HP is pushing for 15% lead mixed with tin while Sony is requesting 5-10% lead mixed with tin (Buetow, 2005). Swatch group implemented lead free operations and components in 2005 (Lederrey, 2006).

Unfortunately they experienced “serious problems with tin whiskers growing inside their quartz crystal resonators, generating short circuits that end the watch’s function (Lederrey, 2006). As a result of the tin whisker failures, Swatch has requested a RoHS exemption to return to using solder containing 10-37% lead (Lederrey, 2006).

Other Legislation

China is also working on a version of RoHS. The China RoHS will ban six hazardous substances including: lead, mercury, cadmium, chromium, PBBs (polybrominated biphenyls), and PBDEs (polybrominated diphenyl ethers) like the EU legislation (Lau, 2006). China will start phasing in its version of RoHS on March 1, 2007 (Lau, 2006).

In the United States lead has been banned from paint, gasoline, and plumbing (Reliability Information Analysis Center, 2006). However, legislation introduced in the 1990's regarding lead-free solders did not become law, and there is currently no new federal legislation in work (Reliability Information Analysis Center, 2006).

Substitute Materials for Tin Lead Alloys

A number of different lead free finishes and solders have been tested with varying degrees of success. Alloying tin with various combinations of silver (Ag), copper (Cu), zinc (Zn), bismuth (Bi), cerium (Ce), and nickel (Ni) (Reliability Information Analysis Center, 2006). A variety of factors affect the suitability of the lead free finishes and solders including: propensity to whisker, availability and cost of the alloy (for instance silver), reliability of the joints, solderability, melting temperature, and wetting characteristics.

Sakuyama and Kutami studied whisker growth on Sn and Sn-Cu plating (Sakuyama & Kutami, 2005). The sample was mechanically stressed by clamping to accelerate the whisker growth process. The Sn-Cu finish grew whiskers in just two hours but stopped growing whiskers after 24 hours, while the Sn plating had a long latency period of about 720 hours before whisker growth started and continued growing whiskers until about 2000 hours (Sakuyama & Kutami, 2005). The Sn plating grew longer whiskers than the

Sn-Cu plating (Sakuyama & Kutami, 2005). Chaung and Yen stated that “the addition of rare-earth elements into Pb-free solders has been reported to be a beneficial effect for their wettability, tensile strength, and creep resistance. However, the current study shows that undesirable rapid whisker growth occurs in Sn_{3.5}AgO.5CuO.5Ce solder BGA packages” (Chuang & Yen, 2006).

Complications from Lead-Free Materials

In addition to whiskering, there are other issues to consider from the lead-free initiative. The Environmental Protection Agency noted that “There is no drop-in replacement for SnPb solder. The switch to lead-free solder affects many aspects of the manufacturing and assembly process” (United States Environmental Protection Agency, 2005). Tin lead solder has a melting point of 183 °C with a maximum reflow temperature 220 °C, while many lead-free alloys have a melting points ranging from 217 – 220°C with processing temperatures around 254° C (Richard Ciocci & Michael Pecht, 2006). The 34° C increase in process temperature is beyond the design temperature of many components and boards used in tin-lead processes (Richard Ciocci & Michael Pecht, 2006). Many existing components require redesign and/or recertification to withstand the higher temperatures associated with lead-free soldering (United States Environmental Protection Agency, 2005).

Another interesting challenge is equipment maintenance and cleaning. At the higher temperatures required for lead-free processes, high concentrations of tin has proven to be corrosive to many metals including stainless steel used in processing equipment (United States Environmental Protection Agency, 2005). The residue from lead free flux requires increased cleaning time, thus increasing costs (United States Environmental Protection Agency, 2005).

Another issue is the reliability of lead free joints. Thermal cycling and vibration tests of the new solder replacements are necessary to determine their reliability. Corbitt tested a lead free solder composed of 96.5% Sn, 3% Ag, and 0.5% Cu, and found that the lead free solder joints “can withstand 1,000 cycles of a three-point bending test and a thermal cycle range of 0-100 °C. Based on the thermal cycling test, the trend suggests a slight increase in the resistance without total failure through 1,000 cycles while the board exhibits a 10% change of resistance at about 2,500 cycles and fail approximately 200 cycles later under the vibration cycling test” (Corbitt et al., 2007). The fatigue life of lead free solder joints has been shown in some studies to be superior to tin-lead joints, while other studies have found the opposite to be true (Puttlitz & Galyon, 2007).

Growth Mechanism Theories

Despite over 50 years of research in whisker growth, a consensus about whisker formation has not been reached (G. T. Galyon & Palmer, 2005). The theories for whisker formation propose three different growth mechanisms: dislocation, oxidation, and recrystallization (Y. Fukuda, 2005). Galyon noted that (G. Galyon, 2004):

There have been more transactions and proceedings whisker publications in the first three years of the 21st century than in the previous 60 years. This whisker research upsurge is due to the impending European Union environmental regulations requiring lead (Pb) removal from electroplated tin films. New analytical techniques, such as focused ion beam (FIB) microscopy and micro-focus X-ray diffraction (XRD), were utilized to gain insight into tin film microstructures and internal stress levels.

These new tools allowed Xu et al. to confirm the one common belief among whisker growth theorists that stress in the Sn coating is the driving force for whisker formation (C. Xu et al., 2002).

Dislocation

Peach proposed an explanation for the cause of whisker growth stating that “each whisker contains a screw dislocation running along its axis” (Peach, 1952). Galyon noted that “Peach...stated that Sn whiskers grew from tin atoms migrating through a screw dislocation at the center of the whisker. These migrating Sn atoms subsequently deposited themselves at the tip” (G. Galyon, 2003).

Eshelby considered the proposal a there may be a dislocation with a screw component running parallel to the axis of the whisker (Eshelby, 1953a). Eshelby later stated that since Koonce and Arnold determined that whiskers grow from the root (Koonce & Arnold, 1953). Thus, Peach’s explanation is not correct (Eshelby, 1953b). Eshelby went on to propose a different dislocation theory where the “surface tension forces a small hump on the surface obviously have the right character (a central pull surrounded by a restraining pressure) to wire-draw it into a whisker according to the intuitive ideas of a plastic flow” (Eshelby, 1953b).

Recrystallization

Van Vlack defines recrystallization as “a process of growing new crystals from previously deformed crystals. Crystals that have been plastically deformed...have more energy than unstrained crystals...given a chance, the atoms will move to form a more perfect, unstrained array...the recrystallization process requires atom movements and rearrangements...which occur more rapidly at high temperatures” (Van Vlack, 1980).

Ellis proposed that whisker growth is the result of a process of grain growth or recrystallization and growth, and that this process may not require dislocation (Ellis, Gibbons, & Treuting, 1958). Ellis further stated (Ellis et al., 1958):

The nucleating crystal of a whisker is small - on the order of size of the cross-section of the whisker. If such a crystal does not exist, it forms by recrystallization before a whisker is generated. The atoms which build the whisker are derived by transfer from the surrounding matrix via the grain boundary. A whisker is the growth of the crystal out of the free surface, as a result of the continual addition of extra atoms either internally or at the base.

Boguslavsky and Bush provided an excellent explanation of recrystallization theory as follows (Boguslavsky & Bush, 2003):

Recrystallization theory postulates that shear strain introduced by plastic deformation is stored in the metal in the form of dislocations (lattice defects). In bulk metals, produced metallurgically from the molten phase, these lattice defects usually are not present in noticeable quantity unless the material is subjected to cold work (plastic deformation at temperatures significantly below melting point). In electroplated tin, however, the metal is formed at the temperatures much below melting point. During plating, energy is stored in the deposit in the form of crystal defects such as vacancies and dislocations. This causes the crystal structure of metal deposits to resemble the structure of cold worked metals, and thus forms the starting point for application of recrystallization principles.

The second important factor that justifies the application of recrystallization/grain growth principles to whisker formation is related to the low recrystallization temperature of tin. Recrystallization temperature is defined as the temperature at which a particular metal with particular amount of cold deformation will completely recrystallize within one hour. Typically, it can be estimated as between 0.4 and 0.7 T_m (where T_m is the melting temperature). It is a well-known fact that in most metals, recrystallization occurs at elevated temperatures. For tin, however, the recrystallization temperature is approximately 30°C, which means that recrystallization will spontaneously occur around room temperature (above and below 30°C), reforming a strain-free structure.

Furuta and Hamamura expanded on the recrystallization theory and derived a formula for whisker growth rate (Furuta & Hamamura, 1969). They determined that the growth rate does not depend on whisker thickness and is proportional to the dislocation energy (Furuta & Hamamura, 1969).

In 2002 Sheng et al. studied two lead-free finishes SnCu and pure Sn. They used a focused ion beam (FIB) to create a cross sectional samples normal and parallel to the

whiskers growth direction (Sheng et al., 2002). The FIB images that were parallel the growth direction revealed the information about the grains in the matrix (Sheng et al., 2002). They observed more precipitates of Cu_6Sn_5 in the grain boundaries of the SnCu finish than in the pure Sn finish and concluded that “The growth of these precipitates at room temperature provides the driving force of spontaneous whisker growth. The existence of a large number of these precipitates in the grain boundaries of SnCu is the reason why whisker growth is faster on the SnCu finish than on the pure Sn finish” (Sheng et al., 2002).

Zhang et al. used atomic force microscopy to study the relationship between the relative evenness of the intermetallic layer (IMC) and the tin whisker growth (Zhang, Egli, Schwager, & Brown, 2005). Zhang et al. assumed that the IMC surface roughness was related to whisker growth propensity (Zhang et al., 2005). Instead they found that the lowest whisker growth was found at the two ends of the spectrum: a very smooth or a very uneven IMC layer (Zhang et al., 2005).

Oxidation

Tu’s theory is that Sn whiskers will grow where there are cracks or weak spots in the oxide layer on surface (Tu, 1994). The stress in the plating caused by the volume change from intermetallic layer formation is relieved through these spots (Tu, 1994).

Since oxidation is believed to cause the surface layers to expand in volume, thus creating stress in the plating, Wolfgang et al. tested this theory by performed experiments to determine the effect of oxidation on whisker growth (Wolfgang, Ogden, Champaign, & Waller, 2005). The tin plated control group samples were exposed to room air (Wolfgang et al., 2005). The other sample groups were exposed to selected water

evaporation rates (Wolfgong et al., 2005). Finally the last group of samples was exposed to an artificial oxidizing environment (Wolfgong et al., 2005). The experiments revealed that whisker formation was accelerated by oxidation (Wolfgong et al., 2005).

Factors that Effect Tin Whisker Growth

Applied Stress

Pressure has been shown to increase whisker growth. Pitt and Henning found by clamping tin coated steel samples under pressure the whisker growth rate increased with increasing pressure (Pitt & Henning, 1964). The turning of nuts and screws can introduce loads that create stress causing whisker growth (Government Electronics and Information Technology Association, 2006).

Damage to the surface such as scratches in the substrate or plating can also introduce stress (Siplon, Ewell, Frasco, Brusse, & Gibson, 2002). Also, bending operations which are applied to many components can cause residual stresses (Dittes, Oberndorff, Crema, & Su, 2006). Bending can take place at the manufacturer as in lead formation in an integrated circuit or during component installation as in the bending of resistor or capacitor leads to install the component in a circuit board.

Internal Stresses

Osterman noted that the “intermetallic compound formation between the plating material and substrate results in compressive stress within the plating” (M. Osterman, 2006) In addition, Osterman stated that “mismatches in coefficient of thermal expansion (CTE) of the tin-based plating material and substrate or underlayer” cause stress within the finish (M. Osterman, 2006). Barsoum et al. proposed an oxidation based process for the growth of whiskers where stress fields result from the relative change in volume due

to the diffusion of oxygen and the formation of an oxide layer (Barsoum, Hoffman, Doherty, Gupta, & Zavaliangos, 2004).

Substrate Material Selection

Arnold noted that substrate material selection had a profound influence on whisker growth (Arnold, 1954). In a two year study, Arnold found that tin applied over iron had “luxuriant whisker growth” while tin applied over brass had extremely short whisker growth (Arnold, 1954). As a guideline for tin whisker mitigation, iNEMI has developed a table of lead-free finishes and the corresponding recommended base materials (International Electronics Manufacturing Initiative, 2005).

Environmental Stresses

Unfortunately there are a number of experiments that appear to have contradictory finding regarding environmental factors. The results are summarized in the following paragraphs from GEIA-STD-0005-2 (Government Electronics and Information Technology Association, 2006):

Temperature: Elevated temperature increases diffusion and formation of intermetallics, so it might accelerate whisker formation. However, high temperatures can also relieve internal stresses.

Barometric Pressure: Pressure seems to have little effect on whisker growth. Whiskers have been observed to grow in both earth-based atmospheric pressures and low-pressure (vacuum) environments. Some theories have been proposed that oxidation may contribute to whisker growth, but because whiskers have been shown to grow under low-pressure (oxygen starved) conditions, it is clear that oxidation is not required for whiskers to form.

Humidity and Moisture: Experiments examining the effects of humidity have been inconclusive. Some results have shown increased growth rate in high humidity (85% - 95% RH), but others show no change.

Thermal Cycling: There is also no consensus on whether temperature cycling affects tin whisker growth. Some experiments, typically cycling between -40° C to +90° C, have shown higher growth rates, but others

have not demonstrated any effect. It may be the case that the impact of thermal cycling on growth is related to the plating material below the tin. Under-plates with higher thermal mismatches with tin may be influenced by cycling while better matched materials may not.

Electric Field: Unlike dendrites, whiskers grow without an applied electric field. There have been studies suggesting that electric field can change the growth rate. However, several studies found that whisker growth is not related to electric bias. However, electric fields can create electrostatic attraction between whiskers and other surfaces and may increase the likelihood of whisker-induced shorts.

Plating and Process Chemistry

Brusse et al. stated that higher current density in the plating process, co-deposited hydrogen, and co-deposited organics (carbon) from "brighteners" in the plating bath create higher stress in the plating (Brusse et al., 2002). Schetty reported that deposit thickness of greater than 8 μm or less than 0.5 μm minimize whisker formation (Schetty, 2001). Kakeshita et al. determined that internal defects of electroplated tin as well as grain size and shape are important factors in the growth of whiskers (Kakeshita, Shimizu, Kawanaka, & Hasegawa, 1982). Smaller grain sizes between 0.2 – 0.8 μm were more prone to whiskering than larger grain sizes of 1 – 8 μm (Kakeshita et al., 1982).

Growth Mitigation Strategies

Alloying with Lead

Pitt and Henning found that by alloying the Sn with Pb from 0 - 50% Pb, that whisker densities decreased as the percentage lead increased (Pitt & Henning, 1964). Although exemptions exist in current legislation for the government and aerospace industries, the military/aerospace industry which once dominated the electronics market in the US now holds only a 1.1% market share (Reliability Information Analysis Center, 2006). Thus, with the market for lead alloyed products shrinking, the availability of lead

alloyed components will likely shrink along with it, reducing the effectiveness of this mitigation strategy.

Underlay

Baliga reported that Agere systems tested the application of a nickel barrier (underlay) between the copper substrate and the matte tin finish (Baliga, 2004). The samples were subjected to accelerated life tests for 15 weeks (Baliga, 2004). The matte tin sample without the nickel barrier did grow whiskers during the test, where the sample with the nickel barrier did not grow tin whiskers during the test (Baliga, 2004). The nickel underlay acts as a barrier to the diffusion of Cu into the Sn (Joint Electron Device Engineering Council, 2006). Sn does diffuse into the nickel which form an intermetallic compound, but it has a much slower growth rate than a SnCu intermetallic compound (Joint Electron Device Engineering Council, 2006).

Conformal Coating

Woodrow and Ledbury evaluated different conformal coatings to determine their effectiveness in tin whisker mitigation (Woodrow & Ledbury, 2005). The conformal coatings were applied over bright tin plated brass coupons (Woodrow & Ledbury, 2005). Although the conformal coating did suppress whisker growth, over time whiskers grew under the coating on all samples and eventually penetrated the thinner coatings (Woodrow & Ledbury, 2005). In the 18 month test performed by Kadesch and Leidecker, none of the whiskers had broken through the Uralane conformal coating (Kadesch & Leidecker, 2000). However, they noted that for short term space missions this coating provides some mitigating effect, but it is not conclusive for long term missions (Kadesch & Leidecker, 2000). Kadesch and Leidecker also noted that quantity

and length of whisker growth was greater at room temperature than at 50 °C which differed from the findings of other researchers (Kadesch & Leidecker, 2000).

Physical Barriers

The placement of a hard non-conductive material as a barrier between conductors can prevent whisker from growing between conductors (Government Electronics and Information Technology Association, 2006). However, it does not eliminate the hazard from loose whiskers (Government Electronics and Information Technology Association, 2006). While this may work for large electrical systems, it is not practical for fine pitch electronics.

Tin Finish Selection (Matte vs. Bright)

The use of matte tin instead of bright tin has been recommended as an effective whisker mitigation strategy (Sriyarunya, Tondtan, & Bansal, 2004). Sriyarunya tested the application of matte Sn over copper and found that after 12 months of storage no whiskers were observed (Sriyarunya et al., 2004). Hashemzadeh's experiments did not indicate the bright tin is more whisker prone than matte tin (Nayeri Hashemzadeh, 2005). However, the bright tin samples did grow the longest whiskers (Nayeri Hashemzadeh, 2005). Smetana noted that matte tin finishes have lower internal stresses and larger grain sizes than bright tin finishes, and that matte tin is less prone to whisker formation than bright tin (Smetana, 2005). Smetana also noted that any supplier's claim of producing a "whisker-free" matte tin finish is most likely premature (Smetana, 2005).

Thickness of Plating

Glazunova's experiments studied tin coating of thickness from 0.5 – 50 μm . Glazunova determined that the maximum rate of growth was seen for plating thicknesses of 2 – 5 μm for tinned copper, 5 – 10 μm for tinned steel and up to 20 μm for tinned brass

(Glazunova & Kudryavtsev, 1963). Whiskers did not form on the 0.5 μm thick coatings (Glazunova & Kudryavtsev, 1963). Rozen, based on his experiments, recommended that electroplated tin should have a minimum thickness of 5 μm to minimize whisker growth (Rozen, 1968).

Heat Treatments

Glazunova studied the effects of heat treatments on tin plated steel with a copper underlay and determined that heat treatments lengthened the incubation period for whisker growth and reduced the rate of whisker growth (Glazunova, 1962). Reflowing the tin finish has been suggested as a mitigation strategy. Xu stated that the theory behind this technique is that the melting (reflow) of the plating relieves the stress in the plating (C. Xu, Fan, Zhang, & Abys, 2004). X-ray diffraction was used to measure the stress in the Sn finish (C. Xu et al., 2004). The stress in the reflowed samples was less than in the as-plated samples (C. Xu et al., 2004). After 18 months of aging no significant stress levels had built up in the reflowed samples (C. Xu et al., 2004). Fukada's experiments showed that heat treating did not always have a mitigating effect on whisker growth (Y. Fukuda, 2005).

Solder Dipping

Solder dipping has been recommended to obtain a Sn-Pb finish to mitigate whiskering on parts that are delivered with a pure tin finish. The risks associated with solder dipping include: thermal damage to the package, exposure of the base metal, and a non uniform finish thickness (Sengupta et al., 2005). Sengupta outlined the flow of the solder dipping process as follows (Sengupta et al., 2005): Apply flux to the part with original finish, preheat, dip, rinse, and then dry. You now have a part with a new Sn-Pb finish.

Hot Tin Dipped Coating

Although, as noted in the introduction, hot-tin dipped coatings have fewer propensities to whisker than electroplated coatings, they have other drawbacks. Hot-tin dipped coatings have greater variation in plating thickness and the multiple processing steps can introduce stresses from handling damage (Government Electronics and Information Technology Association, 2006).

Risk Assessments and the Probability of Electrical Shorts

An application-specific tin whisker risk algorithm was developed by Pinsky of Raytheon in 2003. This risk assessment considers the following factors: conductor spacing, lead content in tin plating, process by which the tin was deposited, tin thickness, material directly beneath the tin, substrate controlling the coefficient of thermal expansion, thermal treatments the tin was subjected to after deposition, conformal coating over the tin, use of mechanical hardware, vulnerability of the system to dysfunction as a result of the presences of small pieces of conductive contaminants, use of conformal coating on conductors in the enclosure, and air flow in the assembly (Pinsky, 2002). The purpose of this algorithm was to quantify the risk that tin whiskers will bridge between conductors for a specific tin plating application (Pinsky, 2002).

In 2005, Hilty and Corman of Tyco Electronics developed a Monte Carlo simulation tin whisker reliability assessment (Hilty & Corman, 2005). The purpose of their work was “to help predict the likelihood for electrical shorting between adjacent leads of a typical component” (Hilty & Corman, 2005). Tin whiskers were grown on two different samples. The first was a plating and substrate selection that had been proven to grow whiskers; the second utilized a plating process and substrate shown to mitigate whisker growth (Hilty & Corman, 2005). After exposing both of these samples to the

same accelerated aging environment, the quantity, length, and growth density were measured (Hilty & Corman, 2005). This data was used to fit the statistical distributions that were utilized by the simulation to determine whisker length (Hilty & Corman, 2005). The locations of the whiskers, the rotation and inclination angles were randomly generated in the simulation (Hilty & Corman, 2005). Whiskers that were long enough and grew at an angle that allowed them to touch an adjacent contact were identified as a failure for the component (Hilty & Corman, 2005). The results of the simulations provide a quantitative assessment of the effectiveness of plating process mitigation in reducing simulated failure rates, as well as the effect of terminal separation distance (Hilty & Corman, 2005). This was the first application of a Monte Carlo simulation for tin whisker risk assessment.

In October 2005, the second tin whisker risk assessment using Monte Carlo simulation was published by Fang at the University of Maryland (Fang, 2005). In addition to developing a simulation to predict the risk of an electrical short from a tin whisker growth from a conductor to an adjacent conductor, this study also developed a simulation to assess the risk of shorts from free whiskers. The author attributed the large difference between the experimental results and the results of the simulation for free whiskers to contact resistance. In the recommendations for future work section, Dr. Fang stated “In order to obtain a more accurate simulation answer, it is recommended to quantify the probability of occurrence of an electrical short given a whisker bridging adjacent exposed conductors physically. This number will be used as an input data to the algorithm to correct the final bridging simulation risk” (Fang, 2005).

CHAPTER 3: PROOF OF CONCEPT EXPERIMENT

Breakdown Voltage Experiment

To demonstrate that the breakdown voltage of the film resistance can be measured, and to show that there is enough variability to generate an empirical probability model, the following proof of concept experiment was performed. From the data gathered in this experiment, a probability distribution was fit. This probability model also facilitated the evaluation of the sample size that was used in the full experiment. In addition, tin whiskers from the same card guides were sectioned using a focused ion beam, and analyzed.

Review Stage

In the published simulations it was assumed that physical contact between a whisker and an exposed contact results in an electrical short. This conservative assumption has been made because the probability of an electrical short from tin whiskers had not yet been determined. The purpose of the experiments was to quantify the probability of an electrical short when a whisker bridges two adjacent exposed electrical contacts.

Contact resistance is the sum of the constriction resistance and the film resistance (R. Holm & Holm, 1967). When two surfaces touch, only a small portion of the area actually makes contact due to unevenness in the surfaces (R. Holm & Holm, 1967). The a-spot is the radius of the circular contact area (R. Holm & Holm, 1967). Current flow is constricted through the smaller area resulting in a constriction resistance (R. Holm & Holm, 1967). Film resistance is due to the build up of tarnish films (oxides, etc.) on the contact surfaces that act in a nearly insulating manner (R. Holm & Holm, 1967).

Slade (Slade, 1999) points out that when the ratio of $(\rho_f / \rho)(d / a)$ is much larger than unity, the effect of constriction resistance is overshadowed by the film resistance, where ρ_f = the resistivity of the film, ρ = the resistivity of the substrate material, d = the film thickness, a = the a-spot radius.

Contact resistance can be measured by putting two metal cylinders in contact with each other in a crossed arrangement under a mechanical load, and measuring the current through the crossed rods and the voltage across the crossed rods (E. Holm, 1962). The a-spot radius can be estimated with the crossed cylinder model developed by Holm (E. Holm, 1962) as shown in equation 3-1. This assumes that the whiskers are cylindrical, which is a simplification, since whiskers are fluted.

$$a = 1.11 \sqrt[3]{(P/E)r} \quad (3-1)$$

In equation 3-1, P = the mechanical load, E = the modulus of elasticity, r = the radius of crossed rods, and a = the radius of the contact surface (E. Holm, 1962). The tip of the micromanipulator which is used to make contact with the tin whiskers is also called the probe. The mechanical load of the probe touching the whisker can be estimated by modeling the whisker as a cantilever beam as shown in Figure 3-1.

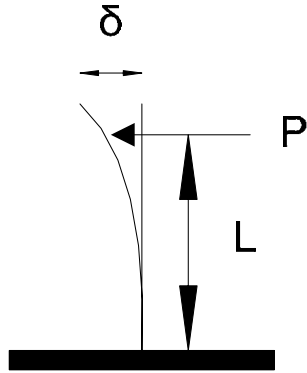


Figure 3-1 Cantilever beam whisker model illustrating the mechanical load placed on a whisker by the micromanipulator probe.

The whisker bending model also assumes that the whiskers are cylindrical. With that assumption stated, P = the force applied to the whisker, L = the distance from the base of the whisker to the applied force, δ = the whisker deflection, I = the moment of inertia, and E = the modulus of elasticity (Timoshenko & Young, 1968). The force applied to the whisker by the tip of the micromanipulator probe is shown in equation 3-2.

$$P = 3EI\delta / L^3 \quad (3.2)$$

The moment of inertia for a circular section is shown in equation 3-3 (Timoshenko & Young, 1968).

$$I = \pi r^4 / 4 \quad (3.3)$$

If we assume a whisker has a diameter of 2 μm , length of 4mm, the probe contacts the whisker at 80% of its length (L = length of whisker x 0.80), and it deflects 5% of its

length ($\delta = \text{length of whisker} \times 0.05$), then using Equation 3-3 the moment of inertia $I = 7.854 \text{ E-}25 \text{ m}^4$. Given that the modulus of elasticity for tin is $E = 41.369 \text{ GPa}$ (Wu et al., 2007), using equation 3-2, the force applied to the whisker $P = 5.949\text{E-}10 \text{ N}$. Since the value for P was calculated, one can determine the spot area radius using equation 3-1, resulting in the value $a = 2.689\text{E-}9\text{m}$.

Since the resistivity of tin at 20°C is $\rho = 11.6\text{E-}8 \text{ }\Omega\text{m}$ (Slade, 1999), and the resistivity of tin oxide at 20°C is $\rho_{\text{oxide}} = 4\text{E}4 \text{ }\Omega\text{m}$ (Samsonov, 1973), if one assumes the oxide film thickness is $d = 50\text{\AA}$ (Schetty, 2004), the ratio of $(\rho_f / \rho)(d / a) = 6.412\text{E}11$. Since the aforementioned ratio is much larger than unity, one can conclude the effect of constriction resistance is overshadowed by the film resistance.

In order to determine the probability of an electrical short from a tin whisker across adjacent exposed leads it is necessary to determine when the film resistance from the oxide layer and any other films breaks down. Conduction can be experienced when the film is ruptured mechanically in some spots, as in switch with wiping action contacts, or is electrically broken down when enough voltage is applied. This type of breakdown is called fritting (R. Holm & Holm, 1967). The breakdown voltage can be seen by examining change in the plots of the whisker voltage and whisker current.

Equipment List

- Microscope - Nikon SMZ1500
- Micromanipulator – Wentworth Laboratories 195RH
- Chassis - National Instruments PXI-1045
- Embedded Controller (computer) - National Instruments PXI-8186
- Current Meter - National Instruments PXI-4071
- Voltage Meter - National Instruments PXI-4070
- Power Supply – Pickering 41-742-001
- True RMS Multimeter - Fluke 87
- Decade Resistor - General Radio Company 1432-Z

Methods

To determine the break down voltage a micromanipulator probe was brought in contact with the side of a tin whisker growing from a tin-plated beryllium copper card guide as illustrated in Figures 3-2, 3-3, and 3-4. The card guide used in this experiment was removed from a Space Shuttle Orbiter Flight Control System (FCS) Ascent Thrust Vector Control (ATVC) Line Replaceable Unit (LRU) that was built in 1989.

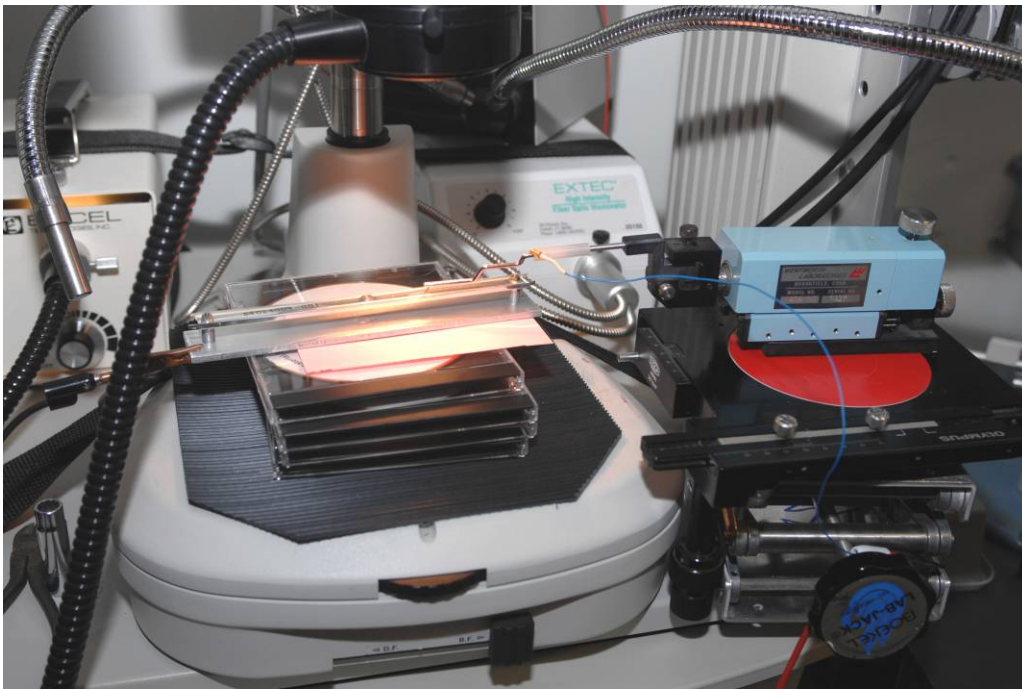


Figure 3-2 Micromanipulator and card guide

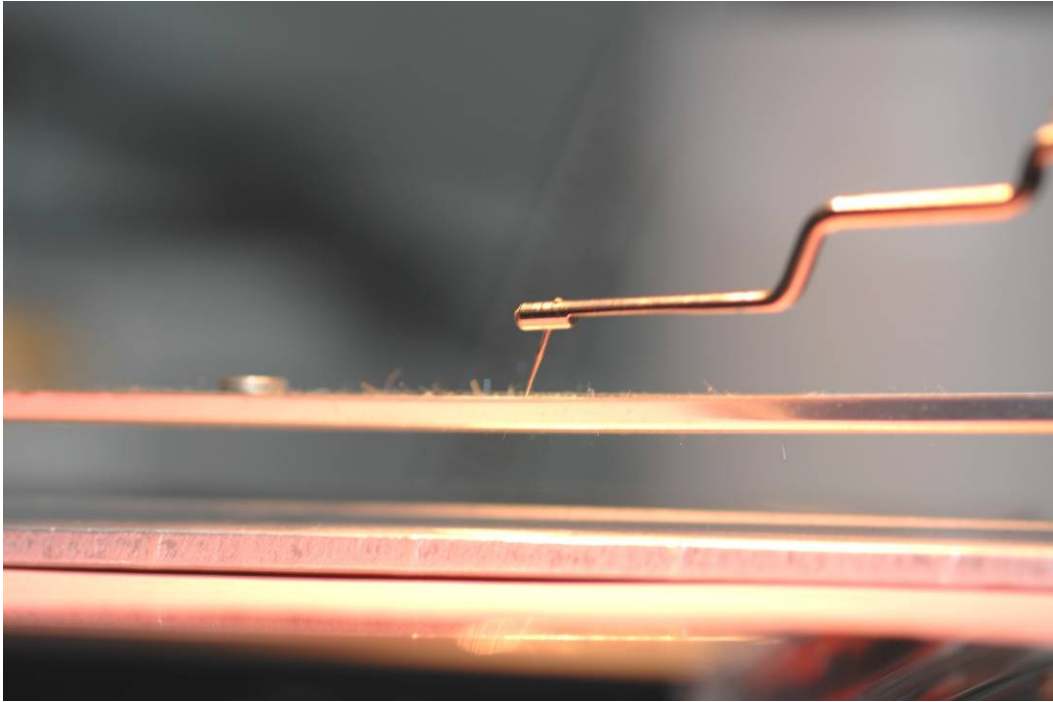


Figure 3-3 Close up photo of micromanipulator probe and whiskers on card guide

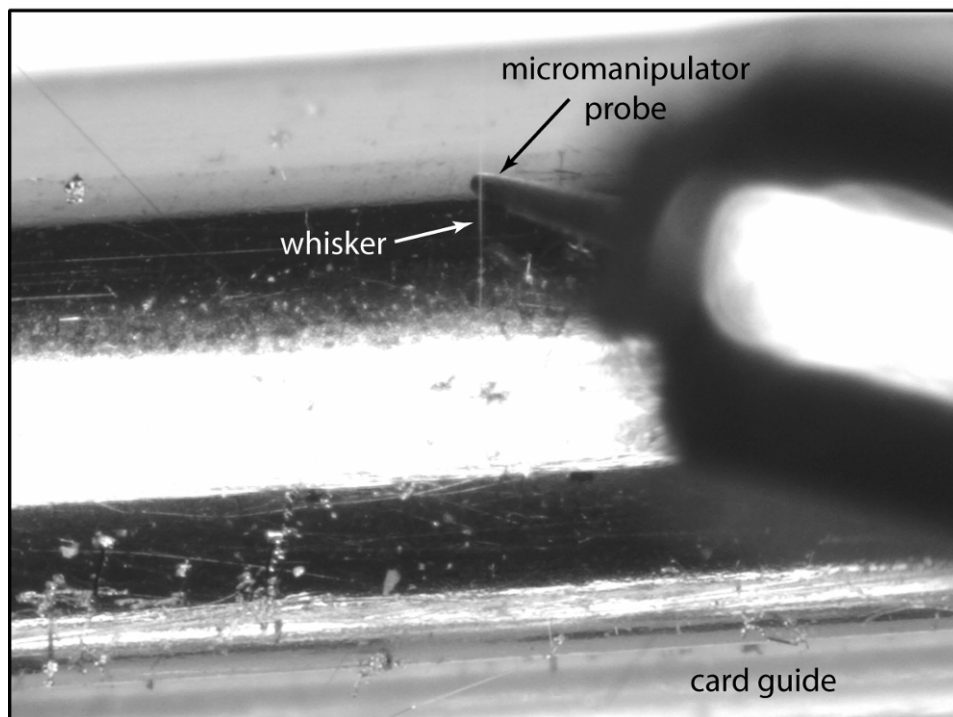


Figure 3-4 The micromanipulator probe touching tin whisker number 20 growing from the card guide.

A PXI automated data acquisition (DAQ) system was used to ensure improved experimental control. PXI is a platform for measurement and automated systems that uses a PC (Personal Computer) (National Instruments, 2004). The acronym PXI stands for (PCI extensions for instrumentation) (National Instruments, 2004). Peripheral component interconnect (PCI) is a specific type of bus that is used in PC's for connecting peripheral devices to the motherboard of the PC (Wikipedia, 2007a). The PXI automated DAQ system is shown in Figure 3-5.

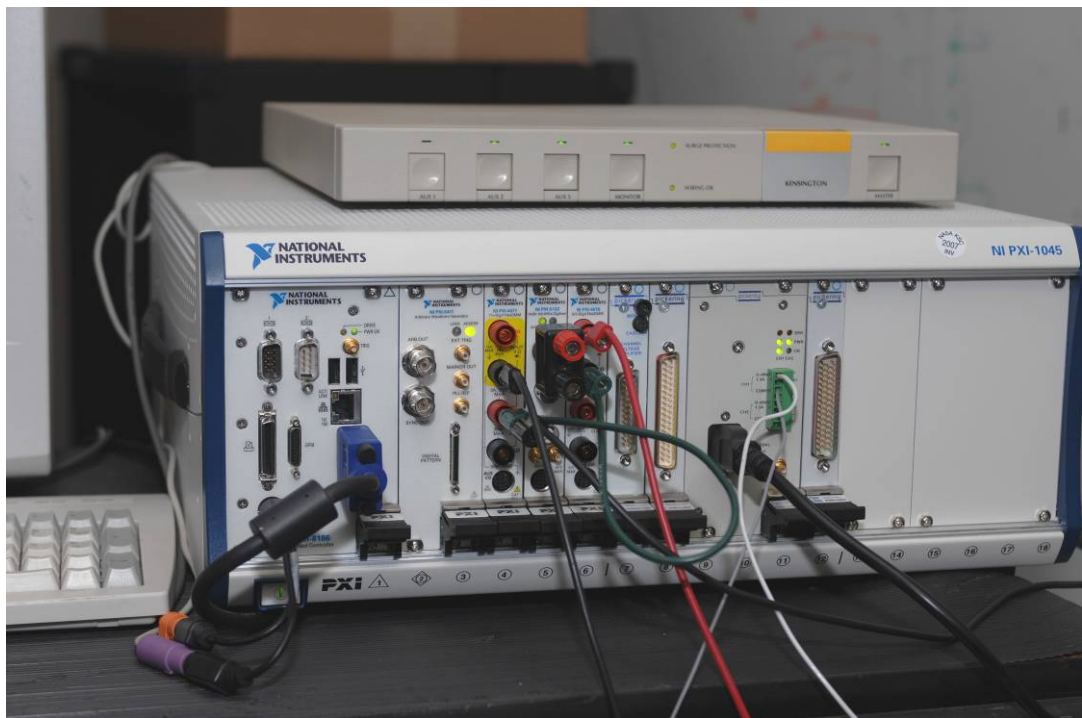


Figure 3-5 PXI chassis with computer, power supply, voltmeter, and currentmeter

DAQ software was written using LabVIEW® to automate both the incrementing of power supply voltage changes as well as the gathering and recording of the voltage and current data for each of the tin whiskers. Once contact was established, as determined with an optical microscope, the power supply voltage was increased from 0 to 45 vdc in 0.1 vdc increments. In addition to automating the recording of the critical data, the

software provided real-time plots of whisker voltage and current as shown in Figure 3-6.

The entire test station and its the cable interconnect diagram are shown in Figures 3-7 and 3-8 respectively.

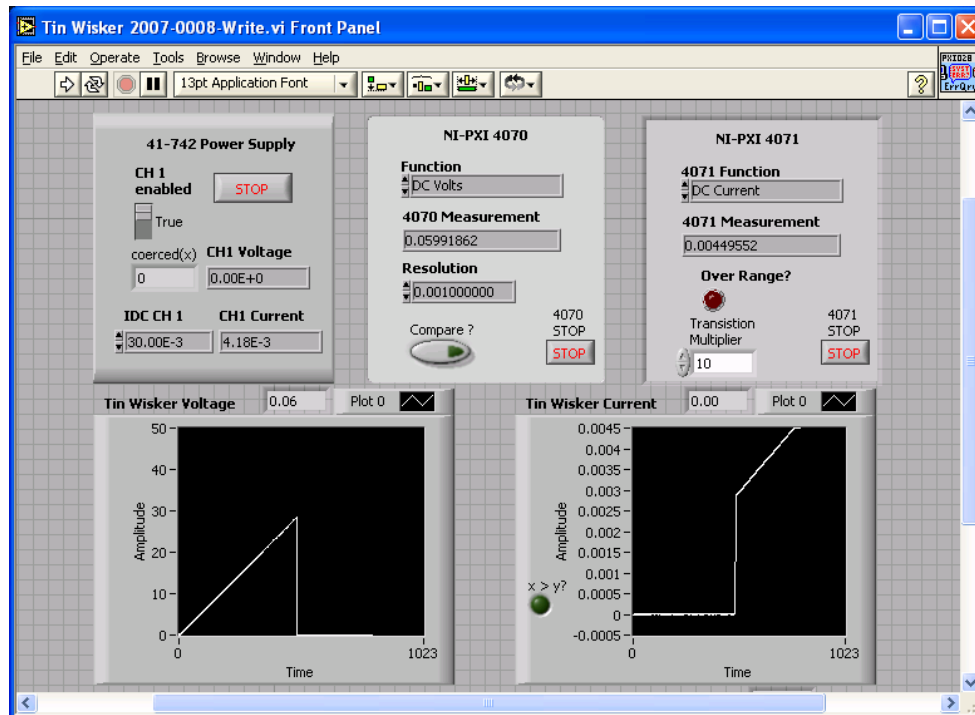


Figure 3-6 Software screen capture for whisker number 27

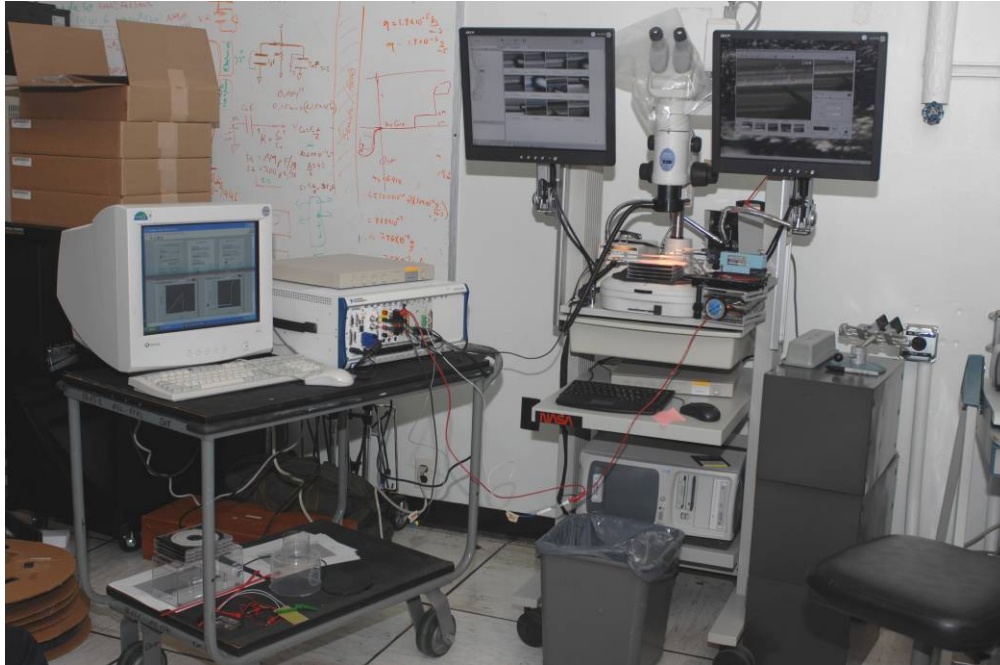


Figure 3-7 Tin whisker test station

Automated Tin Whisker Test Fixture

PXI instrumentation running a Labview program

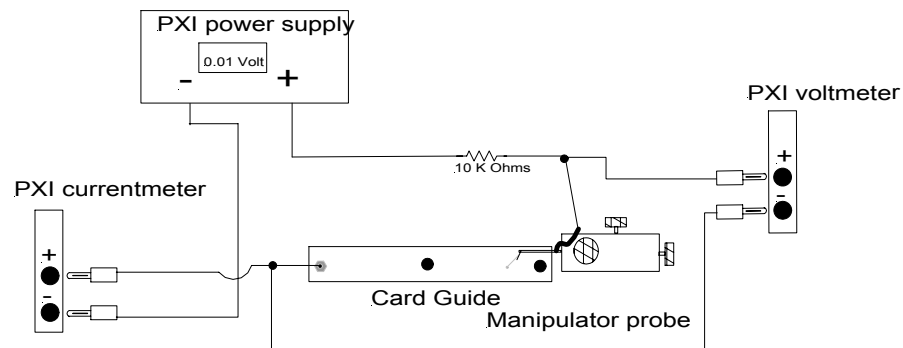


Figure 3-8 Cable interconnect diagram for the tin whisker test station instrumentation

The software captured 3 to 4 samples per second over the entire voltage range. The whisker voltage measurement included the resistance of the micromanipulator probe and lead as well as the card guide. However, the resistance of the whisker prior to film

breakdown is so high, and the lead/probe resistance and the card guide are so low, that they can be represented as a single resistance value, $R_2 = \text{Whisker Resistance}$, in the simplified electrical schematic illustrated in Figure 3-9. To avoid vaporizing the whiskers, a $10\text{ K}\Omega$ resistor was placed in series with the whisker to limit the current through the whisker when the break down voltage was achieved. With the current-limiting resistor in place, the test station was limited to a maximum of 4.5 mA at 45 vdc . The maximum output of the power supply is 45 vdc . The experiment was repeated to develop an empirical probability distribution of shorting as a function of voltage.

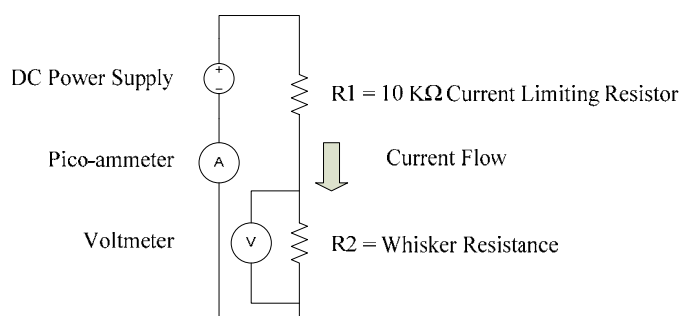


Figure 3-9 Electrical schematic for the tin whisker test station

Validation

The automated test fixture was validated by substituting a calibrated resistor decade box for the micromanipulator, whisker and card guide.

Results

The graphs of whisker voltage, whisker current, and power supply voltage for all 35 whiskers are contained in Appendix B. The point at which a short occurs, when the film resistance breaks down, can easily be seen in Figure 3-11 when the current jumps

from near zero, the nanoamp range, to the milliamp range. Prior to breakdown the majority of the voltage drop is across the whisker due to the high resistance of the film resistance on the whisker. In this state, the whisker voltage reading tracks close to the power supply voltage. The power supply voltage increases linearly from 0 to 45 vdc, then it remains at 45 vdc for a few seconds at the end of the run until the software is given a stop command. After the film has broken down, the majority of the voltage drop is across the current limiting resistor. In this state, the low whisker voltage reading was the result of the small resistance of the whisker, card guide and micromanipulator. Refer to Figures 3.9 and 3-10.

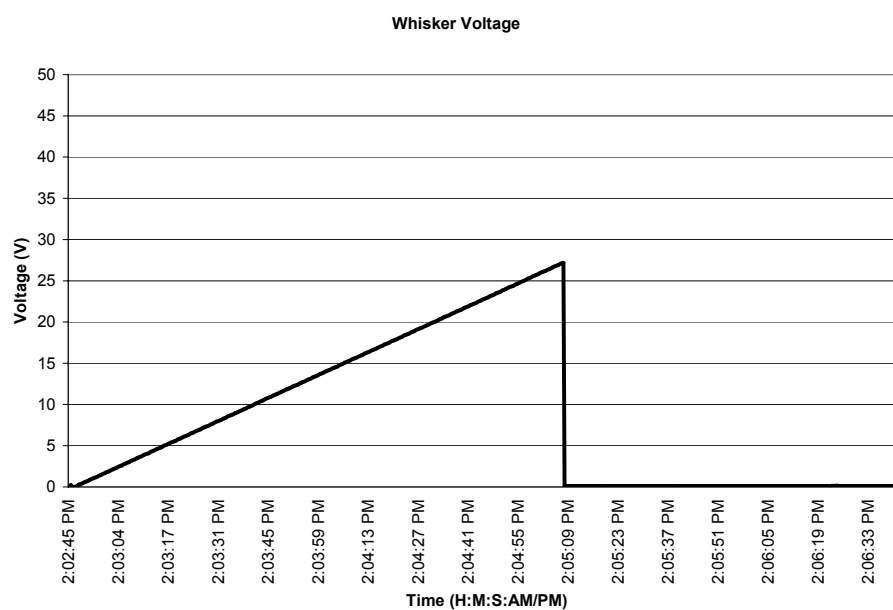


Figure 3-10 Whisker voltage as a function of time plotted for whisker number 32, illustrating a single transition point.

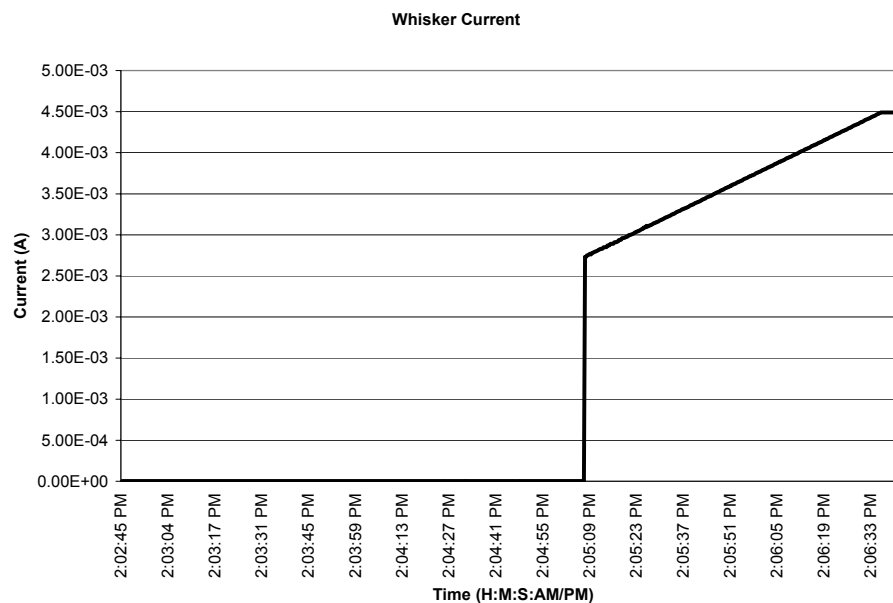


Figure 3-11 Whisker current as a function of time plotted for whisker number 32, illustrating a single transition point.

Although the software had originally been written to stop recording data after the film resistance broke down as determined by the change in whisker current, it was decided to run 35 whiskers to the full range of the test, 0 – 45 vdc, to observe their behavior.

An interesting benefit of running the test from 0 - 45 vdc for all of the whiskers was the opportunity to witness the difference in transitions. A single transition point, as illustrated in Figures 3-10 and 3-11, was exhibited by 20 of the 35 whiskers tested. Multiple transition points, as shown in Figures 3-12 and 3-13, were found in 9 of the 35 whiskers tested.

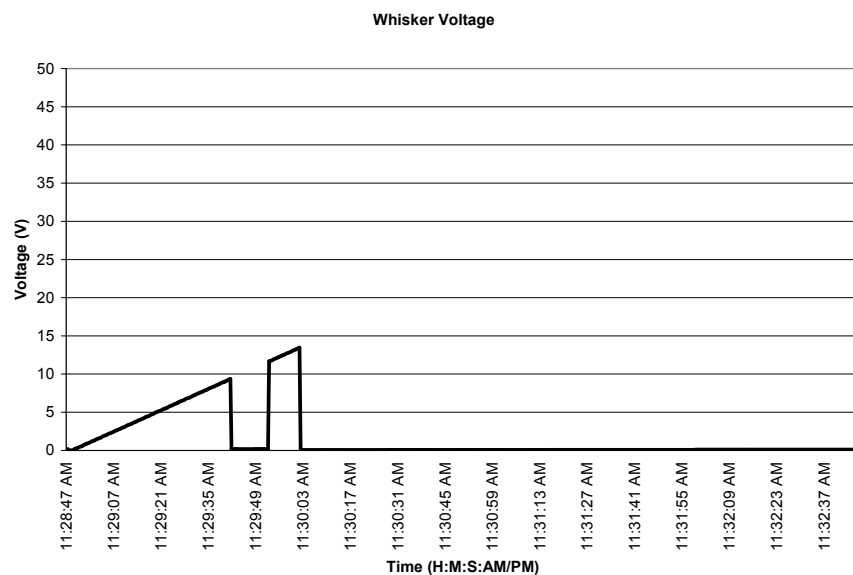


Figure 3-12 Whisker voltage as a function of time plotted for whisker number 4, illustrating multiple transition points.

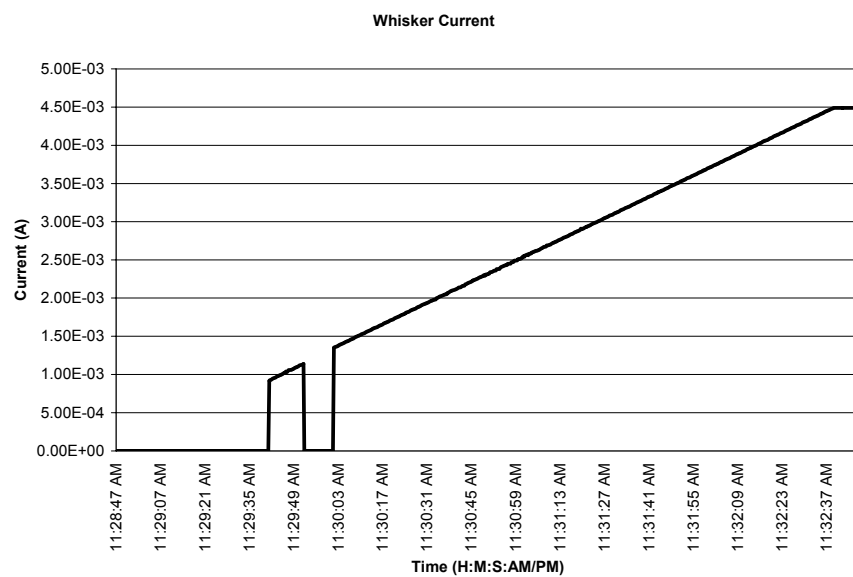
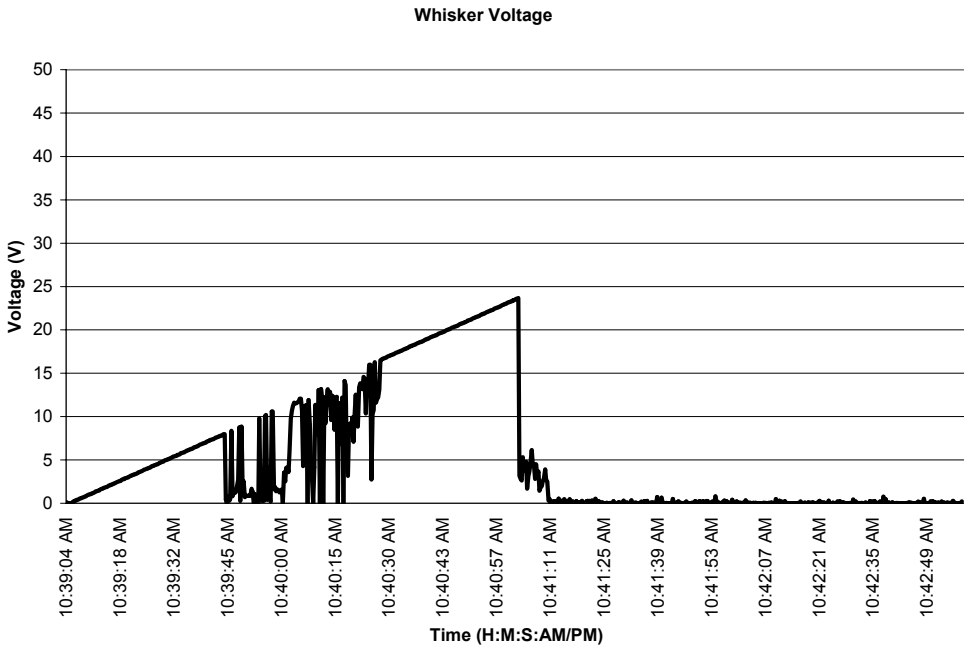


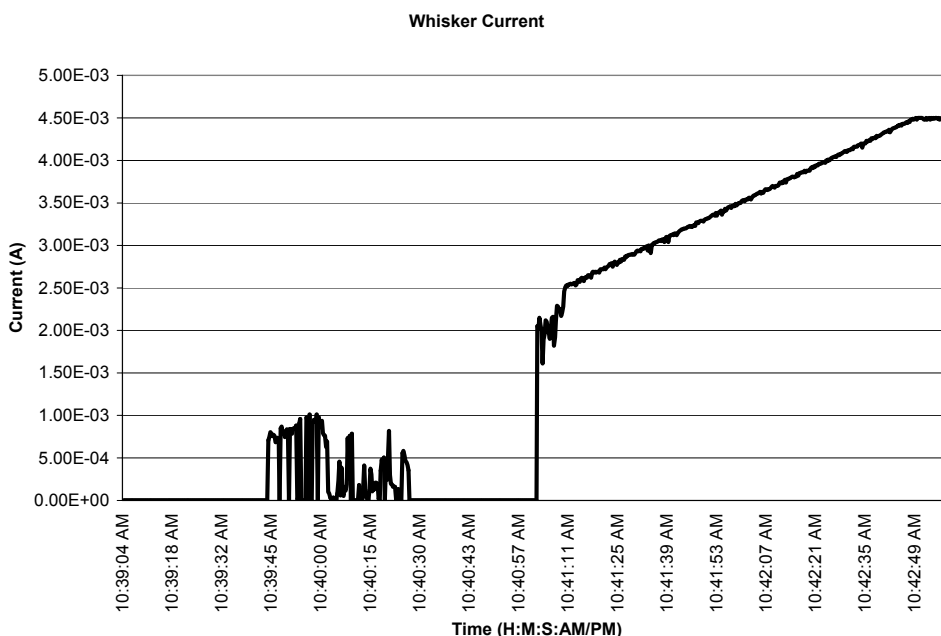
Figure 3-13 Whisker current as a function of time plotted for whisker number 4, illustrating multiple transition points.

Multiple transitions with intermittent contact were present in 6 of the 35 whiskers tested. The intermittent contact may be explained by air currents in the room. Whiskers

are very flexible and can appear to move like grass in the wind when observed under a microscope. Other possible explanations are that the probe was barely making contact with the whisker, or that thermal expansion caused whisker movement. An example of multiple transitions with intermittent contact is shown in Figures 3-14 and 3-15.



Figures 3-14 Whisker voltage as a function of time plotted for whisker number 2, illustrating multiple transition points with intermittent contact.



Figures 3-15 Whisker current as a function of time plotted for whisker number 2, illustrating multiple transition points with intermittent contact.

For the tin whiskers that exhibited multiple transitions and multiple transitions with intermittency, the first occurrence of breakdown was recorded as the breakdown voltage for the whisker. This was chosen because the first time the whisker conducts current in the milliamp range it can cause a short circuit.

The whiskers 17 and 24 conducted up to 3.06 mA and 2.00 mA respectively before metallic conduction ceased. This result is likely caused by either vaporization of the whisker, or the whisker slipping away from the micromanipulator tip because the whisker was being touched too close to the end of the micromanipulator probe.

The voltage level at the transition to metallic conduction current is the voltage level at which the film and oxide layers break down. The breakdown voltages for all thirty five whiskers were recorded in Appendix A. From the data in Appendix A, a cumulative

distribution of the fraction of whiskers that have broken down vs. applied voltage is shown in Figure 3-16 as a stair step shaped plot.

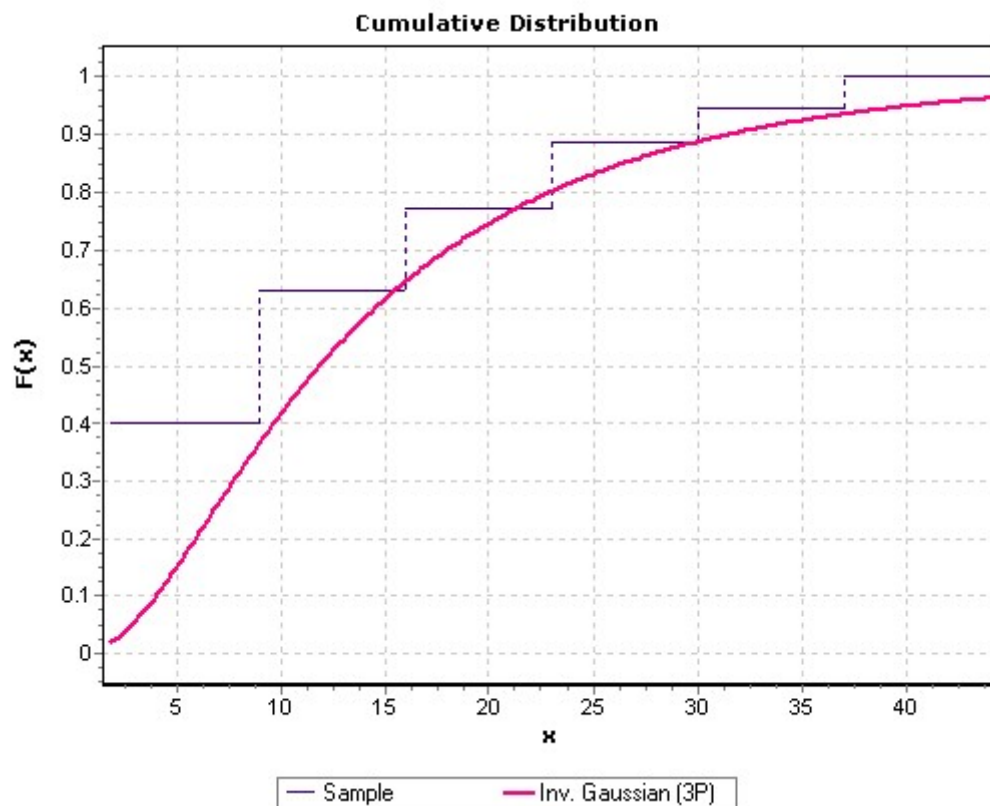


Figure 3-16 Cumulative distribution of sample data and the fitted inverse gaussian (3-parameter) model as a function of voltage.

The smoothed idealization of this is a cumulative distribution function $F(x)$, estimating the probability that the whisker contact resistance, interrogated this way, will break down when the applied voltage has a given value. Then $f(x) = dF(x)/dx$ is the probability density for breakdown at x (Walpole & Myers, 1989). The applied voltage is represented here by the variable x . The breakdown voltages recorded above were analyzed using EasyFit® distribution fitting software to determine the parametric probability distribution that best fits the data. The best fit distribution was the 3-

parameter inverse gaussian distribution. The estimated best fit cumulative distribution function and probability density function are shown in Figures 3-16 and 3-17 respectively. A histogram of the data is also shown in Figure 3-17.

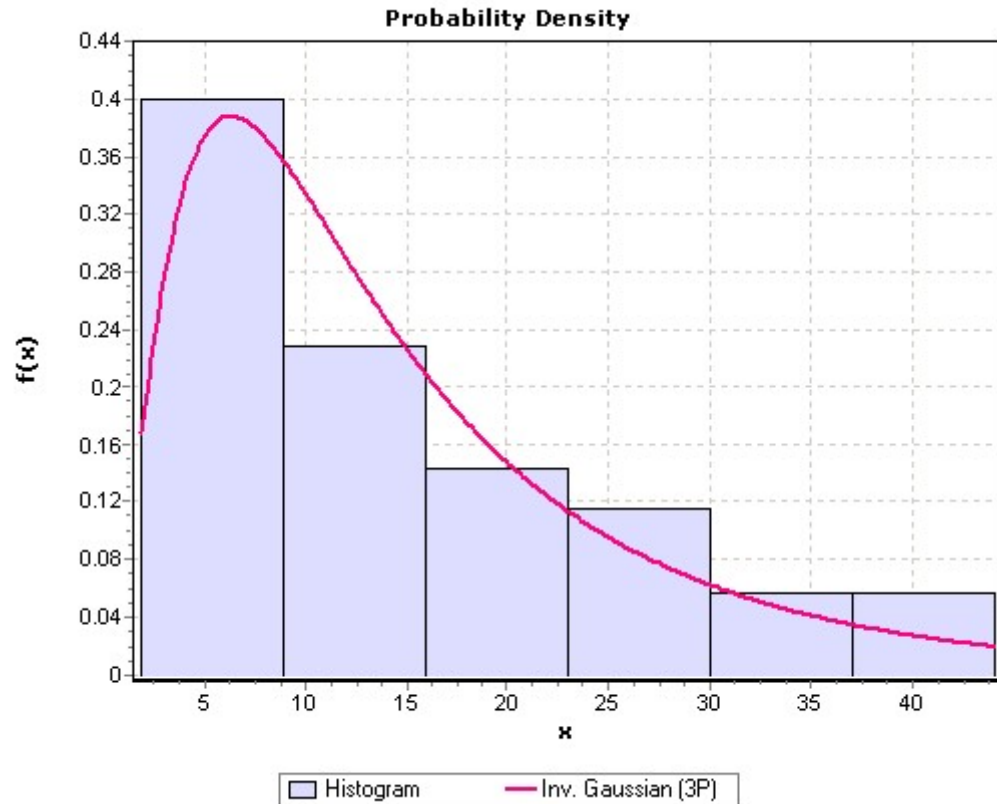


Figure 3-17 Probability density function of inverse gaussian (3-parameter) model as a function of voltage with a histogram of the sample data.

One tool to determine how well a specific model fits the observed data is the P-P plot shown in Figure 3-18. The closer the plot is to being linear, the better the model fits the observed data (Mathwave Technologies, 2007). While the P-P plots help one weed out the distributions that do not fit well, it is often difficult to discern between the good fitting models when the plots are close in the degree of deviation from linearity. The Kolmogorov-Smirnov test was helpful in further analyzing the best fit.

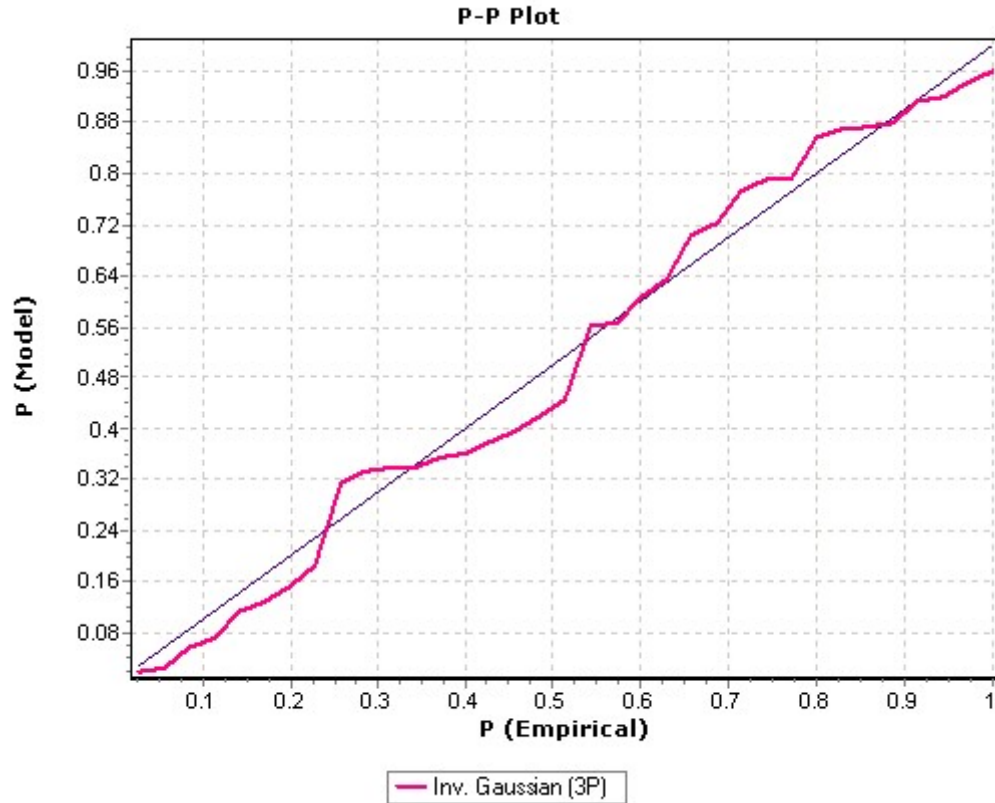


Figure 3-18 The probability-probability (P-P) plot shows how well the data follows the inverse gaussian (3-parameter) distribution.

The results of the Kolmogorov-Smirnov goodness of fit test are shown in Table 3-2. The null hypothesis and alternative hypotheses for this test are: H_0 : The data follows the specified distribution, H_A : The data does not follow the specified distribution (Mathwave Technologies, 2007). At the specified level of significance α , if the test statistic is greater than the critical value, the null hypothesis is rejected. For the values of α given below, the null hypothesis is not rejected.

Table 3-1 Kolmogorov-Smirnov test

KOLMOGOROV-SMIRNOV TEST		
Sample Size	35	
Statistic	0.06676	
Rank	1	
α	Critical Value	Reject?
0.2	0.18086	No
0.15	0.1927	No
0.1	0.20622	No
0.05	0.22988	No
0.01	0.27552	No

The EasyFit® distribution fitting software tested over 40 different distributions before selecting the 3-parameter inverse gaussian as the best fit based on the Kolmogorov-Smirnov test results.

The estimated parameter values for the best fitting 3-parameter inverse gaussian distribution are $\lambda = 31.977$, $\mu = 17.571$, $\gamma = -1.9716$. The probability density function (PDF) for the 3-parameter (3-P) inverse gaussian distribution is shown in equation 3-4 (Mathwave Technologies, 2007):

$$f(x) = \sqrt{\frac{\lambda}{2\pi(x-\gamma)^3}} \exp\left(-\frac{\lambda(x-\gamma-\mu)^2}{2\mu^2(x-\gamma)}\right) \quad (3-4)$$

The cumulative distribution function (CDF) for the 3-parameter inverse gaussian distribution is shown in equation 3-5, where $\Phi(\cdot)$ is the normal cumulative distribution function (Mathwave Technologies, 2007):

$$F(x) = \Phi\left(\sqrt{\frac{\lambda}{x-\gamma}}\left(\frac{x-\gamma}{\mu}-1\right)\right) + \Phi\left(-\sqrt{\frac{\lambda}{x-\gamma}}\left(\frac{x-\gamma}{\mu}+1\right)\right)\exp(2\lambda/\mu) \quad (3-5)$$

Based on the data and the fitted model the expected voltage (mean) where a short will occur is $\mu + \gamma = 15.5994$ vdc, with a variance of $\mu^3/\lambda = 169.6491$ (Koutrouvelis, Canavos, & Meintanis, 2005/6/15).

The proof of concept experiment was the first step in developing an empirical distribution that represents the probability of a free whisker shorting across two exposed contacts. This experiment demonstrated that whisker shorting can be represented as a function of breakdown voltage. However, it is important to consider the limitations of the experiment including the small sample size, the number of conducting surfaces, and the difference and variation between force applied by gravity and the force applied by the micromanipulator probe.

Given that the density of tin is 7300 kg/m^3 (Slade, 1999), for a whisker that has a diameter of $2 \text{ }\mu\text{m}$ and length of 4mm ; the whisker volume will be $1.25\text{E-}14 \text{ m}^3$. The whisker volume multiplied by the density of tin gives the whisker mass of $m = 9.17\text{E-}11 \text{ kg}$. Since $F = ma$ and $a = 9.806\text{m/s}^2$ (Halliday & Resnick, 1981), the force of gravity can be calculated to be $F = 9.0\text{E-}10 \text{ N}$. Since load applied to a whisker at each point of contact $P = F/2 = 4.50\text{E-}10 \text{ N}$ as illustrated in Figure 3-19.

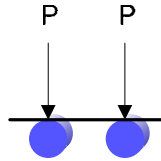


Figure 3-19 Load Applied to Whisker Lying Across Two Conductors

The force applied by the micromanipulator probe to the whisker was calculated above as $P = 5.95\text{E-}10$ N. The force applied to the micromanipulator was greater than that applied by gravity $P = 4.50\text{E-}10$ N. The additional pressure was not enough to physically breach the oxide layer or we would have had breakdown voltages much closer to 0 vdc. However, the difference in pressure could cause a shift in the mean of the distribution. A larger sample experiment with additional experimental controls was performed to better understand the phenomena as recorded in Chapters 4 and 5.

Focused Ion Beam (FIB) Analysis

Methods

Tin whiskers from the same card guide used in the breakdown voltage experiment were cross-sectioned using an FEI 200 TEM FIB with a 30kV Gallium liquid metal ion source. The whiskers were removed from the card guide and placed on a microscopy stub using carbon tape as shown in Figure 3-20.

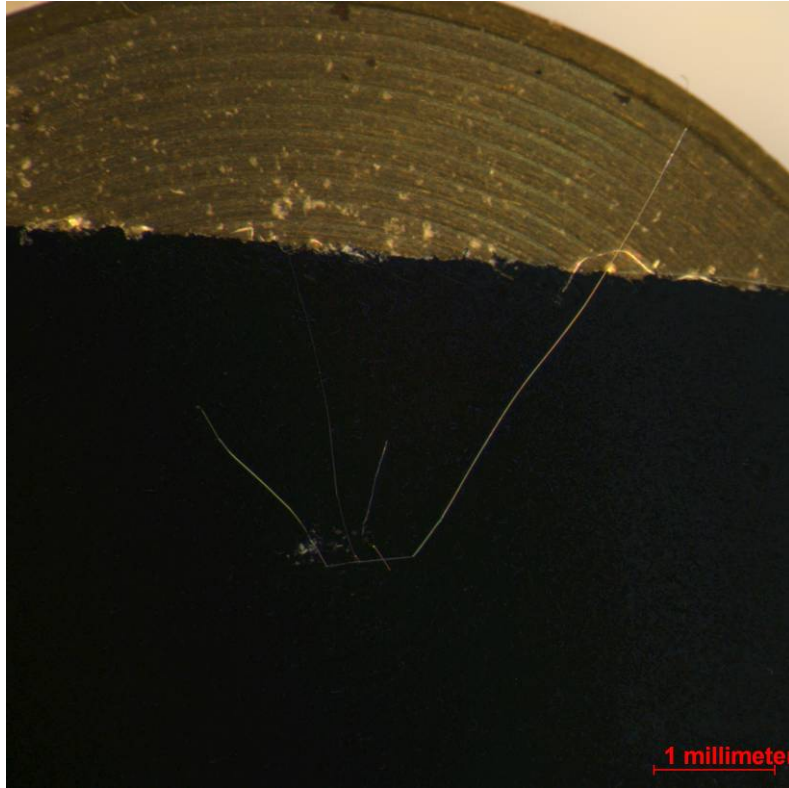


Figure 3-20 Stereomicroscope image showing tin whiskers on carbon tape mounted on a microscopy stub. Magnification: 18X

To make the whiskers conductive for electron and ion imaging, the whiskers were sputter coated with gold-palladium as shown in Figure 3-21.

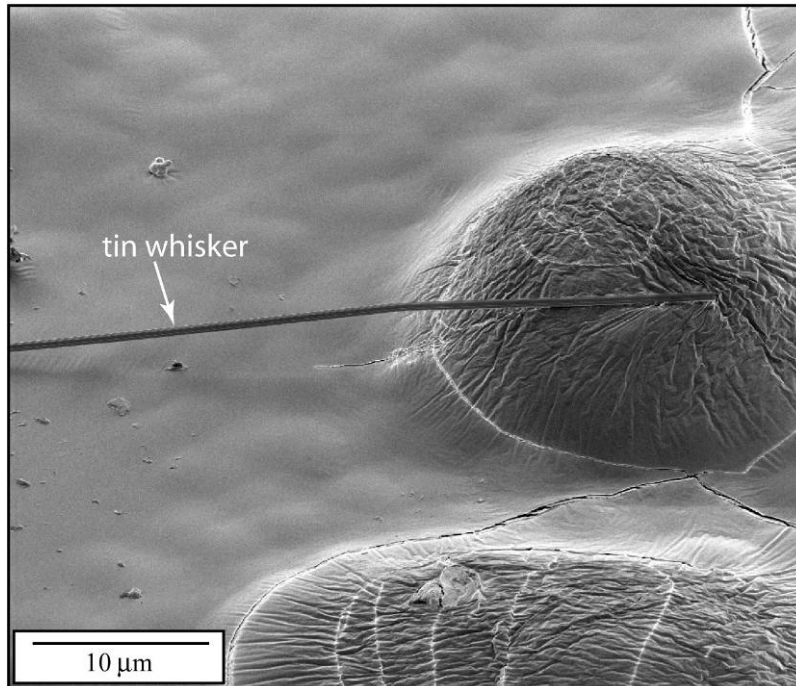


Figure 3-21 FIB image of a tin whisker on the carbon tape substrate that has been sputter coated with gold palladium (NASA/UCF)

Platinum was deposited on the region of interest prior to FIB sectioning in order to preserve the whisker's outer surface. It was observed that the whisker exhibited a fluted shape resembling an extruded surface, as shown in Figure 3-22.

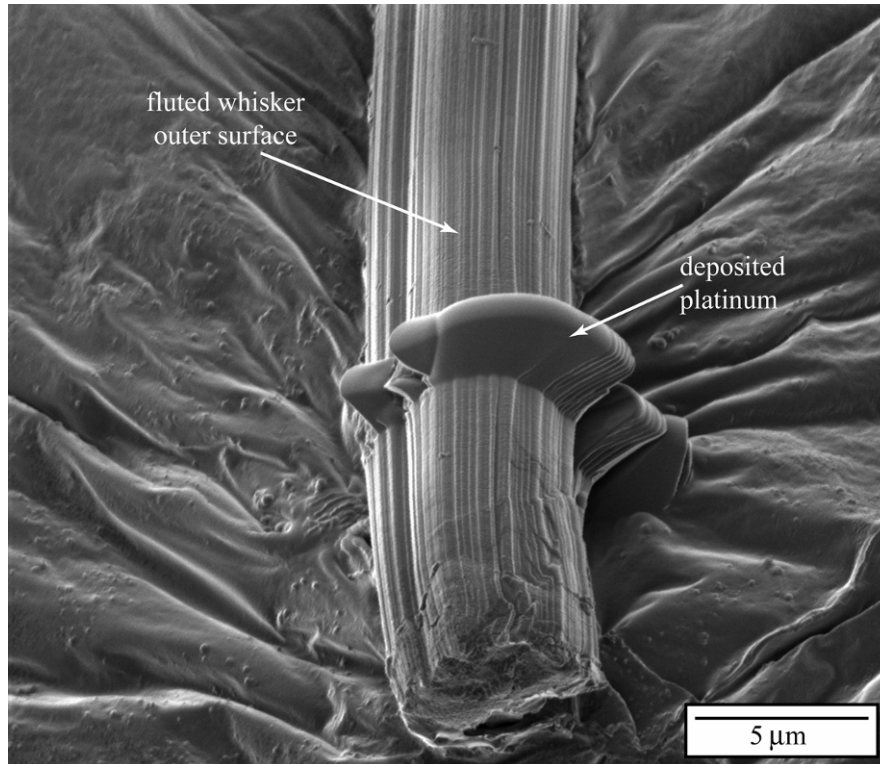


Figure 3-22 FIB image of tin whisker removed from card guide shows a fluted outer surface. Platinum was deposited on the surface prior to sectioning in order to preserve the region of interest (NASA/UCF).

The ion beam was used to mill away whisker material until the desired region of interest to obtain a cross section normal to the whisker's growth direction as shown in Figure 3-23.

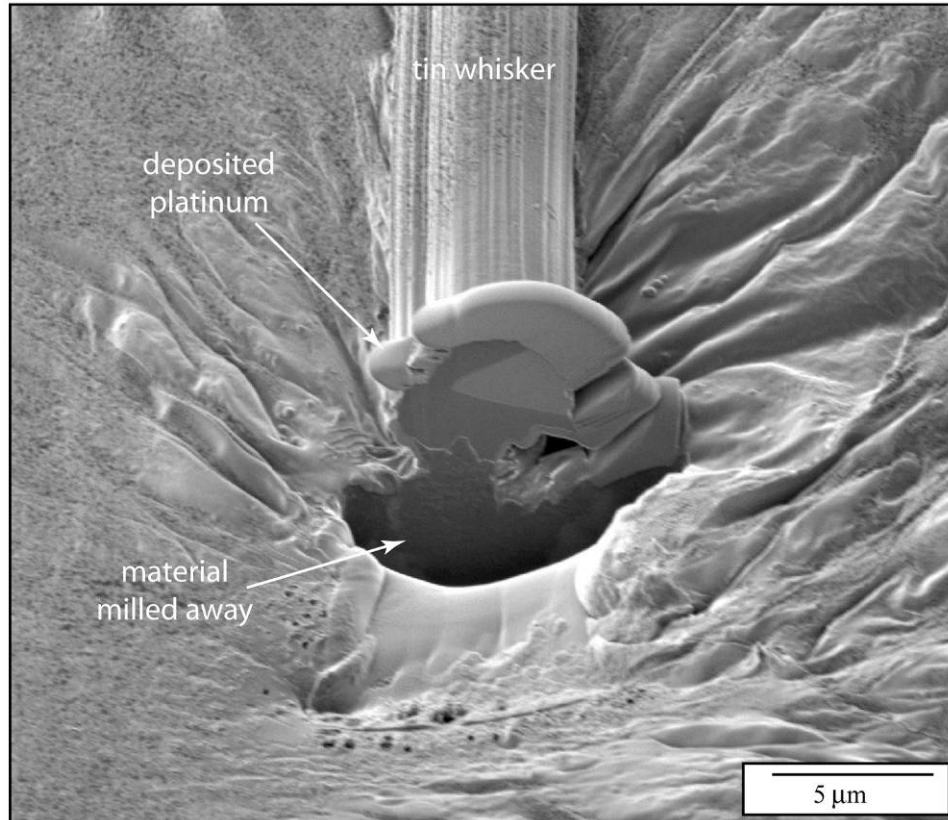


Figure 3-23 FIB image of sectioned whisker after ion beam milling (NASA/UCF).

Results

The FIB cross section in ion channel imaging facilitates the examination of what appears to be grains with varying crystallographic orientations within the tin whisker as illustrated in Figure 3-24. Ion channeling images show contrast from a variance in the crystallographic orientation within a sample and this particular image shows what appear to be three distinct grains (Giannuzzi & Stevie, 2005). In the majority of the tin whisker literature, tin whiskers were considered single crystals. While polycrystalline whiskers are rare, they have been observed before (Joint Electron Device Engineering Council, 2006). The polycrystalline nature of the whiskers was verified in the full experiment using transmission electron microscopy (TEM). The image in Figure 3-24 was taken at a

52° tilt resulting in the semi-elliptical shape. However, the geometry of the cross-section is expected to be more circular. The diameter of the tin whisker is approximately 6.7 μm in the vertical direction and 6.1 μm in the horizontal direction.

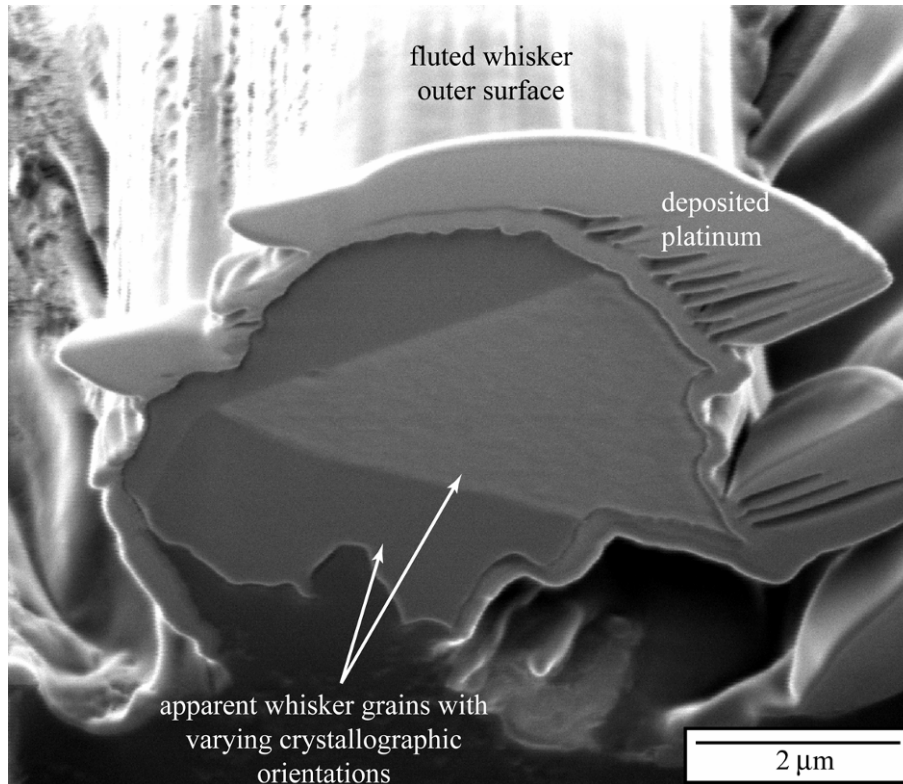


Figure 3-24 FIB image of as-sectioned tin whisker shows apparent variation in grain orientation within the cross-section. Image was taken at a 52° angle from horizontal (NASA/UCF).

An additional two whiskers from the card guide were removed and sectioned by the FIB. These smaller-diameter whiskers exhibited the commonly reported single crystal structure as shown in Figure 3-25. The diameter of the top whisker is approximately 2.4 μm in the vertical direction and 2.0 μm in the horizontal direction. The diameter of the bottom whisker is approximately 1.72 μm in the vertical direction and 2.0 μm in the horizontal direction. Since the cross section of the each tin whisker was not truly

circular, the diameter measurements given above were made along the largest dimension in the stated direction.

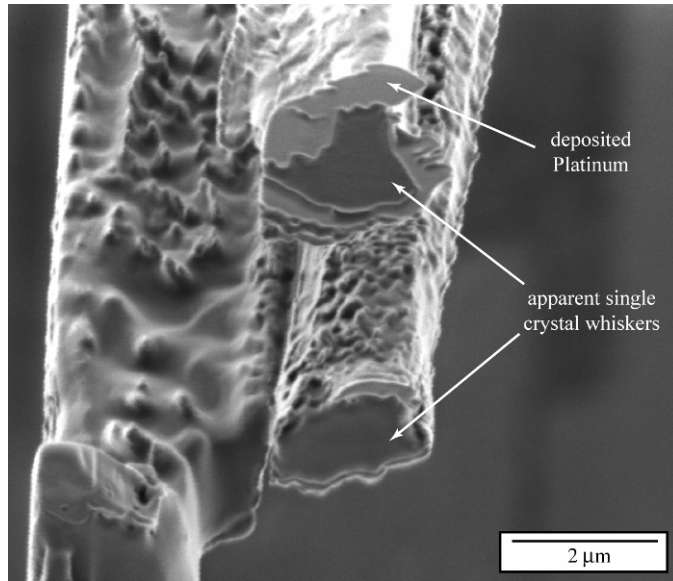


Figure 3-25 FIB image of two as-sectioned tin whiskers that exhibited the expected single-crystal cross section. Image was taken 52° from horizontal (NASA/UCF).

CHAPTER 4: METHODOLOGY

Full Experiment

The full experiment incorporated the lessons learned from the proof of concept experiment. It determined the breakdown voltage for a larger sample ($n = 200$) of whiskers with the objective of obtaining a more comprehensive empirical distribution of breakdown voltage. The observed data was used to determine the best fitting parametric distribution to the breakdown voltage. The associated data analysis also incorporated explorations of possible sources of variability. In addition, transmission electron microscopy was used to study and determine if the whisker that was sectioned in the proof of concept experiment was polycrystalline or a single crystal. Also, a FIB was used to section a sample of one card guide from each ATVC to determine if the plating that grew the whiskers was bright or matte finish.

Whisker Breakdown Voltage Experiment

Equipment

The hardware, software and methods described in the proof of concept experiment were used in the full experiment with the improvements listed below. The test station was validated using a calibrated decade box to ensure that none of the improvements has any adverse effects on the automated test station.



Figure 4-1 Tin whisker test station - full experiment

Improvements

The following improvements were added to the full experiment.

- Improved electrical ground by connecting to card guide instead of card holding fixture.
- Added shielding to wires to minimize noise during low current measurements.
- To minimize the effect of any oxides on the probe, rather than removing the oxide from the tungsten micromanipulator probe with emery cloth, gold plated tungsten micromanipulator tips were used.
- To improve control of the applied pressure, the probe was applied to the whisker on approximately the top 25% of the whisker.
- The probe tip were cleaned every five whiskers with isopropyl alcohol to ensure the gold tip is clean.
- A solderer's helper was modified to allow flexible positioning of the card guide.
- An extension platform for the microscope was fabricated to facilitate clamping of the lab jack.
- A ferrous top plate was fabricated for the lab jack to allow the magnetic base of the micromanipulator to be firmly mounted on the lab jack. The lab jack

provided the coarse X, Y and Z movements, while the micromanipulator provided the fine X, Y and Z movements for probing the tin whiskers.

- Air duct diverters were fabricated to reduce the movement of the whisker during the experiments by air currents.
- A software method of selecting the breakdown voltages from the tin whisker voltage and current data was developed using Microsoft Excel.

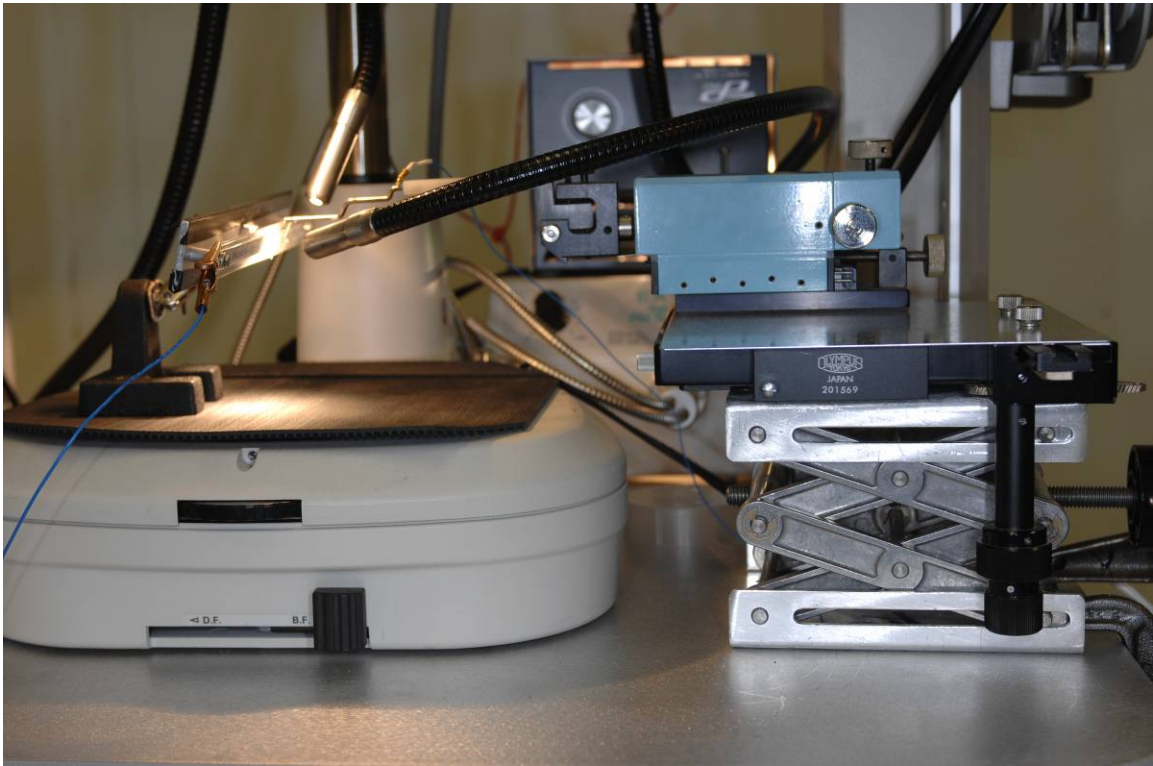


Figure 4-2 Test station - tin whisker probing

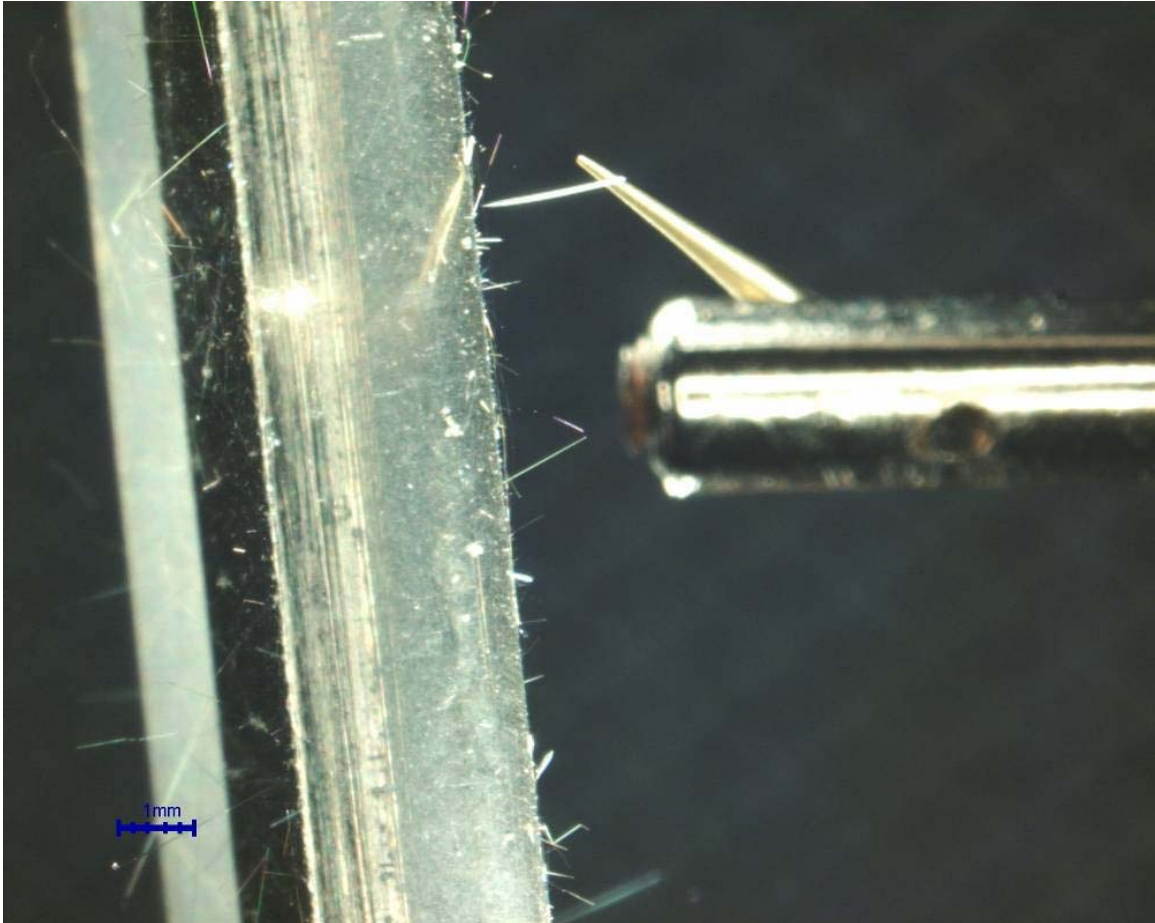


Figure 4-3 Micromanipulator probe in contact with a tin whisker

Method of Sample Selection

Card guides from two different LRUs were available for sampling. The card guides are from ATVC Serial Number 31 and ATVC Serial Number 33. There are 28 card guides from each LRU. Card guides that have been used for other experiments were removed from selection. A number (1-28) was assigned to each card guide from each LRU. Using a table of random numbers 10 card guides were selected from each LRU.



Figure 4-4 ATVC 31 card guides

Five whiskers were tested from the top, and five whiskers were tested from the bottom of each card guide. The result was a sample size of 200 whiskers. The data was recorded in Appendix C:

Analysis of Sample Size

A 3-parameter inverse gaussian distribution was determined as the best fitting parametric distribution to the data collected during the proof of concept experiment. The parameters of this 3-parameter inverse gaussian distribution were estimated as $\mu = 17.571$, $\lambda = 31.977$ and $\gamma = -1.9716$. To gain insight into the population suggested by the data from the proof of concept experiment, 500,000 random numbers, representing breakdown voltages typical for this distribution, were generated and the simulated population is shown Figure 4-5.

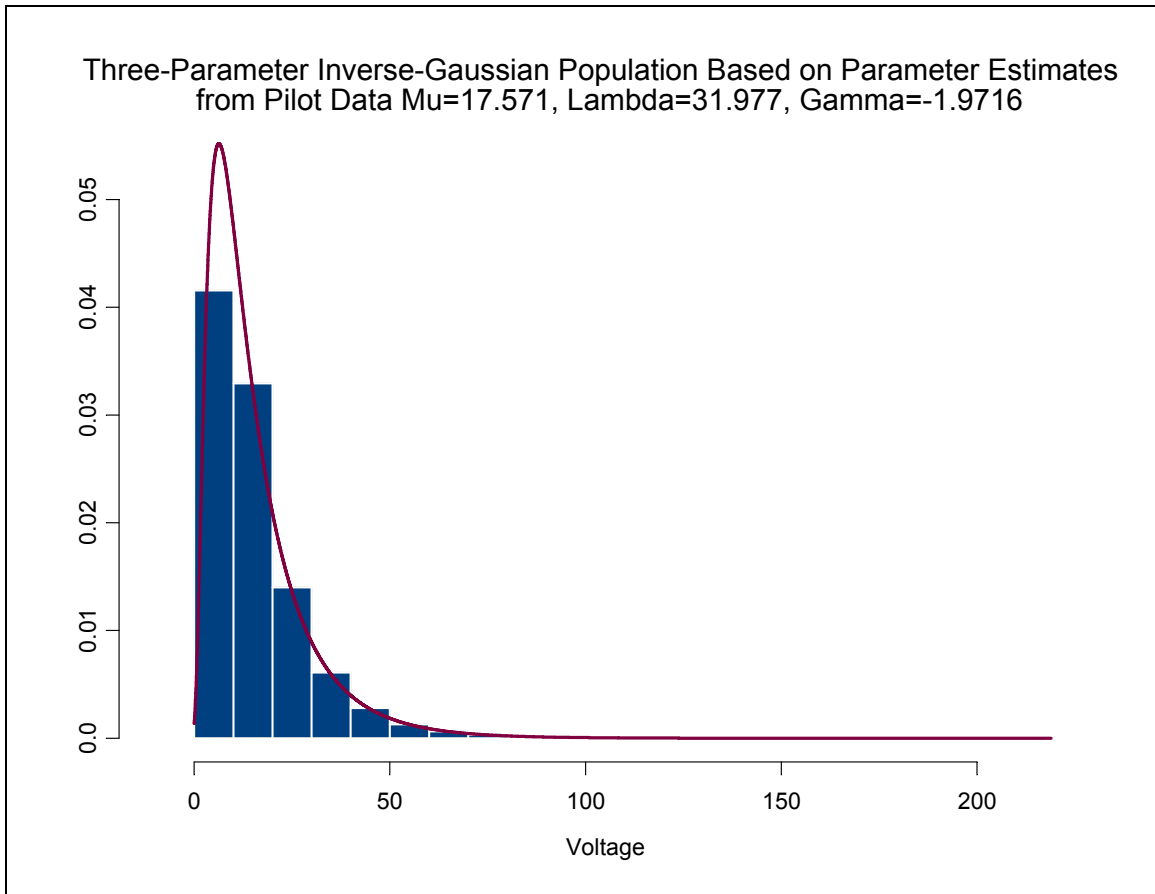


Figure 4-5 Simulated population for 3-parameter inverse gaussian distribution

The summary statistics for this population are shown in Figure 4-6:

Min.	1st Qu.	Median	Mean	3rd Qu.	Max.
-0.6727095	6.7945666	11.8924230	15.5880056	20.2323773	218.9191417

Figure 4-6 Population summary statistics

To gain an understanding of how well a sample size of 200 would estimate the some of the critical parameters of the population (such as the 5th and the 95th percentiles), 5000 random samples of size 200 were generated. The observed values from this simulation were compared to the parameters of the simulated population to determine how “close” they were in estimating some crucial parameters of the population. Estimates of the 5th, 25th, 75th and 95th percentiles of the population as well as the

estimates of the mean and the median were computed and compared. These results are numerically summarized in Figure 4-7 below. Note that the “true values” are based on the assumption that the distribution identified during the proof of concept experiment is the actual distribution of the breakdown voltage.

```

True 5th percentile of the breakdown voltage: 2.841087
[1] "5th Percentile Estimates"
      Min. 1st Qu.  Median      Mean 3rd Qu.    Max.
 1.523943 2.644764 2.913967 2.928684 3.207551 4.727095
[1]
"=====
True 25th percentile of the breakdown voltage: 6.794567
[1] "25th Percentile Estimates"
      Min. 1st Qu.  Median      Mean 3rd Qu.    Max.
 4.864106 6.468616 6.844655 6.854999 7.227740 9.091247
[1]
"=====
True Mean of the breakdown voltage: 15.58801
[1] "Mean Estimates"
      Min. 1st Qu.  Median      Mean 3rd Qu.    Max.
12.41457 14.92909 15.55633 15.57636 16.19635 18.77387
[1]
"=====
True Median of the breakdown voltage: 11.89242
[1] "50th Percentile Estimates"
      Min. 1st Qu.  Median      Mean 3rd Qu.    Max.
 9.256348 11.330888 11.889008 11.919265 12.485658 15.302178
[1]
"=====
True 75th percentile of the breakdown voltage: 20.23238
[1] "75th Percentile Estimates"
      Min. 1st Qu.  Median      Mean 3rd Qu.    Max.
14.85390 19.15161 20.12113 20.18654 21.17835 25.88537
[1]
"=====
True 95th percentile of the breakdown voltage: 40.98433
[1] "95th Percentile Estimates"
      Min. 1st Qu.  Median      Mean 3rd Qu.    Max.
29.15260 37.50809 40.01682 40.36368 42.96036 58.44113
[1]
"=====

```

Figure 4-7 Population values and the numerical summaries of 5000 samples for each of the quantities of interest

The smoothed-histograms in Figure 4-8 provide a visual of the overall performance of these samples in estimating the assumed population quantities of interest.

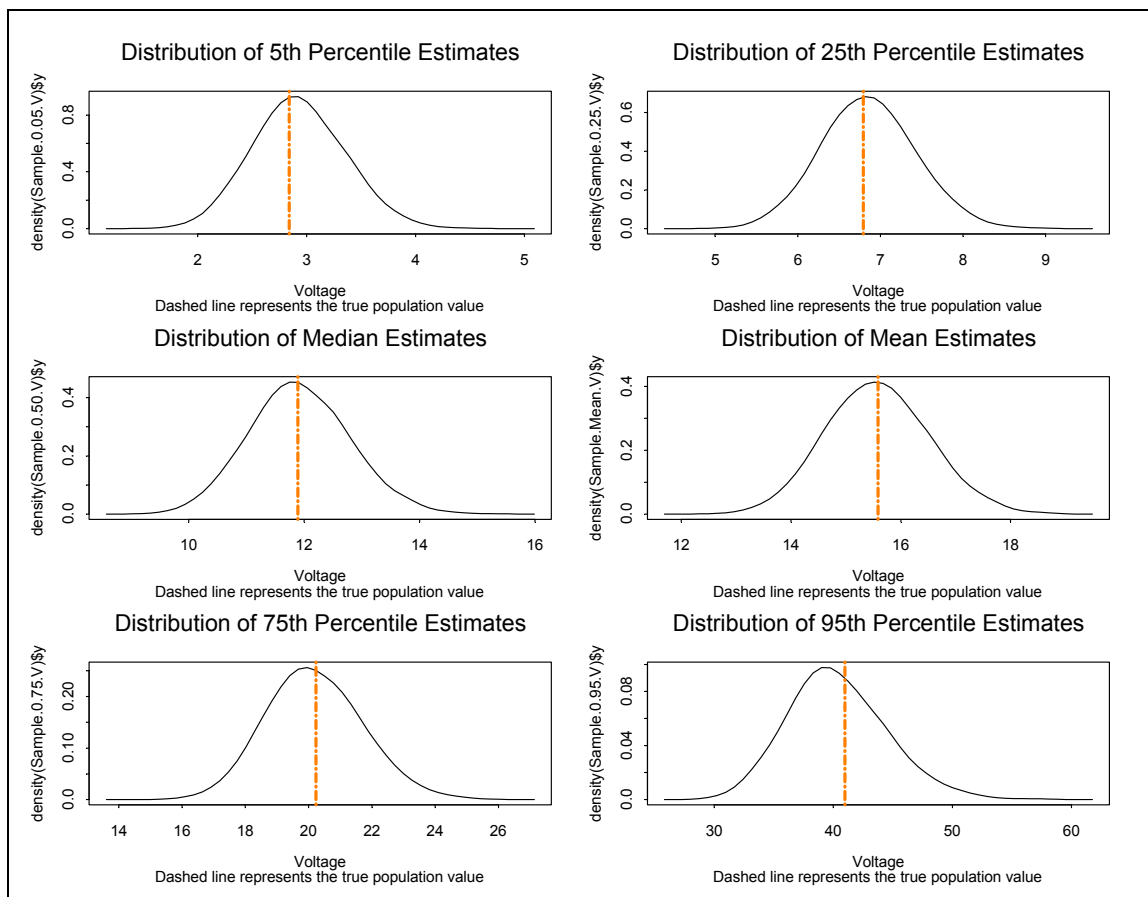


Figure 4-8 Smoothed histograms for sample size evaluation

Based on the numerical summaries and especially the plot above (which are essentially histograms that have been smoothed over), we can expect to do fairly well using a sample size of 200. However, it is important to note the limitations of this analysis, including:

- This approach did not take into account possible censoring (i.e. the possibility that at 45V, the limit of the power supply, a short will not occur). If the assumption is made that the distribution suggested by the proof of concept experiment sample is the true population (which it is clearly a false assumption, but this distribution is the best estimate available) there is approximately a 4% chance that a short will not occur within the limits of the power supply. Since the percentage of values expected to be larger than 45V is 3.6972%, in the full experiment one would expect approximately 8 whiskers to not fail among the sample of 200 that will be tested in the full

experiment. Statistical methods are available to properly accommodate any censoring which may be observed during the full experiment.

- Another very crucial assumption made in this analysis was that the whiskers that come from different card guides and LRUs will perform identically. If this is not the case, there will be more variability which may result in a very different shape for the distribution. Since the data from the proof of concept experiment came from a single card guide, there is no way to know what the influence of using different card guides from different LRUs will be. Thus, the aforementioned simulated setting represents the best case scenario in terms of variability.

Validation

Validation of the automated test station was performed by substituting a calibrated resistor decade box for the micromanipulator, whisker and card guide.

Data Analysis

Using commercially available software, a parametric distribution was selected that best fits the breakdown voltage data observed during the full experiment. The selection was based on probability-probability plots as well as goodness of fit tests. The parameters for the identified distribution were estimated and the relevant interpretations were provided. In addition, possible sources of variability such as the differences across the LRUs, card guides, top and bottom of card guides etc. were explored. The detailed data analysis was performed in Chapter 5.

Sample Preparation for Transmission Electron Microscopy (TEM)

A focused ion beam (FIB) was used to prepare a tin whisker cross sectional sample for TEM examination. The TEM analysis was used to determine if the apparent polycrystalline structure of the tin whisker examined in the proof of concept experiment was truly polycrystalline or a single crystal. The first step was to deposit platinum on top of the region of interest (ROI) along the whisker to protect the whisker outer surface from the ion beam. Next, the ion beam was used to mill trenches on either side of the ROI of

the whisker normal to the direction of growth leaving a small ($< 1 \mu\text{m}$) section of the whisker. A close up of the section at this step is shown in Figure 4-9.

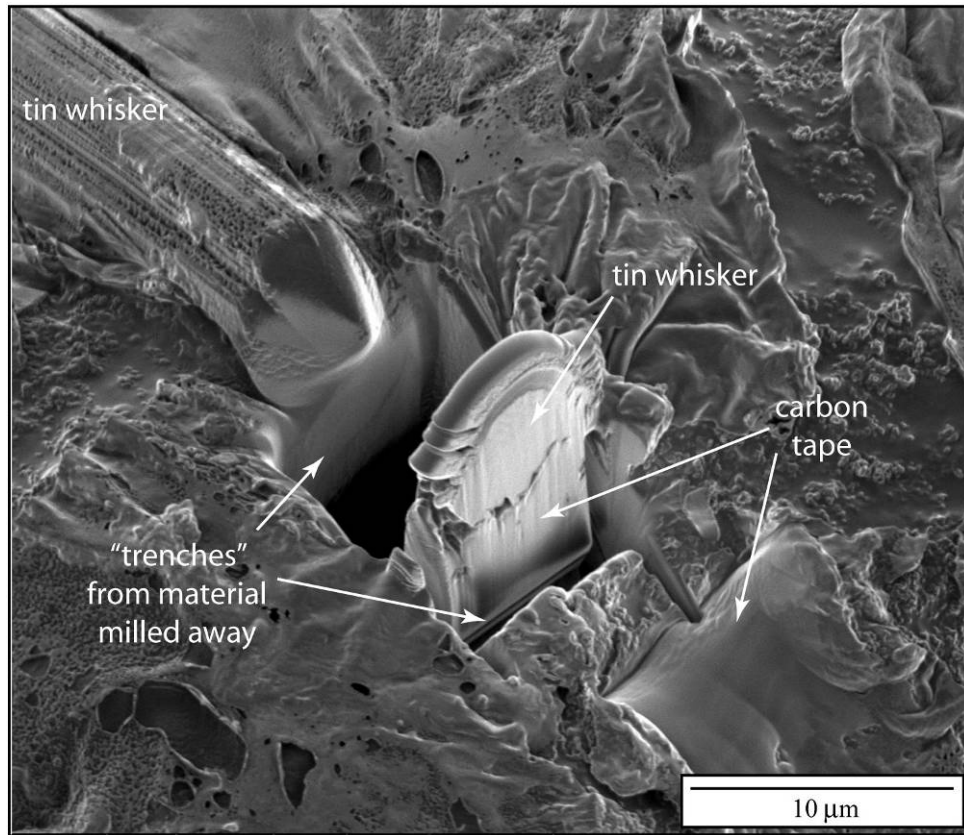


Figure 4-9 FIB image showing a cross section of a tin whisker that has been created by milling out trenches on either side of section. Magnification: 8000X (NASA/UCF)

Once the section was milled to a desired thickness needed for TEM evaluation, an in-situ needle was lowered in preparation for removing the tin whisker section, as shown in Figure 4-10. The needle was spot welded to the whisker section using platinum, and the section was released from the carbon tape by milling away any remaining point of attachment with the FIB, as shown in Figure 4-11.

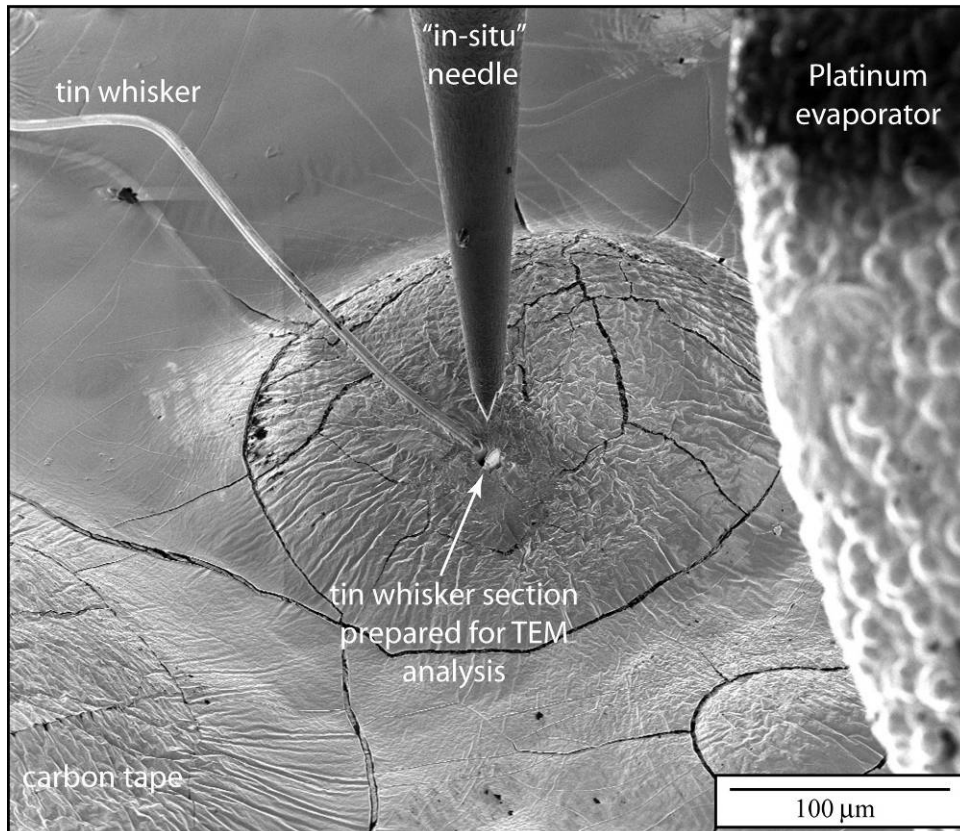


Figure 4-10 FIB image showing the in-situ needle approaching whisker and FIB section.
Magnification: 650X (NASA/UCF)

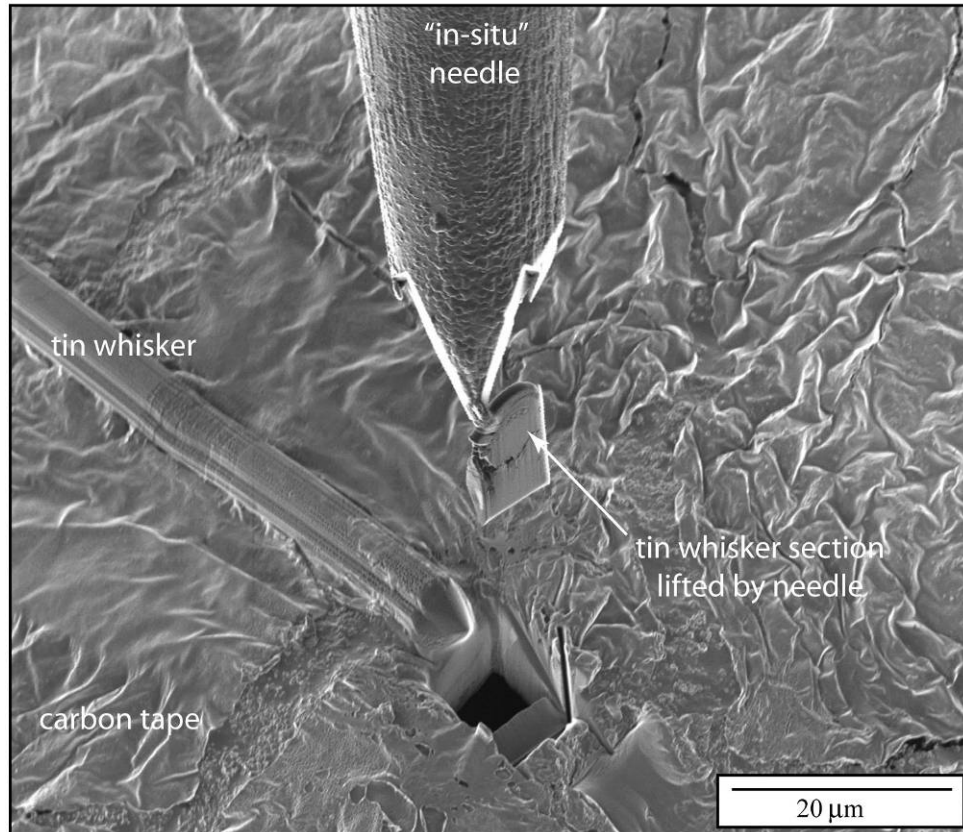


Figure 4-11 FIB image showing removal of tin whisker section using the in-situ needle.
Magnification: 3500X (NASA/UCF)

Next, a conventional TEM copper grid was cut in half, and a small ditch was made with the FIB to accommodate the ROI. In Figure 4-12 the tin whisker section has been lowered and inserted in the copper grid in preparation for TEM examination. The section was first spot welded to the grid, and then released from the in-situ needle. The last step prior to placing the grid and sample into the TEM was to thin out the sample using the FIB until a thickness of $< 1000 \text{ \AA}$.

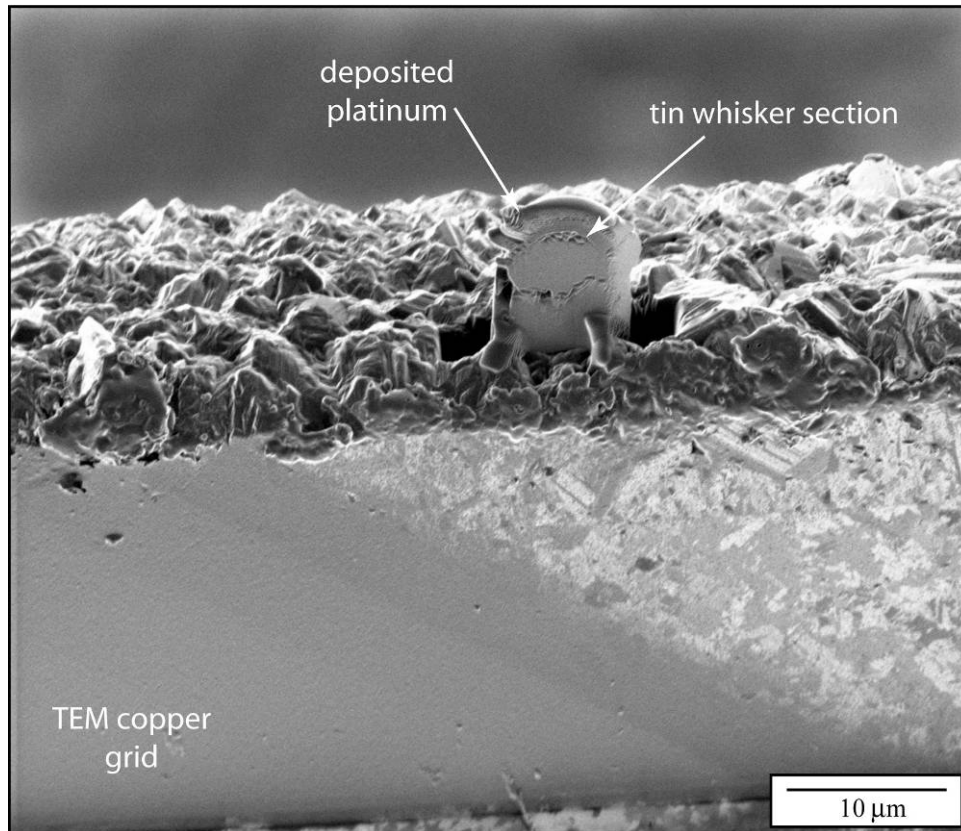


Figure 4-12 FIB image of tin whisker section mounted on copper grid for TEM.
Magnification: 5000X (NASA/UCF)

CHAPTER 5: RESULTS AND DISCUSSION

Full Experiment

Breakdown Voltage Experiment

Tin Whisker Current and Voltage Data and Breakdown Voltage Selection

The current and voltage data gathered for each of the 200 tin whiskers is summarized in the graphs in Appendix D. The breakdown voltage for each of the whiskers was selected first by visual review of the graphs as was done in the proof of concept experiment. To ensure that a more consistent approach was used in the data collection process in the full experiment, a computer based method for selecting the breakdown voltage was developed using Microsoft Excel. All 200 breakdown voltages were verified using both methods.

The breakdown voltages from the full experiment are shown in Appendix C. Since whiskers number 49 and 56 did not breakdown in the 0 to 45 vdc range used in this experiment, these two data points are considered censored. The data analysis software used in the proof of concept experiment EasyFit® does not handle censored data. Therefore, Minitab® was used since it can accommodate censored data.

Data Analysis

The individual value plot shown in Figure 5-1 provides insight into the data. The majority of the data falls between 0 and 10 vdc. The aforementioned figure shows tin whisker breakdown voltages versus Card Guide Side where 1= top and 2 = bottom, Card Guide and LRU Serial Number. The right skewed nature of the data is evident from this plot. The individual values are shown in red and the median values are shown in blue.

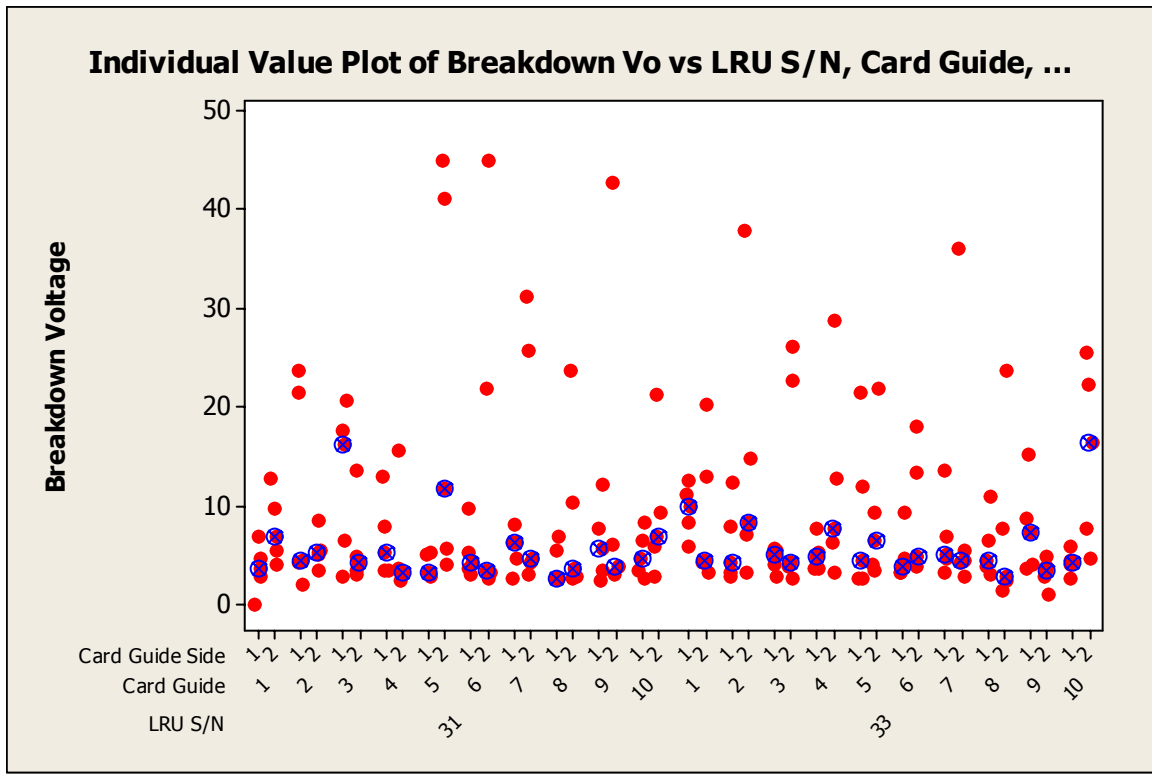


Figure 5-1 Breakdown voltage individual value plot

ANOVA was used to examine the difference between the break down voltage for LRU serial number, card guide, and card guide side. Since ANOVA assumes normality, the data was natural-log transformed. The transformed data is called LogVol. This is a nested ANOVA where:

- The null hypothesis (H_o): The mean breakdown voltages are the same.
- The alternative hypothesis (H_A): At least one of the mean breakdown voltages is different from the rest.

The abbreviated ANOVA is shown Figure 5-2:

Source	DF	F	P
LRU S/N	1	0.43	0.515
Card Guide (LRU S/N)	18	0.64	0.863
Card Guide Side (LRU S/N Card Guide)	20	1.73	0.033
Error	160		
Total	199		

R-Sq (adj) = 3.68%

Figure 5-2 ANOVA natural log transformed data (abbreviated)

The full ANOVA is shown in Appendix E. The P value for card guide side (LRU S/N card guide) is 0.033 which is small and thus the null hypothesis was rejected. This indicates that the voltages associated with the two sides may be different. From the full ANOVA shown in Appendix E, Minitab® identified observations 1, 56, 86, 168, & 178 as outliers based on having a large standardized residual. The first data point was the outlier that stands out the most, and thus warrants further study. Minitab did not identify any observations as influential values.

The residual plots for the natural log transformed data in Appendix E indicate that the first data point where the whisker broke down at 0.06 vdc is an outlier. To examine the influence of this value, the outlier was removed from the data set. The log-transformed data set with the outlier removed is labeled LogVol_1. The abbreviated ANOVA and Residual plots were rerun as shown in Figures 5-3 and Appendix E.

Source	DF	F	P
LRU S/N	1	0.09	0.768
Card Guide (LRU S/N)	18	0.51	0.951
Card Guide Side (LRU S/N Card Guide)	20	1.63	0.051
Error	159		
Total	198		

R-Sq (adj) = 1.39%

Figure 5-3 ANOVA with outlier removed (abbreviated)

The full ANOVA with the outlier removed is shown in Appendix E. From ANOVA shown in Figure 5-3 the P value for card guide side (LRU S/N card guide) is 0.051. This is an improvement, but it still indicates that the voltages associated with the two sides may be different.

The residual plots for the natural log transformed data with outlier removed in Appendix E show a more dispersed and random cloud that indicates that they have improved. Since the residual plot improved with the first data point removed, the first data point is an outlier and may be influential. For additional insight into the data, individual value plots of the breakdown voltage natural log transformed breakdown voltage versus LRU serial number and card guide side while collapsing over card guides are plotted in Figures 5-4 and 5-5.

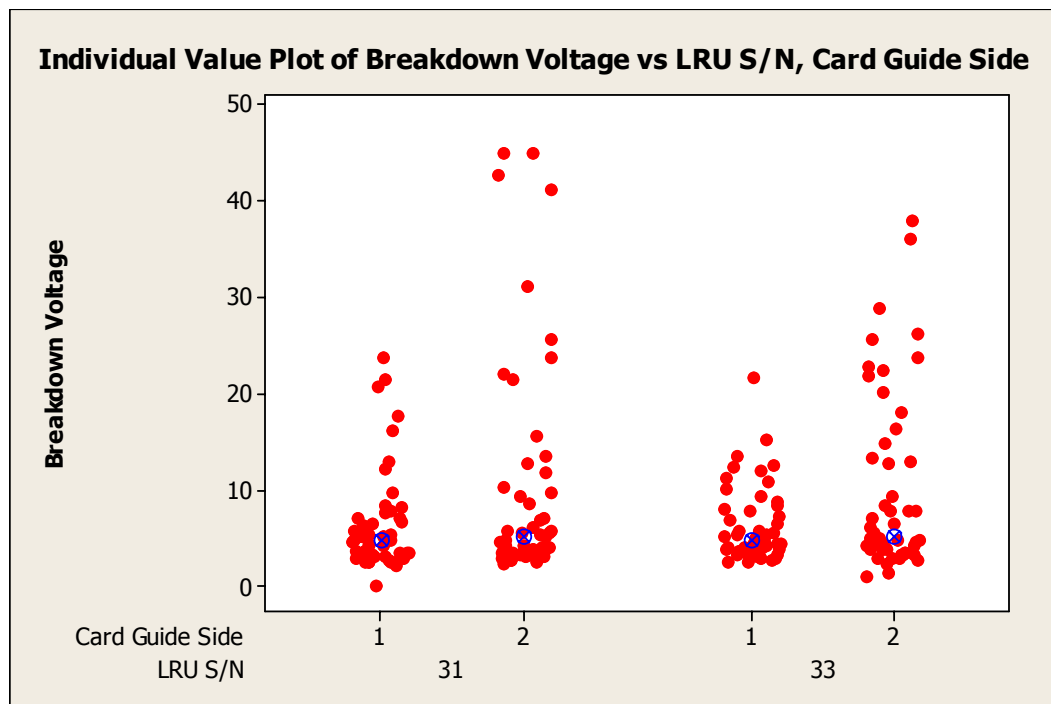


Figure 5-4 Individual value plot collapsing over card guides data not transformed

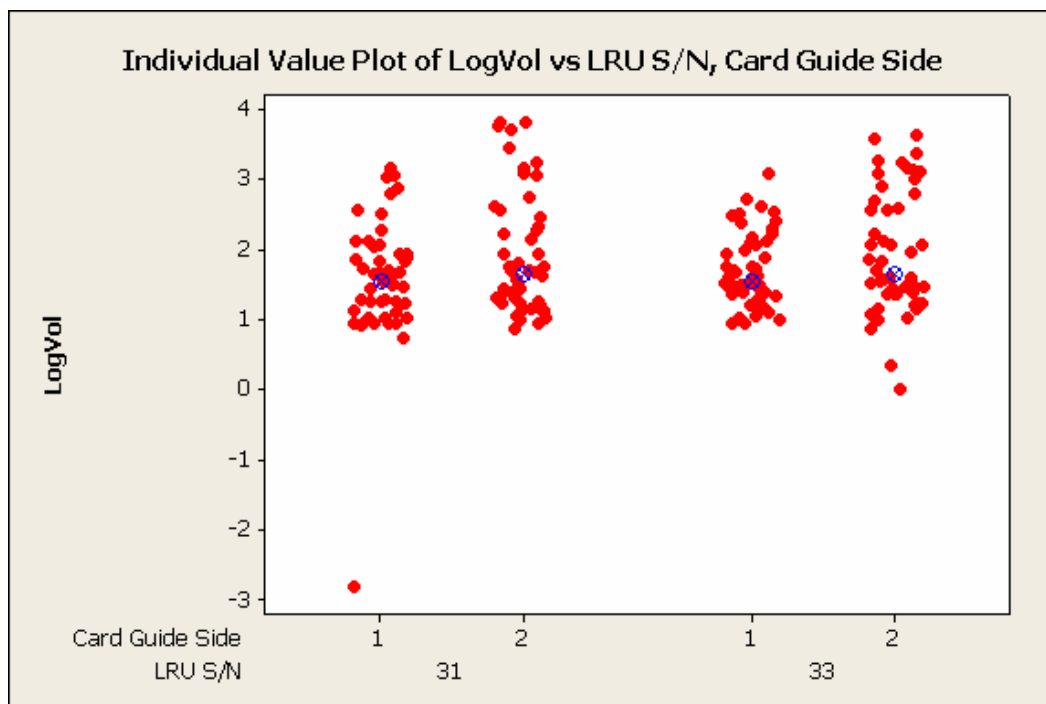


Figure 5-5 Individual value plot collapsing over card guides data transformed

In Figure 5-4 and 5-5, the median value per card guide side is consistent for each plot. The outlier, the first data point, is more evident in the plot of the transformed data shown in Figure 5-5.

Since the breakdown voltage data is definitely not normally distributed, a nonparametric alternative called a Kruskal-Wallis test was used for a similar analysis. The results of this test are shown in Appendix E. The P-value of 0.087 suggests that there may be a difference between the median breakdown voltages for the sides of the card guides. The Kruskal-Wallis test also suggests that the median breakdown voltage for side 2 may be greater than the median breakdown voltage for side 1. However, the purpose of developing this empirical distribution is to characterize the probability of an electrical short circuit from tin whiskers and thus there is no benefit to developing separate distribution for the top and bottom of the card guides. Further in the ANOVA analyses the R-squared (adjusted) values were very small (<5%) and thus accounting for

the card guides and card guide sides in this analysis explains a very small portion of the variability present in breakdown voltage, which also supports the decision of not accounting for these factors in describing the breakdown distribution.

To determine if the outlier has a significant affect on the distribution fitting, the distribution analysis was run on the breakdown voltage data with and without the outlier. By default, Minitab® explores the following 11 distributions for the best fit: weibull, lognormal, exponential, loglogistic, 3-parameter weibull, 3-parameter lognormal, 2-parameter exponential, 3-parameter loglogistic, smallest extreme value, normal, and logistic. The P-P plots and correlation coefficients for the weibull, lognormal, exponential and loglogistic distributions are shown in Figures 5-6 to 5-7 below. The P-P plots and correlation coefficients for the other distributions are shown in Appendix E.

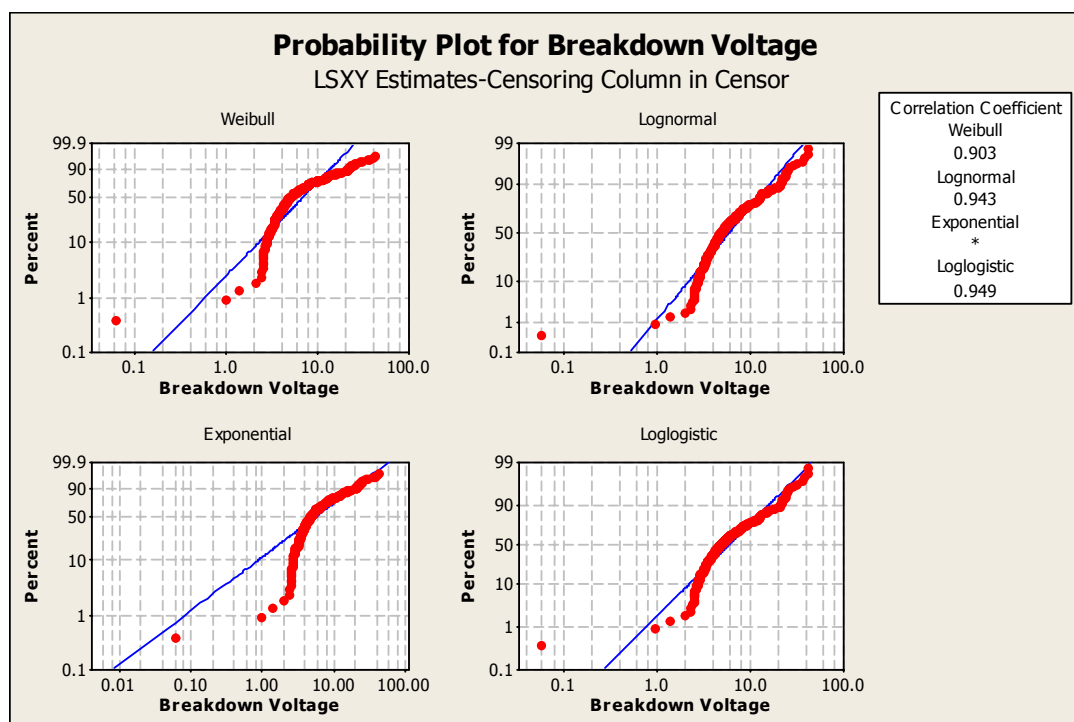


Figure 5-6 P-P plot and correlation coefficient for weibull, lognormal, exponential and loglogistic

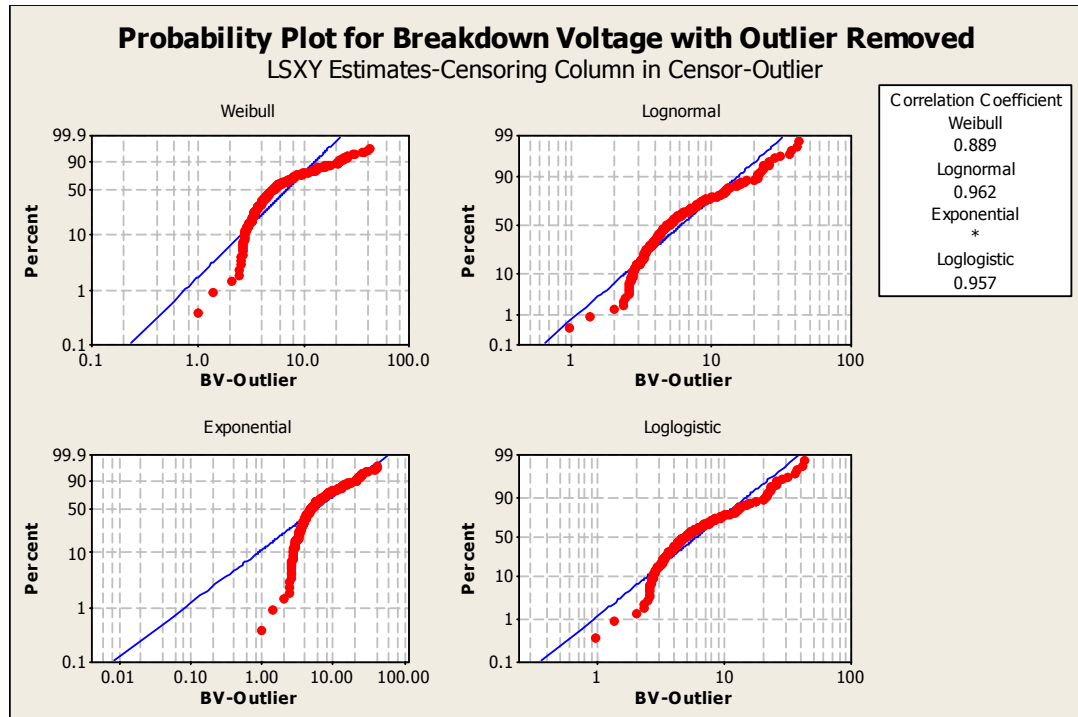


Figure 5-7 P-P plot and correlation coefficient for weibull, lognormal, exponential and loglogistic with outlier removed

From examining the relative linearity of the P-P plots and correlation coefficients in Figures 5-6, Figure 5-7 and Appendix E it is evident that the outlier has little effect on the distribution fitting. Based on these results, and the fact that there is no proof that the outlier is not a legitimate data point, the outlier was retained in the data set.

In the proof of concept experiment the P-P plots were used along with the Kolmogorov-Smirnov test to determine the best fitting distribution. Since Minitab® does not perform the Kolmogorov-Smirnov test; the adjusted Anderson Darling test and correlation coefficient were used in its place, in addition to the P-P plot. The adjusted Anderson-Darling test measures the area between the fitted line (based on chosen model) and the nonparametric step function (based on the plot points) (Minitab Inc., 2003). Precisely, the Anderson-Darling (adjusted) statistic is a squared distance that is weighted

heavier in the tails of the distribution. Smaller Anderson-Darling (adjusted) values indicate that the "fit" of the probability plot is better (Minitab Inc., 2003).

The correlation coefficient reported for each graph (distribution) measures the correlation between the data and what would be expected if the data comes from the specified distribution (represented by the blue line). If the data and the blue line are perfectly correlated, the correlation coefficient would be 1 and that would strongly indicate that the data probably came from the specified distribution. Note that even if one generated the data from a given distribution, typically the correlation coefficient would not equal to 1 due to random variability. However, larger correlation coefficients indicate that the "fit" of the probability plot is better.

The results of the goodness-of-fit tests are shown in Figure 5-8 below.

Goodness-of-Fit

Distribution	Anderson-Darling (adj)	Correlation Coefficient
Weibull	19.144	0.903
Lognormal	5.361	0.943
Exponential	11.840	*
Loglogistic	5.291	0.949
3-Parameter Weibull	20.798	0.905
3-Parameter Lognormal	6.144	0.960
2-Parameter Exponential	11.866	*
3-Parameter Loglogistic	6.071	0.960
Smallest Extreme Value	71.400	0.699
Normal	23.566	0.823
Logistic	22.693	0.825

Figure 5-8 Anderson-Darling (adjusted) and correlation coefficients

Based on the P-P plots and the correlation coefficients, the four best fitting distributions are the lognormal, loglogistic, 3-parameter lognormal, and the 3-parameter loglogistic. Although the correlation coefficients for the 3-parameter lognormal and the 3-parameter loglogistic are larger than the correlation coefficients for the lognormal and the loglogistic distributions, they are close. Therefore, we can apply the principle of

parsimony and narrow the selection of the best fitting models to the lognormal and loglogistic. The lower values in the Anderson-Darling test also support the selection of the lognormal and loglogistic.

The lognormal and loglogistic have good fitting P-P plots; close Anderson-Darling test results and correlation coefficients. Thus, mathematically both distributions fit the empirical data well. The next step in determining the best fitting distribution is to examine the applications of the distributions.

The lognormal is a right skewed distribution and has been used to describe the number of species, the distribution of mineral resources in the Earth's crust, and the length of latent periods of infectious diseases (Limpert, Stahel, & Abbt, 2001). The lognormal distribution has also been used to describe sizes of incomes in economics. The lognormal distribution can be derived "as the asymptotic result of an iterative process of successive breakage of a particle into two randomly size particles. Consider the distribution of small particles such as crushed stones. The histogram of the weights or masses is often skew and is similar to that given by a lognormal distribution" (Crow & Shimizu, 1988).

Shaban states that "The lognormal distribution, like the weibull and the exponential distributions, has been widely used as a life time distribution model" (Crow & Shimizu, 1988). Leon summarized the motivation for selecting the lognormal distribution as follows (Leon, 2003):

The lognormal distribution is a common model for failure times. It can be justified for a random variable that arises from a product of a number of identically distributed independent positive random quantities. It has been suggested as an appropriate model for failure times caused by a degradation process with combinations of random rates that combine multiplicatively. It is widely used to describe time to fracture from fatigue

crack growth in metals. It is useful in modeling failure time of a population of electronic components with a decreasing hazard function (due to a small proportion of defects in the population). It is also useful for describing the failure-time distribution of certain degradation processes

In contrast, the loglogistic distribution has been used in hydrology for flood frequency analysis (Ahmad, Sinclair, & Werritty, 1988), and performed “extremely well” when compared to the pearson type 3, the 3-parameter lognormal and the generalized extreme value models (Ashkar & Mahdi, 2006). The loglogistic has also been used for modeling cancer survival data (Bennett, 1983); and employed in volcanology to characterize bubble populations in volcanic rocks. (Proussevitch, Sahagian, & Tsentalovich, 2007).

Though both of these distributions seem to fit the breakdown voltage data equally well, the wide applicability of the lognormal distribution as well as its close relationship with the gaussian distribution which can be exploited in future applications of the voltage breakdown data make the lognormal distribution the more desirable choice in describing tin whisker breakdown voltage.

The hazard plot for tin whisker breakdown voltage shown in Figure 5-9 below exhibits the expected shape for a lognormal failure rate. Sweet states that “ the lognormal failure rate as a function of time is an increasing followed by a decreasing function, and can be shown to approach zero for large lifetimes and at the initial time” (Sweet, 1990). With zero volts applied, there would be no current through the whisker and thus no breakdown of the film resistance. From the data in the full experiment, there were only two censored data points out of 200 whiskers tested, all other whisker have reached a breakdown voltage by 45 vdc.

A zero hazard rate implies that there will be no failures. More specifically, the zero hazard rate suggested by the log-normal for large voltages implies that the whiskers that survived large voltages may never break down. This may be an unrealistic assumption but these distributions are approximate and they are meant to describe the general properties of the distribution. The extremes of distributions are notoriously difficult to capture and require a very large number of observations to describe accurately. The increasing and then decreasing hazard rate implies that most failures will occur early, as observed, and after that the rate of failure will fall until it reaches 0 at the very extreme voltages. The hazard plot of the lognormal distribution fits the physical phenomena demonstrated by the empirical data, with only a slight divergence in the extreme tail.

The P-P plot in Figure 5-10 shows the 95% confidence interval on the same plot. This plot also shows that the first data point is an outlier.

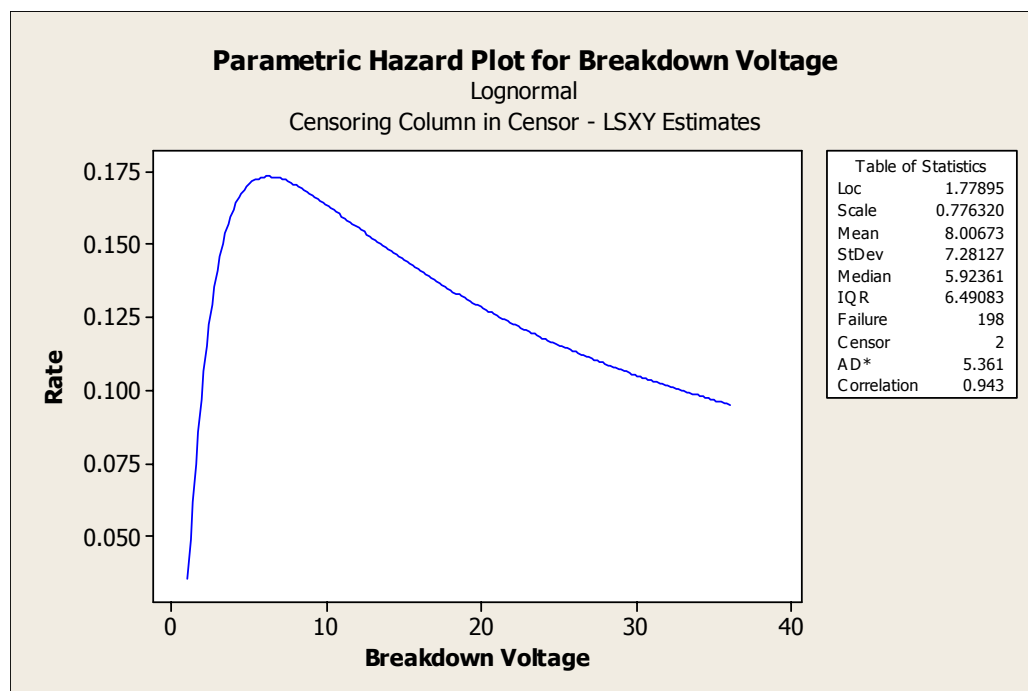


Figure 5-9 Hazard plot for breakdown voltage

The P-P plot for the tin whisker breakdown voltage is shown in Figure 5-10 with the 95% confidence intervals.

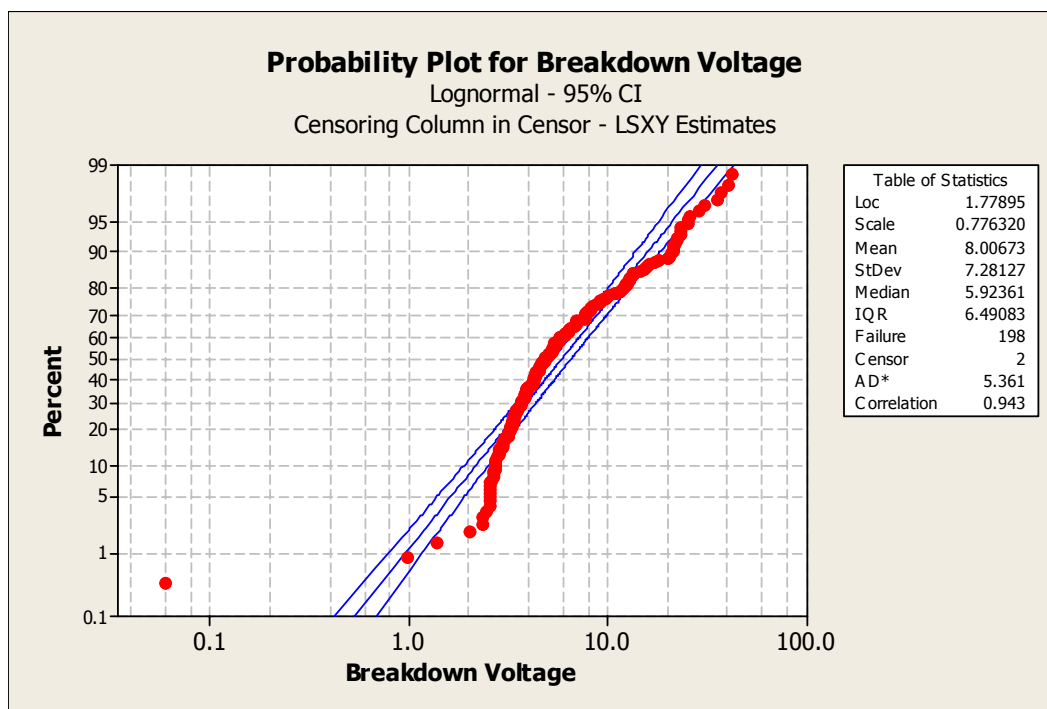


Figure 5-10 P-P plot of tin whisker breakdown voltage with confidence intervals

The distribution analysis for the lognormal distribution is shown in Figure 5-11 below.

Distribution Analysis: Breakdown Voltage

Variable: Breakdown Voltage

Censoring Information Count
 Uncensored value 198
 Right censored value 2

Censoring value: Censor = 1

Estimation Method: Least Squares (failure time(X) on rank(Y))

Distribution: Lognormal

Parameter Estimates

Parameter	Estimate	Standard Error	95.0% Normal CI	
			Lower	Upper
Location	1.77895	0.0549173	1.67131	1.88658
Scale	0.776320	0.0362000	0.708515	0.850614

Log-Likelihood = -593.384

Goodness-of-Fit

Anderson-Darling (adjusted) = 5.361

Correlation Coefficient = 0.943

Characteristics of Distribution

	Estimate	Standard Error	95.0% Normal CI	
			Lower	Upper
Mean (MTTF)	8.00673	0.493631	7.09540	9.03511
Standard Deviation	7.28127	0.768321	5.92090	8.95418
Median	5.92361	0.325309	5.31913	6.59678
First Quartile (Q1)	3.50898	0.211012	3.11885	3.94792
Third Quartile (Q3)	9.99981	0.600653	8.88921	11.2492
Interquartile Range (IQR)	6.49083	0.485280	5.60610	7.51518

Figure 5-11 Lognormal distribution analysis

The PDF and CDF for the lognormal distribution are shown in equations 5-1 and 5-2 below (Minitab Inc., 2003). The location parameter = $\mu = 1.77895$, and the scale parameter = $\sigma = 0.776320$.

The cumulative distribution function (CDF) for the lognormal distribution:

$$F(x) = \int_{-\infty}^x \frac{1}{\sqrt{2\pi}\sigma t} \exp\left[-\frac{(\ln t - \mu)^2}{2\sigma^2}\right] dt \quad (5-1)$$

The probability density function (PDF) for the lognormal distribution:

$$f(x) = \frac{1}{\sigma x \sqrt{2\pi}} \exp\left(-\frac{(\ln(x) - \mu)^2}{2\sigma^2}\right) \tag{5-2}$$

The cumulative distribution function F(x) estimates the probability that the whisker, interrogated this way, will break down when the applied voltage has a given value. Then $f(x) = dF(x)/dx$ is the probability density for breakdown at x (Walpole & Myers, 1989); where x is the applied voltage. The CDF is shown in if Figure 5-13. The PDF along with a histogram of the breakdown voltage data is shown in Figure 5-12.

Based on the data and the fitted model the expected voltage (mean) where a short will occur is 8.00673 vdc, with a standard deviation of 7.28127 vdc. The median tin whisker breakdown voltage is 5.92361 vdc.

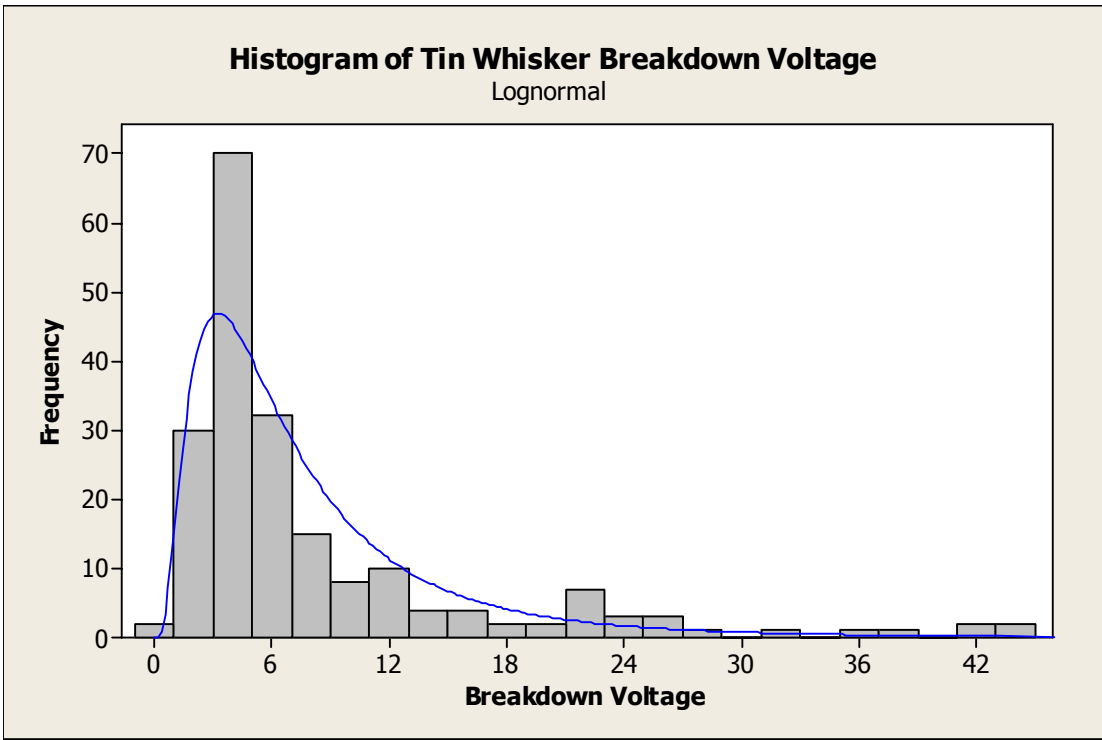


Figure 5-12 Histogram tin whisker breakdown voltages with lognormal distribution

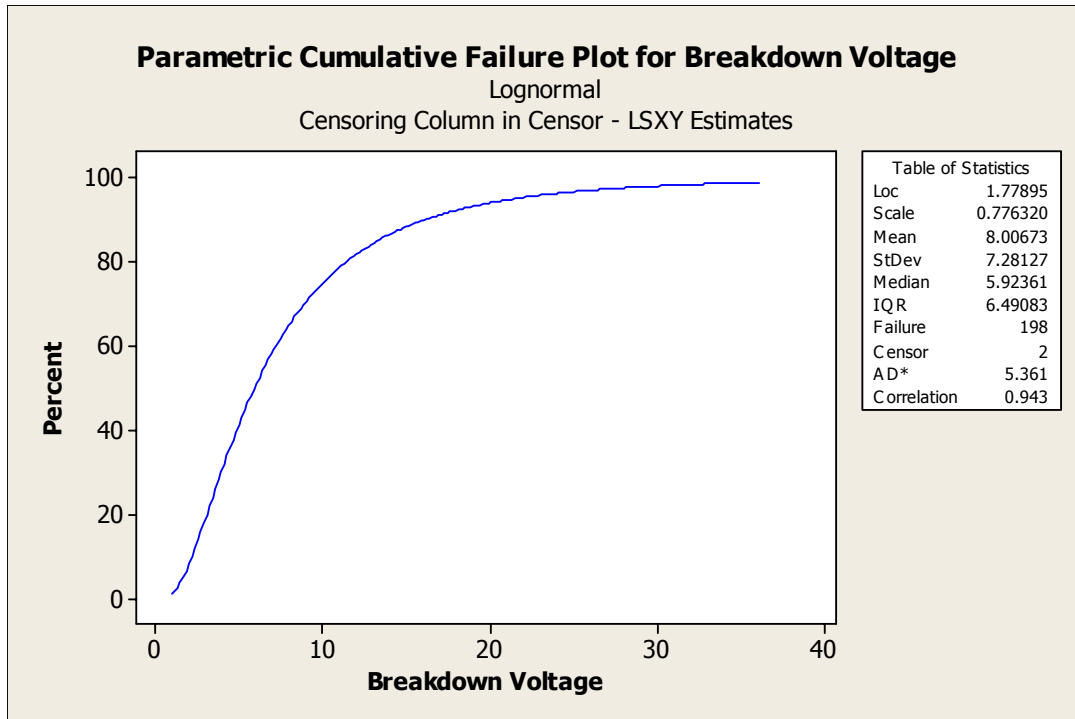


Figure 5-13 Tin whisker CDF of breakdown voltage for lognormal distribution

Explanation of the Linearity Seen in the Voltage and Current Charts

An electrical schematic of the test station is shown in Figure 5-14 below. V_{PS} is the power supply voltage, R_{CL} is the resistance of the current limiting resistor, R_W is the whisker resistance, V_{CL} is the voltage across the current limiting resistor, V_W is the voltage across the resistor, and I is the current through the circuit. The range of the power supply voltage in this experiment was $V_{PS} = 0 - 45\text{vdc}$, and the value of the current limiting resistor was $R_{CL} = 10\text{K}\Omega$. The derivation of the equations necessary to explain the linearity seen in the tin whisker voltage and current charts is shown following the schematic.

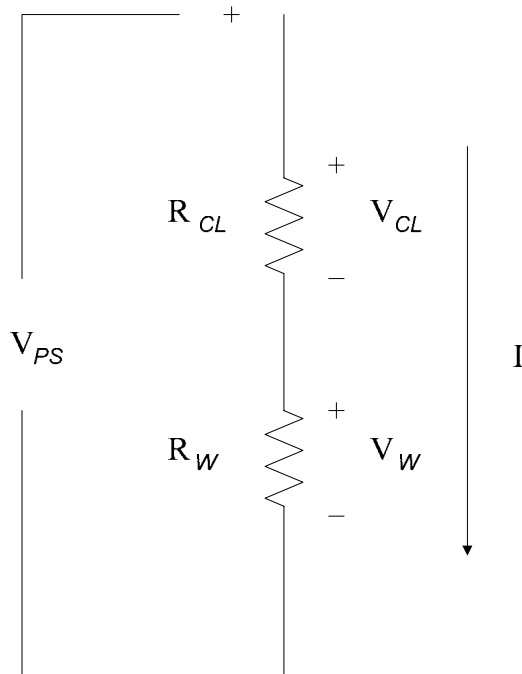


Figure 5-14 Electrical schematic for derivation of equations to explain the tin whisker voltage and current charts

Given Ohm's law and the voltage divider equations from (Durney, Harris, & Alley, 1982) then:

$$V_{CL} = IR_{CL} \text{ and } V_W = IR_W$$

$$\text{Therefore: } \frac{V_{CL}}{V_W} = \frac{IR_{CL}}{IR_W} = \frac{R_{CL}}{R_W}$$

$$\text{Since } V_{PS} = I(R_{CL} + R_W)$$

$$\text{Then: } \frac{V_{CL}}{V_{PS}} = \frac{IR_{CL}}{I(R_{CL} + R_W)} = \frac{R_{CL}}{(R_{CL} + R_W)} \text{ and } \frac{V_W}{V_{PS}} = \frac{IR_W}{I(R_{CL} + R_W)} = \frac{R_W}{R_{CL} + R_W}$$

$$\therefore V_W = V_{PS} \frac{R_W}{R_{CL} + R_W} \text{ and} \quad (5-3)$$

$$I = \frac{V_{PS}}{R_{CL} + R_W} \quad (5-4)$$

Referring to equation 5-3, before the film resistance has broken down, R_W is very large compared to R_{CL} , therefore V_W will increase linearly as V_{PS} increases linearly.

Once the film resistance has broken down, R_W is very small compared to R_{CL} , and thus V_W drops to a very small value. V_W will still increase as V_{PS} increases in this region, but the values are so small they appear as a straight line near zero. Refer to the whisker voltage chart in Figure 5-15.

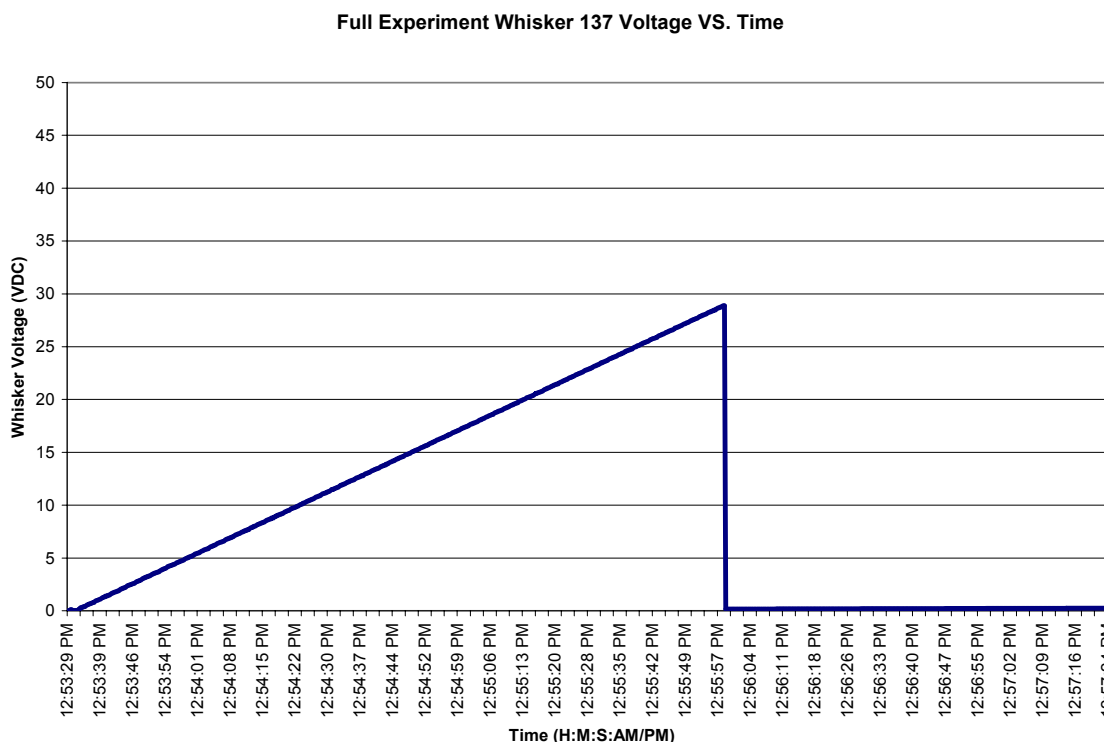


Figure 5-15 Tin whisker number 137 graph of voltage versus time from the full experiment

Referring to equation 5-4, before the film resistance has broken down, R_W is very large compared to R_{CL} , and the current through the whisker, I will be a very small value. The current I will still increase as V_{PS} increases in this region, but the values are so small they appear as a straight line near zero.

Once the film resistance has broken down, R_W is very small compared to R_{CL} , and the current through the whisker, I will increase linearly as V_{PS} increases linearly. Refer to the whisker current in Figure 5-16.

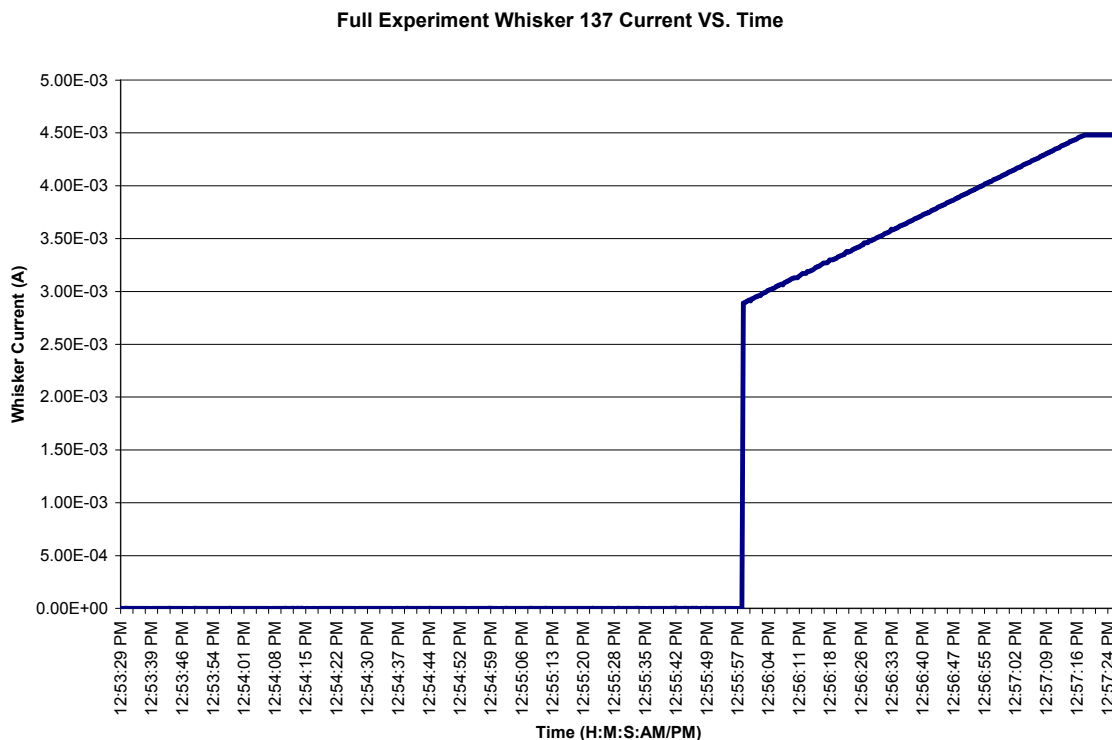


Figure 5-16 Tin whisker number 137 graph of current versus time from the full experiment

The variation will be in the breakdown voltages found for the whiskers.

Tin Whisker Current Carrying Characteristics

Since the power supply was limited to 45 vdc in this experiment, and the current limiting resistor was 10K Ω , the current through the whisker was limited to 4.5 mA.

While the purpose of the experiment was to develop an empirical probability distribution, and not to directly test the maximum current carrying capability of the tin whiskers, the data does yield some quantitative measures. From Table 5-1, 12 of the 200 whiskers, or 6% of the whiskers fused open before the end of the experiment. Thus 6% (95% CI (3.14%, 10.25%)) of the whiskers could not carry 4.5 mA. In addition, 2 of the 200 whiskers, or 1% of the whiskers never conducted because the film resistance did not breakdown from the applied maximum voltage of 45 vdc. Prior to the end of the

experiment, 28 of the 200 whiskers or 14% of the whiskers stopped conducting due to whisker movement, but did not fuse open. The intact whiskers were clearly visible under the microscope. The remainder of the whiskers, 158 out of 200 whiskers, or 79% (95% CI (72.69%, 84.43%)) of the whiskers was able to carry 4.5 mA. In some circuits, this current carrying capability is enough to cause permanent short circuits.

Table 5-1 Tin whisker current carrying characteristics from the full experiment

Full Experiment							
Sequential Whisker Number	Fused Open	Did Not Conduct	Dropped Out at End, Did Not Fuse Open	Sequential Whisker Number	Fused Open	Did Not Conduct	Dropped Out at End, Did Not Fuse Open
2			YES	114	YES		
5			YES	117	YES		
17	YES			122			YES
47			YES	129			YES
49		YES		148			YES
52			YES	153			YES
53	YES			158			YES
56		YES		161	YES		
59			YES	163			YES
64			YES	164	YES		
78	YES			165	YES		
87			YES	166	YES		
88	YES			168	YES		
89			YES	173			YES
92	YES			175			YES
94			YES	176			YES
95			YES	179			YES
100			YES	186			YES
102			YES	194			YES
104			YES	196			YES
111			YES	197			YES
				Total	12	2	28

Comparison of Proof of Concept and Full Experiment Results

The empirical distributions derived from the data gathered in the proof of concept and the full experiments were the inverse gaussian and the lognormal distributions

respectively. It is important to note that EasyFit® was used for fitting the distribution in the proof of concept experiment, and Minitab® was used for fitting the distribution in the full experiment. Minitab® had the capability to handle censored data, and EasyFit® did not. The inverse gaussian distribution is not evaluated by Minitab®, and thus was not a choice in the full experiment. Takagi noted that the probability density functions of the inverse gaussian and the lognormal distributions are similar in shape (Takagi, Kumagai, Matsunaga, & Kusaka, 1997). The probability density functions for both experiments shown in Figure 3-17 and Figure 5-12 and are both right skewed. The larger sample size in the full experiment likely results in a better estimate of the tail of the distribution. Based on the inverse gaussian distribution, 8 censored values were estimated for the full experiment. However, only 2 censored values were obtained in the full experiment which demonstrates a difference in the tails and may be indicative of the need for a slightly different distribution to characterize the data. Increasing the sample size from 35 to 200 tin whiskers improves the accuracy of the empirical distribution in representing the characteristics of tin whisker breakdown voltage.

To aid in comparing the results of the full experiment to proof of concept experiment, the data from the proof of concept experiment was analyzed using Minitab®. The four best fitting distributions were the 3-parameter weibull, the 3-parameter lognormal, the lognormal, and the weibull based on the P-P plots, adjusted Anderson-Darling test, and the correlation coefficient. The P-P plots and goodness of fit test results are in Appendix G. Considering the correlation coefficients for the 3 and 2 parameter distributions are close, based on the principle of parsimony, the selection of the best fitting models can be narrowed to the lognormal and the weibull. The correlation

coefficients for the lognormal and the weibull distributions are both 0.986. However, the Anderson-Darling test statistic is 0.679 for the lognormal and 0.808 for the weibull. A lower value for the test statistic provides the more statistical evidence that the distribution fits the data. From this analysis, it is evident that the proof of concept and full experiments are consistent when using the same software for fitting the distributions.

In the proof of concept experiment all of the tin whiskers selected in the experiment were from one card guide. In the full experiment multiple card guides were randomly selected from two different LRUs. This facilitated the examination of sources of variability. In the full experiment ANOVA analysis was performed to examine possible sources of variability such as the differences across the LRUs, card guide, and card guide side. From the P-values determined in the ANOVA, there was no indication that there was a difference between the mean breakdown voltages by LRU serial number or LRU card guide. However, the P-value from the ANOVA indicated that there may be a difference between the mean breakdown voltages by card guide side. To study this further, the ANOVA analysis was performed with the most significant outlier removed from the data set. The larger P-value indicated an improvement, but still remained suggestive in that voltages between the two sides may be different. The residual plots showed improvement with the outlier removed. The residual plots displayed a more dispersed and random cloud. Thus, the outlier is clearly influential. To gain additional insight into the potential difference between card guide sides, the individual value plots were studied. The median value per card guide side was consistent for each plot.

The best fitting probability models were also run with and without the outlier. The relative linearity of the P-P plots and correlation coefficients showed that the outlier has little effect on the chosen distribution. Thus, the outlier was retained in the data set

Based on the data and the fitted model for the proof of concept experiment, the expected voltage (mean) where a short will occur is 15.5994 vdc, and the median tin whisker breakdown voltage is 11.8924 vdc. Based on the data and the fitted model for the full experiment, the expected voltage (mean) where a short will occur is 8.0067 vdc, and the median tin whisker breakdown voltage is 5.9236 vdc. The shift in the mean and median can partially be explained by the change to a gold plated probe tip in the second experiment, thus eliminating any effect of oxides on the probe tip. Other factors such as the larger and more diverse sample size, and the improvements listed in improvements section of Chapter 4 that facilitate better contact between the micromanipulator probe and the whisker may also contribute to the shift in the mean.

Limitations

Two whiskers in full experiment did not experience a breakdown of the film resistance in the 0 – 45 vdc range of the experiment. This resulted in two censored values out of the two hundred whiskers tested. Increasing the upper voltage limit of the power supply voltage could eliminate the censoring.

The sample size was increased from 35 whiskers in the proof of concept experiment to 200 whiskers in the full experiment. The increased sample size facilitated achieving the objective of obtaining a more comprehensive empirical distribution of breakdown voltage. However, the tails are often the hardest part of a distribution to model. Increasing the sample size to a very large number, say 1000 whiskers, can clarify

the tails of the distribution further. This would provide insight into the validity of the assumption of the lognormal distribution that hazard rate approaches zero.

The difference and variation between force applied by gravity and the force applied by the micromanipulator probe was another limitation in the proof of concept experiment. To improve control of the applied pressure in the full experiment, the probe was applied to the whisker on approximately the top 25% of the whisker. This minimizes the applied pressure, but does not completely eliminate the difference.

Another limitation of this experiment is the number of conducting surfaces. A free whisker falling across two contacts will have two points of contact for breakdown, while the micromanipulator probe contacts the whisker at one point. This is an accepted simplification in this experiment.

Transmission Electron Microscopy (TEM)

During the preliminary tin whisker characterization in the proof of concept experiment, FIB analysis and ion channeling imaging revealed what appeared to be a polycrystalline whisker, that is, one composed of several grains in varying crystallographic orientations (refer to Figure 3-24). In order to determine whether the whisker was polycrystalline, a thin section was prepared for TEM analysis as shown in Figure 5-17. This sample is from a different section of the same tin whisker shown in the Figure 3-24, but is rotated as evident by the location of the deposited platinum layer. Diffraction patterns were taken at four apparent grains, labeled A, B, C and D in Figure 5-17 and are displayed in Appendix F. The TEM images and diffraction patterns were taken using a FEI Tecani F30 TEM with a 30kV Field Emission Source.

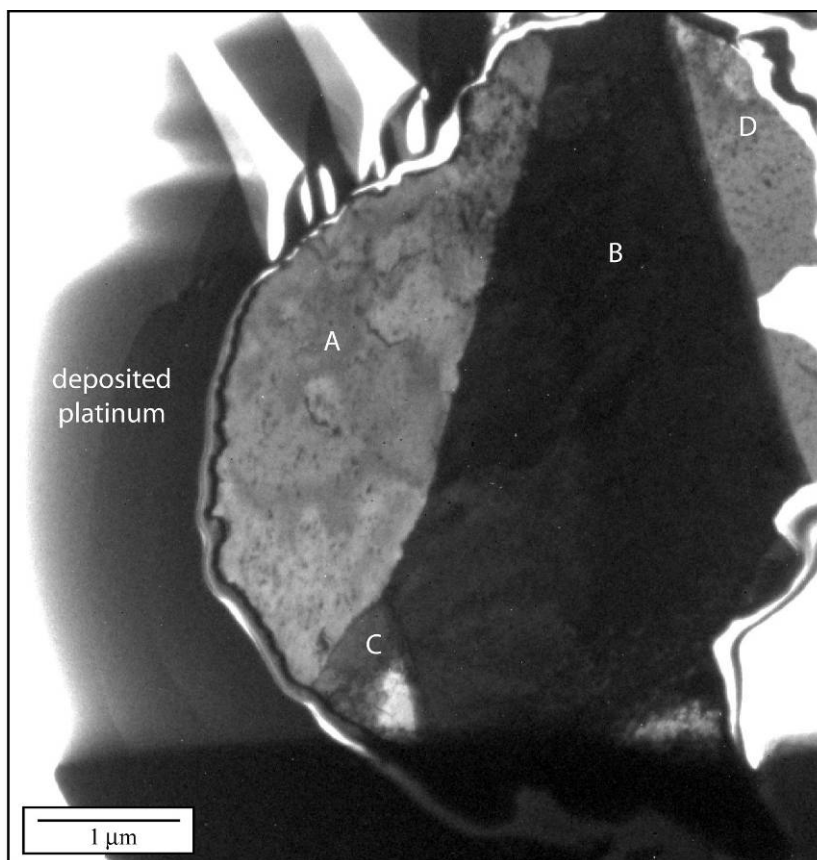


Figure 5-17 TEM Image of the polycrystalline tin whisker and nomenclature used to identify the various grains (A-D). Magnification: 34000X (NASA/UCF)

The diffraction patterns for the areas labeled A, B, C & D are shown in Appendix F. The diffraction patterns for areas A, B & C displayed minor changes in orientation, expected to be low angle grain boundaries, while section D showed a larger orientation mismatch. The contrast in each apparent grain in the TEM image arises from the orientation of each grain relative to the electron beam. Based on the contrast shown in the TEM image in Figure 5-17, we expected B to have the largest mismatch, since areas A, C, and D exhibit similar contrast. High-resolution TEM imaging was used to image an amorphous region between uniform crystal lattices of areas A and B, which clearly delineates a grain boundary between the crystals in the polycrystalline tin whisker, Figure

5-18. Additionally, X-ray energy dispersive spectroscopy (EDS) was used to verify that there were no compositional differences between the grains, all were composed of pure tin (Sn).

From the TEM images and the diffraction patterns it can be definitively stated that the studied card guide whisker was polycrystalline.

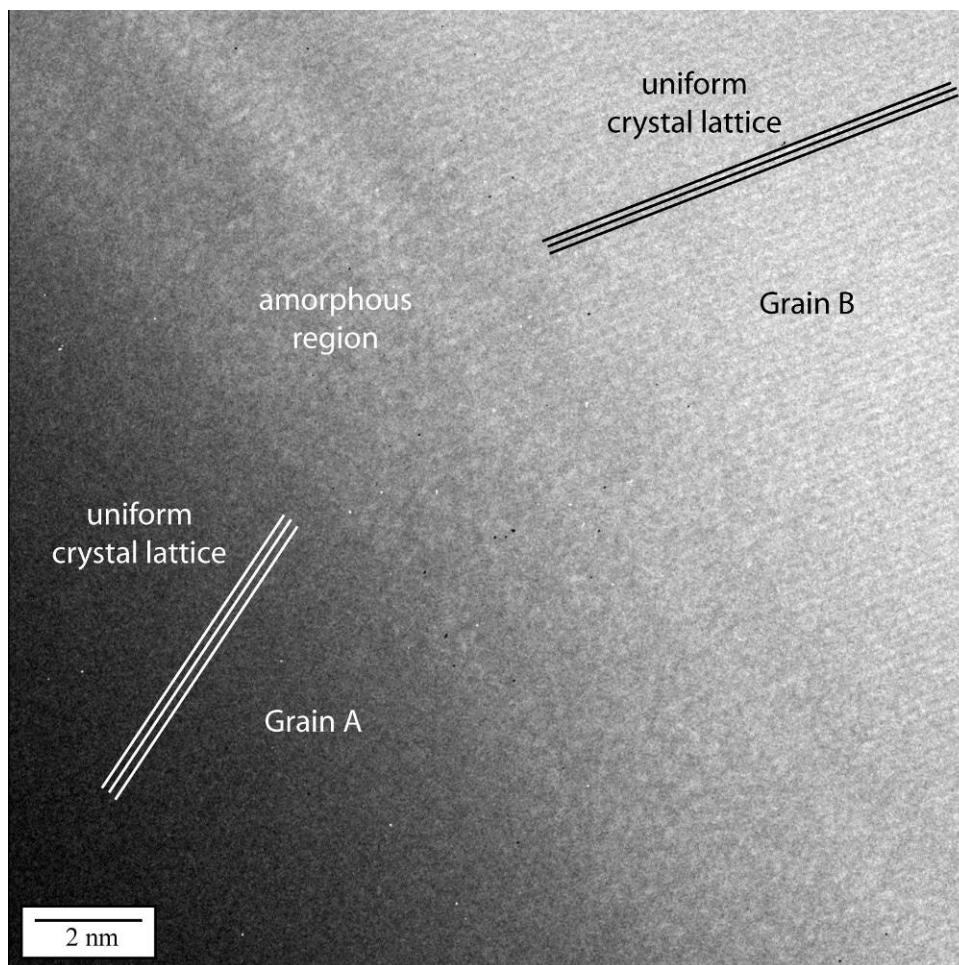


Figure 5-18 High-resolution TEM image of the amorphous region in the polycrystalline tin whisker between the uniform crystal lattices of regions A and B. The amorphous region is a low-angle grain boundary (NASA/UCF). Magnification: 1,000,000X

Card Guide Cross Sections Using a FIB

FIB analysis of two card guides was used to determine the grain size and thickness of the tin plating. Ion channel imaging was used to acquire images showing distinct

grains based on crystal orientation contrast as shown in Figures 5-19 and 5-20. Using a modified line-intercept method, the average grain size for card guide S/N 31 shown in Figure 5-19 was estimated to be $0.350\ \mu\text{m}$ (350 nm), which falls well below the ASTM grain size number (grain size $\gg 14$) (American Society for Testing and Materials, 2006). The figures show the copper-beryllium (Cu-Be) substrate base metal and the tin (Sn) plating. A layer of gold-palladium (Au-Pd) was sputter coated on top of the tin plating prior to the FIB sectioning, and a layer of platinum (Pt) was deposited along the area of interest in the FIB to protect the sample during ion beam etching. The average thicknesses of the layers are as follows: Sn = $6.9\ \mu\text{m}$, Au-Pd = $3.9\ \mu\text{m}$, Pt = $6.2\ \mu\text{m}$. EDS in a field-emission SEM was used to confirm the composition of each layer by running line scans. The presence of beryllium cannot be confirmed using this technique since EDS is limited to picking up elements heavier than Carbon in the periodic table. However, the original drawings show the base metal for the card guide as beryllium-copper.

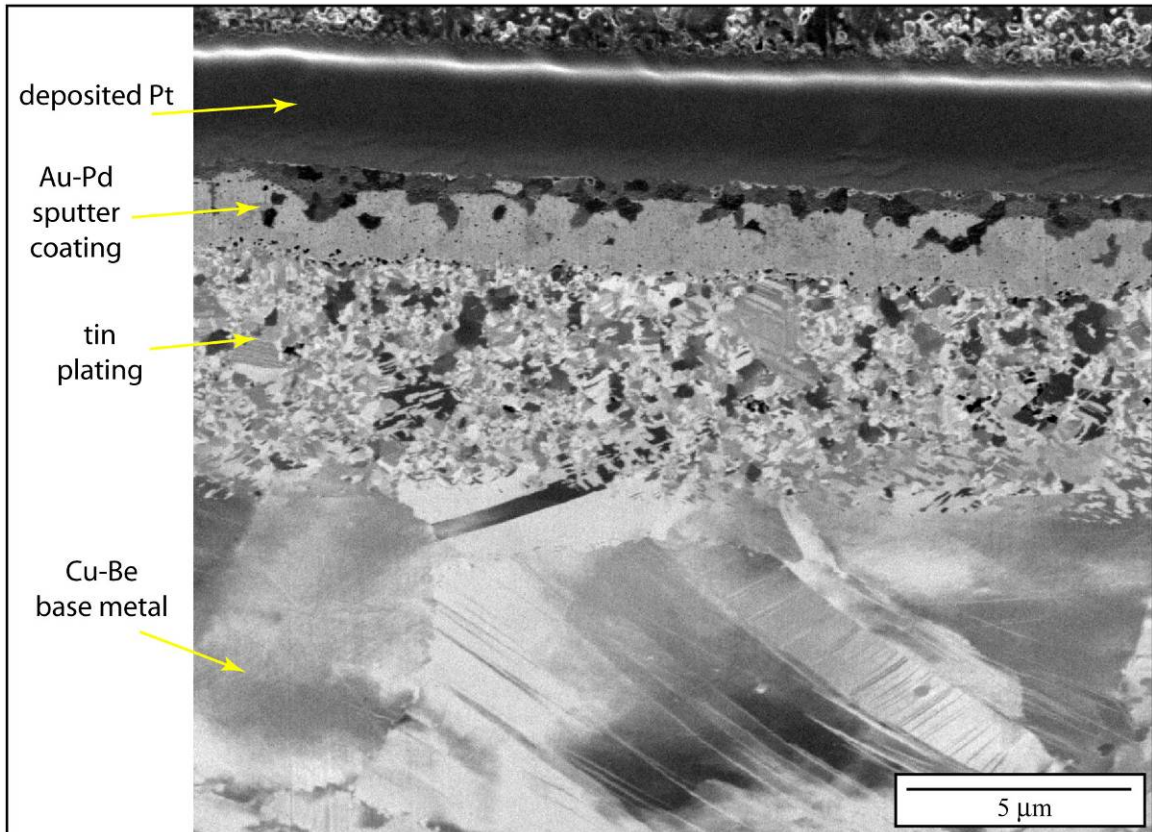


Figure 5-19 FIB ion channeling image of card guide 16 (ATVC S/N 31) cross section showing the distinct layers studied: the expected Cu-Be substrate with larger grains, the Sn plating with nm-sized grains, the Au-Pd sputter coating and finally the deposited Pt used to protect the region during FIB (NASA/UCF). Magnification: 15,000X.

Using the modified line-intercept method on the second card guide (S/N 33), the FIB cross section shown in Figure 5-20 reveals a grain size of 0.290 μm (290 nm) (American Society for Testing and Materials, 2006). This image shows the same layers that were evident in the other card guide and confirmed via EDS: the copper-beryllium substrate, the tin plating, the sputter coated gold-palladium, and finally the deposited platinum used to protect the sample during ion beam etching. The thicknesses of the layers are as follows: Sn = 2.7 μm, Au-Pd = 1.3 μm, Pt = 3.9 μm.

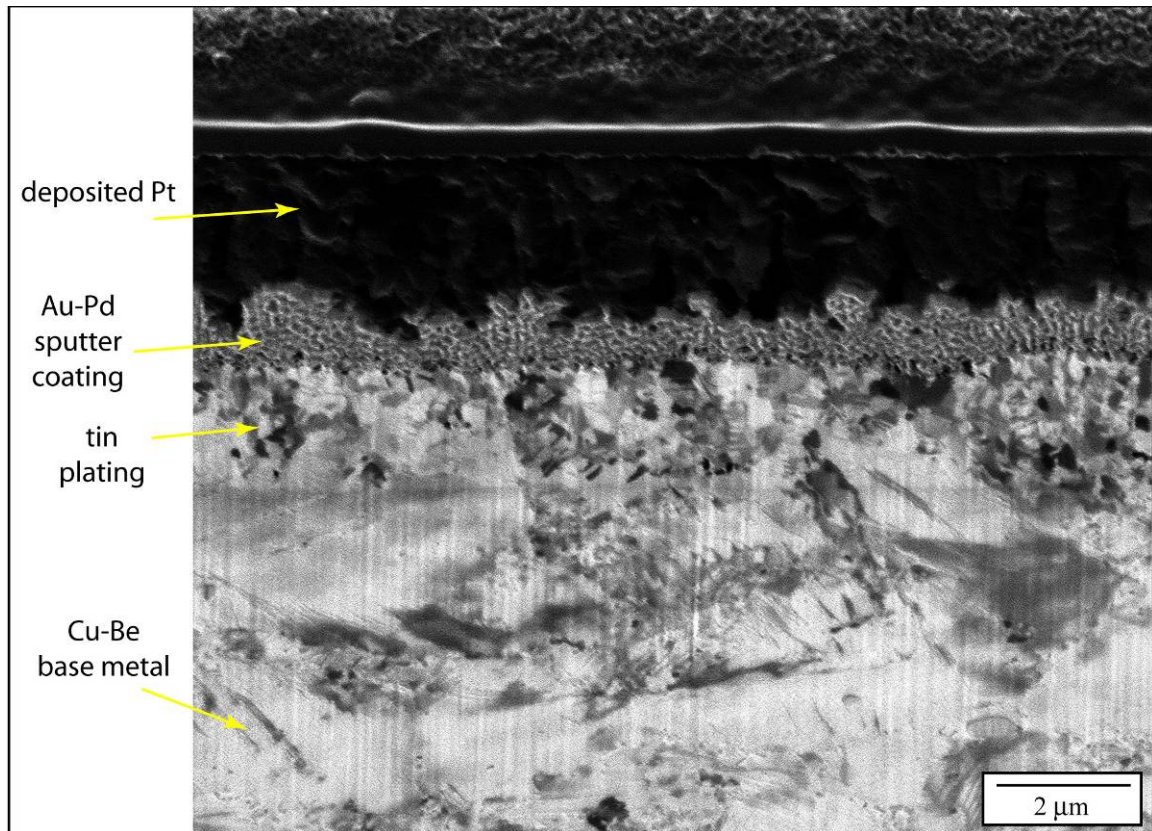


Figure 5-20 FIB ion channeling image of card guide 15 (ATVC S/N 33) cross section showing the distinct layers studied: the expected Cu-Be substrate with larger grains, the Sn plating with nm-sized grains, the Au-Pd sputter coating and finally the deposited Pt used to protect the region during FIB (NASA/UCF). Magnification: 20,000X.

The purpose of measuring the grain size was to quantitatively determine the finish of the tin plating. Shetty classified large grain matte finish as having a grain size between 3-8 μm , fine grain matte finish as having a grain size between 1-2 μm , and bright finish as having a grain size $< 1 \mu\text{m}$ (Schetty, 2004). Based on these criteria, the tin plating used in both ATVC S/N 31 and 33 can be classified as bright finish. While tin finish was not a variable in this experiment, it is a point of interest because bright tin finishes have been associated with greater tin whisker growth than matte tin finishes (Smetana, 2005) (M. Osterman, 2002).

CHAPTER 6: CONCLUSION

In the published simulations it was assumed that physical contact between a whisker and an exposed contact results in an electrical short. This conservative assumption was made because the probability of an electrical short from tin whiskers had not been determined at the time the simulations were written. The purpose of the experiments was to quantify the probability of occurrence of an electrical short from tin whiskers as a function of voltage. This model can be used to improve existing risk simulation models.

The first empirical model to quantify the probability of occurrence of an electrical short circuit from tin whiskers as a function of voltage was developed in the proof of concept experiment. It provided insight into the right skewed shape of the probability model. The 3P-inverse gaussian distribution was used to describe the whisker breakdown voltage in this experiment. This probability model also provided the baseline for a simulation to evaluate the sample size for the full experiment. In the proof of concept experiment a sample size of 35 tin whiskers was used. In the full experiment a sample size of 200 tin whiskers was used to improve the accuracy probability model

The lessons learned from proof of concept experiment also aided in improving the equipment and procedures for the full experiment. Some of the improvements in the full experiment are listed below:

- A solderer's helper was modified to allow flexible positioning of the card guide
- An extension platform for the microscope was fabricated to facilitate clamping of the lab jack
- A ferrous top plate was fabricated for the lab jack to allow the magnetic base of the micromanipulator to be firmly mounted on the lab jack. The lab jack provided the coarse X, Y and Z movements, while the micromanipulator provided the fine X, Y and Z movements for probing the tin whiskers

- To minimize the effect of any oxides on the probe, rather than removing the oxide from the tungsten micromanipulator probe with emery cloth, gold plated tungsten micromanipulator tips were used.
- Added shielding to wires to minimize noise during low current measurements.

The modified solder's helper, extension platform, and the ferrous top plate greatly improved the ability to clearly see and probe the whiskers under a microscope. This also resulted in better photos that aided in determining if a whisker had fused open or moved. The gold plated tungsten micromanipulator tip also eliminated the issue of oxide build up on the micromanipulator tip. This improvement likely resulted in the shift of the mean and median voltage where a short would occur that was seen between the proof of concept and the full experiment. The expected voltage (mean) changed from 15.5994 vdc in the proof of concept experiment to 8.0067 vdc in the full experiment, and the median voltage changed from 11.8924 vdc in the proof of concept experiment to 5.9236 vdc in the full experiment. The lognormal distribution was the best fitting distribution to describe the whisker breakdown voltage in the full experiment.

The addition of the shielding did not eliminate the noise during low current measurements. However, the noise does not affect the ability to clearly see the transition to metallic conduction. Since the noise is only present before the film resistance break down, once the breakdown voltage has been achieved the current readings are no longer noisy.

The data from this experiment also yielded some quantitative measures of the current carrying capability of the tin whiskers. For example: 6% (95% CI (3.14%, 10.25%)) of the whiskers could not carry the maximum current of 4.5 mA used in this experiment. Also, 1% of the whiskers never achieved breakdown voltage, and thus were

classified as censored data points. In addition, 14% of the whiskers stopped conducting at some point during the experiment due to whisker movement. The remaining 79% (95% CI (72.69%, 84.43%)) of the whiskers were able to carry 4.5 mA. This current carrying capacity could cause permanent short circuits in low current applications, or intermittent short circuits in higher current applications.

Three tin whiskers were cross-sectioned using a FIB for study. Two of the whiskers exhibited the commonly reported single crystal structure. These whiskers were smaller in diameter. One whisker showed apparent variation in grain orientation within the cross-section. This indicated that the whisker may be polycrystalline. Further examination was performed using a TEM. High-resolution TEM imaging was used to image an amorphous region between uniform crystal lattices. This clearly delineates a grain boundary between the crystals in the polycrystalline tin whisker. X-ray energy dispersive spectroscopy (EDS) was used to verify that there were no compositional differences between the grains, all were composed of pure tin (Sn). Diffraction patterns were also taken using the TEM. From the TEM images and the diffraction patterns it can be definitively stated that the studied whisker was polycrystalline.

In addition, since bright tin finishes have been associated with greater tin whisker growth than matte tin finishes, two card samples were prepared, one from each LRU, and were sectioned using a FIB. EDS in a field-emission SEM was used to confirm the composition of each layer by running line scans. Ion channel imaging was used to acquire images showing distinct grains based on crystal orientation contrast. Using a modified line-intercept method, the average grain size for card guides was calculated.

Based on the grain size calculation, the tin finish on the card guides was determined to be a bright finish.

Future Work

There are many aspects of the tin whisker phenomena that provide opportunities for future research. One area that would expand on the research performed in this dissertation would be to study the effect of pressure on breakdown voltage. This would require the development of a method measuring pressure applied to the tin whisker either directly or indirectly by measuring whisker deflection, length and diameter and then calculating the pressure.

Expanding the range of the power beyond the 0-45 vdc to determine the upper limit of breakdown voltage would also provide additional insight. By expanding the upper limit one may be able to eliminate the censored data points. Developing a distribution for breakdown voltage using an alternating current power supply and comparing it to the results for the direct current power supply would also provide useful data. If there was a significant difference, both distributions could be used to improve risk simulations based on whether the whiskered circuitry contains ac circuitry, dc circuitry or both.

A free whisker experiment where only the force of gravity is applied to the whiskers would also contribute to the body of knowledge. Given the extremely low mass and small diameter of the whiskers, they are difficult to handle by hand even with a pair of fine tweezers. A micromanipulator with a tweezers attachment for precise control of the whisker removal and placement would be very helpful for this type of experiment. In addition, designing a transparent enclosure for the experiment would minimize the problems associated with loose whisker and air currents in the room.

Most of the current studies of fusing current use small samples of tin whiskers. A large sample experiment is recommended from a variety of controlled sources. Obtaining additional insight into the how much current a whisker can carry before fusing open would provide enhance the understanding of the risk that tin whiskers pose to electronic circuits.

Other variables that could affect tin whisker shorting should also be studied. Some examples of these variables that warrant future study include: whisker shape, whisker length and thickness, and oxidation layer thickness. Another phenomenon related to tin whiskers that warrants further quantification is metal vapor arcing. Obtaining a better understanding of this phenomenon will improve the capability of risk simulations to take this factor into account

LIST OF REFERENCES

- Ahmad, M. I., Sinclair, C. D., & Werritty, A. (1988). Log-logistic flood frequency analysis. *Journal of Hydrology*, 98(3-4), 205-224.
- American Society for Testing and Materials. (2006). *Standard test methods for determining average grain size* (ASTM Standard No. E 112 - 96). West Conshohocken, PA: ASTM International. Retrieved October 29, 2007 from www.astm.org
- Anoplate. (2000). *The trouble with tin: Get the lead out!* Retrieved May 8, 2007, from <http://www.anoplate.com/news/pastnews/fall2000/tin.htm>
- Arnold, S. M. (1954). Hidden cause of failure in electronic equipment: Metal whiskers. *Electrical Manufacturing*, 54(5), 110-114.
- Arnold, S. M. (1956). The growth and properties of metal whiskers. *43rd Annual Convention of the American Electroplaters' Society*, 26-31.
- Arnold, S. M. (1966). Repressing growth of tin whiskers. *Plating*, 53(1), 96-99.
- Arnold, S. M., & Koonce, S. E. (1956). Filamentary growths on metals at elevated temperatures. *Journal of Applied Physics*, 27(8), 964.
- Ashkar, F., & Mahdi, S. (2006). Fitting the log-logistic distribution by generalized moments. *Journal of Hydrology*, 328(3-4), 694-703.
- Baliga, J. (2004). Can nickel barriers eliminate tin whiskers? *Semiconductor International*, 27(12), 38-38.
- Barsoum, M. W., Hoffman, E. N., Doherty, R. D., Gupta, S., & Zavaliangos, A. (2004). Driving force and mechanism for spontaneous metal whisker formation. *Physical Review Letters*, 93(20), 206104-1.
- Bennett, S. (1983). Log-logistic regression models for survival data. *Applied Statistics*, 32(2), 165-171.
- Boguslavsky, I., & Bush, P. (2003). Recrystallization principles applied to whisker growth in tin. *APEX 2003*, Anaheim, CA. S12-4-1-S12-4-10.
- Brusse, J., Ewell, G., & Siplon, J. (2002). Tin whiskers: Attributes and mitigation. *Capacitor and Resistor Technology Symposium*, New Orleans, LA. (22ND) 67-80.
- Brusse, J., & Sampson, M. (2004, November/December). Zinc whiskers: Hidden cause of equipment failure. *IEEE IT Professional*, 6(6) 43-47.
- Buetow, M. (2005). HP, sony seek RoHS exemptions. *Circuits Assembly*, 16(4), 8-8.

- Chen, K., & Wilcox, G. D. (2005). Observations of the spontaneous growth of tin whiskers on tin-manganese alloy electrodeposits. *Physical Review Letters*, 94(6), 066104.
- Chuang, T., & Yen, S. (2006). Abnormal growth of tin whiskers in a Sn₃Ag_{0.5}Cu_{0.5}Ce solder ball grid array package. *Journal of Electronic Materials*, 35(8), 1621.
- Chudnovsky, B. H., Swindler, D. L., & Thompson, J. R. (2001). Silver whiskers growth on power contacts in corrosive industrial atmospheres. 199-207.
- Cobb, H. L. (1946). Cadmium whiskers. *The Monthly Review American Electroplaters Society*, 33(28), 28-30.
- Compton, K. G., Mendizza, A., & Arnold, S. M. (1951). Filamentary growths on metal surfaces—Whiskers. *Corrosion*, 7(10), 327-334.
- Corbid, L. (1989). Constraints on the use of tin plate in miniature electronic packages. *3rd International SAMPE Electronics Conference: Electronic Materials and Processes, Jun 20-22 1989*, 3 773-779.
- Corbitt, N., Ngo, C. C., & Lai, F. C. (2007). Effects of thermal and vibrational cycles on stresses in lead-free solder joints *45th AIAA Aerospace Sciences Meeting and Exhibit*, Reno, Nevada. (AIAA-2007-619) 1-8.
- Crawford, M. (2004). *Zinc whiskers found in war memorial*. Retrieved September 26, 2006, from <http://www.computerworld.com.au/index.php/id;613452630;relcomp;1>
- Crow, E. L., & Shimizu, K. (1988). Lognormal distributions theory and applications. In E. L. Crow, & K. Shimizu (Eds.), *History, genesis, and properties* (1st ed., pp. 1-26). New York, New York: Marcel Dekker.
- Daddonna, P. (2005, July 4,). Reactor shutdown: Dominion learns big lesson from A tiny 'tin whisker'. [Electronic version]. *The Day*, pp. 1-5. Retrieved August 30, 2006 from http://nepp.nasa.gov/whisker/reference/tech_papers/2005-dadonna-nuclear-reactor-shutdown.pdf
- Davis, J. H. (1966). The effect of high elastic uniaxial strain on the resistivity and the superconducting transition temperature of tin whiskers. (Clemson University). *DAI-B*, 27 (12), 4520.
- Davy, G. (2002). *Relay failure caused by tin whiskers*. Retrieved September 9, 2006, from http://nepp.nasa.gov/whisker/reference/tech_papers/davy2002-relay-failure-caused-by-tin-whiskers.pdf
- Dittes, M., Oberndorff, P., Crema, P., & Su, P. (2006). Tin whisker formation - a stress relieve phenomenon. *AIP Conference Proceedings*, (816), 348-59.

- Downs, J. (1994). The phenomenon of zinc whisker growth and the rotary switch (or, how the switch industry captured the abominable snowman). *Metal Finishing*, 23-25.
- Dunn, B. D. (1987). Mechanical and electrical characteristics of tin whiskers with special reference to spacecraft systems. *ESA Journal*, 12(1), 1-17.
- Dunn, B. D. (1997). Chapter 7 - whisker growths. *Metallurgical assessment of spacecraft parts, materials and processes* (pp. 515-548). Chichester, UK: John Wiley & Sons in association with Praxis Publishing.
- Dunn, B. D., Burke, W. R., & Battrick, B. (1987). *Laboratory study of tin whisker growth* (No. ESA STR-223). Netherlands: European Space Agency. Retrieved June 23, 2006 from http://nepp.nasa.gov/whisker/reference/tech_papers/dunn1987-a-lab-study-of-tin-whisker-growth.pdf
- Durney, C. H., Harris, L. D., & Alley, C. L. (1982). In Van Valkenburg M. E. (Ed.), *Electric circuits: Theory and engineering applications* (1st ed.). New York, NY: Holt, Rinehart and Winston.
- Egashira, M., Matsumoto, T., Shimizu, Y., & Iwanaga, H. (1988). Gas-sensing characteristics of tin oxide whiskers with different morphologies. *Sensors and Actuators*, 14(3), 205-213.
- Ellis, W. C., Gibbons, D. F., & Treuting, R. C. (1958). Growth of metal whiskers from the solid. In R. H. Doremus, B. W. Roberts & D. Turnbull (Eds.), *Growth and perfection of crystals* (1st ed., pp. 102-120). New York, NY: John Wiley and Sons.
- Eshelby, J. D. (1953a). Screw dislocations in thin rods. *Journal of Applied Physics*, 24(2), 176-179.
- Eshelby, J. D. (1953b). A tentative theory of metallic whisker growth. *Physical Review*, 91, 755-756.
- European Union. (2003a). Directive 2002/95/EC of the European parliament and of the council of 27 January 2003 on the restriction of the use of certain hazardous substances in electrical and electronic equipment. *Official Journal of the European Union*, (February 13), L 37/19-L 37/23. Retrieved September 10, 2006, from http://eur-lex.europa.eu/LexUriServ/site/en/oj/2003/l_037/l_03720030213en00190023.pdf
- European Union. (2003b). Directive 2002/96/EC of the European parliament and of the council of 27 January 2003 on waste electrical and electronic equipment (WEEE). *Official Journal of the European Union*, (February 13), L 37/24-L 37/37. Retrieved September 10, 2006, from http://eur-lex.europa.eu/LexUriServ/site/en/oj/2003/l_037/l_03720030213en00240038.pdf

- Fang, T. (2005). Tin whisker risk assessment studies. University of Maryland, College Park). *DAI-B*, 66 (12), 6874. Retrieved June 7, 2006 from <https://drum.umd.edu/dspace/handle/1903/3079>
- Fang, T., Osterman, M., & Pecht, M. (2006). Statistical analysis of tin whisker growth. *Microelectronics Reliability*, 46(5/6), 846-849.
- Fisher, R. M., Darken, L. S., & Carroll, K. G. (1954). Accelerated growth of tin whiskers. *Acta Metallurgica*, 2(3), 368-373.
- Food and Drug Administration. (1986). *Tin whiskers - problems, causes, and solutions*. Retrieved October 30, 2006, from http://www.fda.gov/ora/inspect_ref/itg/itg42.html
- Fukuda, Y., Osterman, M., & Pecht, M. (2007). Length distribution analysis for tin whisker growth. *Electronics Packaging Manufacturing, IEEE Transactions on*, 30, 36-40.
- Fukuda, Y. (2005). Experimental investigations of whisker formation on tin platings. University of Maryland, College Park). *DAI-B*, 66 (12), 6875.
- Furuta, N., & Hamamura, K. (1969). Growth mechanism of proper tin-whisker. *Japanese Journal of Applied Physics*, 8(12), 1404-10.
- Galyon, G. (2003). *Annotated tin whisker bibliography*. Retrieved November 9, 2006, from http://thor.inemi.org/webdownload/newsroom/TW_biblio-July03.pdf
- Galyon, G. T. (2005). Annotated tin whisker bibliography and anthology. *Electronics Packaging Manufacturing, IEEE Transactions on [see also Components, Packaging and Manufacturing Technology, Part C: Manufacturing, IEEE Transactions on]*, 28(1), 94-122.
- Galyon, G. T., & Palmer, L. (2005). An integrated theory of whisker formation: The physical metallurgy of whisker formation and the role of internal stresses. *Electronics Packaging Manufacturing, IEEE Transactions on [see also Components, Packaging and Manufacturing Technology, Part C: Manufacturing, IEEE Transactions on]*, 28(1), 17-30.
- Galyon, G. (2004). A history of tin whisker theory: 1946 to 2004. *SMTAI International Conference*, Chicago, IL.
- Giannuzzi, L., & Stevie, F. (Eds.). (2005). *Introduction to focused ion beams: Instrumentation, theory, techniques and practice* (1st ed.). New York, New York: Springer US.
- Glazunova, V. K. (1962). A study of the influence of certain factors on the growth of filamentary tin crystals. *Kristallografiya*, 7(5), 761-768.

- Glazunova, V. K., & Kudryavtsev, N. T. (1963). An investigation of the conditions of spontaneous growth of filiform crystals on electrolytic coatings. *Zhurnal Prikladnoi Khimii*, 36(3), 543-550.
- Gluck, P. (1978). On current carrying superconducting tin whiskers. *Physics Letters A*, 66(5), 425-426.
- Government Electronics and Information Technology Association. (2006). *Standard for mitigating the effects of tin whiskers in aerospace and high performance electronic systems* (GEIA STANDARD No. GEIA-STD-0005-2). Arlington, VA: Government Electronics and Information Technology Association Standards & Technology Department.
- Hada, Y., Morikawa, O., & Togami, H. (1978). Study of tin whiskers on electromagnetic relay parts. *Proceedings of the 26th Relay Conference, 25-26 April 1978*, 9-1.
- Halliday, D., & Resnick, R. (1981). *Fundamentals of physics* (2nd ed.). New York, NY: John Wiley & Sons, Inc.
- Harris, P. (1994). The growth of tin whiskers. *International Tin Research Institute*, 1-19.
- Herring, C., & Galt, J. K. (1952). Elastic and plastic properties of very small metal specimens. *Physical Review*, 85(6), 1060-1061.
- Hilty, R. D., & Corman, N. E. (2005). Tin whisker reliability assessment by Monte Carlo simulation. *IPC/JEDEC Lead-Free Symposium*, San Jose, CA.
- Holm, E. (1962). Introductory lecture on fundamentals. *Engineering Seminar on Electric Contact Phenomena*, 1-13.
- Holm, R., & Holm, E. (1967). *Electric contacts theory and application* (4th ed.). New York: Springer-Verlag.
- Hunsicker, H. Y., & Kempf, L. W. (1947). Aluminum alloys for bearings. *SAE Quarterly Transactions*, 1(1), 6-26.
- International Electronics Manufacturing Initiative. (2005). *Recommendations on lead-free finishes for components used in high reliability products*. Unpublished manuscript.
- Jiang, B., & Xian, A. -. (2006). Discontinuous growth of tin whiskers. *Philosophical Magazine Letters*, 86(8), 521-527.
- Joint Electron Device Engineering Council. (2006). *Current tin whiskers theory and mitigation practices guideline* (Guideline No. JP002). Arlington, Virginia; Bannockburn, Illinois.: JEDEC Solid State Technology Association; IPC,. Retrieved November 11, 2006 from <http://www.jedec.org/DOWNLOAD/search/JP002.pdf>

- Kadesch, J. S., & Leidecker, H. (2000). Effects of conformal coat on tin whisker growth. Paper presented at the *Proceedings of IMAPS Nordic, the 37th IMAPS Nordic Annual Conference*, 108-116. Retrieved May 26, 2006 from http://nepp.nasa.gov/WHISKER/reference/tech_papers/kadesch2000-paper-effects-of-conformal-coat-on-tin-whisker-growth.pdf
- Kakeshita, T., Shimizu, K., Kawanaka, R., & Hasegawa, T. (1982). Grain size effect of electro-plated tin coatings on whisker growth. *Journal of Materials Science*, 17(9), 2560-6.
- Keming Chen, & Wilcox, G. D. (2005). Observations of the spontaneous growth of tin whiskers on tin-manganese alloy electrodeposits. *Physical Review Letters*, 94(6), 066104-1.
- Koonce, S. E., & Arnold, S. M. (1953). Growth of metal whiskers. *Journal of Applied Physics*, 24(3), 365-366.
- Koutrouvelis, I. A., Canavos, G. C., & Meintanis, S. G. (2005/6/15). Estimation in the three-parameter inverse gaussian distribution. *Computational Statistics & Data Analysis*, 49(4), 1132-1147.
- Lau, J. H. (2006). Key differences between EU RoHS and china RoHS (as of august 7, 2006). *Global SMT & Packaging*, (October 2006), December 2006. http://www.trafalgar2.com/documents/Technical_Articles/6.09-lau.pdf
- Lederrey, P. (2006). *Requested exemption from requirements of article 4(1) of directive 2002/95/EC*. Unpublished manuscript.
- Leidecker, H., & Brusse, J. (2006). *Tin whiskers: A history of documented electrical system failures - A briefing prepared for the space shuttle program Office*. Retrieved December 3, 2006, from http://nepp.nasa.gov/whisker/reference/tech_papers/2006-Leidecker-Tin-Whisker-Failures.pdf
- Leidecker, H., Brusse, J., Sampson, M. & Kadesch, J. (2006). *NASA Goddard Space Flight Center tin whisker (and other metal whisker) homepage*. Retrieved January 22, 2007, from <http://nepp.nasa.gov/whisker/>
- Leon, R. V. (2003). *Location-scale-based parametric distributions*. Retrieved November 23, 2007, from <http://web.utk.edu/~leon/rel/Fall03pdfs/567Unit4Handout.pdf>
- Levy, P. W., & Kammerer, O. (1955). "Spiral polygon" tin whiskers. *Journal of Applied Physics*, 26(9), 1182-1183.
- Limpert, E., Stahel, W. A., & Abbt, M. (2001). Log-normal distributions across the sciences: Keys and clues. *Bioscience*, 51(5), 341-352.

- Lutes, O. S., & Maxwell, E. (1955). Superconducting transitions in tin whiskers. *Physical Review*, 97(6), 1718-1720.
- Mason, M. S., & Eng, G. (2006). *Tin plasmas at 28 V in 1 atm of air* No. ATR-2006(8004)-2). El Segundo, California: The Aerospace Corporation.
- Mathwave Technologies. (2007). *EasyFit* (3.2nd ed.). Dnepropetrovsk, Ukraine: Mathwave Technologies. Retrieved May 21, 2007, from <http://www.mathwave.com/products/easyfit.html>
- Meyer, J. D., & Tidecks, R. (1977). Investigation of the current induced phase transition of superconducting tin whiskers with several potential probes. *Solid State Communications*, 24(9), 639-641.
- Minitab Inc. (2003). *Minitab release 14 statistical software* (14.1st ed.). State College, Pennsylvania: Minitab Inc. Retrieved October 11, 2007, from <http://www.minitab.com/products/>
- Nakadaira, Y., Matsuura, T., Tsuriya, M., Nhat, D. V., Kangas, R., Conrad, J., et al. (2001). Pb-free plating for peripheral/leadframe packages. 213-218.
- National Instruments. (2004). *LabVIEW* (7.1st ed.). Austin, Texas: National Instruments. Retrieved March 23, 2007, from <http://www.ni.com/labview/>
- Nayeri Hashemzadeh, M. (2005). *Study of tin whisker growth and their mechanical and electrical properties*. Retrieved November 5, 2006, from <http://www.diva-portal.org/liu/abstract.xsql?dbid=4491>
- Nishimi, K. (2007). Space shuttle program tin whisker mitigation. *International Symposium on Tin Whiskers*, The Samuel Riggs IV Alumni Center, University of Maryland, College Park, MD 20742. 1-16.
- Nordwall, B. D. (1986). Air force links radar problems to growth of tin whiskers. *Aviation Week & Space Technology*, 124(26), 65.
- Osterman, M. (2002). *Mitigation strategies for tin whiskers.*, 2006, from <http://www.calce.umd.edu/lead-free/tin-whiskers/>
- Osterman, M. (2006). *Assessing the risk posed by tin whiskers*. Retrieved November 27, 2006, from <http://www.calce.umd.edu/lead-free/STMAKeyNote.pdf>
- Peach, M. O. (1952). Mechanism of growth of whiskers on cadmium. *Journal of Applied Physics*, 23(12), 1401-1403.
- Pinsky, D. (2002). *Tin whisker application specific risk assessment algorithm*. Retrieved January 16, 2007, from https://www.reliabilityanalysislab.com/tl_dp_0312_TinWhiskerRiskAssessmentAlgorithm.asp

- Pitt, C. H., & Henning, R. G. (1964). Pressure-induced growth of metal whiskers. *Journal of Applied Physics*, 35(2), 459-460.
- Powell, B. E., & Skove, M. J. (1965). Elastic strength of tin whiskers in tensile tests. *Journal of Applied Physics*, 36(4), 1495-1496.
- Proussevitch, A., Sahagian, D., & Tsentalovich, E. (2007). Statistical analysis of bubble and crystal size distributions: Formulations and procedures. *Journal of Volcanology and Geothermal Research*, 164(3), 95-111.
- Puttlitz, K., & Galyon, G. (2007). Impact of the ROHS directive on high-performance electronic systems. *Journal of Materials Science: Materials in Electronics*, 18(1-3), 347-365.
- Reliability Information Analysis Center. (2006). Working to get the lead out. *The Journal of the Reliability Information Analysis Center, Second Quarter*, December 4, 2006. Retrieved December 4, 2006, from <http://quanterion.com/RIAC/Publications/RIACJournal/PDFFiles/2006Q2.pdf>
- Richard Ciocci, & Michael Pecht. (2006). Learning from the migration to lead-free solder. *Soldering & Surface Mount Technology*, 18(3), 14-18.
- Rozen, M. (1968). Practical whisker growth control methods. *Plating*, 5(11), 1155-1160.
- Sabbagh, N. A. J., & McQueen, H. J. (1975). Tin whiskers: causes and remedies. *Metal Finishing*, 73(3), 27-31.
- Sakuyama, S., & Kutami, M. (2005). Substitute materials for complete elimination of hazardous substances - study of whisker growth on lead-free plating. *Fujitsu Scientific and Technical Journal*, 41(2), 217-224.
- Samsonov, G. V. (1973). *The oxide handbook* (C. N. Turton, T. I. Turton Trans.). (1st English ed.). New York, NY: IFI /Plenum Data Corporation.
- Schetty, R. (2001). Minimization of tin whisker formation for lead-free electronics finishing. *Circuit World*, 27(2), 17-20.
- Schetty, R. (2004). Electrodeposited tin properties & their effect on component finish reliability. *2004 International Conference on Business of Electronic Product Reliability and Liability*, Shanghai, China. 29-34.
- Sengupta, S., Das, D., Ganesan, S., Pecht, M., Lin, T. Y., & Rollins, W. (2005). Effects of re-finishing of terminations by solder-dipping on plastic quad flatpack electronic parts. *Proceedings of 7th Electronic Packaging Technology Conference (EPTC 2005)*, Grand Copthorne Waterfront, Singapore. , 2 768-773.

- Sheng, G. T. T., Hu, C. F., Choi, W. J., Tu, K. N., Bong, Y. Y., & Nguyen, L. (2002). Tin whiskers studied by focused ion beam imaging and transmission electron microscopy. *Journal of Applied Physics*, 92(1), 64.
- Silverstein, S. (1998, August 17 - 23). Reasons for failure lost with galaxy 4. *Space News*, 3-20.
- Siplon, J. P., Ewell, G. J., Frasco, E., Brusse, J. A., & Gibson, T. (2002). Tin whiskers on discrete components: The problem. *Proceedings of the 28th International Symposium for Testing and Failure Analysis, Nov 3-7 2002*, 421-434.
- Slade, P. G. (1999). In Slade P. G. (Ed.), *Electrical contacts principles and applications* (1st ed.). Boca Raton, FL: CRC Press Taylor & Francis Group.
- Smetana, J. (2005). Minimizing tin whiskers. *SMT Surface Mount Technology Magazine*, 19(8), 36-38.
- Sriyarunya, A., Tondtan, J., & Bansal, D. (2004). Matte tin (Sn) plating: Whisker growth study. 281-288.
- Stevens, C. (2001). Relay failures induced by the growth of tin whiskers: A case study. *IEEE Boston Reliability Chapter 38th Annual Spring Reliability Symposium*, Boston, MA. 1-6.
- Sweet, A. L. (1990). On the hazard rate of the lognormal distribution. *Reliability, IEEE Transactions on*, 39(3), 325-328.
- Takagi, K., Kumagai, S., Matsunaga, c., & Kusaka, Y. (1997). Application of inverse gaussian distribution to occupational exposure data. *The Annals of Occupational Hygiene*, 41(5), 505-514.
- Teverovsky, A. (2003). *Gold whiskers: Introducing a new member to the family*. Retrieved July 20, 2006, from http://nepp.nasa.gov/whisker/other_whisker/gold/index.htm
- Timoshenko, S., & Young, D. H. (1968). *Elements of strength of materials* (5th ed.). 450 West 33rd Street, New York, N.Y. 10001: Van Nostrand Reinhold Company.
- Tu, K. N. (1973). Interdiffusion and reaction in bimetallic Cu-Sn thin films. *Acta Metallurgica*, 21(4), 347-354.
- Tu, K. N. (1994). Irreversible processes of spontaneous whisker growth in bimetallic Cu-Sn thin-film reactions. *Physical Review B (Condensed Matter)*, 49(3), 2030-4.
- United States Environmental Protection Agency. (2005). *Solders in electronics* (Summary Document No. EPA-744-S-05-001). Washington, D.C.: United States Environmental Protection Agency. Retrieved October 30, 2006 from <http://www.epa.gov/dfe/pubs/solder/lca/lca-summ2.pdf>

- Van Vlack, L. H. (1980). In Robbins T., Howe M. E. (Eds.), *Elements of materials science and engineering* (4th ed.). Reading, Massachusetts: Addison Wesley.
- Van Westerhuyzen, D. H., Backes, P. G., Linder, J. F., Merrell, S. C., & Poeschel, R. L. (1992). Tin whisker induced failure in vacuum. *ISFA '92: The 18th International Symposium for Testing & Failure Analysis*, Los Angeles, CA. 407-412.
- Walpole, R. E., & Myers, R. H. (1989). *Probability and statistics for engineers and scientists* (4th ed.). New York, NY: Macmillan Publishing Company.
- Wikipedia. (2007a). *The peripheral component interconnect*. Retrieved May 24, 2007, from http://en.wikipedia.org/wiki/Peripheral_Component_Interconnect
- Wikipedia. (2007b). *Superconductivity*. Retrieved May 12, 2007, from <http://en.wikipedia.org/wiki/Superconductivity>
- Wolfgong, W. J., Ogden, B., Champaign, R., & Waller, B. (2005). Surface oxidation as a tin whisker growth mechanism. *Circuits Assembly*, 16(12), 24-27.
- Woodrow, T. A., & Ledbury, E. A. (2005). Evaluation of conformal coatings as a tin whisker mitigation strategy. *IPC/JEDEC 8th International Conference on Pb-Free Electronic Components and Assemblies*, San Jose, CA. 1-25.
- Wu, C., Kumar, V., Bailey, R., Liao, J., L'Esperance, F. & Baker, G. (2007). *Engineering fundamentals*. Retrieved March 03, 2007, from http://www.efunda.com/materials/elements/element_info.cfm?Element_ID=Sn
- Xu, C., Zhang, Y., Fan, C., Abys, J., Hopkins, L., & Stevie, F. (2002). Understanding whisker phenomenon - driving force for the whisker formation. *Proceedings of the IPC SMEMA Council APEX*, S06-2-1-S06-1-6.
- Xu, C., Fan, C., Zhang, Y., & Abys, J. A. (2004, February). Whisker prevention. [Electronic version]. *OnBoard Technology*, 30-34.
- Zhang, W., Egli, A., Schwager, F., & Brown, N. (2005). Investigation of Sn-Cu intermetallic compounds by AFM: New aspects of the role of intermetallic compounds in whisker formation. *IEEE Transactions on Electronics Packaging Manufacturing*, 28(1), 85-93.

APPENDIX A

Proof of Concept Experiment Breakdown Voltage Data

TIN WHISKER BREAKDOWN VOLTAGE DATA

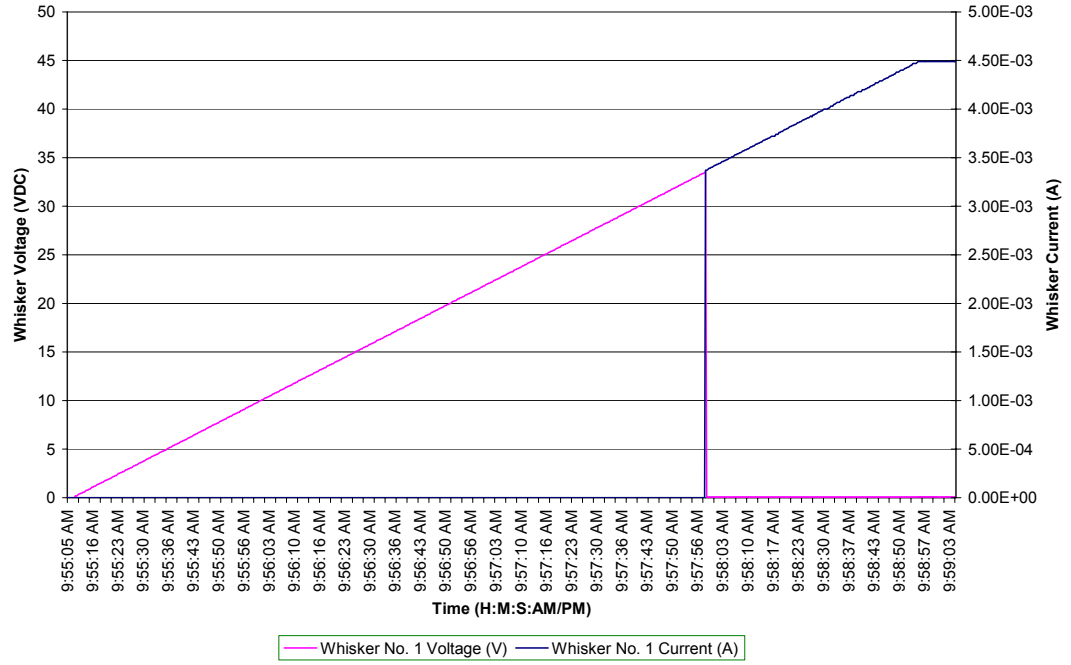
Whisker Number	Transitions ^a	Whisker Voltage
1	S	33.57
2	M/I	7.99
3	M/I	3.39
4	M	9.29
5	M	3.08
6	M	15.68
7	S	13.48
8	S	8.49
9	M/I	13.57
10	S	2.09
11	M/I	10.69
12	S	1.89
13	S	10.09
14	M	28.17
15	M/I	8.38
16	M	4.29
17	M	29.27
18	S	38.96
19	S	18.09
20	S	22.49
21	S	22.49
22	S	18.89
23	S	5.09
24	M	9.59
25	S	5.68
26	M/I	8.48
27	S	28.48
28	S	4.58
29	S	44.05
30	M	8.89
31	M	8.79
32	S	27.18
33	S	14.79
34	S	21.28
35	S	34.77

^a The abbreviations in the transitions column are defined as follows: S = single transition, M = multiple transitions, M/I = multiple transitions with intermittent contact

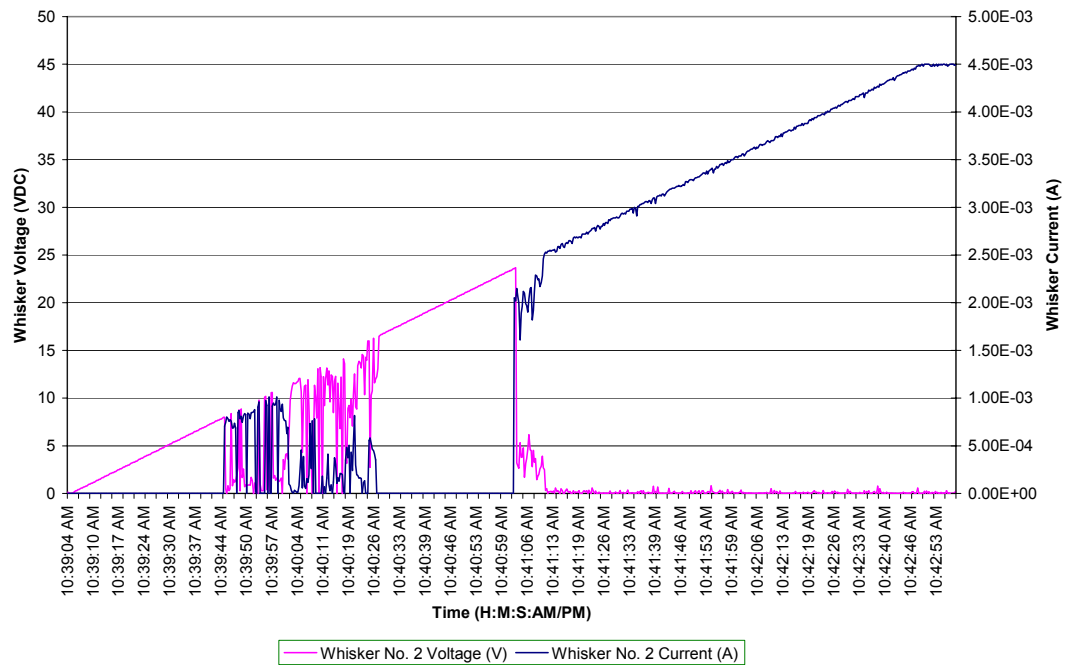
APPENDIX B

Proof of Concept Experiment Tin Whisker Data Graphs

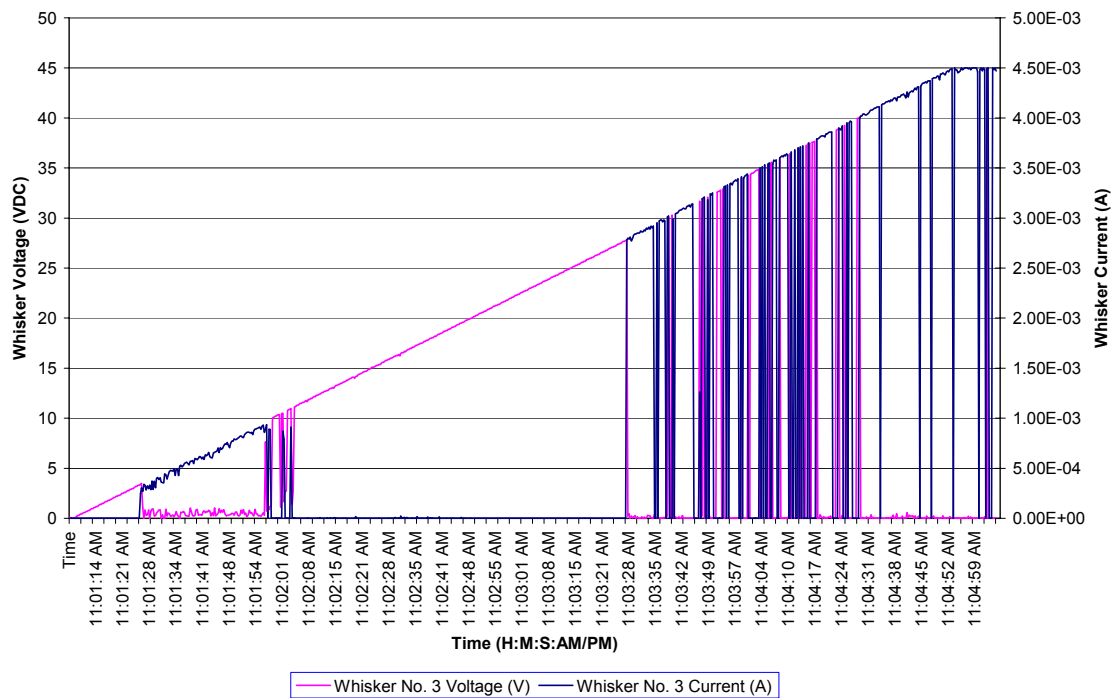
Whisker Breakdown Voltage POC Test Data



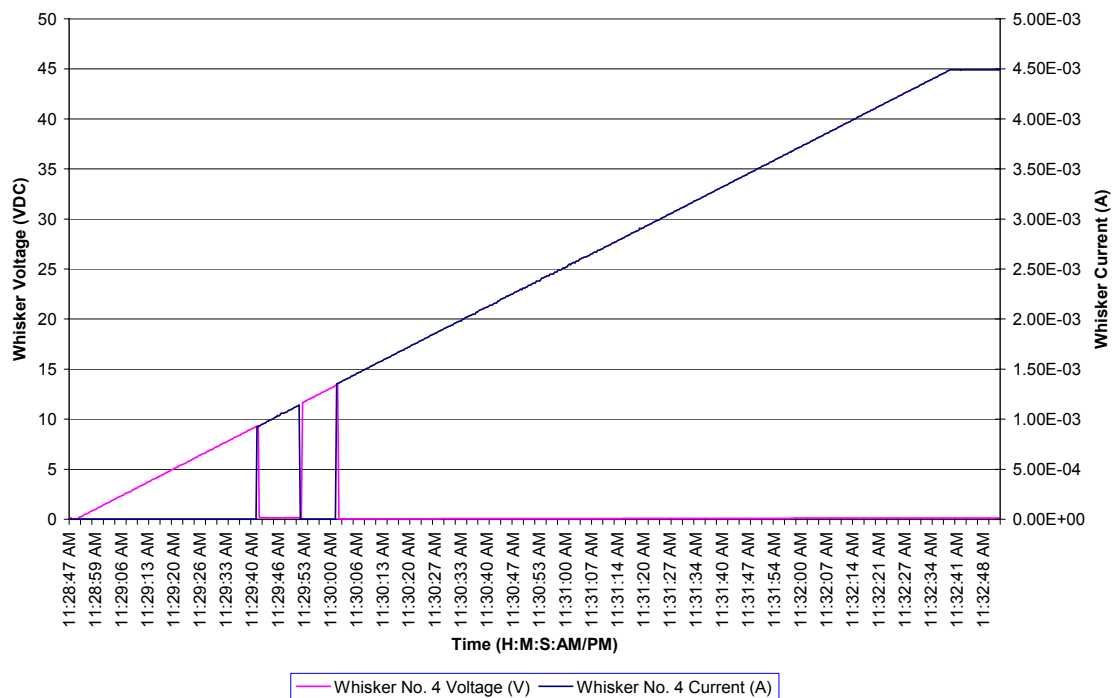
Whisker Breakdown Voltage POC Test Data



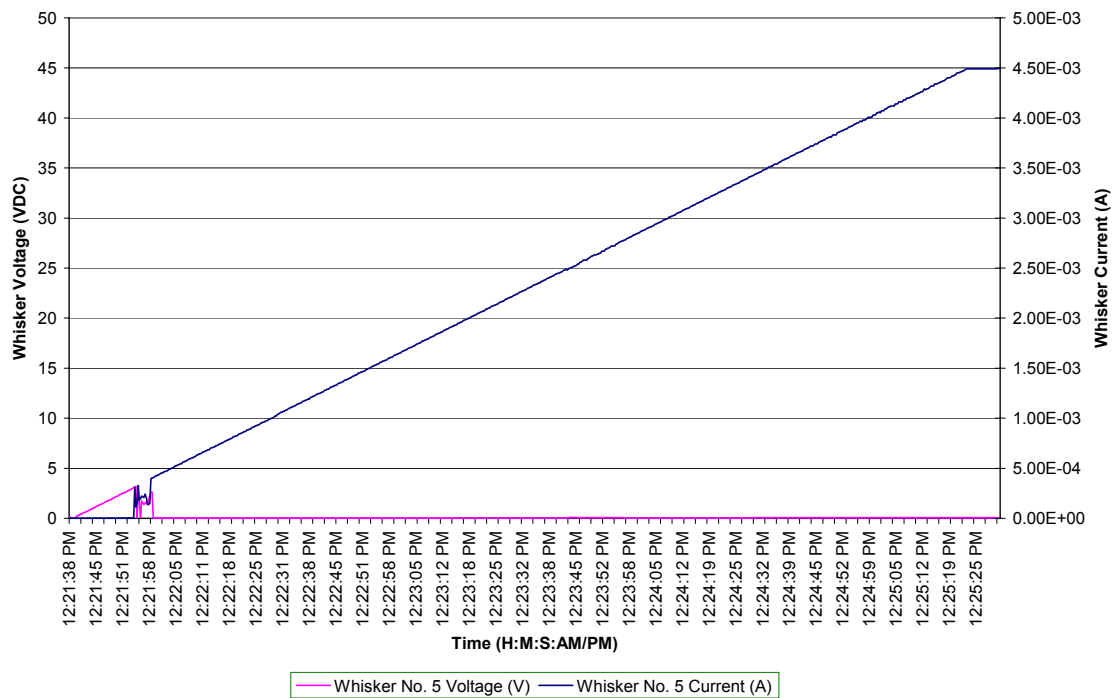
Whisker Breakdown Voltage POC Test Data



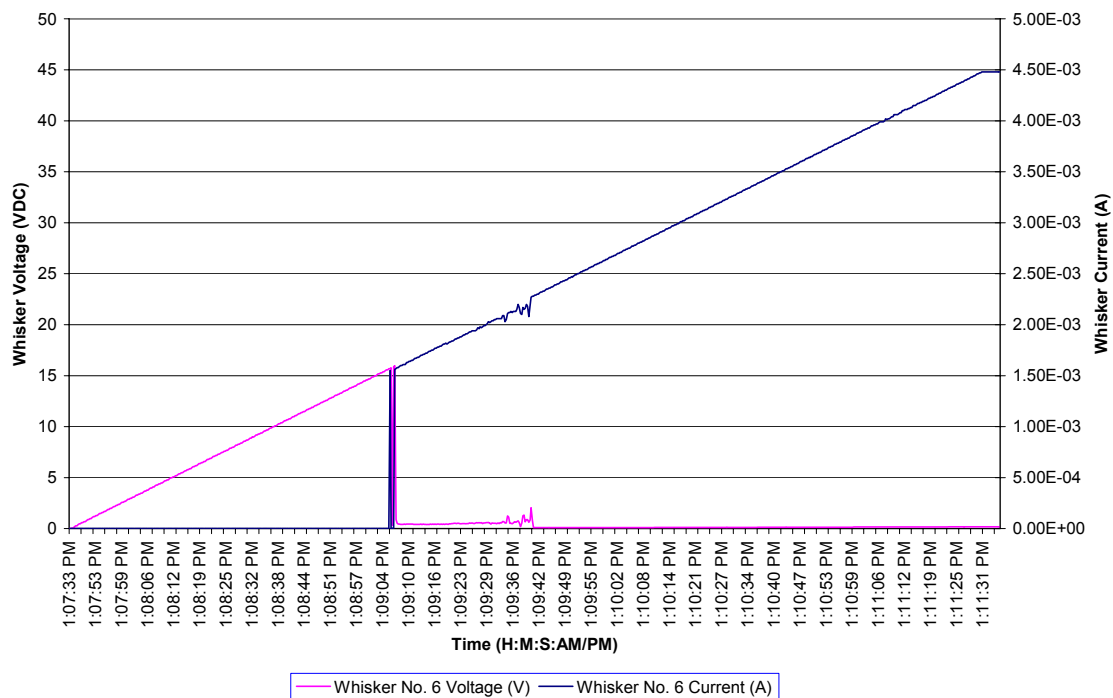
Whisker Breakdown Voltage POC Test Data



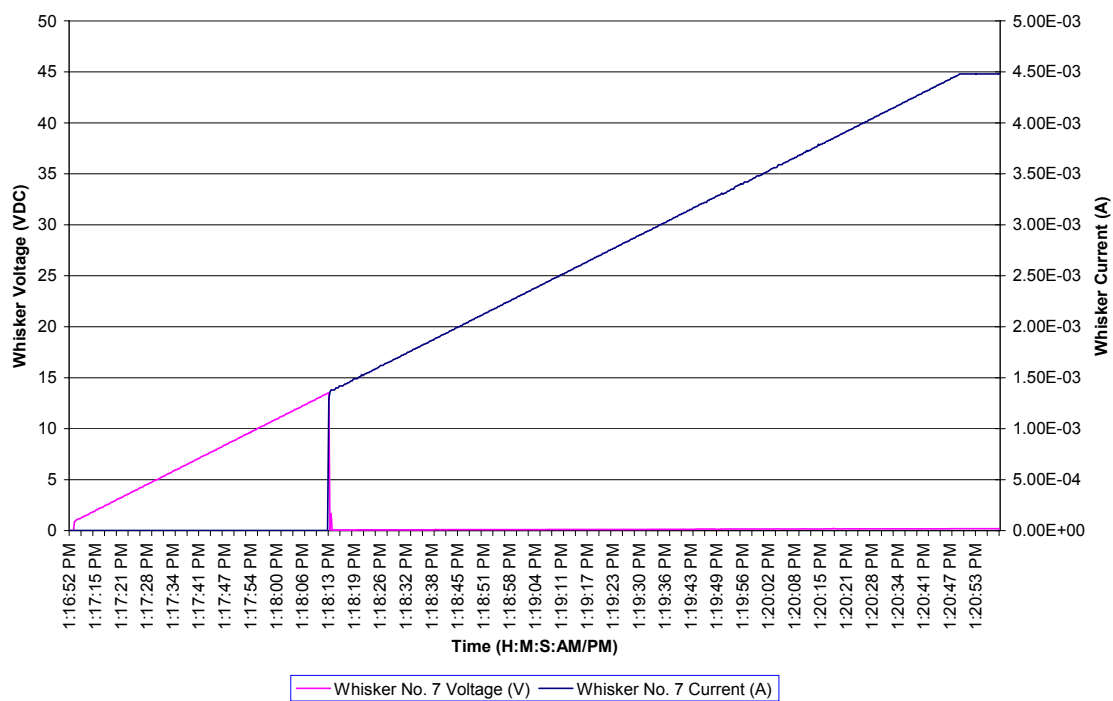
Whisker Breakdown Voltage POC Test Data



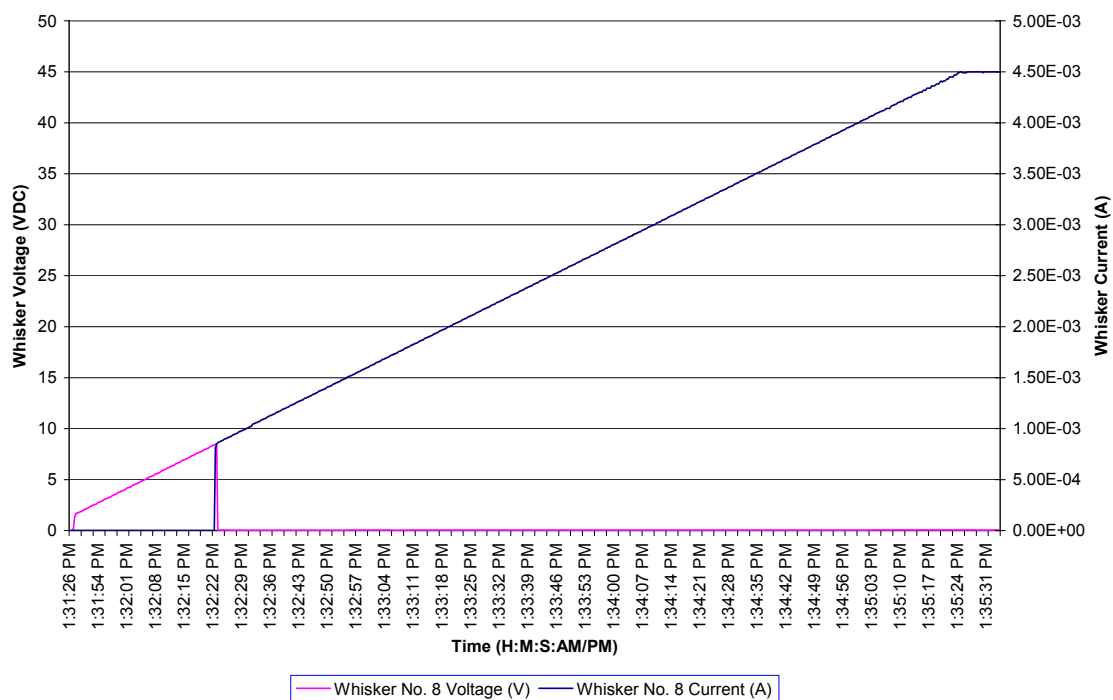
Whisker Breakdown Voltage POC Test Data



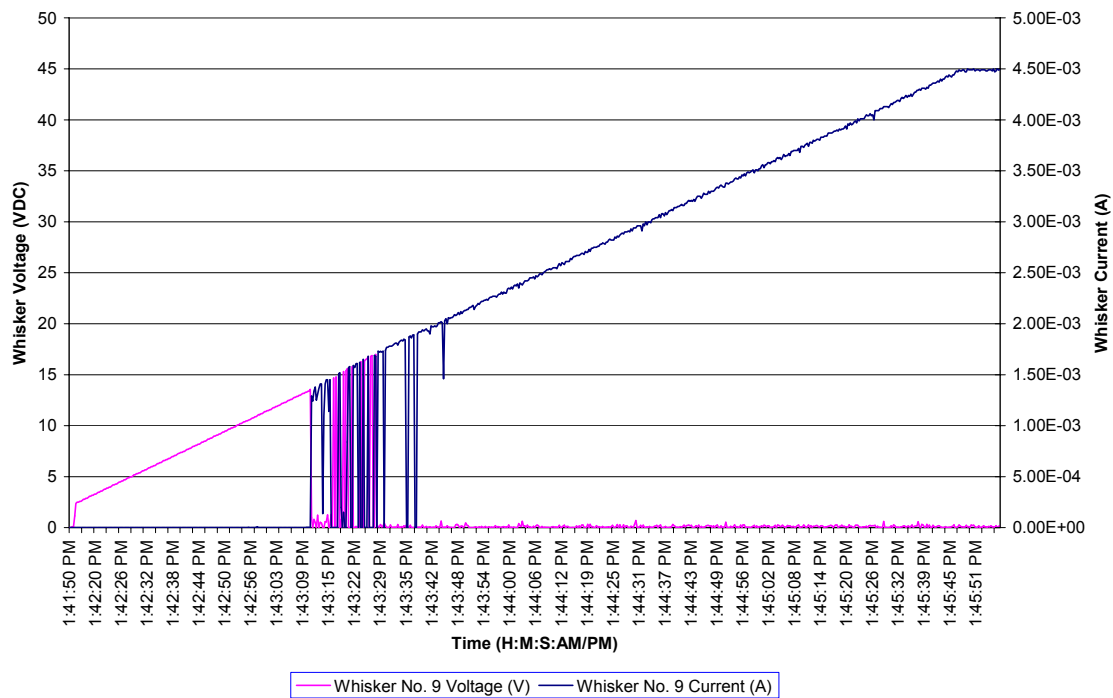
Whisker Breakdown Voltage POC Test Data



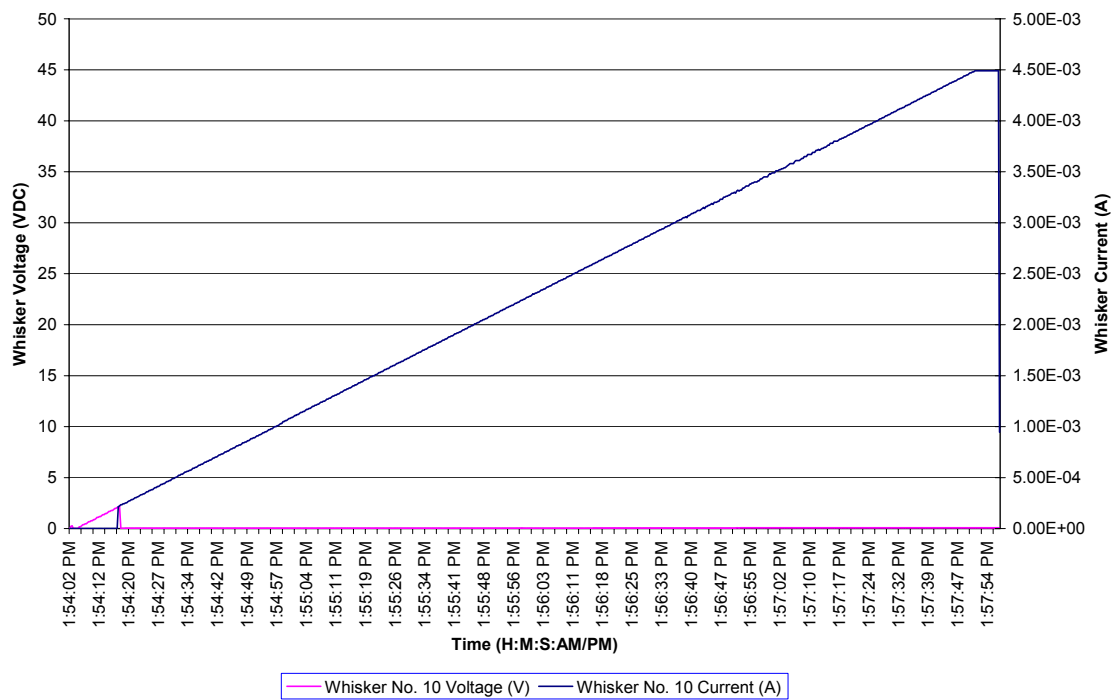
Whisker Breakdown Voltage POC Test Data



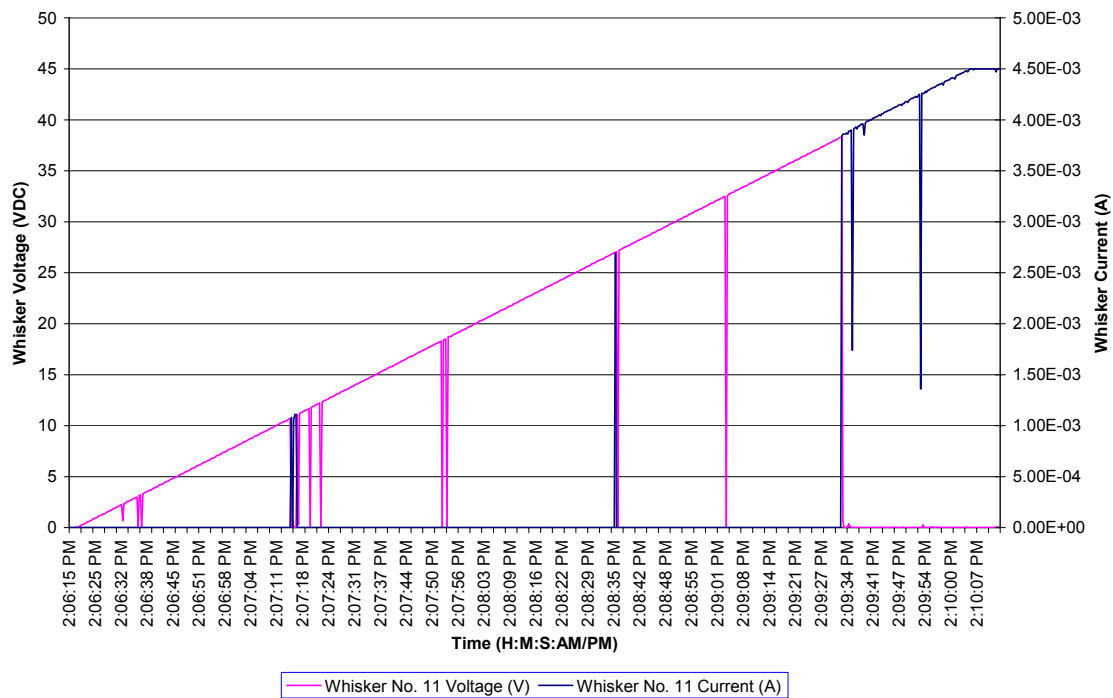
Whisker Breakdown Voltage POC Test Data



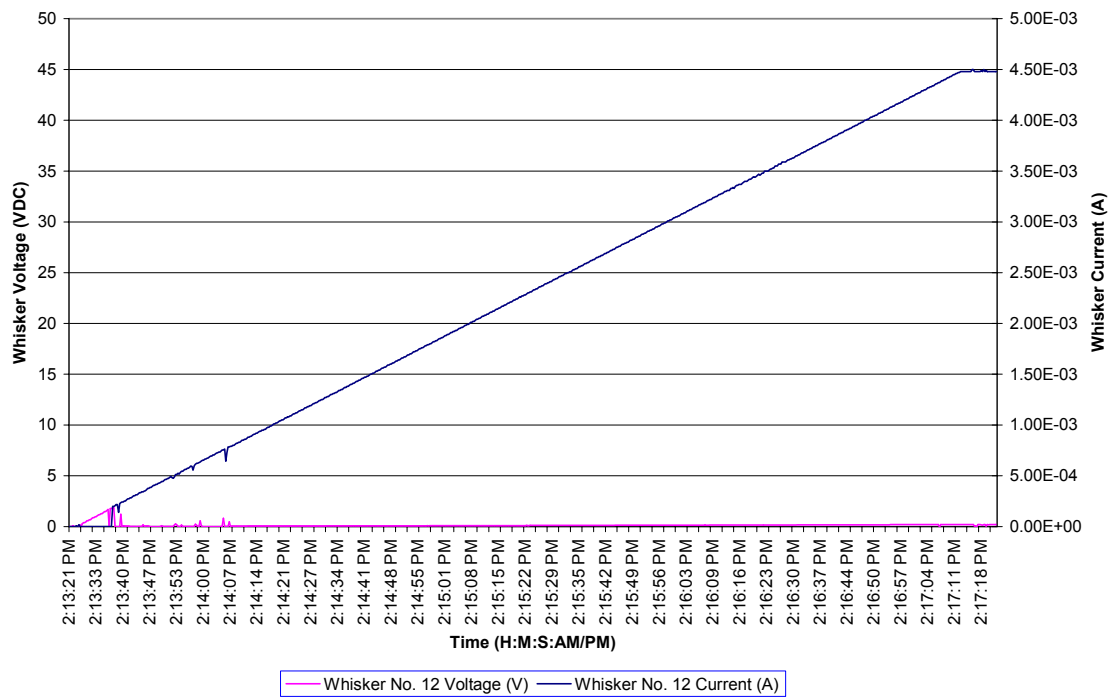
Whisker Breakdown Voltage POC Test Data



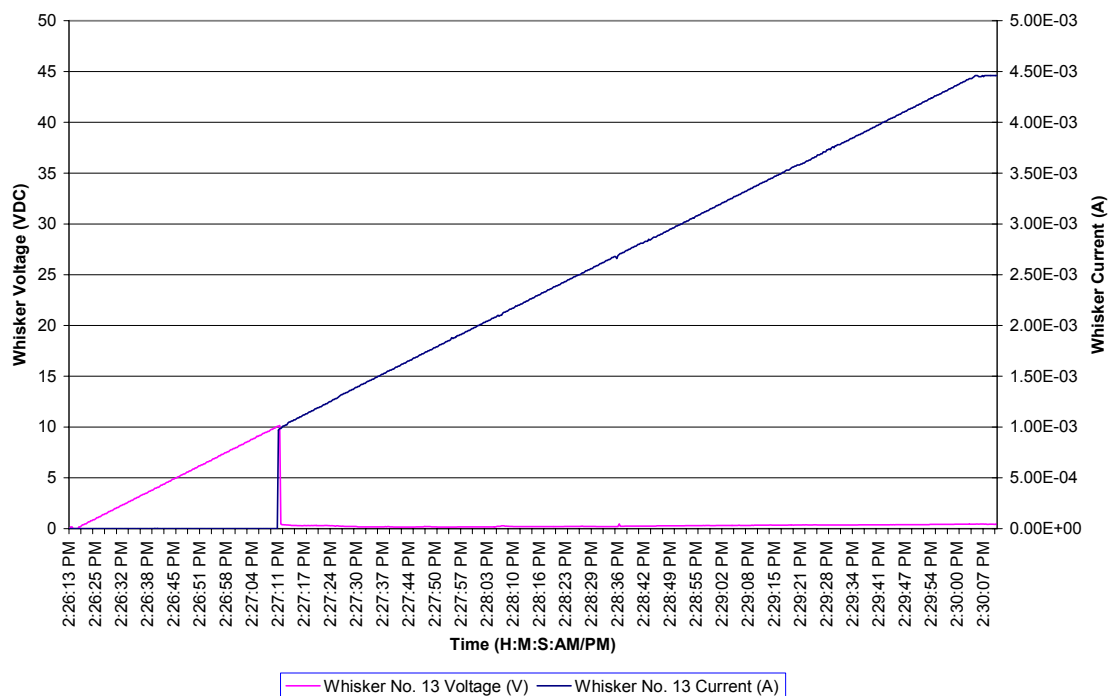
Whisker Breakdown Voltage POC Test Data



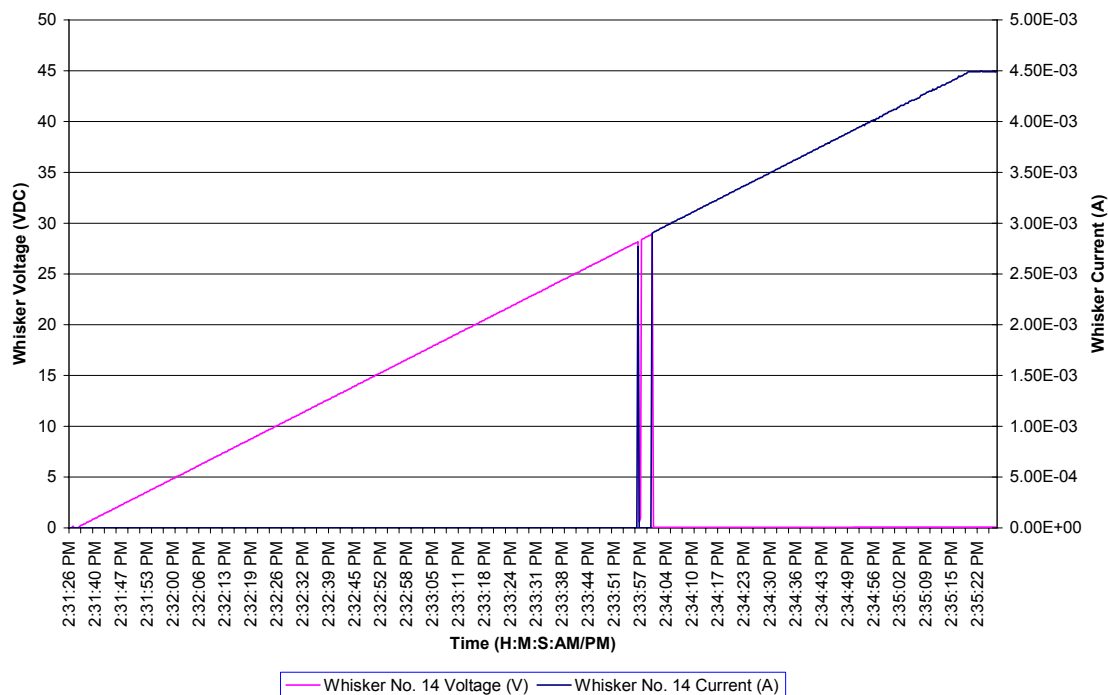
Whisker Breakdown Voltage POC Test Data



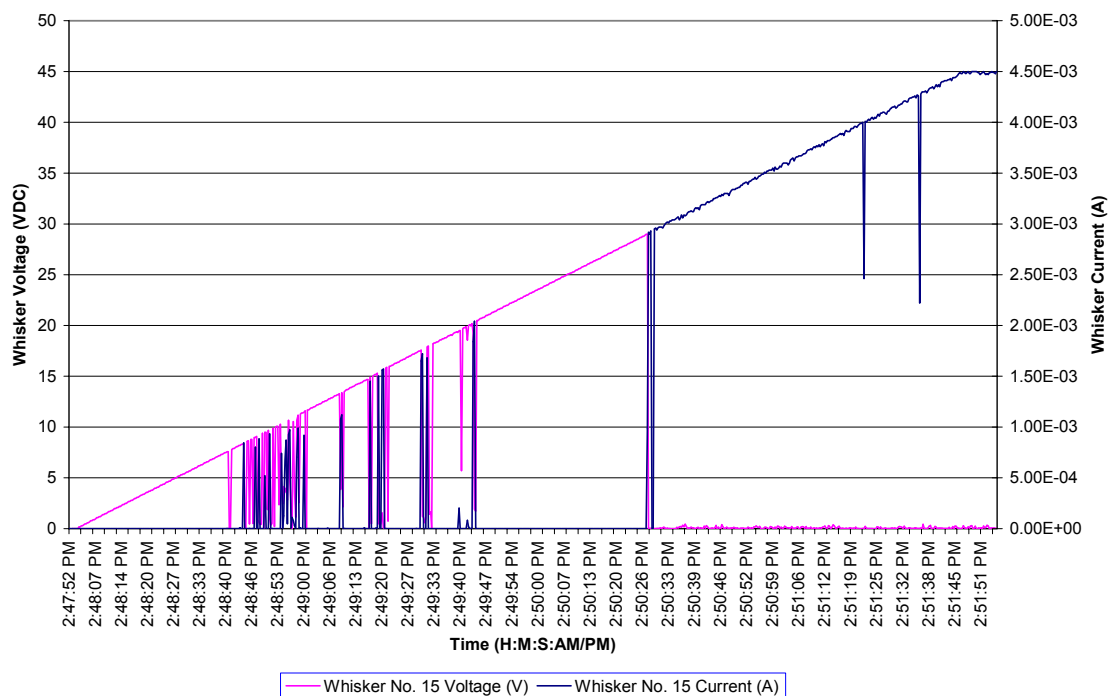
Whisker Breakdown Voltage POC Test Data



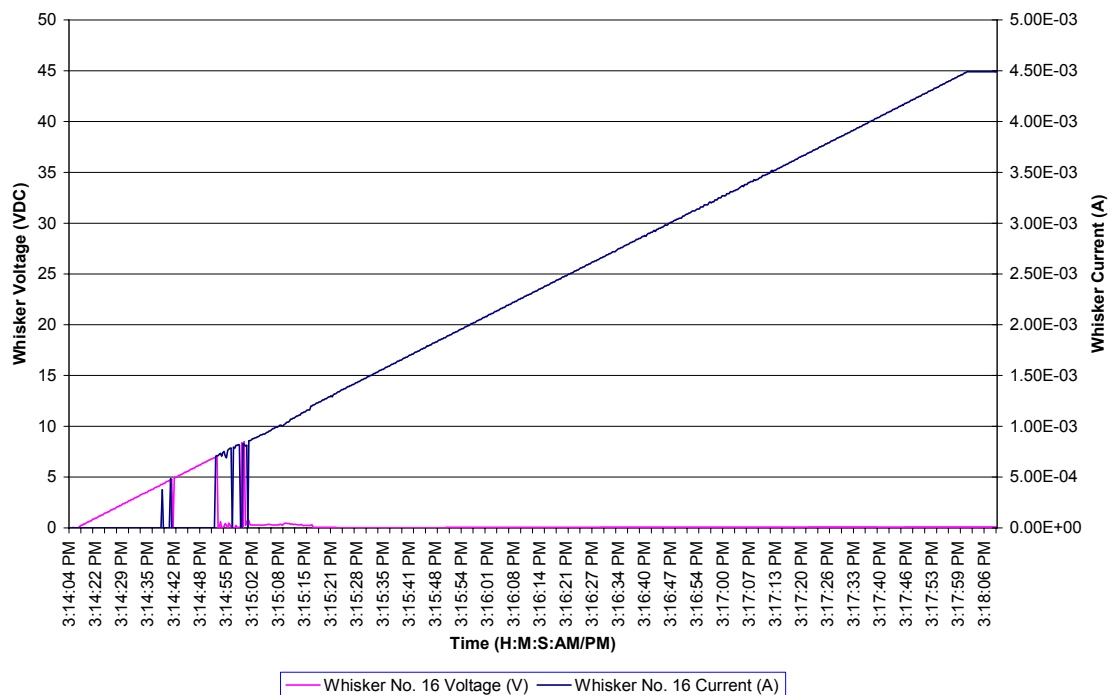
Whisker Breakdown Voltage POC Test Data



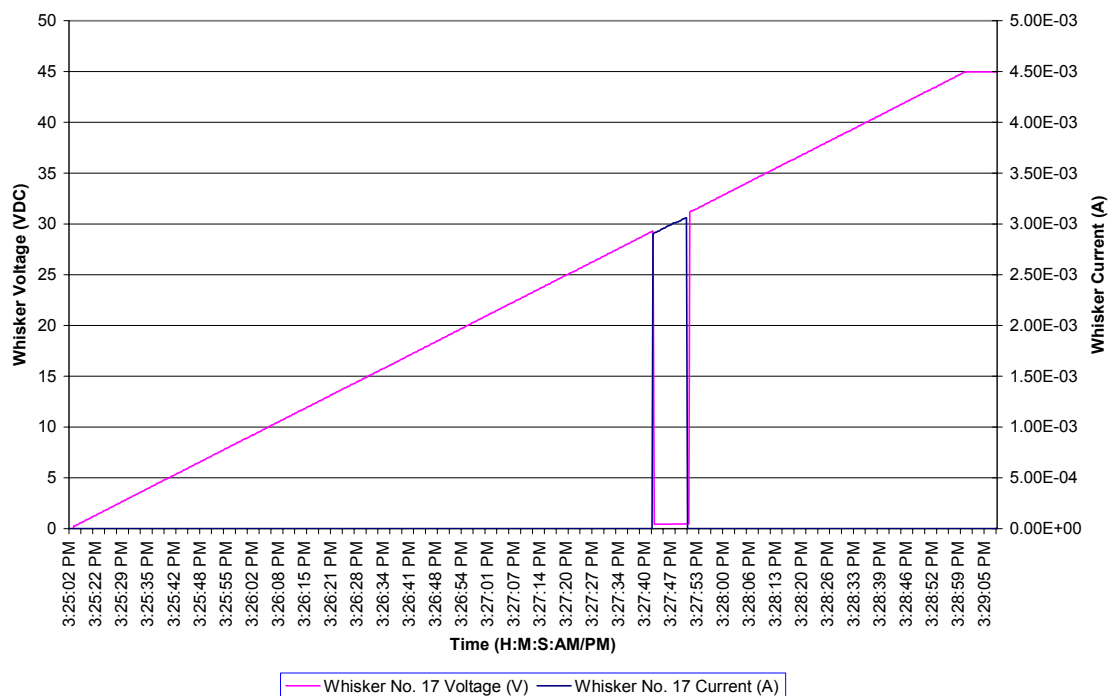
Whisker Breakdown Voltage POC Test Data



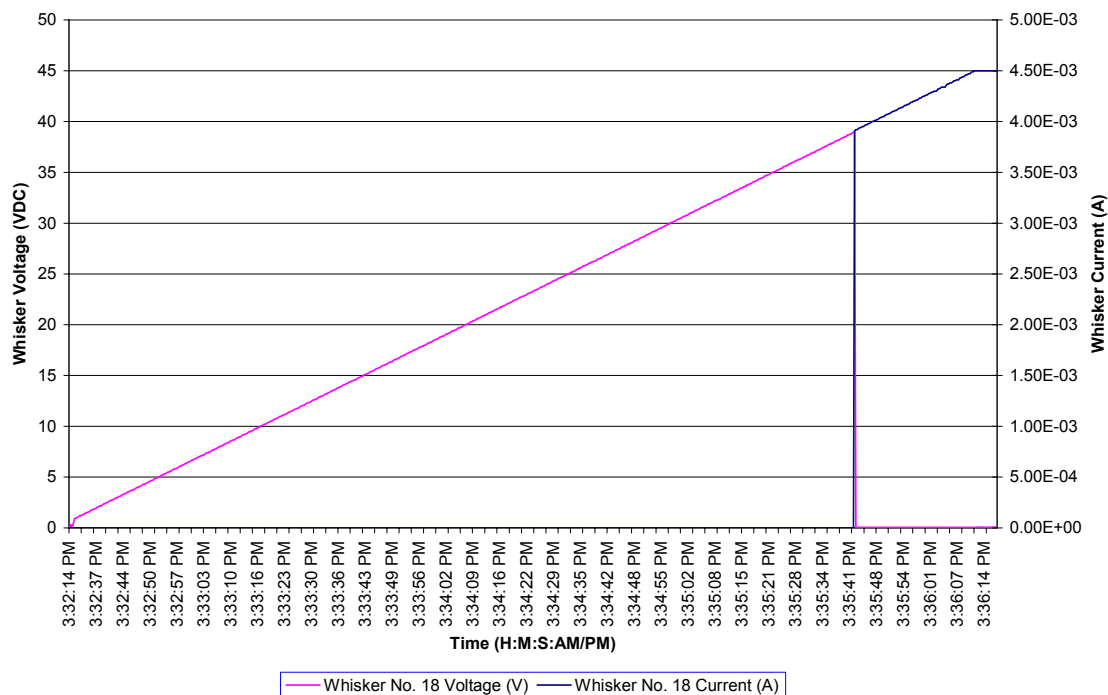
Whisker Breakdown Voltage POC Test Data



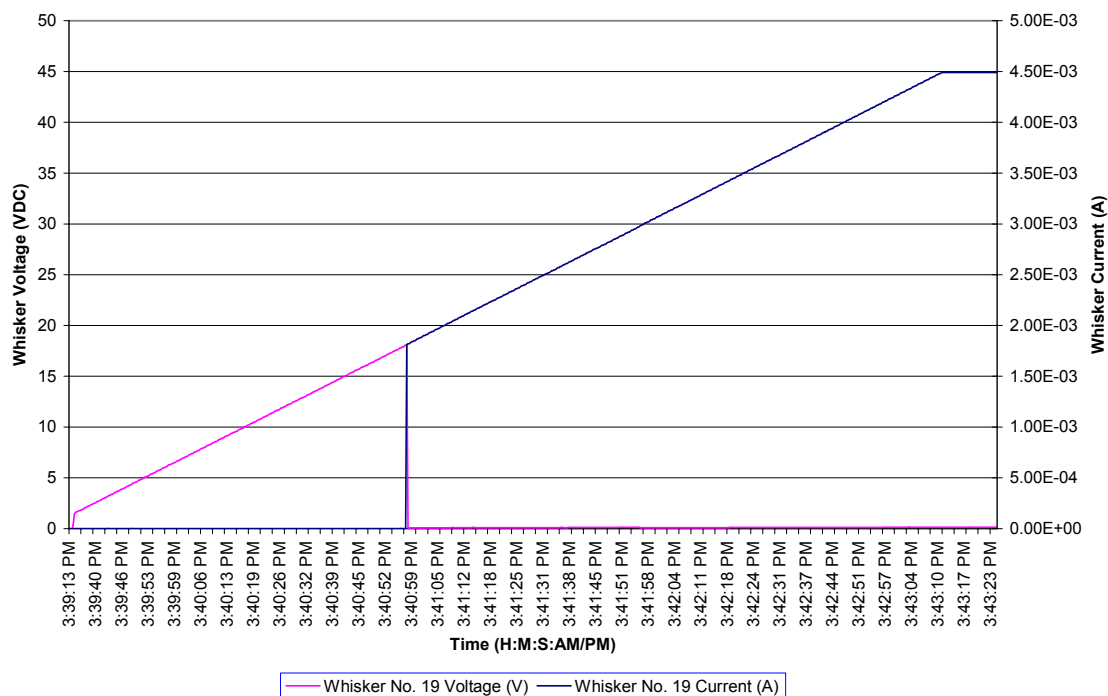
Whisker Breakdown Voltage POC Test Data



Whisker Breakdown Voltage POC Test Data



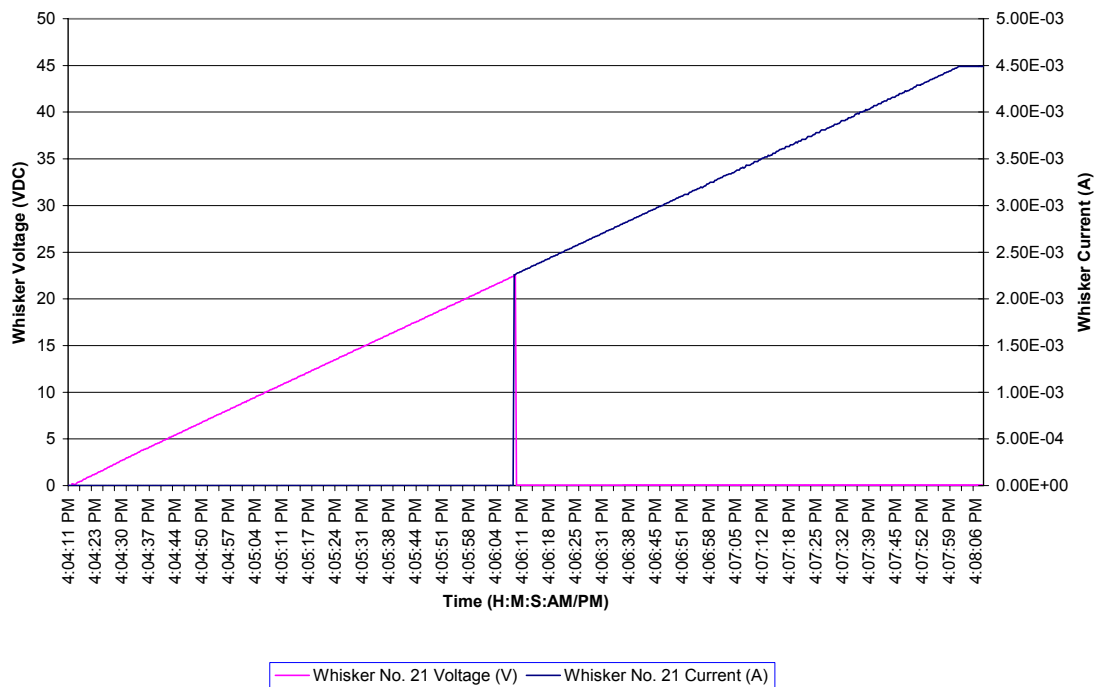
Whisker Breakdown Voltage POC Test Data



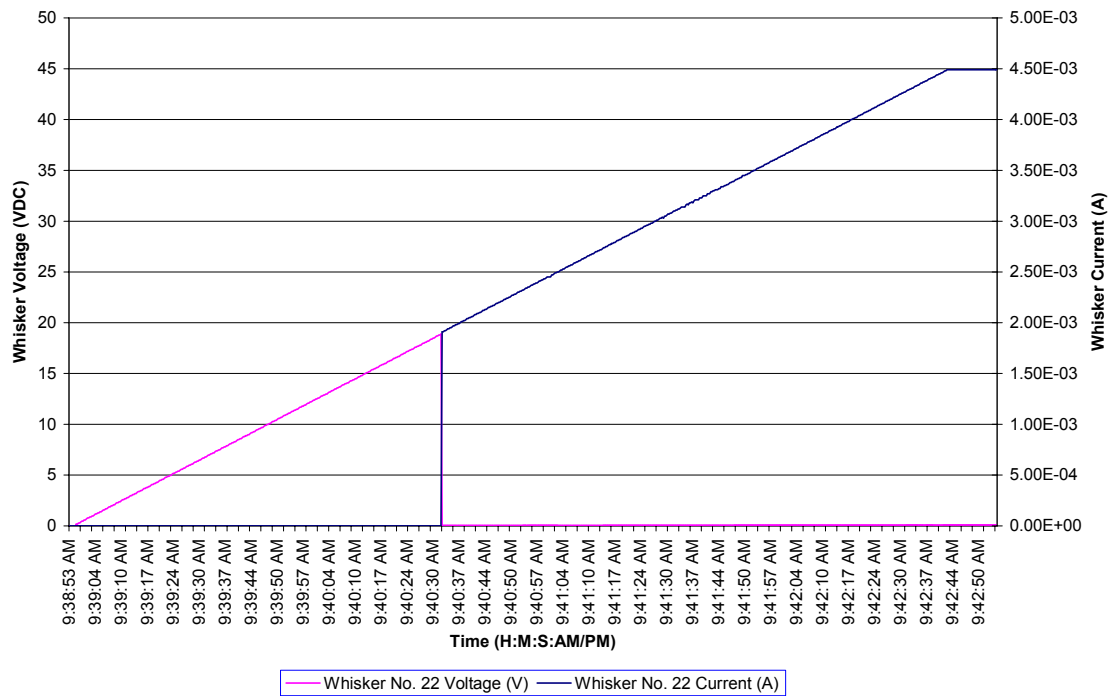
Whisker Breakdown Voltage POC Test Data



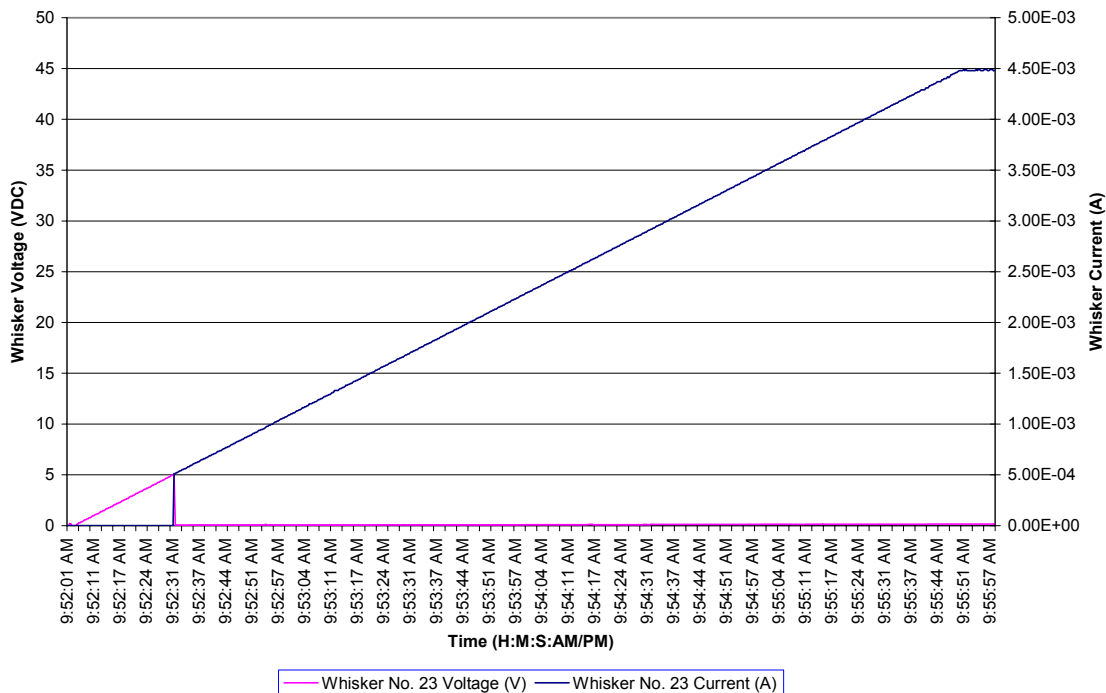
Whisker Breakdown Voltage POC Test Data



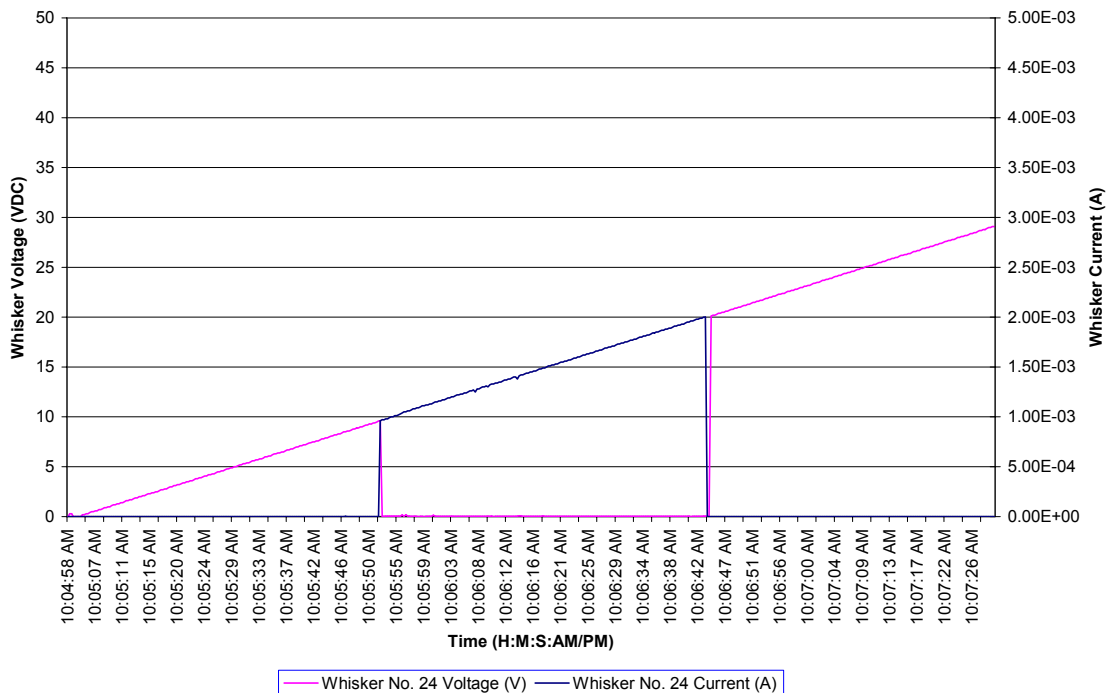
Whisker Breakdown Voltage POC Test Data



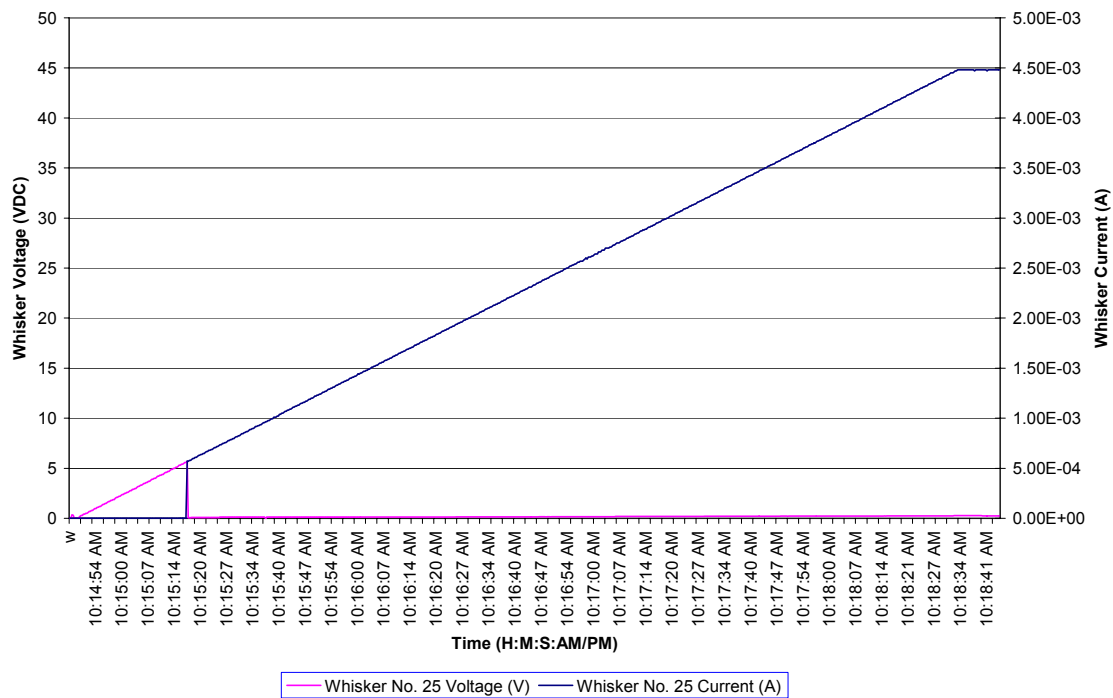
Whisker Breakdown Voltage POC Test Data



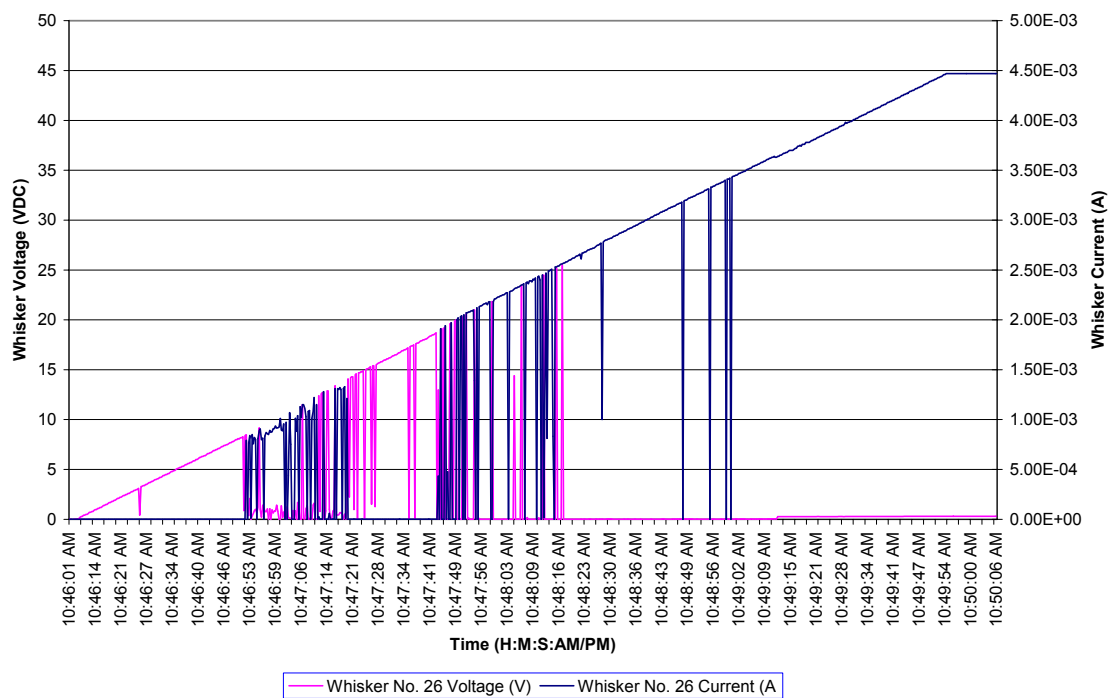
Whisker Breakdown Voltage POC Test Data



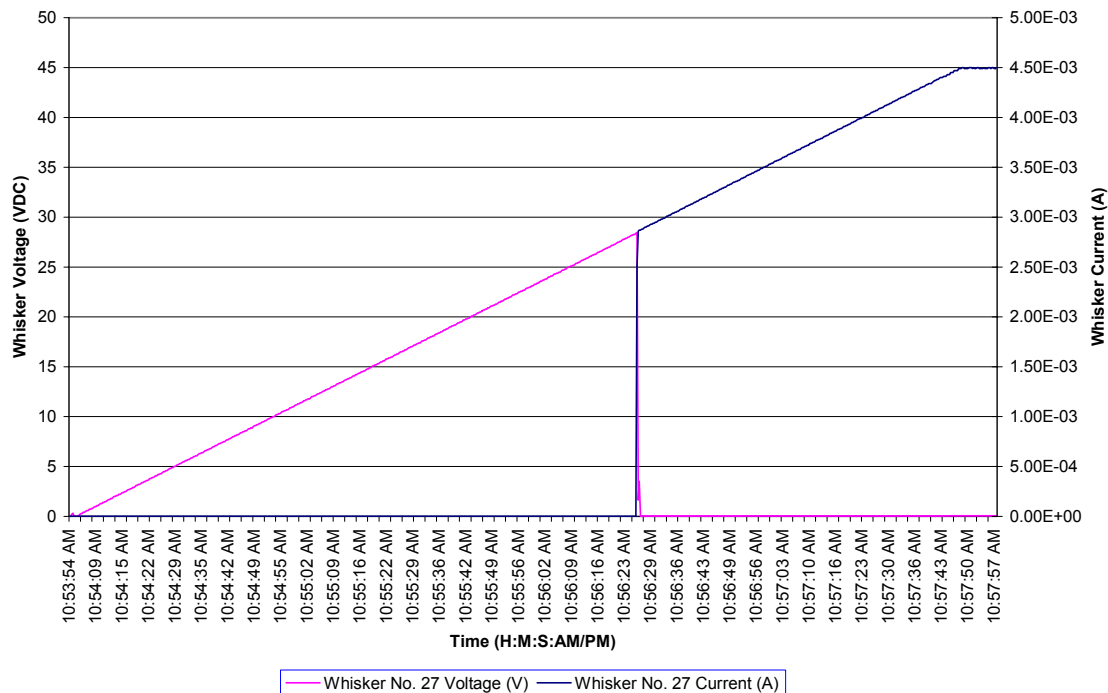
Whisker Breakdown Voltage POC Test Data



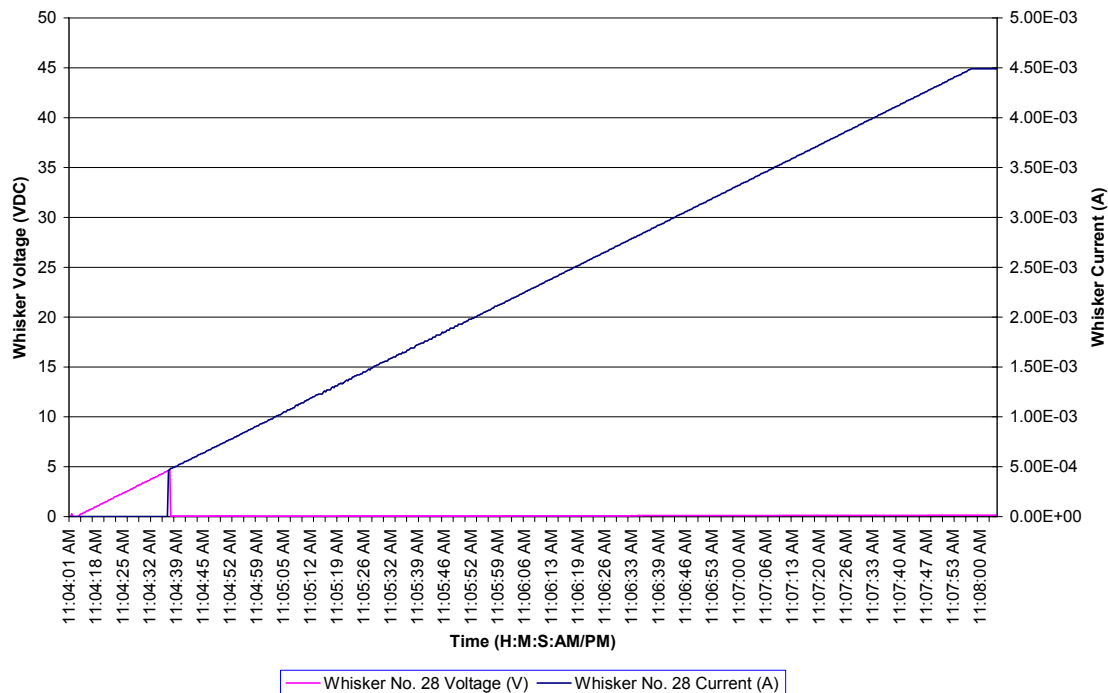
Whisker Breakdown Voltage POC Test Data



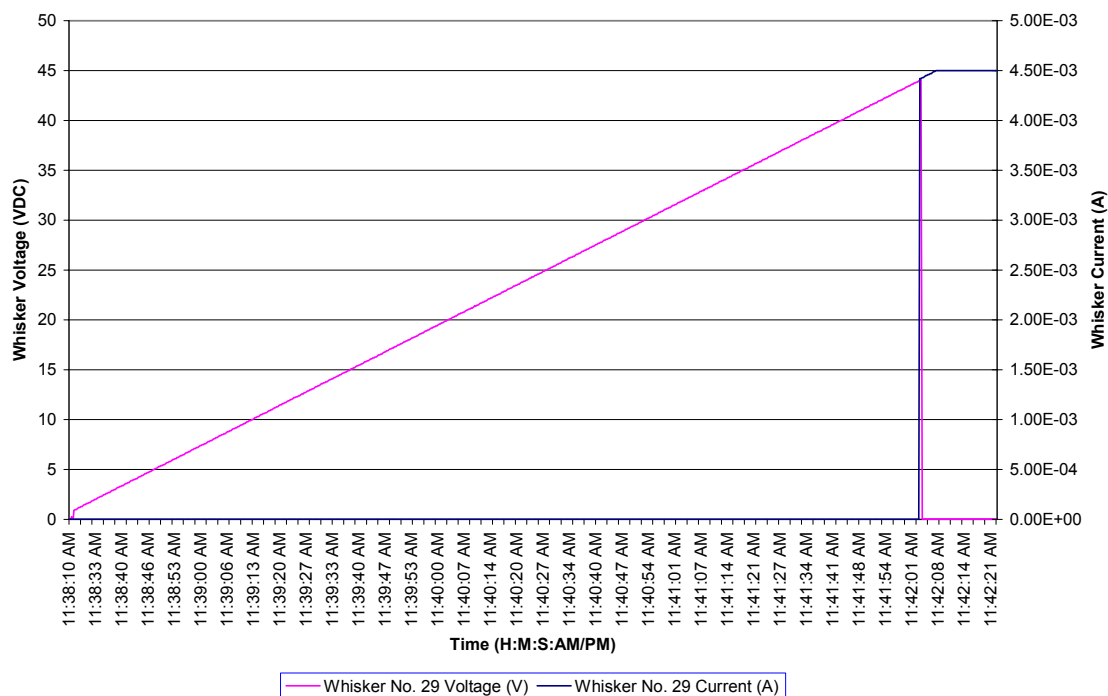
Whisker Breakdown Voltage POC Test Data



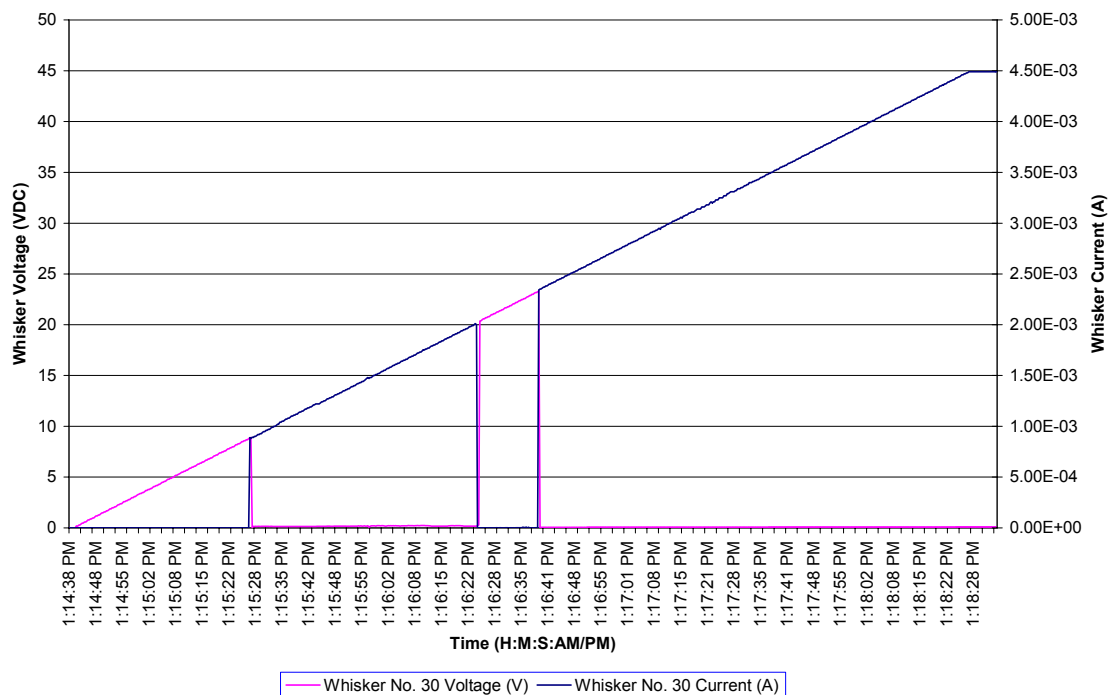
Whisker Breakdown Voltage POC Test Data



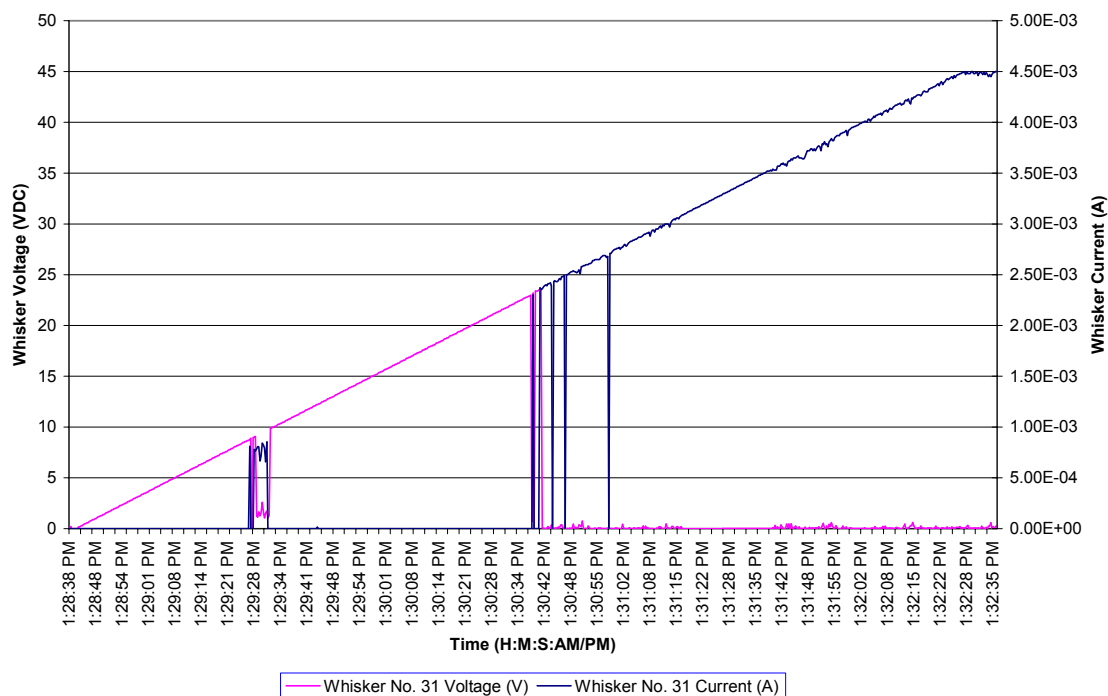
Whisker Breakdown Voltage POC Test Data



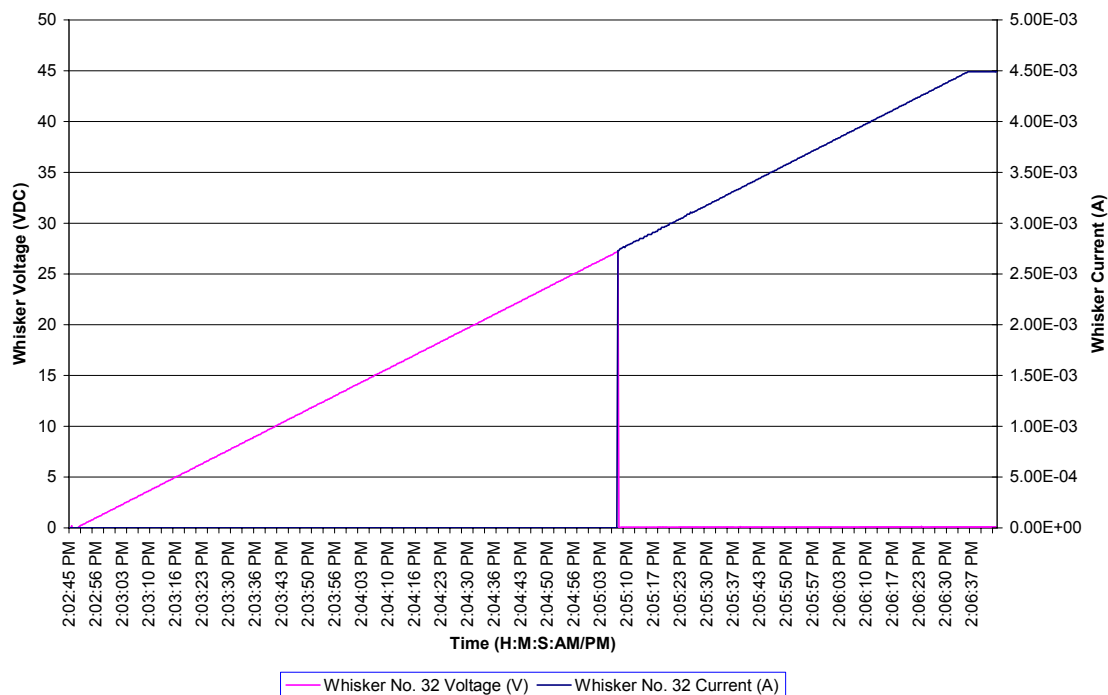
Whisker Breakdown Voltage POC Test Data



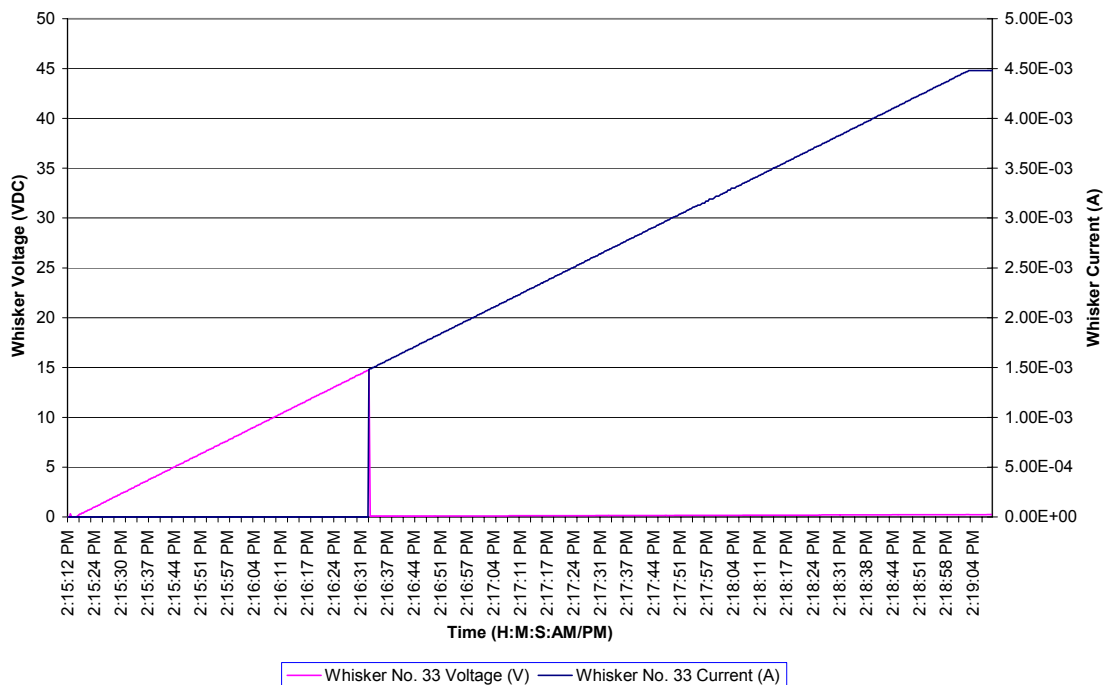
Whisker Breakdown Voltage POC Test Data



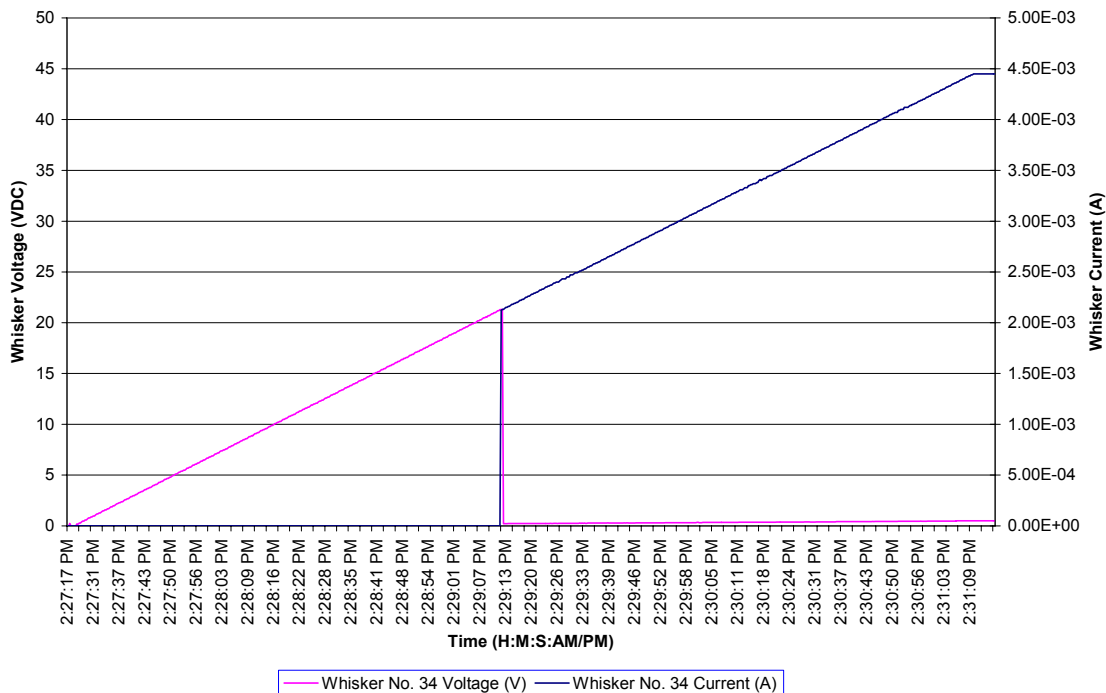
Whisker Breakdown Voltage POC Test Data



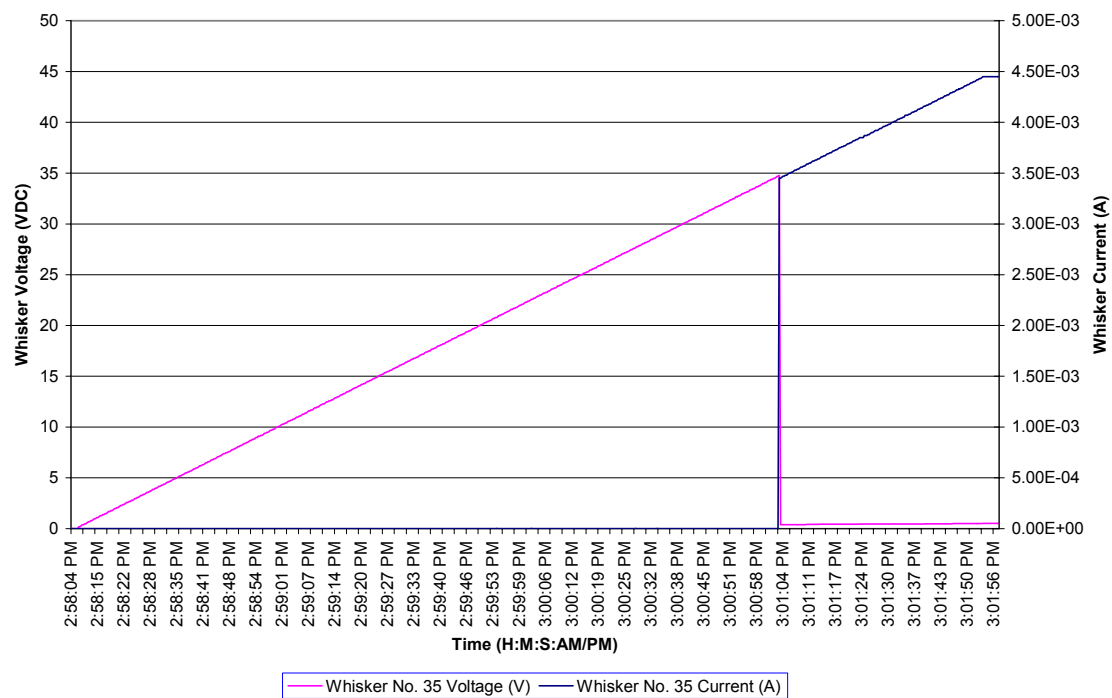
Whisker Breakdown Voltage POC Test Data



Whisker Breakdown Voltage POC Test Data



Whisker Breakdown Voltage POC Test Data



APPENDIX C

Full Experiment Breakdown Voltage Data

Whisker Number	Test Date	Sequence of Card Guide Selected	Card Guide Number	Card Guide Orientation	ATVC Serial Number	Breakdown Voltage
1	7/18/2007	1	15	Top	31	0.06
2	7/18/2007	1	15	Top	31	2.78
3	7/18/2007	1	15	Top	31	4.59
4	7/18/2007	1	15	Top	31	6.98
5	7/18/2007	1	15	Top	31	3.6
6	7/18/2007	1	15	Bottom	31	12.78
7	7/18/2007	1	15	Bottom	31	5.48
8	7/18/2007	1	15	Bottom	31	9.69
9	7/18/2007	1	15	Bottom	31	3.99
10	7/18/2007	1	15	Bottom	31	6.98
11	7/18/2007	2	2	Top	31	4.19
12	7/18/2007	2	2	Top	31	23.79
13	7/18/2007	2	2	Top	31	2.06
14	7/18/2007	2	2	Top	31	4.39
15	7/18/2007	2	2	Top	31	21.48
16	7/18/2007	2	2	Bottom	31	5.29
17	7/18/2007	2	2	Bottom	31	5.48
18	7/18/2007	2	2	Bottom	31	8.58
19	7/18/2007	2	2	Bottom	31	3.39
20	7/18/2007	2	2	Bottom	31	5.09
21	7/19/2007	3	28	Top	31	16.19
22	7/19/2007	3	28	Top	31	17.59
23	7/19/2007	3	28	Top	31	6.39
24	7/19/2007	3	28	Top	31	20.78
25	7/19/2007	3	28	Top	31	2.78

Whisker Number	Test Date	Sequence of Card Guide Selected	Card Guide Number	Card Guide Orientation	ATVC Serial Number	Breakdown Voltage
26	7/19/2007	3	28	Bottom	31	4.19
27	7/19/2007	3	28	Bottom	31	2.98
28	7/19/2007	3	28	Bottom	31	13.58
29	7/19/2007	3	28	Bottom	31	4.77
30	7/19/2007	3	28	Bottom	31	3.47
31	7/19/2007	4	24	Top	31	7.88
32	7/19/2007	4	24	Top	31	3.49
33	7/19/2007	4	24	Top	31	5.3
34	7/19/2007	4	24	Top	31	3.48
35	7/19/2007	4	24	Top	31	12.98
36	7/19/2007	4	24	Bottom	31	3.28
37	7/19/2007	4	24	Bottom	31	3.68
38	7/19/2007	4	24	Bottom	31	3.29
39	7/19/2007	4	24	Bottom	31	15.59
40	7/19/2007	4	24	Bottom	31	2.39
41	7/20/2007	5	25	Top	31	3.3
42	7/20/2007	5	25	Top	31	3.09
43	7/20/2007	5	25	Top	31	5.19
44	7/20/2007	5	25	Top	31	5.09
45	7/20/2007	5	25	Top	31	2.79
46	7/20/2007	5	25	Bottom	31	41.15
47	7/20/2007	5	25	Bottom	31	3.98
48	7/20/2007	5	25	Bottom	31	11.79
49	7/20/2007	5	25	Bottom	31	Censored
50	7/20/2007	5	25	Bottom	31	5.77

Whisker Number	Test Date	Sequence of Card Guide Selected	Card Guide Number	Card Guide Orientation	ATVC Serial Number	Breakdown Voltage
51	7/20/2007	6	3	Top	31	5.37
52	7/20/2007	6	3	Top	31	2.97
53	7/20/2007	6	3	Top	31	3.6
54	7/20/2007	6	3	Top	31	9.79
55	7/20/2007	6	3	Top	31	4.27
56	7/20/2007	6	3	Bottom	31	Censored
57	7/20/2007	6	3	Bottom	31	3.38
58	7/20/2007	6	3	Bottom	31	2.68
59	7/20/2007	6	3	Bottom	31	21.99
60	7/20/2007	6	3	Bottom	31	3.19
61	7/23/2007	7	22	Top	31	6.19
62	7/23/2007	7	22	Top	31	8.19
63	7/23/2007	7	22	Top	31	4.69
64	7/23/2007	7	22	Top	31	2.65
65	7/23/2007	7	22	Top	31	6.2
66	7/23/2007	7	22	Bottom	31	31.18
67	7/23/2007	7	22	Bottom	31	25.67
68	7/23/2007	7	22	Bottom	31	4.58
69	7/23/2007	7	22	Bottom	31	3.09
70	7/23/2007	7	22	Bottom	31	4.25
71	7/23/2007	8	21	Top	31	2.58
72	7/23/2007	8	21	Top	31	5.39
73	7/23/2007	8	21	Top	31	2.57
74	7/23/2007	8	21	Top	31	6.98
75	7/23/2007	8	21	Top	31	2.58

Whisker Number	Test Date	Sequence of Card Guide Selected	Card Guide Number	Card Guide Orientation	ATVC Serial Number	Breakdown Voltage
76	7/23/2007	8	21	Bottom	31	3.68
77	7/23/2007	8	21	Bottom	31	23.68
78	7/23/2007	8	21	Bottom	31	2.88
79	7/23/2007	8	21	Bottom	31	2.58
80	7/23/2007	8	21	Bottom	31	10.29
81	7/24/2007	9	4	Top	31	7.68
82	7/24/2007	9	4	Top	31	3.39
83	7/24/2007	9	4	Top	31	5.67
84	7/24/2007	9	4	Top	31	2.49
85	7/24/2007	9	4	Top	31	12.19
86	7/24/2007	9	4	Bottom	31	42.73
87	7/24/2007	9	4	Bottom	31	3.89
88	7/24/2007	9	4	Bottom	31	6.08
89	7/24/2007	9	4	Bottom	31	3.79
90	7/24/2007	9	4	Bottom	31	2.98
91	7/24/2007	10	8	Top	31	8.38
92	7/24/2007	10	8	Top	31	2.58
93	7/24/2007	10	8	Top	31	3.54
94	7/24/2007	10	8	Top	31	6.59
95	7/24/2007	10	8	Top	31	4.68
96	7/24/2007	10	8	Bottom	31	9.3
97	7/24/2007	10	8	Bottom	31	2.77
98	7/24/2007	10	8	Bottom	31	5.78
99	7/24/2007	10	8	Bottom	31	21.39
100	7/24/2007	10	8	Bottom	31	6.9

Whisker Number	Test Date	Sequence of Card Guide Selected	Card Guide Number	Card Guide Orientation	ATVC Serial Number	Breakdown Voltage
101	7/25/2007	1	8	Top	33	5.78
102	7/25/2007	1	8	Top	33	11.19
103	7/25/2007	1	8	Top	33	8.38
104	7/25/2007	1	8	Top	33	12.5
105	7/25/2007	1	8	Top	33	9.99
106	7/25/2007	1	8	Bottom	33	4.28
107	7/25/2007	1	8	Bottom	33	3.17
108	7/25/2007	1	8	Bottom	33	20.19
109	7/25/2007	1	8	Bottom	33	12.98
110	7/25/2007	1	8	Bottom	33	4.4
111	7/25/2007	2	13	Top	33	3.3
112	7/25/2007	2	13	Top	33	2.88
113	7/25/2007	2	13	Top	33	12.38
114	7/25/2007	2	13	Top	33	4.28
115	7/25/2007	2	13	Top	33	7.99
116	7/25/2007	2	13	Bottom	33	14.78
117	7/25/2007	2	13	Bottom	33	7.09
118	7/25/2007	2	13	Bottom	33	3.18
119	7/25/2007	2	13	Bottom	33	8.39
120	7/25/2007	2	13	Bottom	33	37.96
121	7/26/2007	3	18	Top	33	4.08
122	7/26/2007	3	18	Top	33	5.1
123	7/26/2007	3	18	Top	33	5.59
124	7/26/2007	3	18	Top	33	2.78
125	7/26/2007	3	18	Top	33	5.39

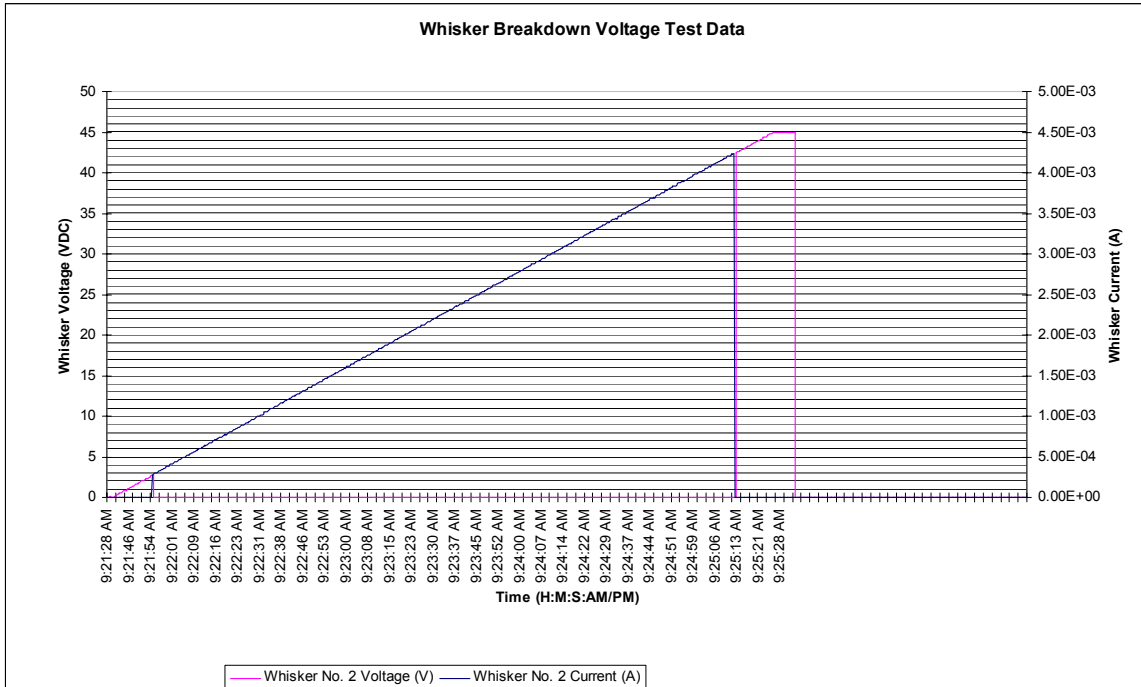
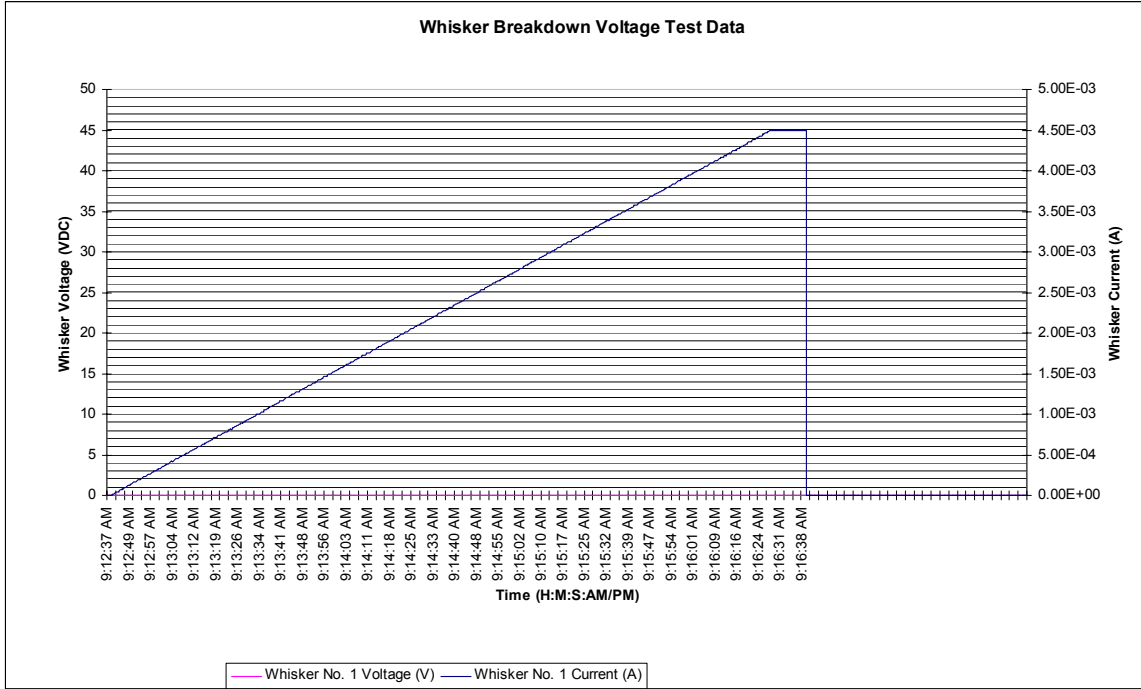
Whisker Number	Test Date	Sequence of Card Guide Selected	Card Guide Number	Card Guide Orientation	ATVC Serial Number	Breakdown Voltage
126	7/26/2007	3	18	Bottom	33	22.78
127	7/26/2007	3	18	Bottom	33	26.18
128	7/26/2007	3	18	Bottom	33	4.19
129	7/26/2007	3	18	Bottom	33	3.88
130	7/26/2007	3	18	Bottom	33	2.69
131	7/26/2007	4	16	Top	33	4.88
132	7/26/2007	4	16	Top	33	3.59
133	7/26/2007	4	16	Top	33	3.68
134	7/26/2007	4	16	Top	33	7.79
135	7/26/2007	4	16	Top	33	5.29
136	7/26/2007	4	16	Bottom	33	12.78
137	7/26/2007	4	16	Bottom	33	28.89
138	7/26/2007	4	16	Bottom	33	6.19
139	7/26/2007	4	16	Bottom	33	3.3
140	7/26/2007	4	16	Bottom	33	7.78
141	7/27/2007	5	6	Top	33	21.59
142	7/27/2007	5	6	Top	33	2.57
143	7/27/2007	5	6	Top	33	2.69
144	7/27/2007	5	6	Top	33	4.39
145	7/27/2007	5	6	Top	33	11.89
146	7/27/2007	5	6	Bottom	33	9.29
147	7/27/2007	5	6	Bottom	33	3.99
148	7/27/2007	5	6	Bottom	33	6.39
149	7/27/2007	5	6	Bottom	33	3.38
150	7/27/2007	5	6	Bottom	33	21.87

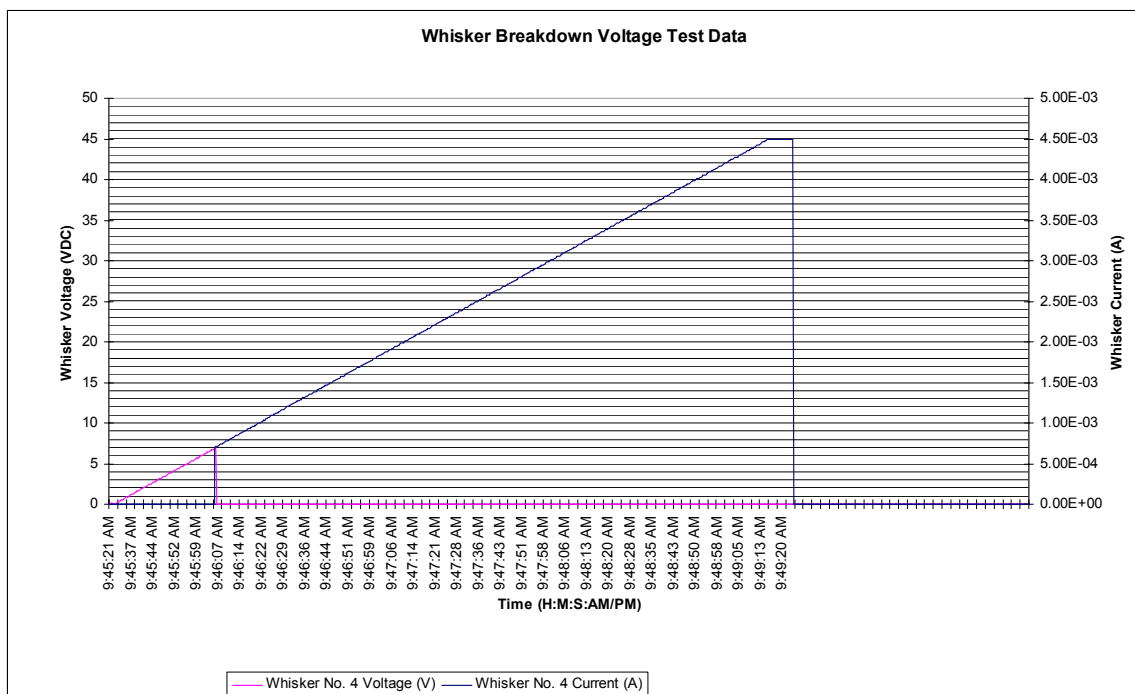
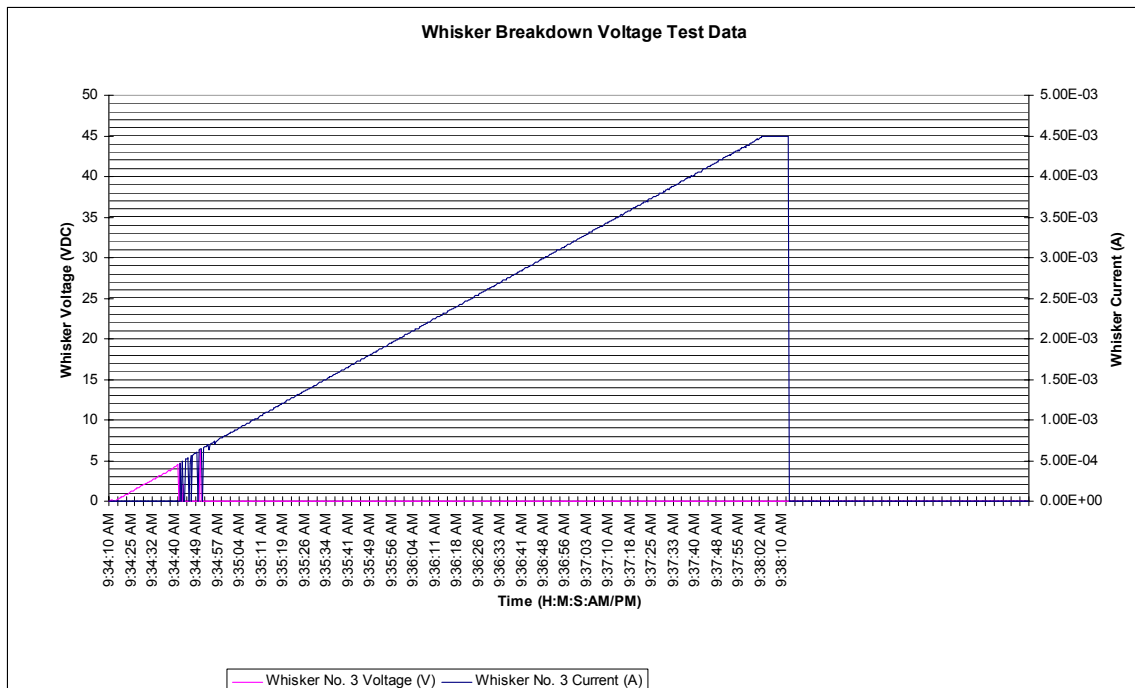
Whisker Number	Test Date	Sequence of Card Guide Selected	Card Guide Number	Card Guide Orientation	ATVC Serial Number	Breakdown Voltage
151	7/27/2007	6	23	Top	33	3.29
152	7/27/2007	6	23	Top	33	3.88
153	7/27/2007	6	23	Top	33	4.58
154	7/27/2007	6	23	Top	33	3.19
155	7/27/2007	6	23	Top	33	9.29
156	7/27/2007	6	23	Bottom	33	13.29
157	7/27/2007	6	23	Bottom	33	4.89
158	7/27/2007	6	23	Bottom	33	4.88
159	7/27/2007	6	23	Bottom	33	3.88
160	7/27/2007	6	23	Bottom	33	18.07
161	7/30/2007	7	2	Top	33	4.58
162	7/30/2007	7	2	Top	33	3.3
163	7/30/2007	7	2	Top	33	13.58
164	7/30/2007	7	2	Top	33	6.89
165	7/30/2007	7	2	Top	33	4.99
166	7/30/2007	7	2	Bottom	33	4.55
167	7/30/2007	7	2	Bottom	33	2.88
168	7/30/2007	7	2	Bottom	33	36.06
169	7/30/2007	7	2	Bottom	33	4.28
170	7/30/2007	7	2	Bottom	33	5.48
171	7/30/2007	8	14	Top	33	4.39
172	7/30/2007	8	14	Top	33	2.98
173	7/30/2007	8	14	Top	33	6.48
174	7/30/2007	8	14	Top	33	3.79
175	7/30/2007	8	14	Top	33	10.89

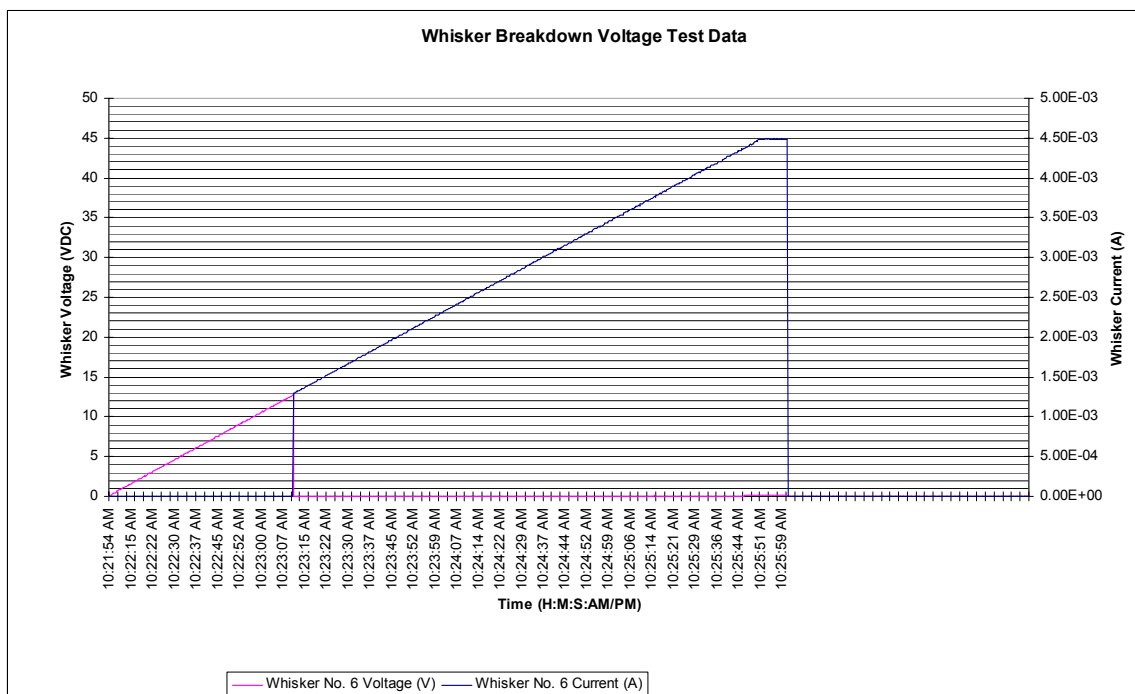
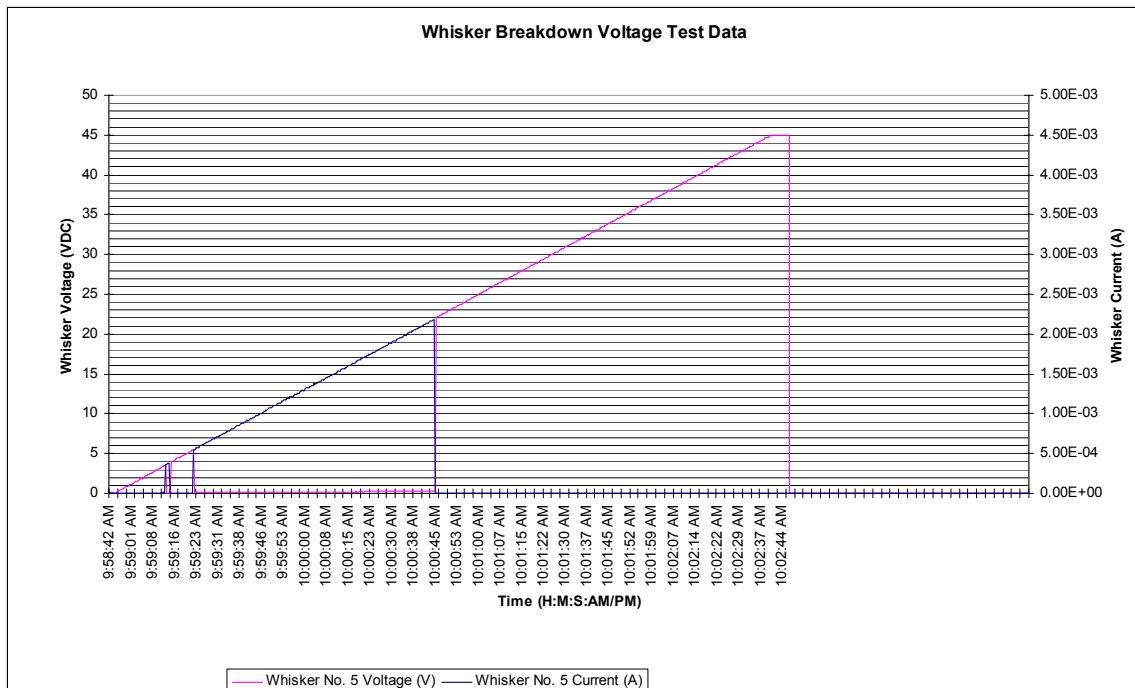
Whisker Number	Test Date	Sequence of Card Guide Selected	Card Guide Number	Card Guide Orientation	ATVC Serial Number	Breakdown Voltage
176	7/30/2007	8	14	Bottom	33	7.78
177	7/30/2007	8	14	Bottom	33	2.89
178	7/30/2007	8	14	Bottom	33	23.67
179	7/30/2007	8	14	Bottom	33	2.39
180	7/30/2007	8	14	Bottom	33	1.39
181	7/31/2007	9	9	Top	33	8.77
182	7/31/2007	9	9	Top	33	3.67
183	7/31/2007	9	9	Top	33	3.99
184	7/31/2007	9	9	Top	33	15.3
185	7/31/2007	9	9	Top	33	7.2
186	7/31/2007	9	9	Bottom	33	3.88
187	7/31/2007	9	9	Bottom	33	0.99
188	7/31/2007	9	9	Bottom	33	4.78
189	7/31/2007	9	9	Bottom	33	3.39
190	7/31/2007	9	9	Bottom	33	2.78
191	7/31/2007	10	21	Top	33	4.28
192	7/31/2007	10	21	Top	33	3.99
193	7/31/2007	10	21	Top	33	2.58
194	7/31/2007	10	21	Top	33	5.79
195	7/31/2007	10	21	Top	33	4.39
196	7/31/2007	10	21	Bottom	33	4.69
197	7/31/2007	10	21	Bottom	33	25.58
198	7/31/2007	10	21	Bottom	33	16.36
199	7/31/2007	10	21	Bottom	33	22.37
200	7/31/2007	10	21	Bottom	33	7.78

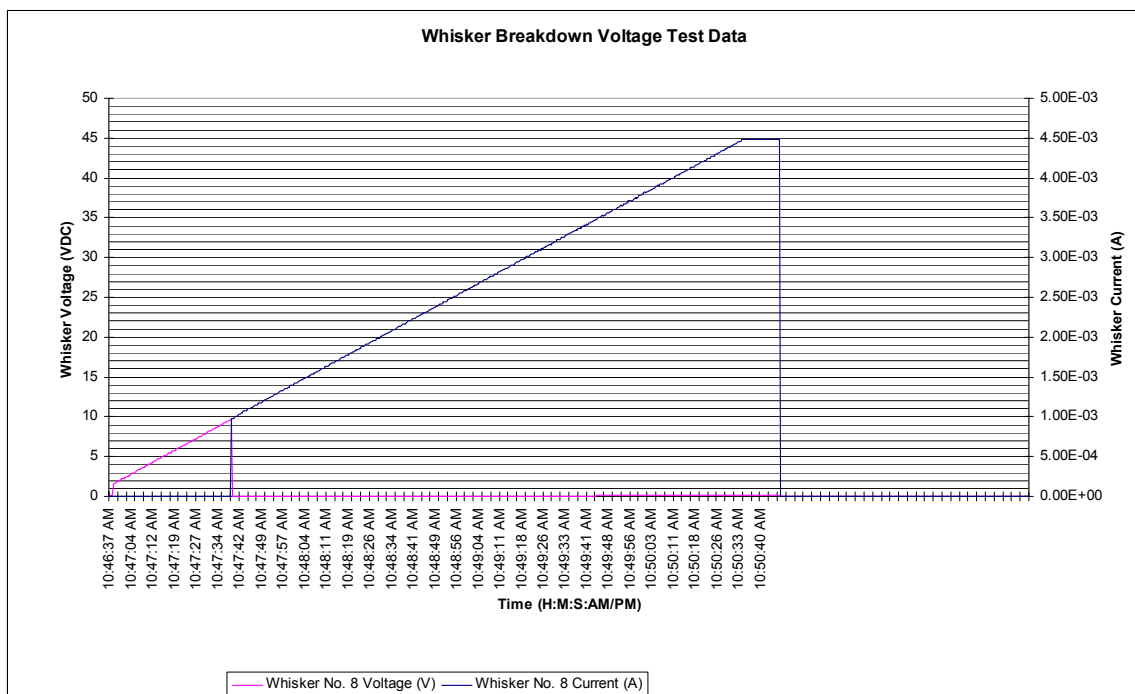
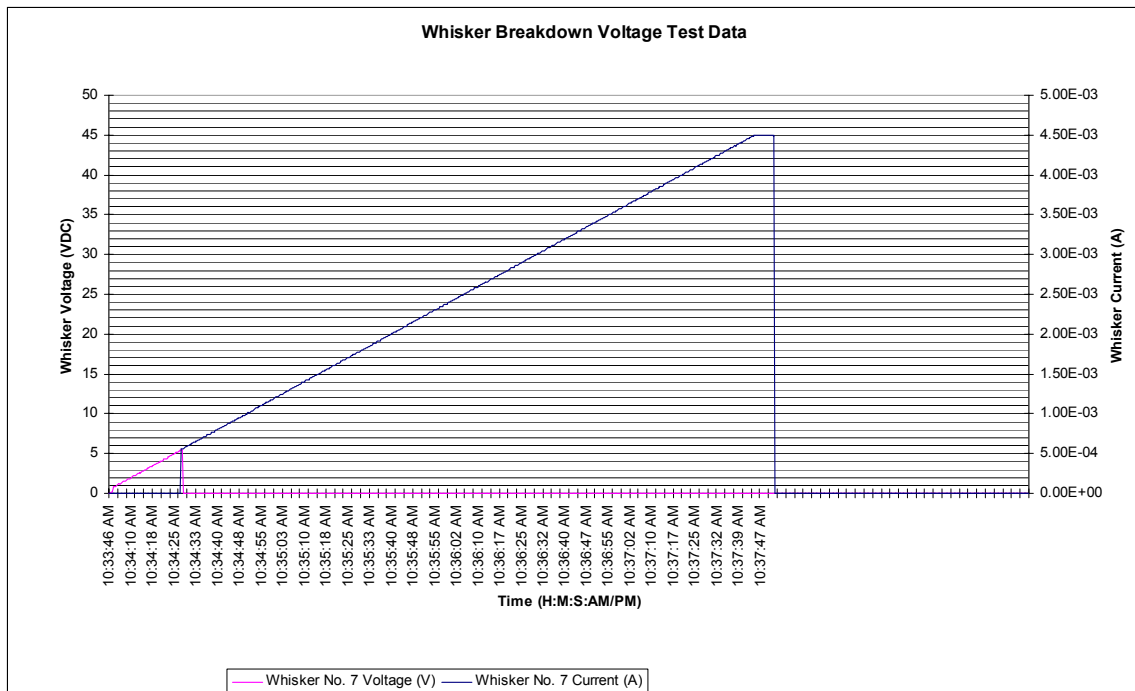
APPENDIX D

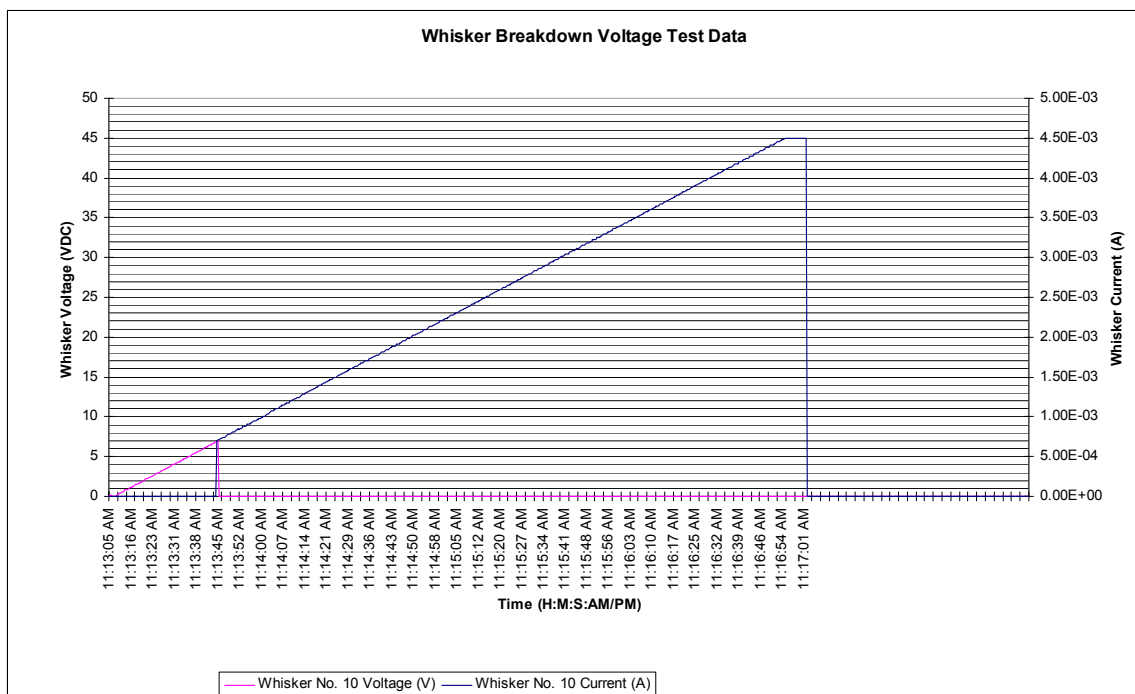
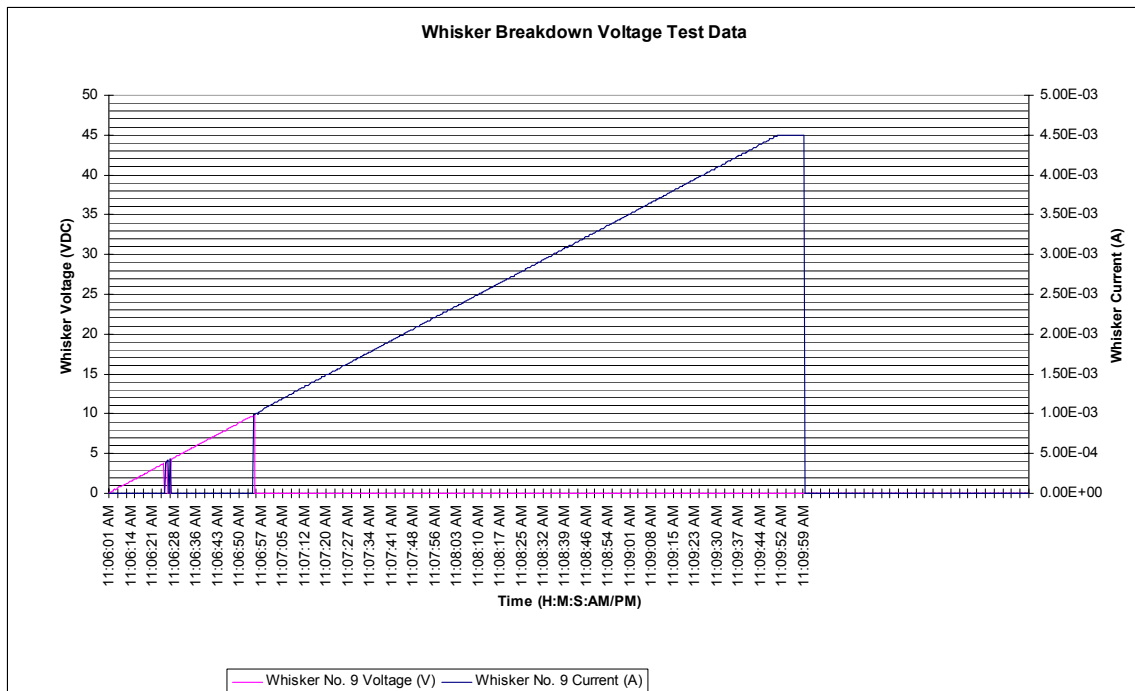
Full Experiment Tin Whisker Data Graphs

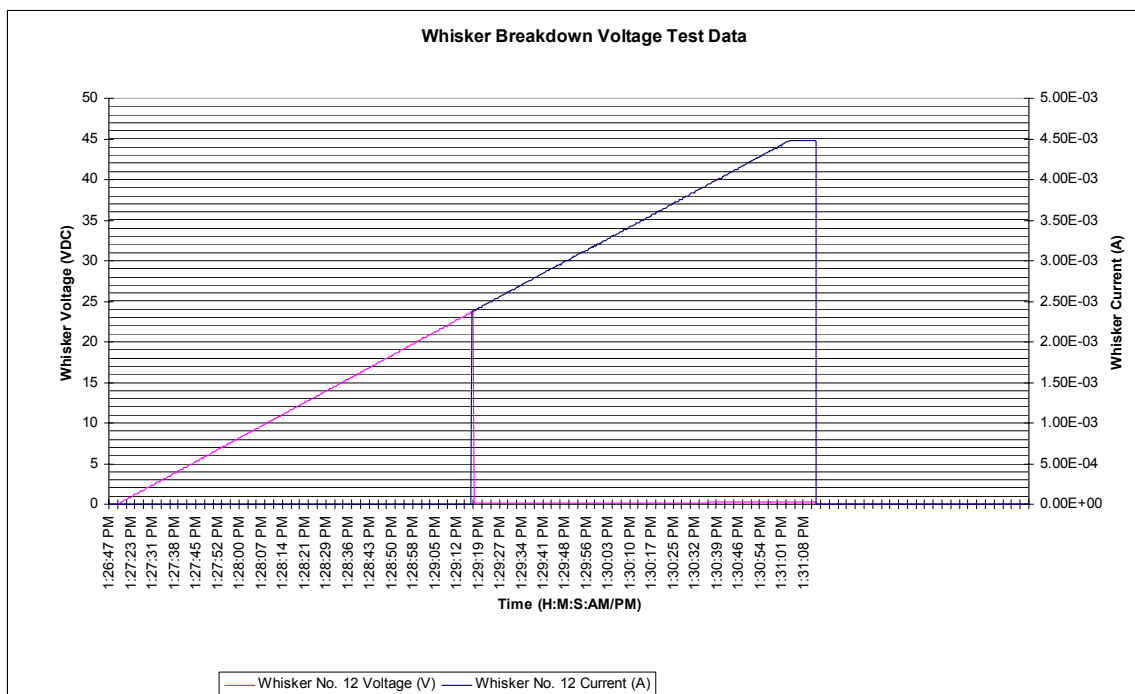
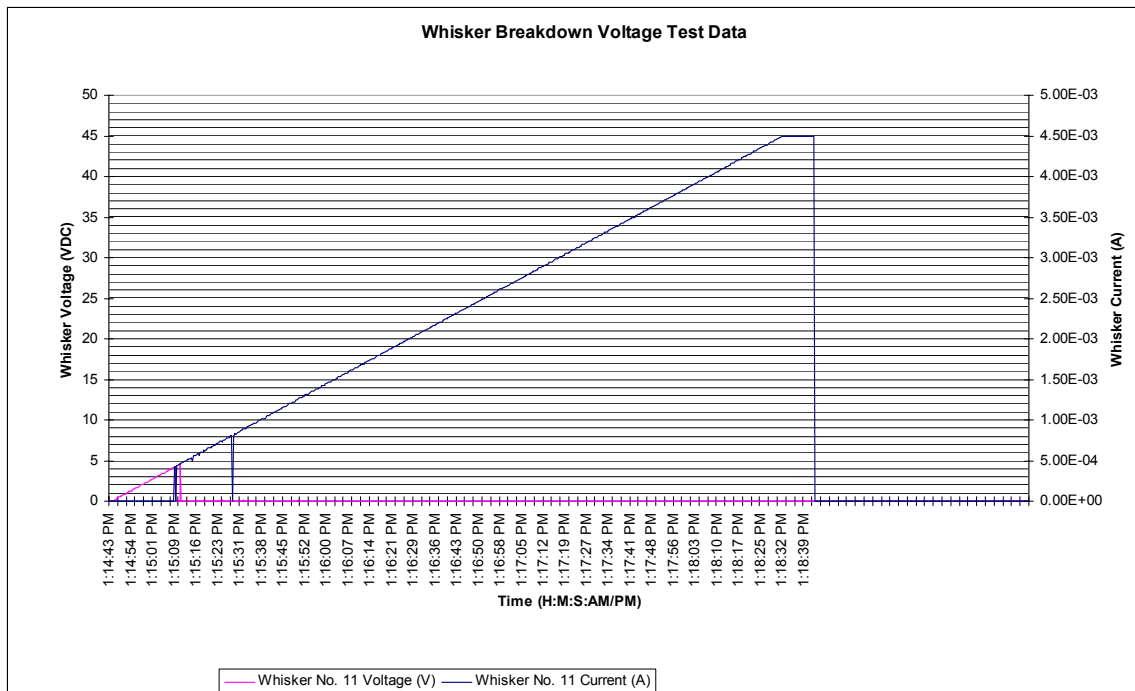


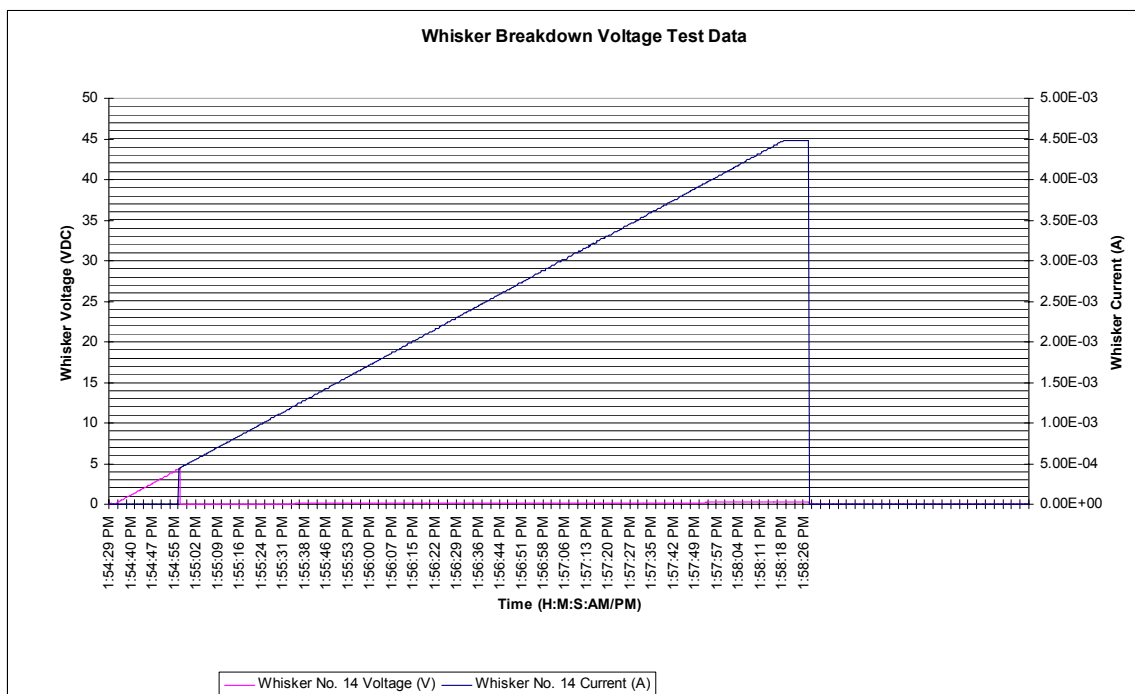
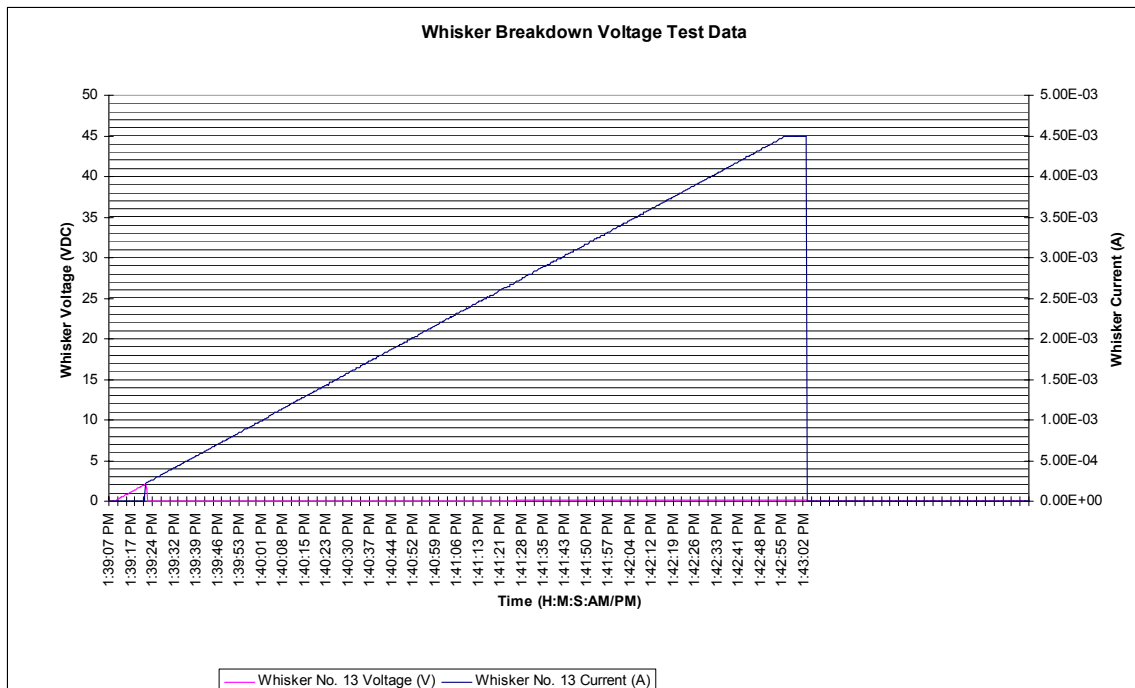


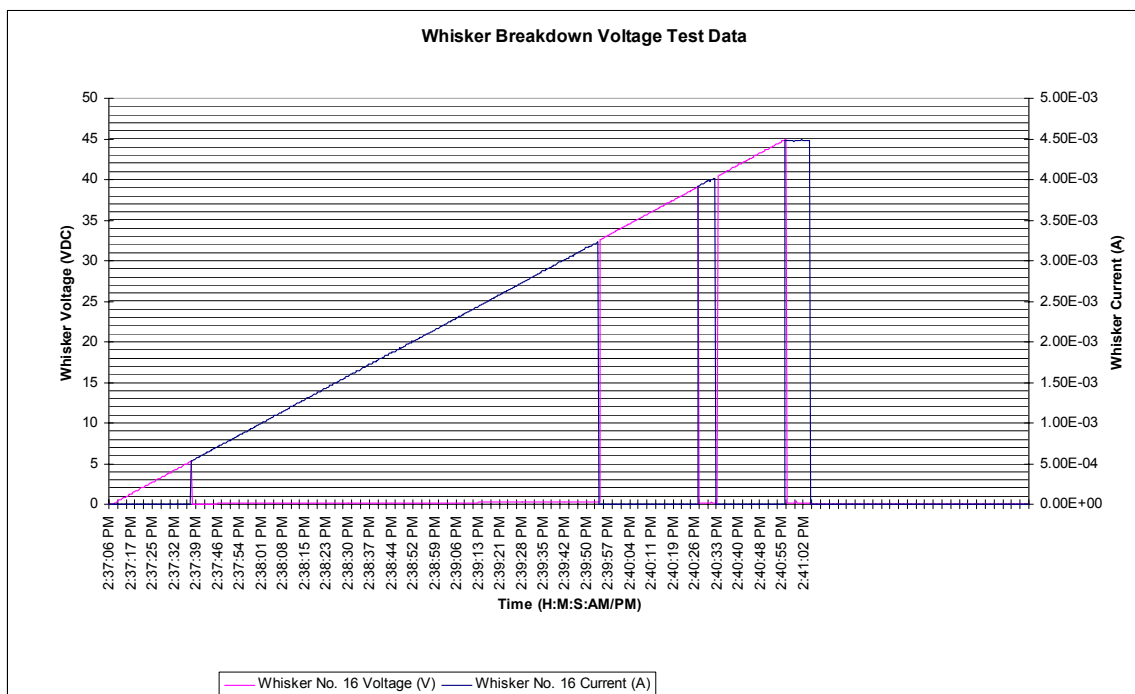
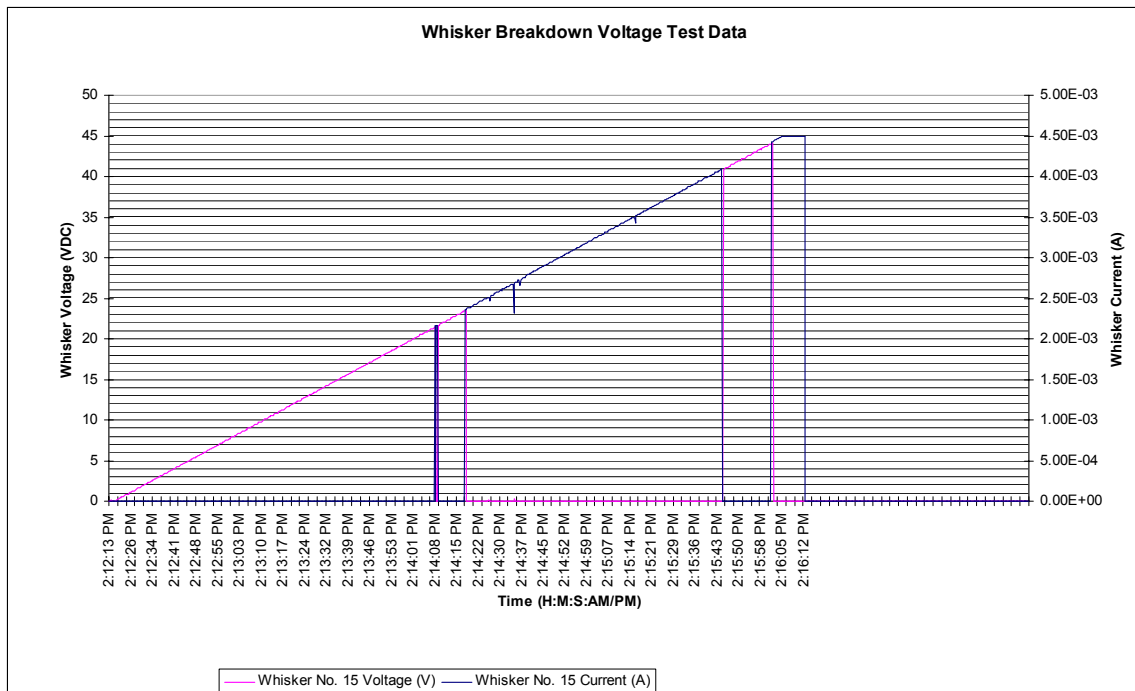


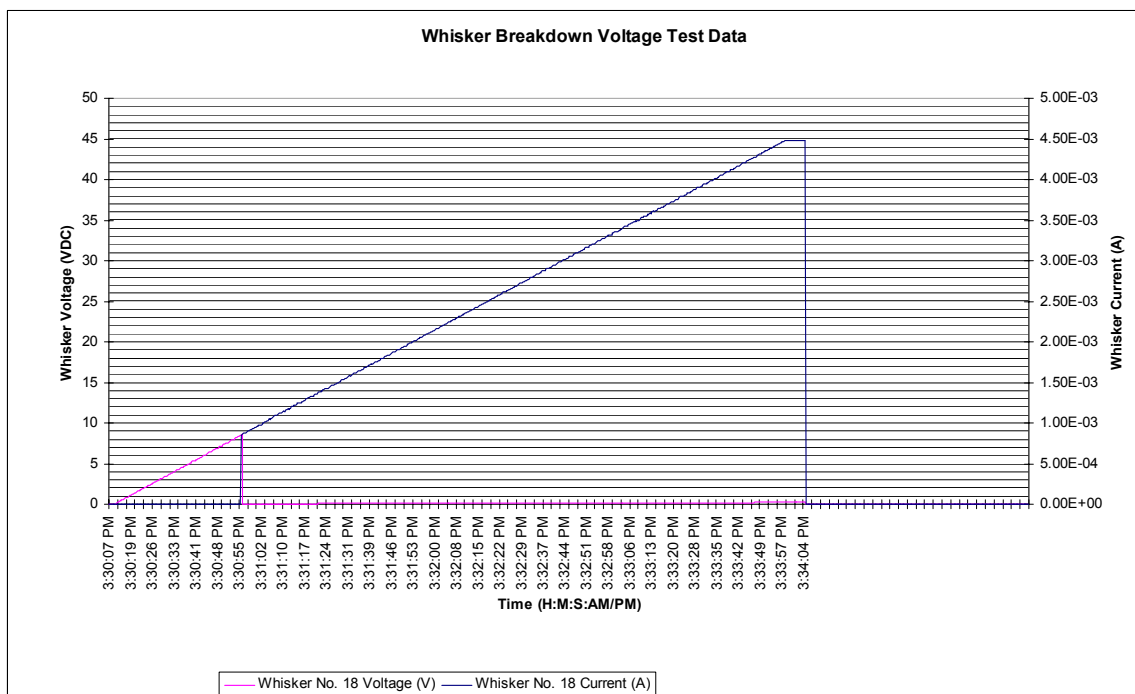
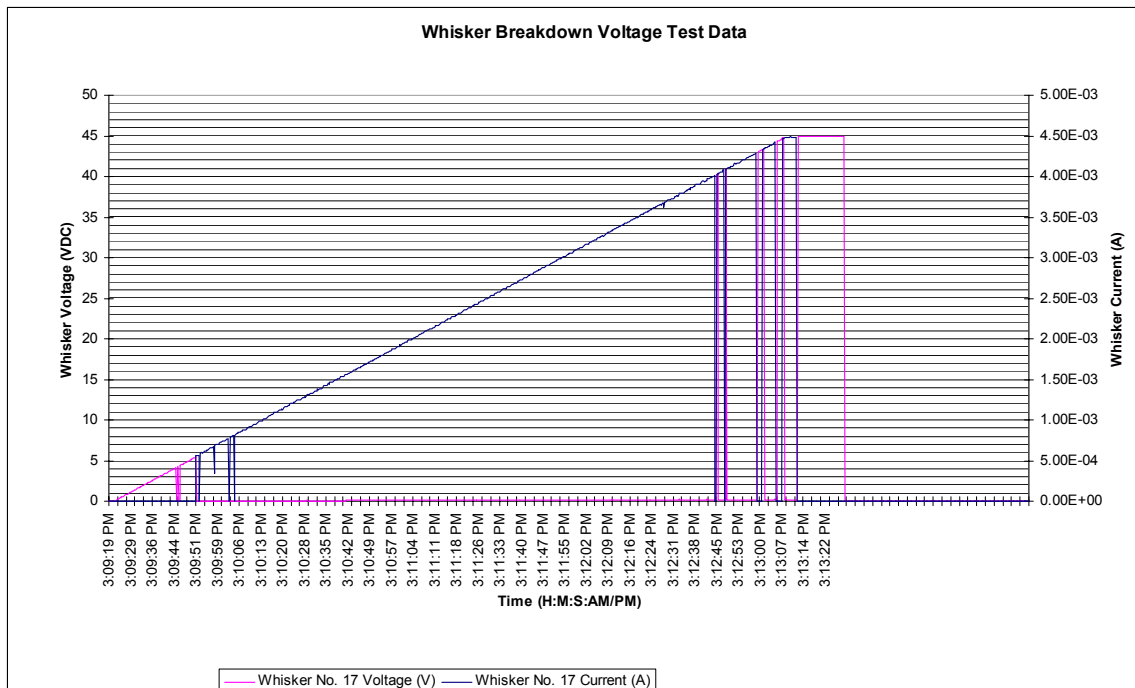


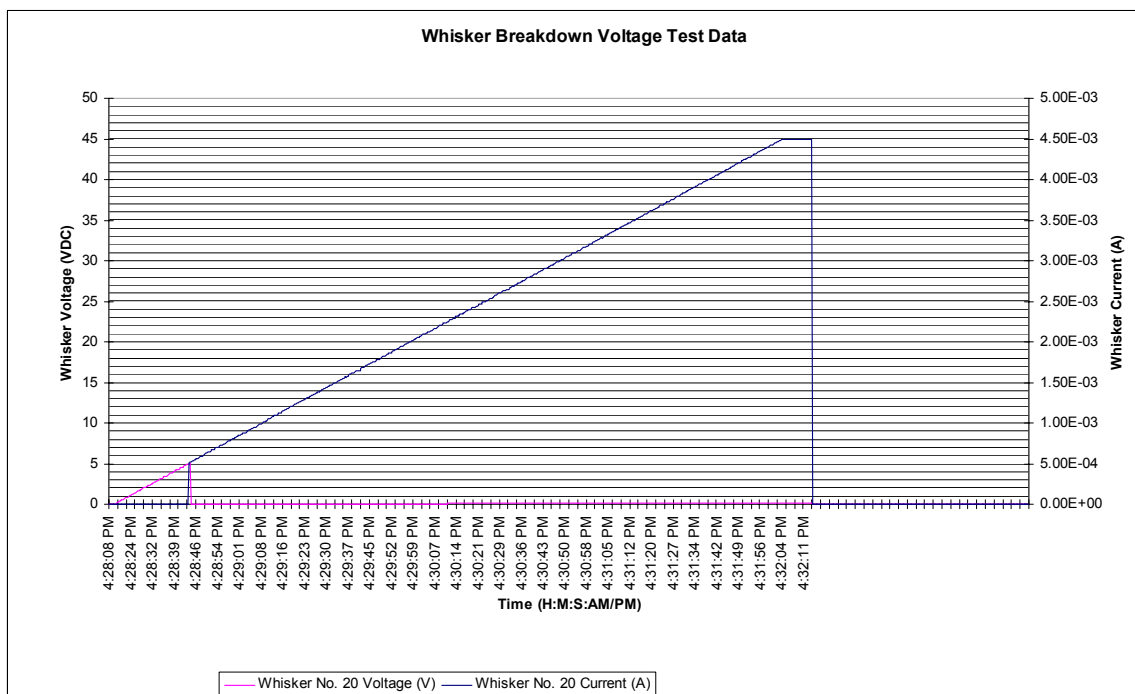
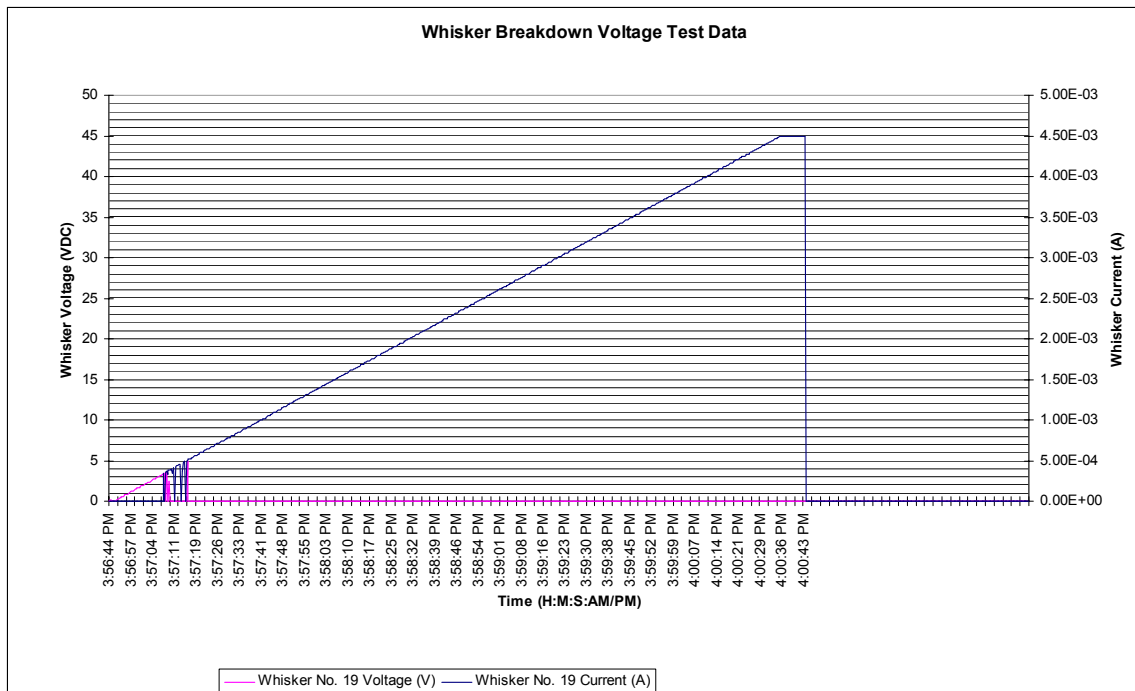


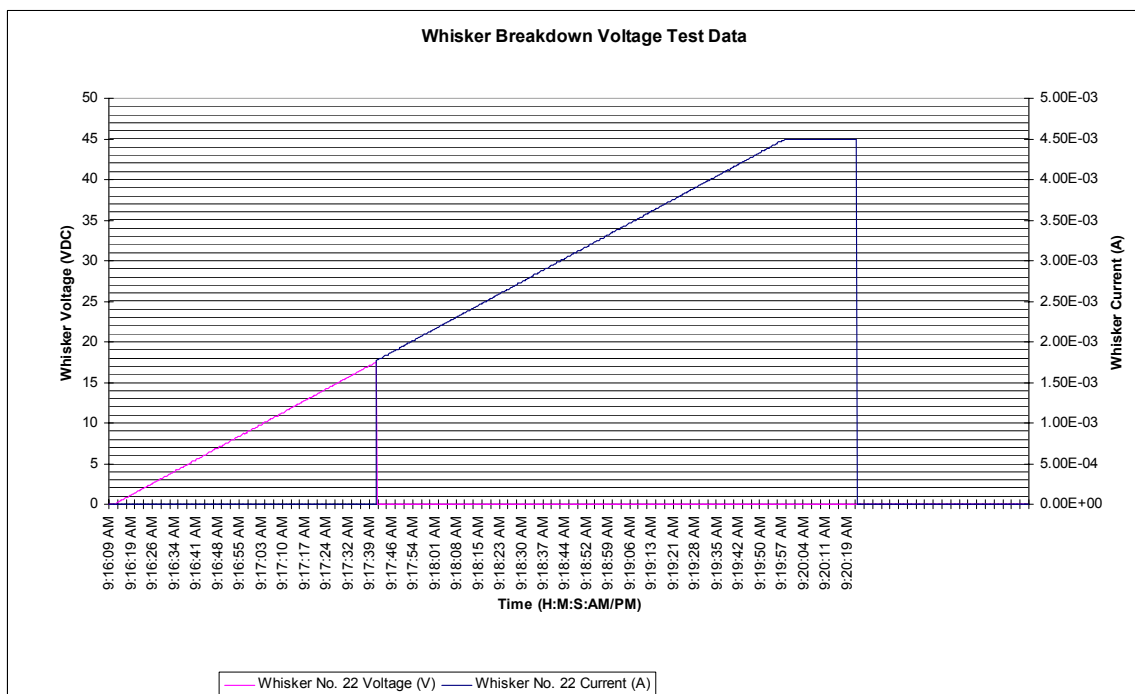
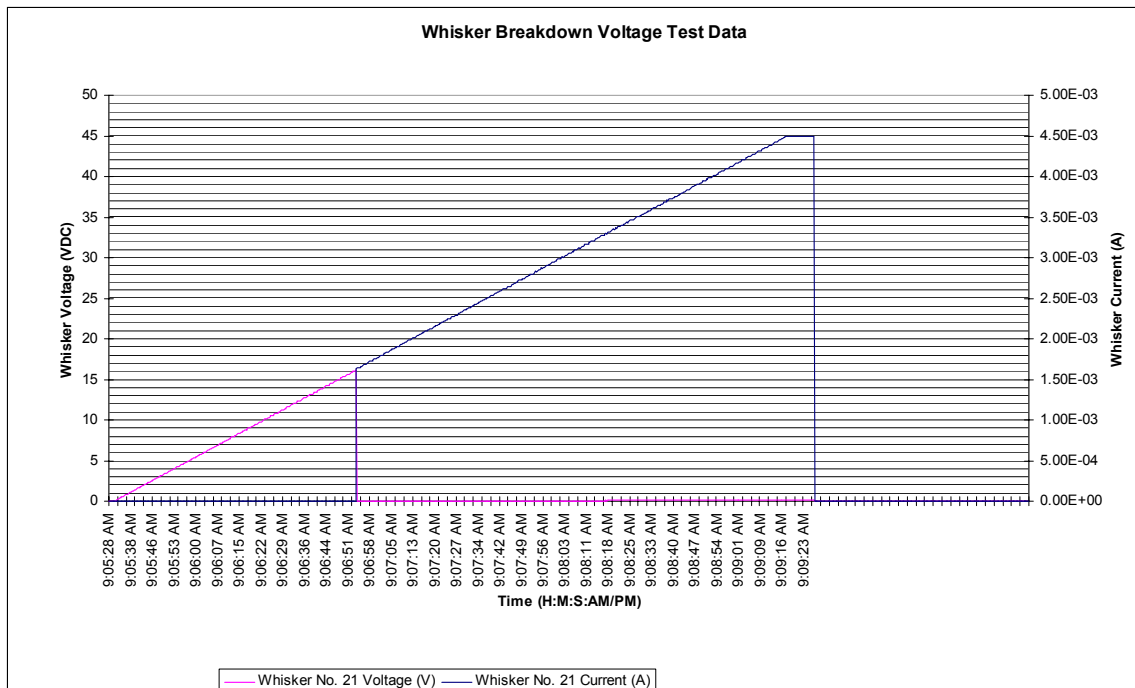


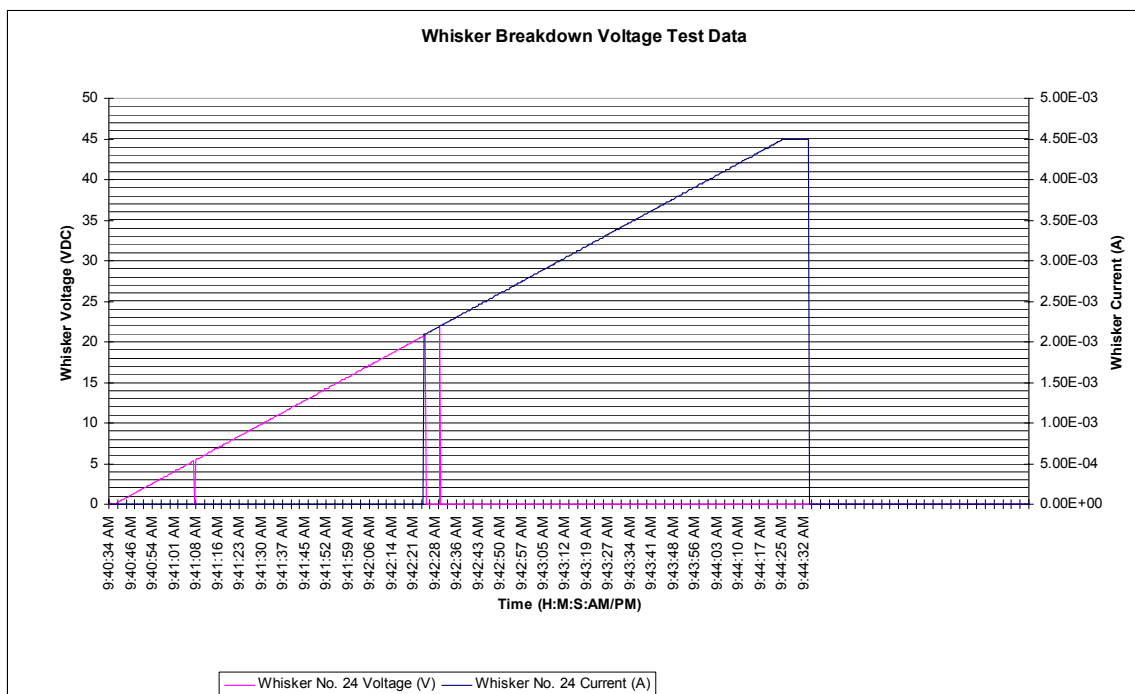
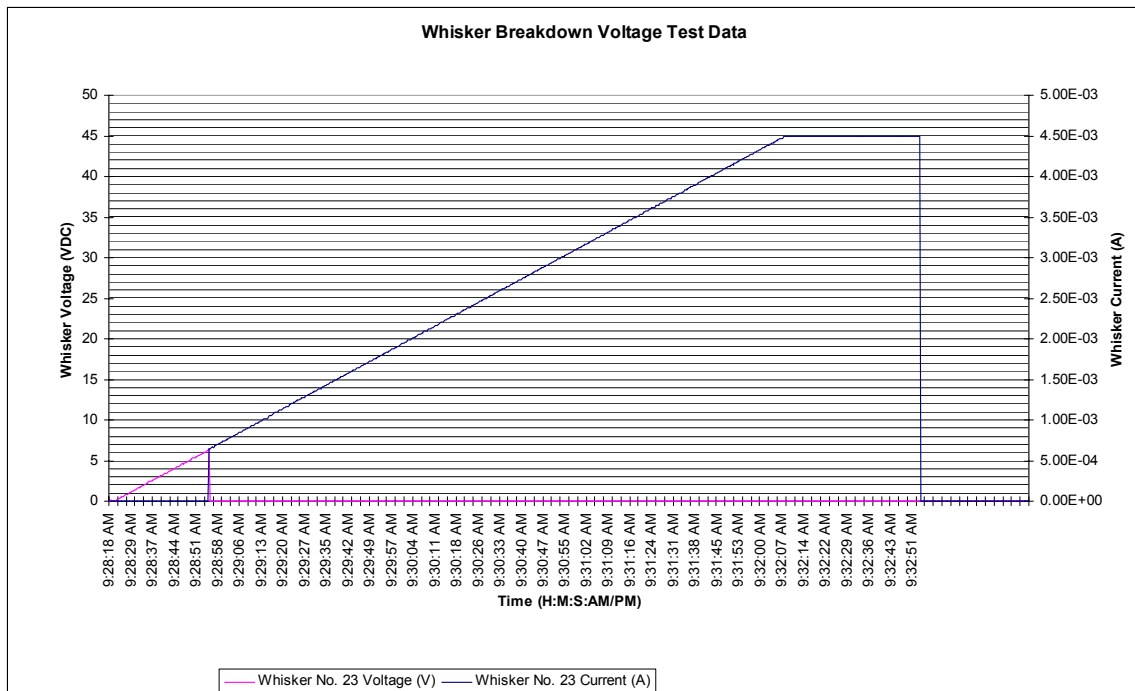


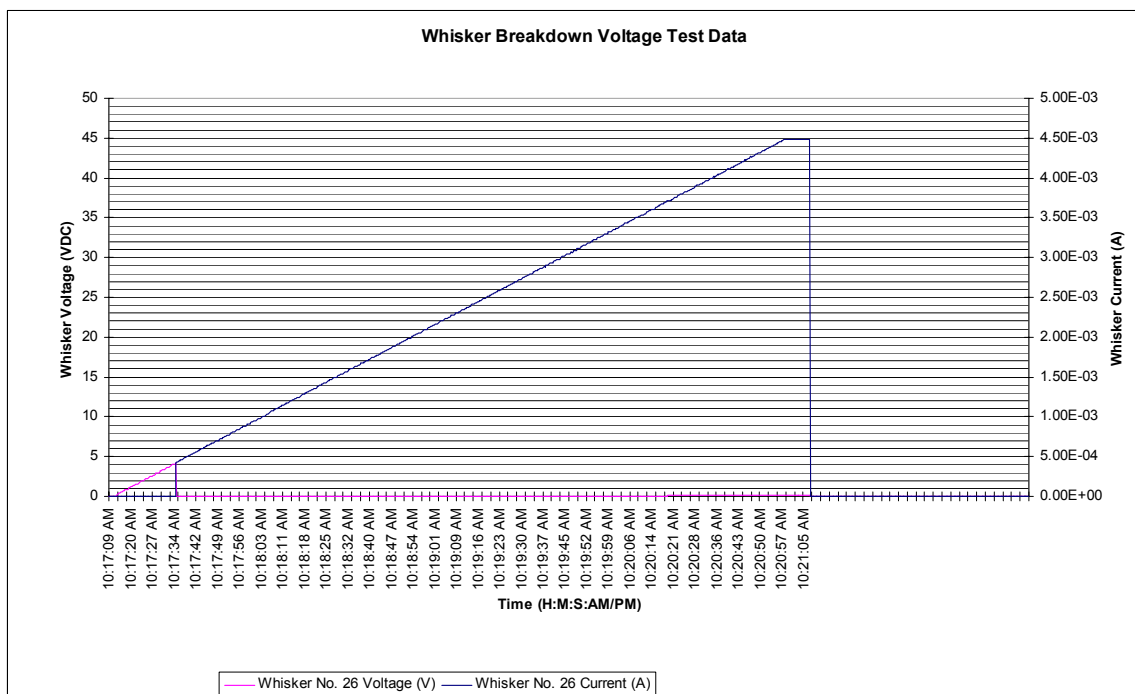
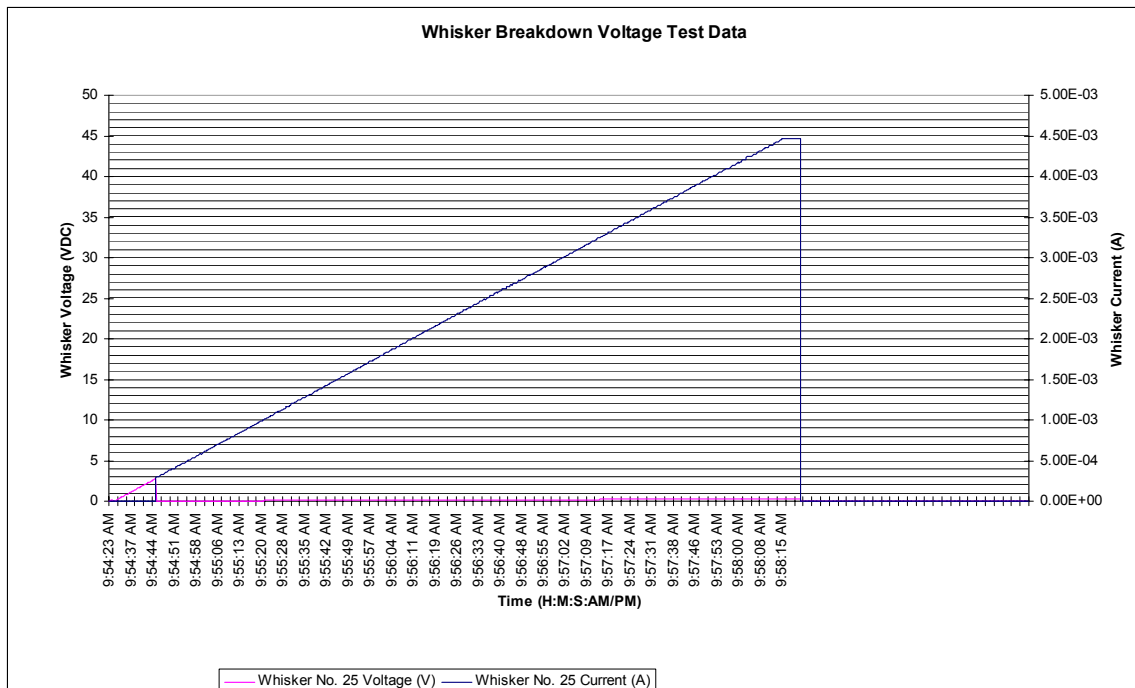


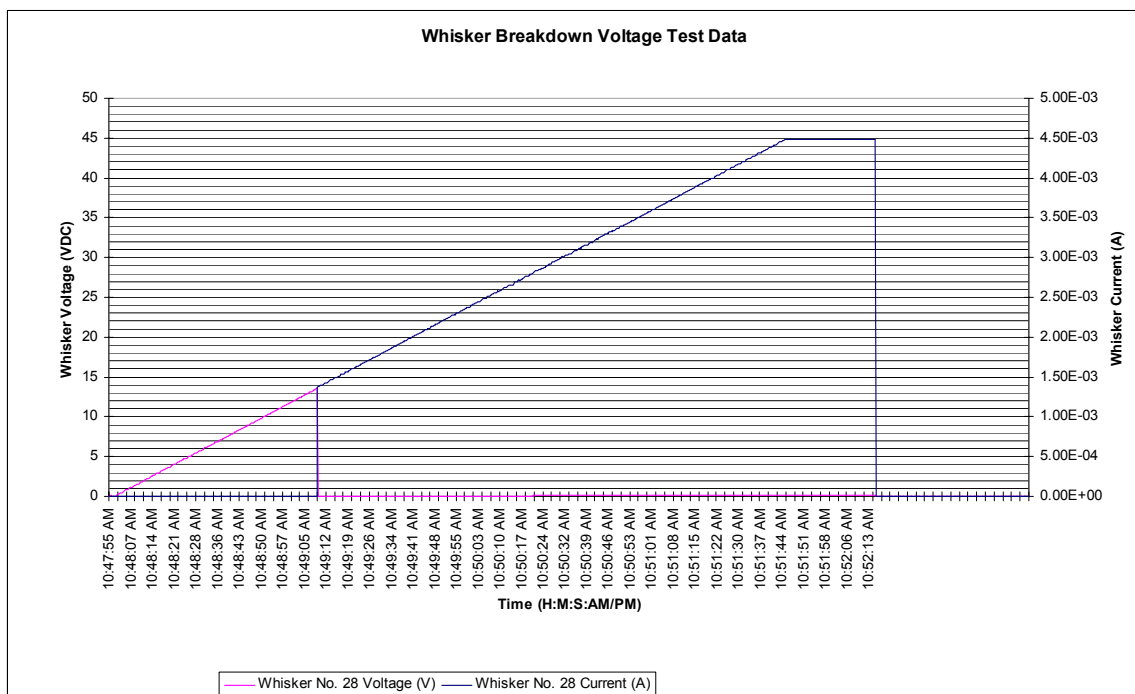
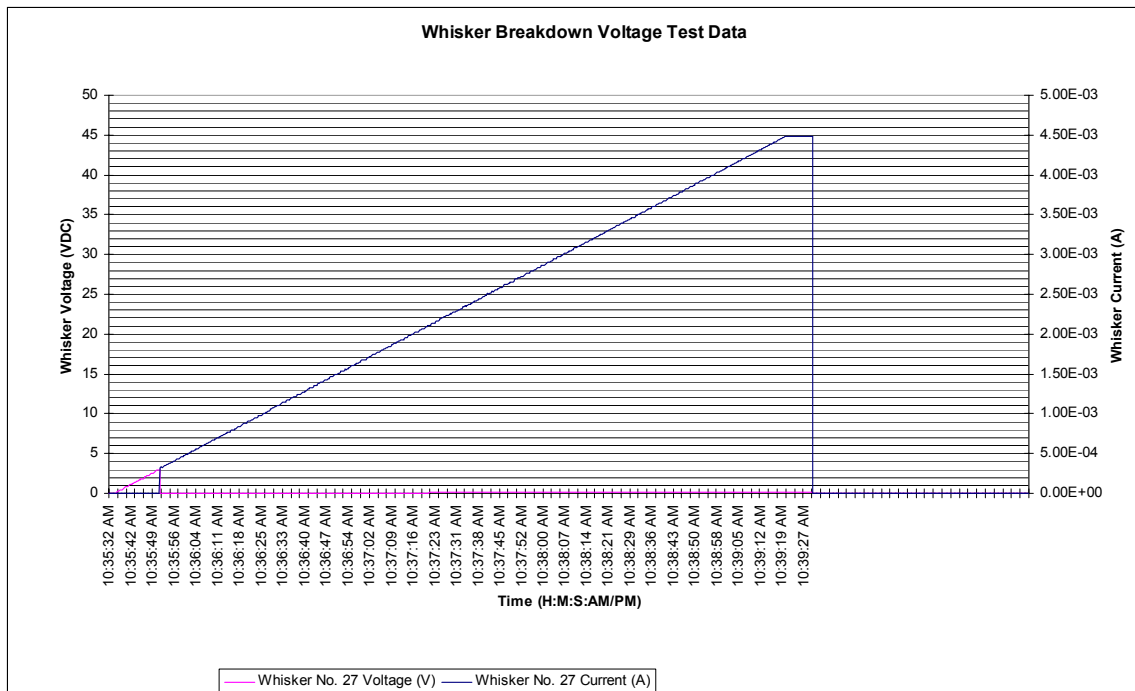


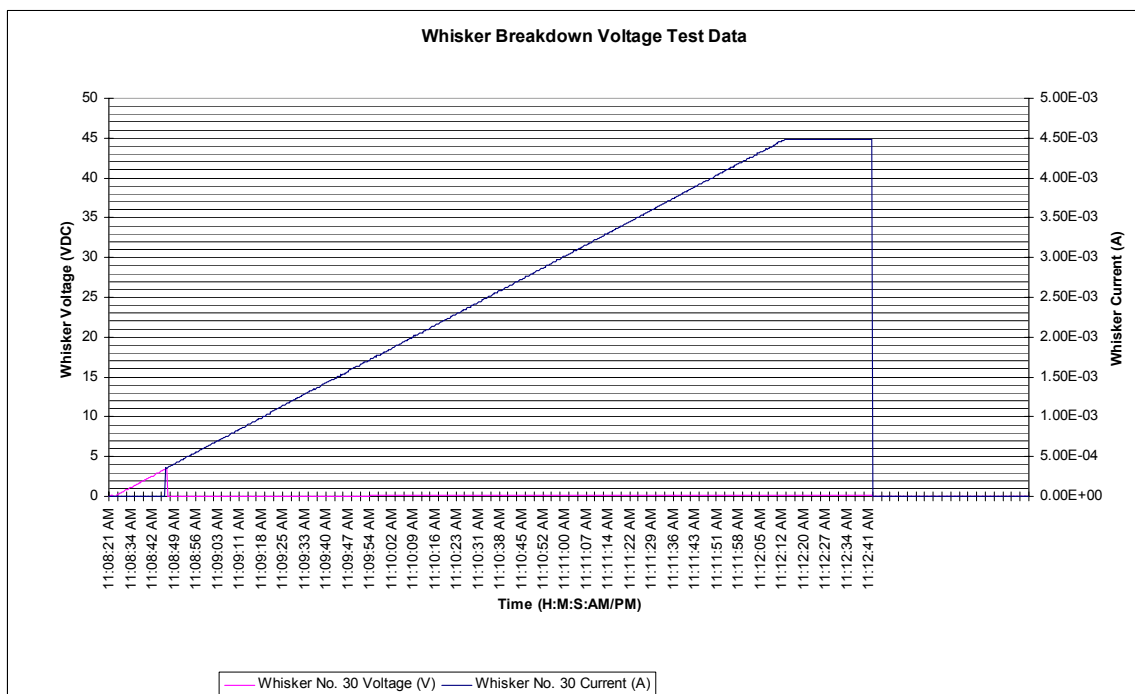
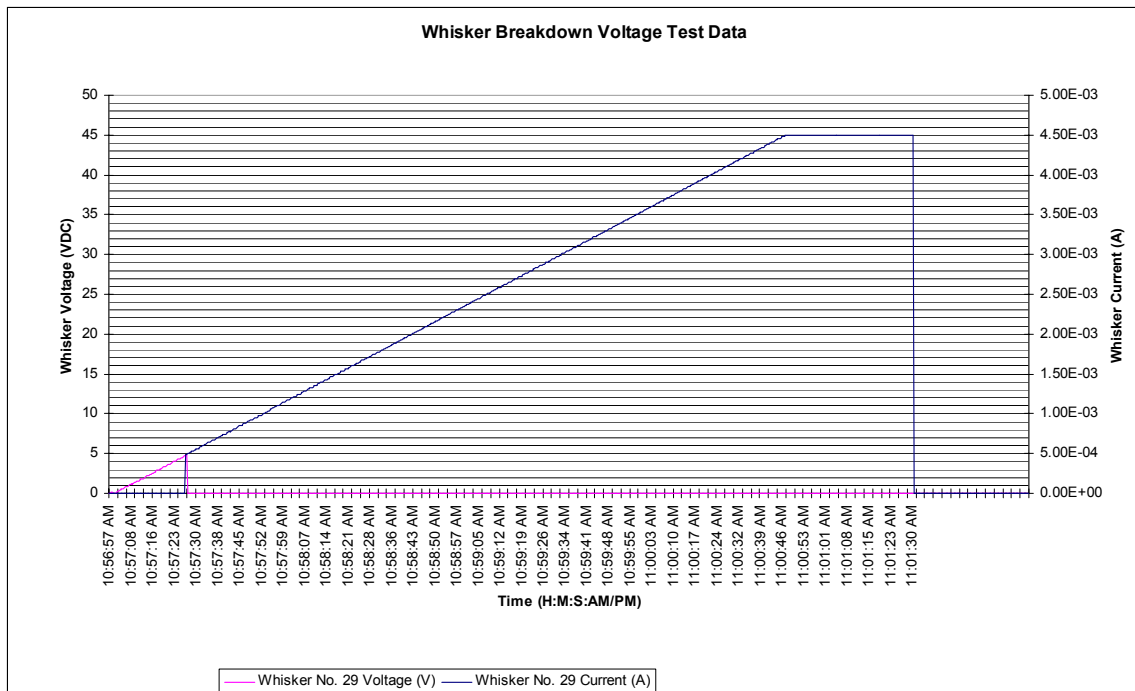


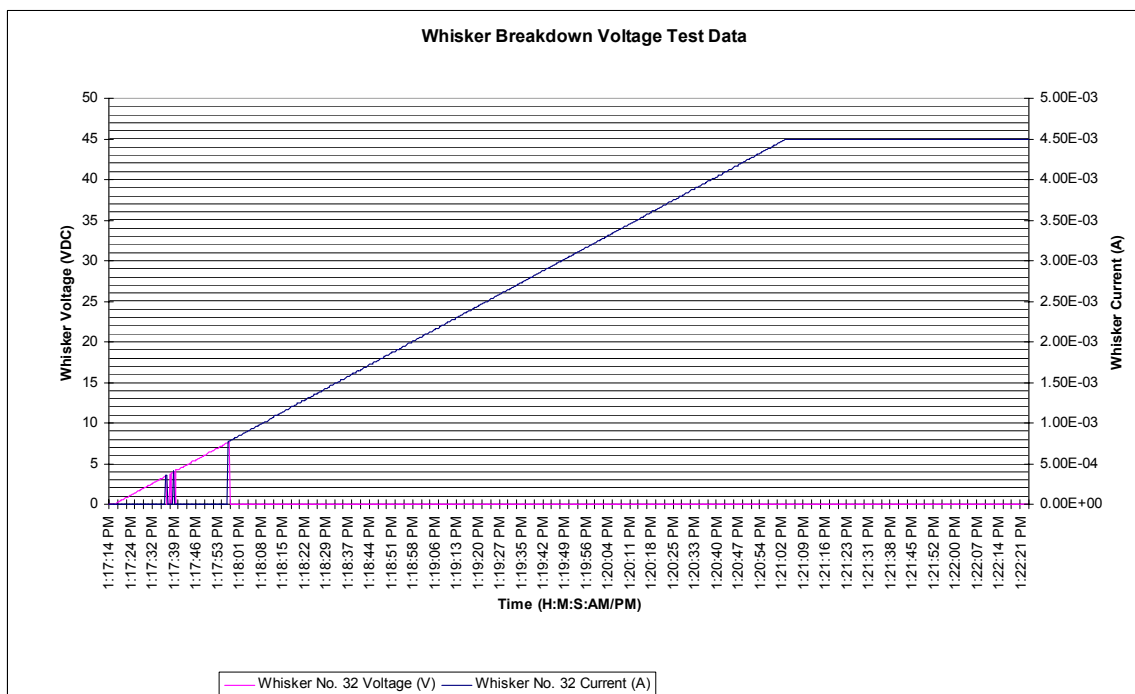
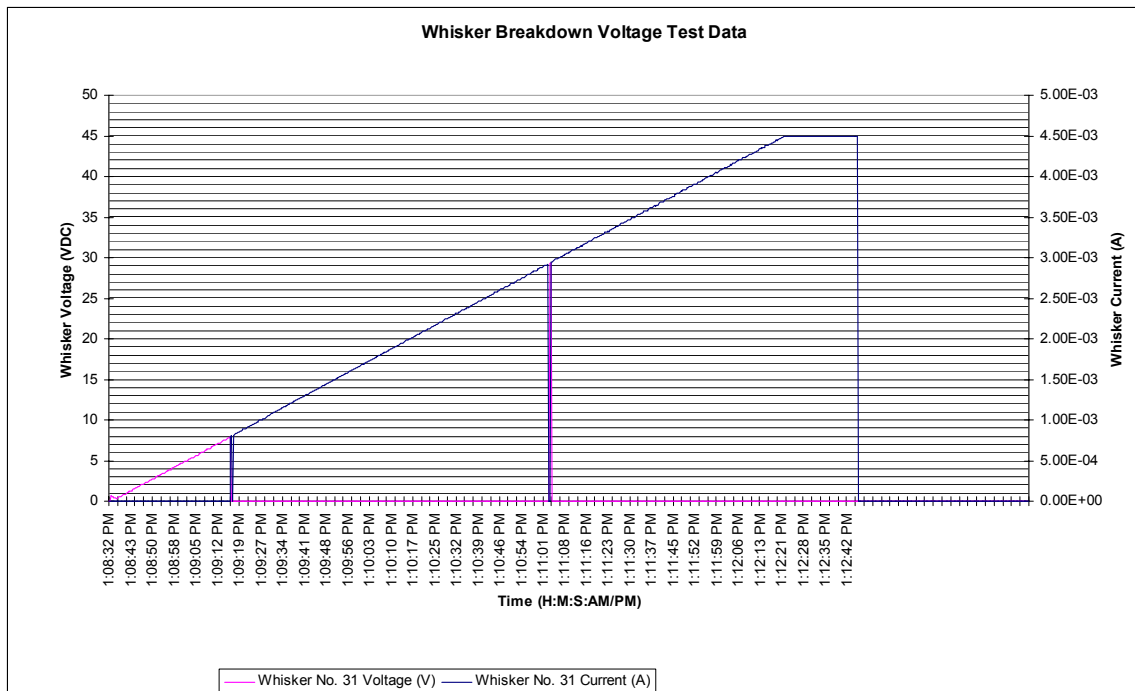


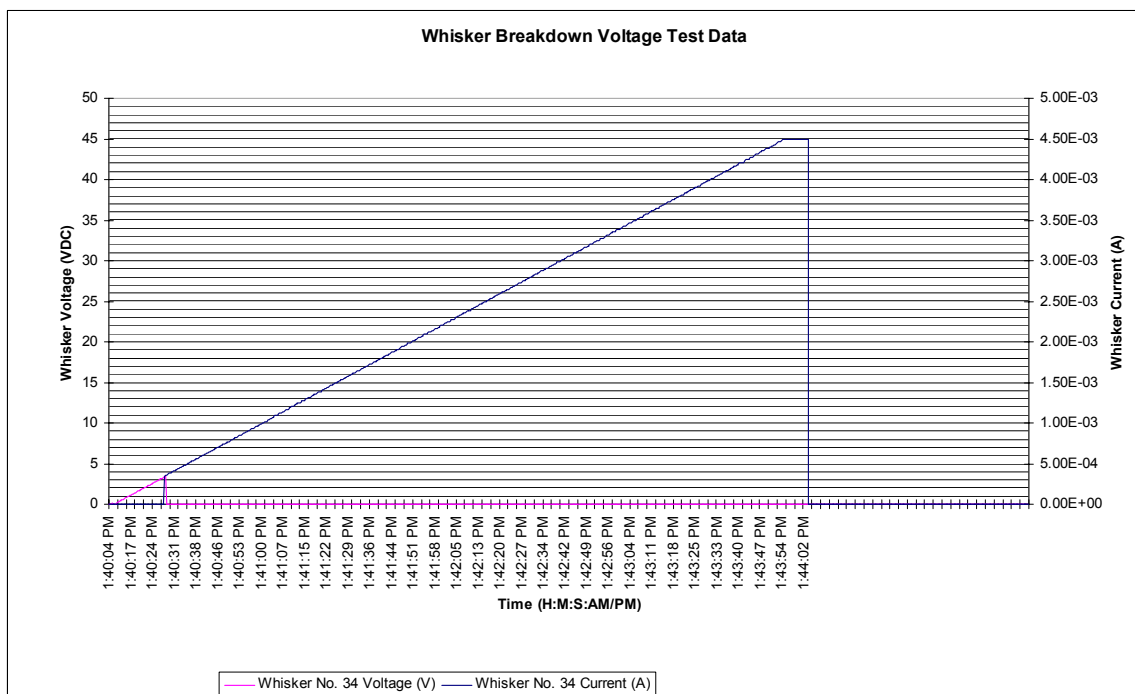
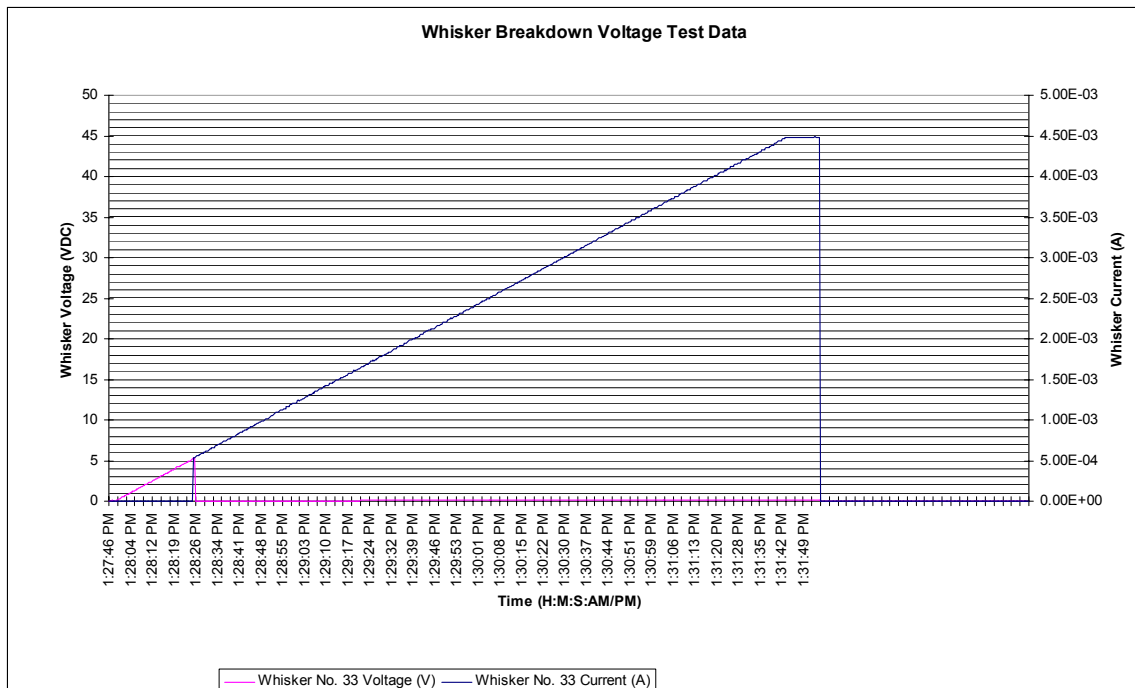


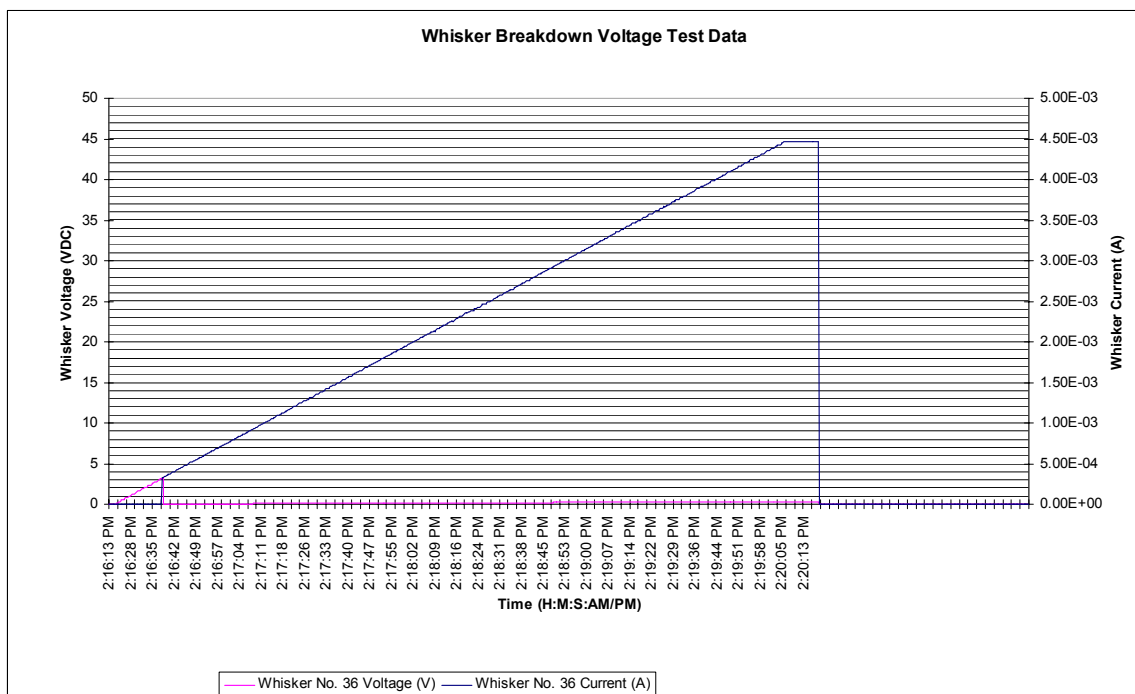
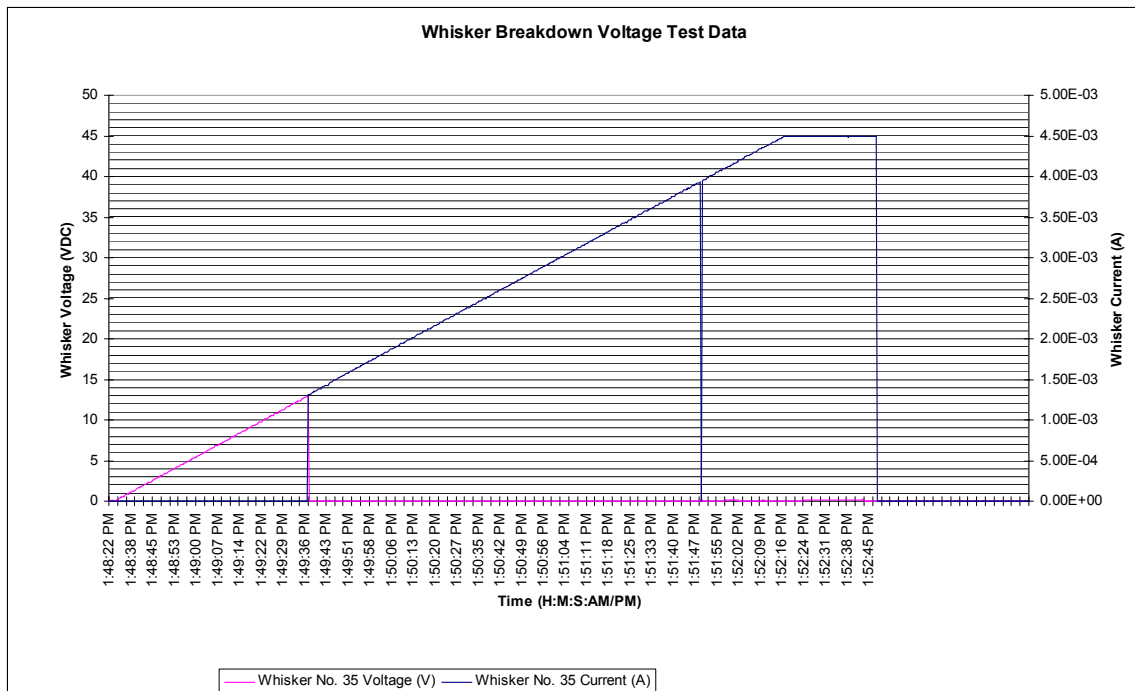


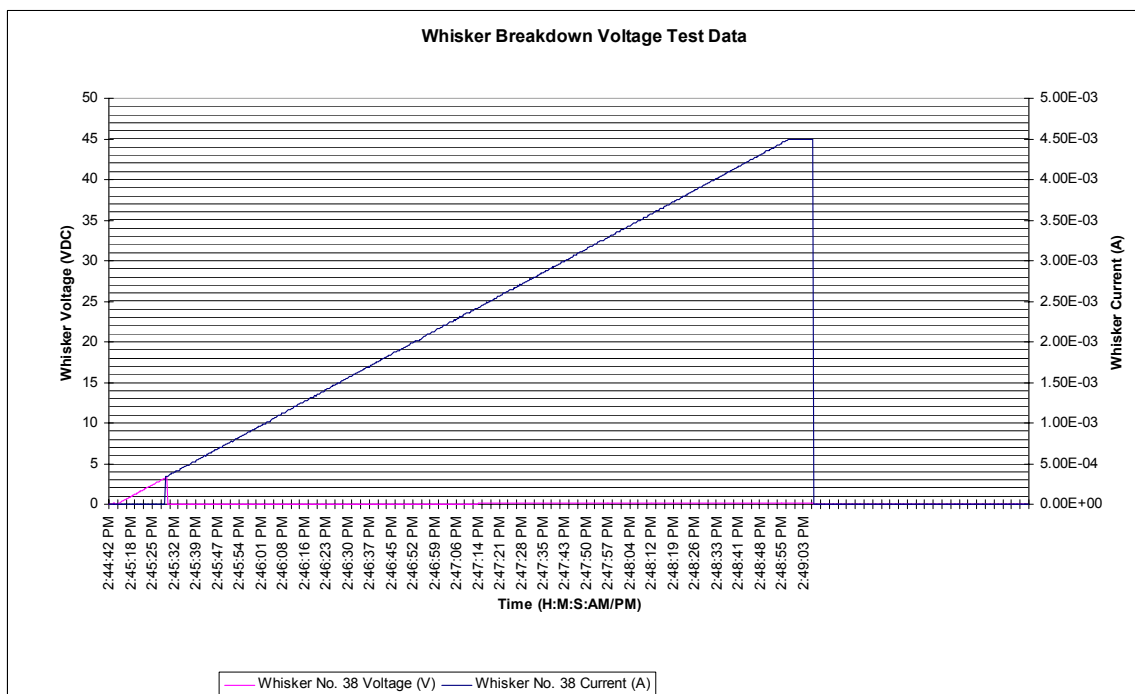
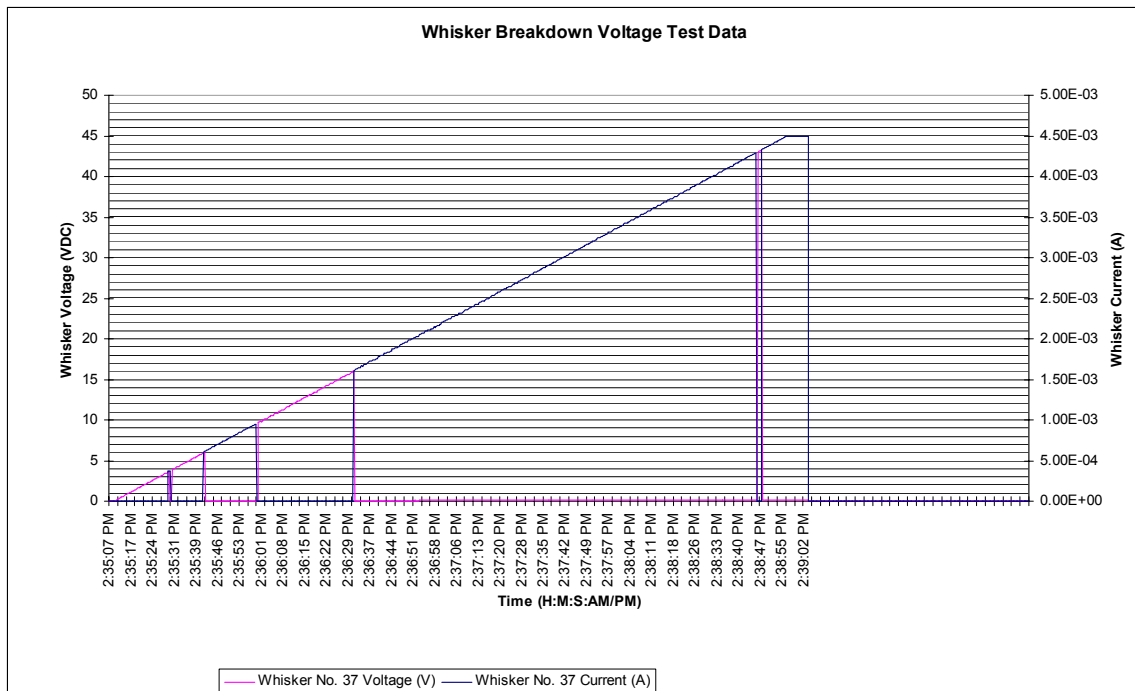


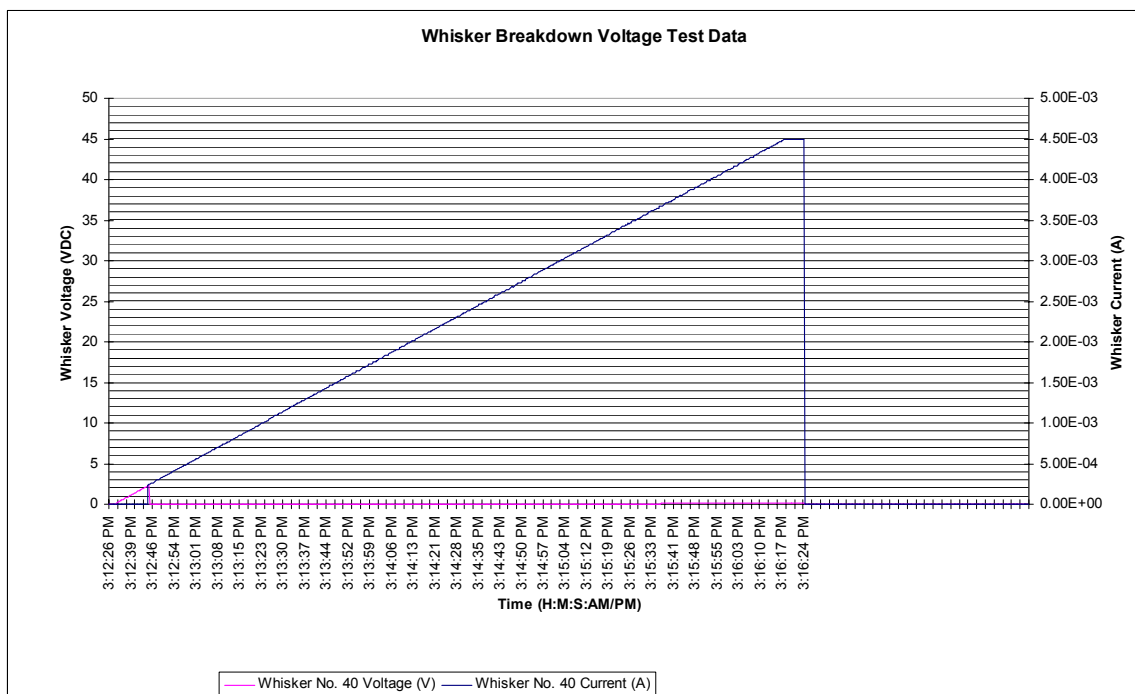
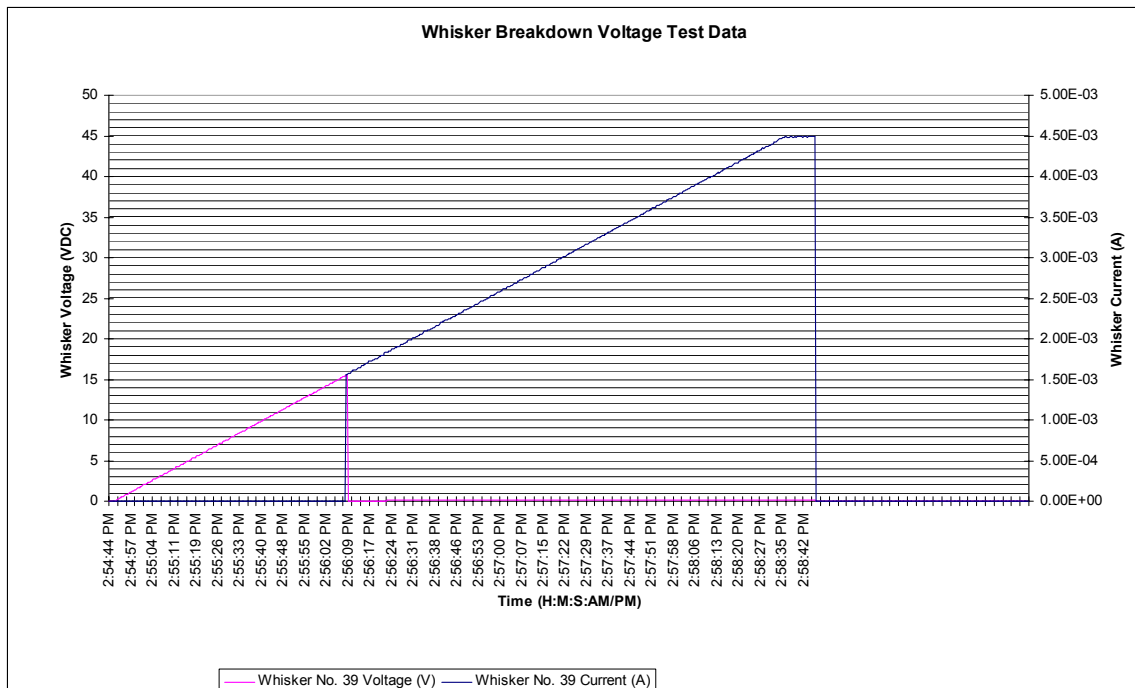


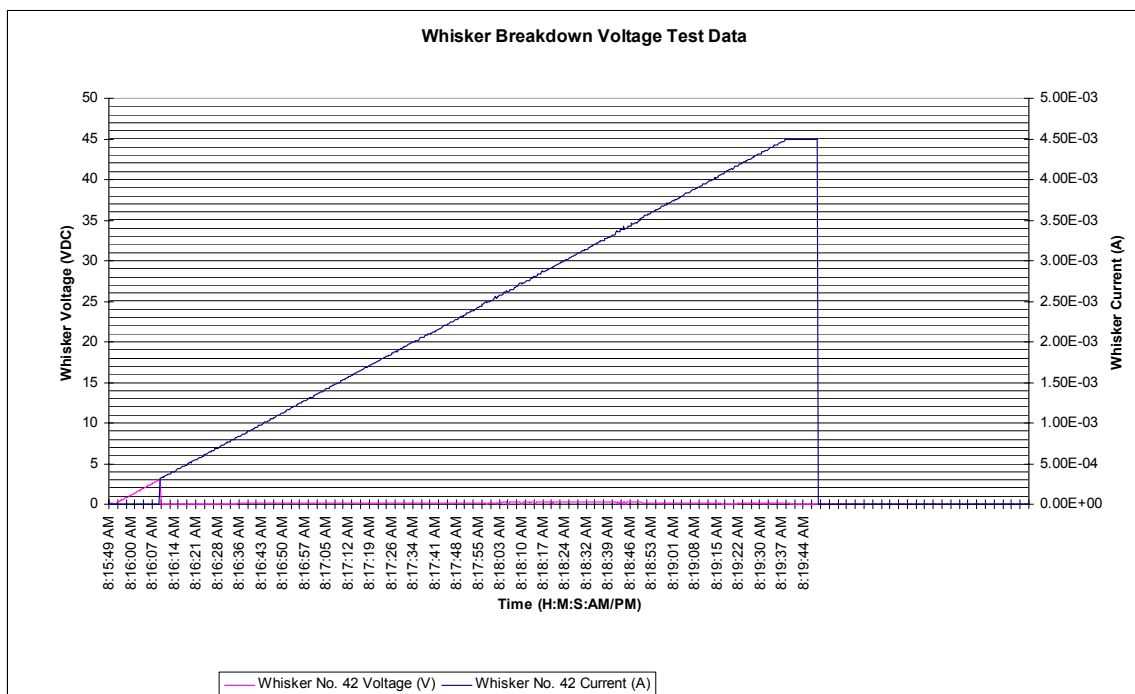
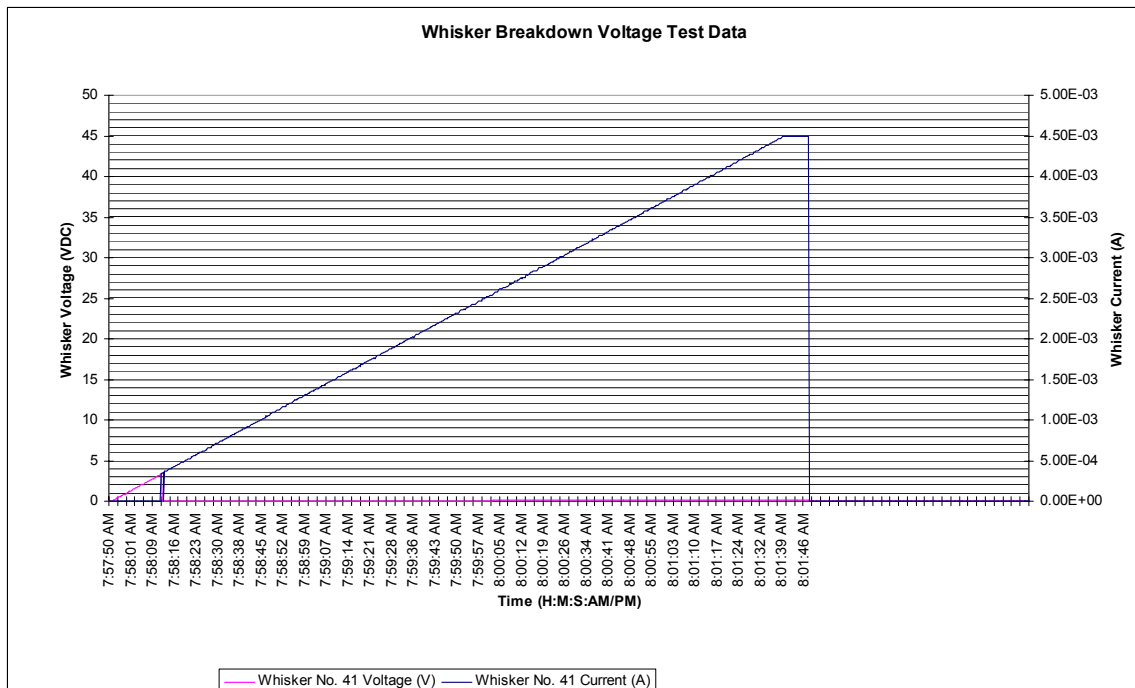


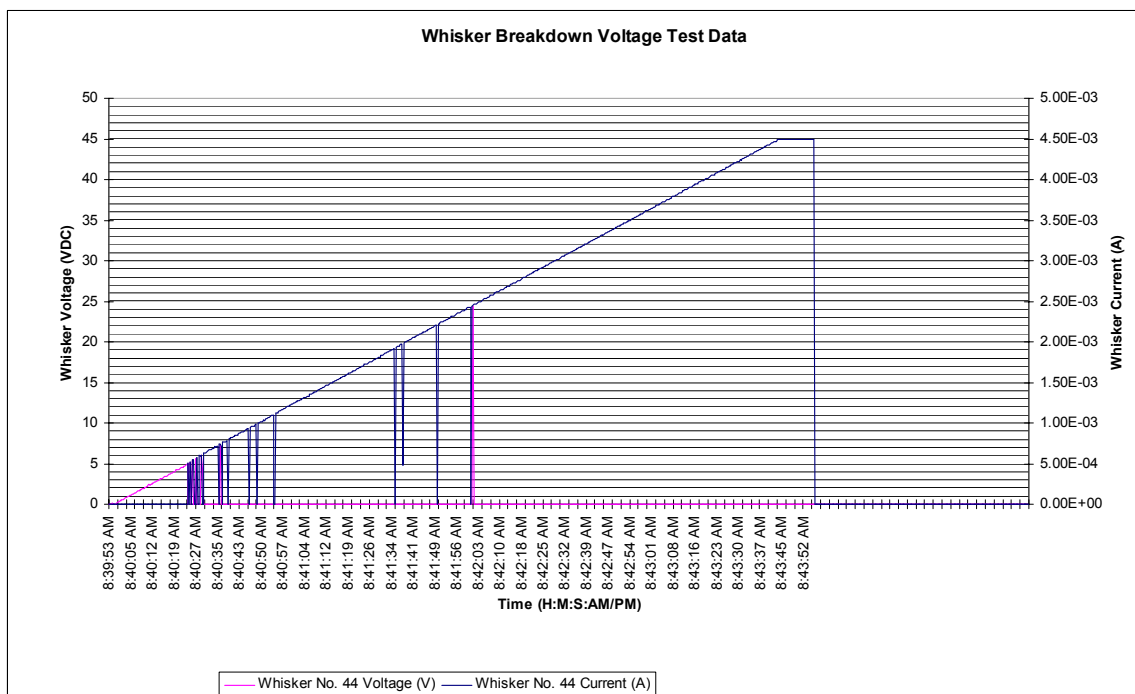
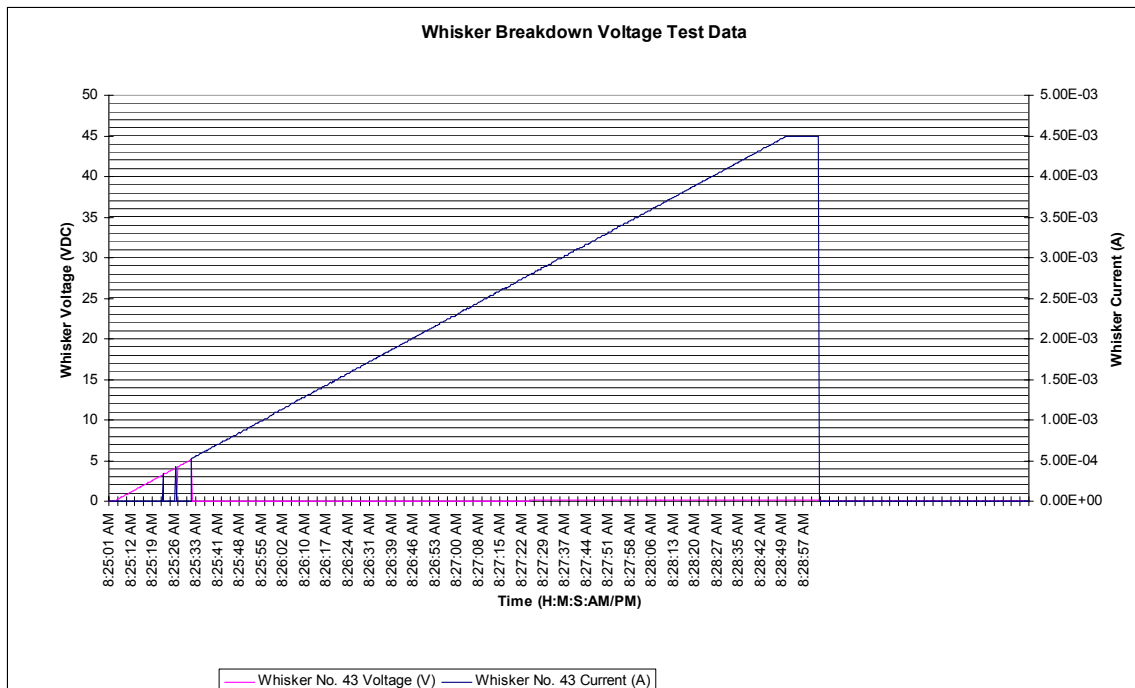


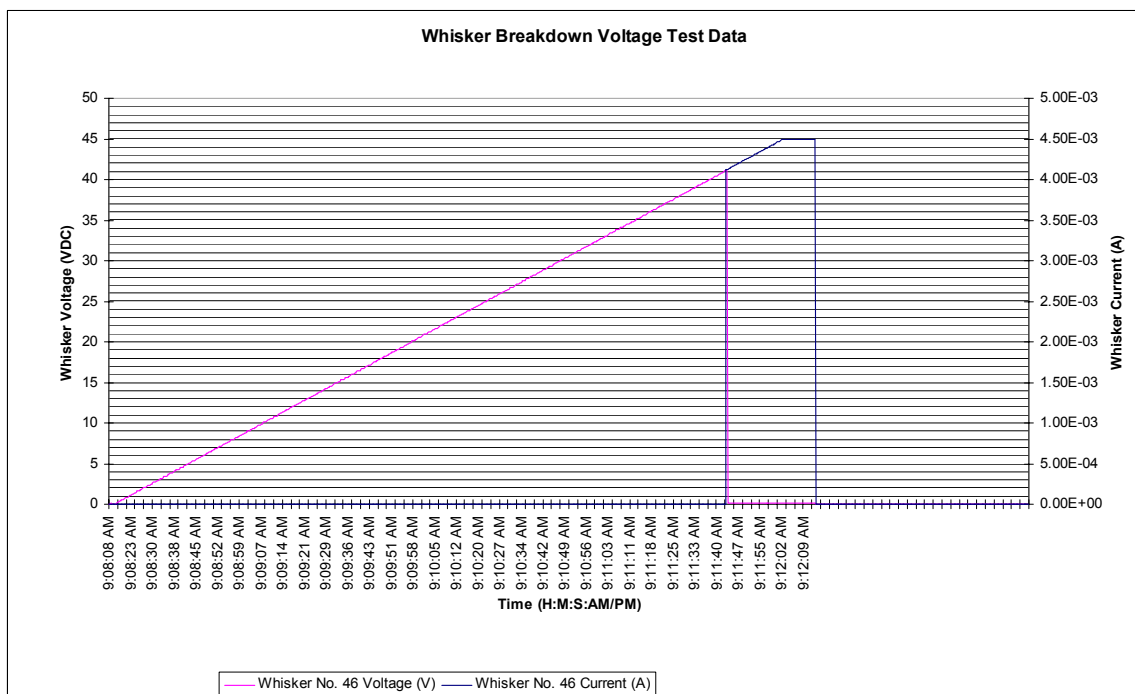
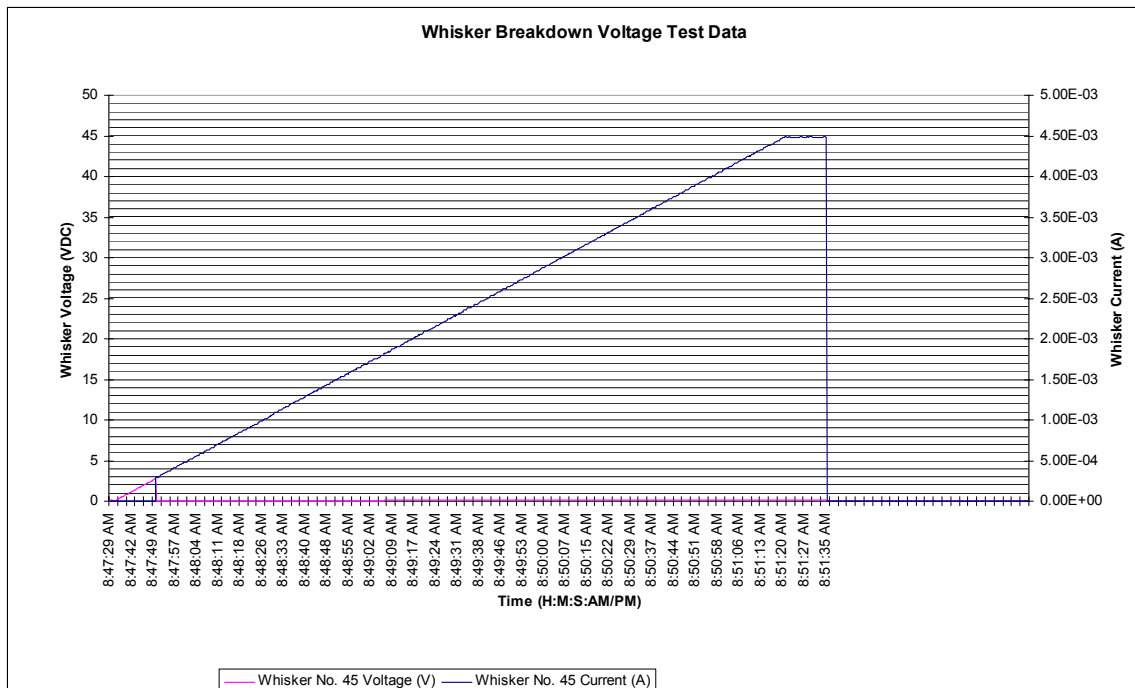


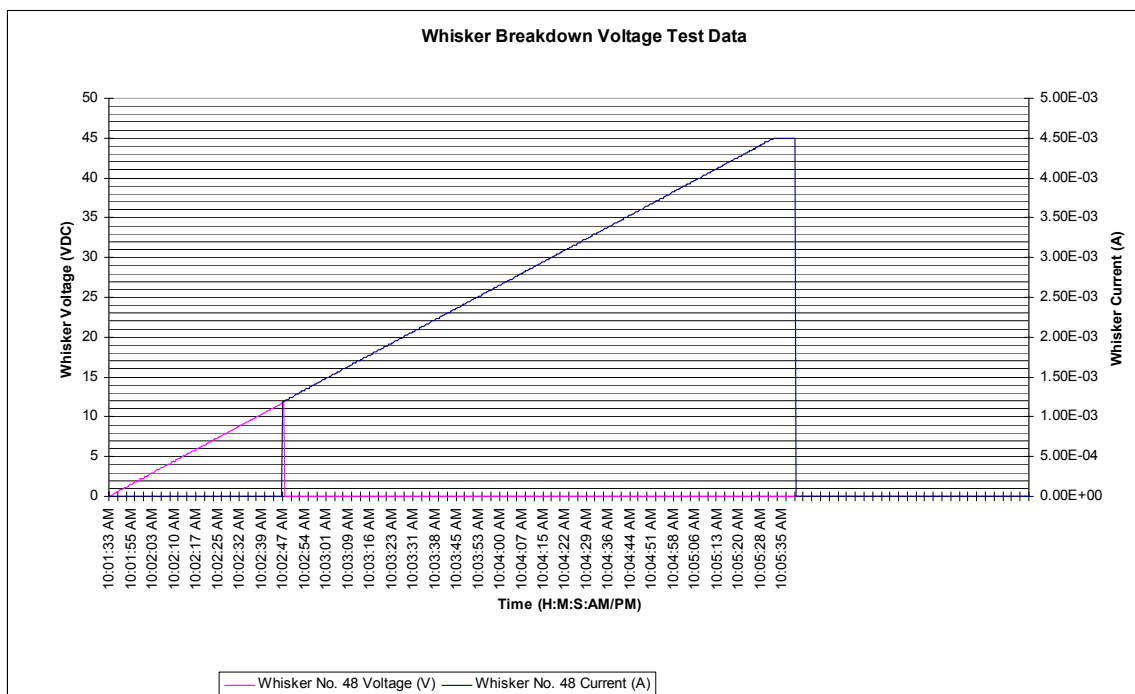
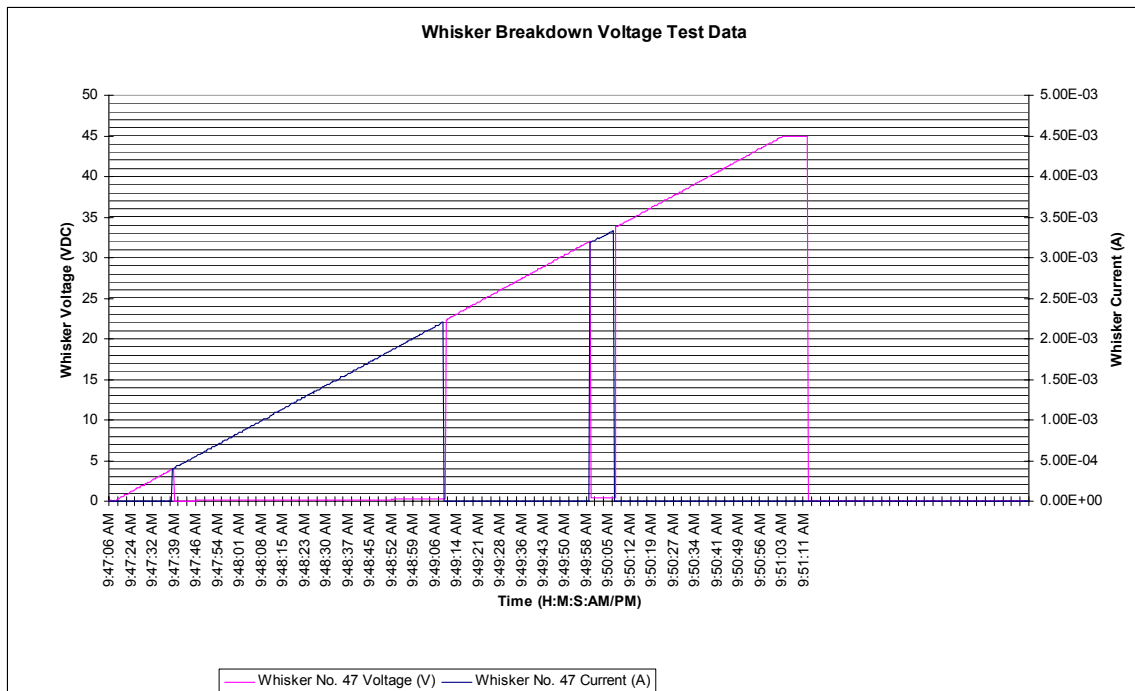


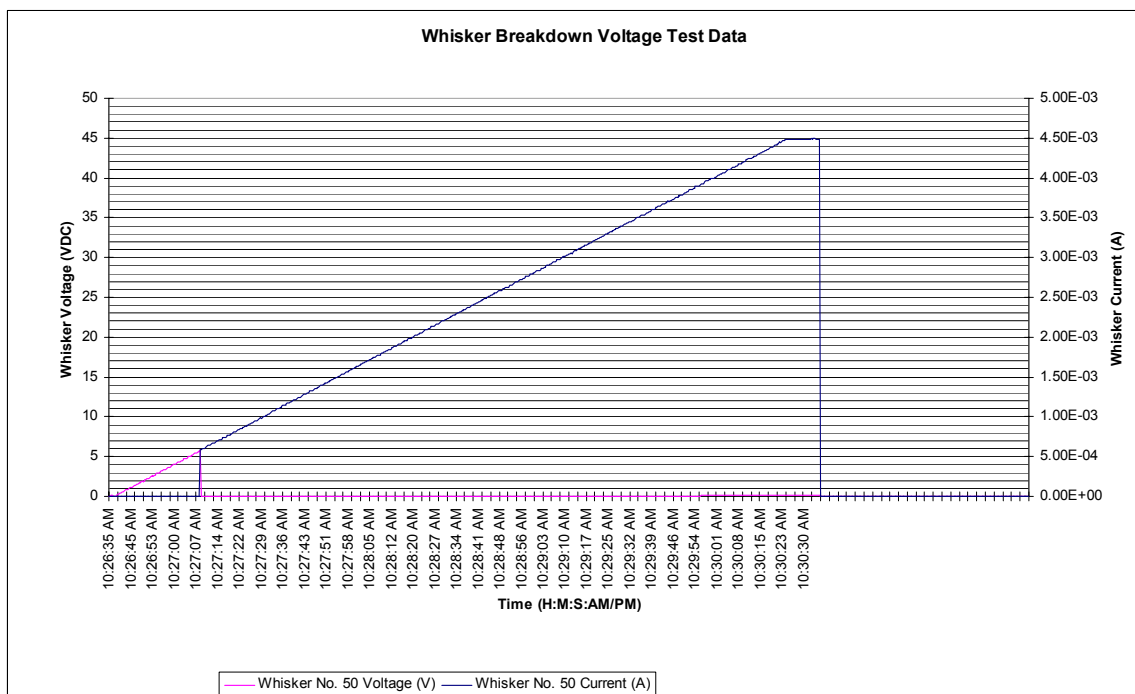
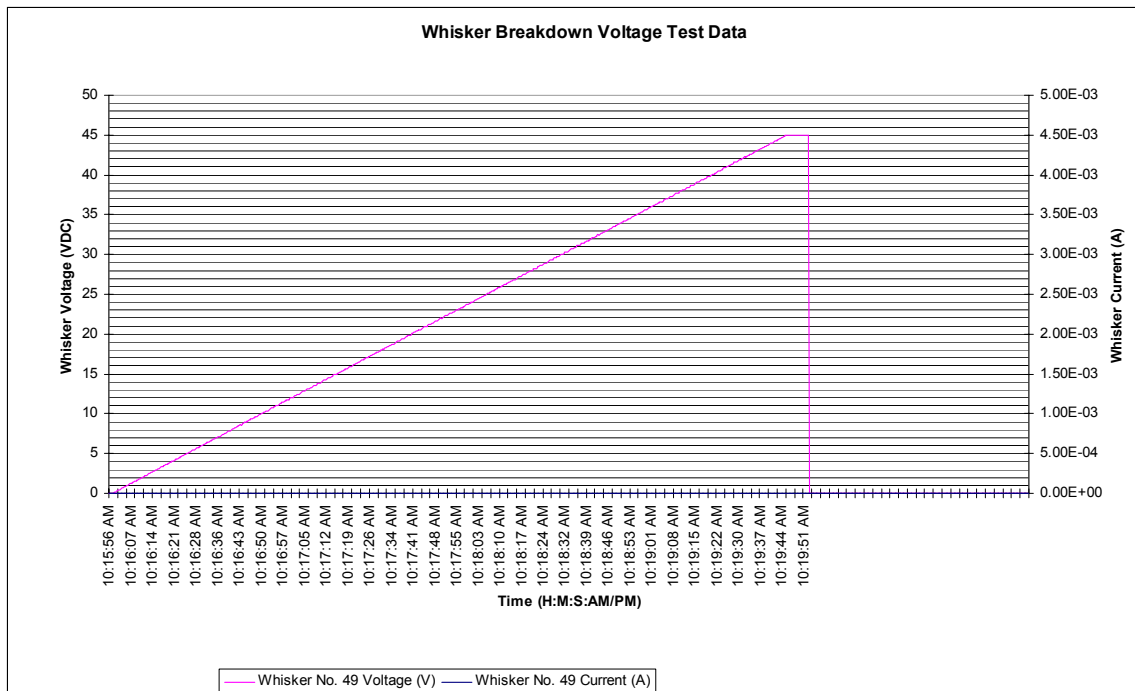


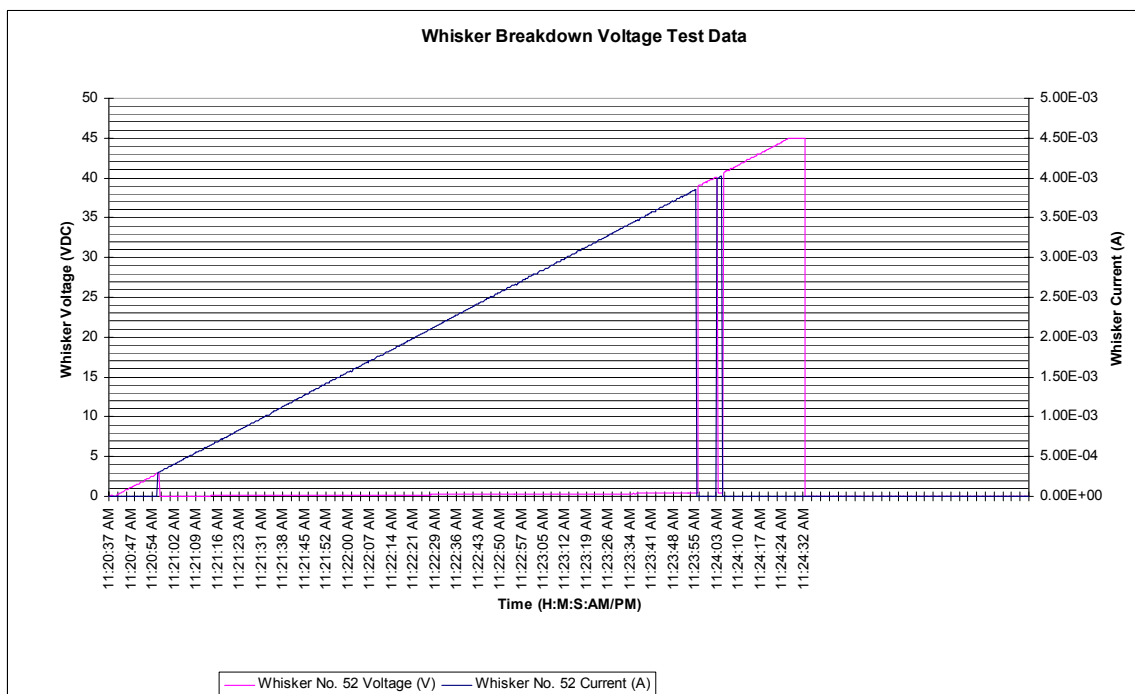
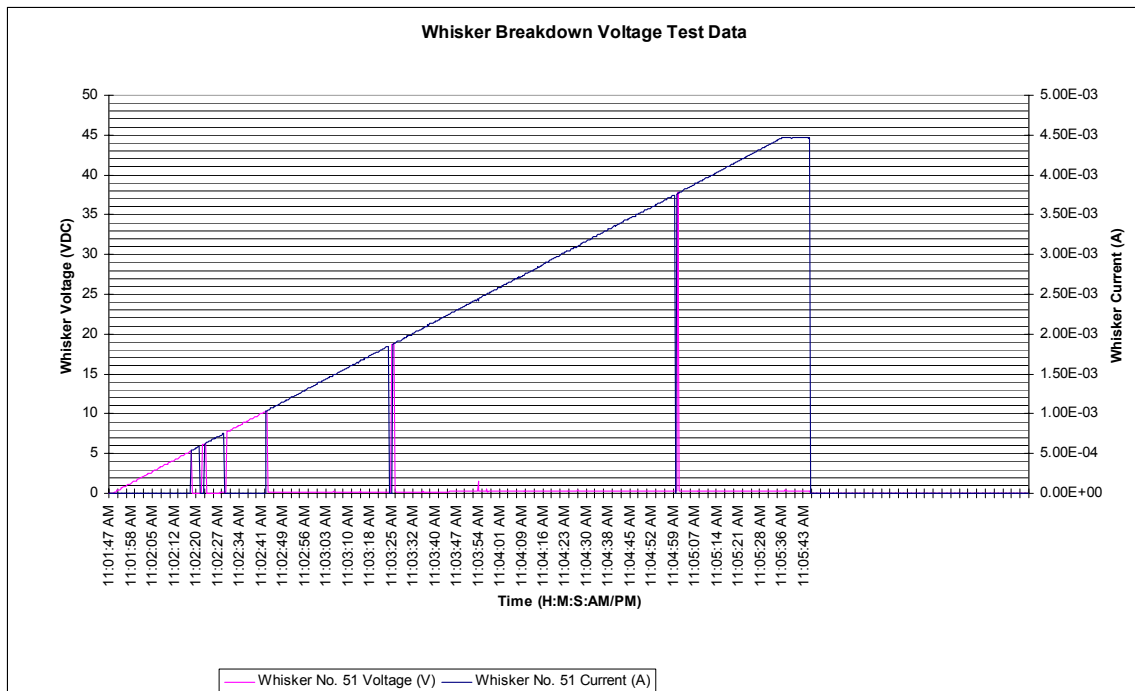


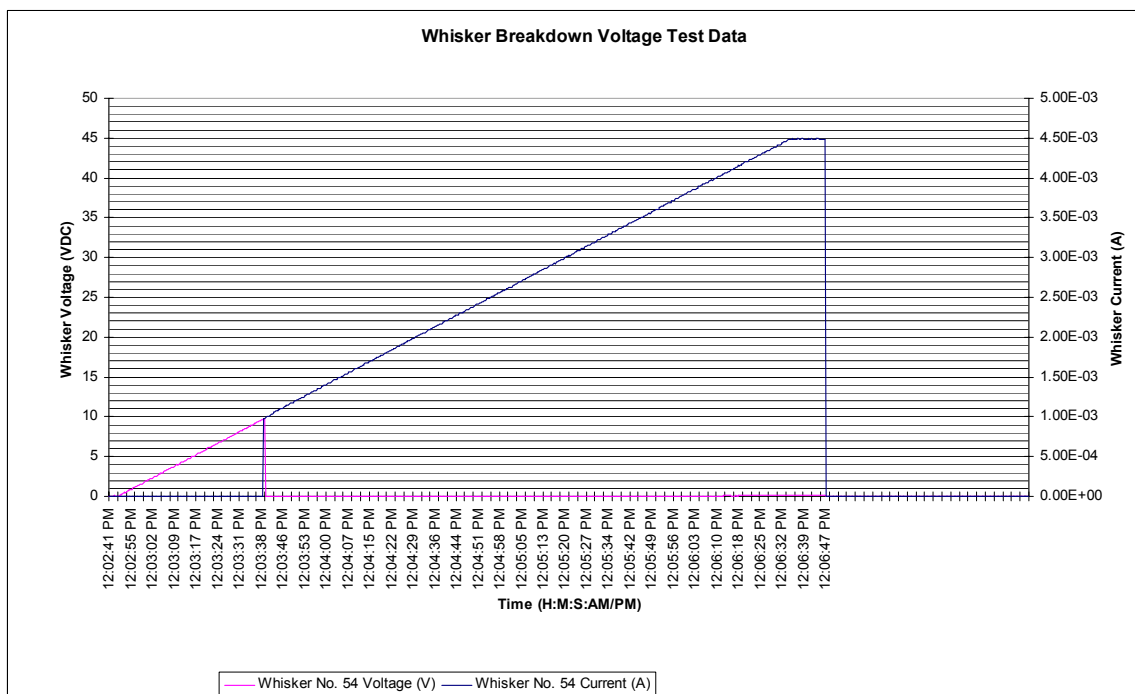
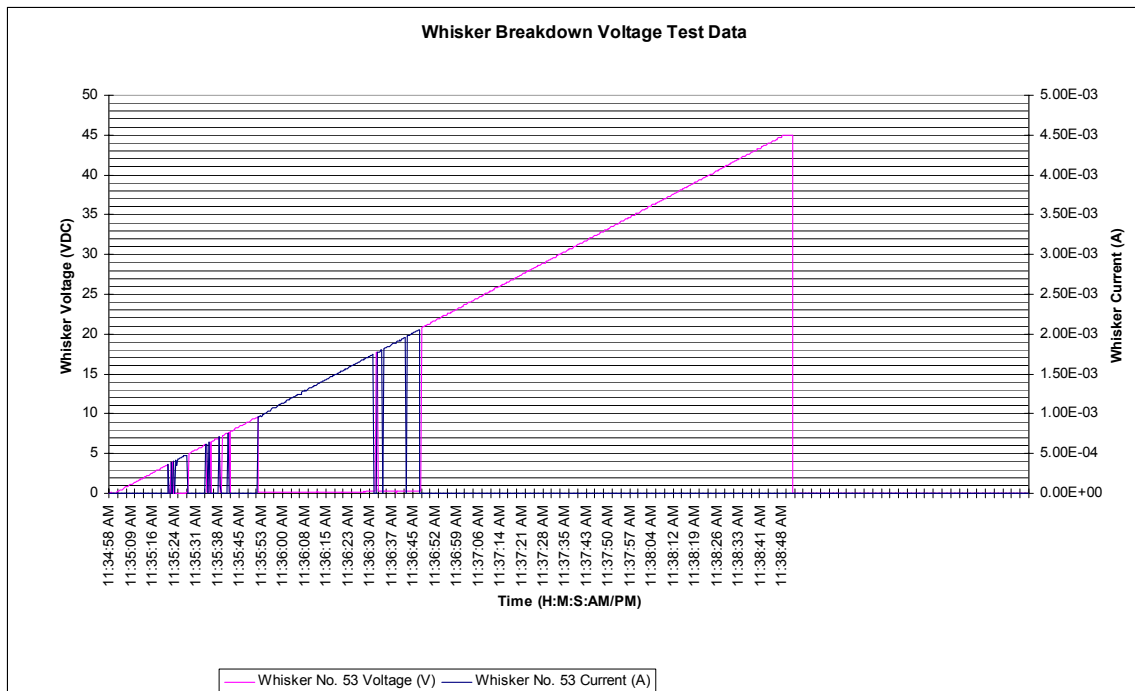


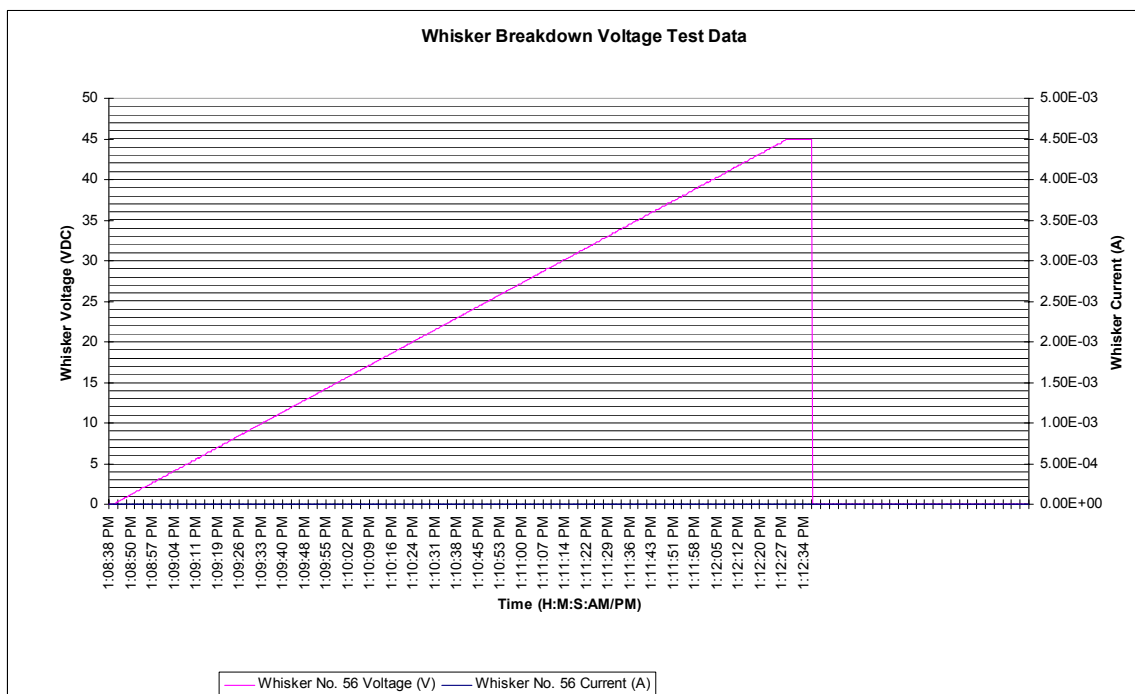
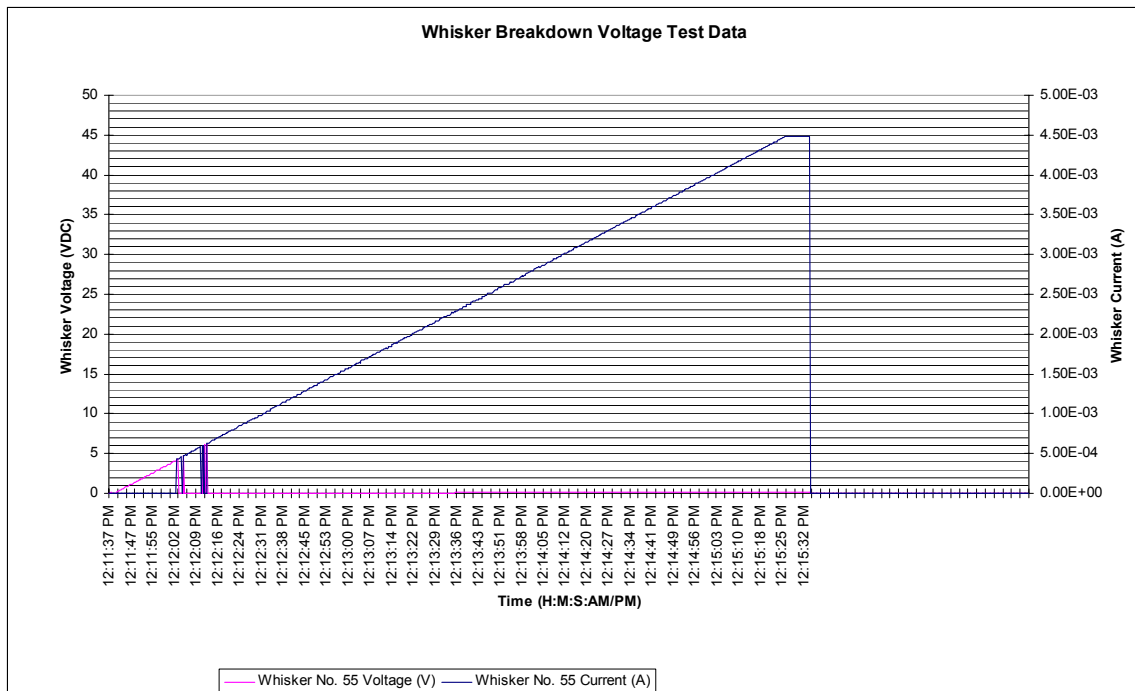


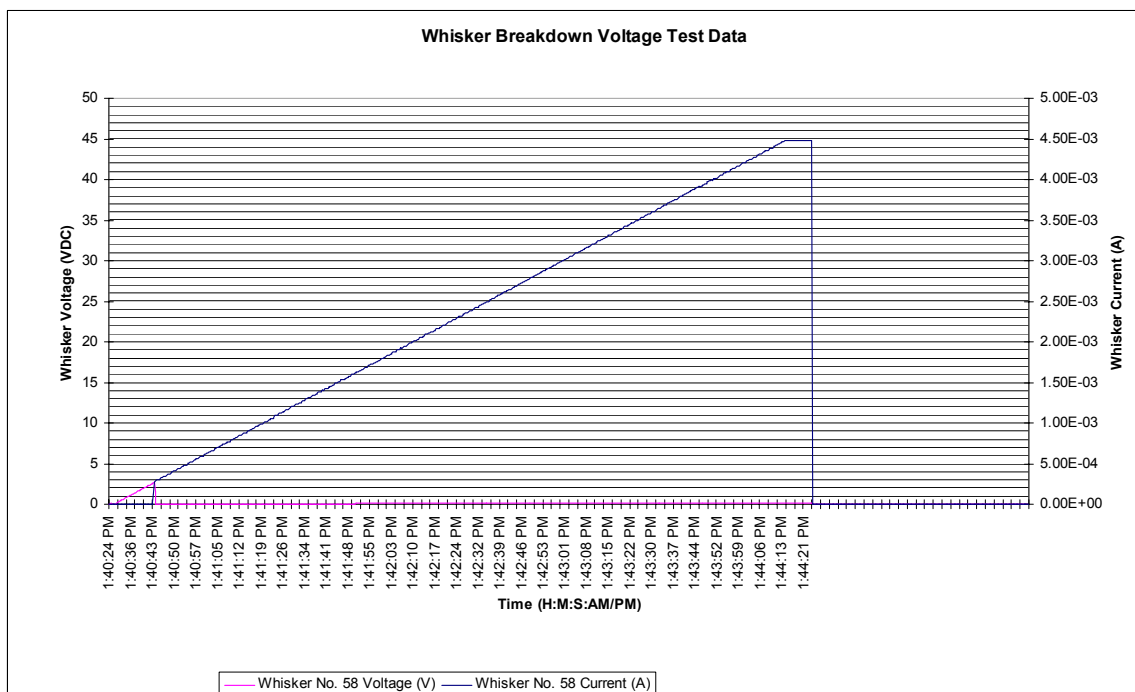
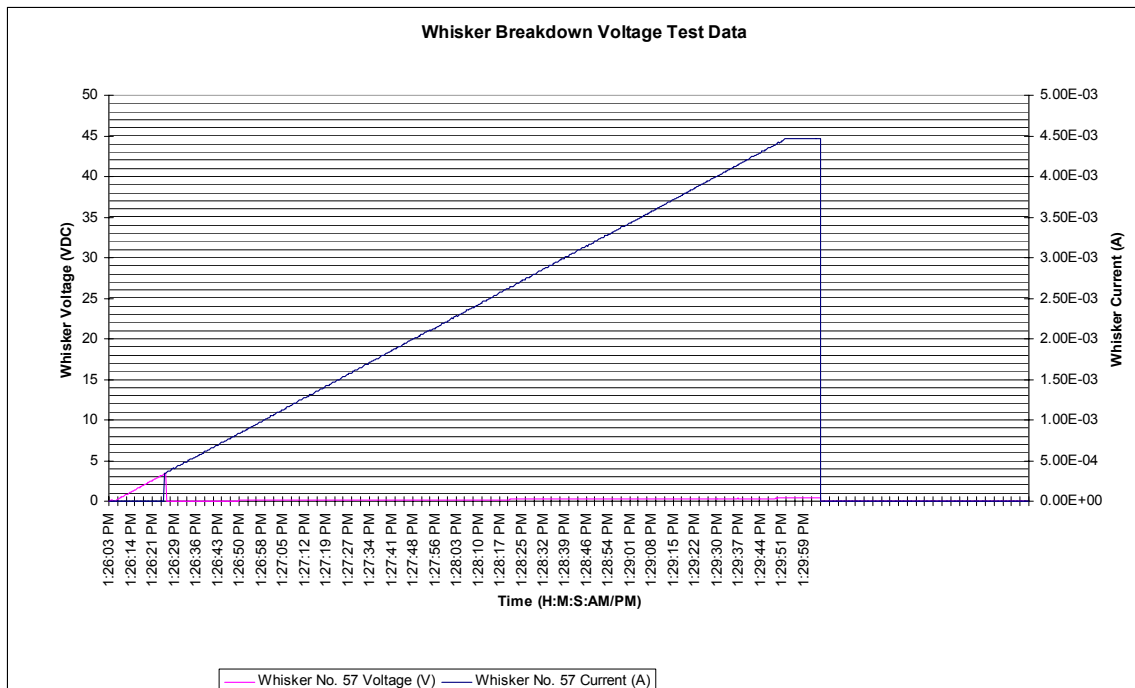


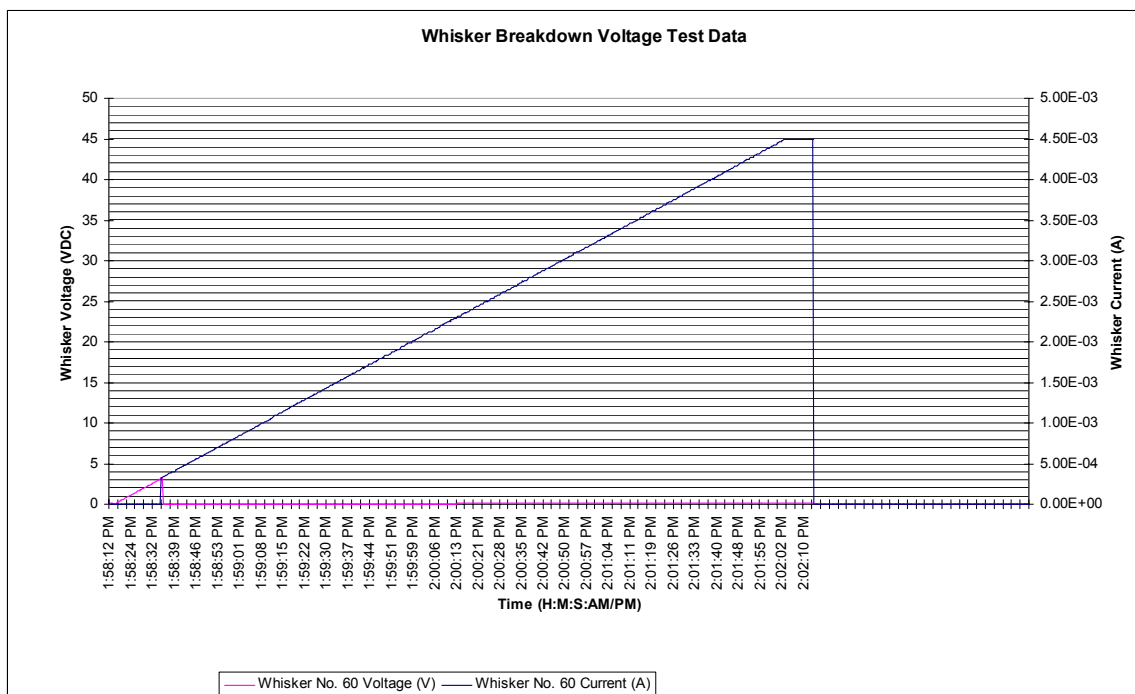
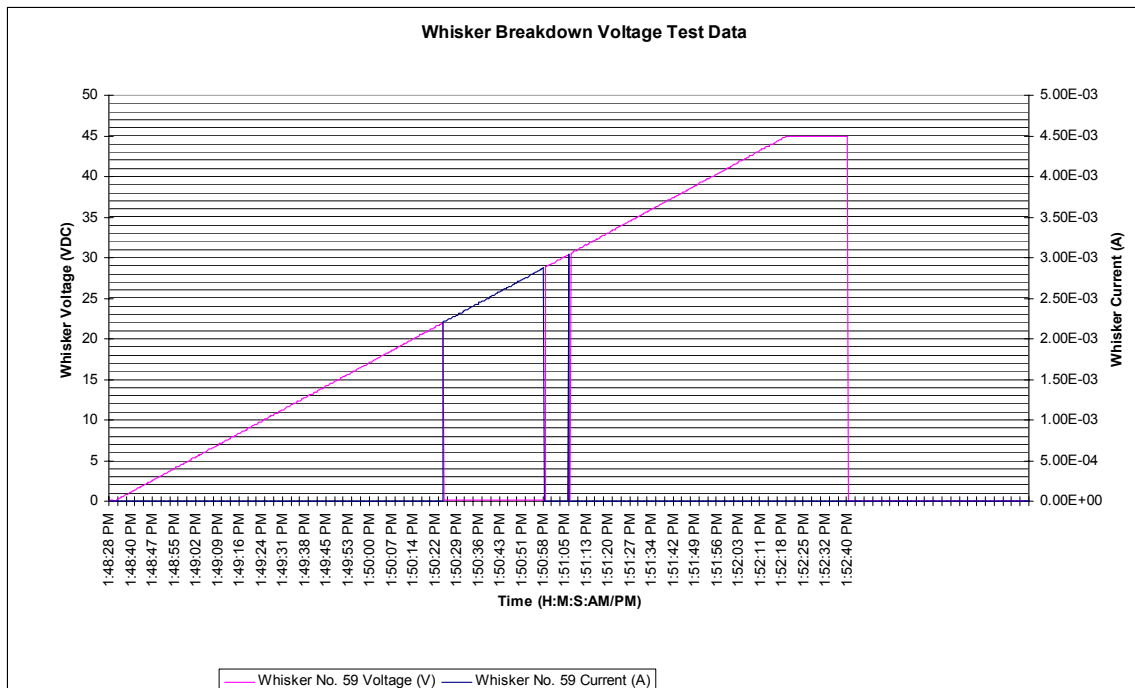


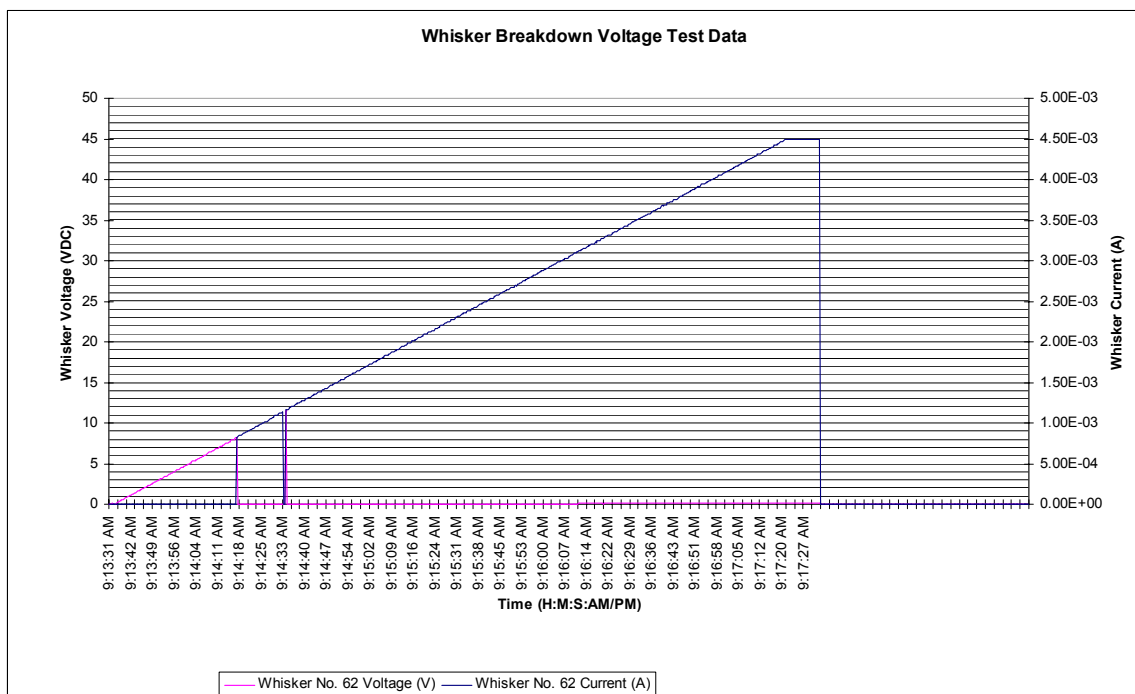
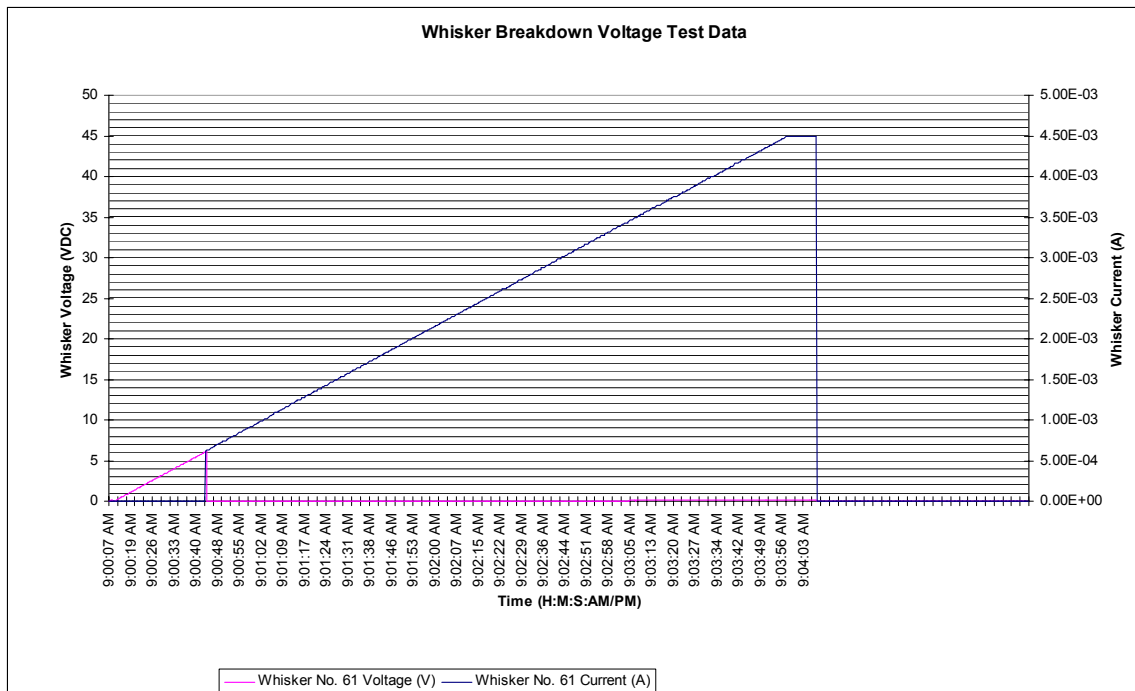


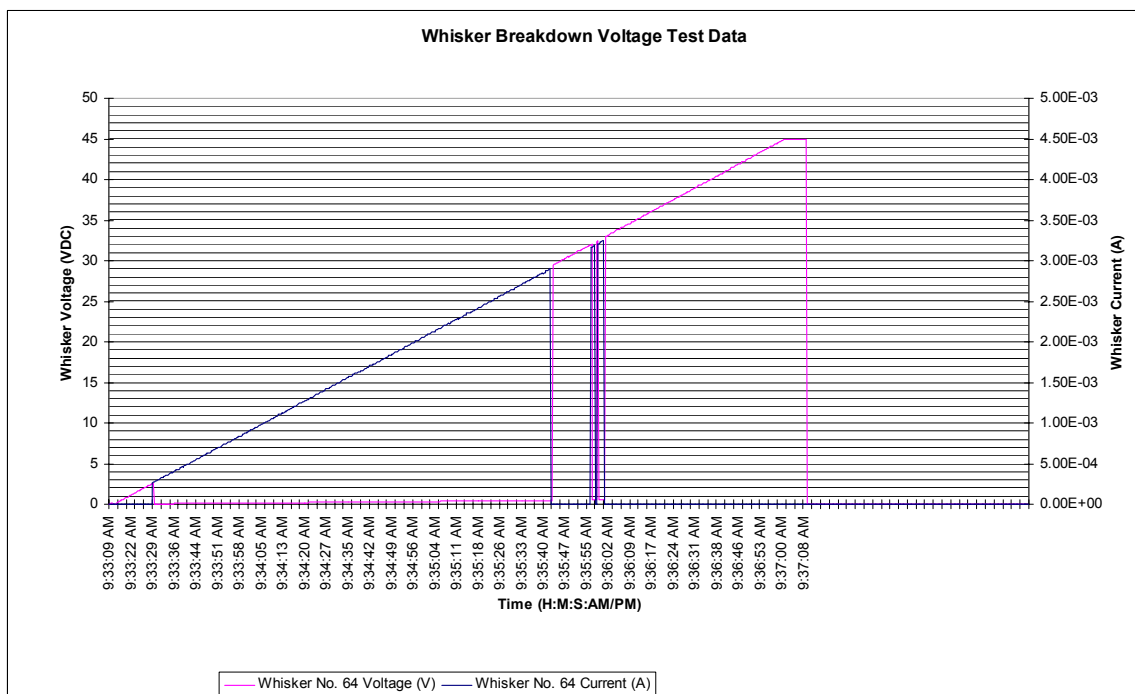
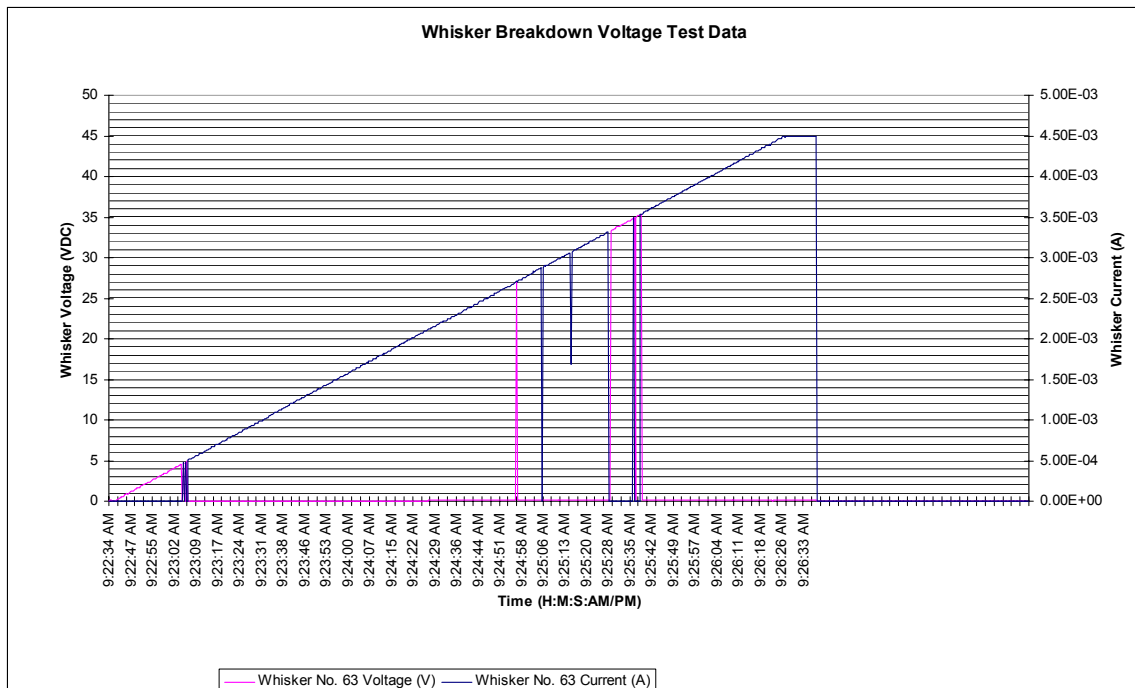


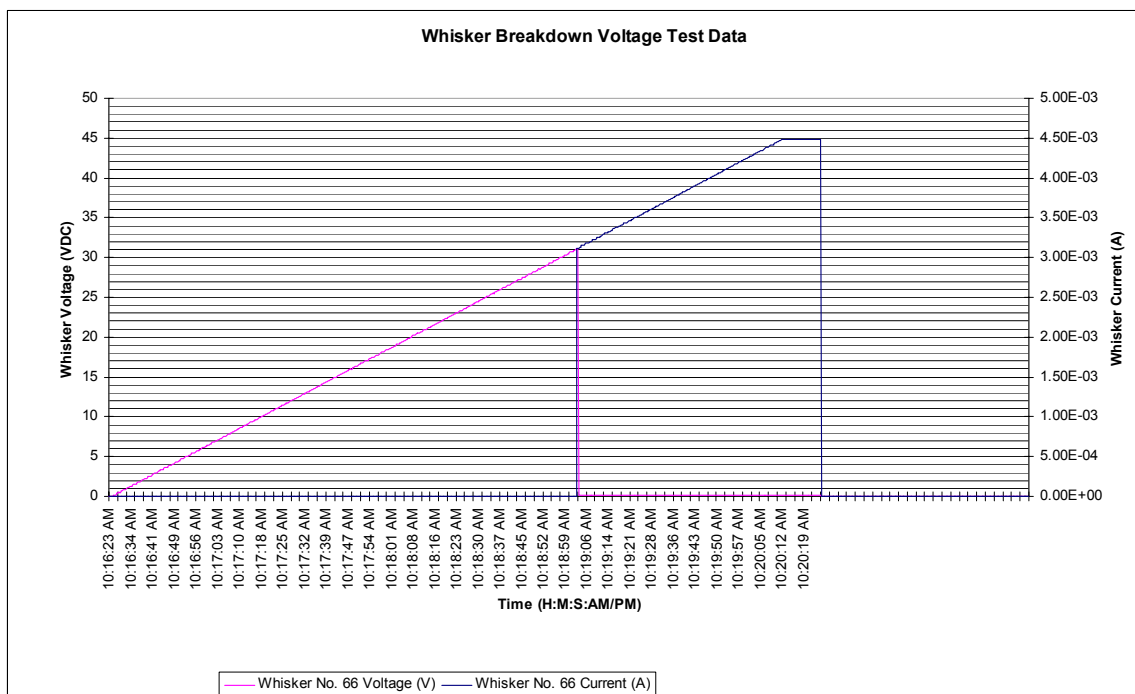
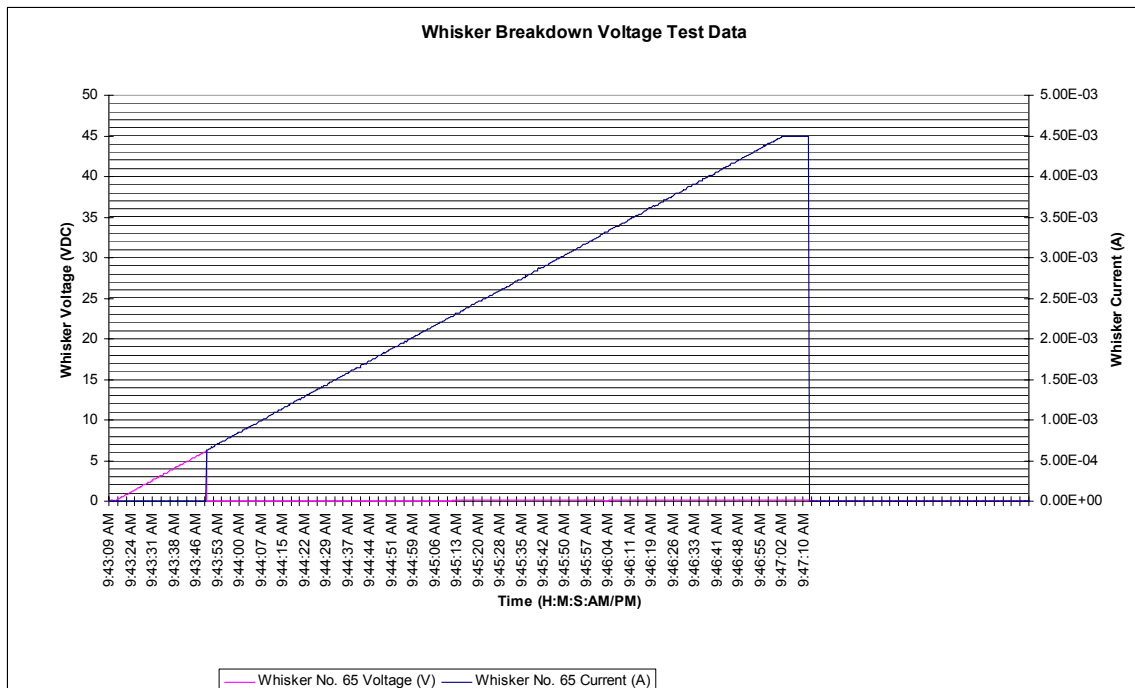


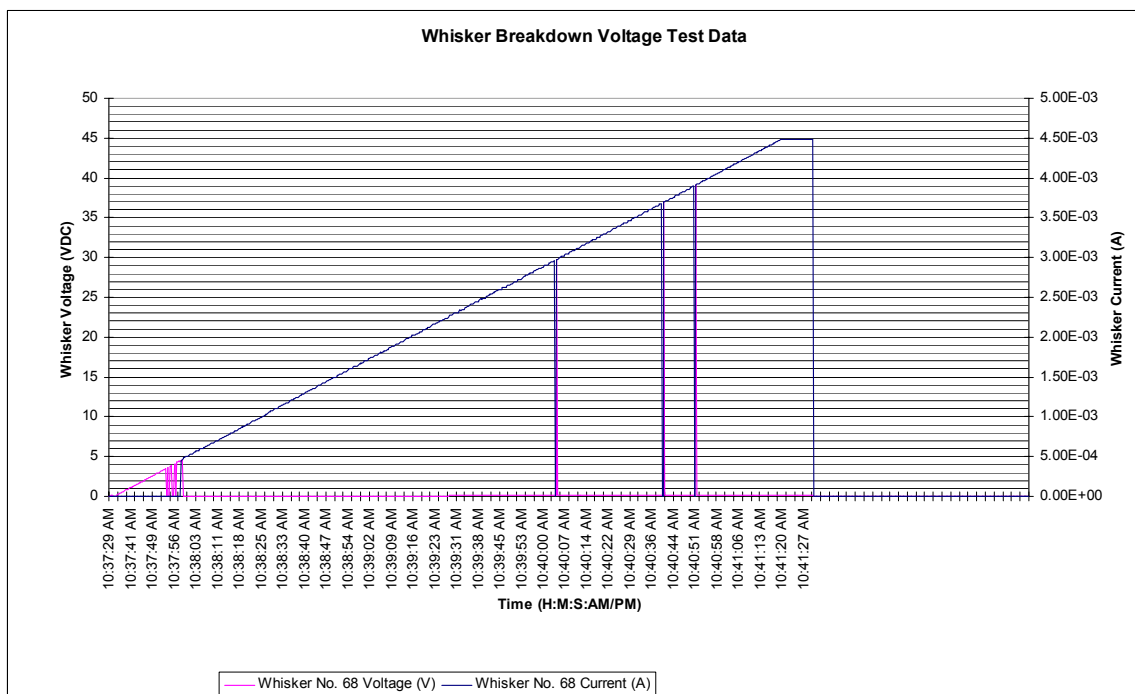
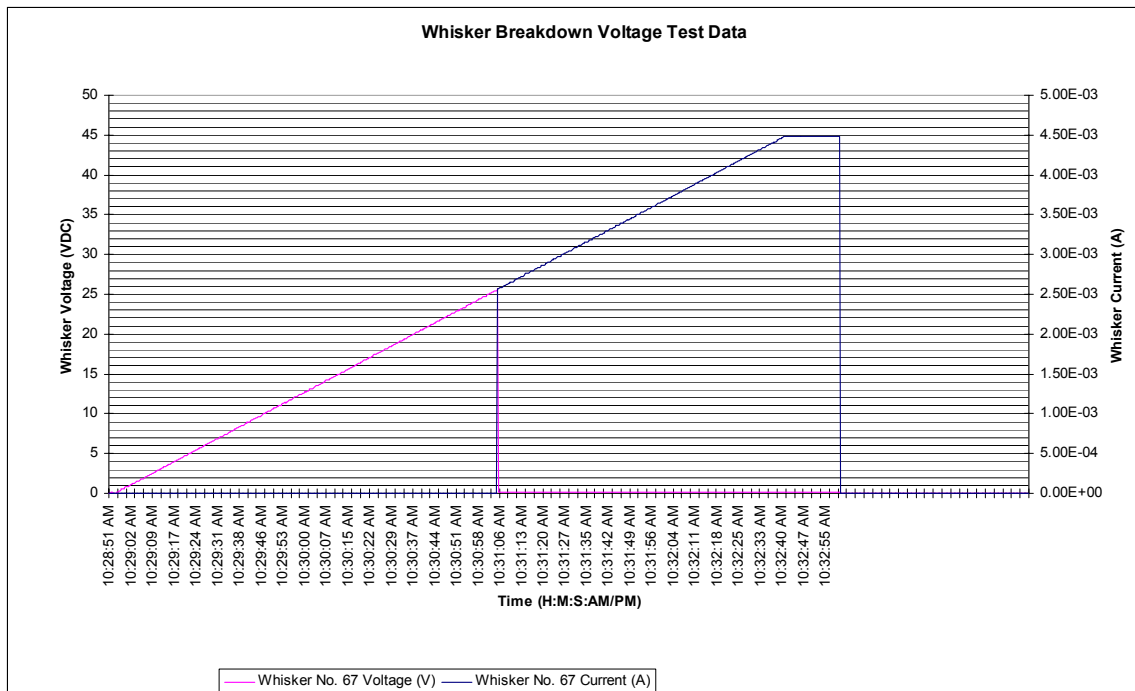


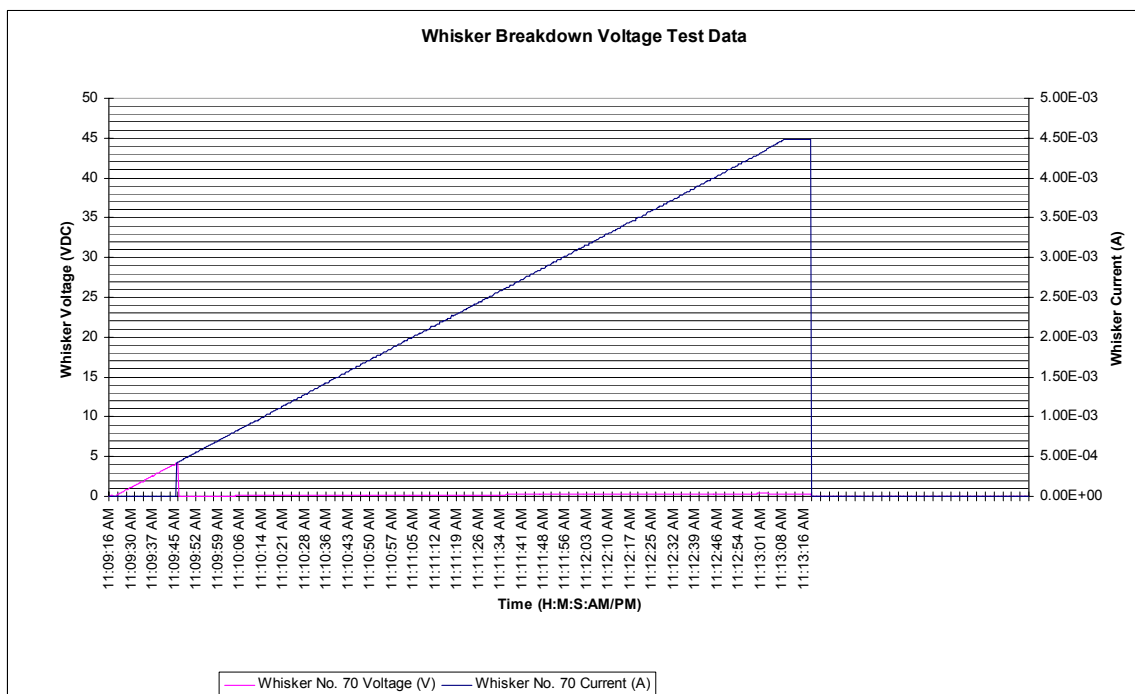
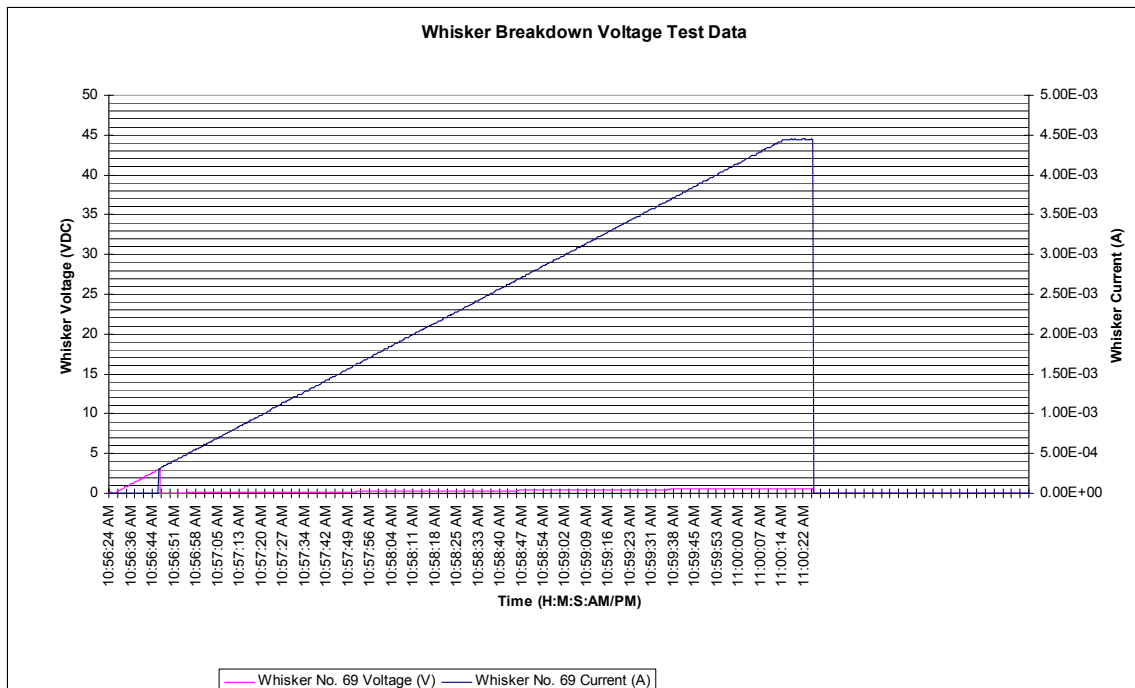


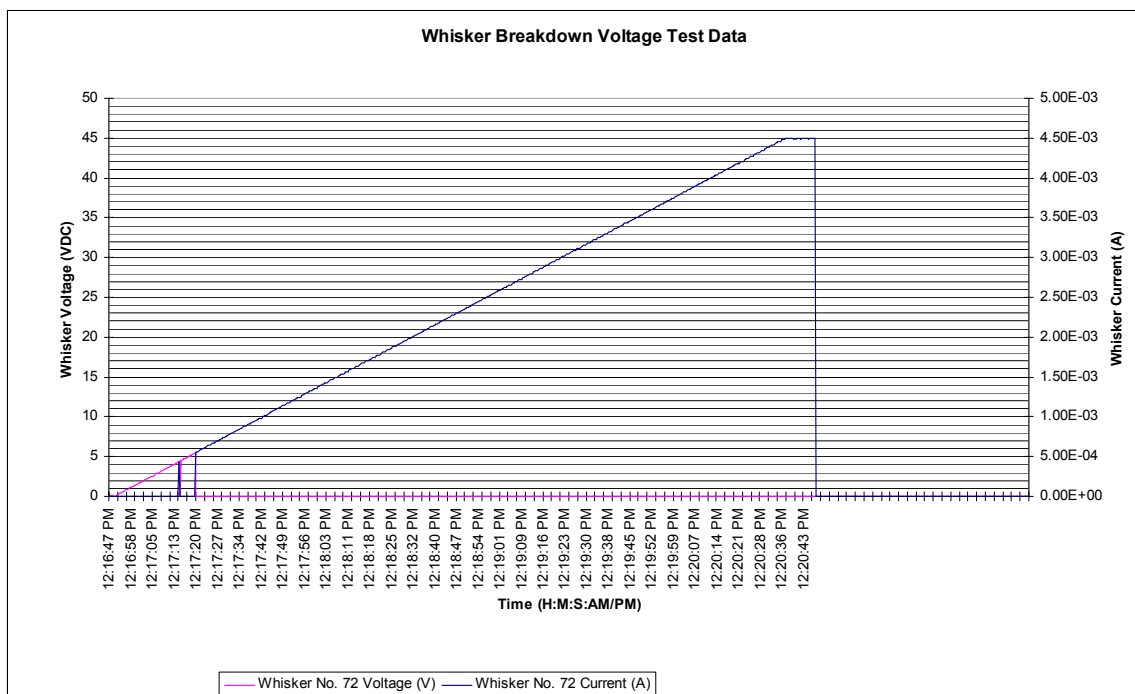
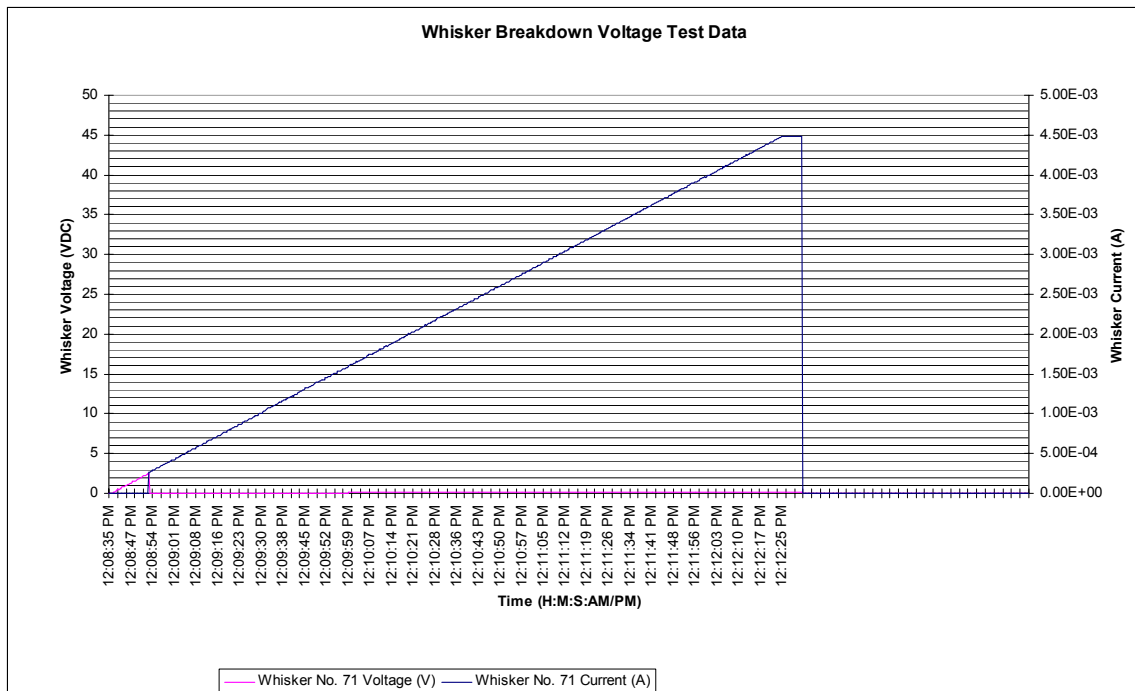


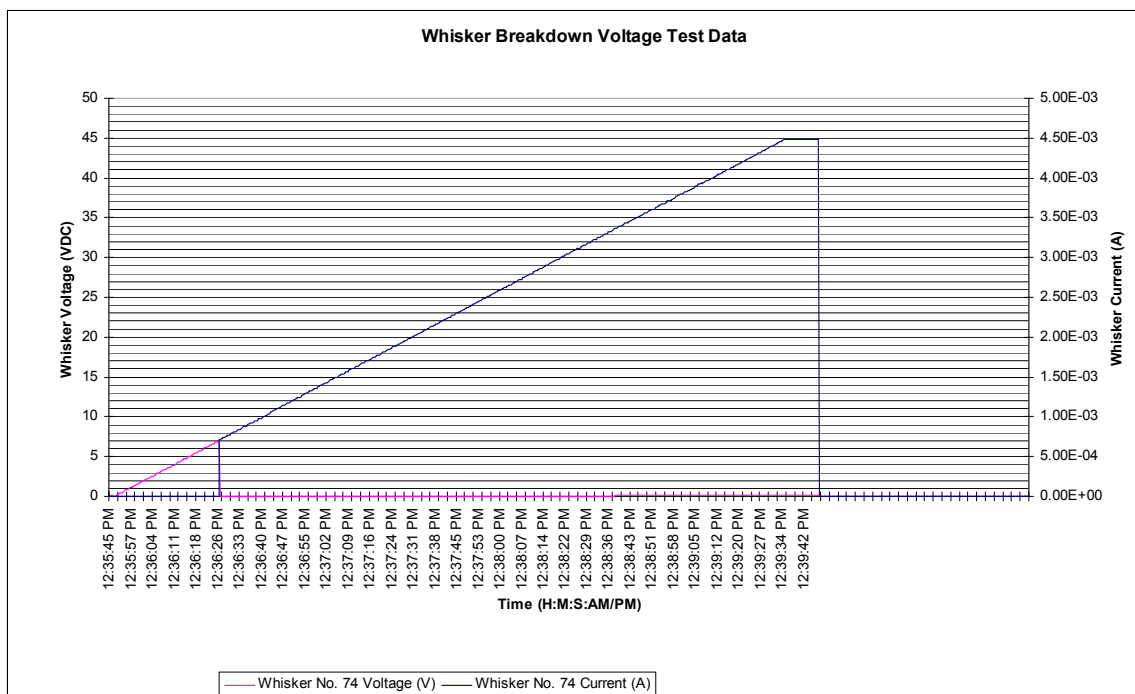
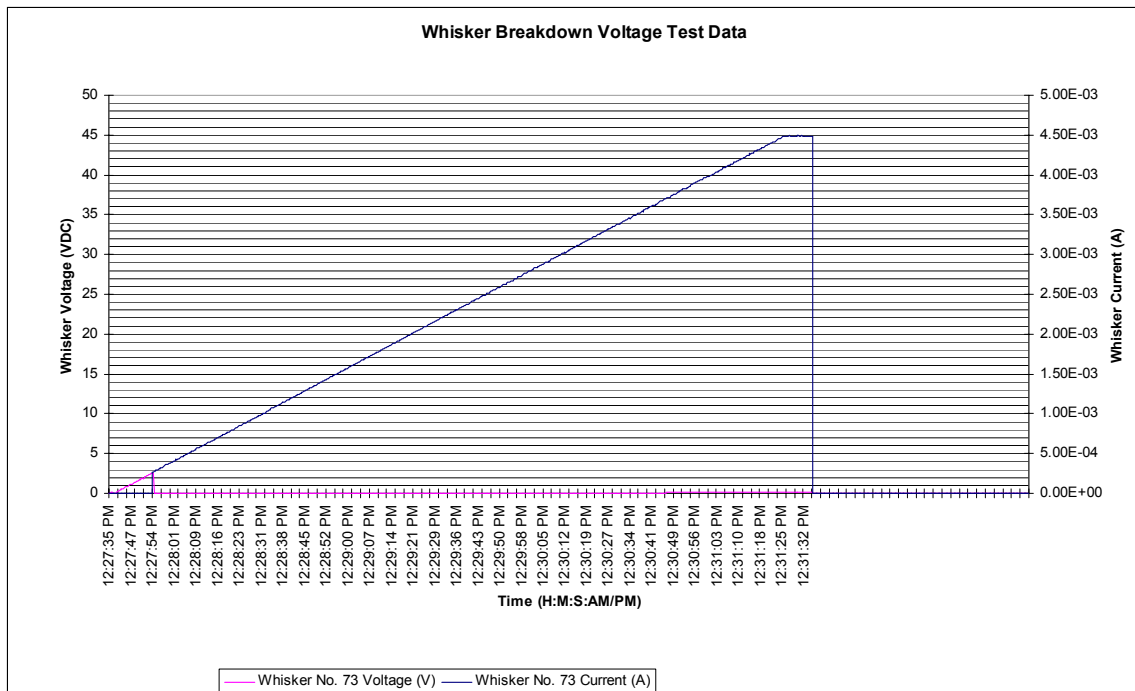


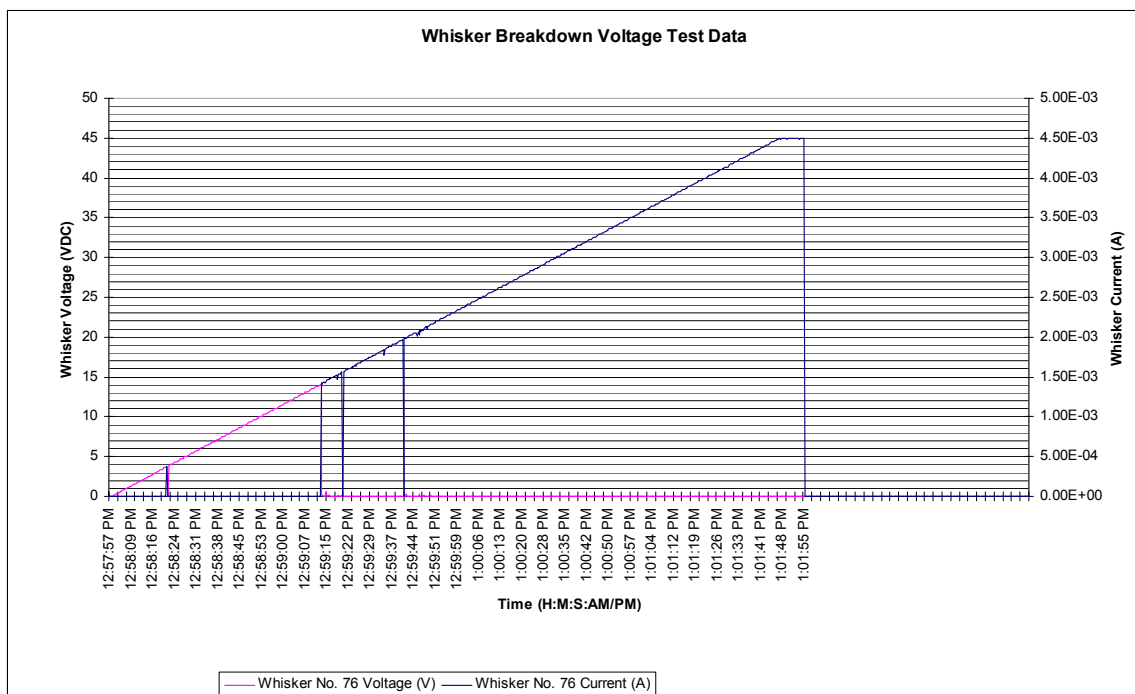
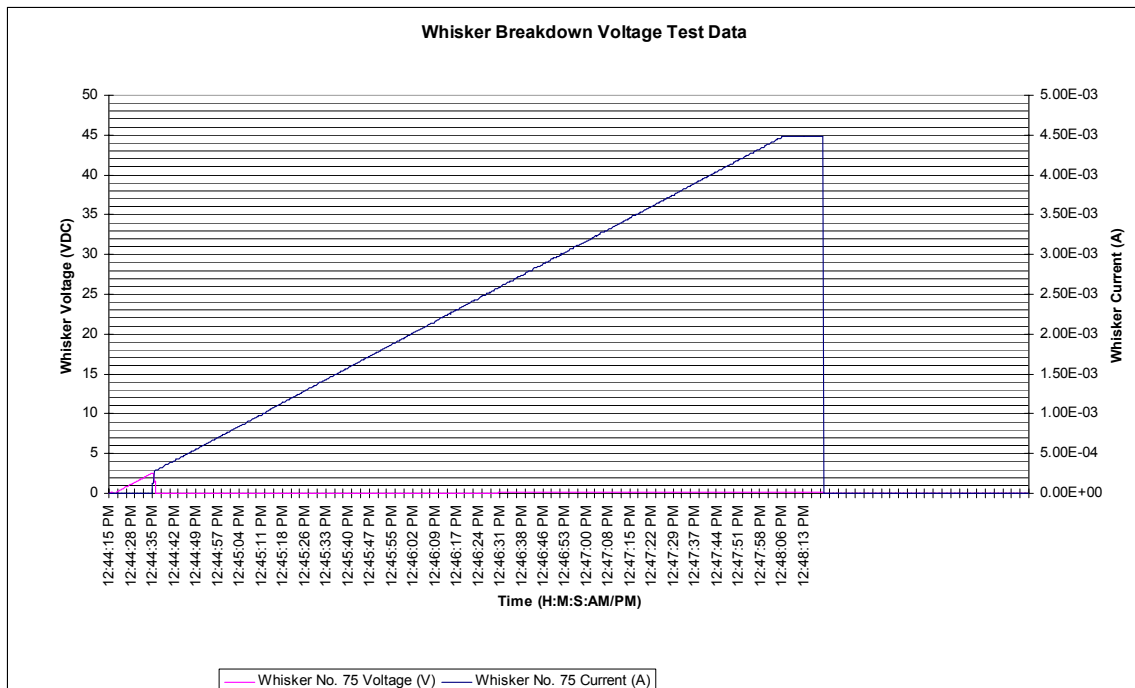


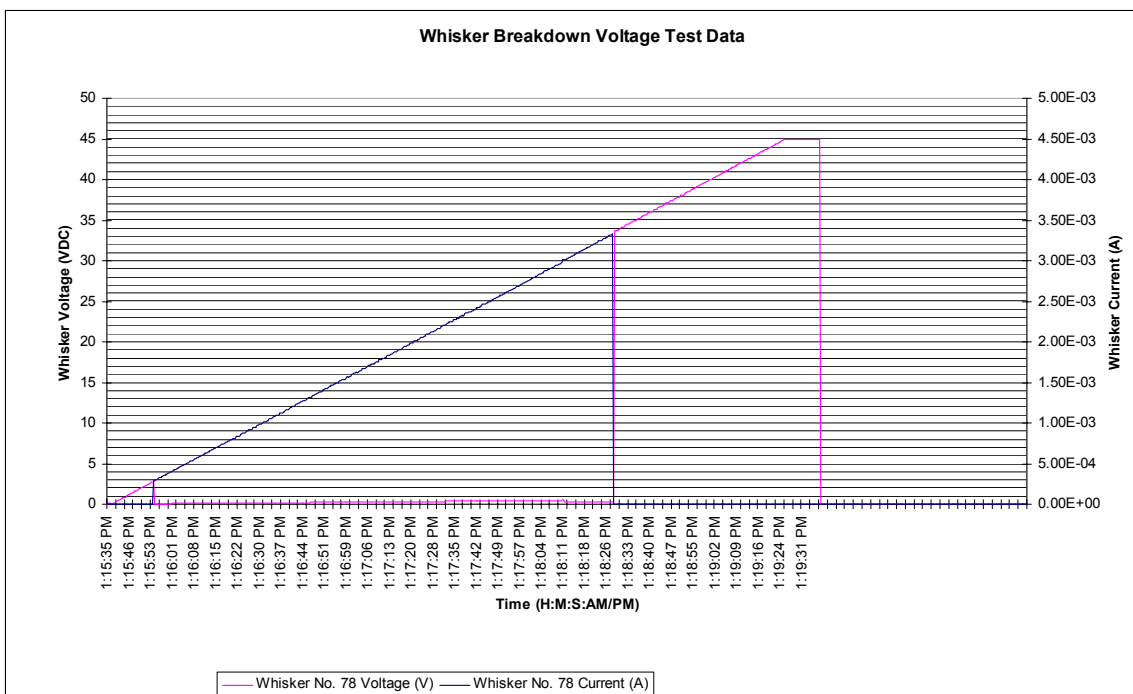
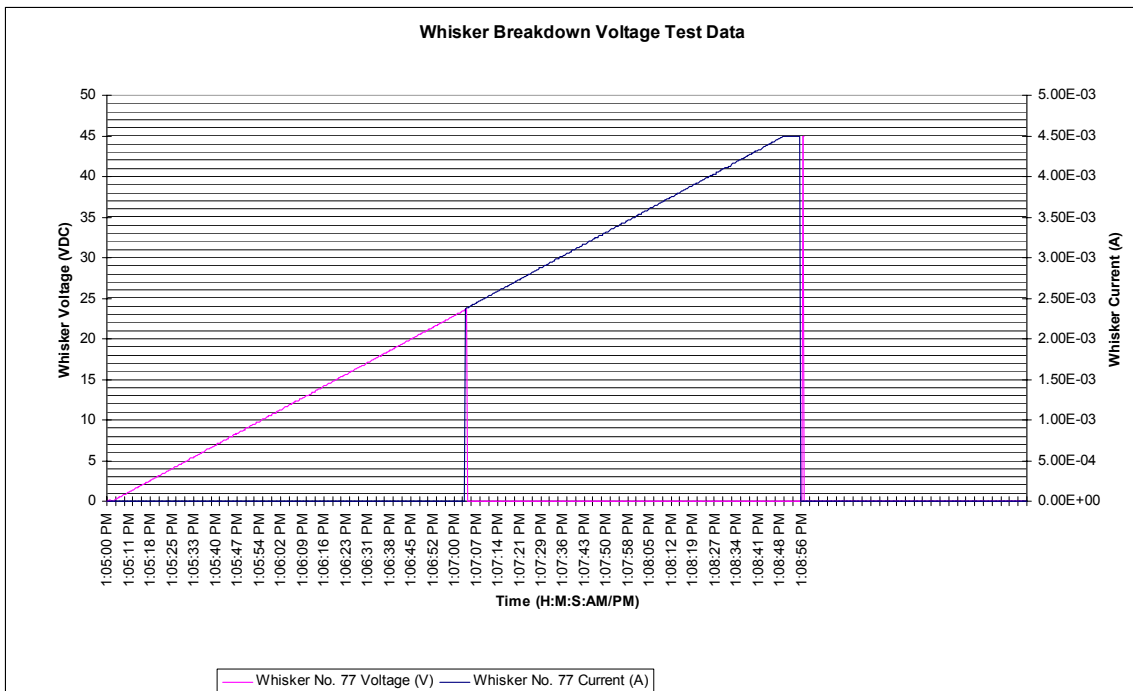


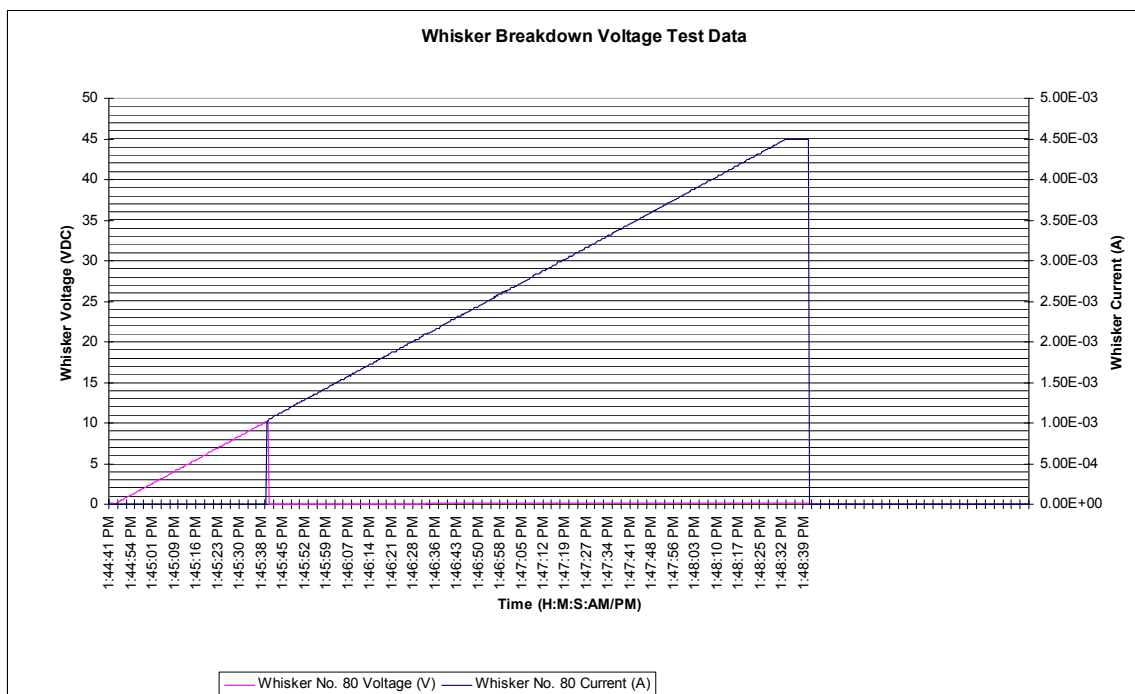
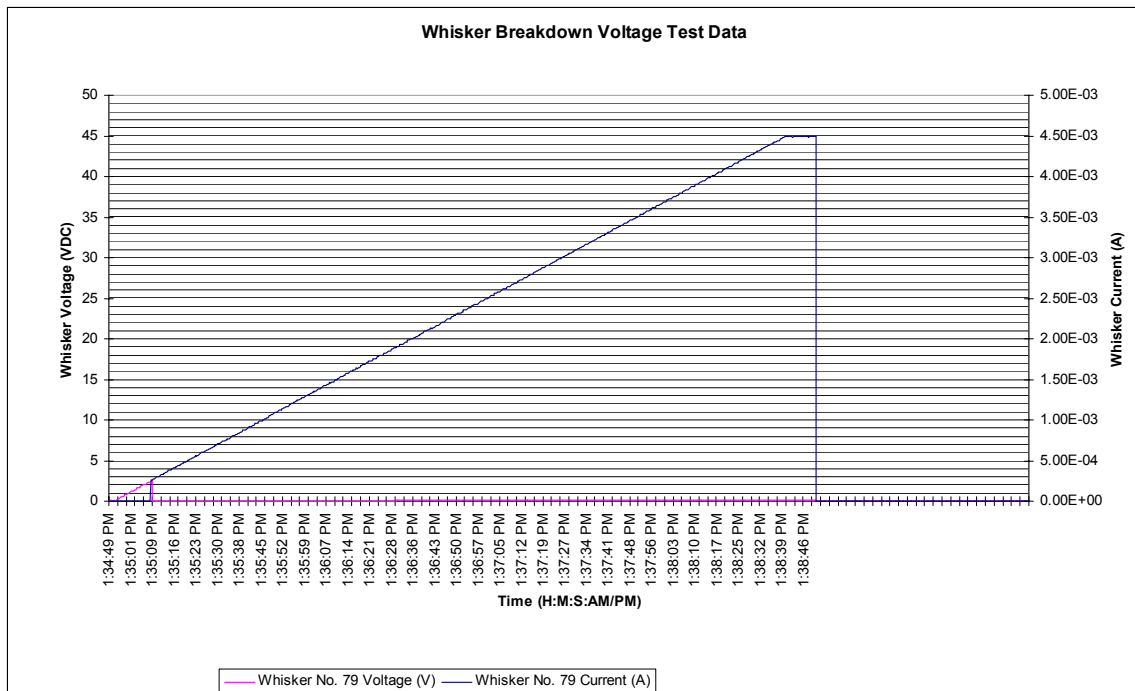


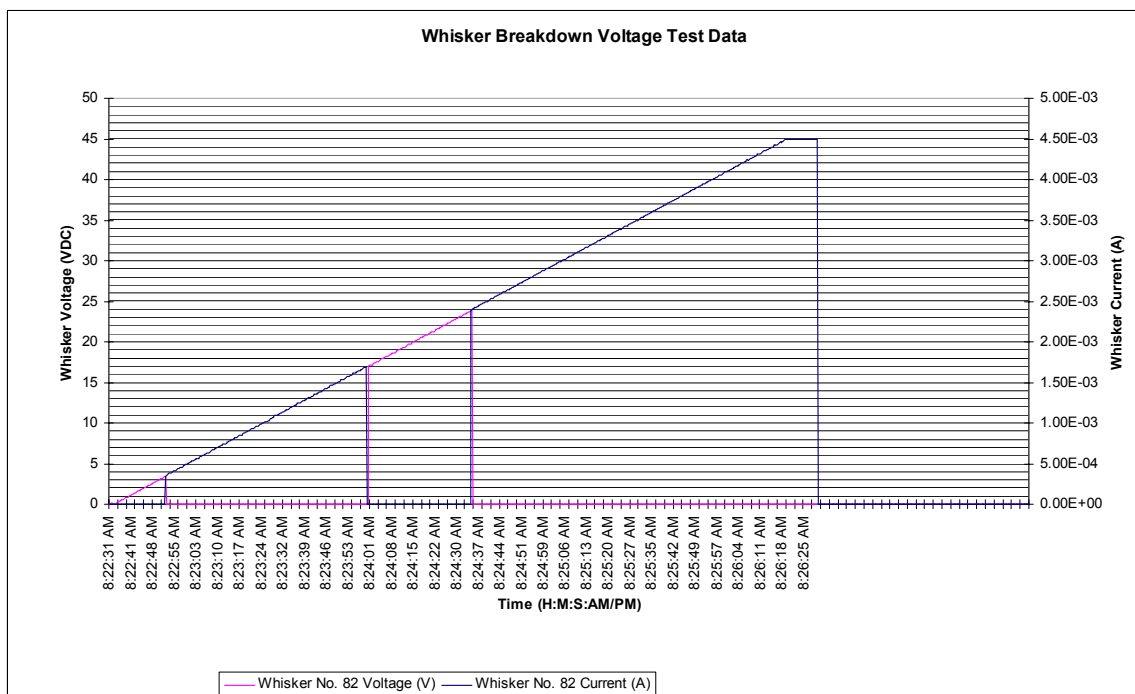
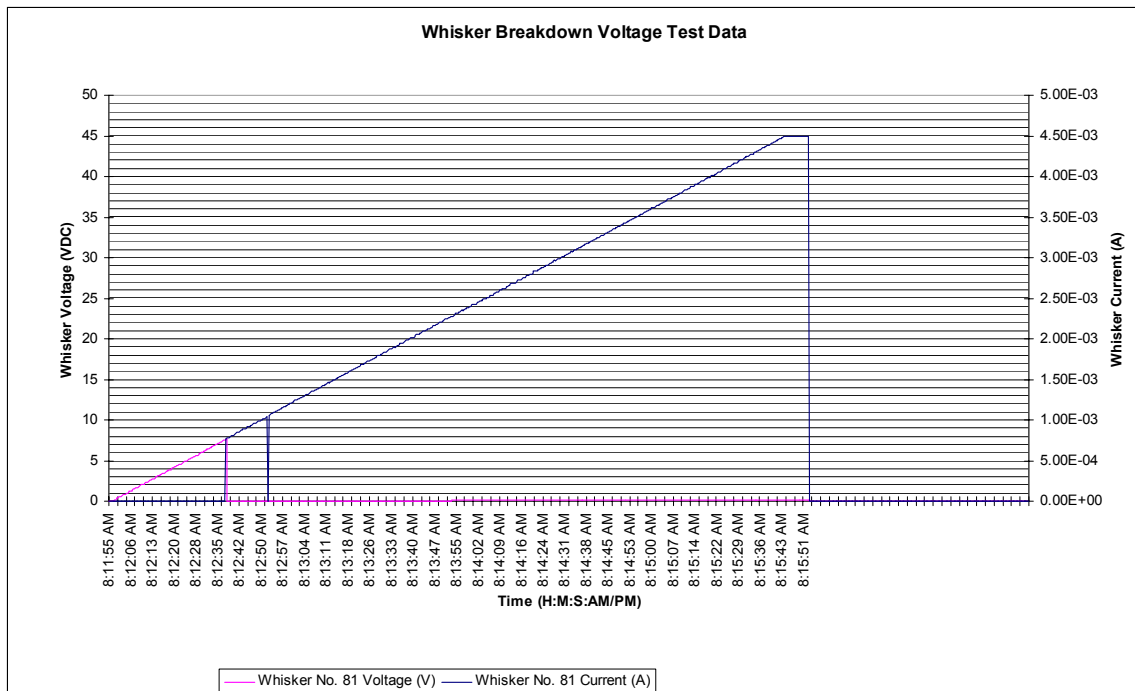


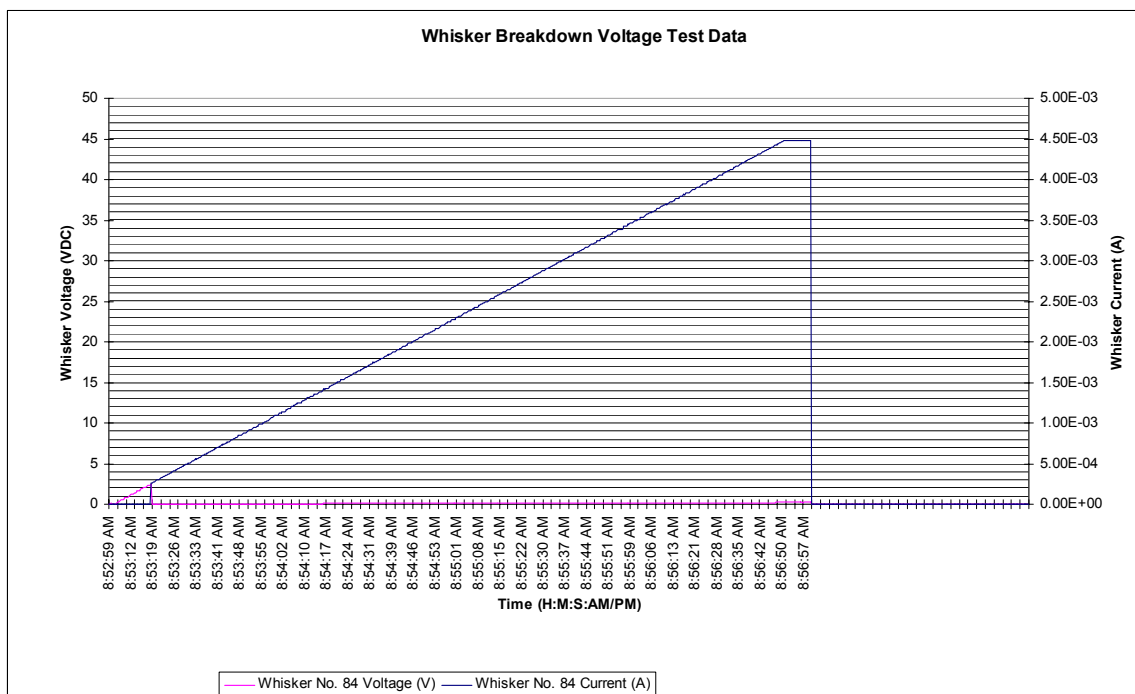
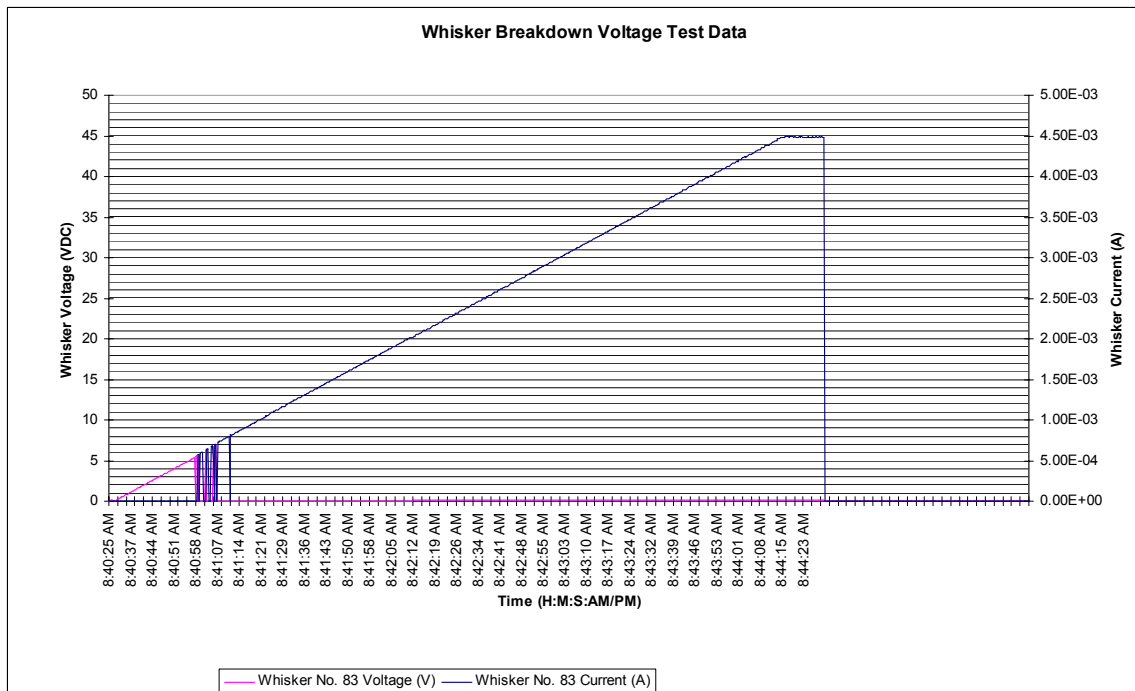


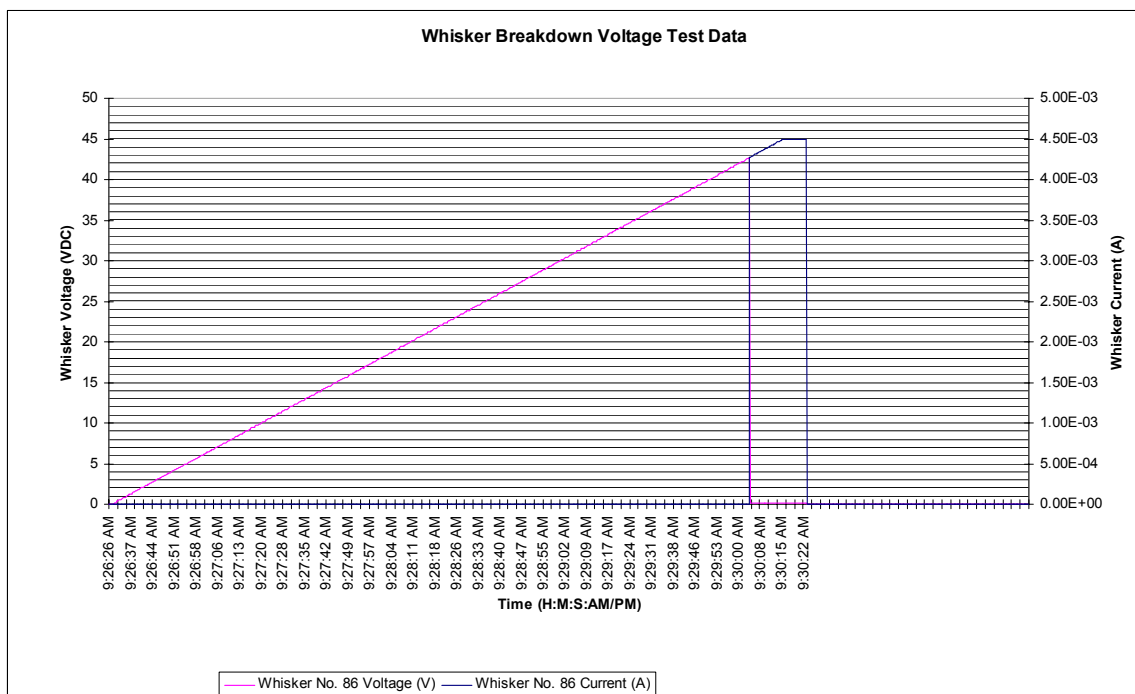
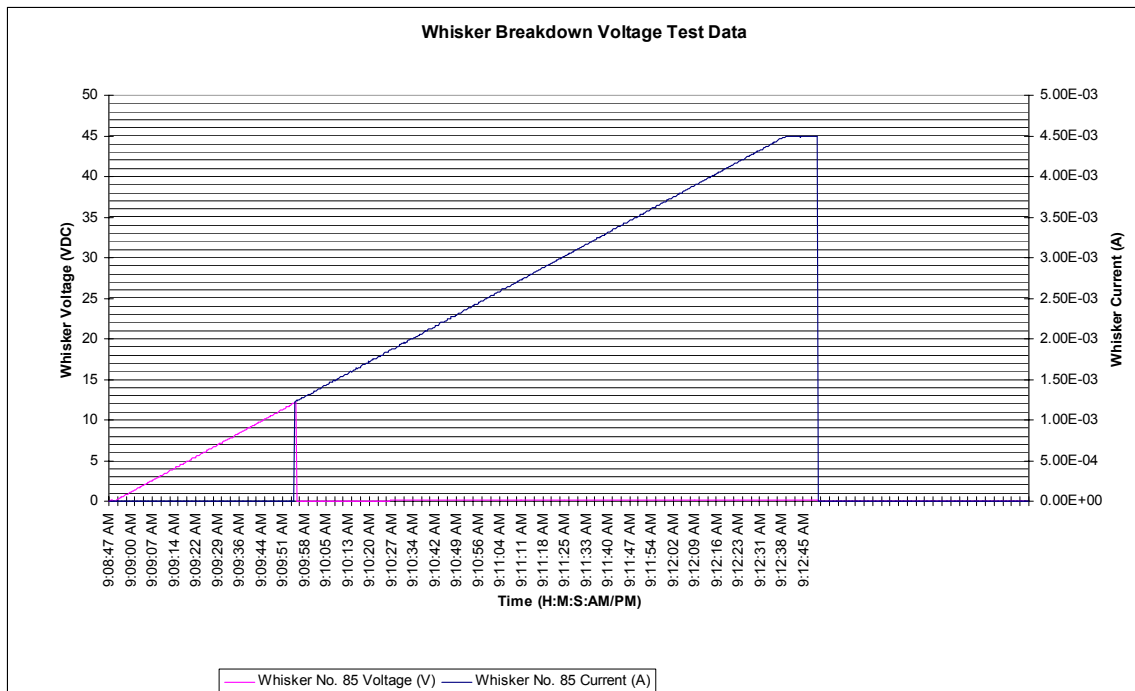


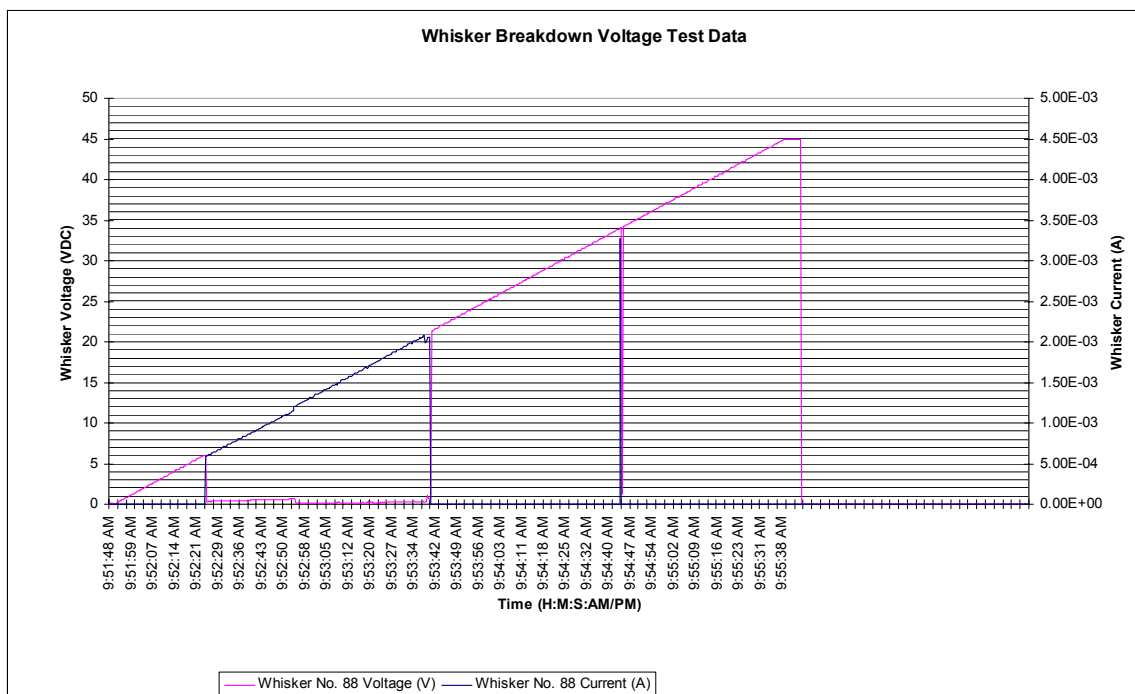
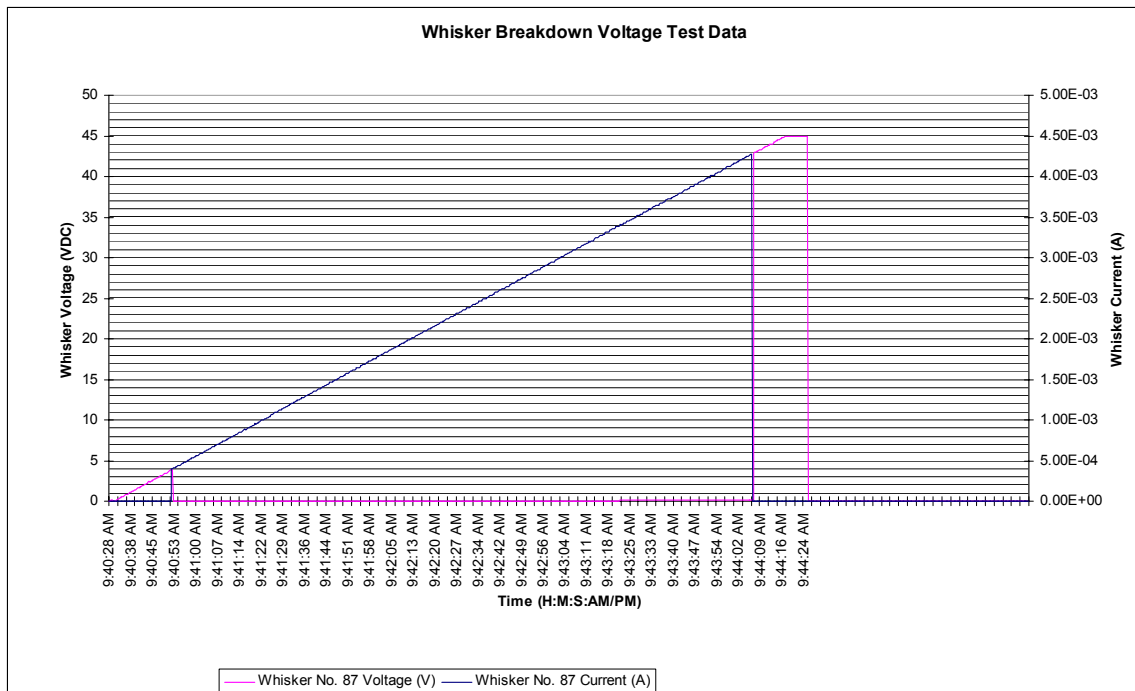


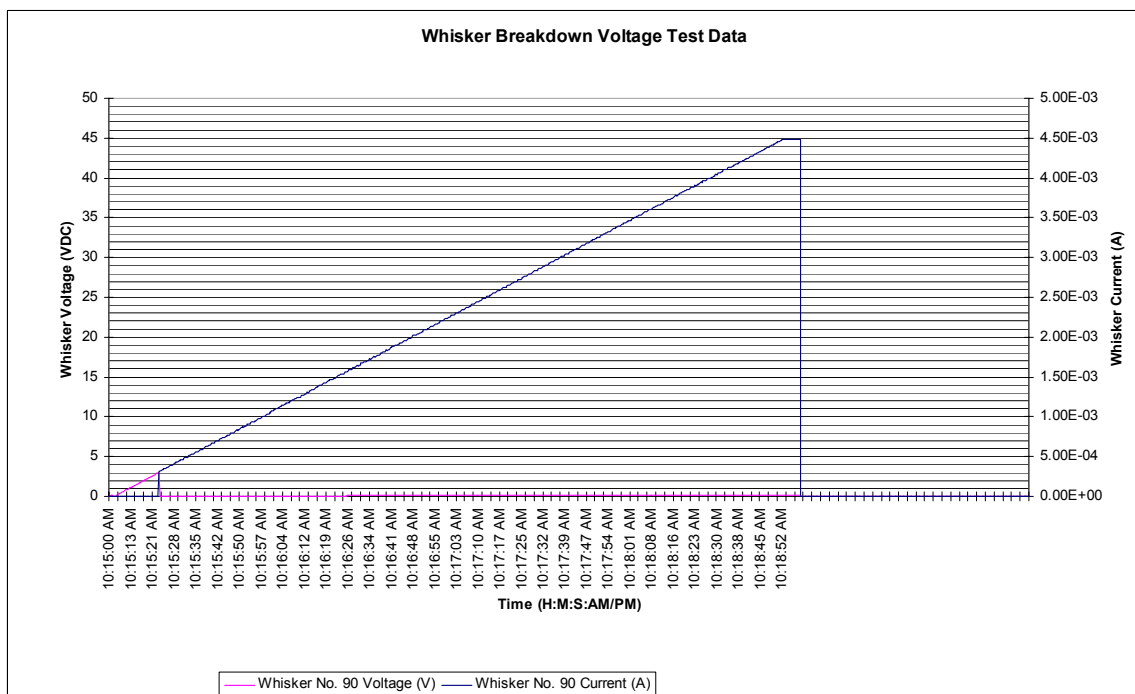
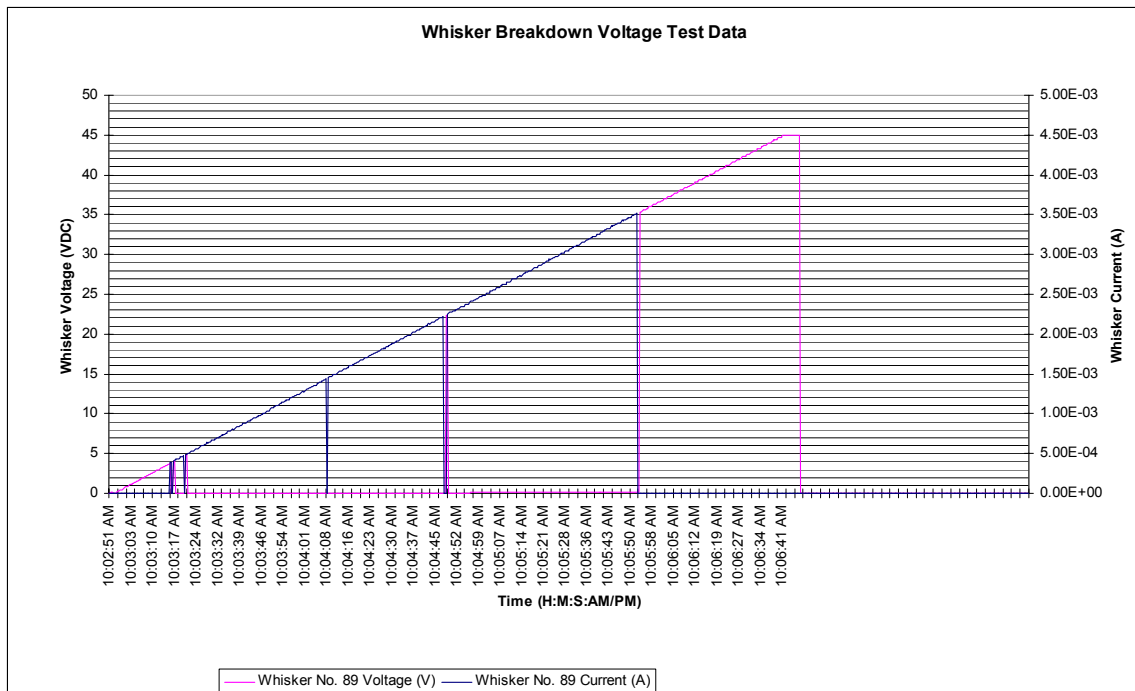


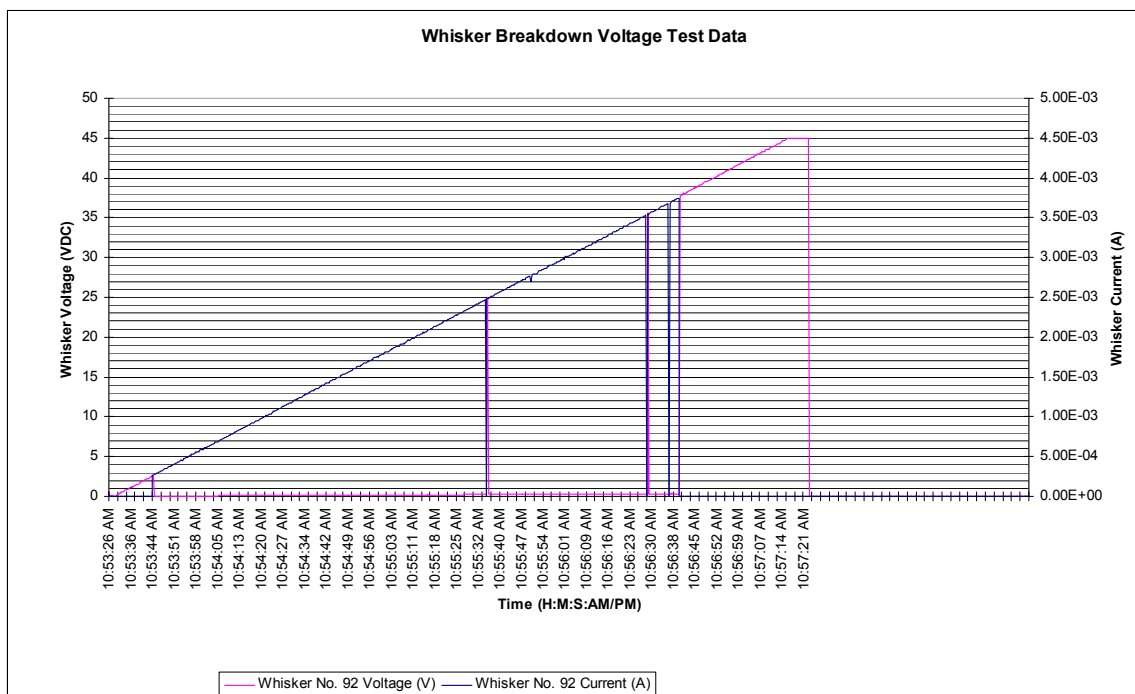
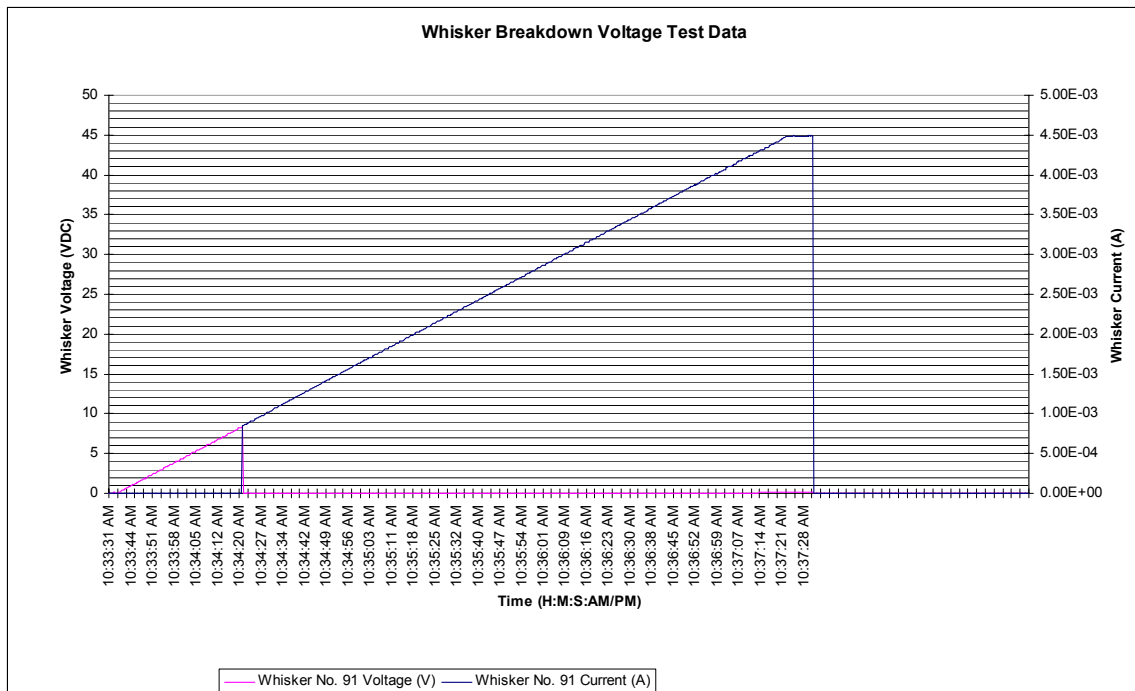


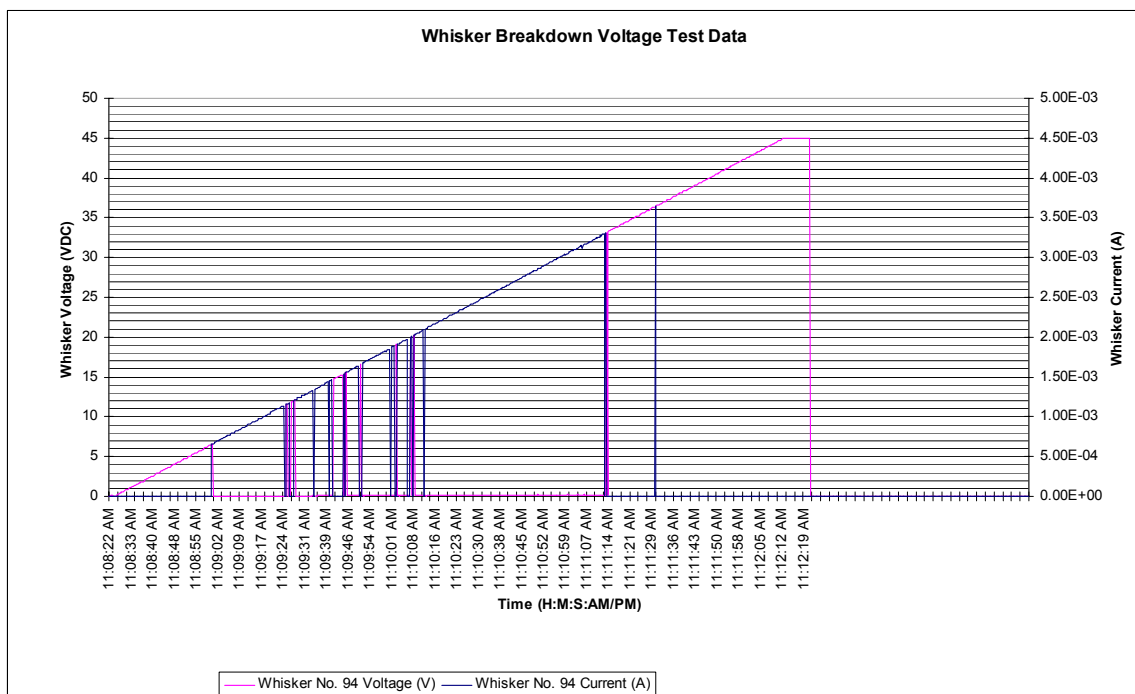
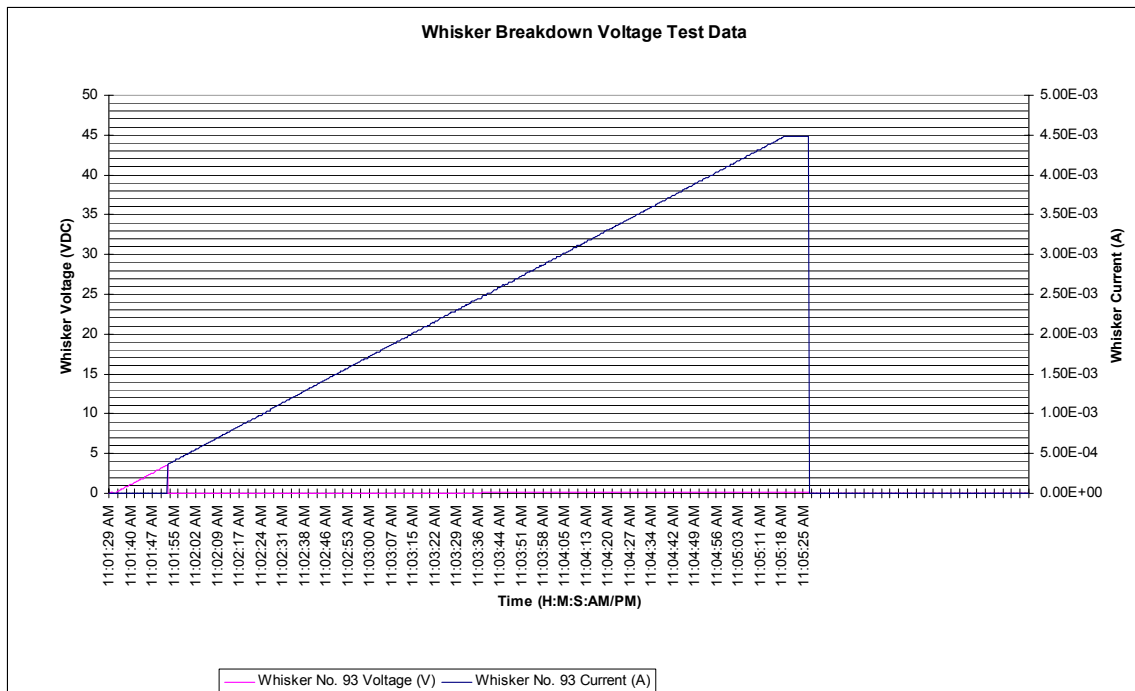


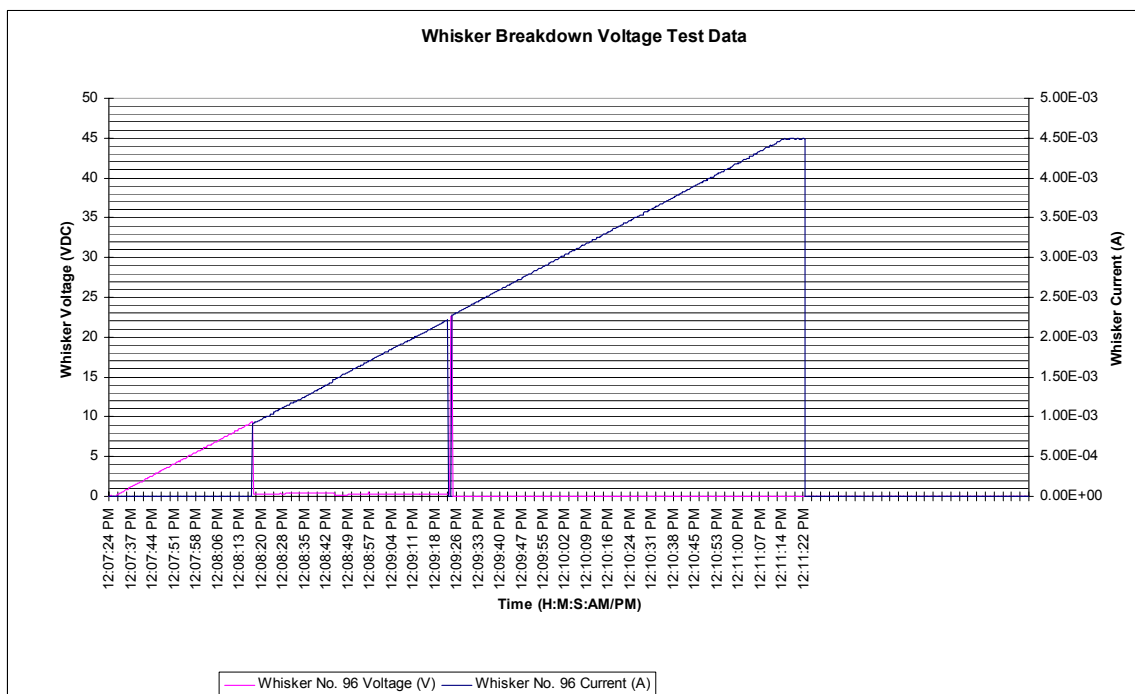
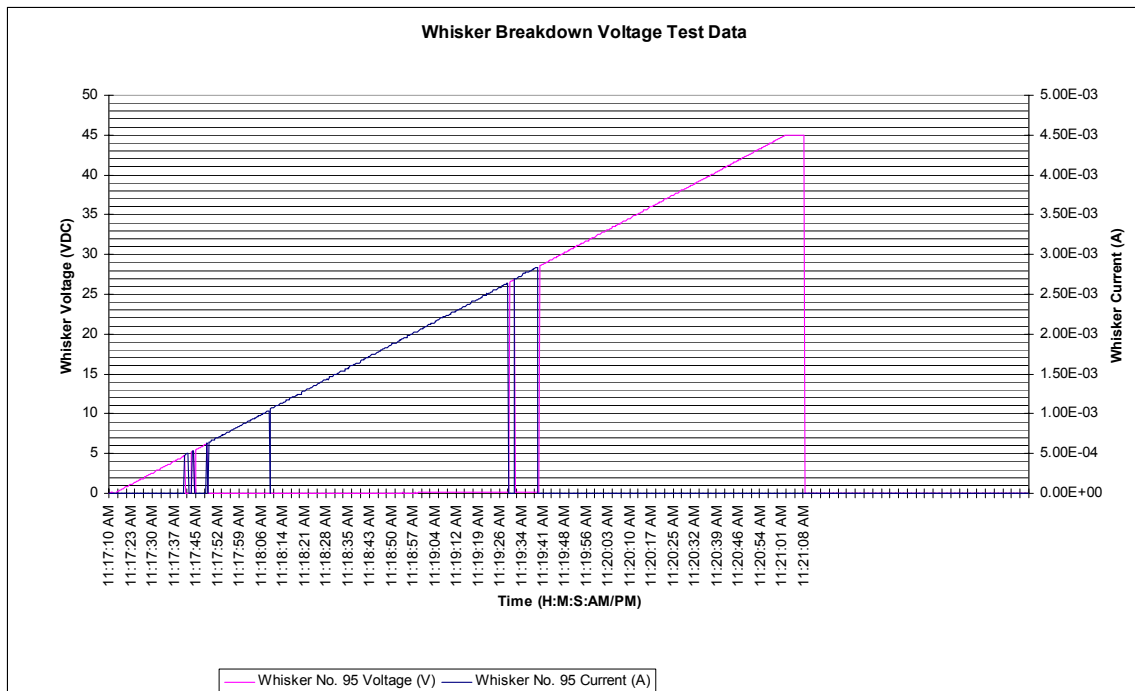


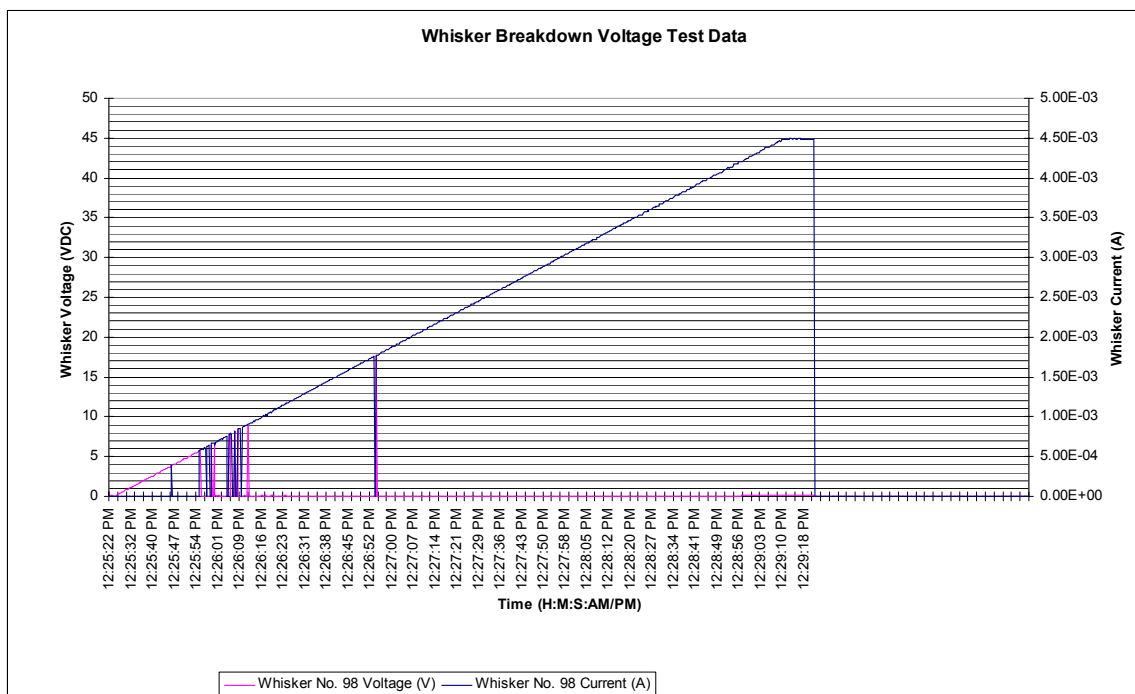
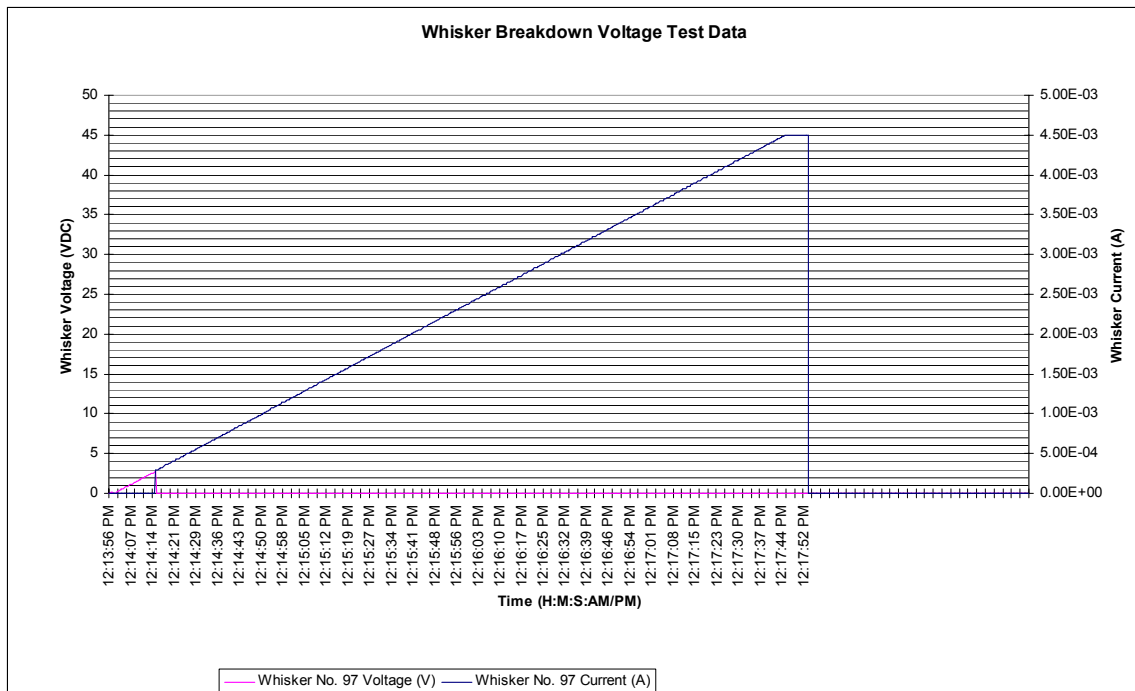


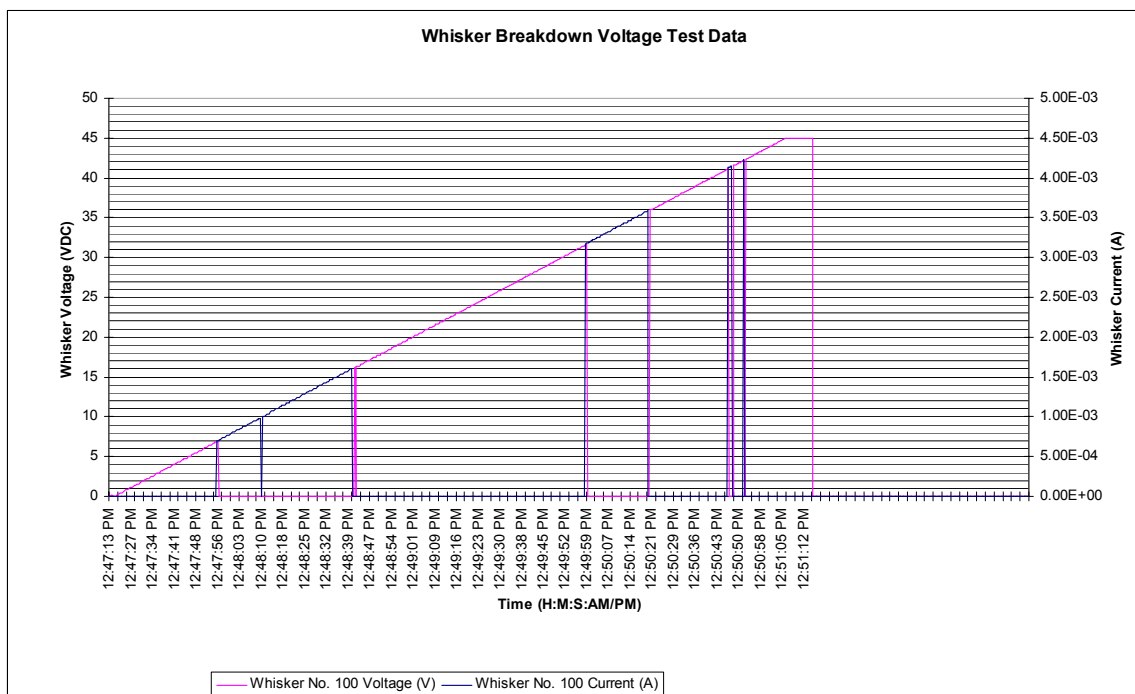
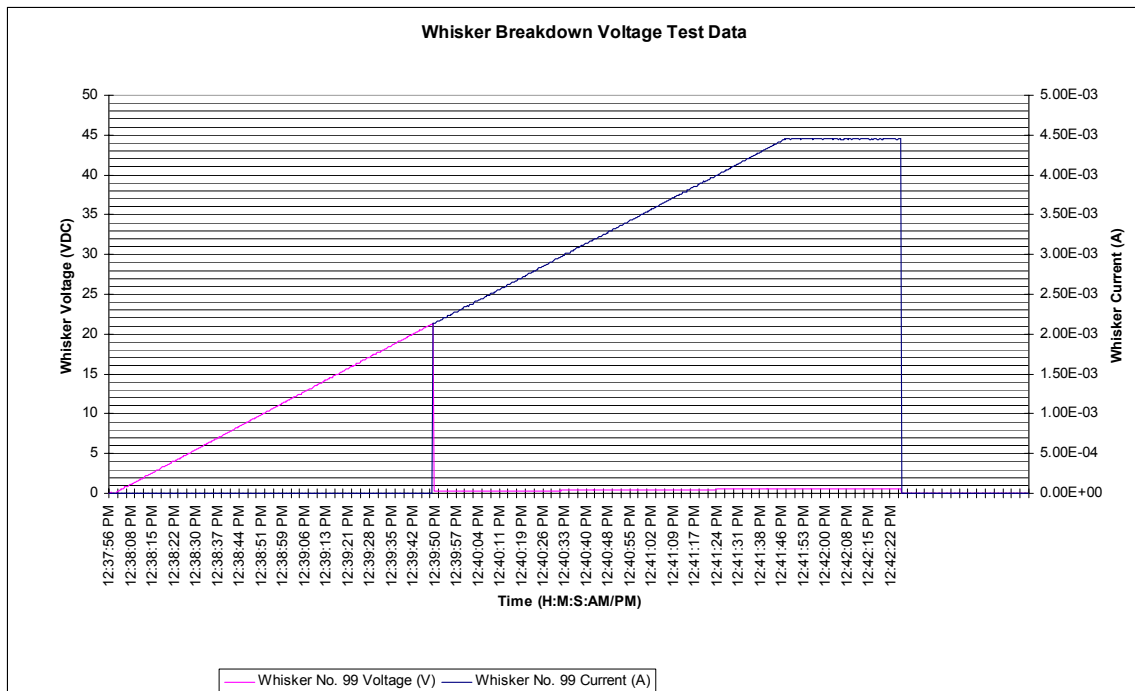


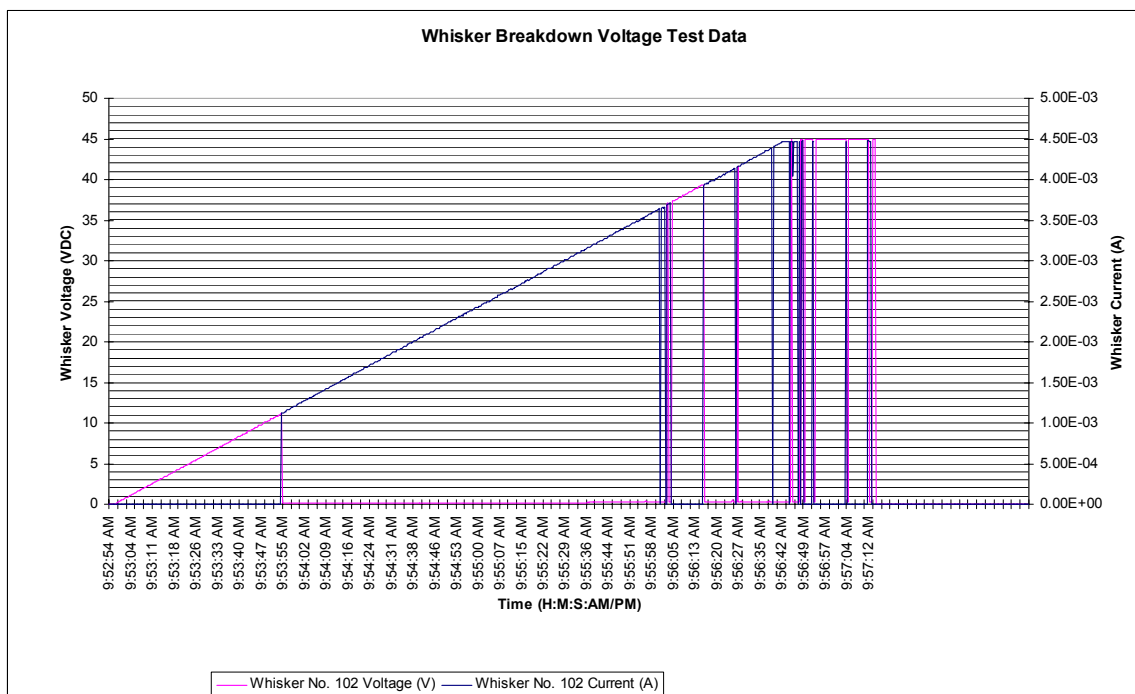
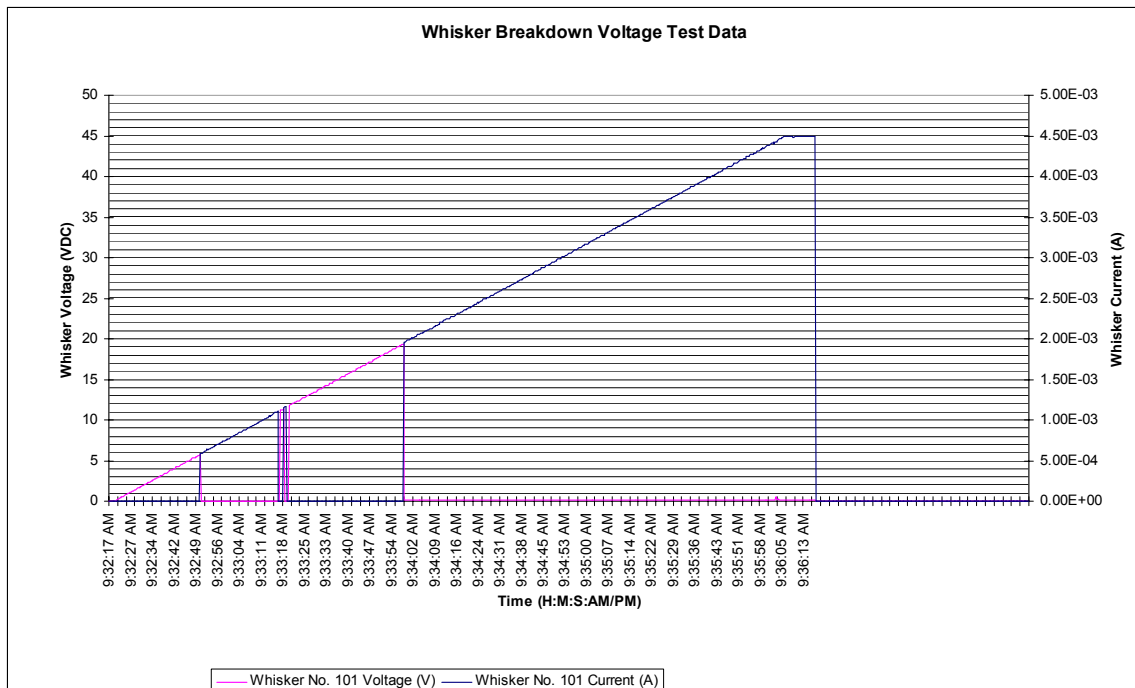


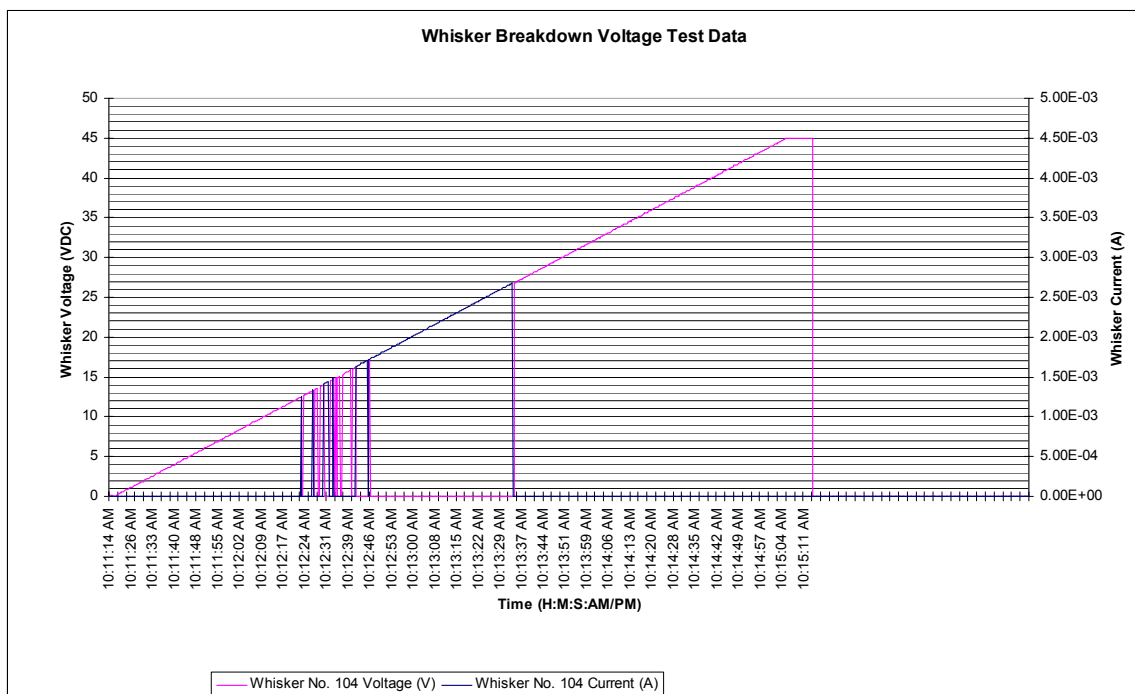
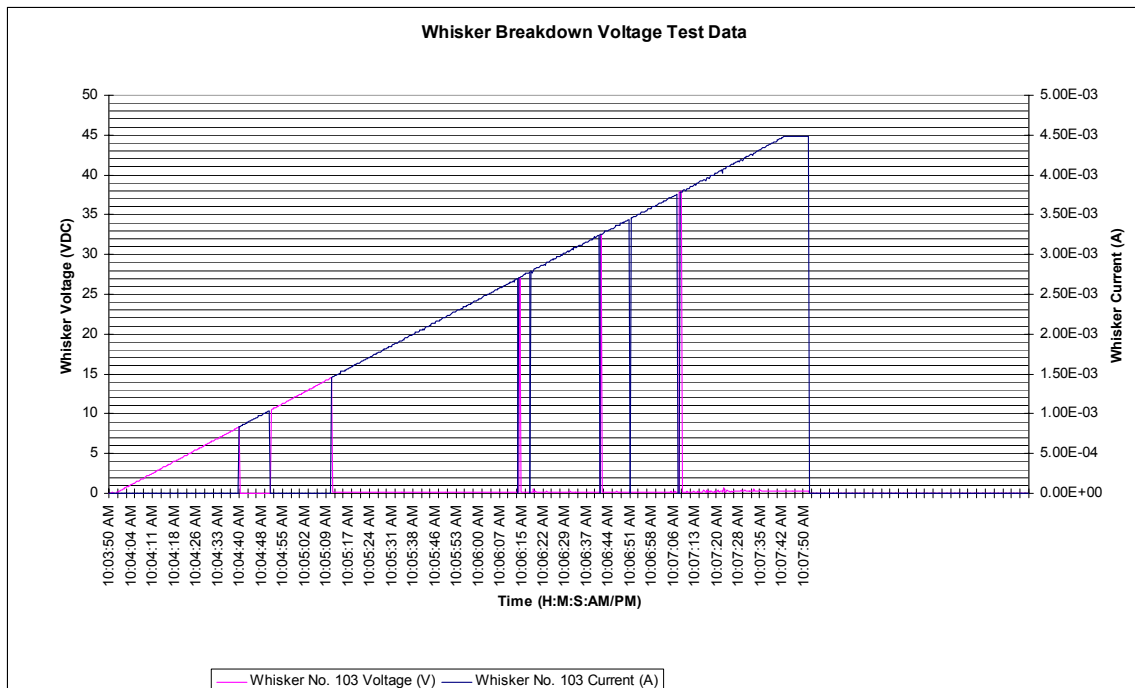


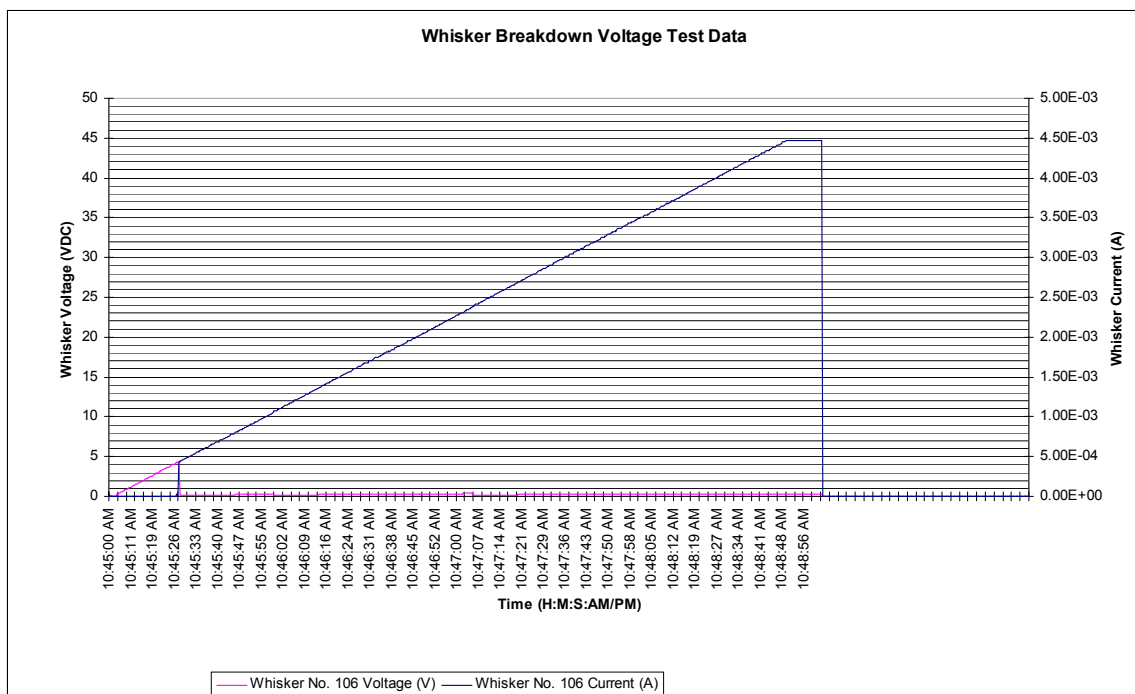
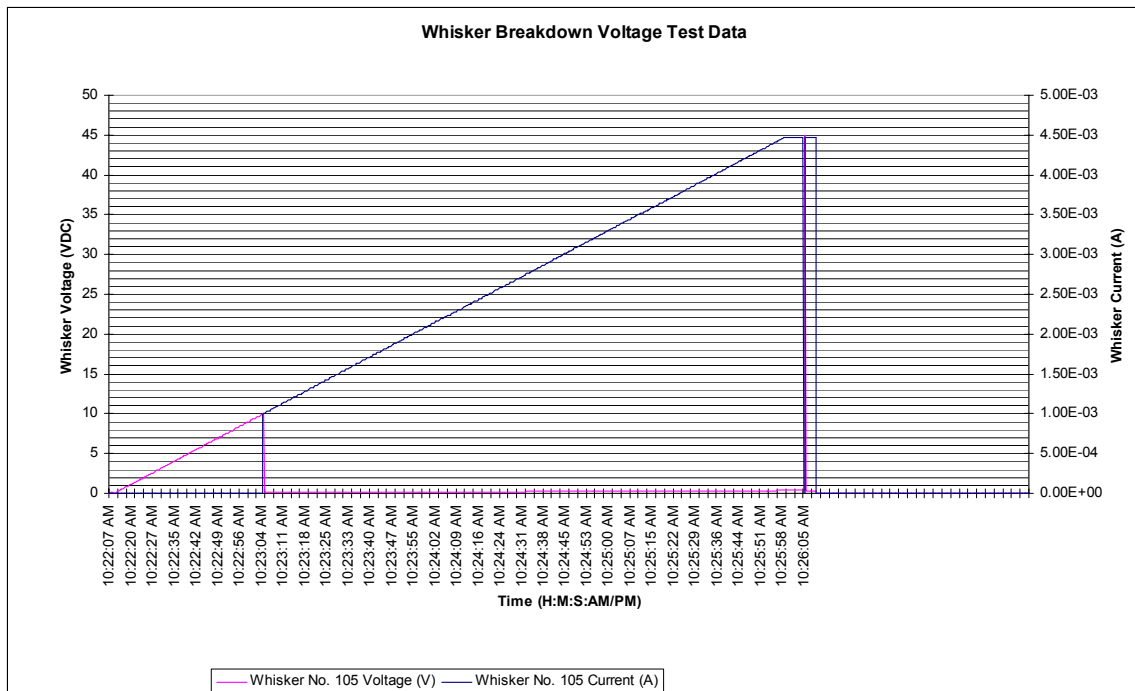


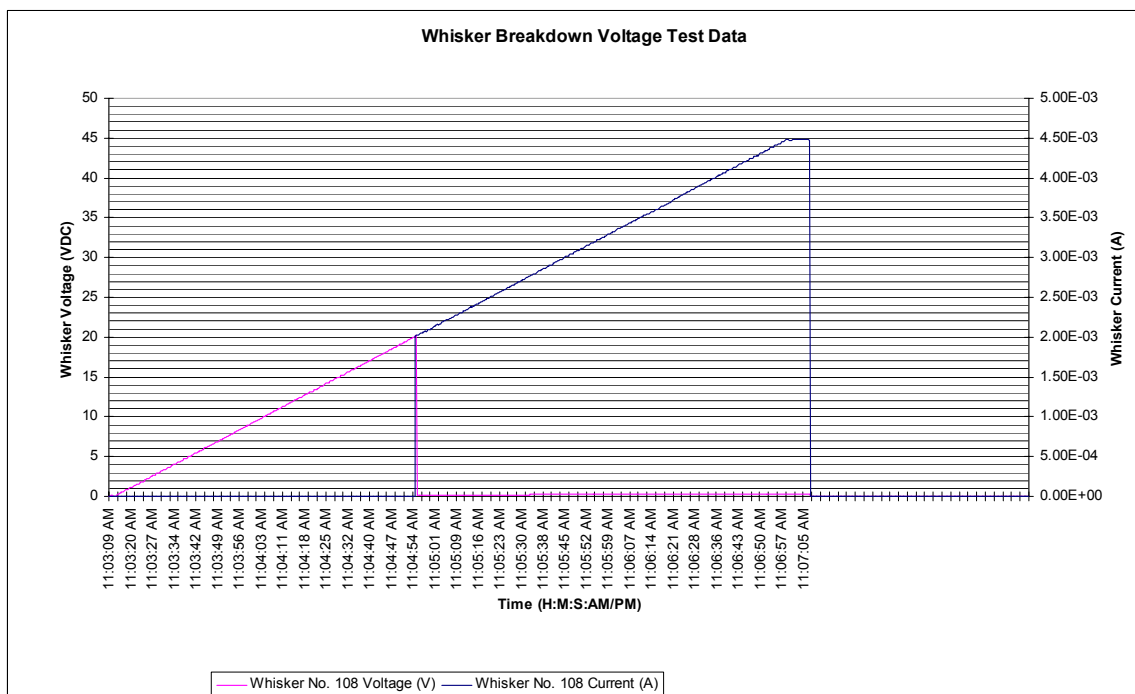
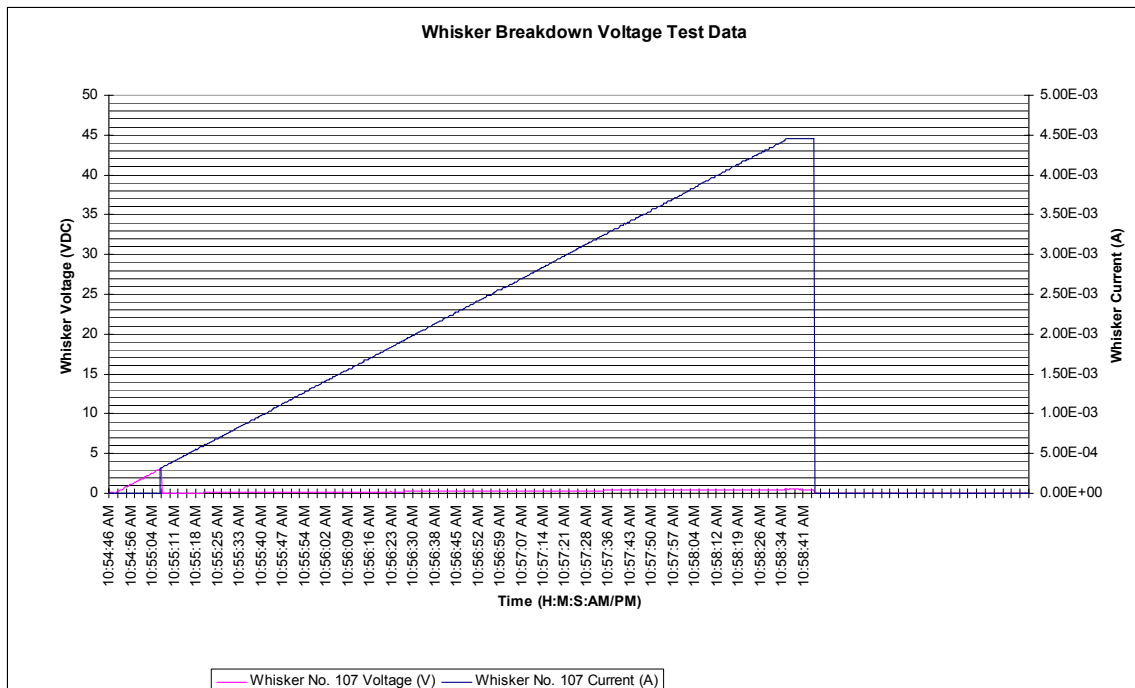


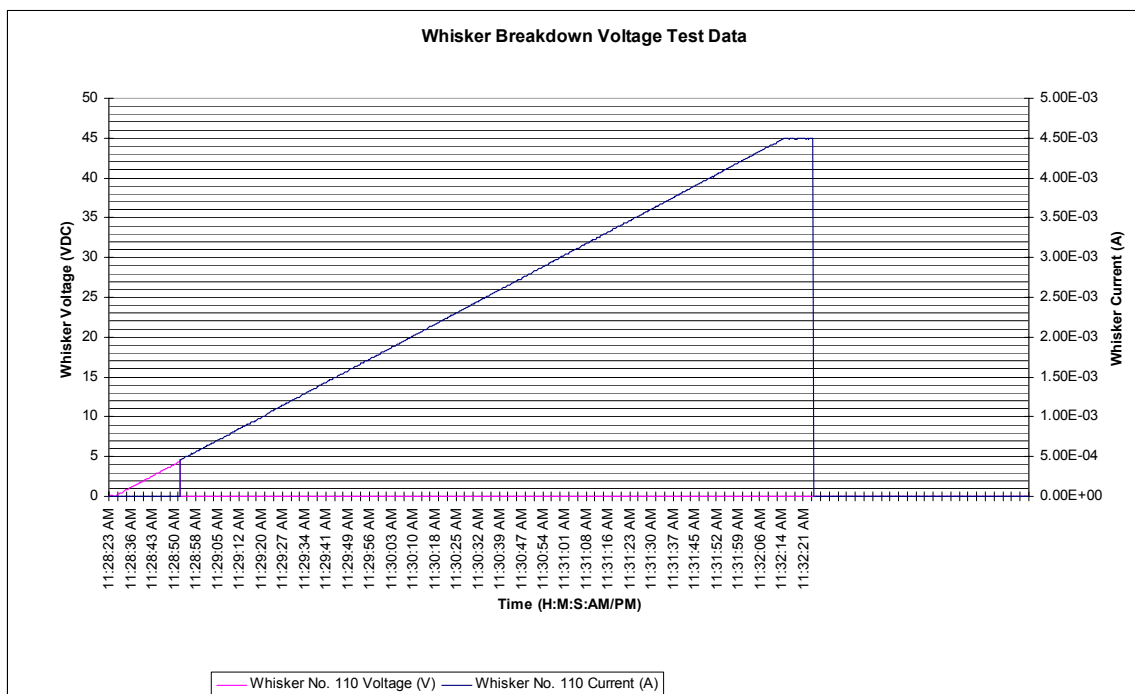
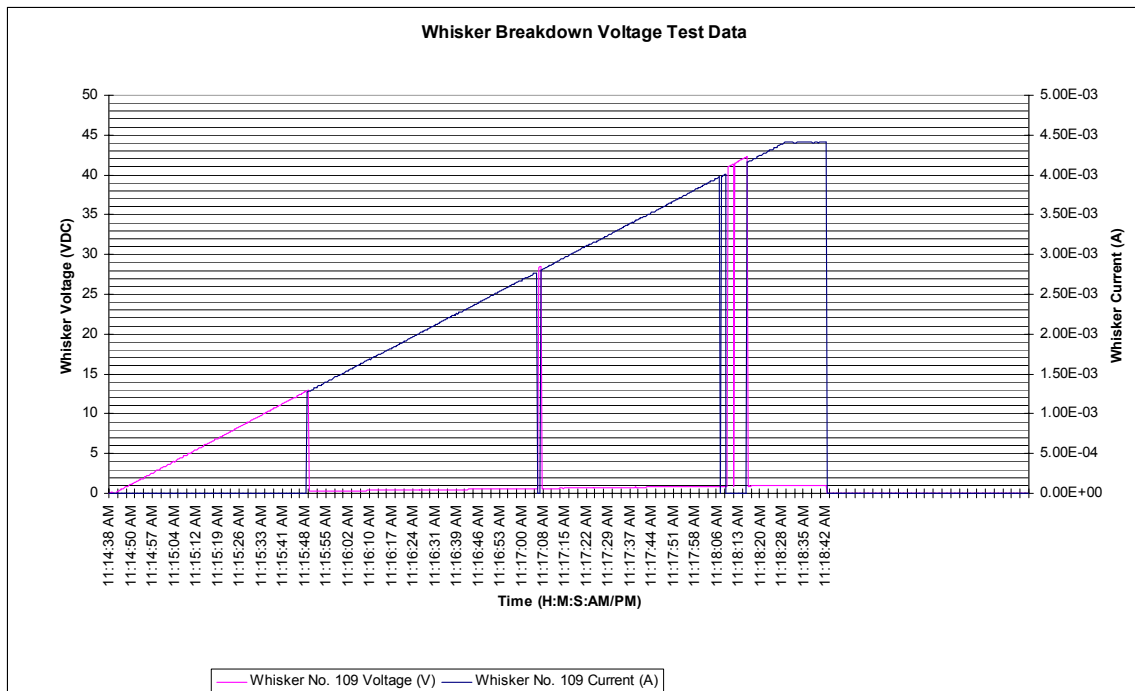


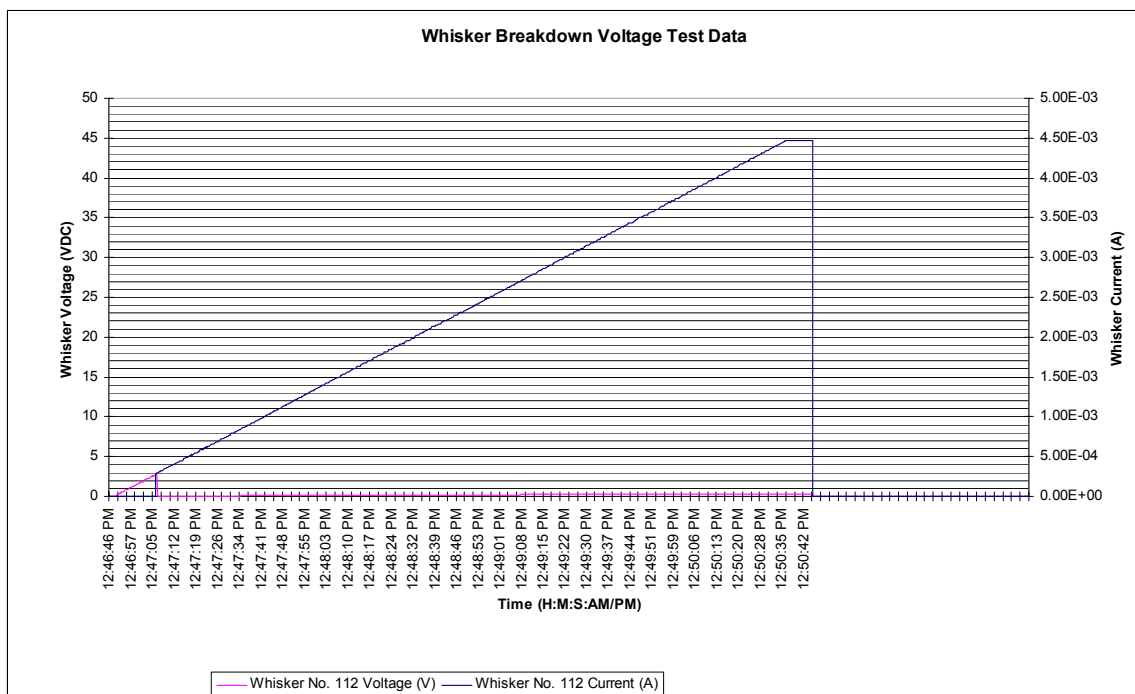
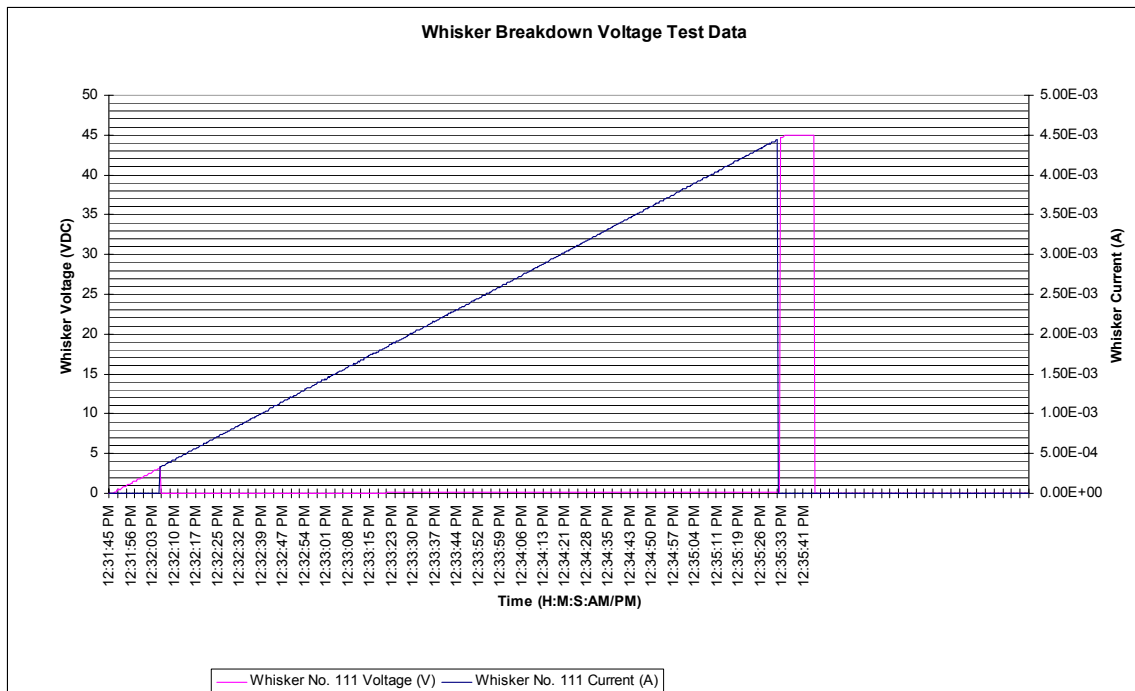


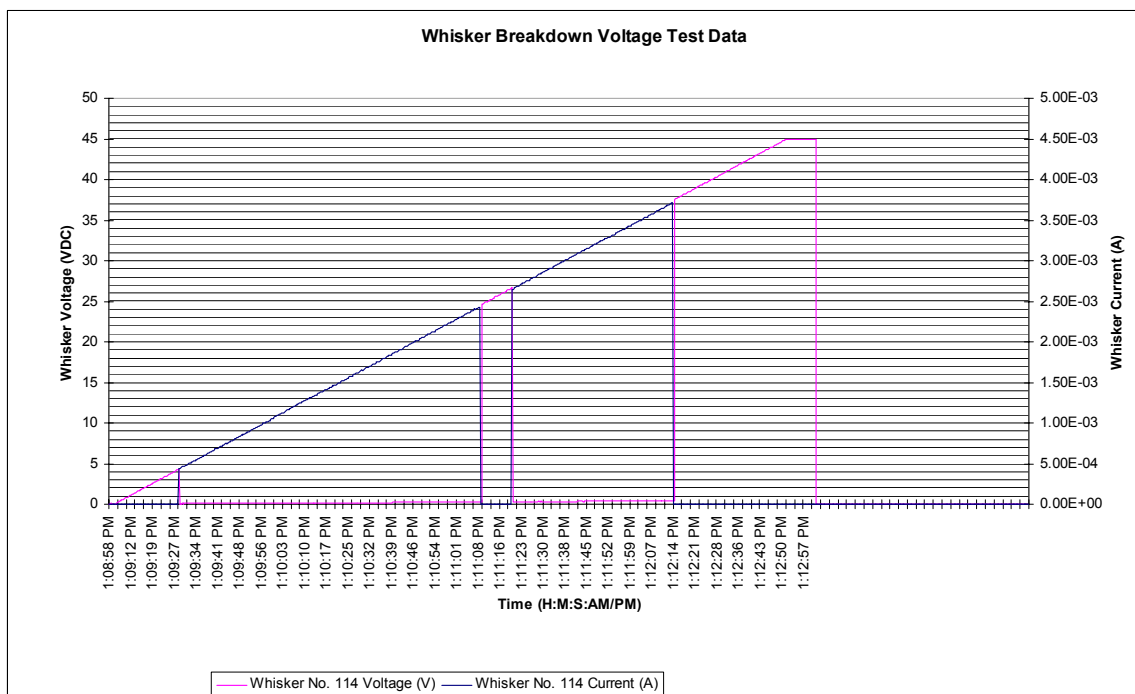
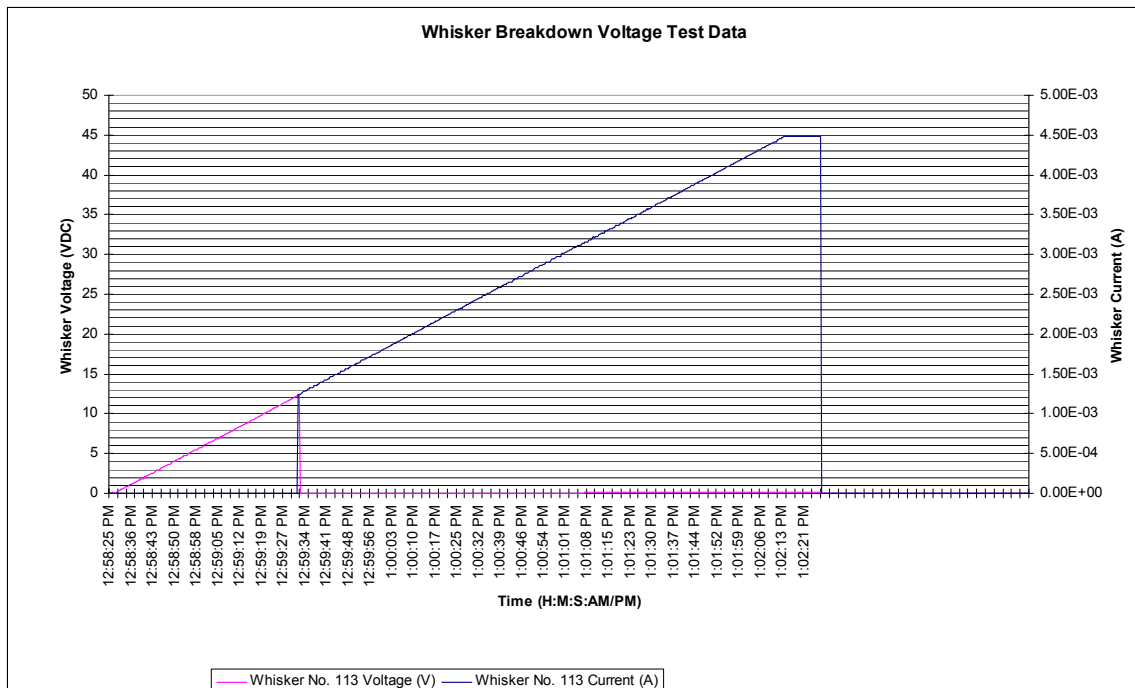


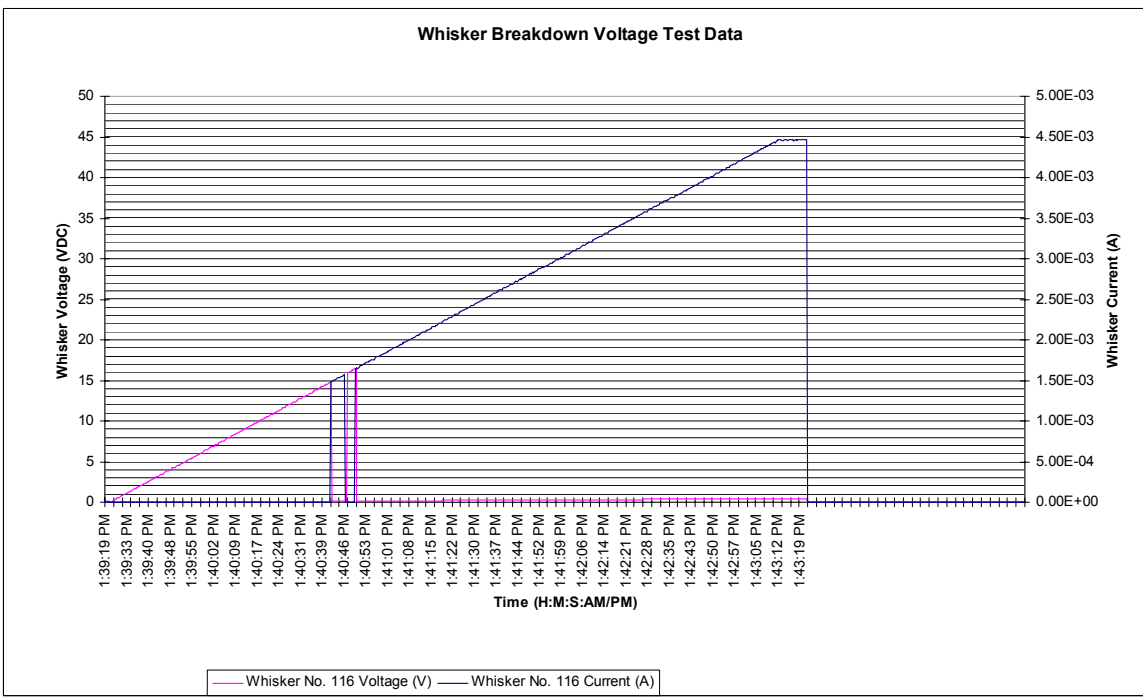
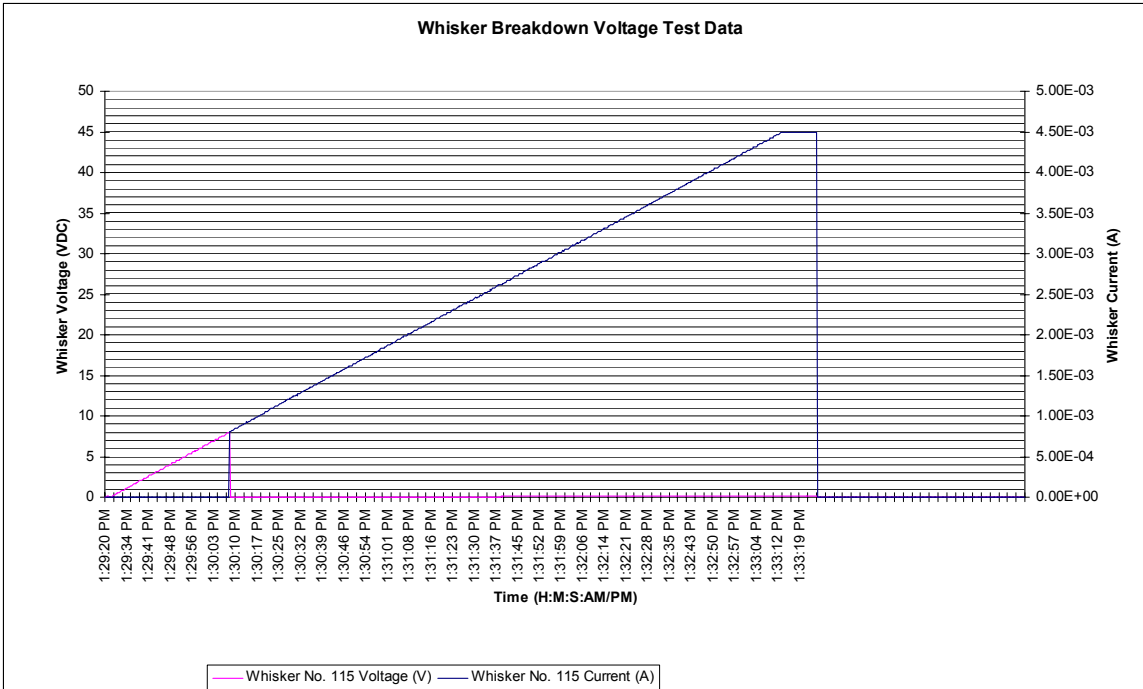


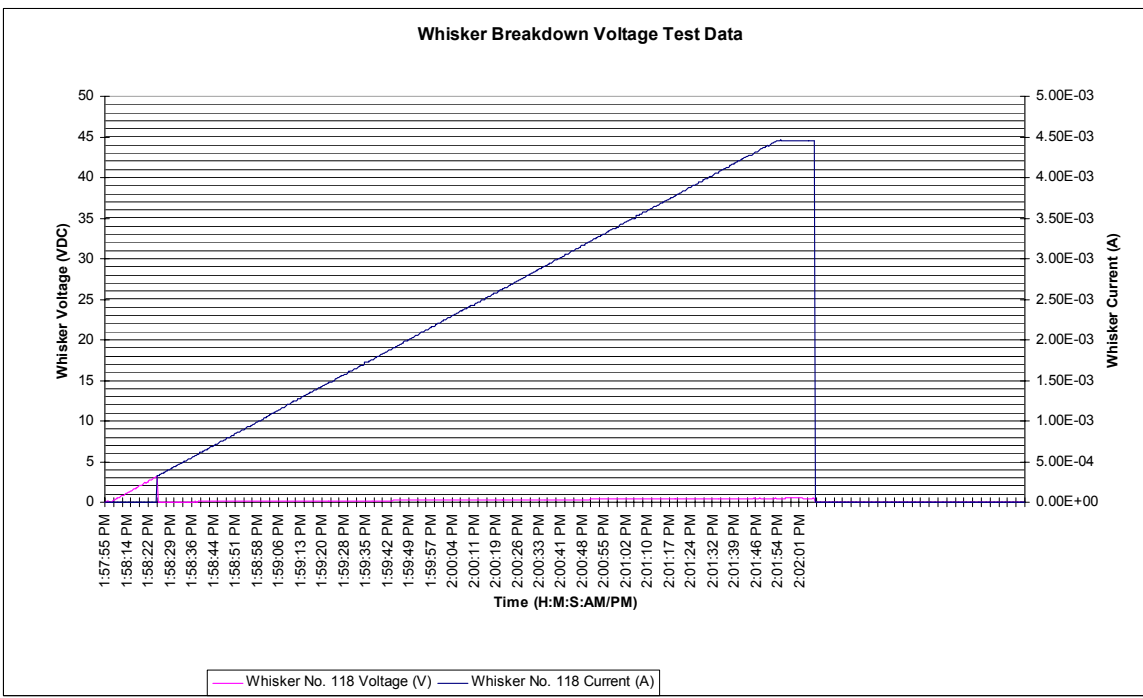
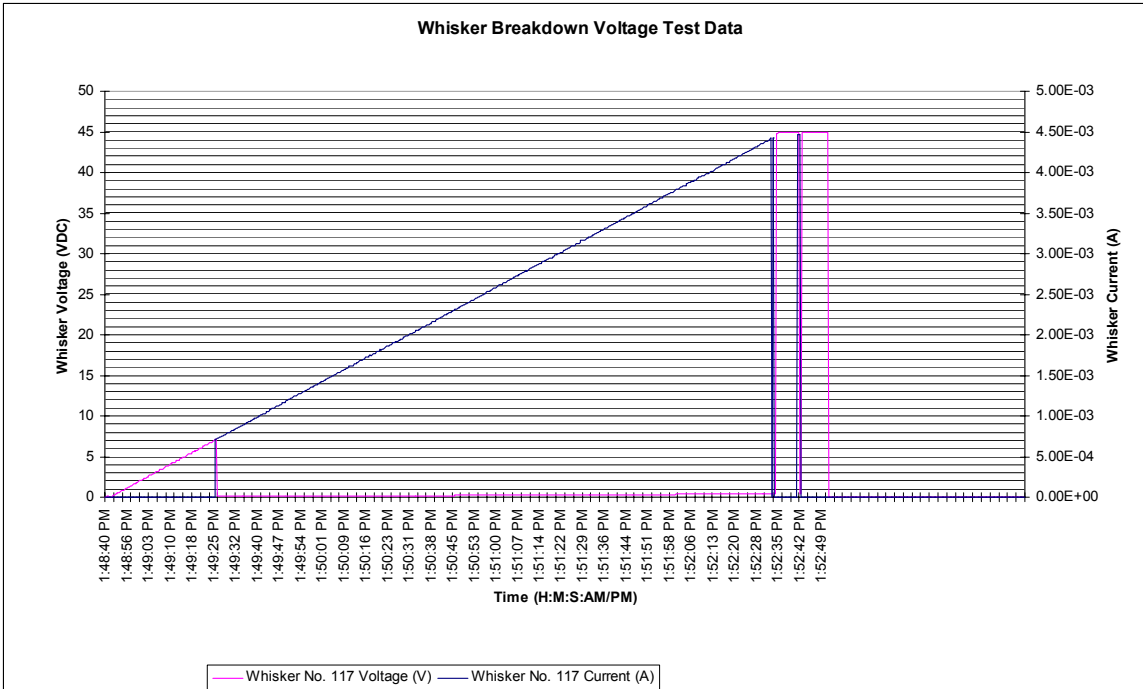


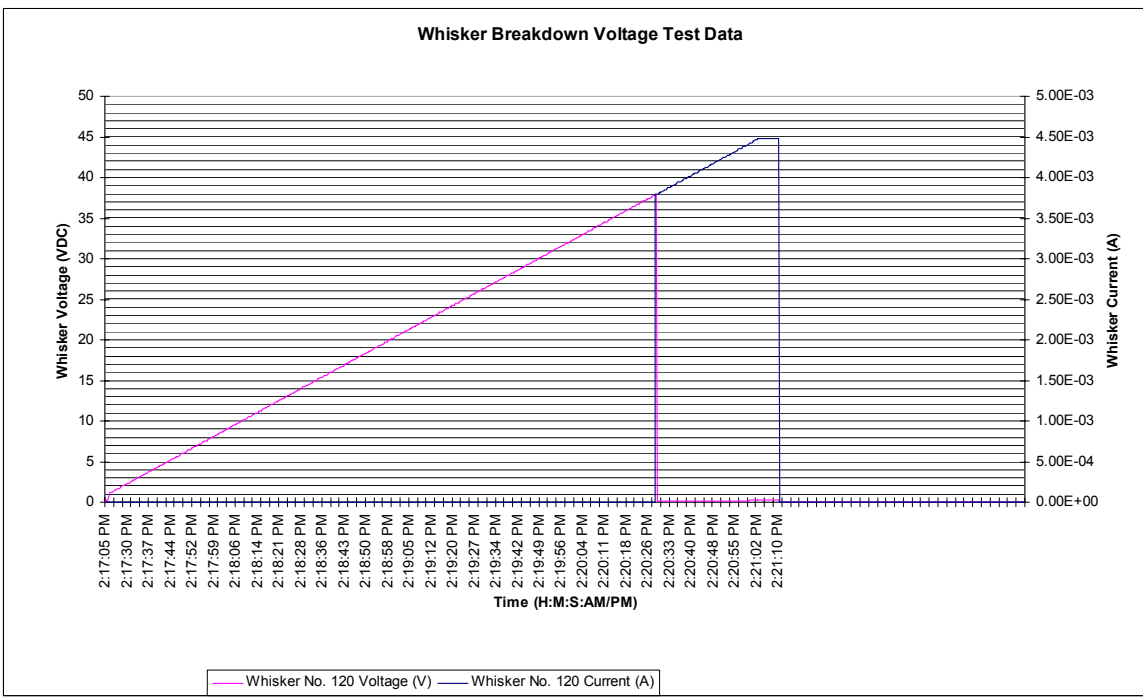
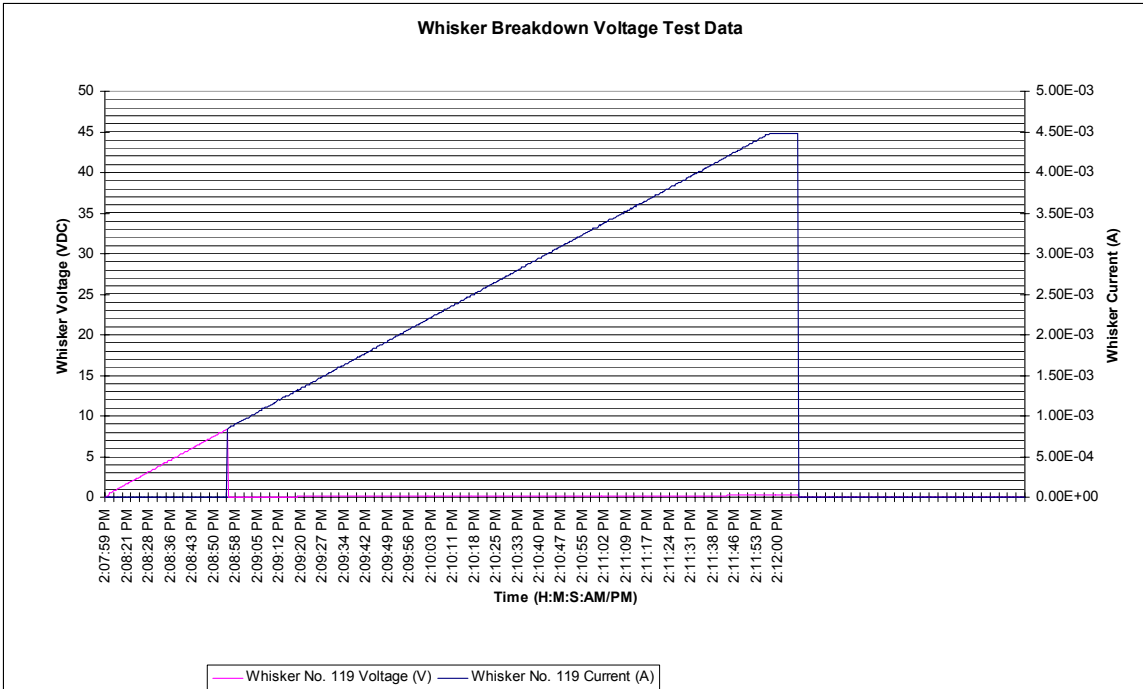


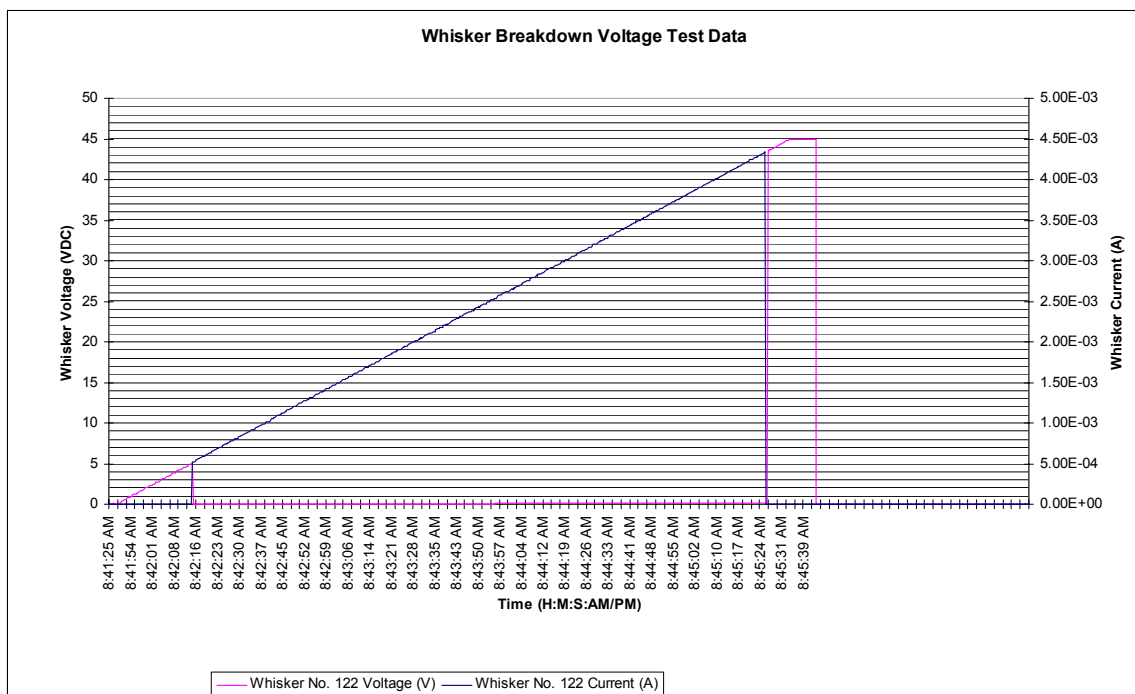
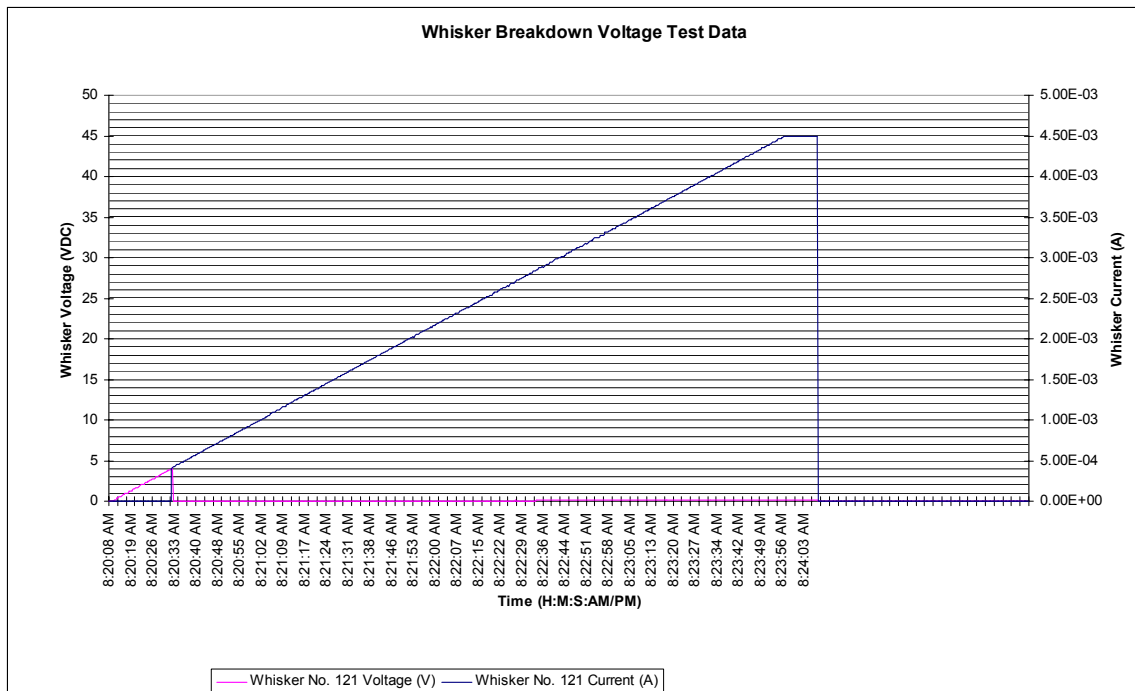


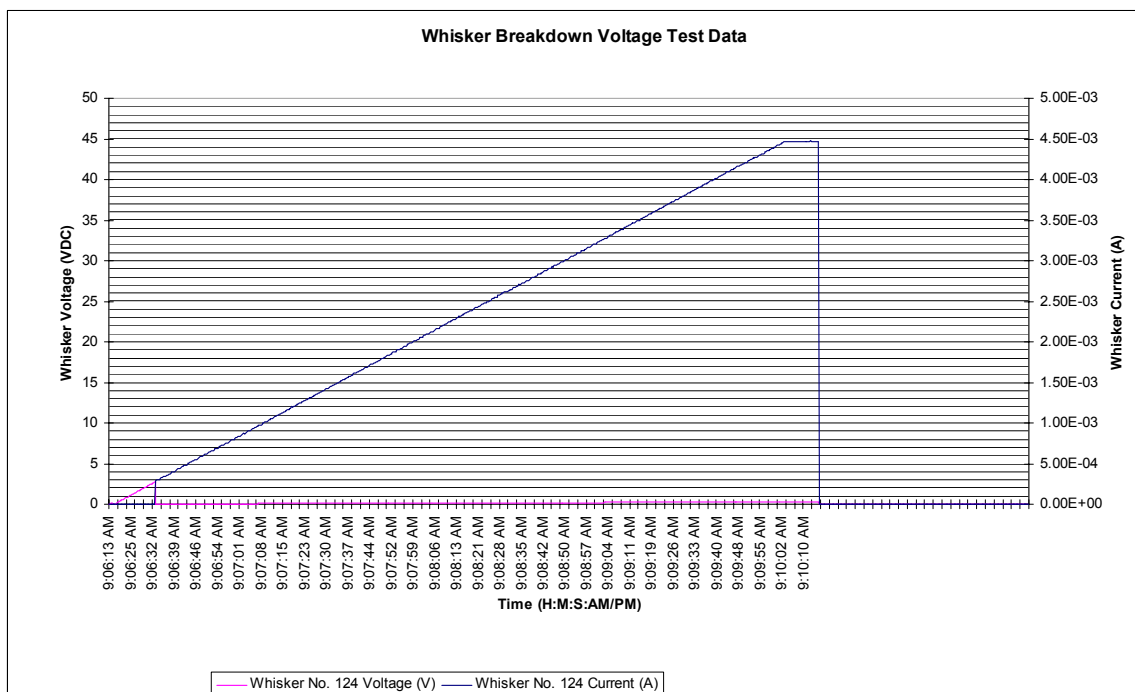
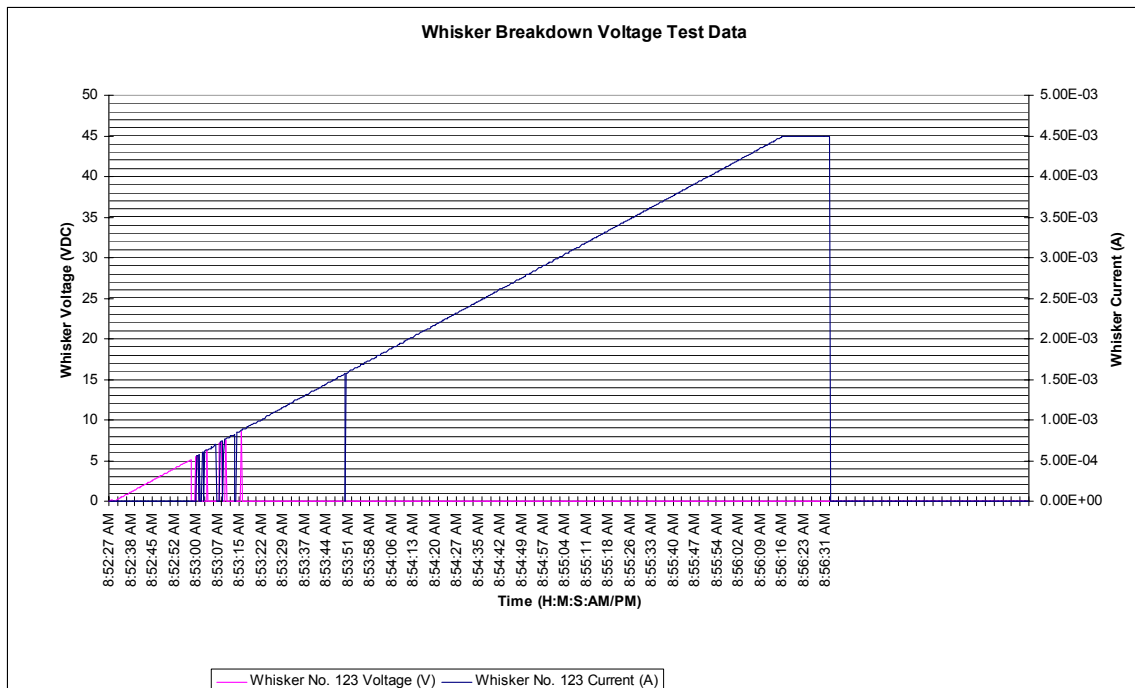


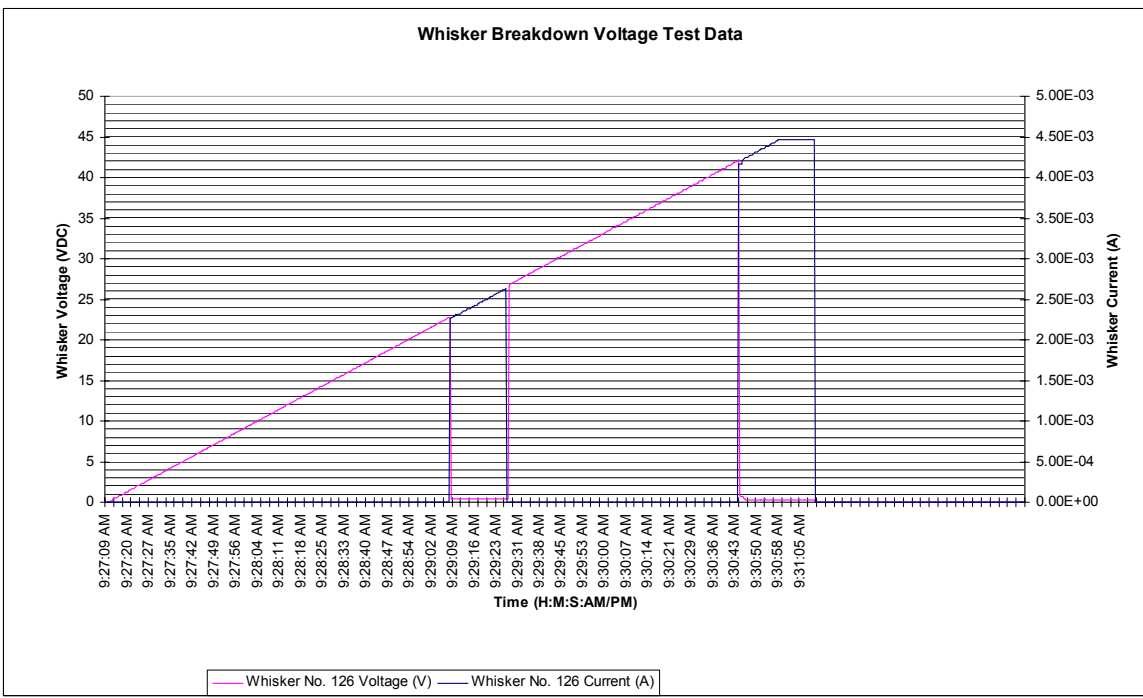
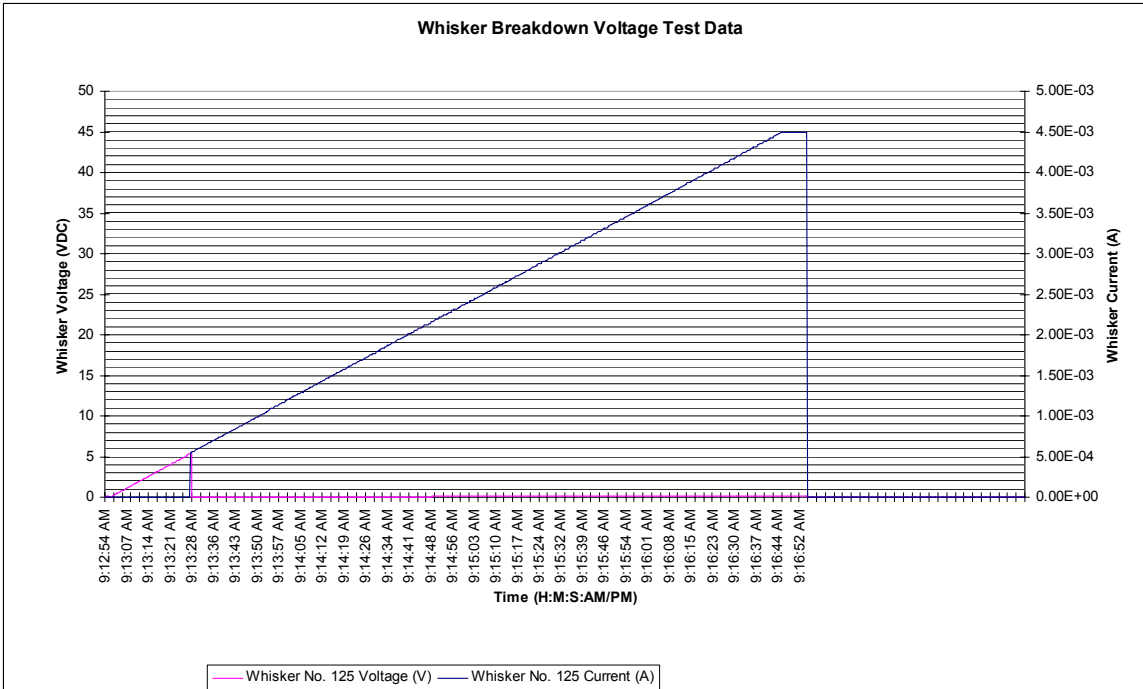


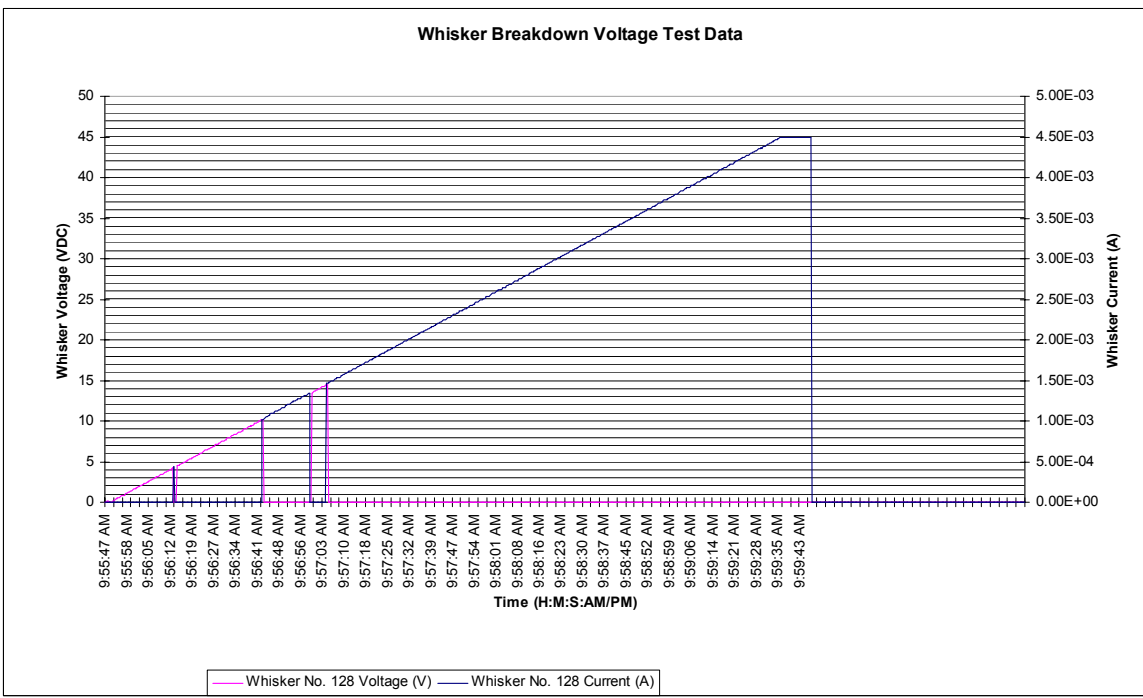
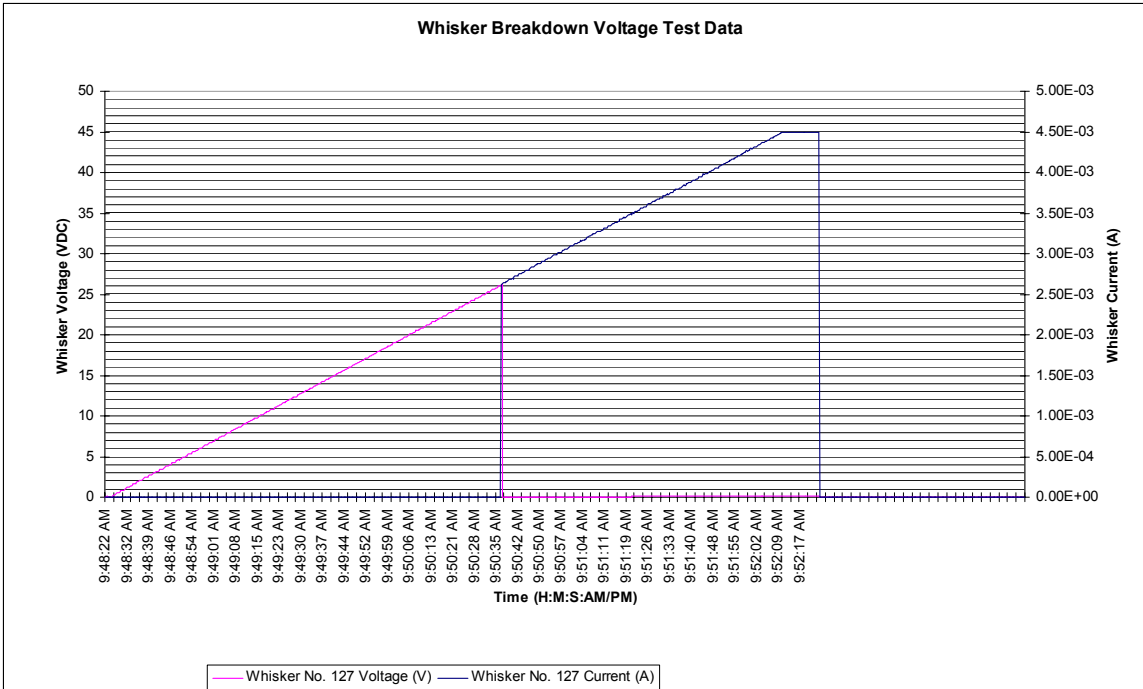


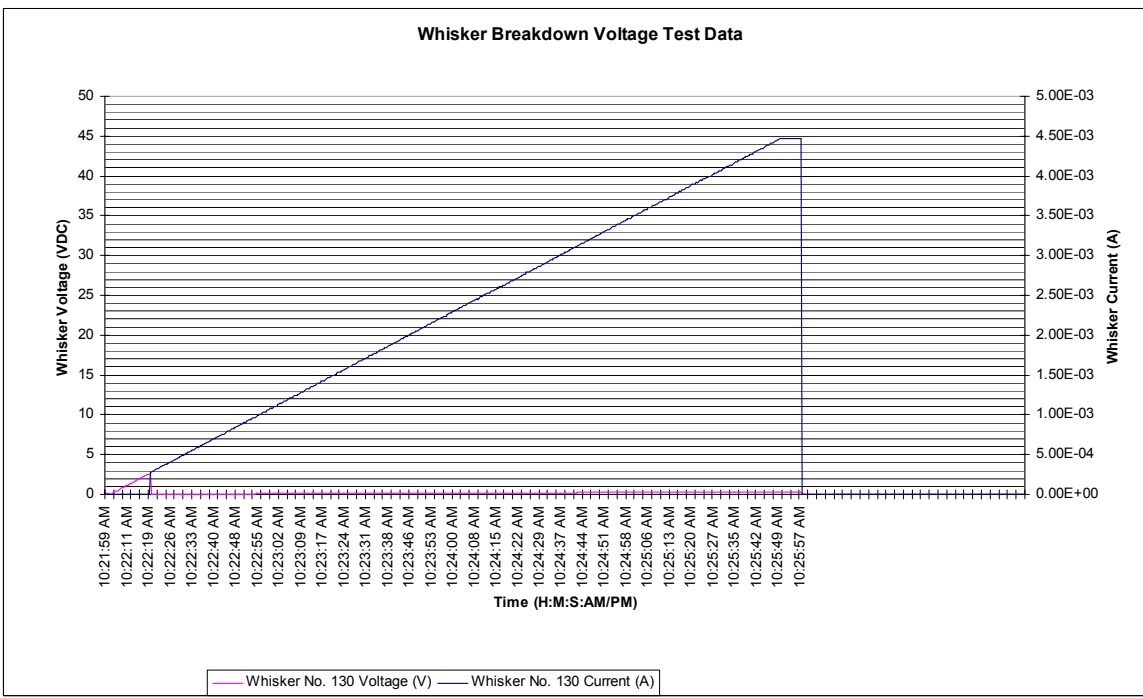
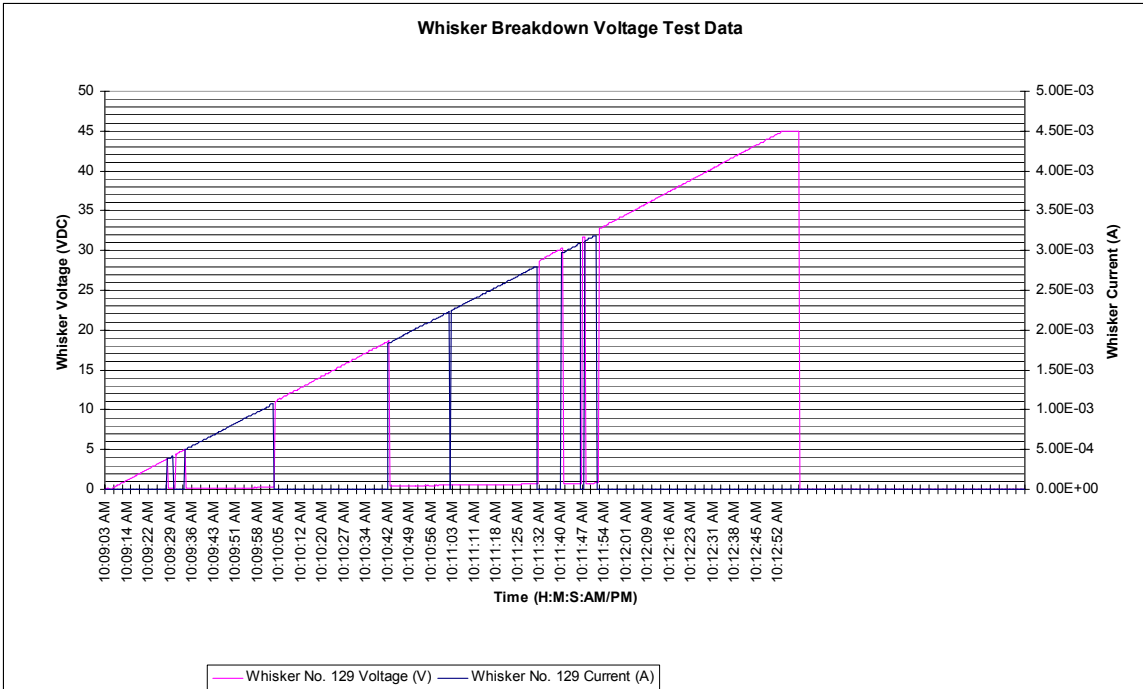


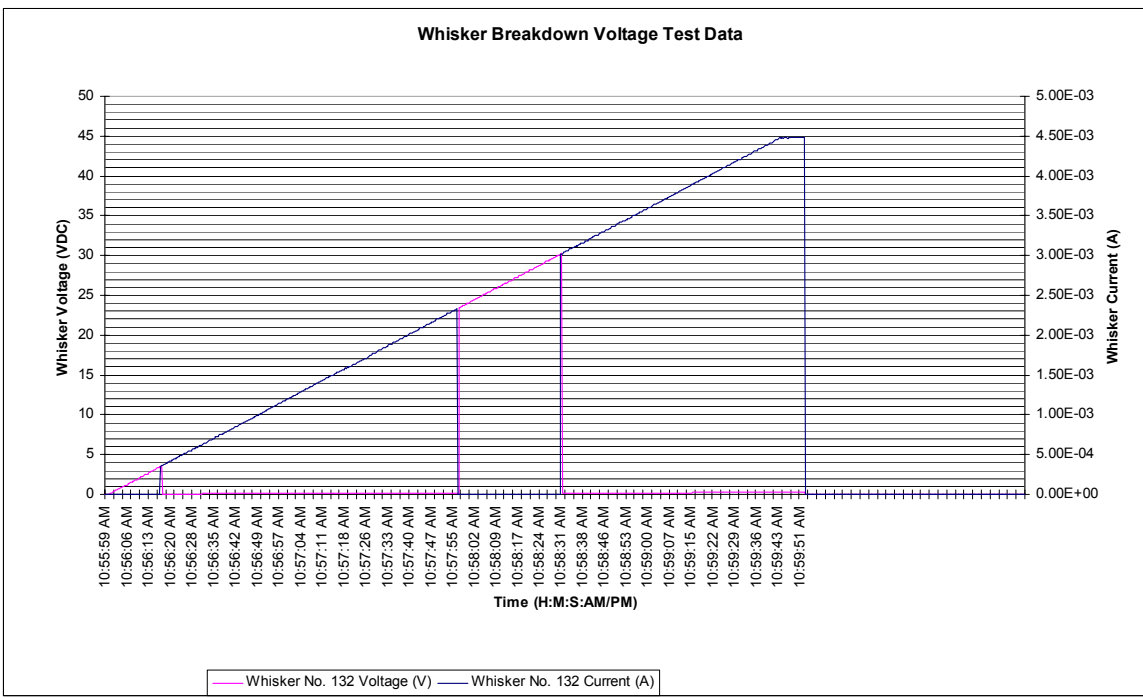
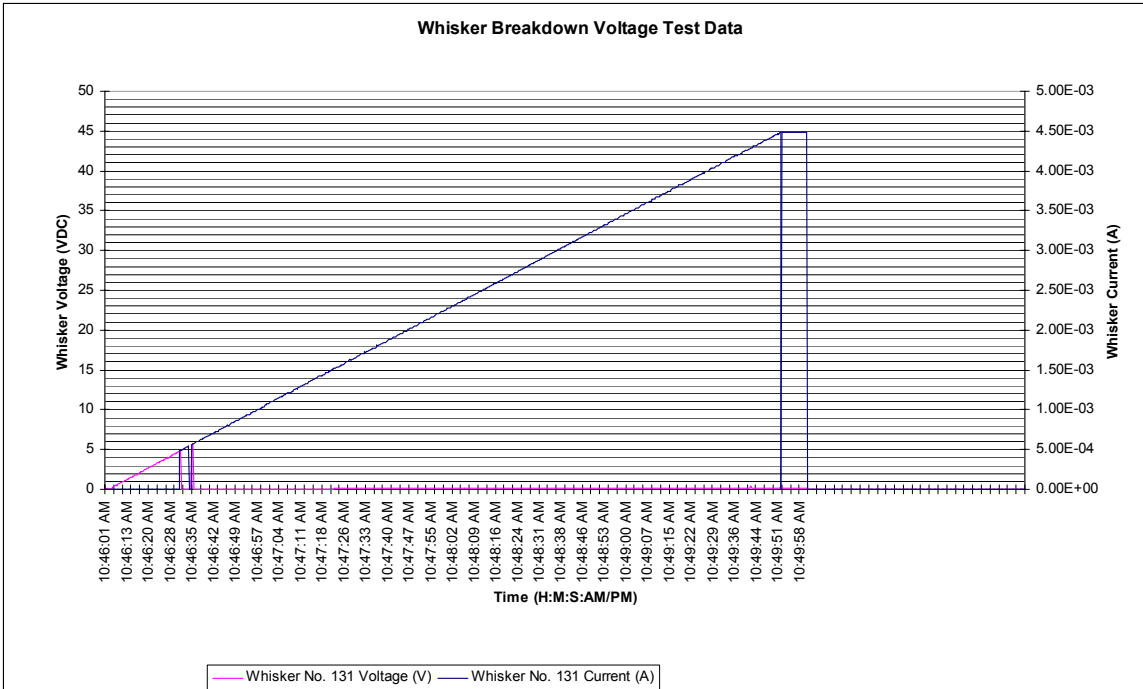


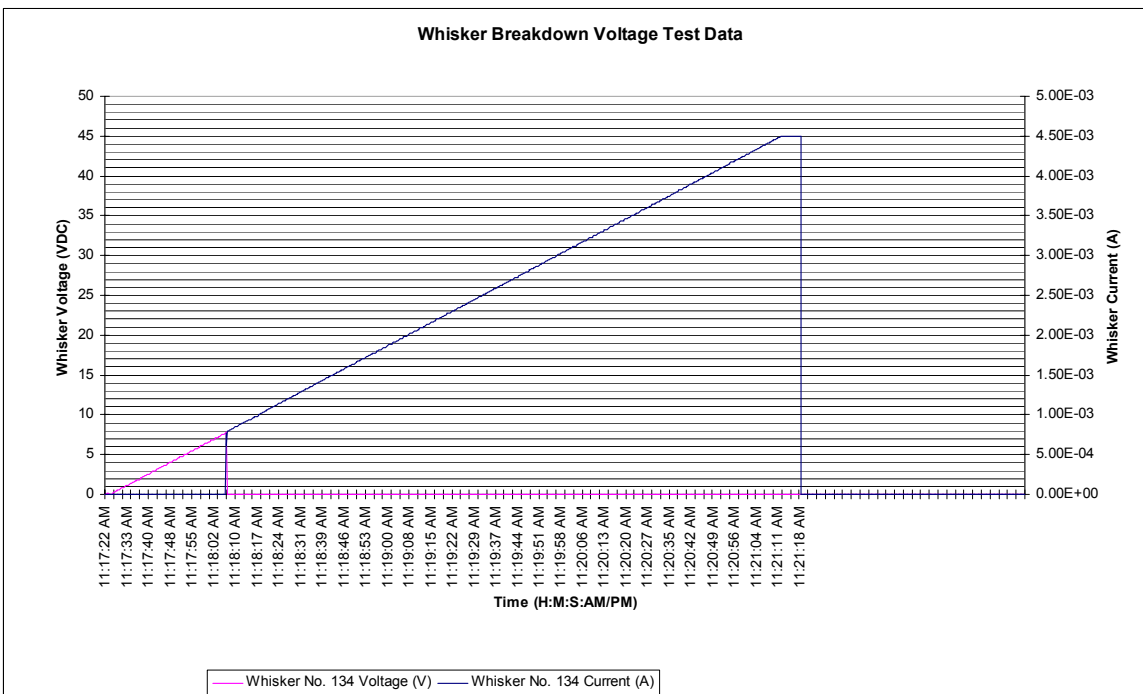
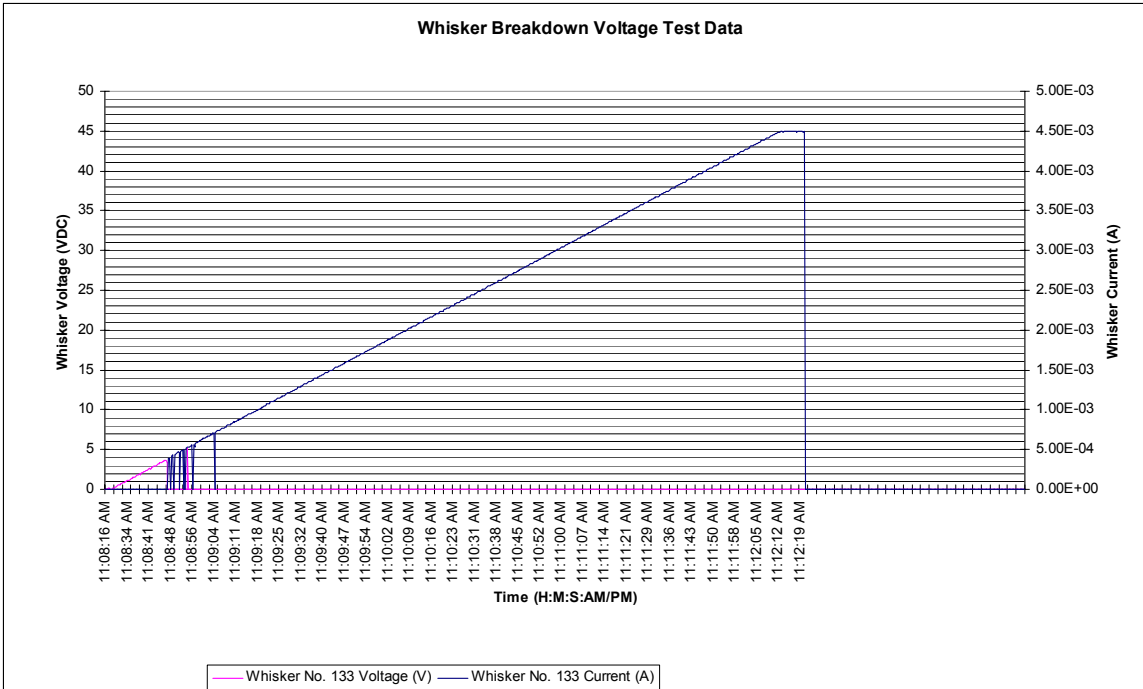


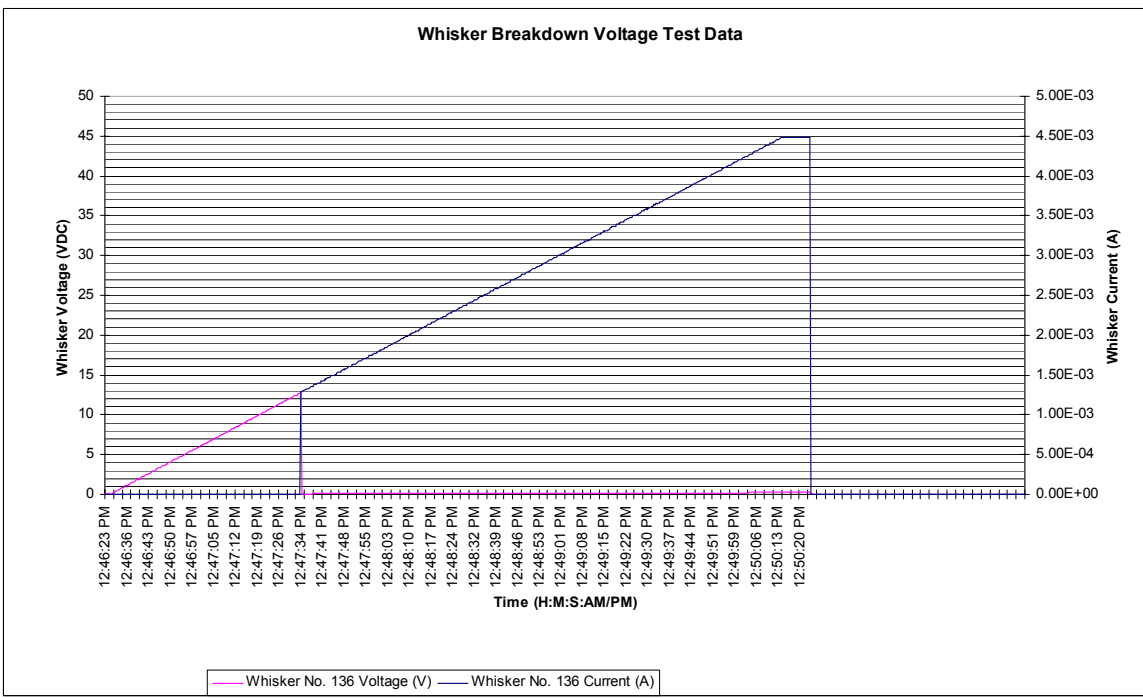
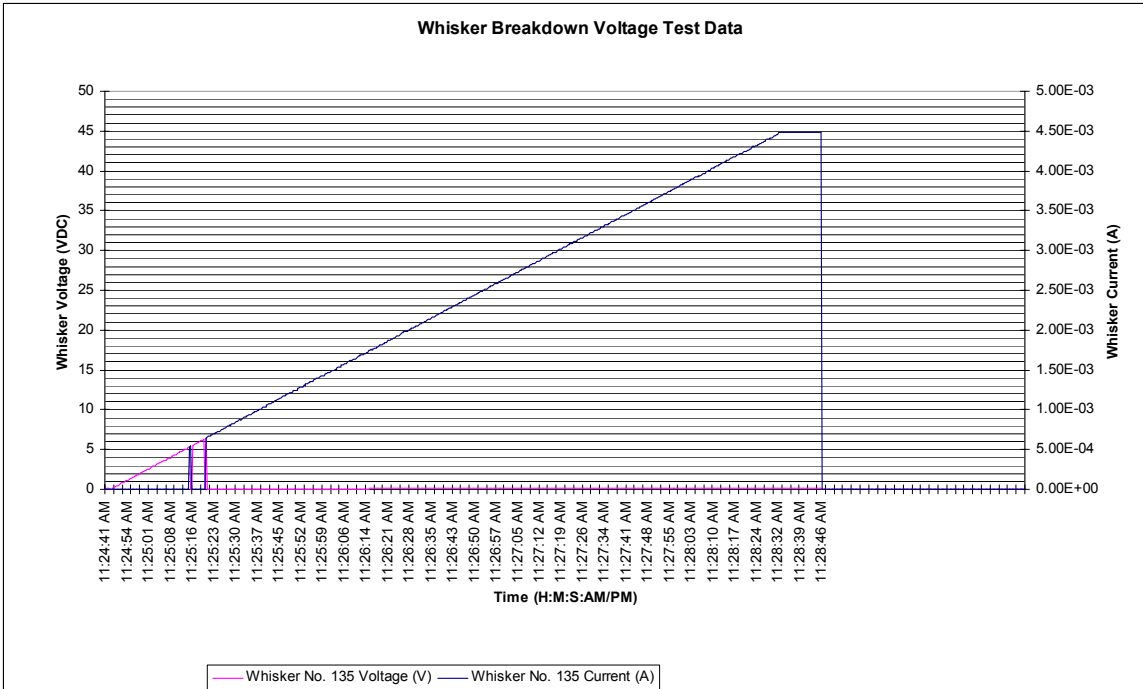


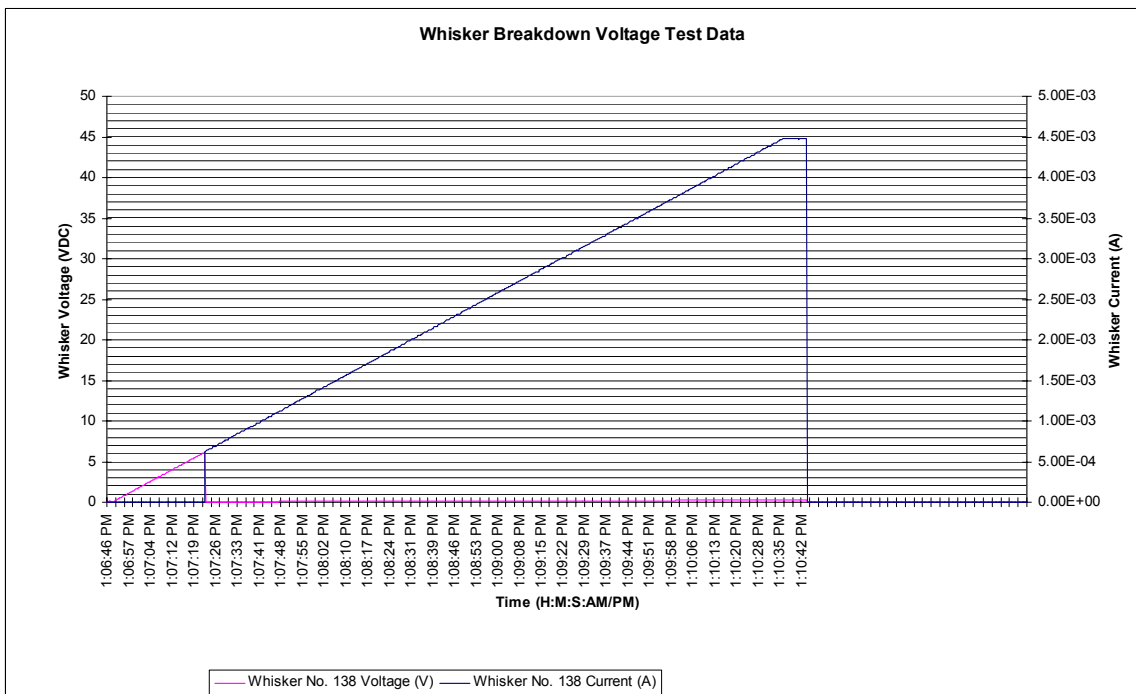
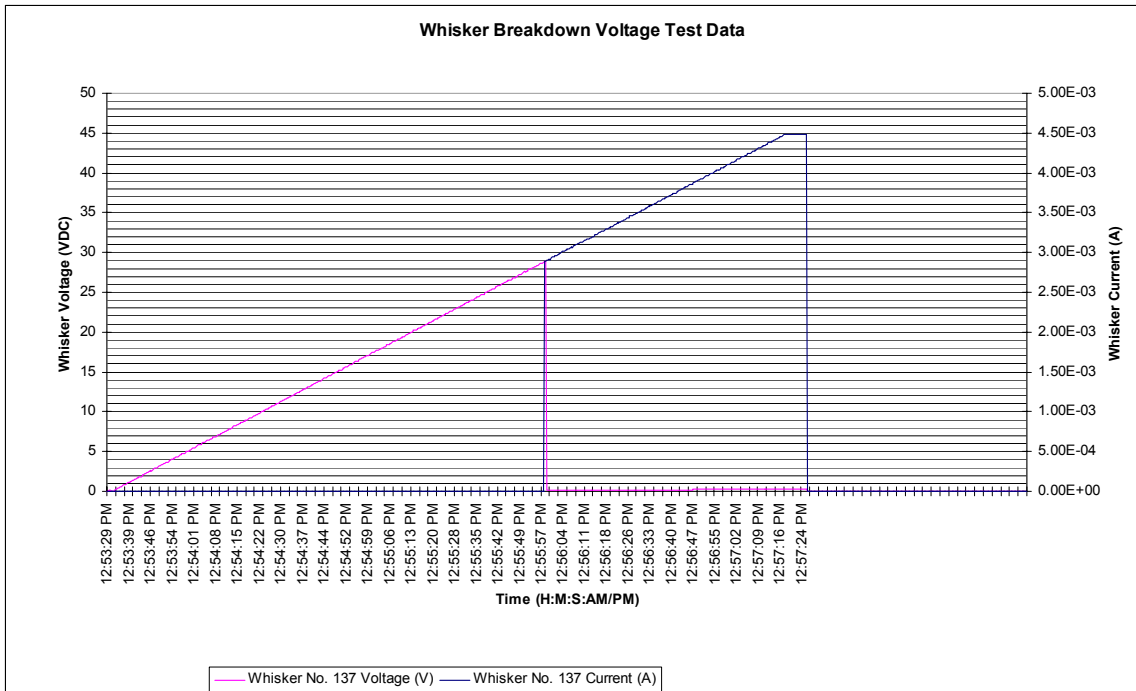


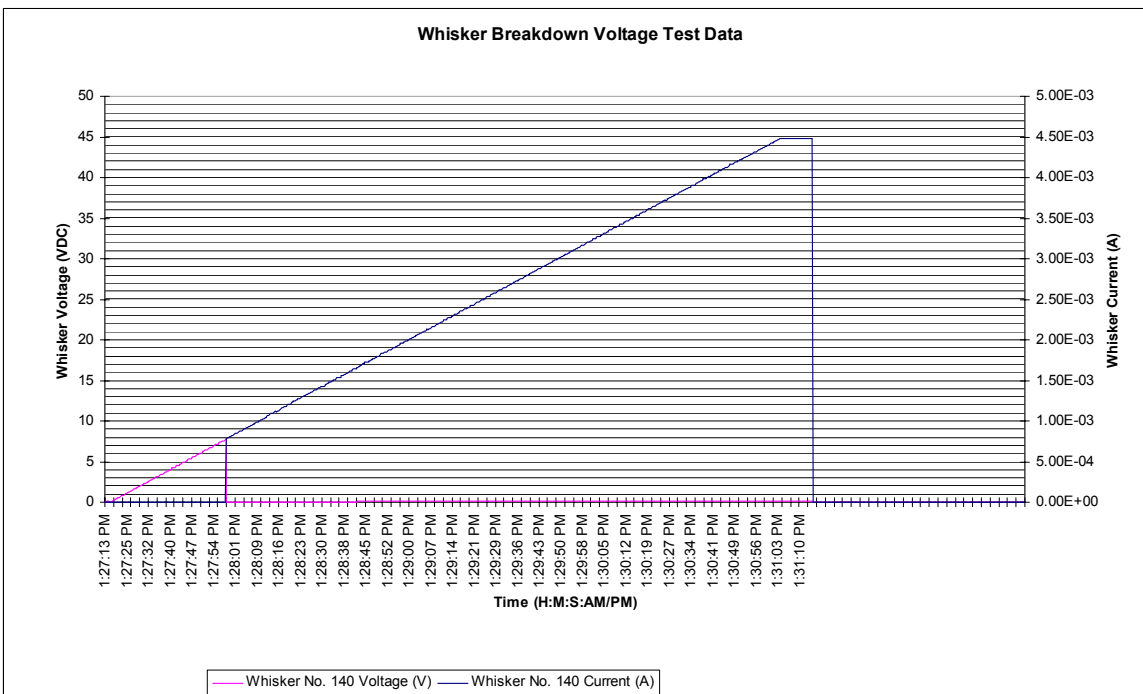
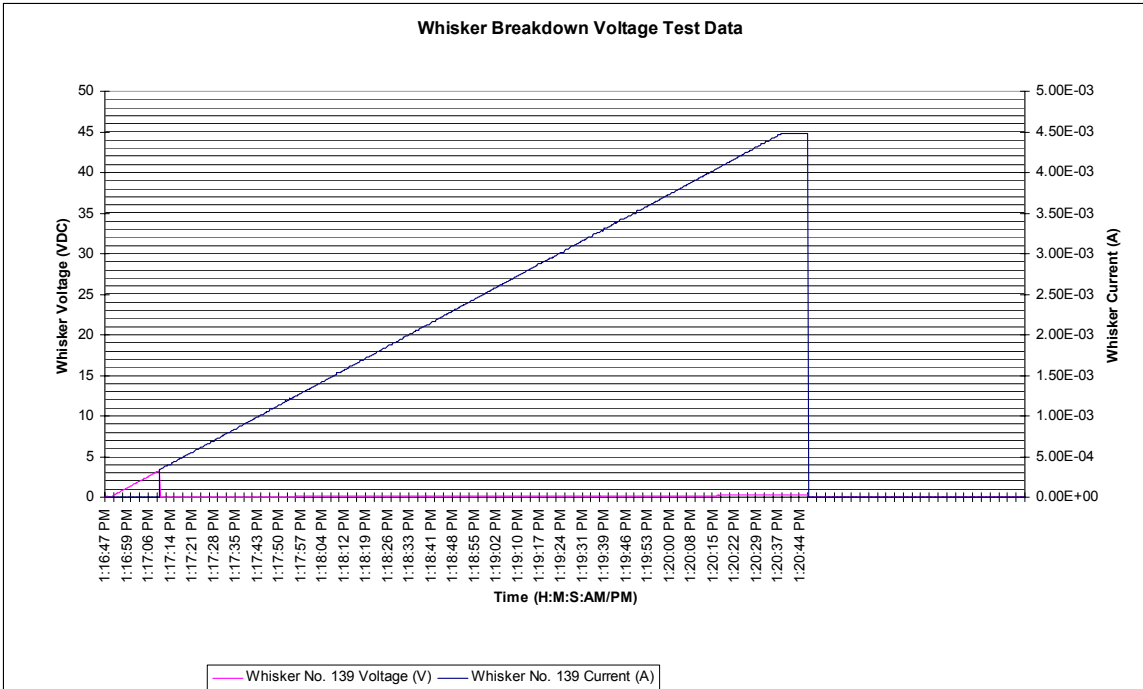


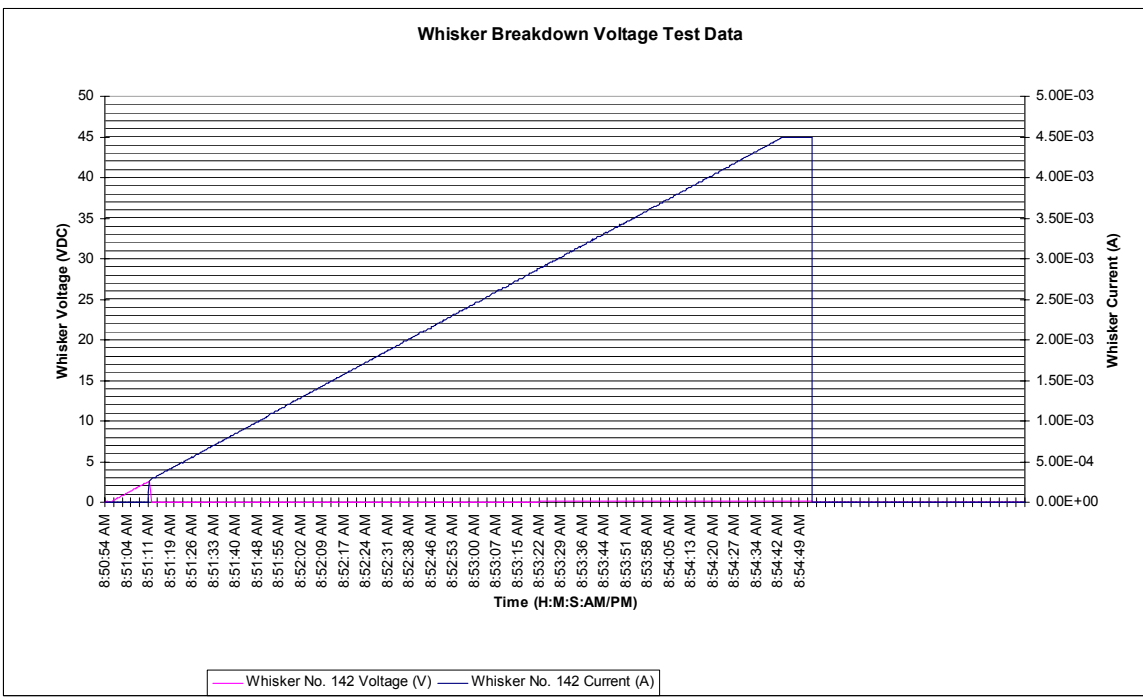
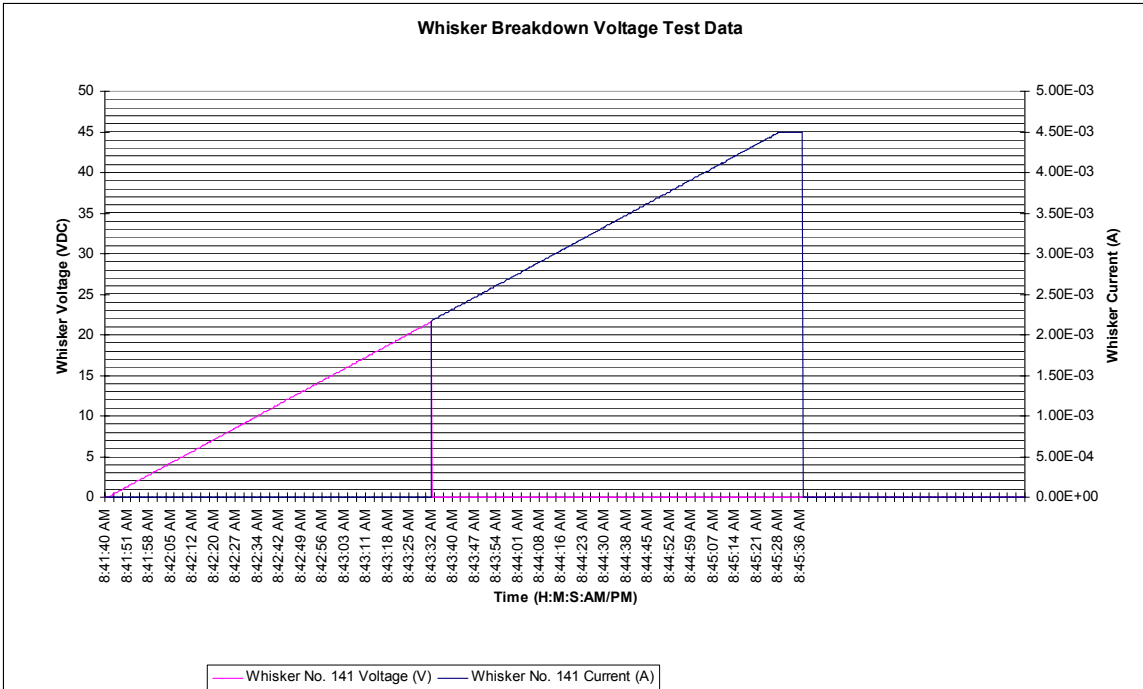


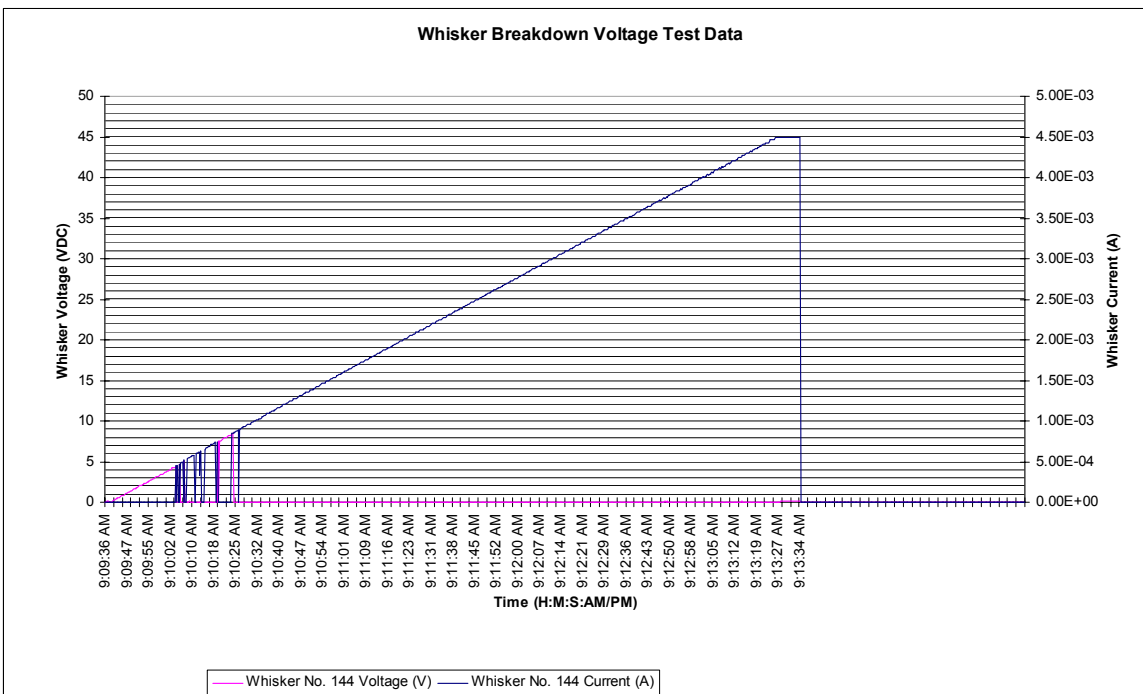
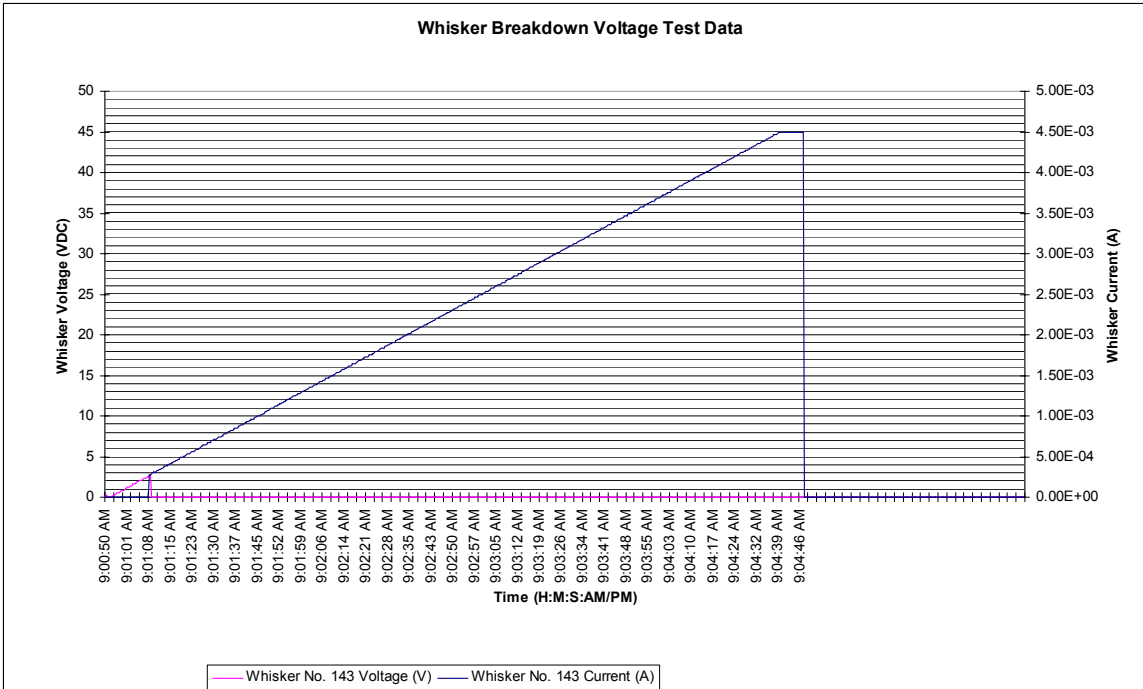


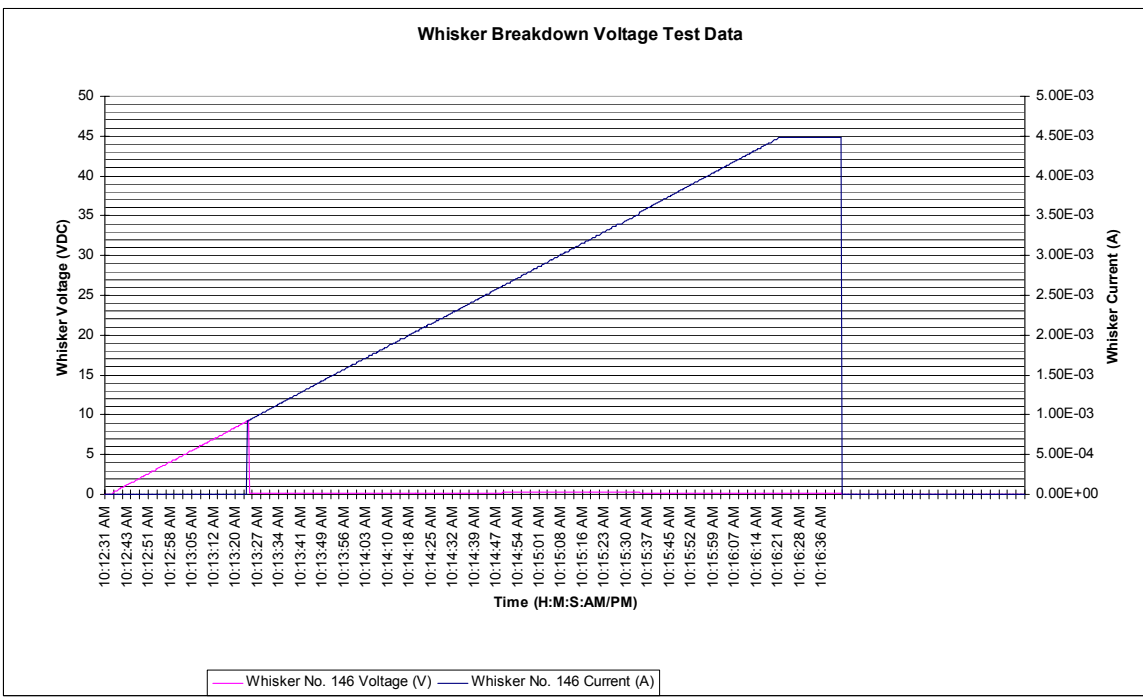
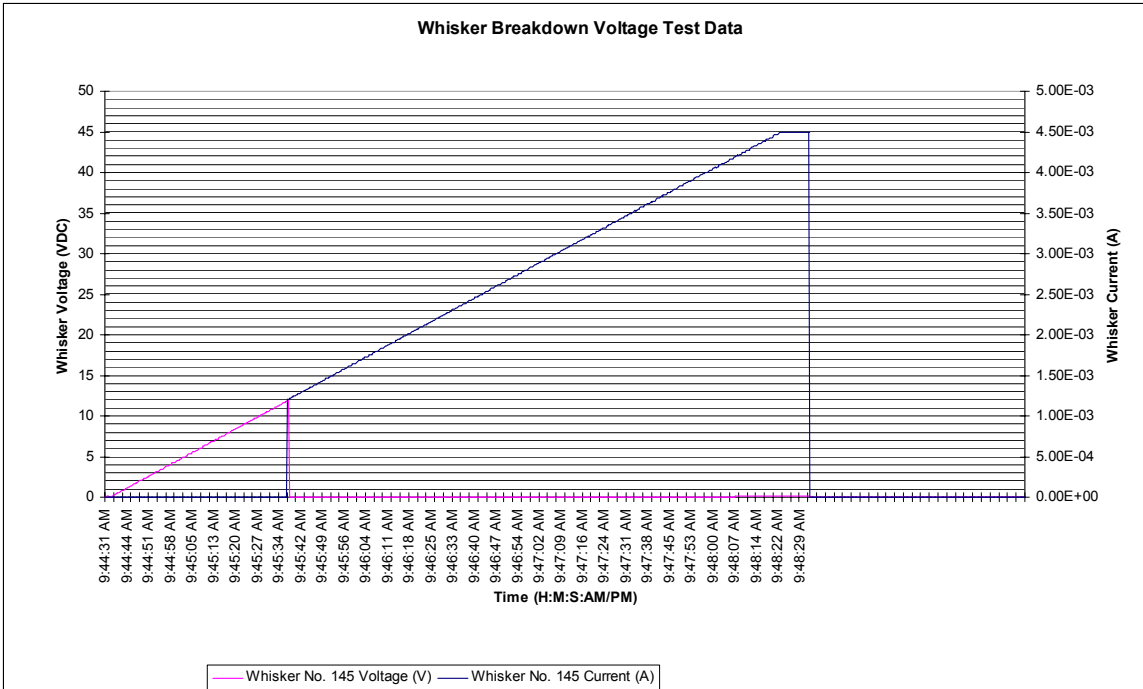


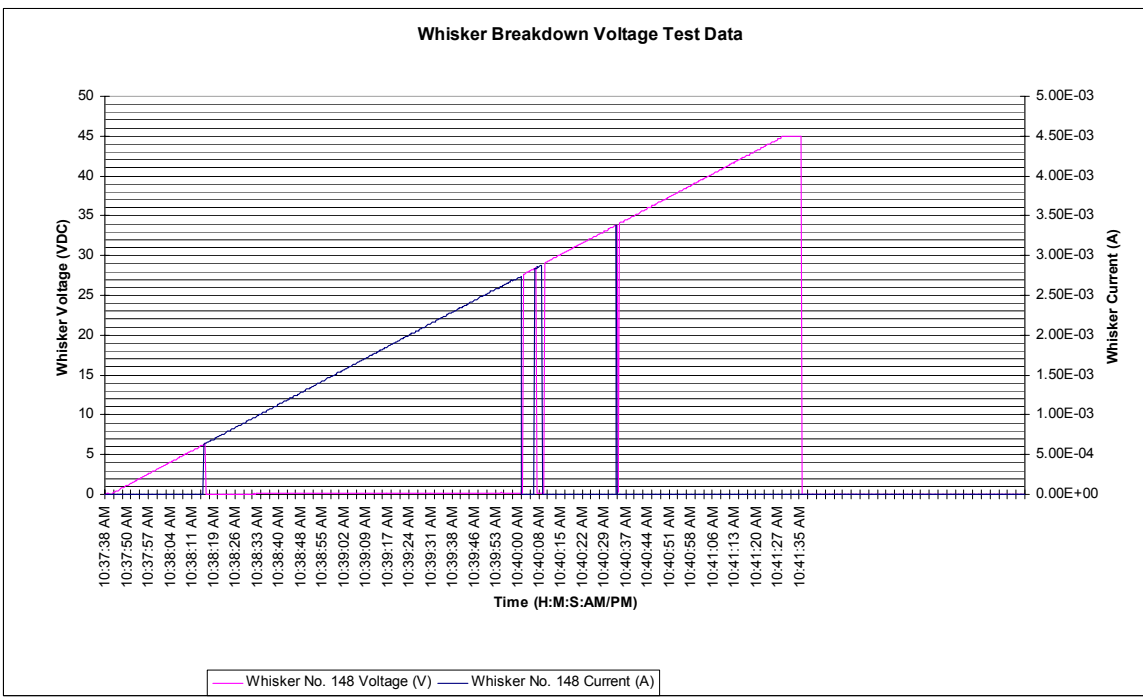
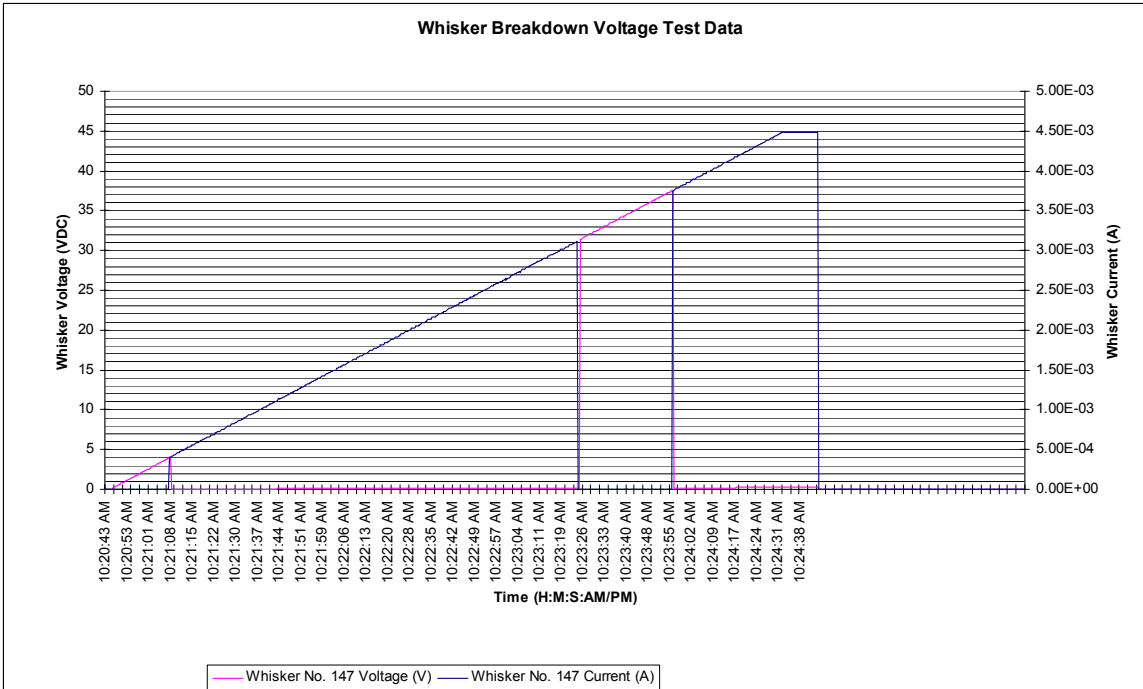


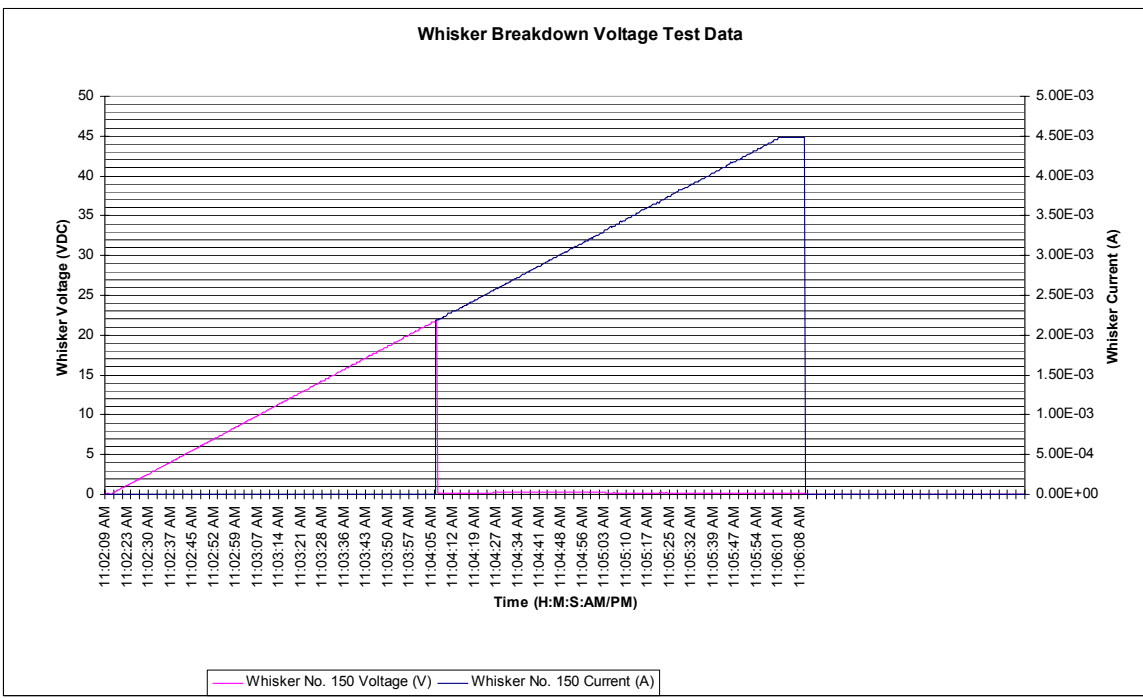
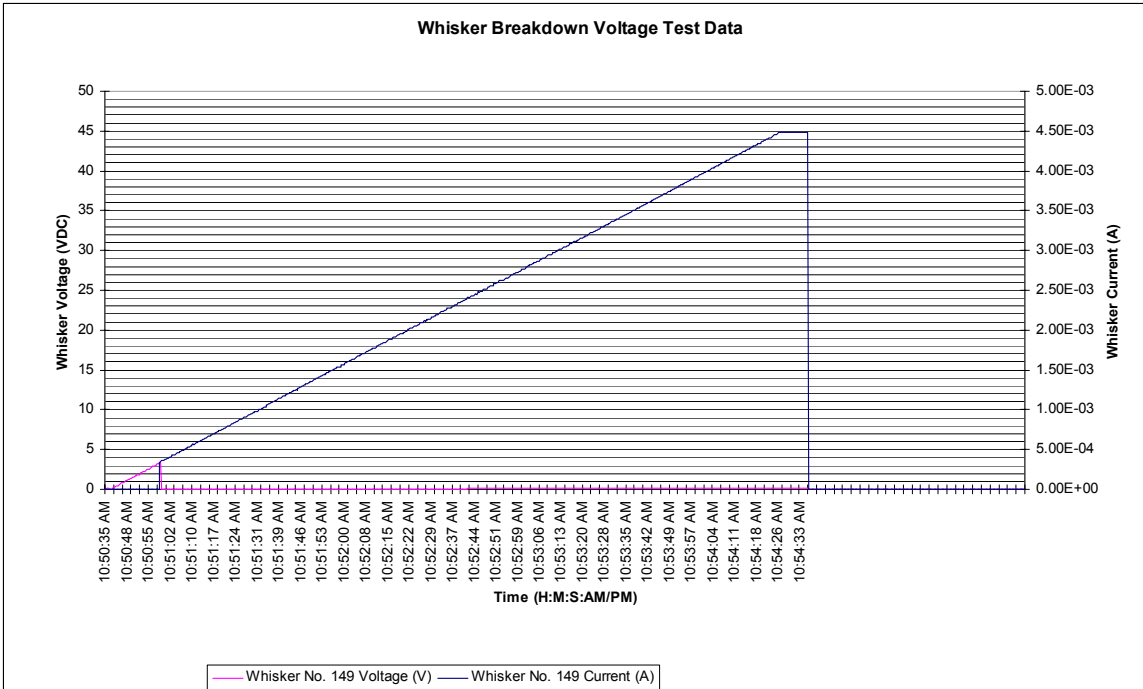


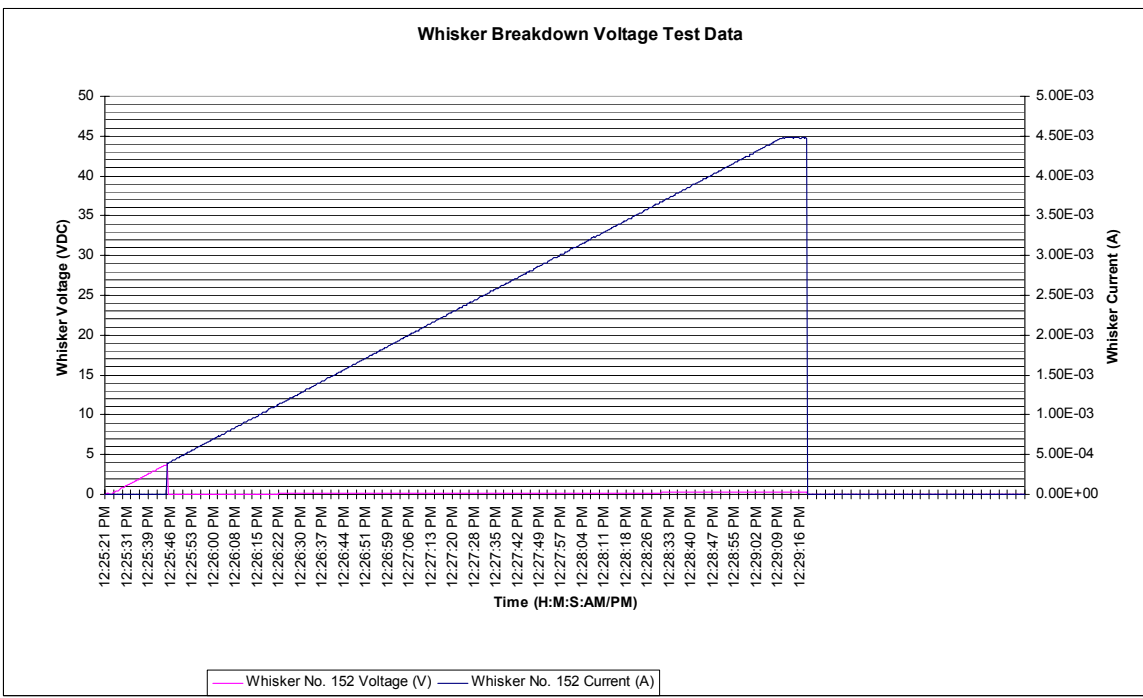
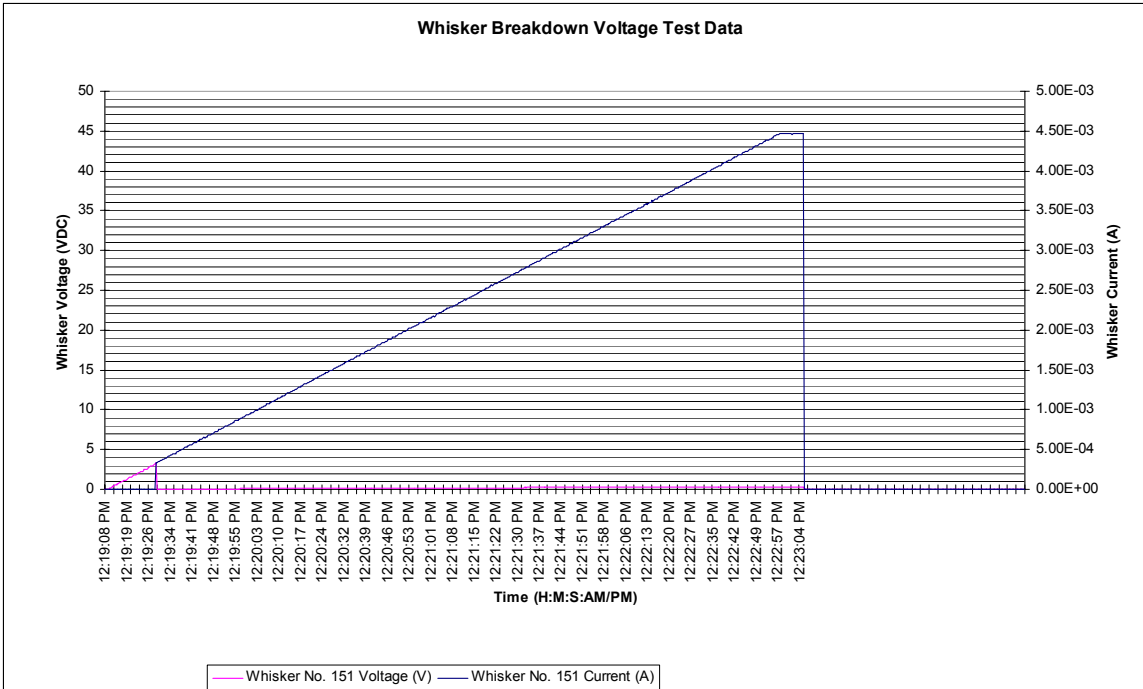


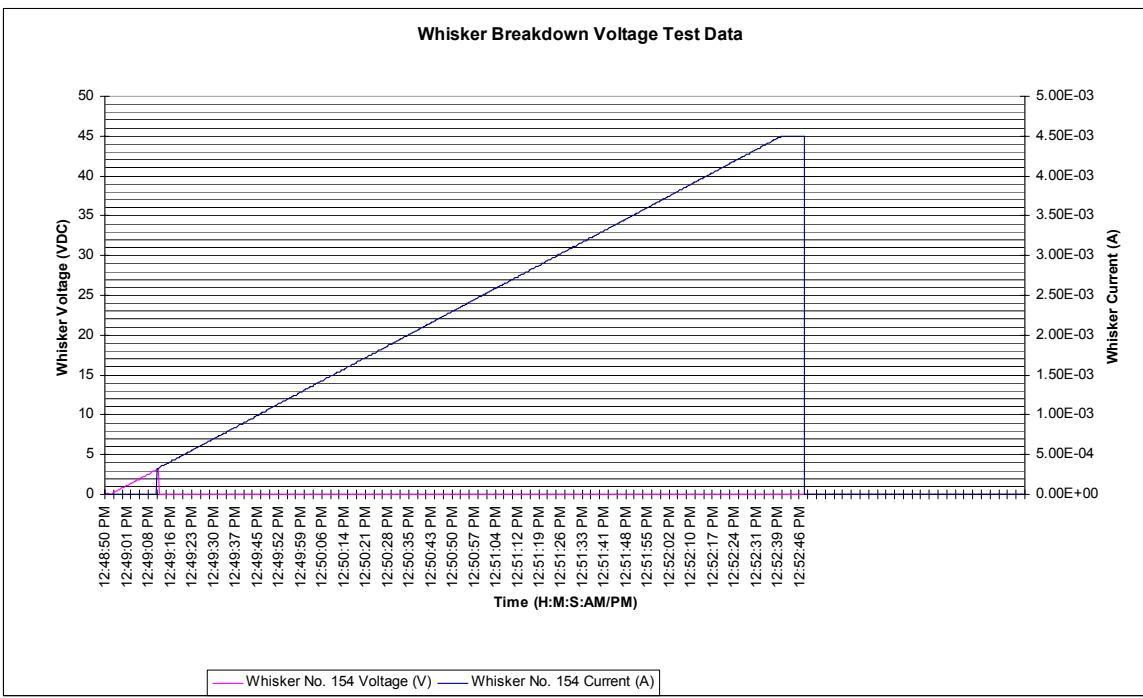
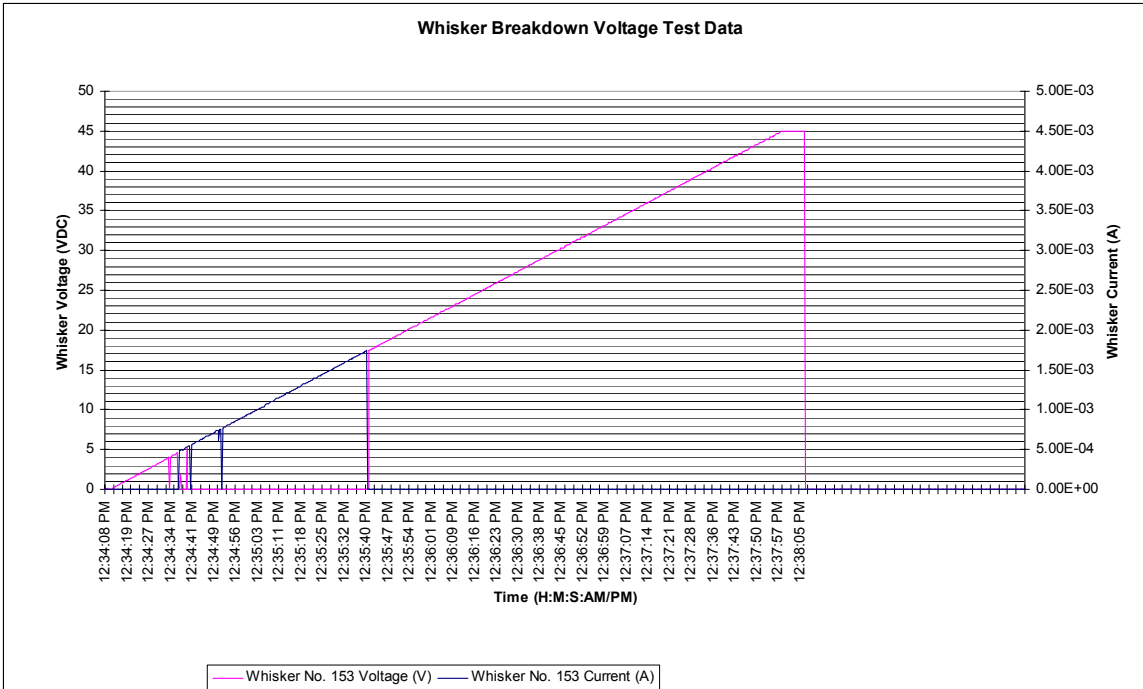


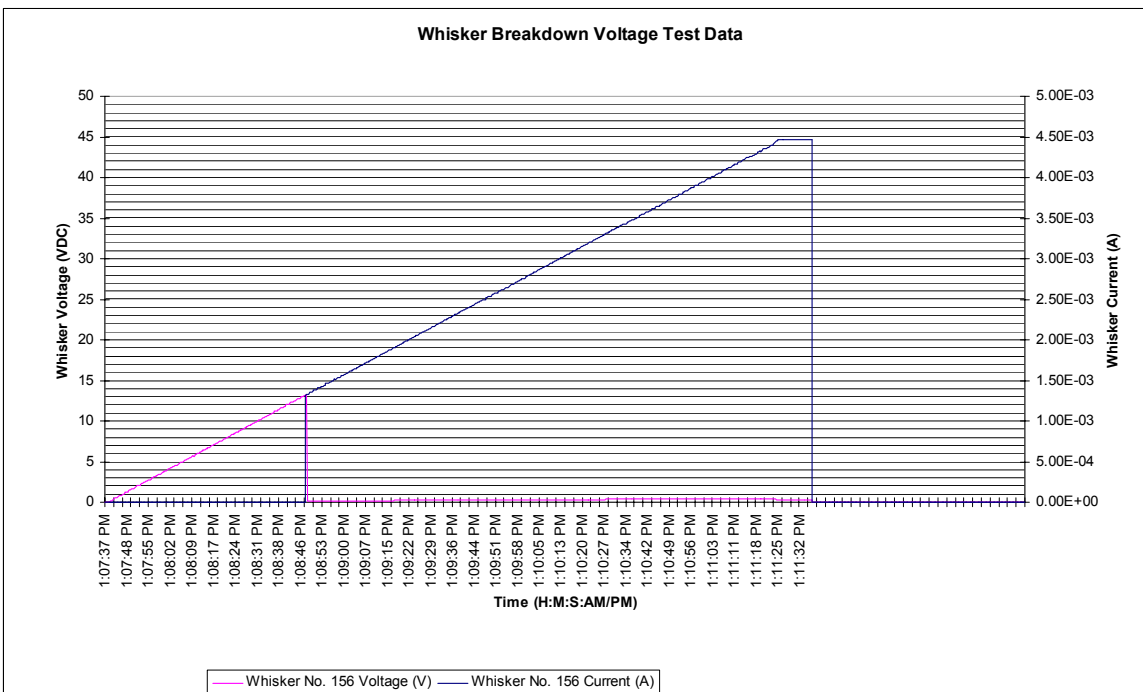
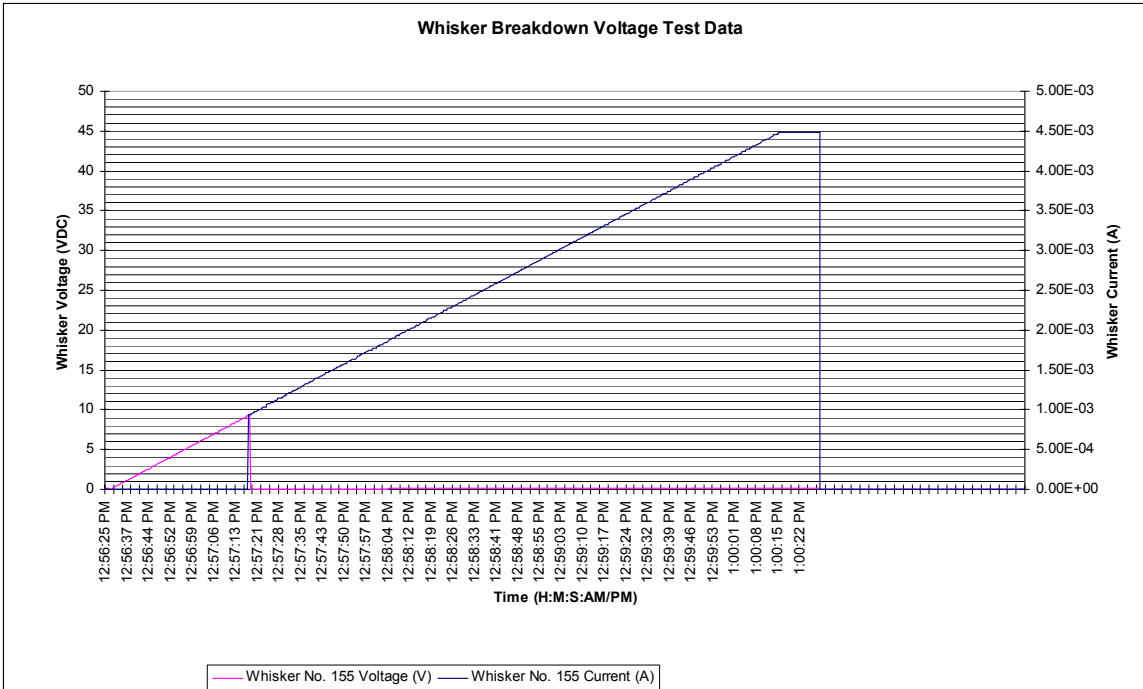


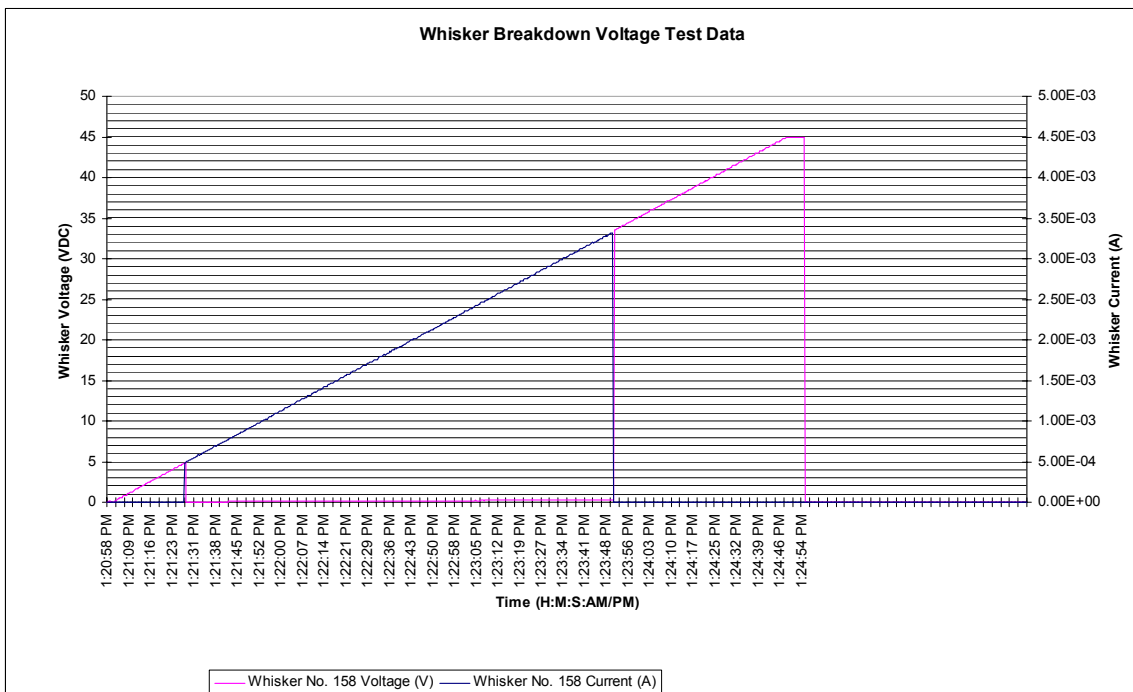
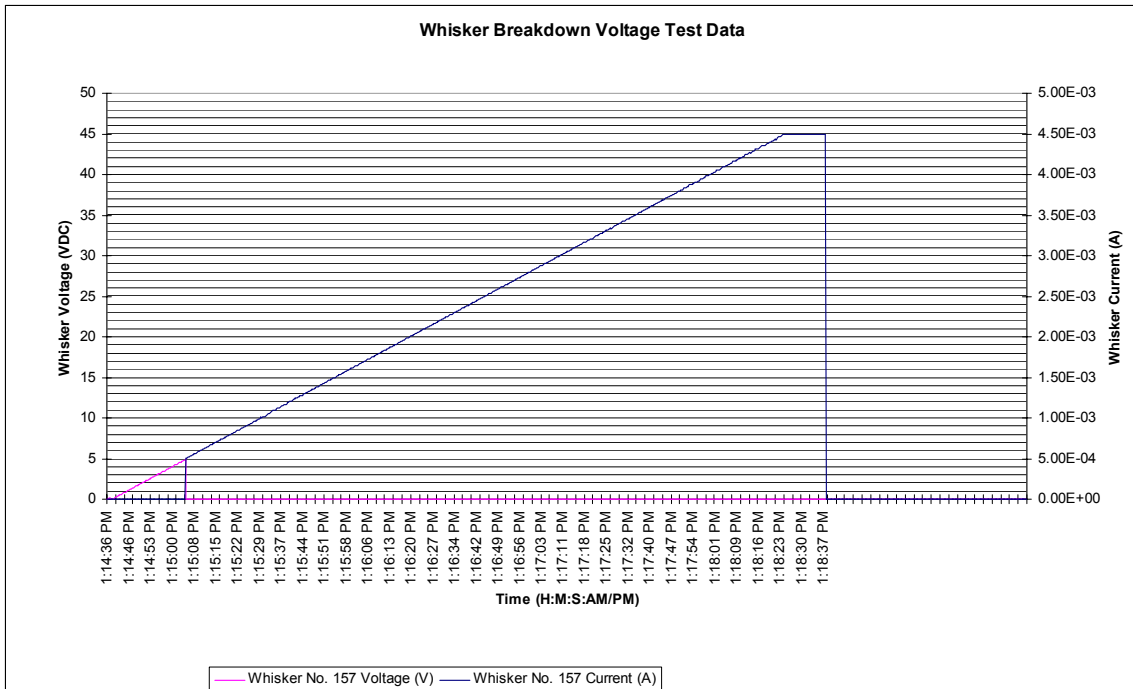


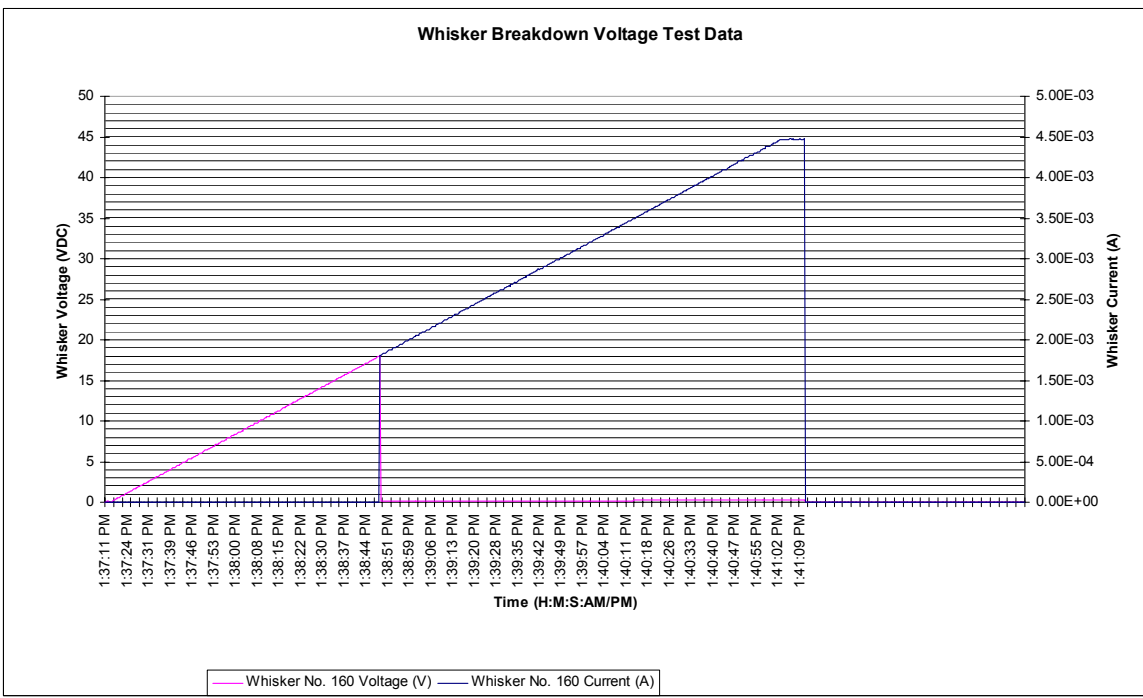
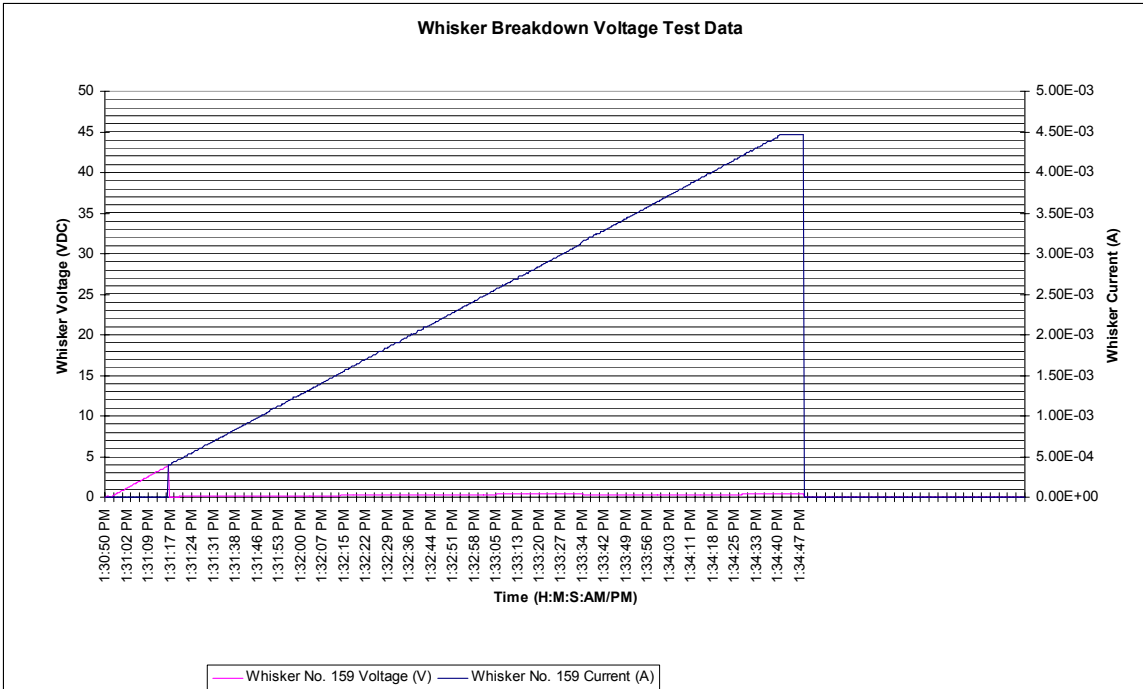


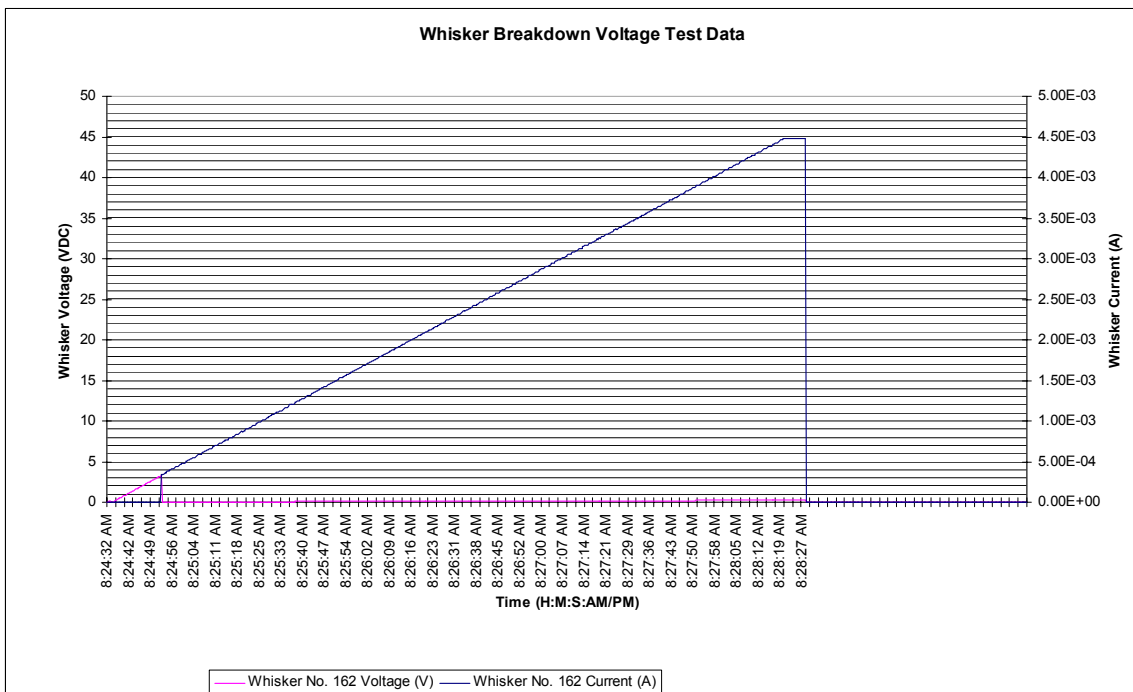
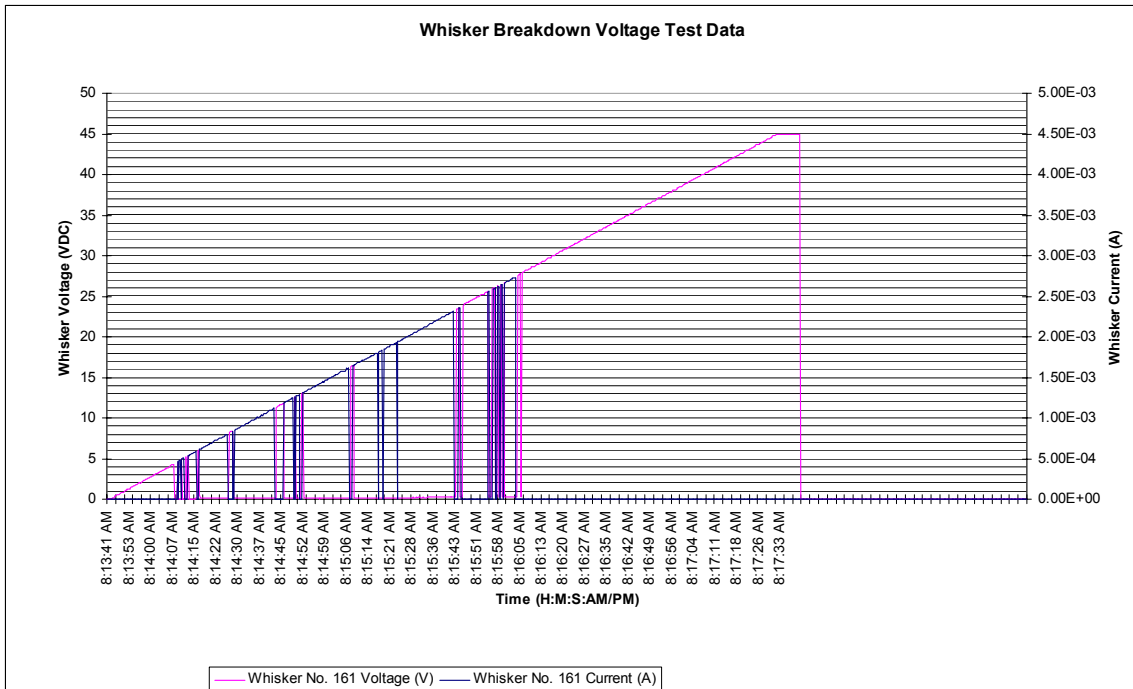


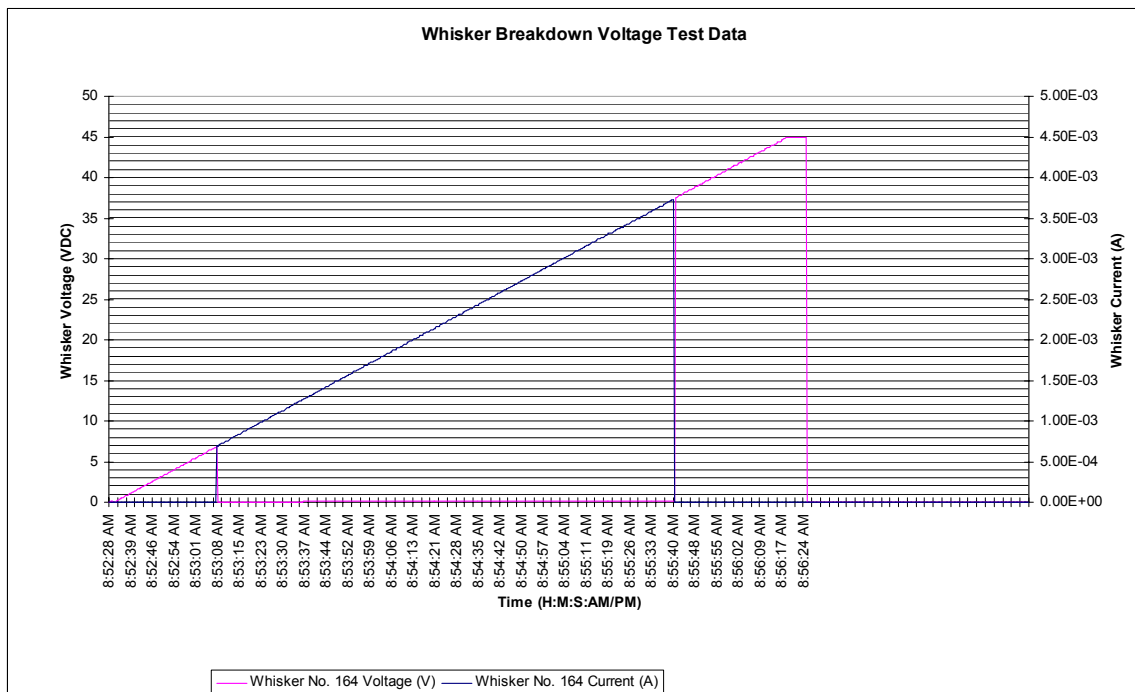
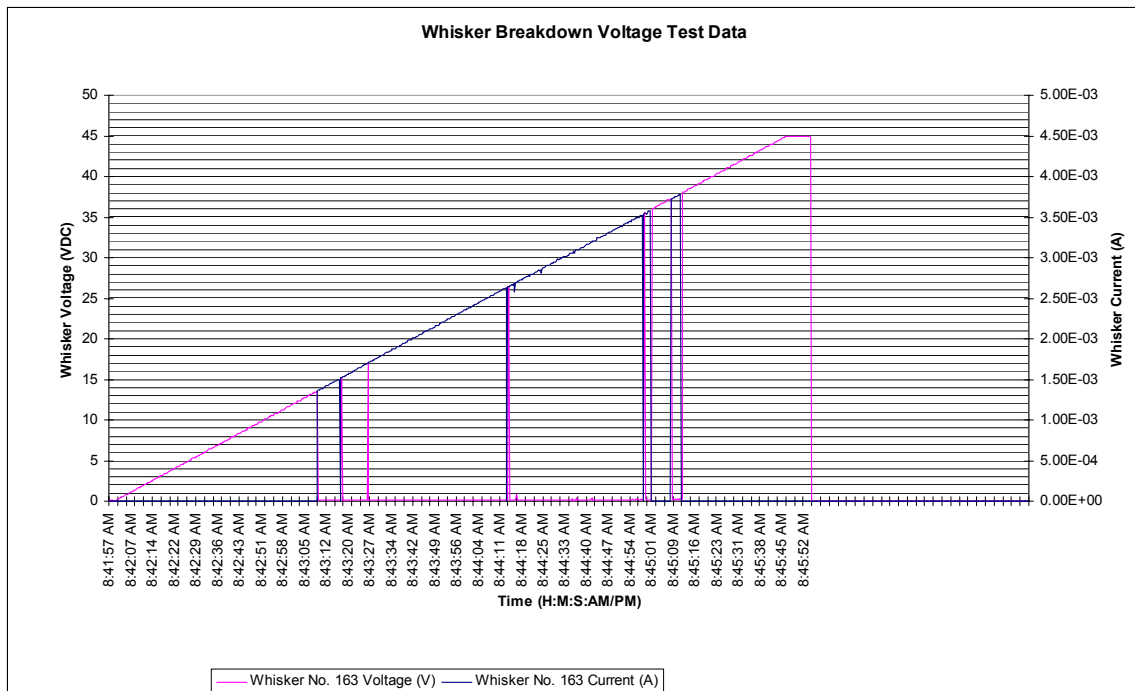


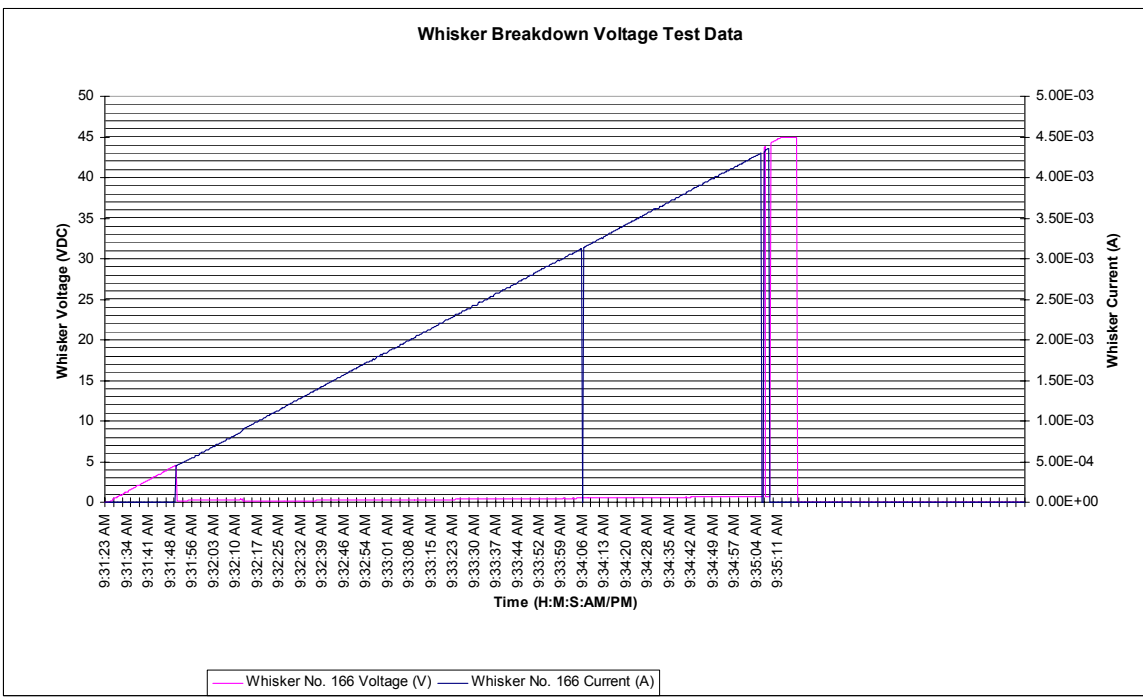
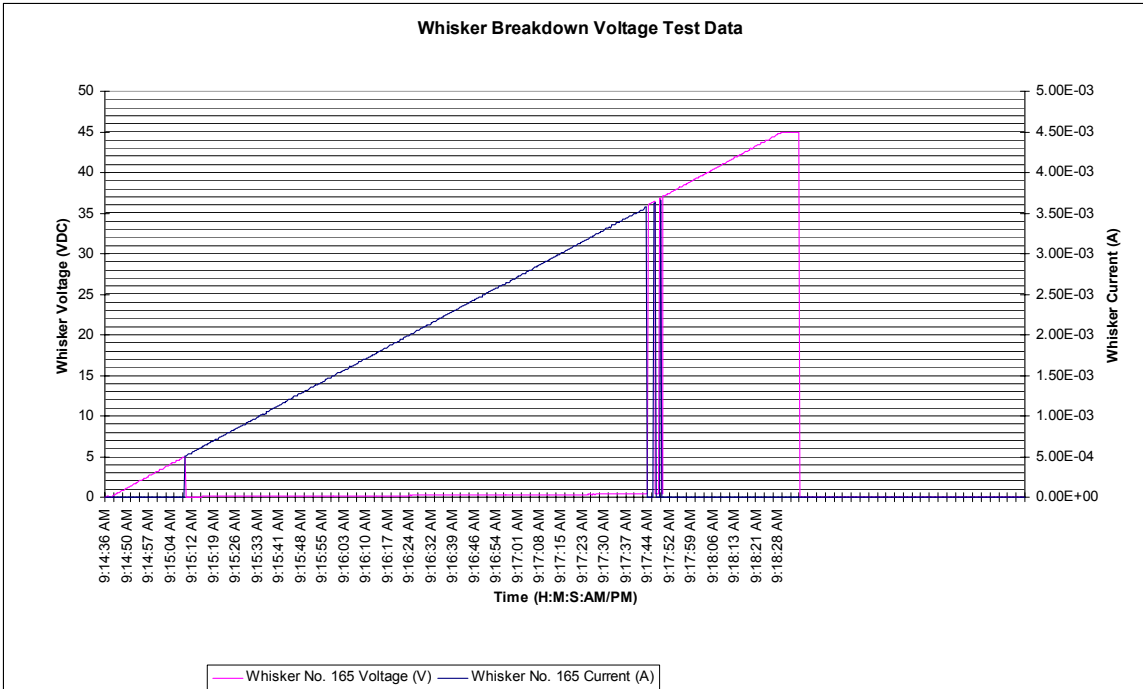


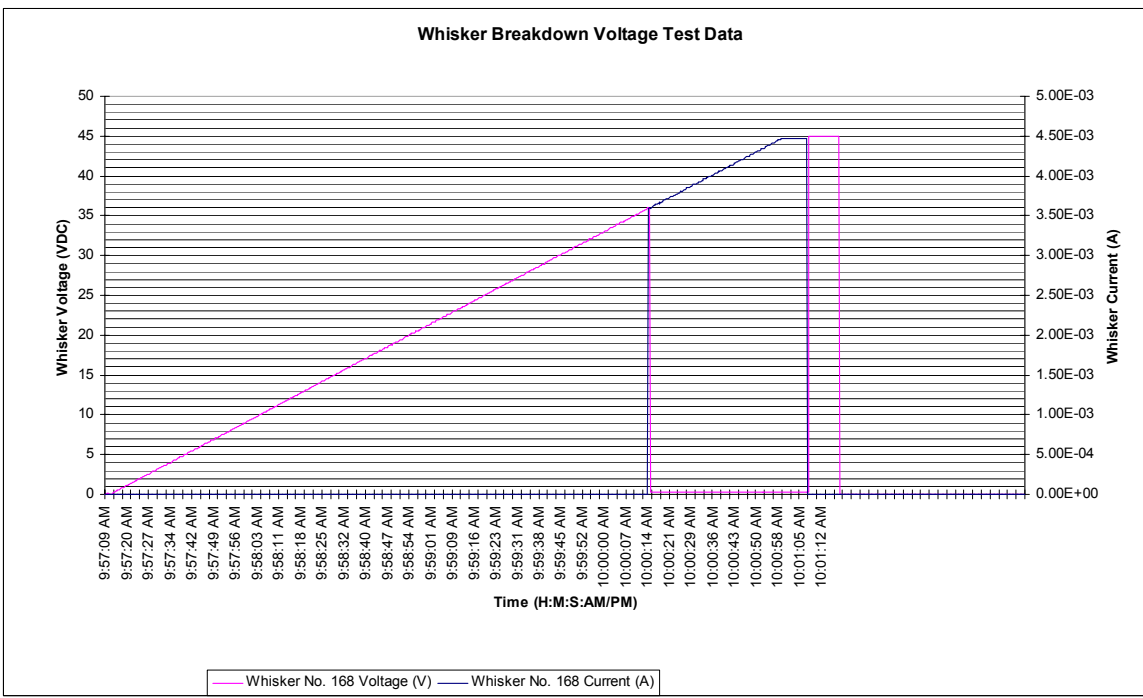
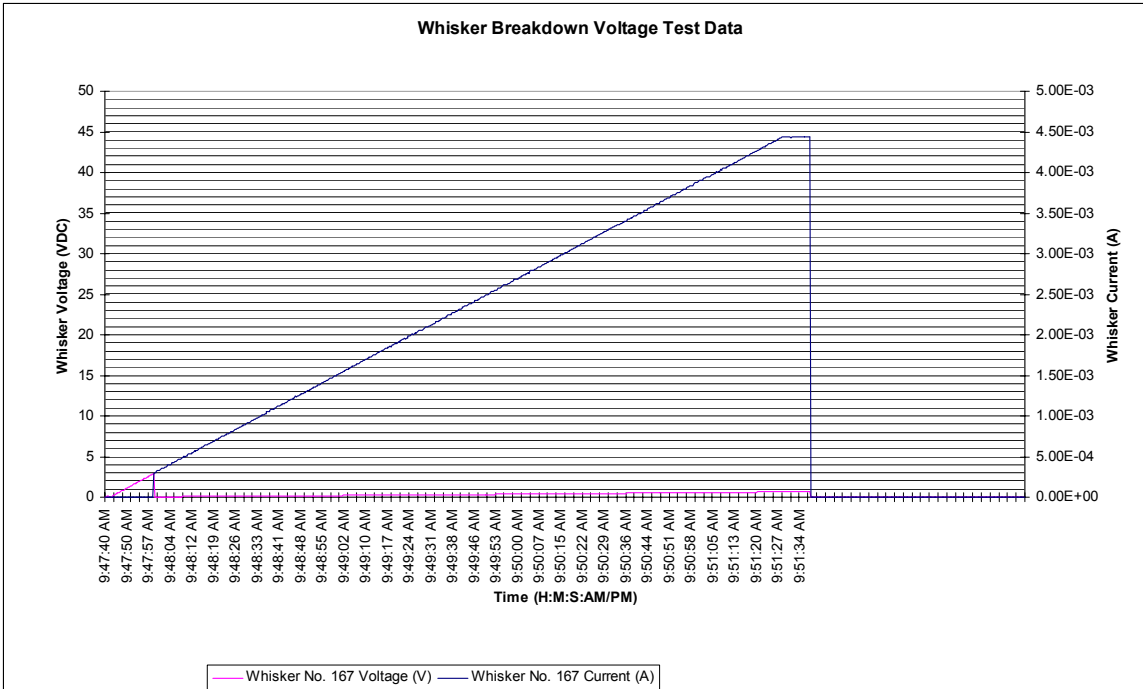


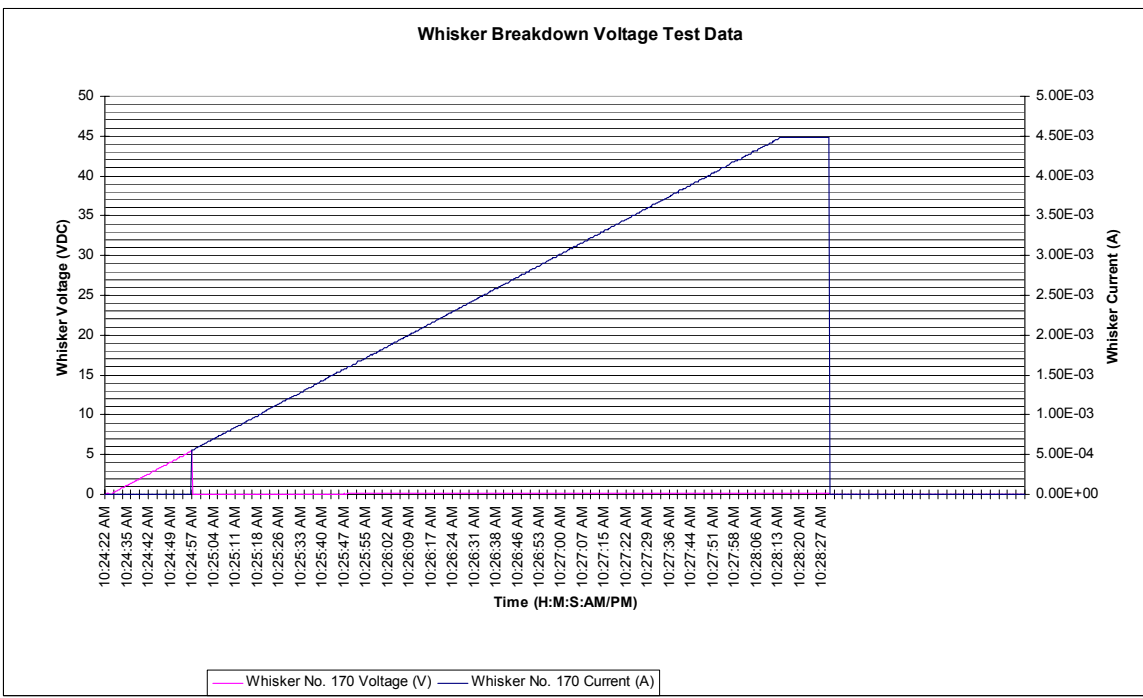
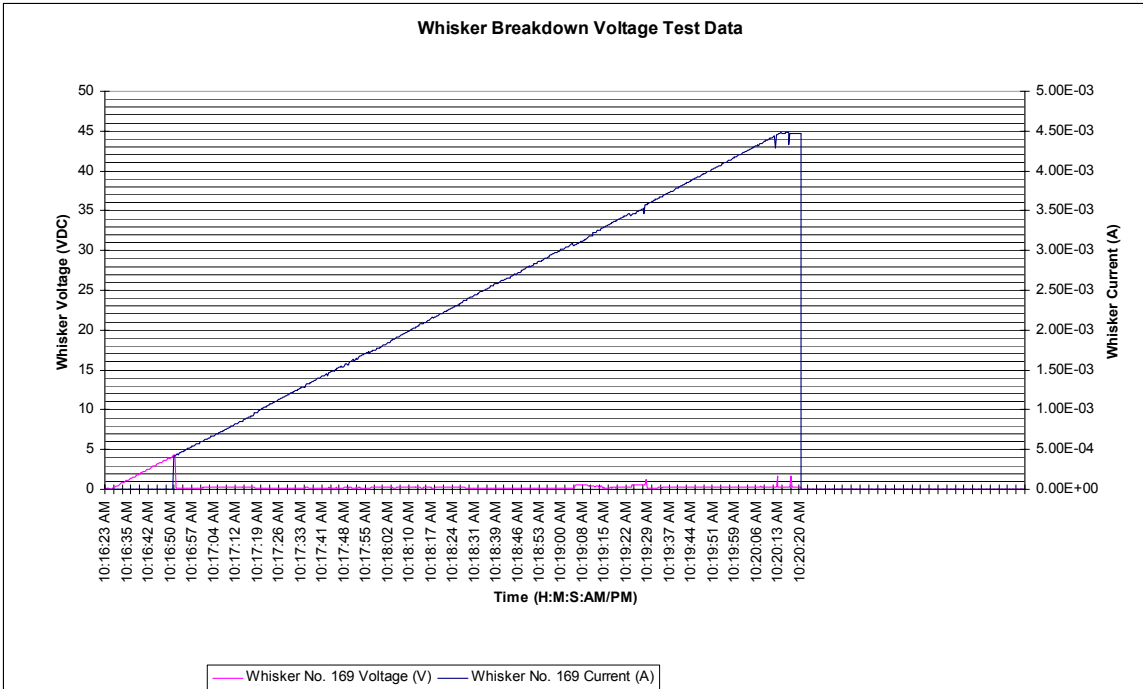


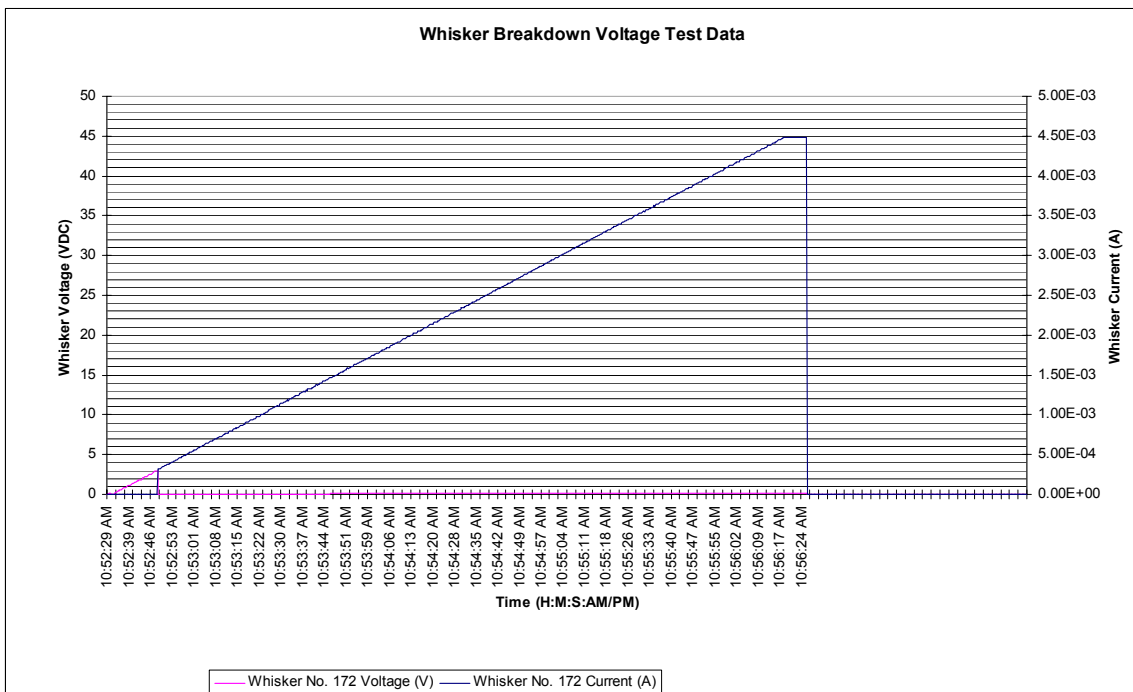
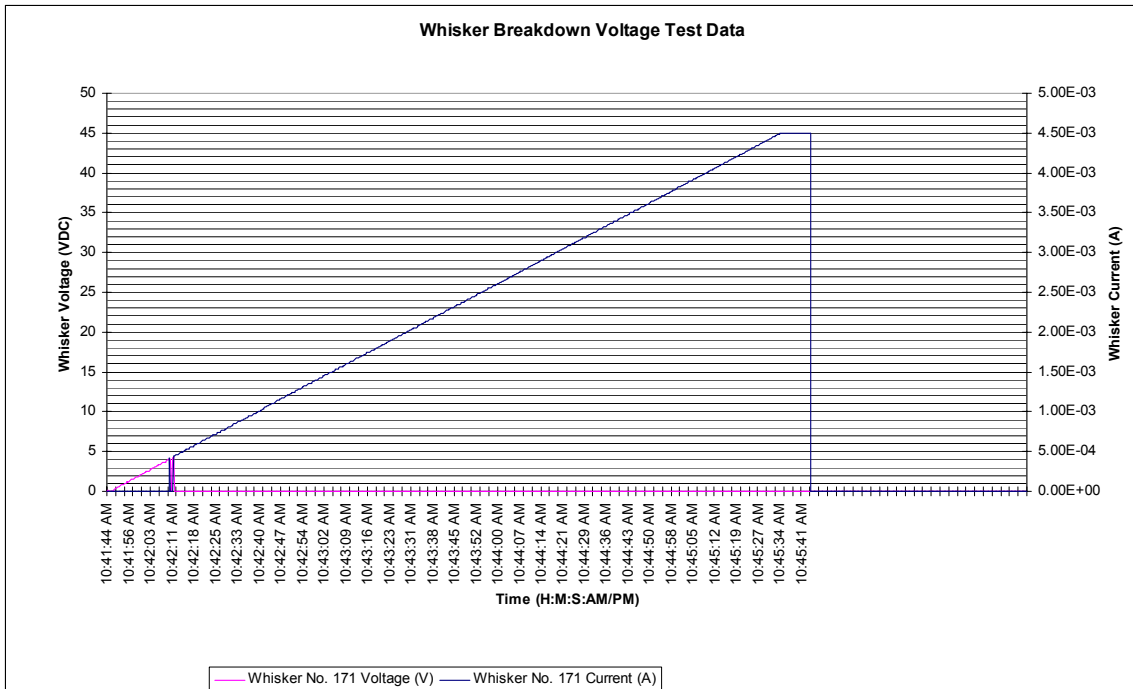


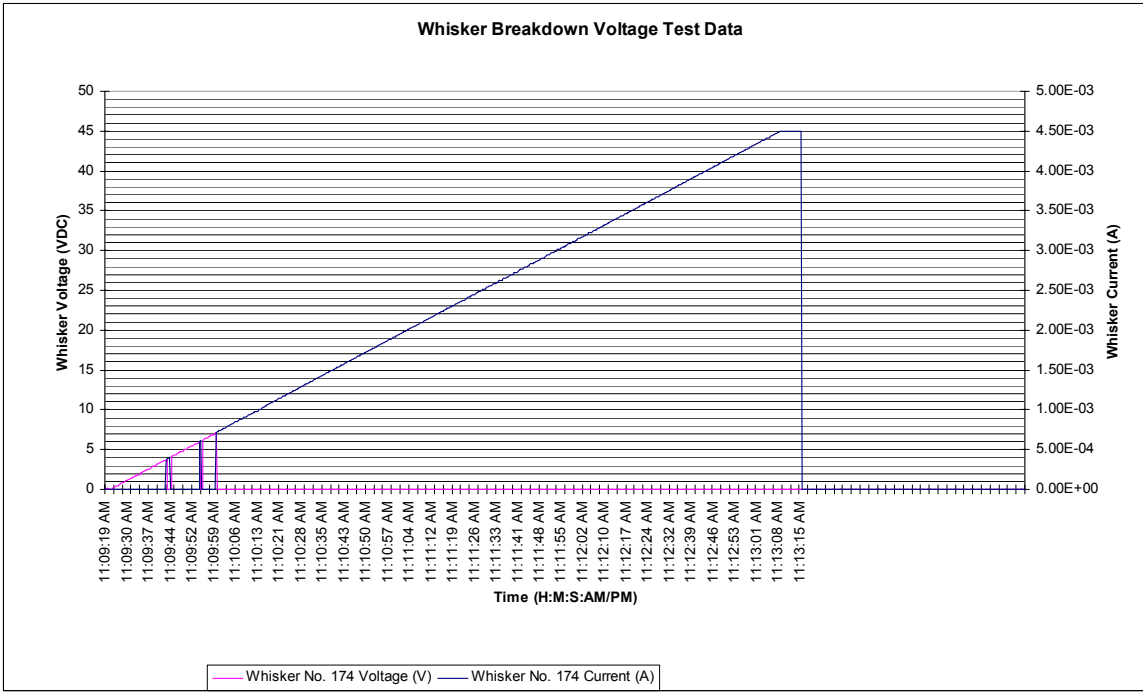
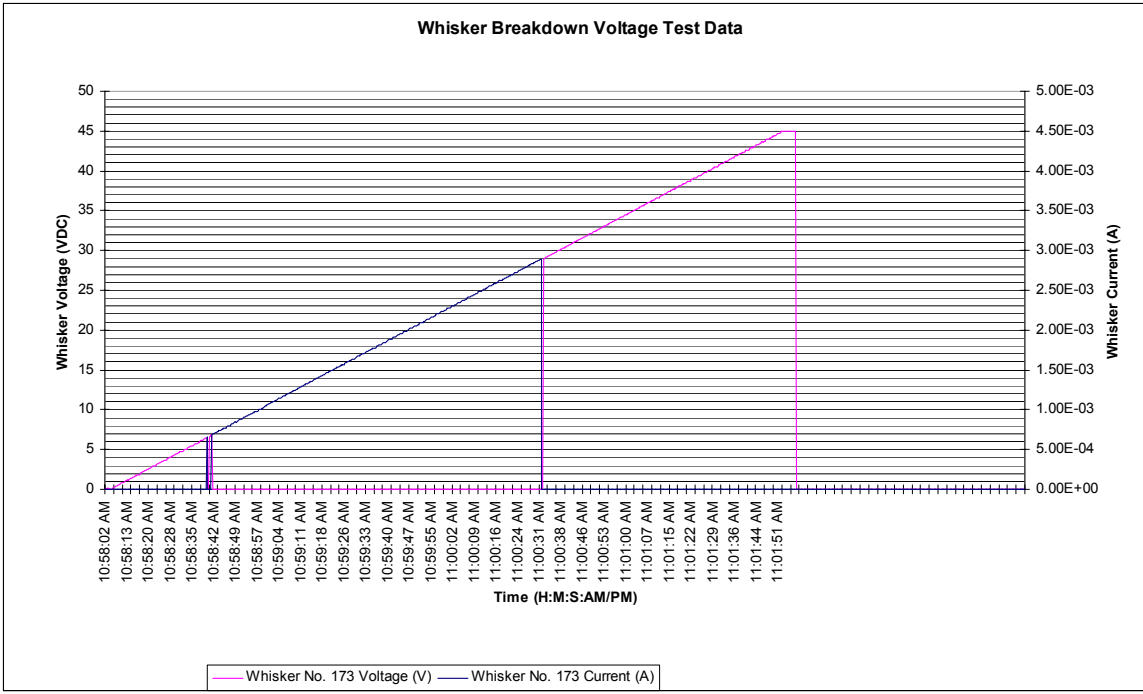


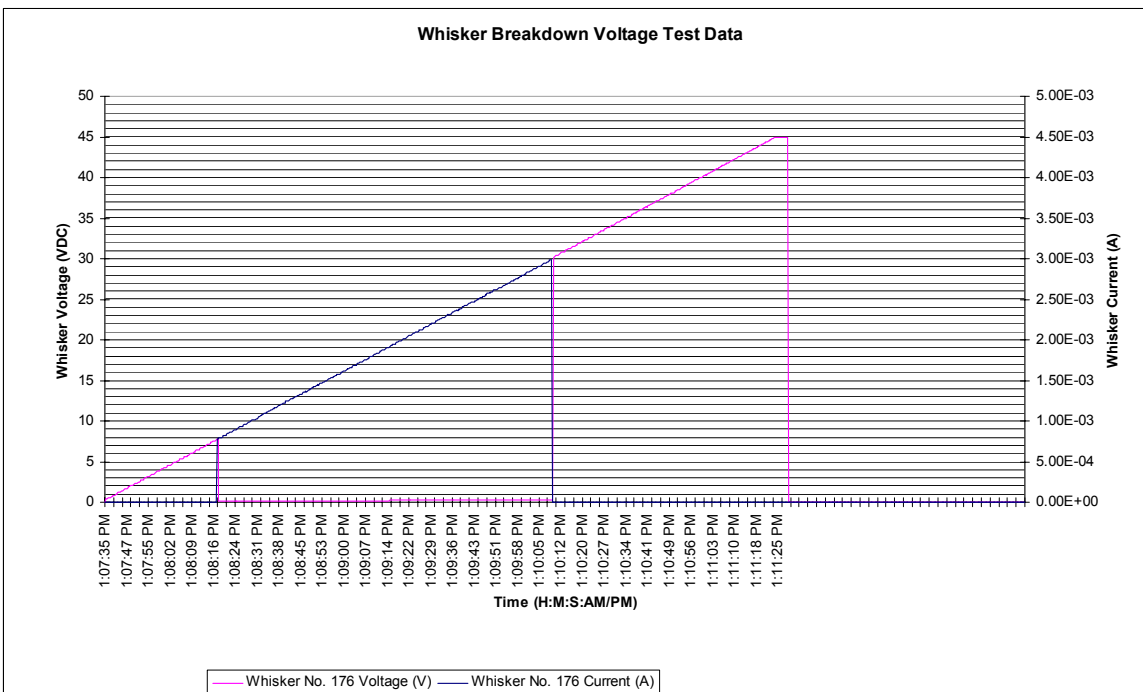
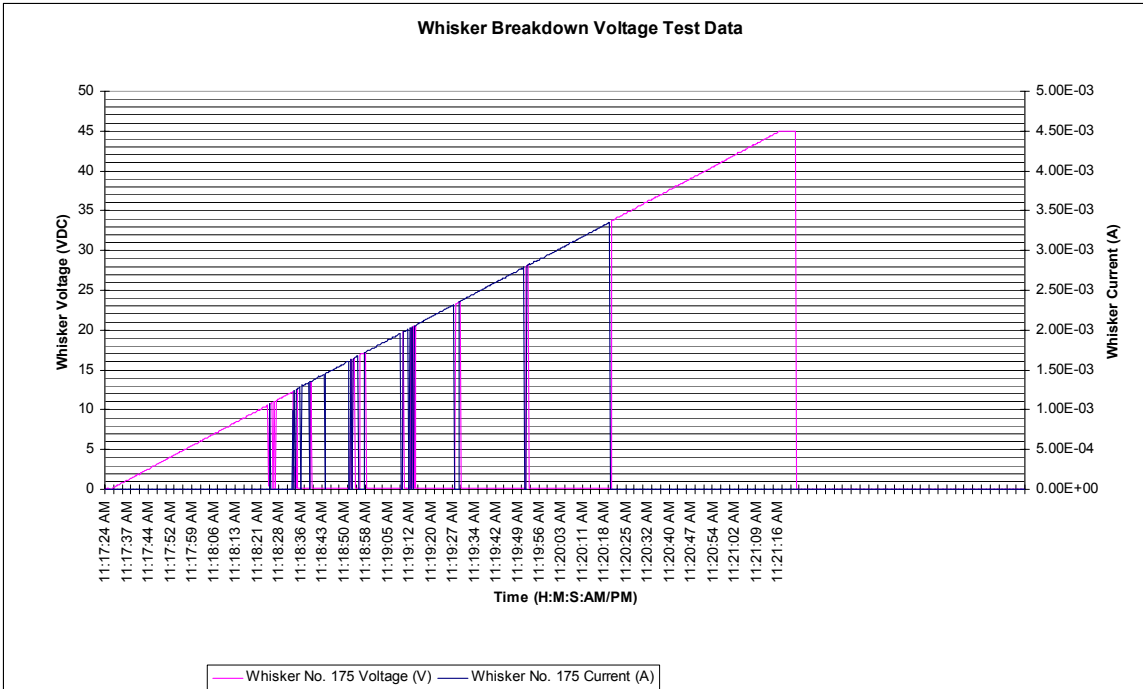


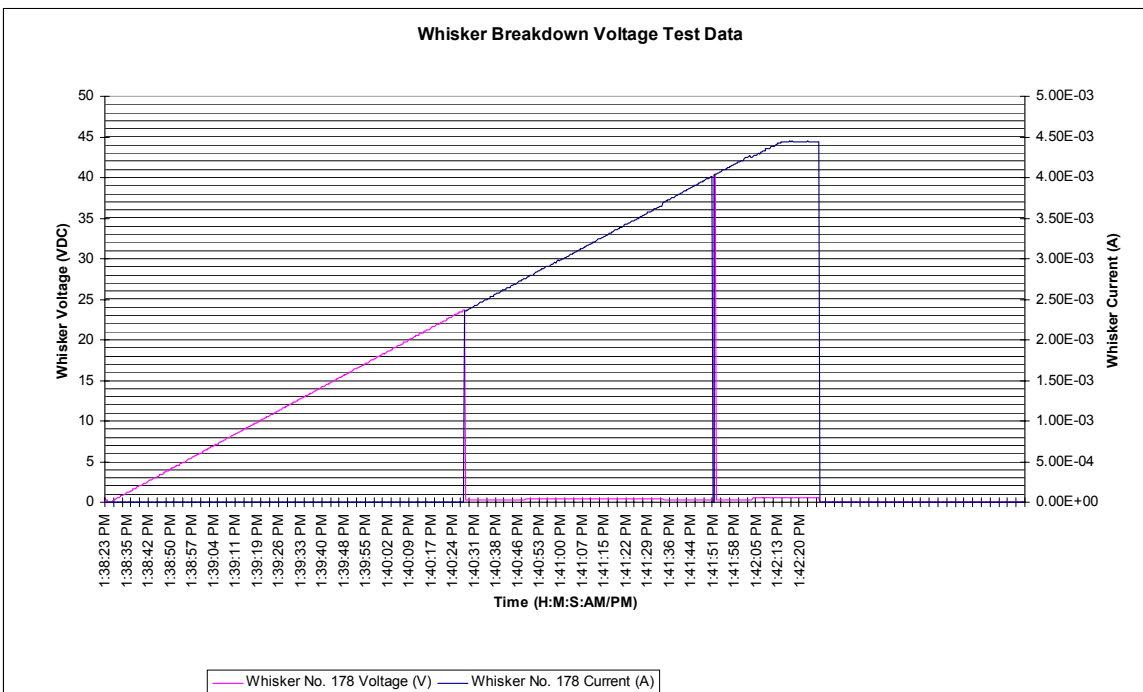
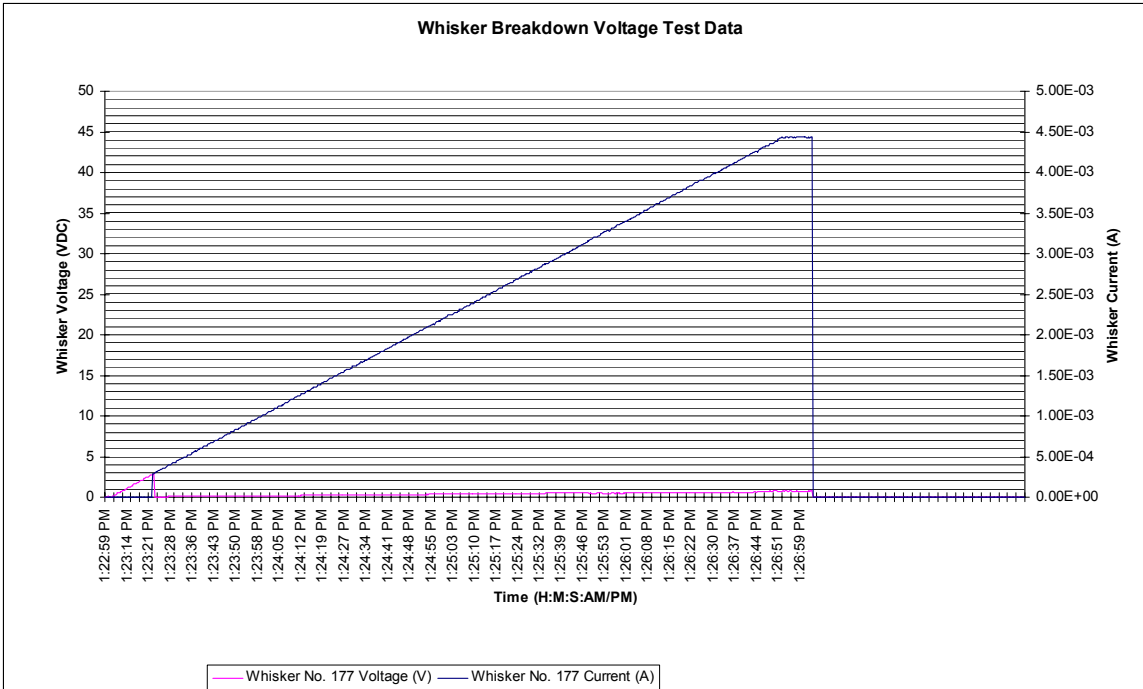


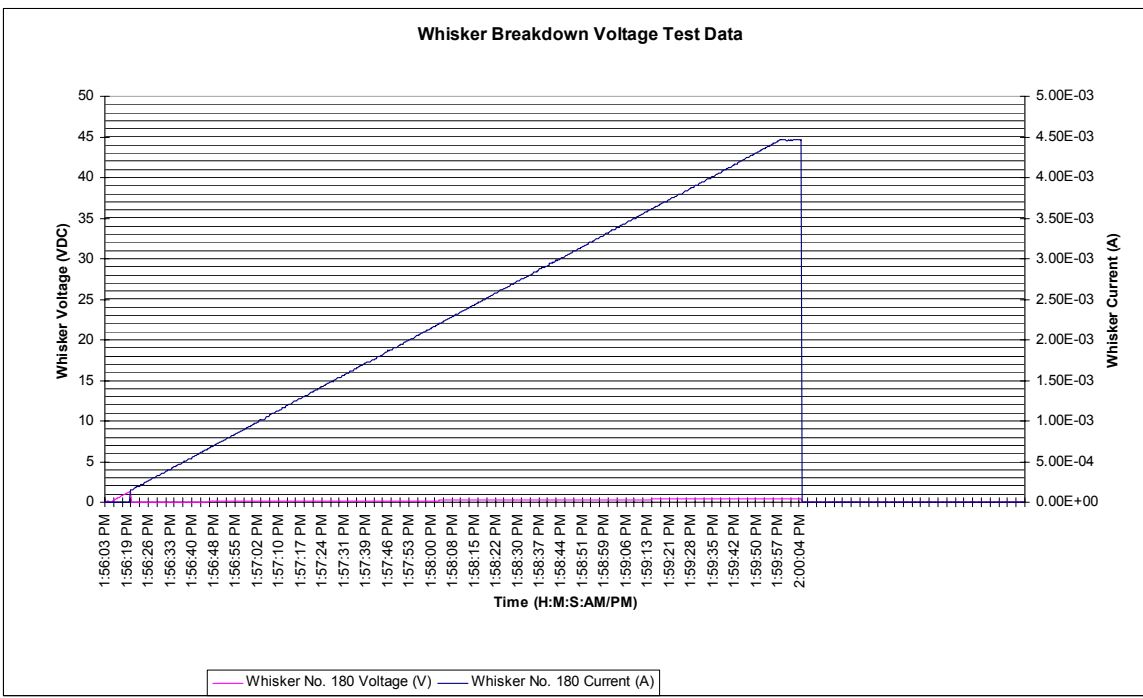
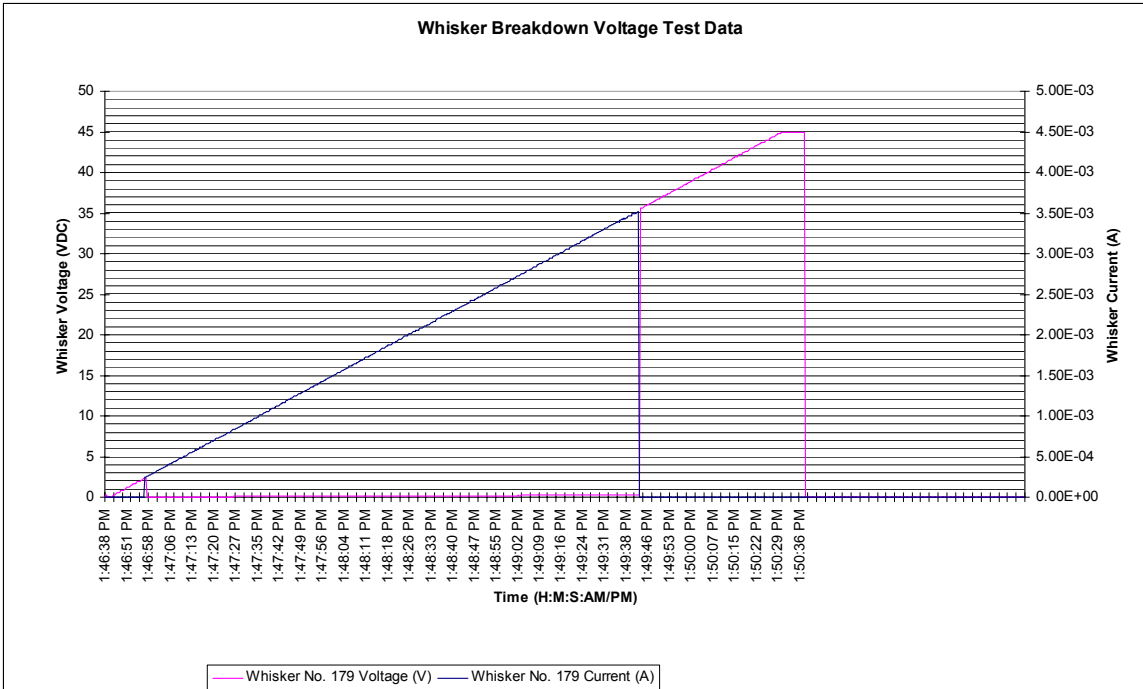


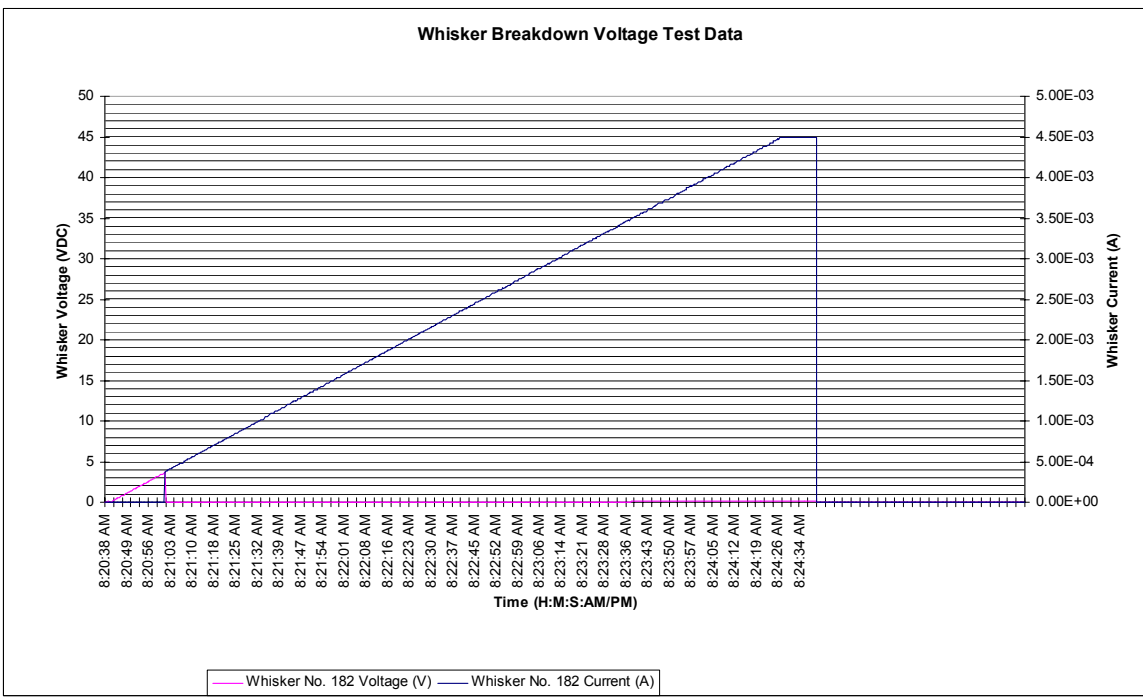
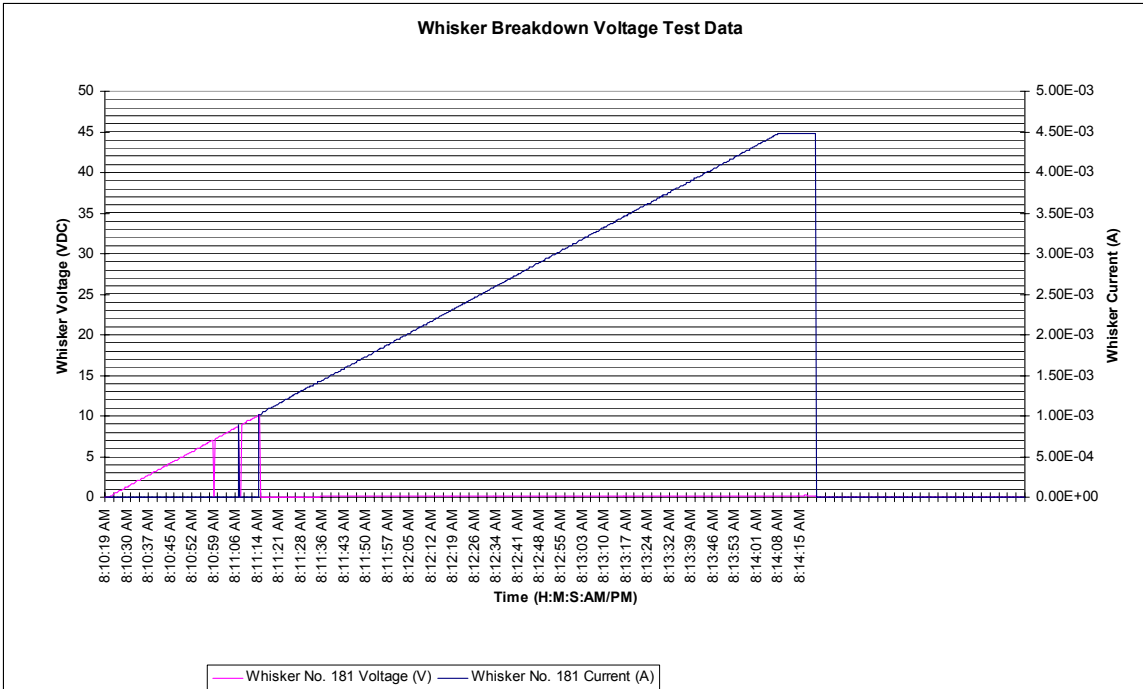


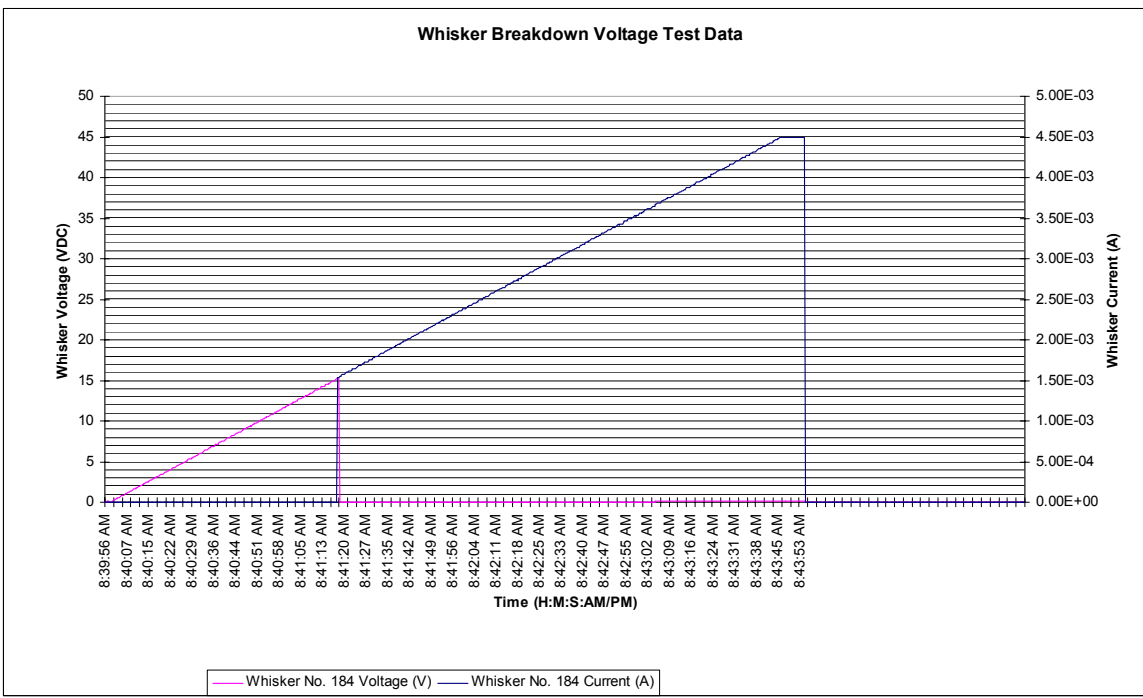
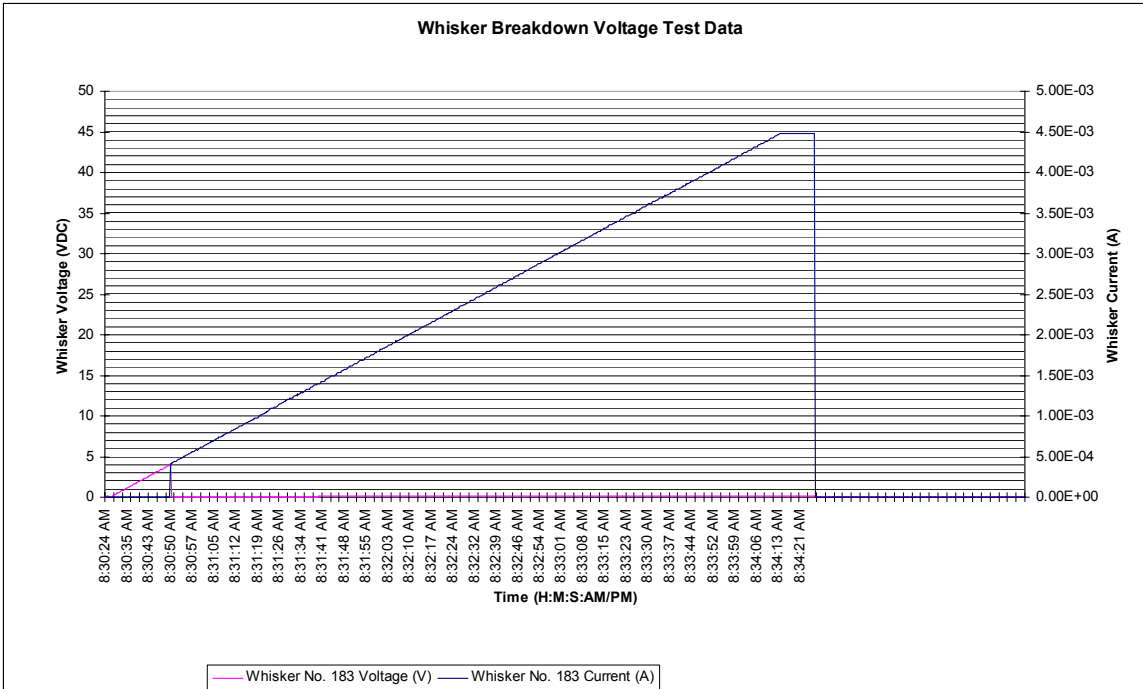


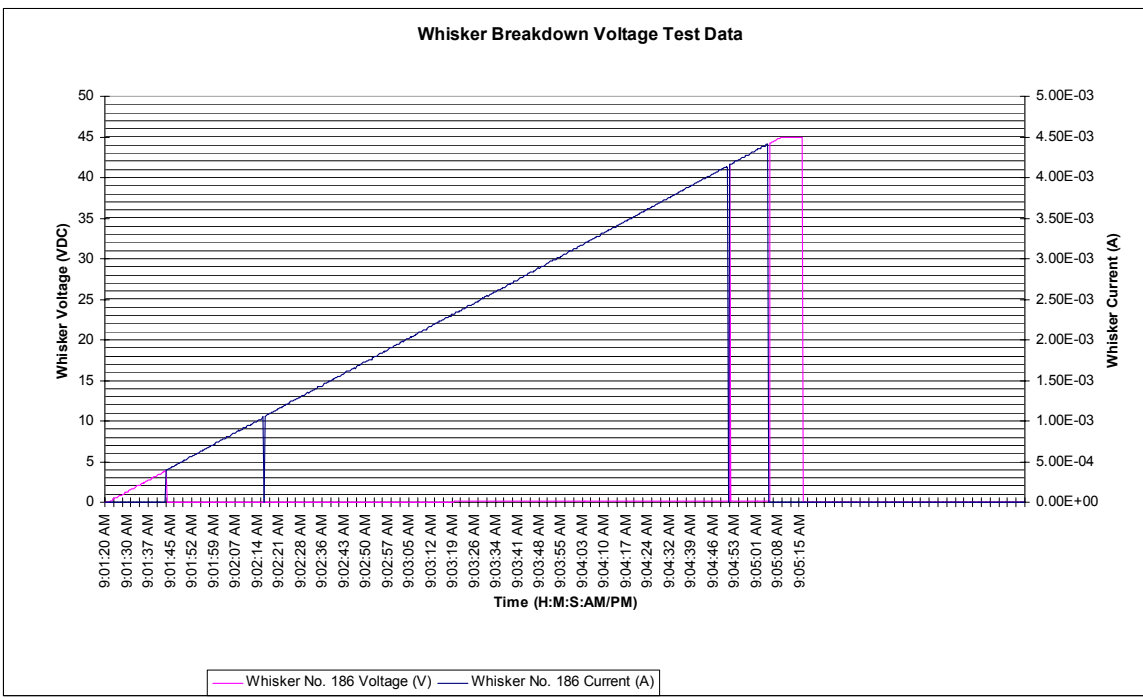
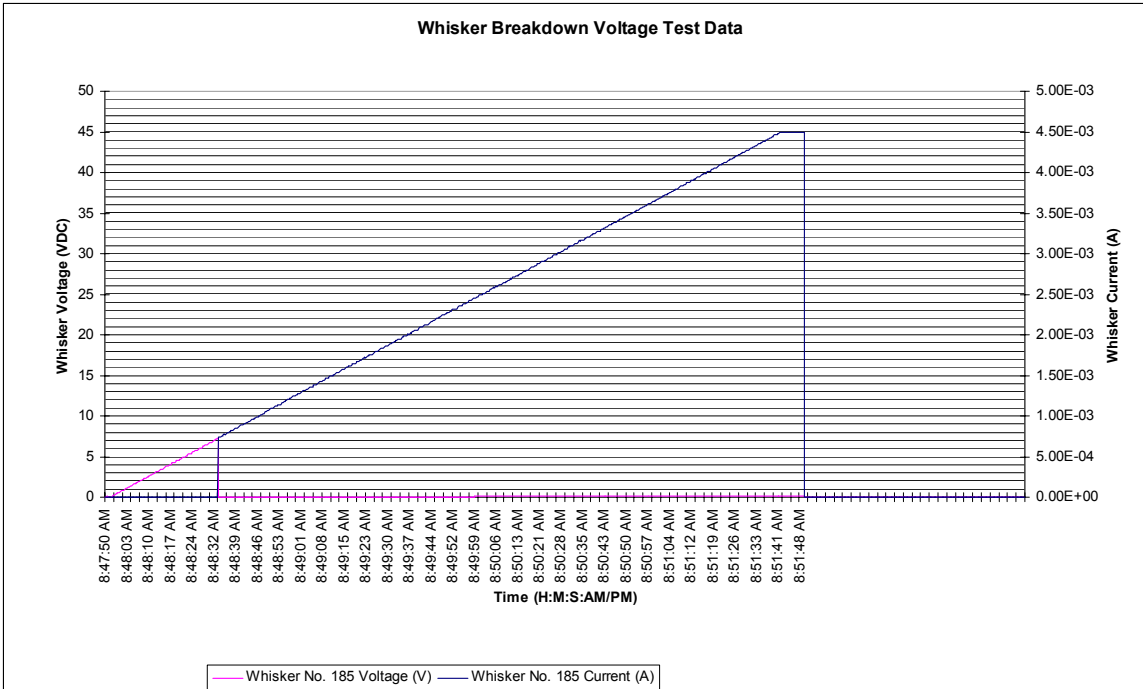


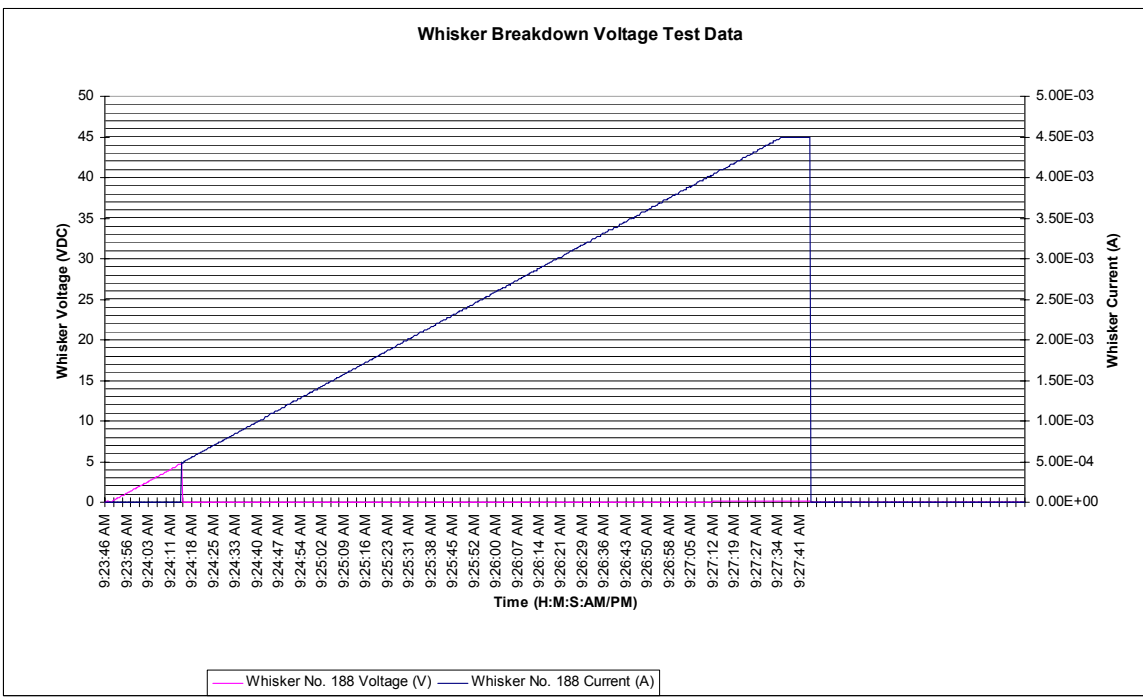
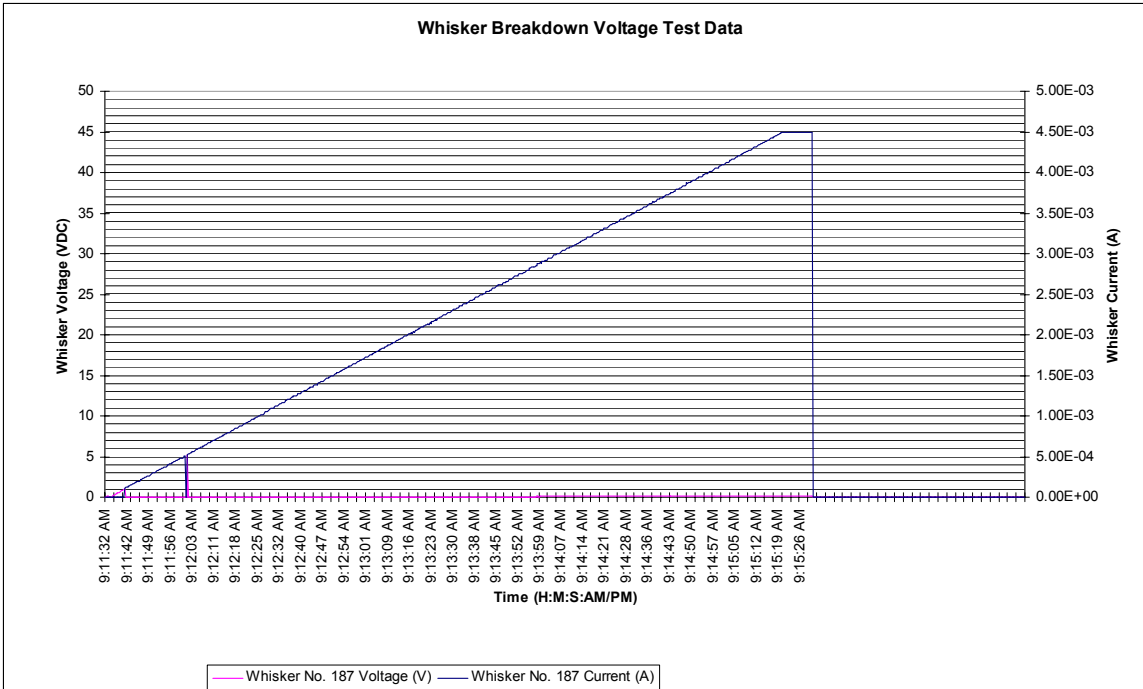


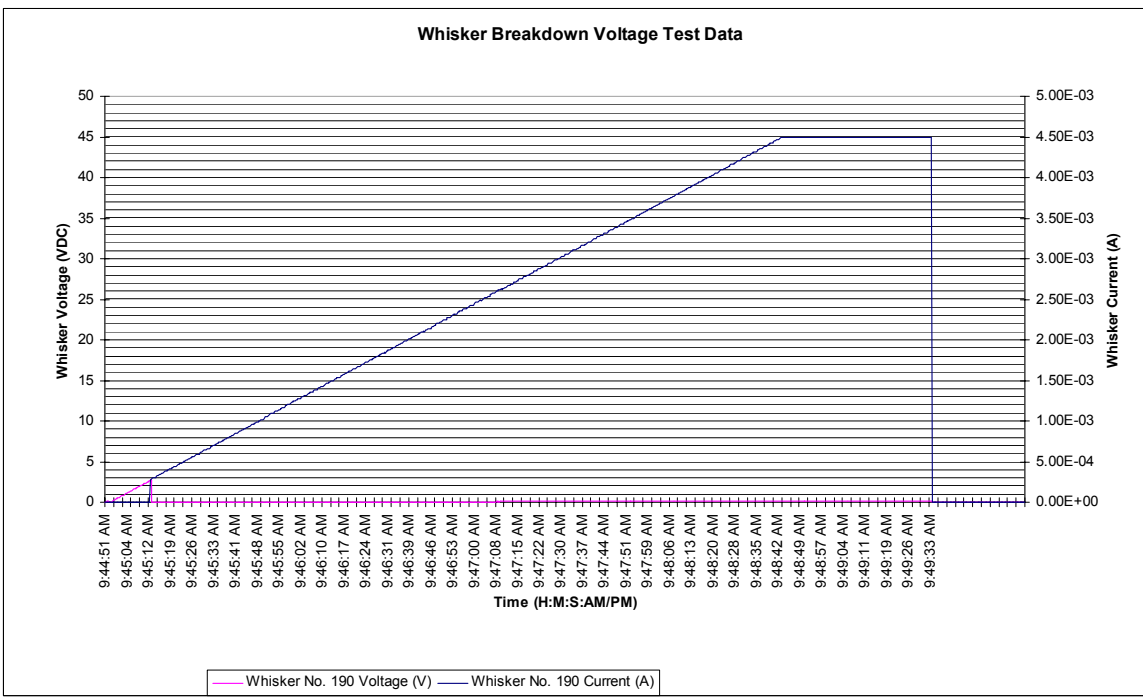
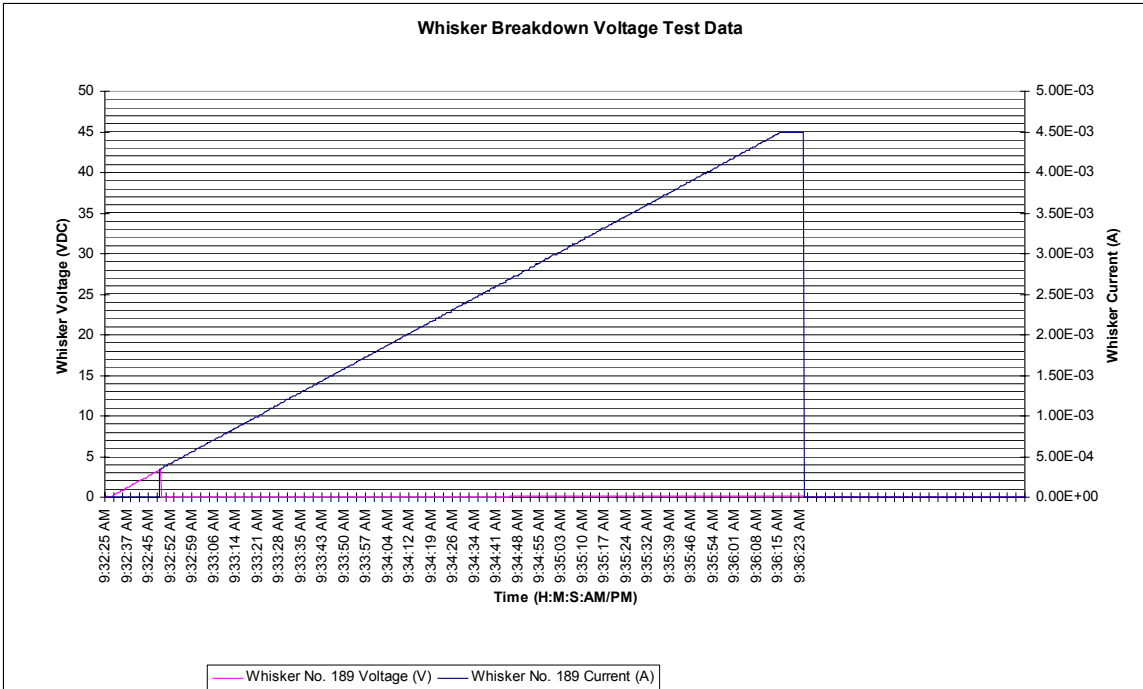


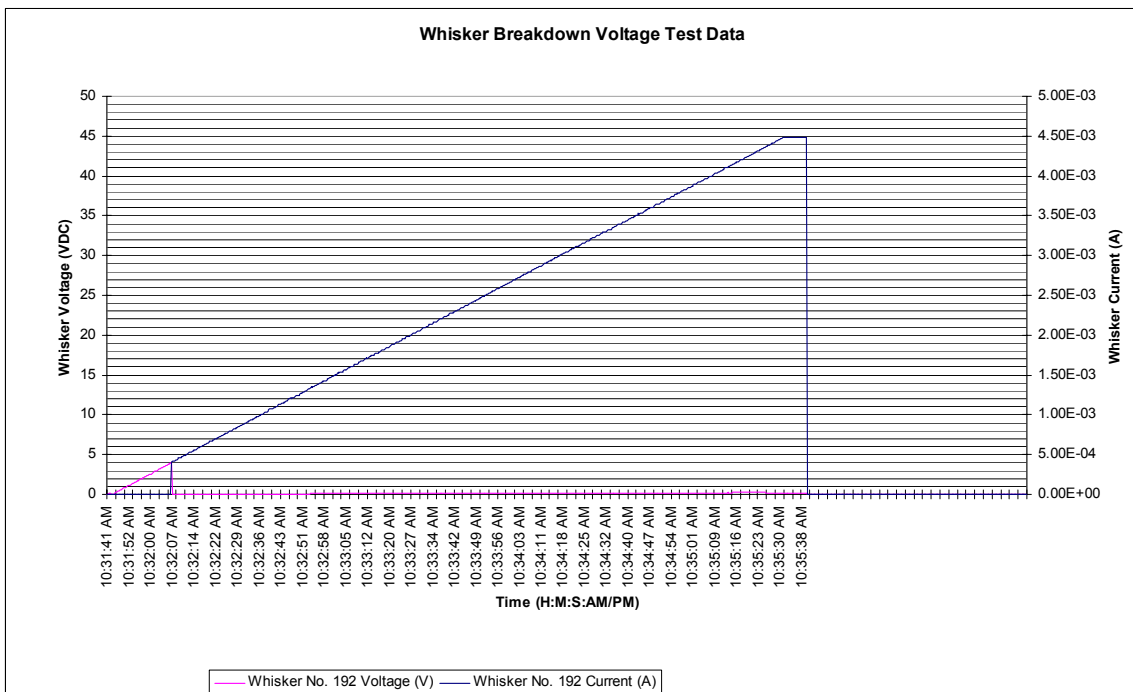
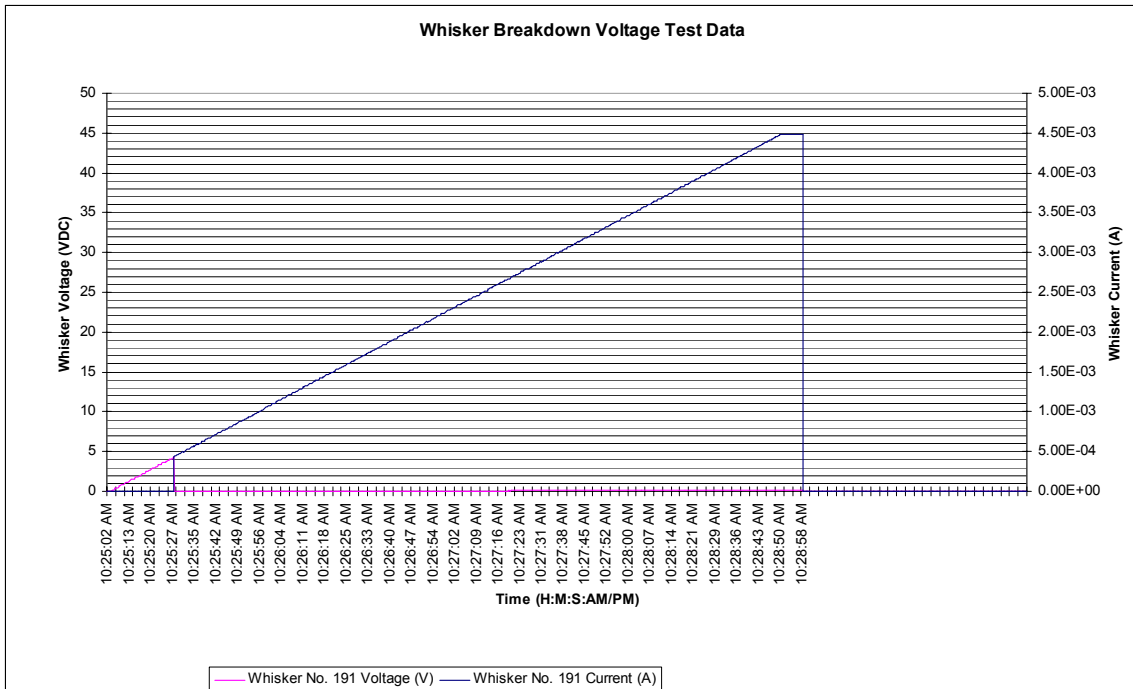


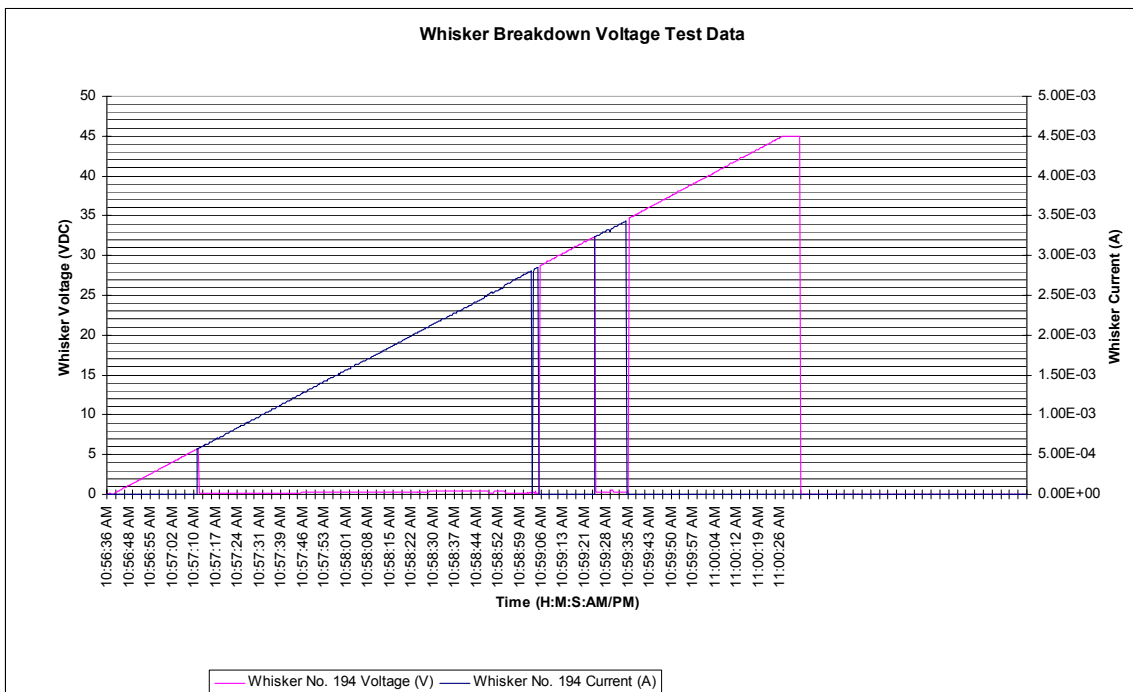
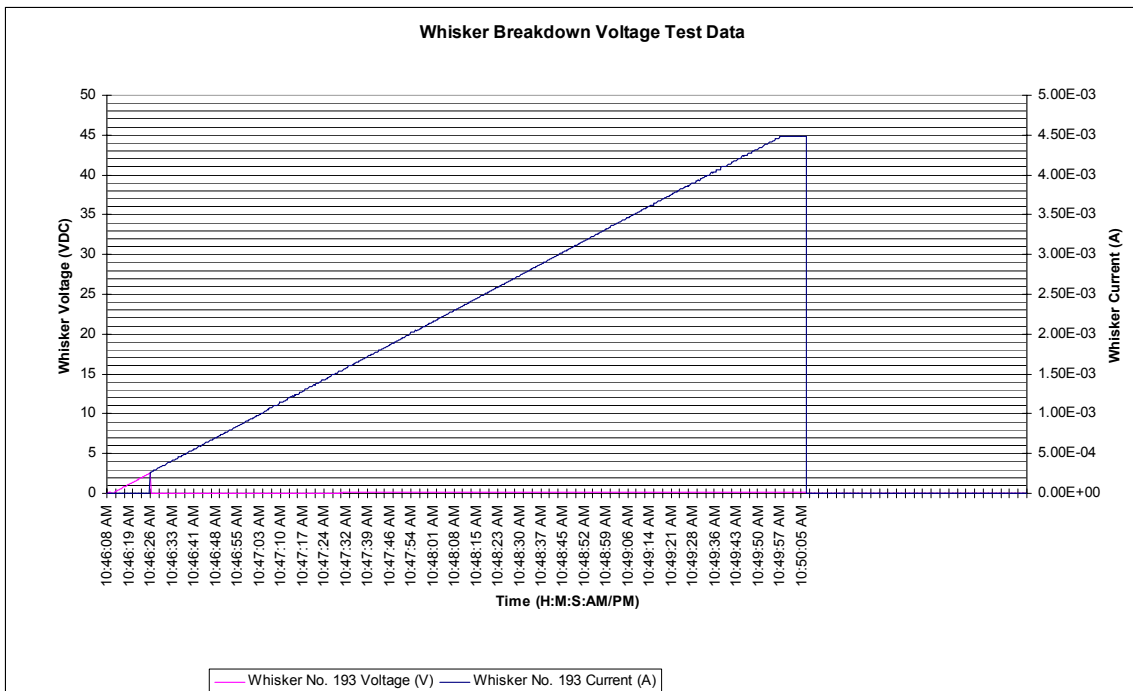


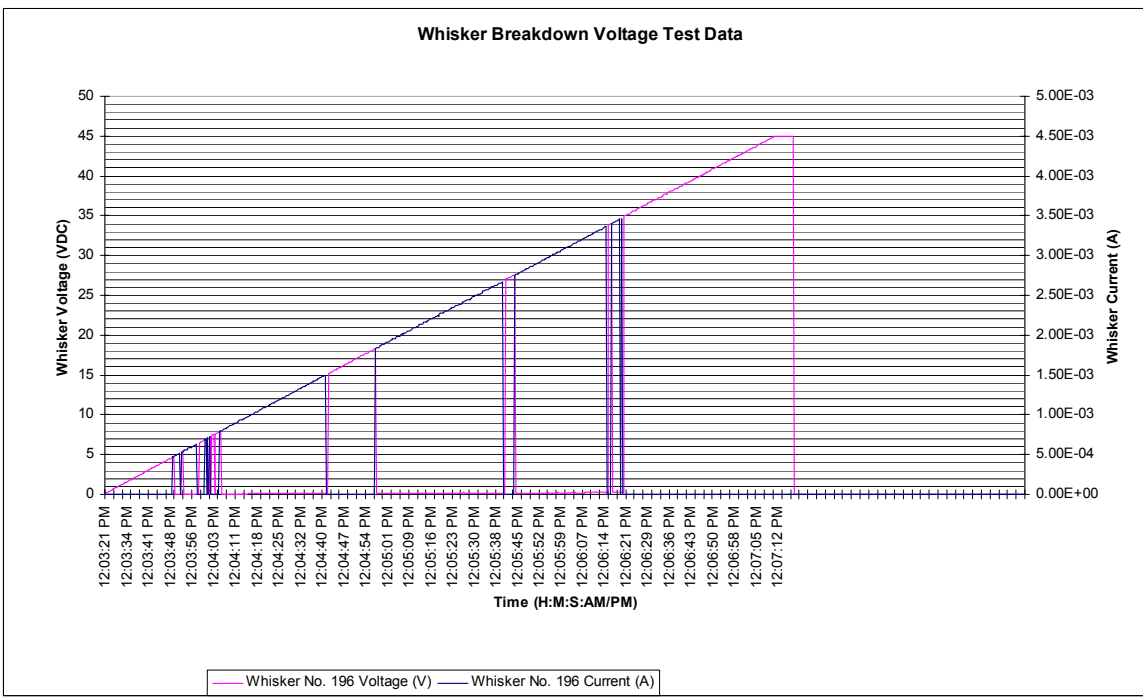
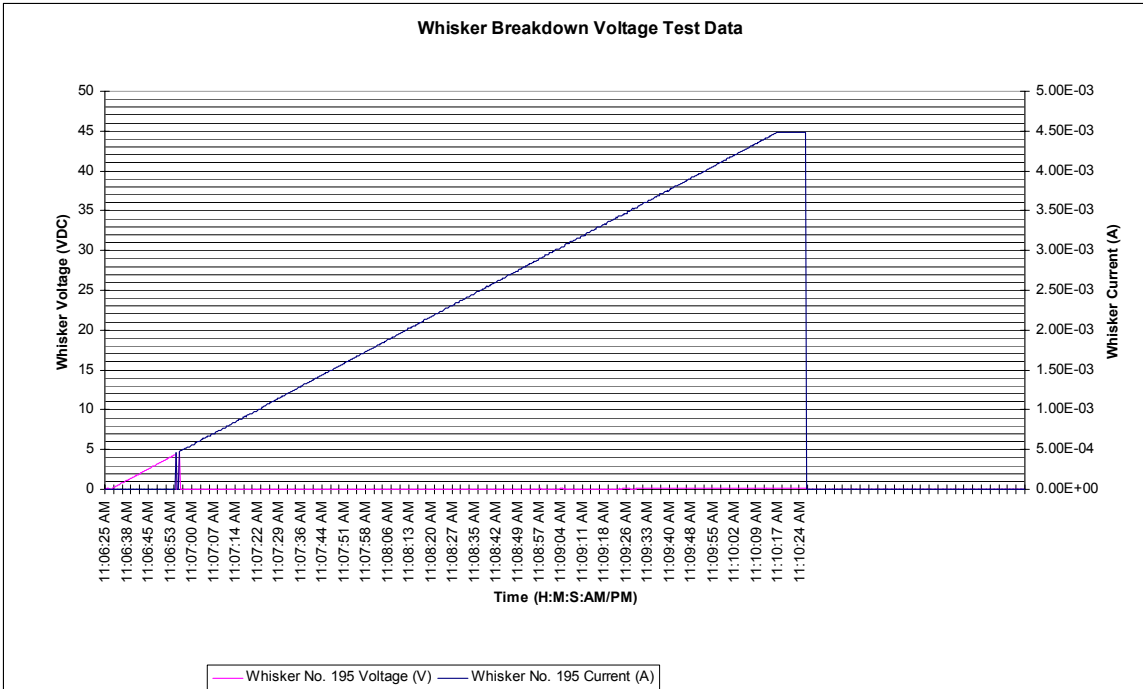


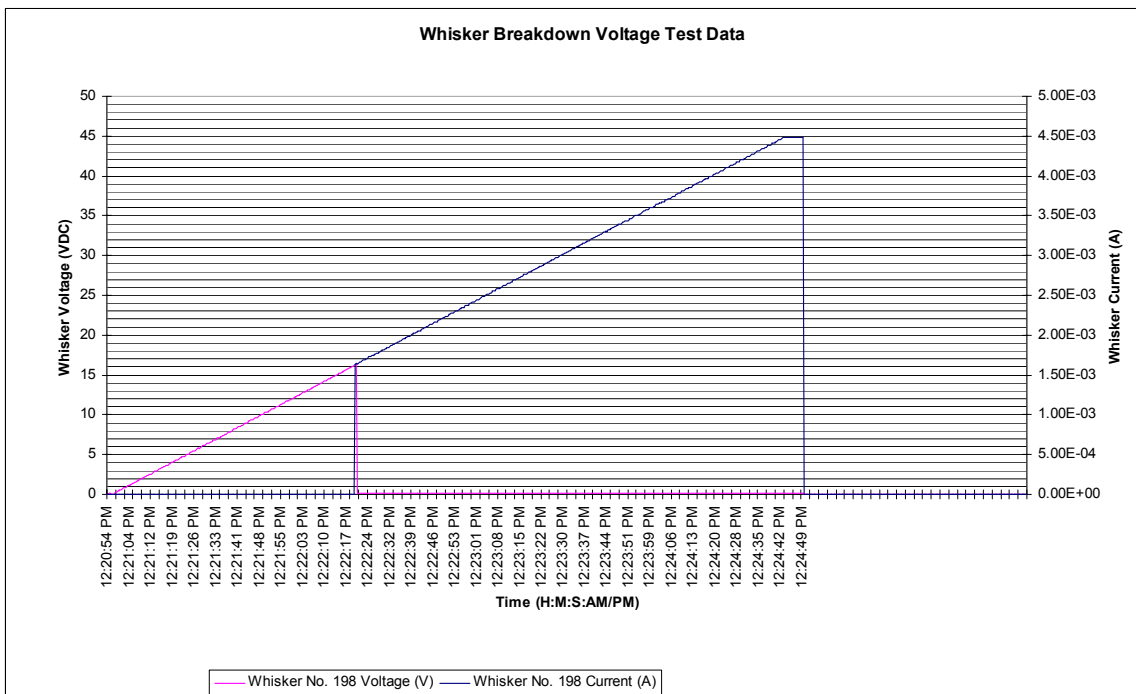
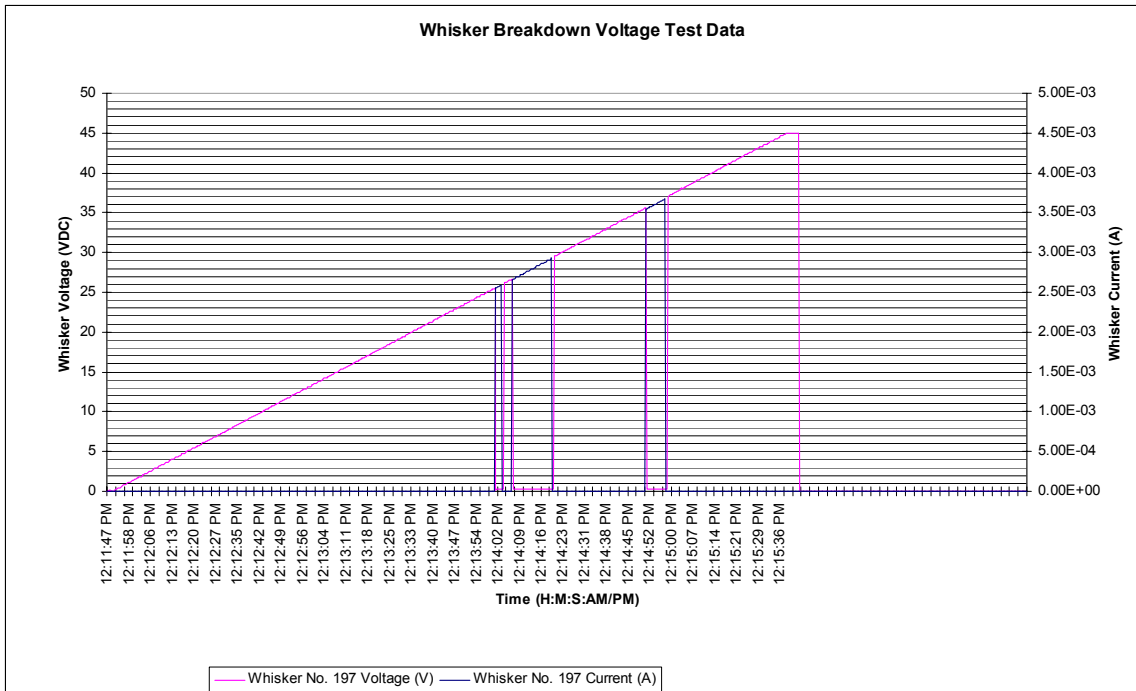


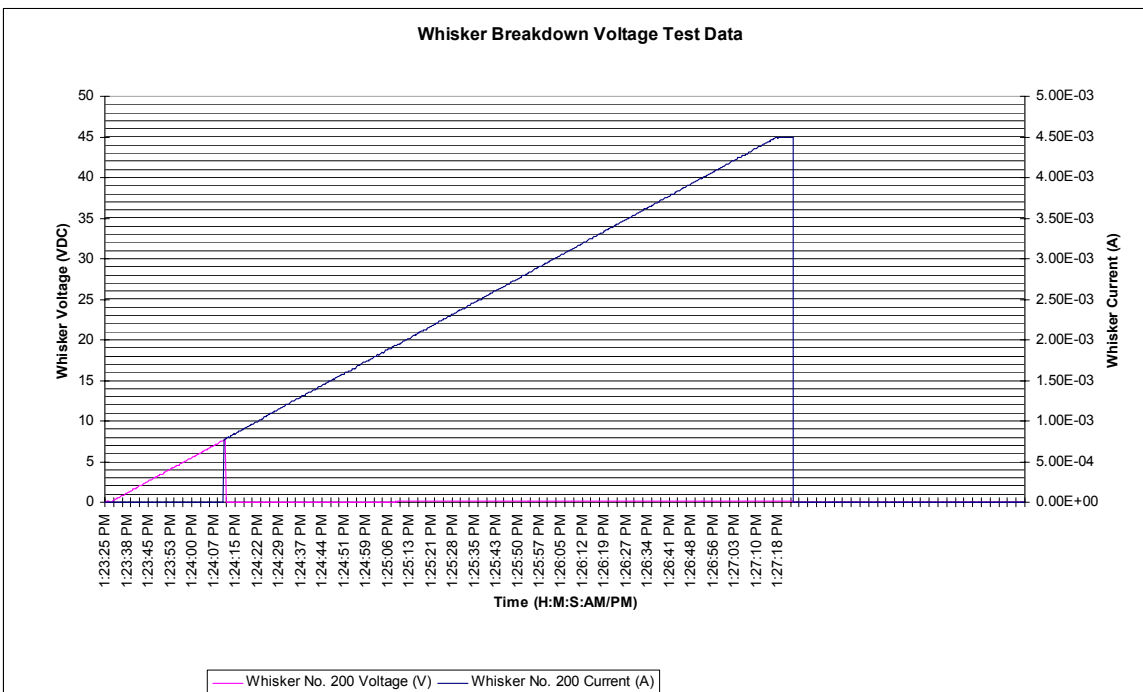
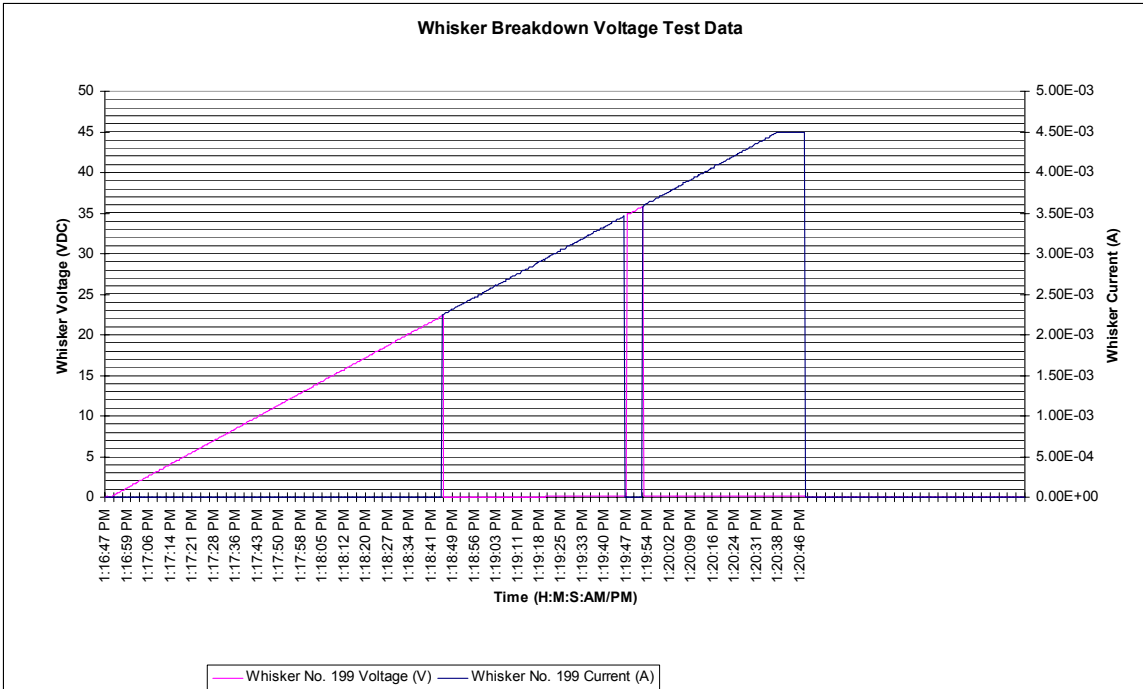












APPENDIX E

Statistical Analysis for the Full Experiment

ANOVA for Natural Log Transformed Data

General Linear Model: LogVol versus LRU S/N, Card Guide, Card Guide Side

Factor	Type	Levels
LRU S/N	fixed	2
Card Guide(LRU S/N)	fixed	20
Card Guide Side(LRU S/N Card Guide)	fixed	40

Factor	Values
LRU S/N	31, 33
Card Guide(LRU S/N)	1, 2, 3, 4, 5, 6, 7, 8, 9, 10, 1, 2, 3, 4, 5, 6, 7, 8, 9, 10
Card Guide Side(LRU S/N Card Guide)	1, 2, 1, 2, 1, 2, 1, 2, 1, 2, 1, 2, 1, 2, 1, 2, 1, 2, 1, 2, 1, 2, 1, 2, 1, 2, 1, 2, 1, 2, 1, 2

Analysis of Variance for LogVol, using Adjusted SS for Tests

Source	DF	Seq SS	Adj SS	Adj MS	F
LRU S/N	1	0.2716	0.2716	0.2716	0.43
Card Guide(LRU S/N)	18	7.3596	7.3596	0.4089	0.64
Card Guide Side(LRU S/N Card Guide)	20	22.0855	22.0855	1.1043	1.73
Error	160	102.0241	102.0241	0.6377	
Total	199	131.7408			

Source	P
LRU S/N	0.515
Card Guide(LRU S/N)	0.863
Card Guide Side(LRU S/N Card Guide)	0.033
Error	
Total	

S = 0.798530 R-Sq = 22.56% R-Sq(adj) = 3.68%

Unusual Observations for LogVol

Obs	LogVol	Fit	SE Fit	Residual	St Resid
1	-2.81341	0.59138	0.35711	-3.40479	-4.77 R
56	3.80666	2.05219	0.35711	1.75447	2.46 R
86	3.75490	1.86852	0.35711	1.88638	2.64 R
168	3.58518	1.86263	0.35711	1.72255	2.41 R
178	3.16421	1.49552	0.35711	1.66868	2.34 R

R denotes an observation with a large standardized residual.

ANOVA for Natural Log Transformed Data with Outlier Removed

General Linear Model: LogVol_1 versus LRU S/N, Card Guide, Card Guide S

Factor	Type	Levels
LRU S/N	fixed	2
Card Guide(LRU S/N)	fixed	20
Card Guide Side(LRU S/N Card Guide)	fixed	40

Factor	Values
LRU S/N	31, 33
Card Guide(LRU S/N)	1, 2, 3, 4, 5, 6, 7, 8, 9, 10, 1, 2, 3, 4, 5, 6, 7, 8, 9, 10
Card Guide Side(LRU S/N Card Guide)	1, 2, 1, 2, 1, 2, 1, 2, 1, 2, 1, 2, 1, 2, 1, 2, 1, 2, 1, 2, 1, 2, 1, 2, 1, 2

Analysis of Variance for LogVol_1, using Adjusted SS for Tests

Source	DF	Seq SS	Adj SS	Adj MS	F
LRU S/N	1	0.0381	0.0482	0.0482	0.09
Card Guide(LRU S/N)	18	5.0137	5.0481	0.2804	0.51
Card Guide Side(LRU S/N Card Guide)	20	17.9550	17.9550	0.8978	1.63
Error	159	87.5333	87.5333	0.5505	
Total	198	110.5401			

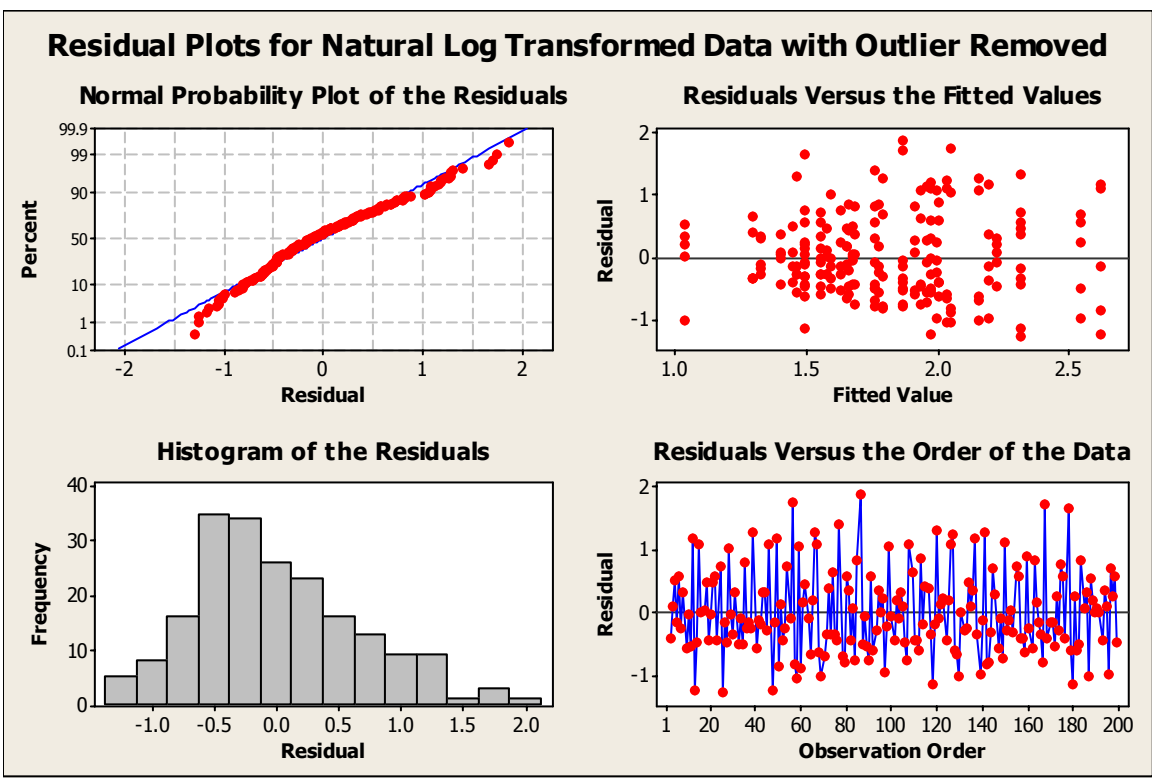
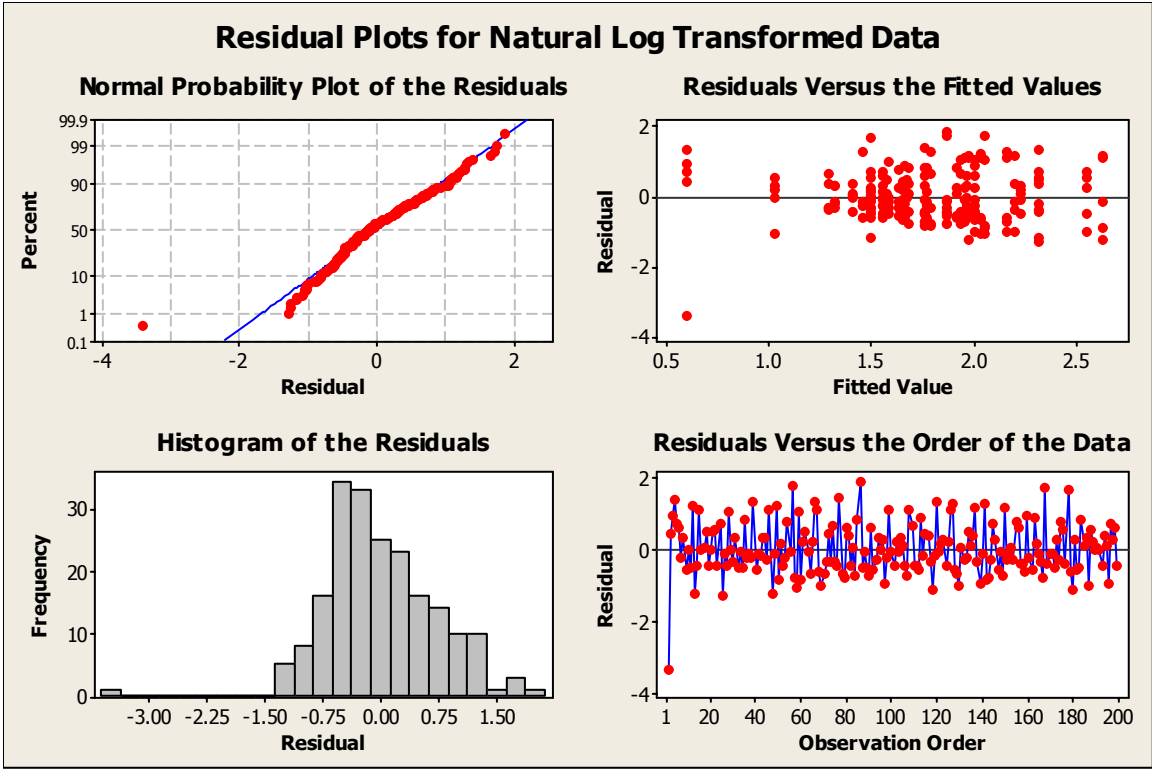
Source	P
LRU S/N	0.768
Card Guide(LRU S/N)	0.951
Card Guide Side(LRU S/N Card Guide)	0.051
Error	
Total	

S = 0.741973 R-Sq = 20.81% R-Sq(adj) = 1.39%

Unusual Observations for LogVol_1

Obs	LogVol_1	Fit	SE Fit	Residual	St Resid
56	3.80666	2.05219	0.33182	1.75447	2.64 R
77	3.16463	1.76086	0.33182	1.40377	2.12 R
86	3.75490	1.86852	0.33182	1.88638	2.84 R
168	3.58518	1.86263	0.33182	1.72255	2.60 R
178	3.16421	1.49552	0.33182	1.66868	2.51 R

R denotes an observation with a large standardized residual.



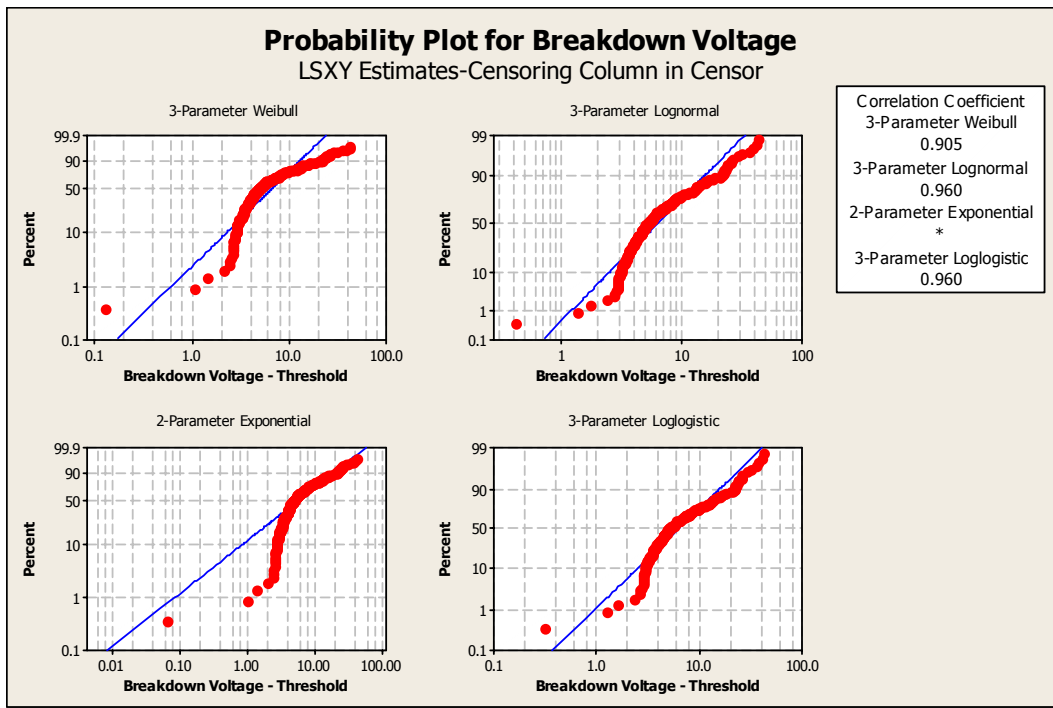
Kruskal-Wallis Test: Breakdown Voltage versus Card Guide Side

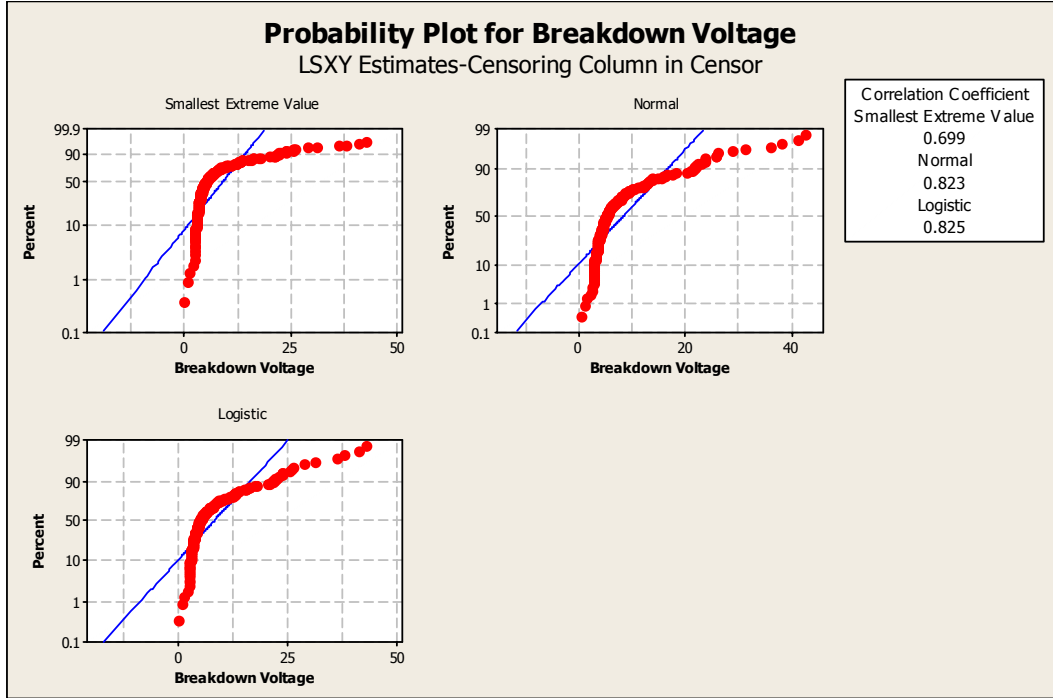
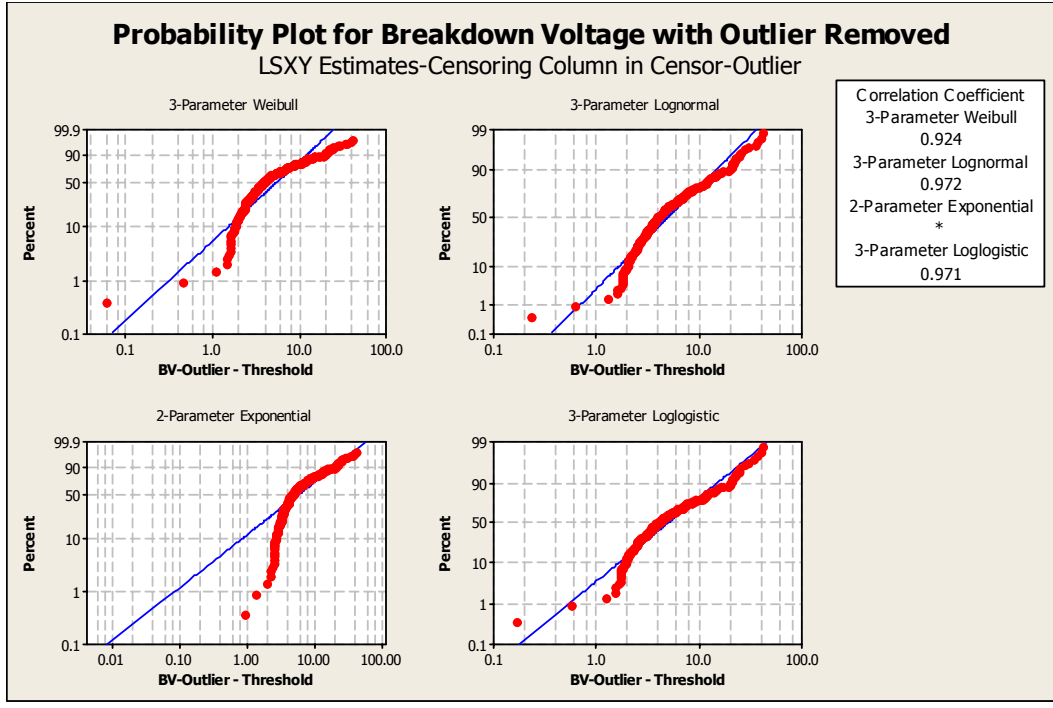
Kruskal-Wallis Test on Breakdown Voltage

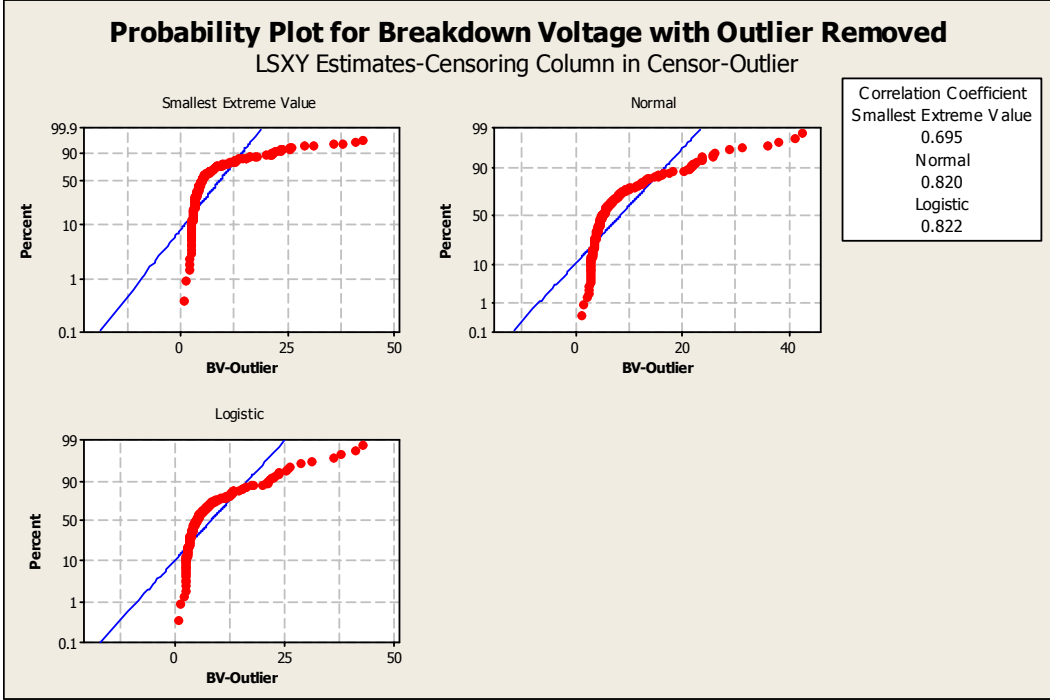
Card
Guide

Side	N	Median	Ave Rank	Z
1	100	4.685	93.5	-1.71
2	100	5.190	107.5	1.71
Overall	200		100.5	

H = 2.93 DF = 1 P = 0.087
H = 2.93 DF = 1 P = 0.087 (adjusted for ties)





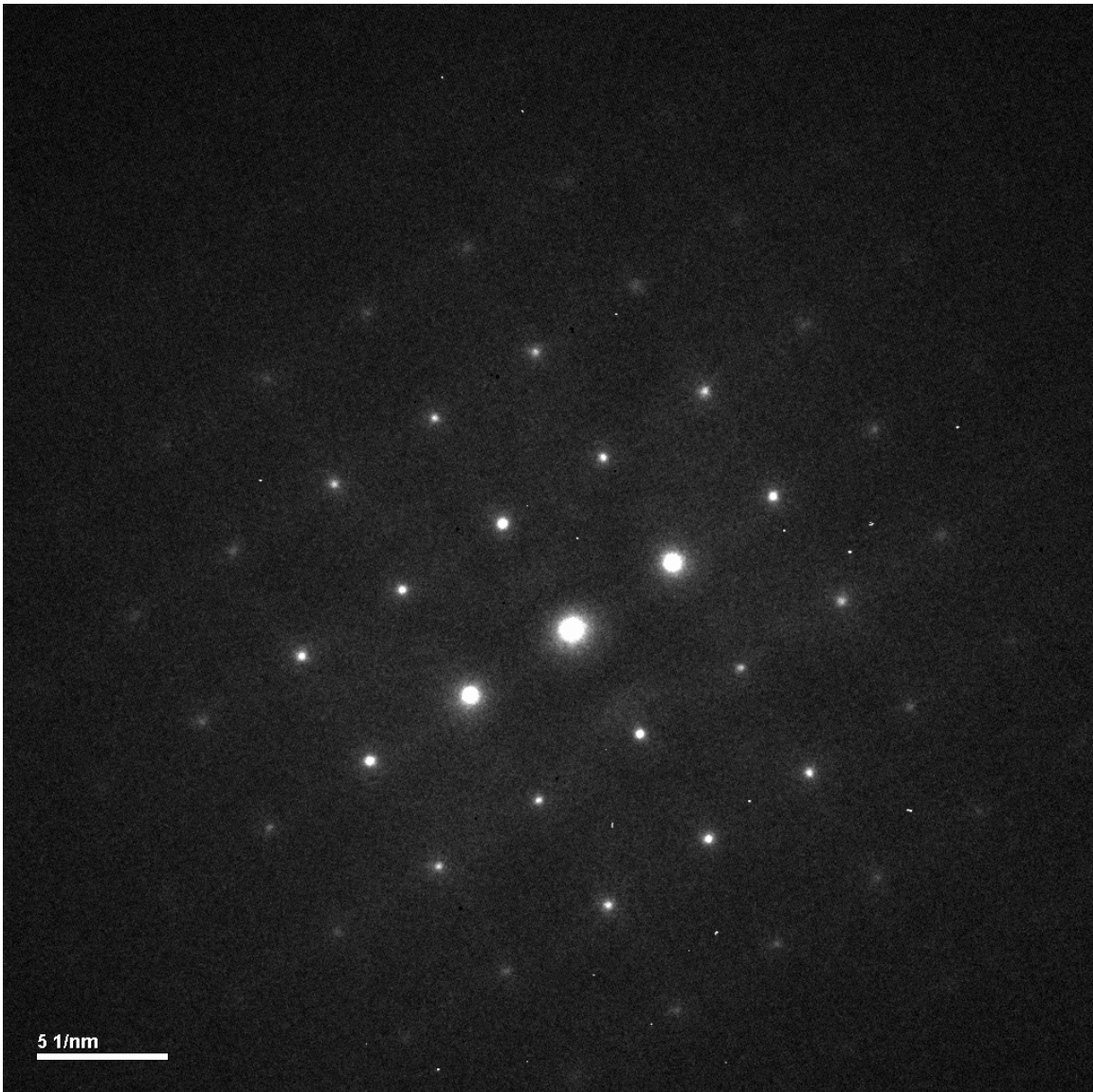


APPENDIX F

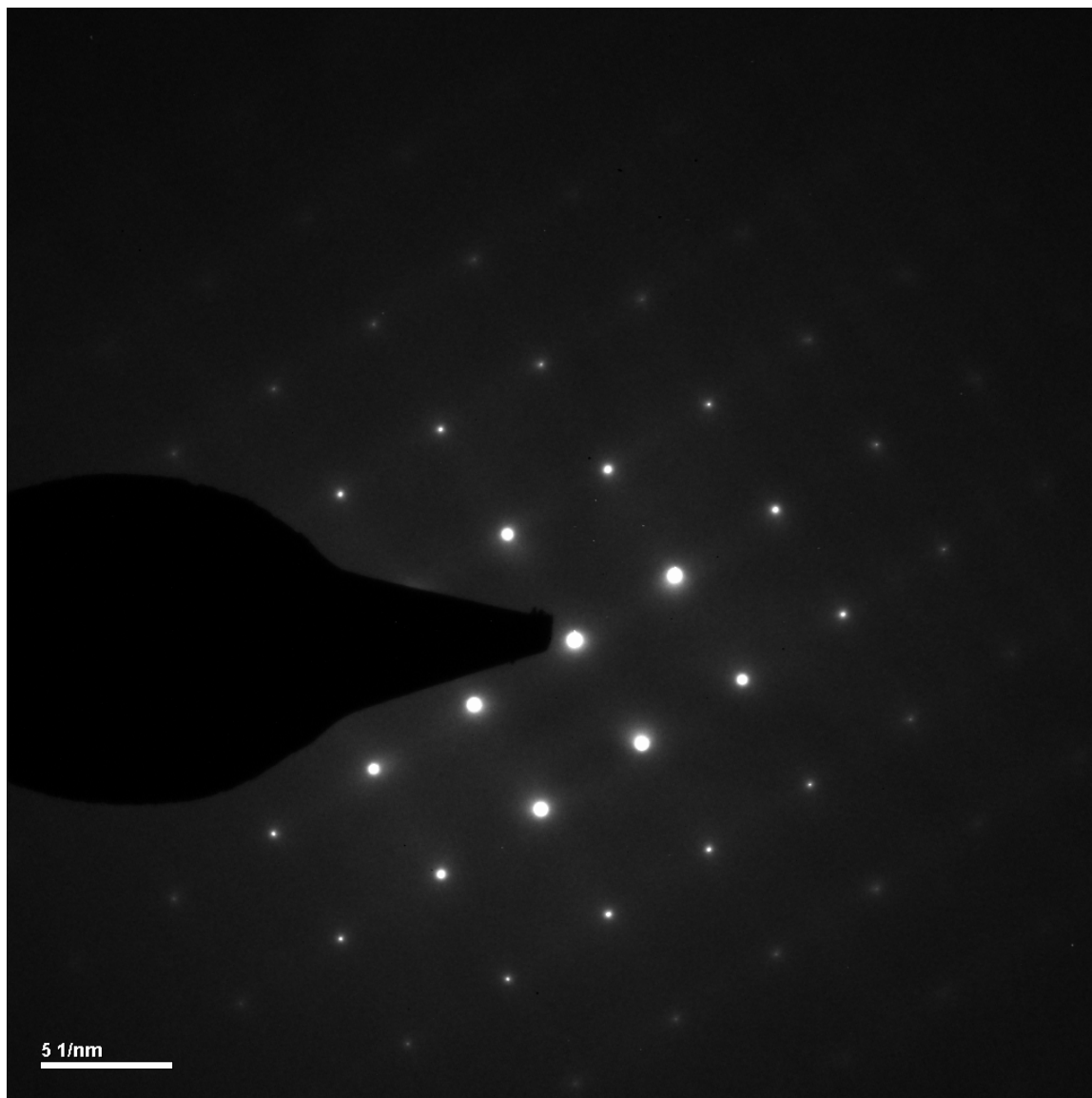
Diffraction Patterns

The diffraction patterns taken in the TEM for each of the four sections in the tin whisker cross section prepared via FIB and discussed in Chapter 5 are shown here. The diffraction patterns are used to determine the orientation of each grain.

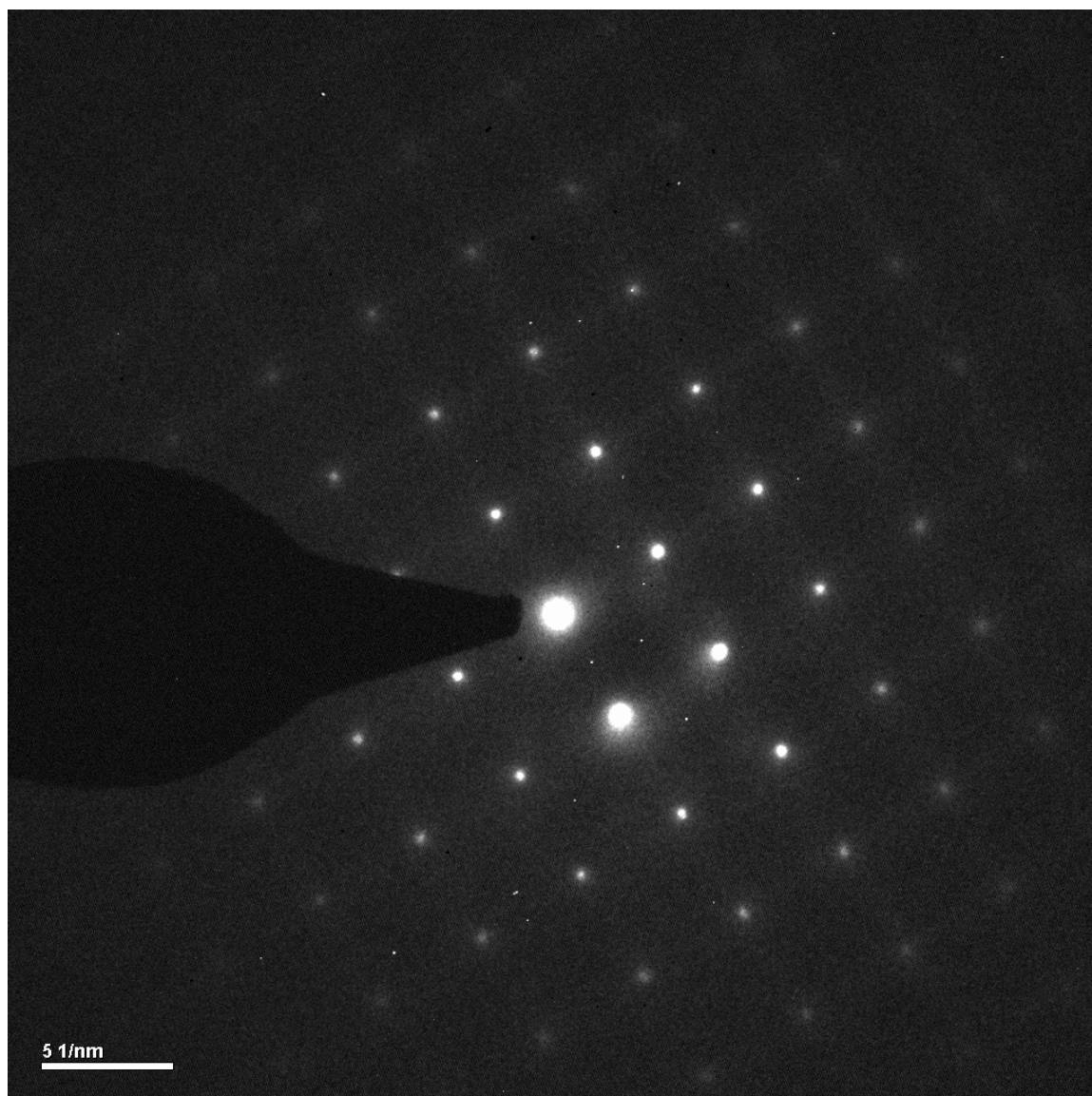
Diffraction Pattern for Polycrystalline Whisker Section A



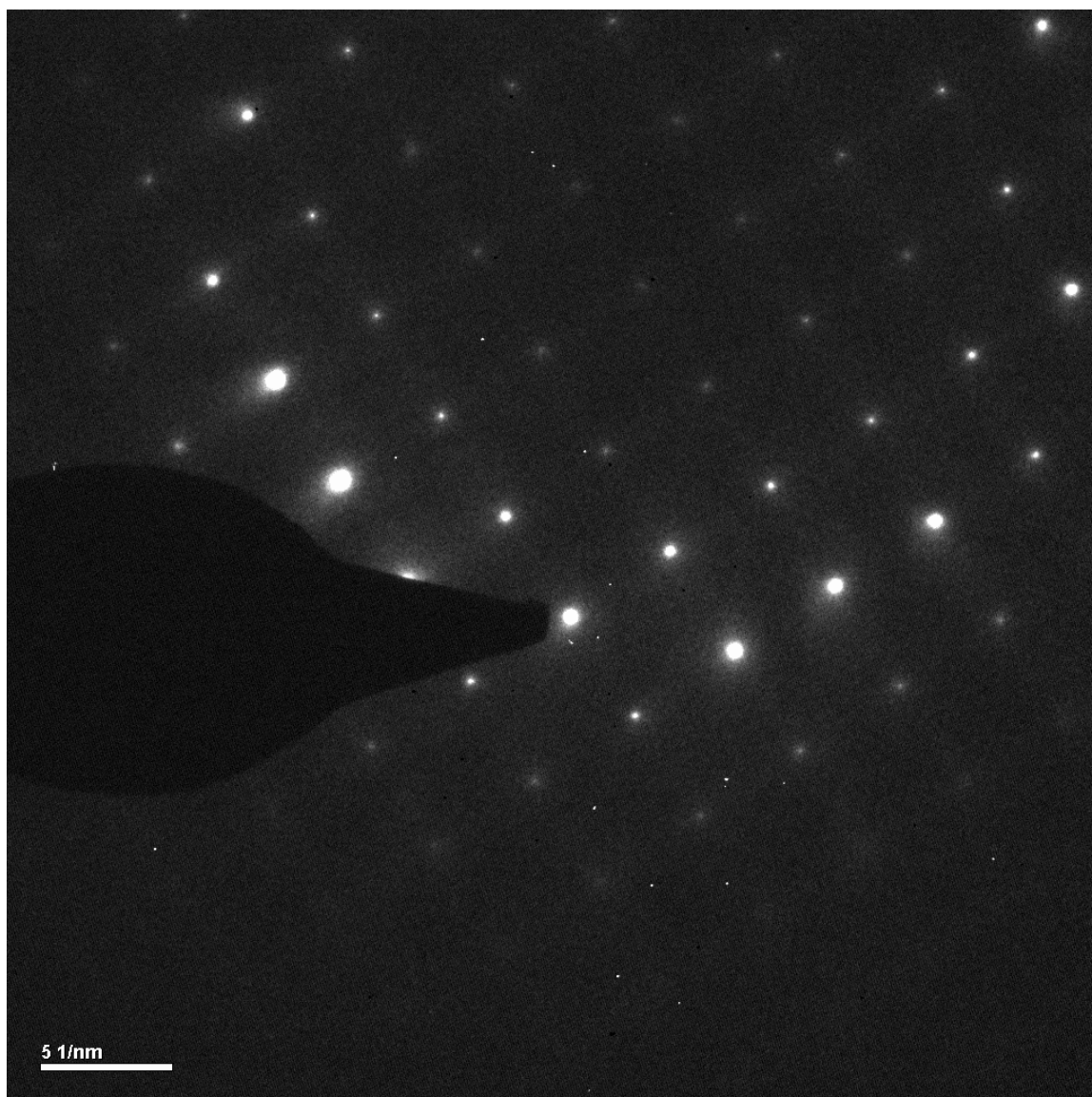
Diffraction Pattern for Polycrystalline Whisker Section B



Diffraction Pattern for Polycrystalline Whisker Section C



Diffraction Pattern for Polycrystalline Whisker Section D

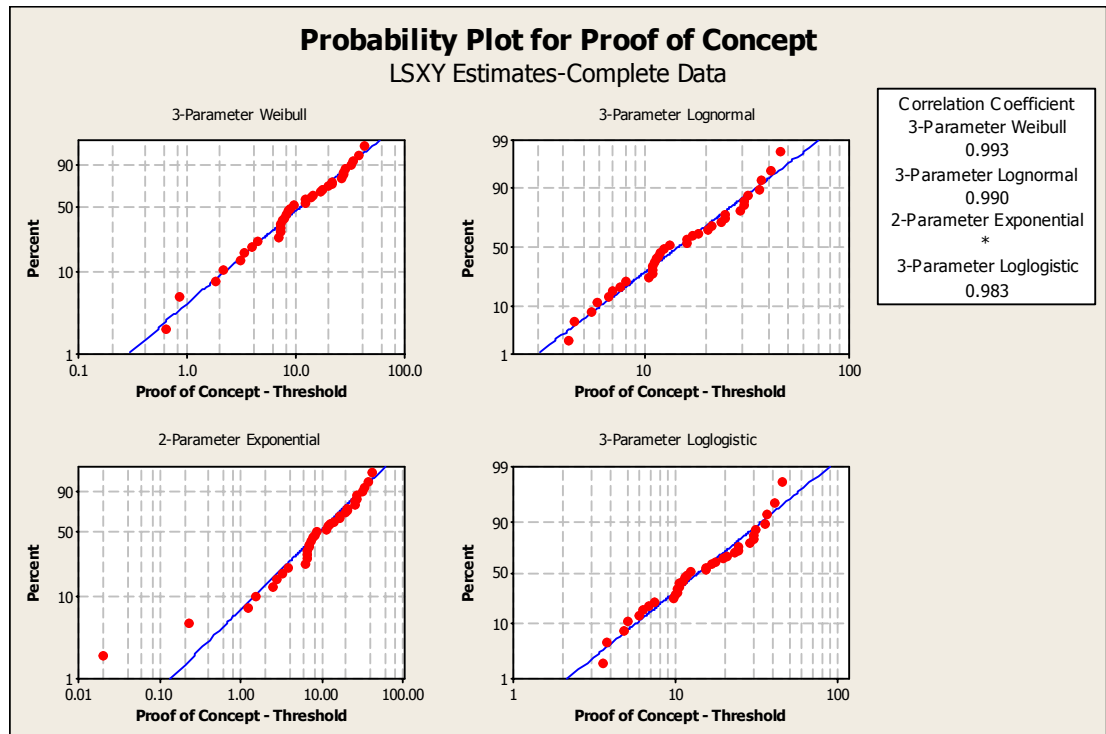


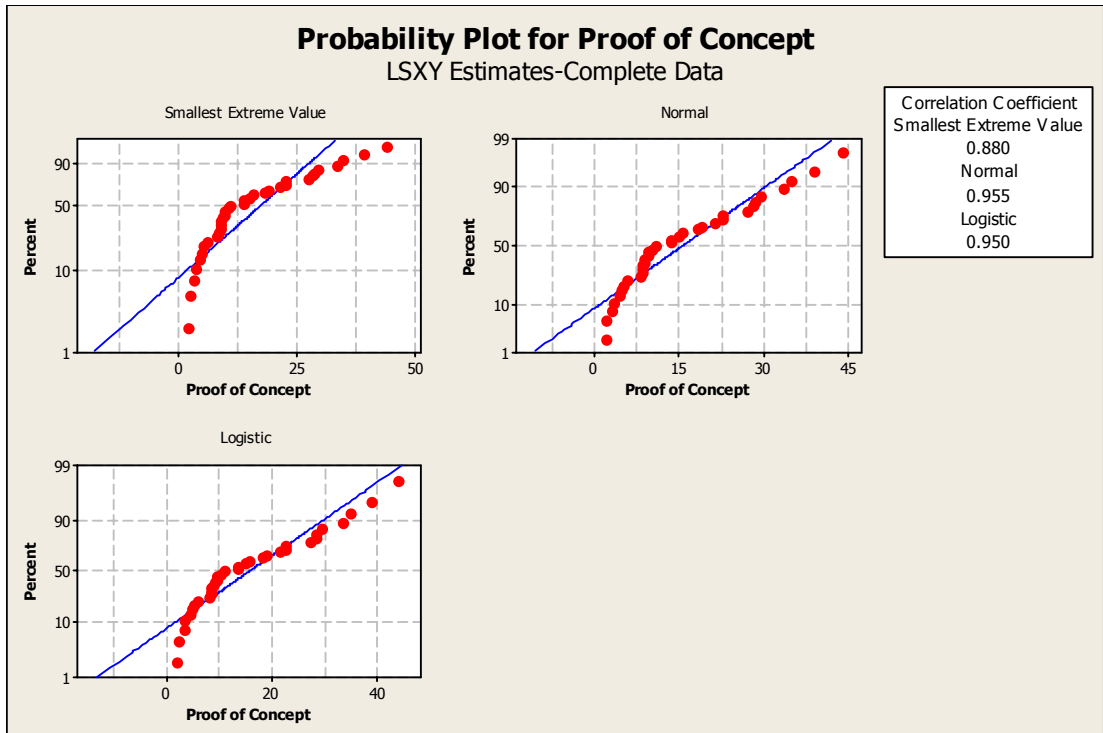
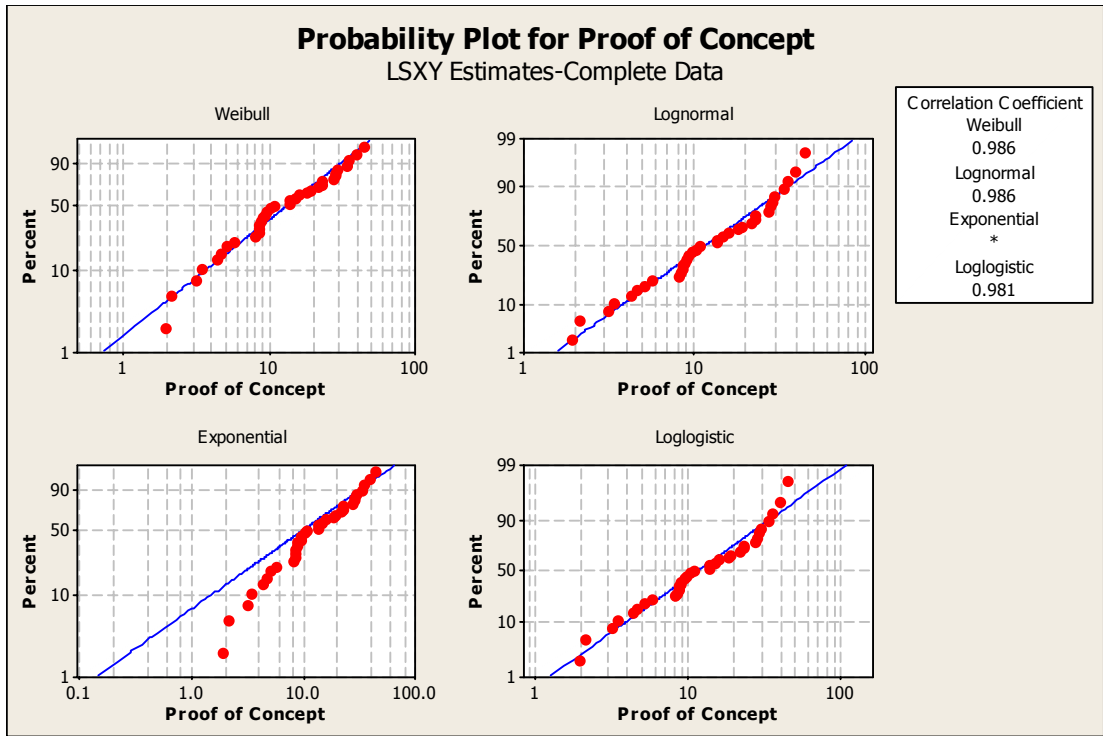
APPENDIX G

Comparative Statistical Analysis for the Proof of Concept

Goodness of Fit Test using Minitab on POC data

Distribution	Anderson-Darling (adj)	Correlation Coefficient
Weibull	0.808	0.986
Lognormal	0.679	0.986
Exponential	2.208	*
Loglogistic	0.776	0.981
3-Parameter Weibull	0.570	0.993
3-Parameter Lognormal	0.640	0.990
2-Parameter Exponential	0.976	*
3-Parameter Loglogistic	0.770	0.983
Smallest Extreme Value	5.091	0.880
Normal	1.535	0.955
Logistic	1.630	0.950





VITA

Karim J. Courey received the Master of Business Administration degree from the Florida Institute of Technology, Melbourne, Florida, in 1993, and the Bachelor of Electrical Engineering degree from Cleveland State University, Cleveland, Ohio, in 1986.

He is currently a Principal Engineer with the Orbiter Sustaining Engineering Office for the National Aeronautics and Space Administration, Lyndon B Johnson Space Center in Texas. His duty location is at John F. Kennedy Space Center in Florida. He has over twenty years of experience in the Space Shuttle Program in a wide range of positions including Systems Engineer, Design Engineer, Design Engineering Manager, Logistics Engineer, and currently a Principal Engineer for Orbiter Electrical and Avionics Systems. He has worked for Lockheed, Lockheed Martin, and United Space Alliance before joining NASA in 2001.

Mr. Courey is a licensed Professional Engineer in the state of Texas. He also received a NASA Johnson Space Center Fellowship to perform doctoral research at the University of Miami during the 2006-2007 academic calendar years.

Permanent Address: 4895 St. James Ave., Titusville, Florida 32780

